STRUCTURAL DYNAMICS OF MODULAR BRIDGE EXPANSION JOINTS RESULTING IN ENVIRONMENTAL NOISE EMISSIONS AND FATIGUE

Eric John Ancich

A thesis submitted in fulfilment of the requirements for the Degree of Doctor of Philosophy (By Publication)

Faculty of Engineering and Information Technology
University of Technology, Sydney
Australia

February 2011

CERTIFICATE OF AUTHORSHIP/ORIGINALITY

I certify that the work in this thesis has not previously been submitted for a degree nor has it been submitted as part of the requirements for a degree except as fully acknowledged within the text.

I also certify that the thesis has been written by me. Any help that I have received in my research work is acknowledged. In addition, I certify that all information sources and literature used are indicated in the thesis.

Eric John Ancich

Production Note:
Signature removed prior to publication.

ACKNOWLEDGEMENTS

Firstly, I would like to express my sincere gratitude to my principal supervisor, Professor Bijan Samali for his guidance and inspiration in all aspects throughout my study. His unselfish help and kindly advice have been invaluable.

I am extremely grateful to Dr. Khalid Aboura for his valuable advice and assistance with the mathematical formulation of the Elliptical Loading Model.

I also acknowledge the contributions of the co-authors of the various papers set out in Appendices A-N.

Special mention needs to be made of the role of the Roads and Traffic Authority of NSW (RTA) in funding the research and the assistance of many RTA colleagues in facilitating that research.

Finally, the results reported in this thesis would not have been possible were it not for the involvement of my RTA colleague, Mr Gordon Chirgwin. He single-handedly negotiated the funding gauntlet and was always able to ensure that the necessary funds were available for whatever experimental tangent I proposed. With the benefit of hindsight, it is clear that these experimental tangents led directly to the development of the high damping bearing solution that was used to successfully fatigue proof the modular bridge expansion joint installed in the western abutment of Anzac Bridge. However, at the time, these tangents were generally regarded as highly unconventional.

PUBLICATIONS

The following technical papers have been published based on the work in this thesis:

Journal Publications:

1. Ancich E.J., Chirgwin G.J. and Brown S.C. (2006). Dynamic Anomalies in a Modular Bridge Expansion Joint, *Journal of Bridge Engineering*, Vol. 11, No. 5, 541-554.

2. Ancich E.J. and Brown S.C. (2004). Engineering Methods of Noise Control for Modular Bridge Expansion Joints, *Acoustics Australia*, Vol. 32, No. 3, 101-107.

Conference Papers:

3. Ancich E.J. and Brown S.C. (2009). Premature Fatigue Failure in a Horizontally Curved Steel Trough Girder Bridge, *Proc. International Association for Bridge & Structural Engineering (IABSE) Symposium,* Bangkok, Thailand.

4. Ancich E.J., Chirgwin G.J., Brown S.C. & Madrio H. (2009). Fatigue Implications of Growth in Heavy Vehicle Loads and Numbers on Steel Bridges, *Proc. International Association for Bridge & Structural Engineering (IABSE) Symposium,* Bangkok, Thailand.

5. Ancich E.J., Chirgwin G.J., Brown S.C. & Madrio H. (2009). Fatigue Sensitive Cope Details in Steel Bridges and Implications from Growth in Heavy Vehicle Loads and Numbers, *Proc. 7th Austroads Bridge Conference*, Auckland, New Zealand.

6. Ancich E.J. (2007). Dynamic Design of Modular Bridge Expansion Joints by the Finite Element Method, *Proc. International Association for Bridge & Structural Engineering (IABSE) Symposium,* Weimar, Germany.

7. Ancich E.J., Forster G. and Bhavnagri V. (2006). Modular Bridge Expansion Joint Specifications and Load Testing, *Proc. 6th Austroads Bridge Conference*, Perth, Western Australia, Australia.

8. Ancich E.J. and Bradford P. (2006). Modular Bridge Expansion Joint Dynamics, *Proc. 6th World Congress on Joints, Bearings, and Seismic Systems for Concrete Structures*, Halifax, Nova Scotia, Canada.

9. Ancich E.J. and Chirgwin G.J. (2006). Fatigue Proofing of an In-service Modular Bridge Expansion Joint, *Proc. 6th World Congress on Joints, Bearings, and Seismic Systems for Concrete Structures*, Halifax, Nova Scotia, Canada.

10. Ancich E.J. and Bhavnagri V. (2006). Fatigue Comparison of Modular Bridge Expansion Joints Using Multiple Bridge Design Code Approaches, *Proc. 6th World Congress on Joints, Bearings, and Seismic Systems for Concrete Structures*, Halifax, Nova Scotia, Canada.

11. Ancich E.J., Brown S.C. and Chirgwin G.J. (2004). The Role of Modular Bridge Expansion Joint Vibration in Environmental Noise Emissions and Joint Fatigue Failure, *Proc. Acoustics 2004 Conference*, Surfers Paradise, Queensland, Australia, 135-140.

12. Ancich E.J. and Brown S.C. (2004). Modular Bridge Joints – Reduction of noise emissions by use of Helmholtz Absorber, *Proc. 5th Austroads Bridge Conference*, Hobart, Tasmania, Australia.

13. Ancich E.J., Brown S.C. and Chirgwin G.J. (2004). Modular Deck Joints – Investigations into structural behaviour and some implications for new joints, *Proc. 5th Austroads Bridge Conference*, Hobart, Tasmania, Australia.

Internal Reports:

14. Ancich E.J. (2000). A Study of the Environmental Noise Generation & Propagation Mechanisms of Modular Bridge Expansion Joints, *RTA Environmental Technology Report No. 000203*, Roads & Traffic Authority of NSW, Sydney, NSW, Australia.

TABLE OF CONTENTS

Chapter 3

Structural Dynamics Investigation

Chapter 4

Elliptical Loading Model

Chapter 5

Conclusions and Suggestions for Future Work

Appendix A

Ancich E.J. (2000). A Study of the Environmental Noise Generation & Propagation Mechanisms of Modular Bridge Expansion Joints, *RTA Environmental Technology Report No. 000203*, Roads & Traffic Authority of NSW, Sydney, NSW, Australia.

Appendix B

Ancich E.J. and Brown S.C. (2004a). Modular Bridge Joints – Reduction of noise emissions by use of Helmholtz Absorber, *Proc. 5th Austroads Bridge Conference*, Hobart, Tasmania, Australia.

Appendix C

Ancich E.J., Brown S.C. and Chirgwin G.J. (2004). The Role of Modular Bridge Expansion Joint Vibration in Environmental Noise Emissions and Joint Fatigue Failure, *Proc. Acoustics 2004 Conference*, Surfers Paradise, Queensland, Australia, 135-140.

Appendix D

Ancich E.J. and Brown S.C. (2004b). Engineering Methods of Noise Control for Modular Bridge Expansion Joints, *Acoustics Australia*, Vol. 32, No. 3, 101-107.

Appendix E

Ancich E.J., Brown S.C. and Chirgwin G.J. (2004). Modular Deck Joints – Investigations into structural behaviour and some implications for new joints, *Proc. 5th Austroads Bridge Conference*, Hobart, Tasmania, Australia.

Appendix F

Ancich E.J. and Bhavnagri V. (2006). Fatigue Comparison of Modular Bridge Expansion Joints Using Multiple Bridge Design Code Approaches, *Proc. 6th World Congress on Joints, Bearings, and Seismic Systems for Concrete Structures*, Halifax, Nova Scotia, Canada.

Appendix G

Ancich E.J. and Chirgwin G.J. (2006). Fatigue Proofing of an In-service Modular Bridge Expansion Joint, *Proc. 6th World Congress on Joints, Bearings, and Seismic Systems for Concrete Structures*, Halifax, Nova Scotia, Canada.

Appendix H

Ancich E.J. and Bradford P. (2006). Modular Bridge Expansion Joint Dynamics, *Proc. 6th World Congress on Joints, Bearings, and Seismic Systems for Concrete Structures*, Halifax, Nova Scotia, Canada.

Appendix I

Ancich E.J., Forster G. and Bhavnagri V. (2006). Modular Bridge Expansion Joint Specifications and Load Testing, *Proc. 6th Austroads Bridge Conference*, Perth, WA, Australia.

Appendix J

Ancich E.J., Chirgwin G.J. and Brown S.C. (2006). Dynamic Anomalies in a Modular Bridge Expansion Joint, *Journal of Bridge Engineering*, Vol. 11, No. 5, 541-554 (With permission from ASCE).

Appendix K

Ancich E.J. (2007). Dynamic Design of Modular Bridge Expansion Joints by the Finite Element Method, *Proc. International Association for Bridge & Structural Engineering (IABSE) Symposium,* Weimar, Germany.

Appendix L

Ancich E.J., Chirgwin G.J., Brown S.C. & Madrio H. (2009). Fatigue Sensitive Cope Details in Steel Bridges and Implications from Growth in Heavy Vehicle Loads and Numbers, *Proc. 7th Austroads Bridge Conference*, Auckland, New Zealand.

Appendix M

Ancich E.J. and Brown S.C. (2009). Premature Fatigue Failure in a Horizontally Curved Steel Trough Girder Bridge, *Proc. International Association for Bridge & Structural Engineering (IABSE) Symposium,* Bangkok, Thailand.

Appendix N

Ancich E.J., Chirgwin G.J., Brown S.C. & Madrio H. (2009). Fatigue Implications of Growth in Heavy Vehicle Loads and Numbers on Steel Bridges, *Proc. International Association for Bridge & Structural Engineering (IABSE) Symposium,* Bangkok, Thailand.

List of Tables

List of Figures

Notations

f_{lim}	Stress at limit state for fatigue
f^*_u	Computed Stress for ultimate design load
f_t	Tyre pulse frequency (Hz)
f_p	Wheel/beam pass frequency (Hz)
V	Vehicle speed (m/s)
G	*S*pacing between centre beams (m)
L_p	Sound Pressure Level (dB)
L_{eq}	Equivalent Continuous Sound Pressure Level (dB)
L_t	Tyre patch length (m)
b	Width of the centre beam top flange (m)
ϖ	Forcing radian frequency (rads/s)
ω_n	Natural radian frequency (rads/s)
m_B	Effective mass of the centre beam
m_V	Effective mass of the vehicle
$P(t)$	Unit vehicle (pulse) excitation with a maximum value of 1
P	Sound pressure (Pa)
P_{ref}	Reference pressure (20μPa)
x_0	Co-ordinate of the first beam node
Δt_T	Tyre pulse duration
N	Number of centre beams
f^*_f	Computed stress for fatigue design load
Φ_f	Capacity reduction factor
H	Longitudinal live load
W_x	Axle load
W_{xu}	Factored axle load for strength design
W_{xf}	Factored axle load for fatigue design
χ	Dynamic amplification factor (DAF)
γ_u	Strength limit state factor
γ_f	Fatigue limit state factor
β	Distribution factor
f_{lim}	Fatigue stress range limit

f_{TH}	Fatigue threshold limit
$J_{s,max}$	Maximum joint opening at serviceability limit state
$J_{s,min}$	Minimum joint opening at serviceability limit state
J_f	Joint opening at fatigue limit state
ε_{dyn}	Strain range due to the vehicle travelling at designated speed (peak-to-peak)
ε_{stat}	Strain range due to vehicle travelling at crawl (slow roll) speed (zero-to-peak)
δ_{dyn}	Maximum displacement due to the vehicle travelling at designated speed
δ_{stat}	Maximum displacement due to the vehicle travelling at crawl (slow roll) speed
DAF	Dynamic amplification factor
MBEJ	Modular bridge expansion joint
OEM	Original equipment manufacturer
RTA	Roads & Traffic Authority of NSW (Australia)

ABSTRACT

Whilst the use of expansion joints is common practice in bridge construction, modular bridge expansion joints are designed to accommodate large longitudinal expansion and contraction movements of bridge superstructures. In addition to supporting wheel loads, a properly designed modular joint will prevent rain water and road debris from entering into the underlying superstructure and substructure. Modular bridge expansion joints (MBEJs) are widely used throughout the world for the provision of controlled pavement continuity during seismic, thermal expansion, contraction and long-term creep and shrinkage movements of bridge superstructures and are considered to be the most modern design of waterproof bridge expansion joint currently available. Modular bridge expansion joints are subjected to more load cycles than other superstructure elements, but the load types, magnitudes and fatigue-stress ranges that are applied to these joints are not well defined. MBEJs are generally described as single or multiple support bar designs. In the single support bar design, the support bar (beam parallel to the direction of traffic or notionally parallel in the case of the swivel joist variant) supports all the centre beams (beams transverse to the direction of traffic) using individual sliding yoke connections (for the swivel joist variant, the yoke connection is characterised as a one-sided stirrup and swivels rather than slides). In the multiple support bar design, multiple support bars individually support each centre beam using a welded connection.

Environmental noise complaints from home owners near bridges with modular expansion joints led to an engineering investigation into the noise production mechanism. It was generally known that an environmental noise nuisance occurred as motor vehicle wheels passed over the joint but the mechanism for the generation of the noise nuisance has only recently been described. Observation suggested that the noise generation mechanism involved possibly both parts of the bridge structure and the joint itself as it was unlikely that there was sufficient acoustic power in the simple tyre impact to explain the persistence of the noise in the surrounding environment.

Engineering measurements were undertaken at two bridges and subsequent analysis led to the understanding that dominant frequency components in the sound pressure field inside the void below the joint were due to excitation of structural modes of the joint and/or acoustic modes of the void. This initial acoustic investigation was subsequently overtaken by observations of fatigue induced cracking in centre beams and the welded support bar connection. A literature search revealed little to describe the structural dynamics behaviour of MBEJs but showed that there was an accepted belief amongst academic researchers dating from around 1973 that the loading was dynamic. In spite of this knowledge, some Codes-of-Practice and designers still use a static or quasi-static design with little consideration of the dynamic behaviour, either in the analysis or the detailing. In an almost universal approach to the design of modular bridge expansion joints, the various national bridge design codes do not envisage that the embedded joint may be lightly damped and could vibrate as a result of traffic excitation. These codes only consider an amplification of the static load to cover sub-optimal installation impact, poor road approach and the dynamic component of load. The codes do not consider the possibility of free vibration after the passage of a vehicle axle.

Codes also ignore the possibilities of vibration transmission and response reinforcement through either following axles or loading of subsequent components by a single axle. What the codes normally consider is that any dynamic loading of the expansion joint is most likely to result from a sudden impact of the type produced by a moving vehicle '*dropping*' onto the joint due to a difference in height between the expansion joint and the approach pavement.

In climates where snow ploughs are required for winter maintenance, the expansion joint is always installed below the surrounding pavement to prevent possible damage from snow plough blades. In some European states (viz. Germany), all bridge expansion joints are installed some 3-5mm below the surrounding pavement to allow for possible wear of the asphaltic concrete. In other cases, height mismatches may occur due to sub-optimal installation.

However, in the case of dynamic design, there are some major exceptions with Standards Australia (2004) noting that for modular deck joints "…*the dynamic load allowance shall be determined from specialist studies, taking account of the dynamic characteristics of the joint*…" It is understood that the work reported in Appendices B-E was instrumental in the Standards Australia committee decisions. Whilst this Code recognizes the dynamic behavior of MBEJs, there is no guidance given to the designer on the interpretation of the specialist study data. AASHTO (2004), Austrian Guideline RVS 15.45 (1999) and German Specification TL/TP-FÜ 92 (1992) are major advancements as infinite fatigue cycles are now specified and braking forces considered but there is an incomplete recognition of the possibility of reinforcement due to in-phase (or notionally in-phase) excitation or the coupled centre beam resonance phenomenon described in Chapter 3.

This thesis investigates the mechanism for noise generation and propagation through the use of structural dynamics to explain both the noise generation and the significant occurrence of fatigue failures world-wide. The successful fatigue proofing of an operational modular joint is reported together with the introduction of an elliptical loading model to more fully explain the observed fatigue failure modes in the multiple support bar design.

CHAPTER 1

What are Modular Bridge Expansion Joints?

1.1 Introduction

Above a certain length, all bridges require some provision for expansion and contraction. In the simplest case, the bridge deck and its supporting sub-structure will expand or contract due to the normal day/night temperature fluctuations and for the greater temperature fluctuations associated with the different seasons. For Portland cement concrete structures, provision must also be made for long-term effects such as creep and shrinkage. Concrete creep is normally defined as the deformation of the structure under sustained load. Basically, long term pressure or stress on concrete can make it change shape. The main component of this deformation usually occurs in the direction the force is being applied. Like a concrete column becoming more compressed or a beam bending. Creep does not necessarily cause concrete to fail or break apart and is allowed for when concrete structures are designed. It is, however, a property of concrete that is poorly understood and only recently have bridge design codes made adequate provision for the effects of creep.

1.2 Types of Bridge Expansion joints

Ramberger (2002) provides a comprehensive summary of the most common types of bridge expansion joints. For bridges with large continuous spans, such as Sydney's Anzac Bridge (main span 345m), the requisite provision for expansion could be anywhere from 500mm to several metres and this expansion space must be filled in a suitable way to permit vehicular traffic to cross the gap. Historically, only two designs of expansion joints were capable of fulfilling this requirement. The oldest design is the roller shutter joint and more recently the modular bridge expansion joint (MBEJ). Figure 1.1 shows a typical cross-section of a roller shutter joint.

The only known example of this design in Australia is in Melbourne's Westgate Bridge. Roller Shutter joints are not considered water-proof and contain a number of wear-prone components. They are now seldom used in new bridge construction and frequently replaced with MBEJs as existing bridges are rehabilitated. However, a recent European Patent (EP 0 382 681 B1) claims to be longer wearing and more water proof.

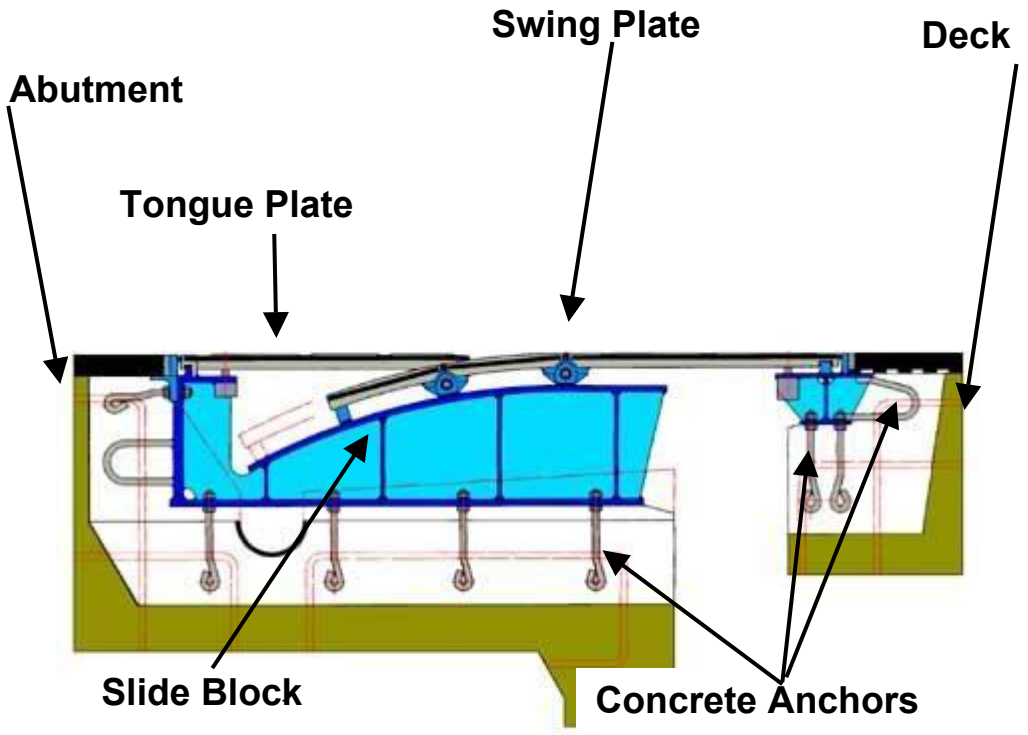

Figure 1.1 Typical cross-section of a roller shutter joint

MBEJs are considered to be the most modern design of water-proof bridge expansion joint currently available. The basic water-proof MBEJ design appears to have been patented around 1960 in Germany but the original patent has now expired and several dozen manufacturers now exist throughout the world but most copy some or all components of the expired patent. MBEJs are generally described as single or multiple support bar designs. In the *single* support bar design, the support bar (beam parallel to the direction of traffic or notionally parallel for the swivel joist variant) supports all the centre beams (beams transverse to the direction of traffic).

In the *multiple* support bar design, multiple support bars individually support each centre beam. Figure 1.2 shows a typical welded multiple support bar design.

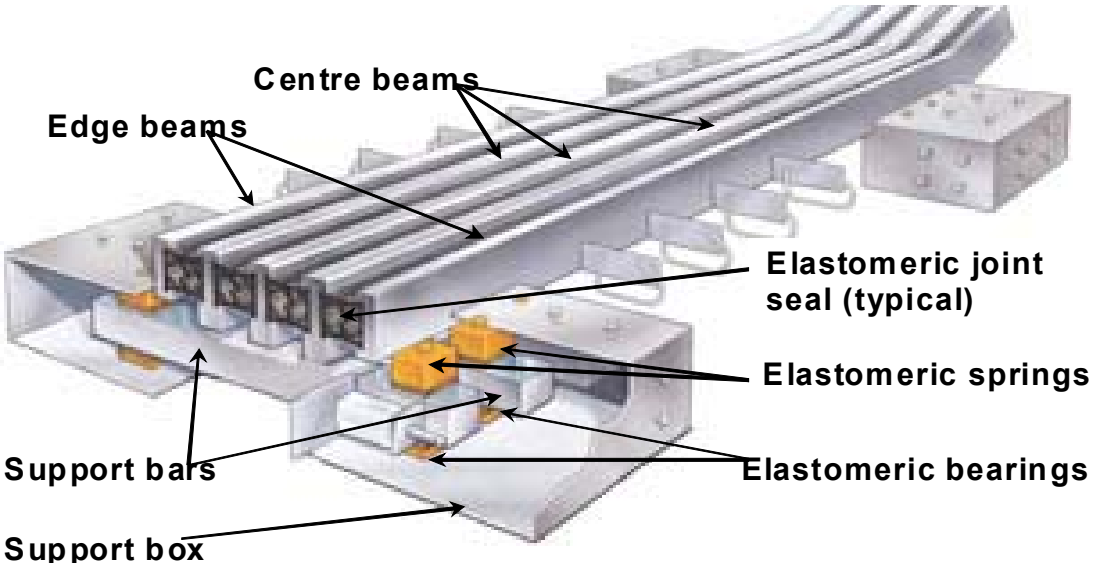

Figure 1.2 Example of a multiple support bar MBEJ design

MBEJs typically employ mechanisms to maintain equidistant centre beam spacing over the full range of joint movement. Equidistant devices include elastomeric springs, steel springs or mechanical linkages such as pantographs (the so-called '*lazy tong*'). The MBEJ installed into the northern abutment of the Karuah River Bridge on the Pacific Highway is a single support bar design and is shown in Figure 1.3 during installation. The seven sliding yokes welded to the soffit of each centre beam are clearly visible and the light blue coloured elastomeric springs of the equidistant device may be seen at the top left of the figure. The MBEJ design is so described because the expansion capability may be increased in a modular fashion by the addition of further centre beam and sealing element combinations. Centre beam widths are not standardised but 63.5mm predominates in the US and 80-90mm predominates in Europe. Other manufacturers follow European or US designs.

The maximum sealing element opening is standardised at 80mm although some jurisdictions in Europe permit the opening to increase to 100mm when noise reducing plates (See Chapter 2) are attached (Fobo, 2004).

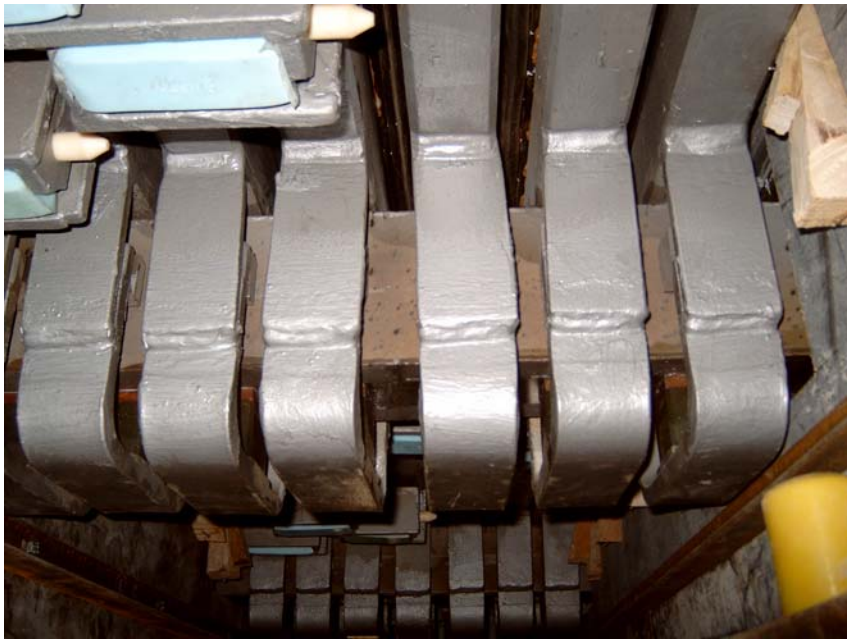

Figure 1.3 Example of a single support bar MBEJ design

Figure 1.4 shows the older style centring mechanism using steel springs. The use of steel springs has fallen out of favour with manufacturers but have considerable benefits over elastomers. In their Figure 2.12, Dexter *et al.* (2002) show a failed elastomeric spring used for centre beam centring. Similar failures have occurred in a number of RTA owned bridges in NSW.

In addition to this "crumbling" type failure, some elastomeric springs have a degree of compression set whereby the spring fails to return to its original shape after load relaxation.

Figure 1.5 shows examples of the typical "crumbling" type failure of elastomeric springs at Taree (NSW).

The manufacturer is unable (or unwilling) to identify the cause of the failures. The still intact elastomeric spring shows unrecovered deformation (compression set).

Figure 1.4 Steel spring centring mechanism at Cowra (NSW)

Figure 1.5 Failed elastomeric springs at Taree (NSW) also showing compression set

1.3 Summary

The need for expansion joints in bridges has been outlined and the typical designs of large movement bridge expansion joints discussed. The joint design known as the MBEJ has been shown to be the preferred design where water proofness was required. MBEJs were shown to come in two typical variations and the methods for achieving and maintaining equal centre beam spacing identified.

CHAPTER 2

Modular Bridge Expansion Joint Noise

2.1 Generation & Propagation

Above approximately 60-70 km/hr for cars and 70-80 km/hr for trucks, road traffic noise is largely dominated by tyre/pavement noise. The mechanism for tyre/pavement noise generation is largely well understood (Bernhard & Wayson, 2005) and involves a combination of factors but is exacerbated by the roughness profile of the pavement. All designs of bridge expansion joints produce a characteristic increase in the noise level above that generated by the general traffic. This is due principally to the discontinuity and a not un-common height mismatch between adjacent sections. In climates where snow ploughs are required for winter maintenance, the expansion joint is always installed below the surrounding pavement to prevent possible damage from snow plough blades. In some European states (viz. Germany), all bridge expansion joints are installed some 3-5mm below the surrounding pavement to allow for possible wear of the asphaltic concrete. In other cases, height mismatches may occur due to sub-optimal installation.

Because of their unique design, modular bridge expansion joints (MBEJs) are potentially the noisiest bridge expansion joints but the mechanism for noise generation from MBEJs has not been well understood. A number of studies have investigated possible noise generation mechanisms of MBEJs and it was suggested from these studies that one mechanism may be related to resonances of the air column within the gap formed by the rubber sealing element between adjacent centre beams and vehicle tyres (Martner, 1996, Ravshanovich, 2007, Ravshanovich *et al.,* 2007). This is similar to the basic tyre/pavement noise generation mechanism described by Bernhard & Wayson (2005). Ravshanovich (2007) describes this above joint noise generation mechanism as "*space compression sound*" between centre beams.

In the late 1990's, the Roads and Traffic Authority of NSW (RTA) received environmental noise complaints from homeowners near bridges with MBEJs with one house being some 500 metres from the bridge in a semi-rural environment. This suggested that the noise generation mechanism involved possibly both parts of the bridge structure and the joint itself as it was unlikely that there was sufficient acoustic power in the simple tyre impact or temperature and wind gradients to explain the persistence of the noise in the surrounding environment. MBEJs as a source of environmental noise have been identified by Martner (1996), Barnard & Cuninghame (1997) and Fobo (2004) but little was known about the generation and propagation mechanism although Barnard & Cuninghame (1997) pointed to the possible role of acoustic resonances.

An experimental investigation was undertaken into the noise production and propagation mechanism and the investigation identified modal vibration frequencies of the MBEJ coupling with acoustic resonances in the chamber cast into the bridge abutment below the MBEJ (See Ancich, 2000, Ancich & Brown, 2004a, Ancich *et al.,* 2004 and Ancich & Brown, 2004b) – also see Appendices A-D) with Ravshanovich (2007); Ravshanovich *et al.* (2007) and Matsumoto *et al.* (2007) appearing to have come to the same conclusion independently. Subsequent work by Ghimire (2007), Ghimire *et al.* (2007), Ghimire *et al.* (2008), Ghimire (2008) and Ghimire *et al.* (2009) has confirmed this earlier work both analytically by the use of Boundary Element Method (BEM) modelling and experimentally.

2.2 Noise Control Methods

There are three basic engineering noise control methods available. These are:

- Helmholtz Absorber in the abutment void space below the MBEJ;
- Partial acoustic encapsulation of the MBEJ; and
- Attachment of "*noise-reducing plates*" to the top surface of the edge and centre beams.

2.2.1 Helmholtz Absorber

The successful use of a Helmholtz absorber was reported by Ancich & Brown (2004a), Ancich *et al.* (2004) and Ancich & Brown (2004b) (See also Appendices B-D).

This noise control method is particularly attractive to Bridge Asset Owners as a retrofit option. The reported noise reduction of 9-10 dBA is equal to or better than the other known methods. Figure 2.1 shows the trialled installation at Tom Ugly's Bridge in Sydney.

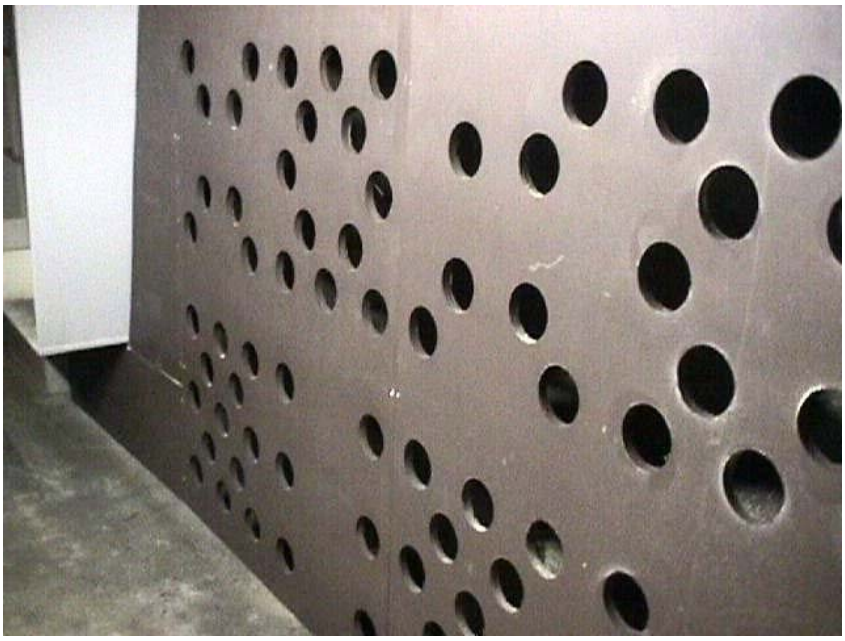

Figure 2.1 Helmholtz absorber installation at Tom Ugly's Bridge

The limitation of a Helmholtz absorber installation is that it requires an initial experimental investigation to identify the modal frequencies of the MBEJ and sufficient clear space in the abutment void to allow installation. Because the method must be tailored to each bridge/MBEJ combination, it is not attractive to MBEJ manufacturers.

2.2.2 Partial Encapsulation

Figure 2.2 shows the partial encapsulation of the MBEJ installation in the Itztal Bridge on the A73 in Upper Franconia (Germany). The joint visible in the opened section is a single support bar variant known as a swivel joist (support bar) joint.

In this type of design, centre beam equidistance is maintained by a mechanical linkage that is an integral part of the design. The swivelling joists (support bars) are free to rotate over a limited arc and as they rotate, the attached centre beams move apart or come together in a uniform manner.

Figure 2.2(a) Partially encapsulated joint – Itztal Bridge (Germany)

(Courtesy Maurer-Söhne GmbH)

Figure 2.2(b) Partial MBEJ encapsulation

(Courtesy Maurer-Söhne GmbH)

By partially encapsulating the joint and lining the encapsulation with acoustically absorbent material, the reverberant noise level above the roadway is reduced.

Also, the noise produced by the vibration of the joint entering the void space is partially absorbed and partially reflected by the enclosure. If the vibration induced noise is sufficiently reduced there will be a reduction in the amplification from coupling with acoustic resonances in the chamber cast into the bridge abutment below the MBEJ. Whilst partial encapsulation is a viable noise abatement option, it does limit the ease with which the MBEJ may be periodically inspected.

2.2.3 Noise Reducing Plates

Martner (1996) discussed the noise reduction obtained by welding triangular or diamond shaped steel elements to the top surface of centre beams. The reported results appear to relate to early experiments to develop the noise reducing plates now offered by a number of manufacturers. However, current designs all appear to be variations of a common theme.

They all appear to work by minimising or reducing the discontinuity between adjacent centre beams so that the noise resulting from the tyre impact and resulting sidewall vibration (viz. Section 2.1) is reduced because there is no longer a longitudinal gap between adjacent centre beams for the vehicle tyre to cross.

This reduced tyre impact then translates into reduced centre beam vibration and a lessened interaction between the modal frequencies of the joint and acoustic resonances in the chamber cast into the bridge abutment below the MBEJ. Figures 2.3(a & b) show the two most common European designs for noise reducing plates. Figure 2.4 shows the comparison between various joint designs and an MBEJ fitted with noise reducing plates. The difference between a treated and untreated MBEJ is of the order of 5 dBA. However, it should be noted that Figure 2.4 only relates to the noise reduction above the roadway.

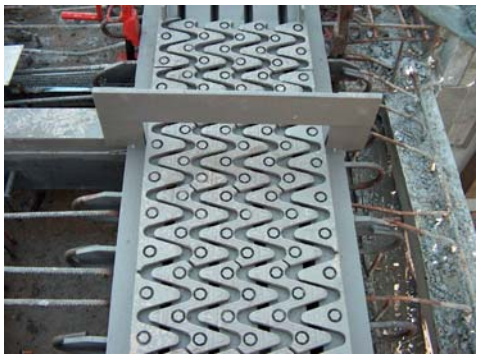

Figure 2.3(a) Bolted sinus plates

(Courtesy Mageba SA)

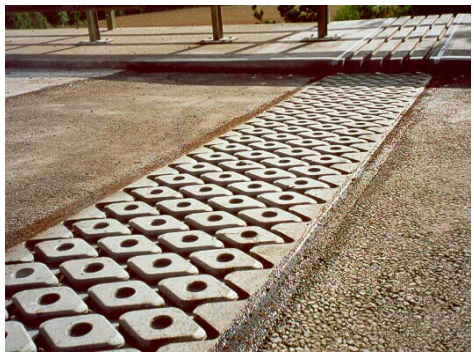

Figure 2.3(b) Welded rhombic plates

(Courtesy Maurer-Söhne GmbH)

The use of noise reducing plates is effective as a noise abatement option particularly as new joints may be purchased with the plates already attached. As a retrofit options, there are problems (and costs) associated with the need for an increase in the height of the pavement each side of the joint. Also, as the present design of noise reducing plates has been developed for the European standard centre beam width of 80-90mm, attachment to other width centre beams is problematical. The main defect with the use of noise reducing plates, for both new or retrofit applications, is the greatly reduced access to the rubber sealing element to remove damaging road debris. There is a potential fatigue issue associated with the attachment of noise reducing plates to the top surface of centre beams. Fritsche (2003) has tested bolted sinus plates for one European manufacturer. Whilst the commissioned tests were intended for approval according to TL/TP-FÜ 92, they show centre beam fracture occurred after some 3 x 10^6 cycles at a wheel load that was progressively stepped from approximately 30% of the design wheel load specified in RTA QA Specification B316 (after 2 x 10^6 cycles) to approximately 60% above that design load. As an SN curve has not been produced, it is not possible to extrapolate cycles to failure at the design wheel load. However, Metzger (2010) advises that testing of a similar centre beam, without the sinus plate attachment, produced a greater level of fatigue resistance. Ravshanovich (2007) also sees fatigue of the noise reducing plate attachment as a potential problem. The fatigue issues with MBEJs will be covered more fully in Chapter 3.

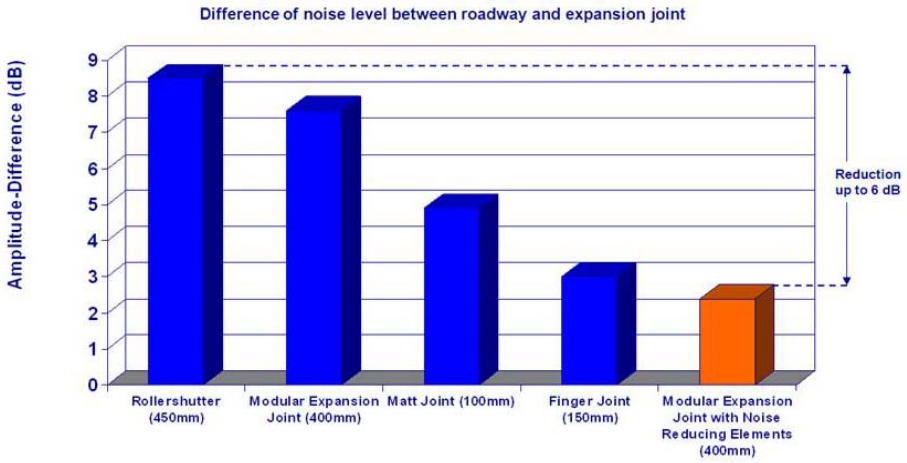

Figure 2.4 Noise reduction comparison (Courtesy Mageba SA)

Watson and Delattre (2008) present a noise level comparison between an MBEJ manufactured and installed in accordance with the RTA's QA Specification B316 and a new generation of finger plate joint described as a Sealed Aluminium Finger Joint (SAFJ) as shown in Figure 2.5. In their Table 1, they show a measurement result (at 100m) for the MBEJ of L_{eq} = 80 dBA and for the SAFJ (at 200m) of L_{eq} = 74 dBA. The measurement results for both joints are considered to be in the acoustic far-field. Accordingly, the measurement at 100m may be corrected for the difference in distance using Equation 1.

$$\Delta L_p = 20 \log_{10}\left(\frac{d1}{d2}\right) \qquad (1)$$

where, ΔL_p = Difference in noise levels

d_1 = First measurement distance

d_2 = Second measurement distance

Using Equation 1 it will be seen that, at a common distance of 200m, both measurements are equal.

Whilst it may seem surprising that an MBEJ and a finger plate joint have virtually identical noise emissions at 200m (considering the greater difference shown in Figure 2.4**),** the hypothesis is presented that the low noise emissions of the reported MBEJ are entirely due to the greater centre beam and support bar stiffnesses required to comply with RTA QA Specification B316 and the high standard of the installation.

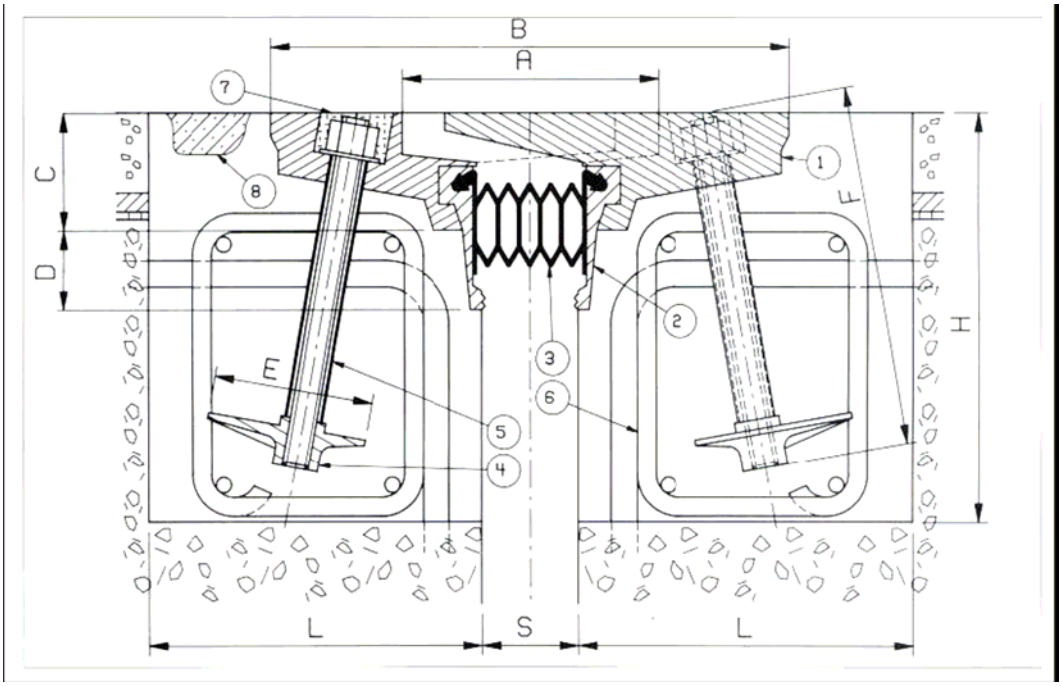

Figure 2.5 Sealed aluminium finger joint [after Watson & Delattre (2008)]

Equation 2 shows the relationship between natural frequency and beam stiffness.

$$\omega_n = \sqrt{EI / \mu l \text{^} 4} \qquad (2)$$

where, ω_n = Natural frequency, radians/sec

E = Young's Modulus

I = Moment of Inertia of beam cross-section

μ = Mass per unit length of beam

l = Length of beam

As the stiffness of centre beams and support bars increases, so do their respective natural frequencies. If the increase is sufficient, there will be a reduction in the number of modal vibration frequencies of the MBEJ able to couple with acoustic resonances in the chamber cast into the bridge abutment below the MBEJ. A simple analogy to this hypothesis would be plucking a stringed musical instrument that does not have a resonator box.

Figure 2.6 shows an MBEJ being installed in one carriageway of the Karuah River Bridge. The attention to detail by ensuring that there are no vertical discontinuities between the approach pavement and the MBEJ is clearly evident in the spirit level.

Figure 2.6 Karuah MBEJ during installation

Spuler *et al.* (2007) provide an extensive comparison between cantilever finger joints, sliding finger joints, modular joints with noise reducing plates and single gap expansion joints (identical to MBEJs but without centre beams) with noise reduction. Whilst their paper provides valuable information relating to initial cost, maintenance cost, drainage, etc. there is no information relating to how noise emissions are affected other than a figure identical to Figure 2.4.

Ravshanovich (2007), Ravshanovich *et al.* (2007) and Matsumoto *et al.* (2007) report a series of noise reduction experiments on the same MBEJ. Noise reduction was attempted by filling the space between the top surface of the centre beam and the rubber sealing element to reduce or eliminate the discontinuity as vehicles cross the joint. Unfortunately, they have chosen to report their results in terms of Sound Pressure (Pa) rather than the more common Sound Pressure Level (dB). Equation 3 shows the relationship between Sound Pressure (Pa) and Sound Pressure Level (dB).

$$L_p = 20 \log (p/p_{ref}) \quad (3)$$

where L_p = Sound Pressure Level, dB

p = Sound Pressure, Pa

p_{ref} = Reference Sound Pressure, 0.00002 Pa

Direct comparison with other reported results is further complicated as the Sound Pressure results are unweighted. Approximate conversion of their measurements to Sound Pressure Level suggests that Ravshanovich (2007), Ravshanovich *et al.* (2007) and Matsumoto *et al.* (2007) have achieved noise reductions (above the joint) of the order of 5-10 dB. This is broadly in line with other reported results.

2.3 Summary

The noise generation and propagation mechanisms for MBEJs have been identified and discussed. Noise generation was shown to have an above joint component where the mechanism was virtually identical to the more general tyre/pavement noise generation.

There was also a below joint component to the noise and this was shown to involve modal vibration frequencies of the MBEJ coupling with acoustic resonances in the chamber cast into the bridge abutment below the MBEJ. There were three basic engineering noise control methods shown to be available and these were discussed together with their relative merits.

CHAPTER 3

Structural Dynamics Investigation

3.1 Introduction

Whilst the use of expansion joints is common practice in bridge construction, modular bridge expansion joints (MBEJs) are designed to accommodate large longitudinal expansion and contraction movements and rotations of bridge superstructures. In addition to supporting wheel loads, a properly designed modular joint will prevent rainwater and road debris from entering into the underlying superstructure and substructure. MBEJs are subjected to more load cycles than other superstructure elements, but the load types, magnitudes and fatigue-stress ranges that are applied to these joints are not well defined (Dexter *et al.,* 1997).

Structural dynamics studies were carried out on the MBEJ installed in the western abutment of Sydney's Anzac Bridge which was opened to traffic on 4th December 1995. The Anzac Bridge is a cable-stayed bridge spanning a portion of Sydney Harbour on the western approach to the Central Business District and is of reinforced/prestressed concrete construction carrying 8 lanes of traffic and a combined pedestrian/bicycle way. The 805 metre long concrete structure comprises six spans with three cable-stayed central spans. With a main span of 345 metres, the bridge is the longest span cable-stayed bridge in Australia. There are two MBEJs installed into Anzac Bridge. A small 3-seal joint is located in the deck at Pier 1 and a larger 9-seal joint is located in the western abutment.

Following three and a half years of operation of Anzac Bridge, the fractured remains of a number of the lower anti-friction bearings from the MBEJ were observed on the floor of the western abutment void space. Typical bearings are shown in Figure 3.1. The left hand side bearing is a laminated elastomer and the right hand side bearing was machined from polyoxymethylene (POM). The yellow coloured disks are low friction inserts.

The absence of these lower anti-friction bearings, which were discovered during a routine inspection, would cause bending moments in the supported centre beams to be at least doubled due to the increased unsupported span.

There is little in the published literature to describe the structural dynamics behaviour of MBEJs, however Ostermann (1991) reported the theoretical and practical dynamic response of a MBEJ and Roeder (1993) reported the results of an analytical modal analysis study (FEM) of a swivel joist design MBEJ.

Figure 3.1 Anzac Bridge MBEJ support bar bearings

Roeder noted that "…*the modes were closely spaced, and many hundreds would be needed to include the predominate portion of the mass in three-dimensional vibration…"*

However, this observation is considered to only apply to the swivel joist design. Earlier, Köster (1986) had set out the principal dynamic aspects of good design and argued against the prevailing static design philosophy with the comment "…*Static calculations often lead to contrary solutions when trying to reach a higher level of security for a bridge by assuming fictitious and higher loads. The reason is that stiffer constructions are less elastic which causes them to react harder to wheel impacts than an elastic construction would*…" Subsequent researchers (Tschemmernegg, 1973 & 1991, Agarwal, 1991, Roeder, 1995, Dexter *et al.,* 1997, Crocetti, 2001) had repeatedly noted that the loading was dynamic in spite of many Bridge Design Codes used throughout the world still specifying a static or quasi-static load case. Roeder (1993) noted that the dynamic response of MBEJs was complex and field measurements of the dynamic response would assist in evaluating the dynamic behaviour. This recommendation was adopted and an experimental modal analysis study (Ewins, 1999) was undertaken to gain a better understanding of the structural dynamics behaviour of the Anzac Bridge MBEJ.

Schwammenhoefer (2001) reported that the Federal Ministry of Transport (Austria) had experienced premature fatigue failure of MBEJs and had replaced joints for both serviceability (fatigue) and noise protection (excessive environmental noise generation) reasons. MBEJ are also known to have been replaced in recent years in both Canada and the USA for predominantly serviceability reasons. Possibly the highest profile in-service failure involved the 3rd Lake Washington Bridge in Seattle, USA. Approximately 6 months after the bridge was opened to traffic in 1989, the asset owner (Washington State Department of Transportation) received numerous noise complaints about the expansion joints. Some relatively minor shim adjustments of the elastomeric bearings were undertaken but within one year, cracks in the centre beams similar to Figure 3.2 were observed.

Figure 3.2 Centre beam cracking – 3rd Lake Washington Bridge
After Roeder (2004)

Roeder (1993) considered that the precise cause of this fatigue problem could not be determined but identified a number of contributing factors. Perhaps the most significant was large compressive stresses introduced by truck wheel loads combined with residual (tensile) stresses near the stirrup-to-centre-beam weld causing the entire cyclic compressive stress to be in cyclic tension.

Fatigue cracks were also observed at Pheasant's Nest Bridge on the Hume Highway (opened December 1980) and Mooney Mooney Creek Bridge on the F3 Freeway (opened December 1986). The MBEJs installed into both bridges are multiple support bar designs and are essentially identical having been supplied by the same European manufacturer. Figure 3.3 shows the typical locations for fatigue cracks in multiple support bar designs. Type A, B & C cracks were observed at Pheasant's Nest and many developed complete structural failure. At Mooney Mooney Creek, only Type B cracks were observed of which some developed complete failure. Several weld repair exercises were attempted at both bridges but these proved to be only stop-gap solutions as fatigue cracks continued to develop. The Pheasant's Nest and Mooney Mooney Creek Bridge joints were replaced progressively by the RTA between 2003 and 2005.

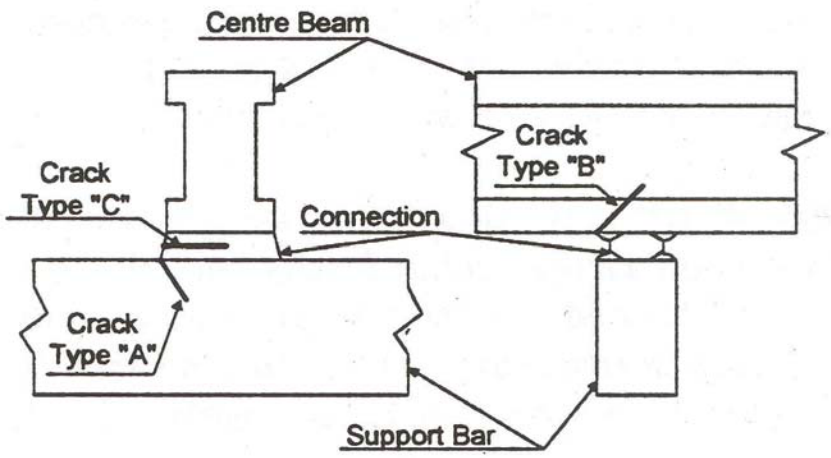

Figure 3.3 Established fatigue crack patterns – multiple support bar designs

3.2 Experimental Modal Analysis

This study of the Anzac Bridge MBEJ identified the major natural modal frequencies (all lightly damped) and, importantly, provided an insight into the source of the previously unidentified dominant frequency at 71 Hz observed during the initial noise investigation (See Appendices A-D). The vibrational modes identified include a translational (bounce/bending) mode where all parts of the MBEJ are vibrating in phase at the same frequency and vertical bending modes for the centre beams where the first three bending modes are strongly excited.

Roeder (1993) reports theoretical translational modes and Ostermann (1991) shows an analytically determined (FEM) vertical mode at 87 Hz that exhibits elements of the whole body (bounce/bending) mode. Table 3.1 presents a summary of the resulting frequency and associated damping for each natural mode identified. Figure 3.4 shows a sample plot depicting the characteristic shape of Mode 1 at 71 Hz. Mode 1 was characterised by in-phase displacement of all structural beams. This translational mode is best described as fundamental bounce of the MBEJ on the linear bearing pads. Significant bending of the centre beams and support bars is also evident.

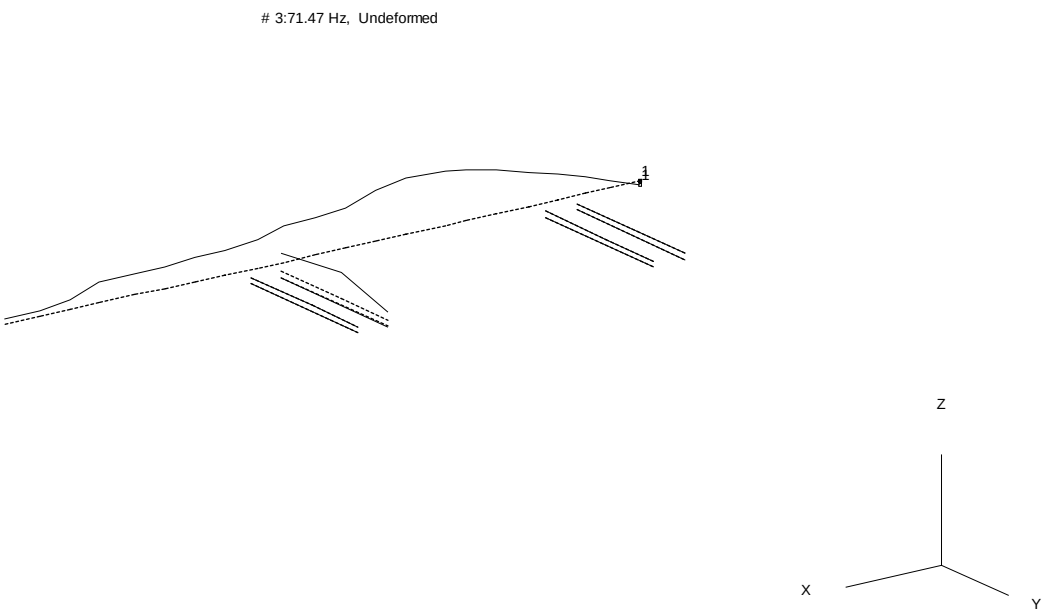

Figure 3.4 Mode 1 at 71 Hz

Table 3.1 Summary of measured modal frequencies and damping (% of Critical)

Mode Number	Mode Type	Centre Frequency, Hz	Damping, %
1	Whole body bounce	71	1.7
2	1st Bending	85	1.3
3a	2nd Bending	91	1.4
3b	Similar to Mode 3	97	1.3
4	3rd Bending	119	1.1
5	4th Bending	126	2.1

It is particularly interesting to note that the translational mode and the first centre beam bending mode are predominantly excited by typical traffic flow. Furthermore, Table 3.1 confirms that typical traffic across the MBEJ excites the joint at the identified natural modes.

3.3 Finite Element Modelling

A finite element (FE) model of the Anzac Bridge MBEJ was developed using NASTRAN (MSC Visual Nastran for Windows 2003). The Anzac Bridge MBEJ consists of two interleaved single support bar structures and previous experimental modal analysis studies (Appendix J) had demonstrated only very light, almost negligible coupling between the two structures. The FE model developed was a representation of one complete single support bar structure, comprising six support bars and four centre beams. Support bars and centre beams were represented by beam elements. The precise centre beam and support bar cross sections were mapped and section properties developed by NASTRAN. The centre beam-to-support bar yoke connection was represented by a MDOF spring/damper element. Support bar springs and bearings were also represented by MDOF spring/damper elements. The modelling is more fully described in Appendix K.

Table 3.2 shows a summary of the resulting natural modal frequencies with a description of the associated mode shapes. The predicted modes are remarkably similar to the experimentally observed modes (Ancich *et al.,* 2006).

However, there are some interesting differences. For instance, the experimentally observed bounce/bending mode at 71 Hz actually appears to be two very closely spaced modes. The FEM Mode 1 at 71 Hz is predominantly bending with some in-phase support bar bounce whereas Mode 2 at 72 Hz is predominantly in-phase support bar bounce with some bending. Mode 3 at 85 Hz is virtually identical to the experimental mode at the same frequency. Mode 4 at 98 Hz is also virtually identical to the two similar experimental modes at 91 Hz and 97 Hz respectively. Finally, Mode 5 at 101 Hz appears to combine the major elements of the separate experimental modes at 119 Hz and 125 Hz respectively. Similar modes were produced by Reid and Ansourian (2004).

Table 3.2 Summary of analytical natural modal frequencies – Anzac Bridge MBEJ

Mode No	Mode Shape Description	Natural frequency from FEM, Hz	Natural frequency of similar mode from EMA, Hz
1	Fundamental Bounce/Bending	71	71
2	Fundamental Bounce/Bending	72	Not Identified
3	First Centre Beam Vertical Bending Mode	85	85
4	Second Vertical Centre Beam Bending	98	91
5	Third Vertical Centre Beam Bending	101	97

In order to more confidently predict the dynamic amplification factors associated with modular joint structures, a procedure was developed that utilized measured strain data to simulate the force time history of a vehicle drive over.

A typical slow roll strain time history was '*calibrated*' to simulate a force time history. This single time history was replicated at time spacings to match the approximate trailer tri-axle spacing of 1.2m. Figure 3.5 shows a plot of this virtual wheel load force profile and Figure 3.6 shows a sample force time history for a 62-km/hr drive over. A time delay was applied to the time history for each centre beam to represent the appropriate drive over speed and nominal 1.2m axle spacing. It is interesting to note that whilst most studies (including Appendix K) have used an essentially sinusoidal waveform input (half sine), Roeder (1993) used a triangular waveform.

There is by no means a universal acceptance of the most representative loading model. Steenbergen (2004) questioned the validity of the half sine wave input model but used an excitation pulse almost identical to that used in Appendix K. Whilst sinusoidal loading is the most common, it is proposed (based on observation) that an elliptical loading model is more appropriate. This will be discussed in more detail in Chapter 4.

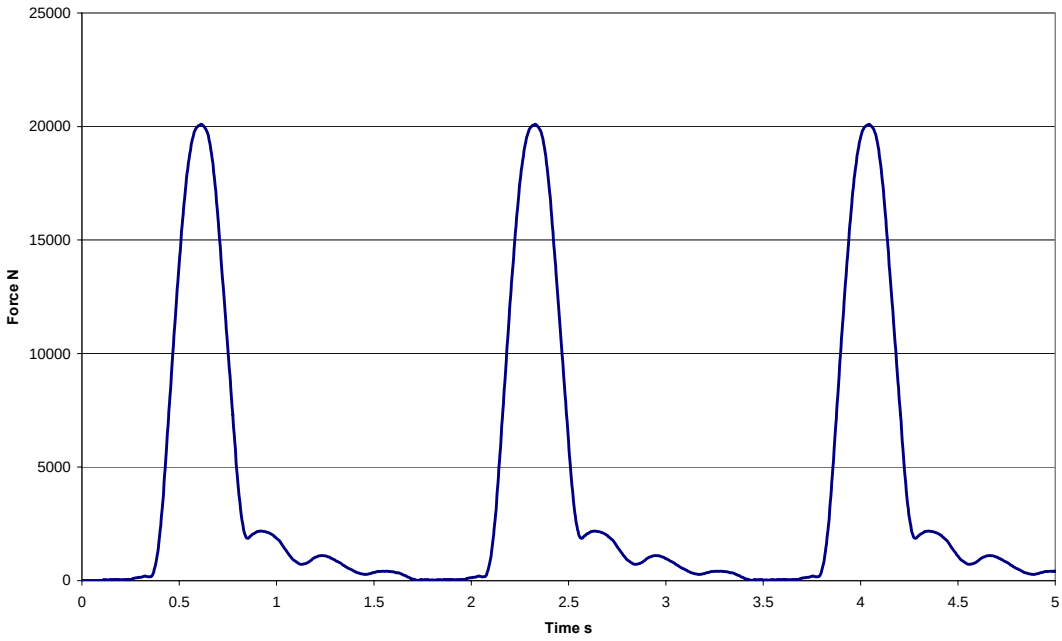

Figure 3.5 Plot of virtual wheel load force profile

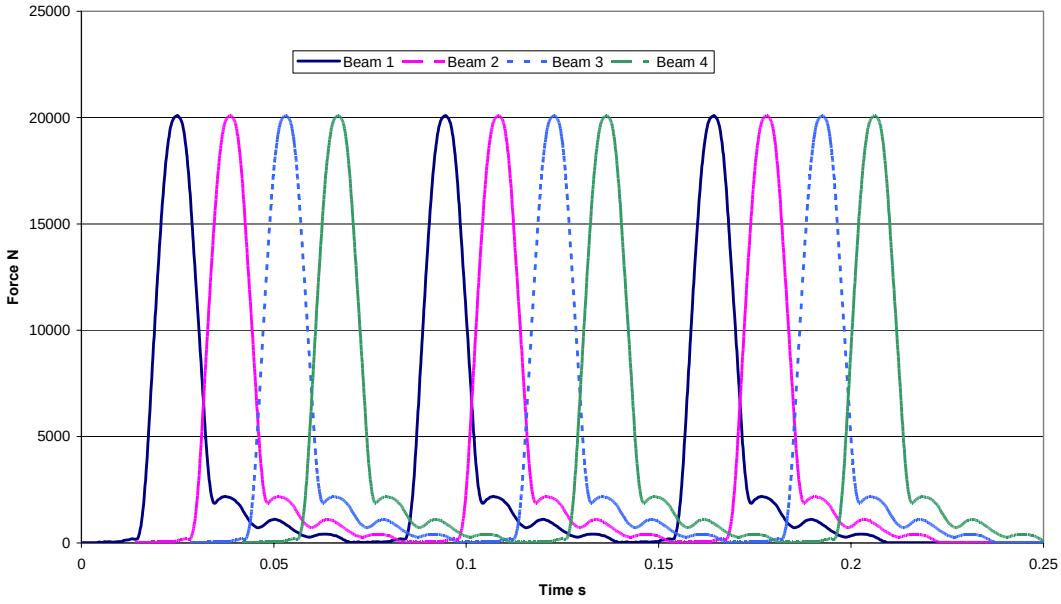

Figure 3.6 Sample force time history for a 62 km/hr drive over (Anzac)

Ostermann (1991) applied two axle transients to a single centre beam but there are no time waveforms to determine the phase relationship between these two transients and the structural response. By comparison, Medeot (2003) applied five axle transients (at 1.2m spacing) to a single centre beam and his time waveforms clearly indicate that successive axle pulses were almost perfectly out-of-phase with the dominant structural response, (i.e. not at resonance with any major natural modes of the structure). Whilst Roeder (1993) modelled an entire MBEJ, it appears from the load duration data published that he used a single triangular pulse excitation. Steenbergen (2004) also modelled an entire MBEJ but only considered a single axle excitation.

3.4 Coupled Centre Beam Resonance

The phenomenon described as *Coupled Centre Beam Resonance* was first observed experimentally by Ancich *et al.* (2004) (see also Appendices C, E, G, H & J) and later confirmed by FE modelling [Ancich (2007) and Appendix K]. Figure 3.7 shows an actual manifestation of the phenomenon.

This strain gauge time waveform shows the six axles of a semi-trailer driving over the Anzac Bridge MBEJ with six discernable peaks corresponding with each axle. Whilst the vibration induced by the steer axle has almost fully decayed by the time the first of the tandem axles crosses the joint, the second tandem axle crossing is reinforced by the continuing vibration induced by the first tandem axle. The three axles of the tri-axle show similar reinforcement even though the vibration induced by the tandem axles has fully decayed by the time the first of the tri-axles crosses the joint.

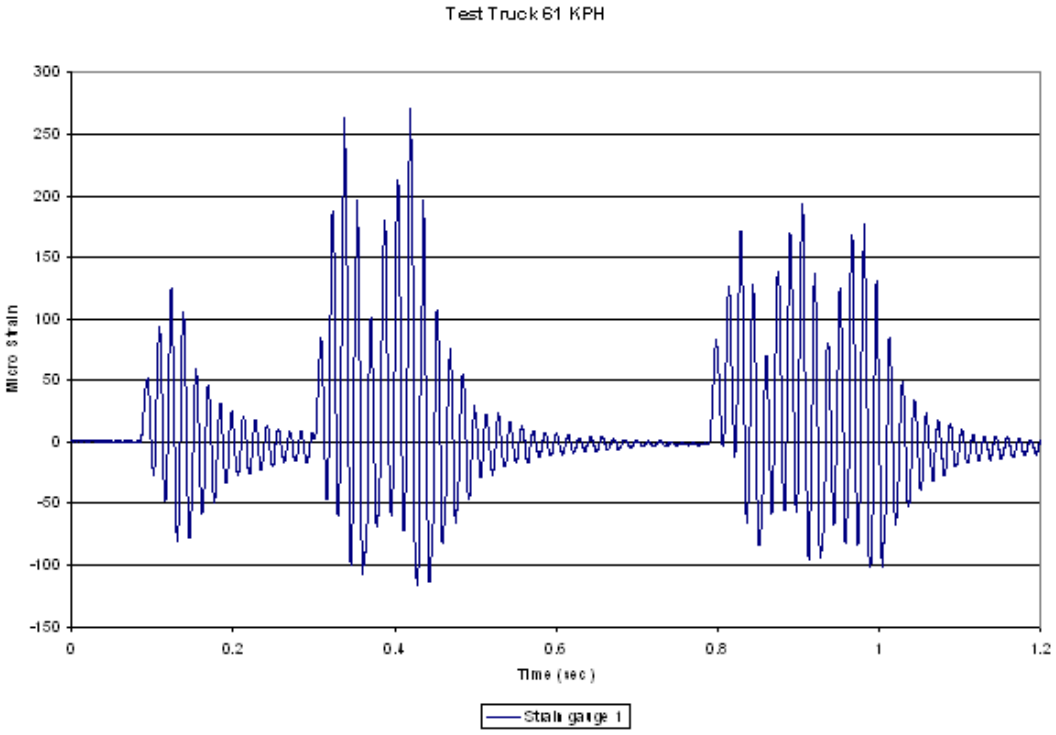

Figure 3.7 Coupled centre beam resonance

It appears that coupled centre beam resonance occurs in the single support bar design because vehicle induced vibration at the first contacted centre beam is transmitted to the other centre beams because they are all attached to a common support bar. The other centre beams are already vibrating before the vehicle tyre reaches them.

In a similar fashion, vibrational energy feeds back to the first and subsequent centre beams after the vehicle tyre has crossed them for as long as there are remaining centre beams. A simple analogy might be a guitar where all six strings are tuned to produce the same musical note. Plucking any string induces resonant vibration in the other five.

Figure 3.8 shows the quasi-static slow roll result at the same strain gauge.

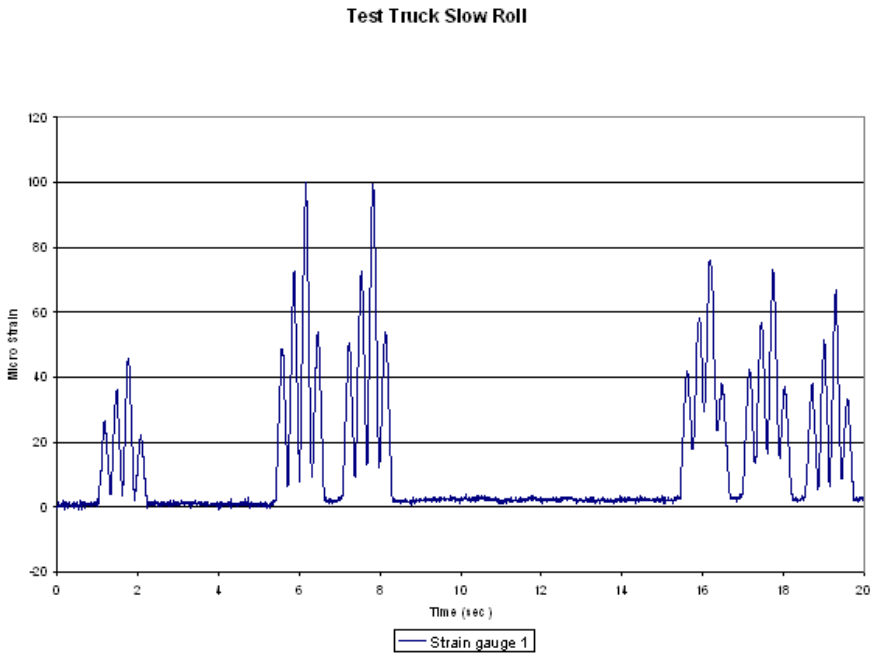

Figure 3.8 Quasi-static strain

A simple comparison between Figures 3.7 and 3.8 shows that the quasi-static slow roll produced 100 με (0-Pk) and the 61-km/hr drive over produced 385 με (Pk-Pk).

This simple comparison indicates a dynamic amplification factor (DAF) of at least 3.8 times static. Furthermore, not only the peak dynamic strains are at least 3.8 times the quasi-static but further observation of Figure 3.7 shows that the steer and tandem axles of the truck produce at least 16 cycles of vibration (per vehicle passage) where the dynamic strain equals or exceeds the quasi-static strain of 100 με (0-Pk).

Similarly, the tri-axles of the trailer produce at least 14 cycles of vibration (per vehicle passage) where the dynamic strain equals or exceeds the quasi-static strain of 100 με (0-Pk). The simple addition of these events shows that each heavy vehicle passage, of the load configuration of the test vehicle, produces around 30 vibration cycles where the dynamic strain equals or exceeds the quasi-static strain of 100 με (0-Pk). This is attributed to coupled centre beam resonance.

The phenomenon is almost entirely restricted to the single support bar design and was confirmed by FEM as the basis of the dynamic behaviour.

For the phenomenon of coupled centre beam resonance to manifest, it is considered that multiple in-phase axle pulses need to be applied to the full joint. Whilst some in-service load configurations may result in notionally out-of-phase excitation, notionally in-phase excitation will frequently occur and is clearly a worst-case for fatigue assessment. Furthermore, it is highly likely that at least 1 in every 10,000 heavy goods vehicles will be at the maximum permissible axle loading and travelling at a speed such that the MBEJ is excited partially or notionally in-phase. It was found experimentally that the impact of coupled centre beam resonance may be mitigated by damping and this will be discussed further in Section 3.6 to follow.

3.5 Strain Gauge Measurements

A series of static and dynamic strain gauge tests were undertaken on the Anzac Bridge MBEJ to clarify modular expansion joint strains and dynamic response. These results are reported in Appendices E & J.

The main aims of the strain gauge measurements were to:

1. Measure strains in critical modular expansion joint elements at potential areas of high stress, as indicated by an experimental modal analysis.
2. Measure static strains for a test vehicle loaded to the maximum legal axle load for Australia.

3. Measure dynamic strains for the same test vehicle over a range of vehicle speeds.
4. Determine maximum measured dynamic amplification factors.
5. Determine maximum measured dynamic stress, both positive (same sense as static) and negative (opposite sense to static).

3.5.1 Strain Gauge Locations

Figure 3.9 represents a plan view diagram of the eastbound kerbside lane of Anzac Bridge and shows the six strain gauge locations (SG1 to SG6).

All gauges were of a linear type and orientated in the anticipated principal stress direction (i.e. parallel to the long axis of the respective structural members).

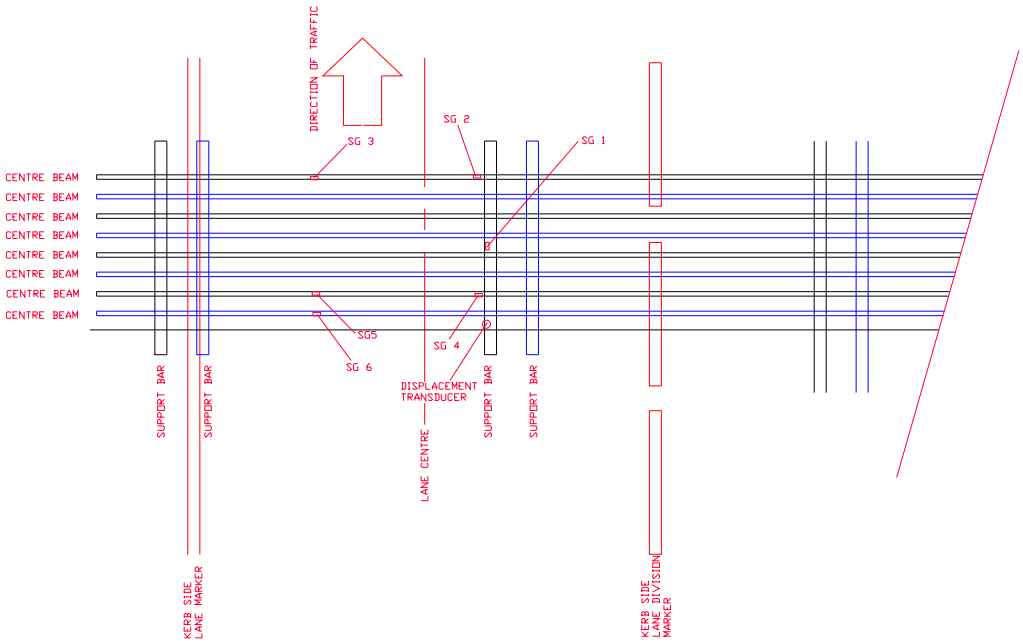

Figure 3.9 Plan view eastbound kerbside lane - six strain gauge locations (SG1 to SG6)

3.5.2 Test Vehicle Loading

Figure 3.10 shows the test vehicle loading arrangement used. The test truck was loaded to the maximum legal axle load for Australia and had a gross vehicle mass (GVM) of 42 tonnes.

Bridge Evaluation & Assessment - Test Truck loading

Axle loads from loading arrangements

Dimensions of Volvo Prime Mover F75155 and Brentwood Low Loader F02726
Test Load Vehicle A

Truck description

Steer axle (tare)	4.26 t	Steer to tandem	3.58 m	Block mass	0.99 t
Tandem (tare)	4.64 t	Spacing of tandem	1.37 m	Space for crane	3.44 m
Trailer (tare at king-pin)	4.28 t	Tandem to tridem	6.70 m	Max reach required	5.99 m
Trailer tridem (tare)	8.66 t	Spacing of tridem	1.27 m	(assumes crane in centre of trailer)	
King pin offset from centre of tandem	0.20 m	Spacing of tridem	1.27 m	Distribution to prime mover	
King-pin to front of trailer	0.63 m	King-pin to centre of tridem	8.85 m	King-pin to steer	5%
Length of tray	11.84 m	Centre of rear axle to end	1.09 m	King-pin to tandem	95%
No of blocks at goose-neck	4	Front of trailer to centre of block	3.60 m		

Block loading

Modular Expansion Joint Testing - ANZAC BRIDGE, WESTERN ABUTMENT

Block Position	Block position 1	2	3	4	5	6	7		Group loads (t) Steer	Tandem	Tridem	Total
								Tare	4.46	8.72	8.66	21.84
Loading level	No of blocks per position							Tare+bl	4.58	11.23	9.99	25.80
1	1	1	0	1	2	2	2	Load 1	4.66	12.83	17.22	34.71
2	2	2	2	2	2	4	2	Load 2	4.82	16.05	20.76	41.64

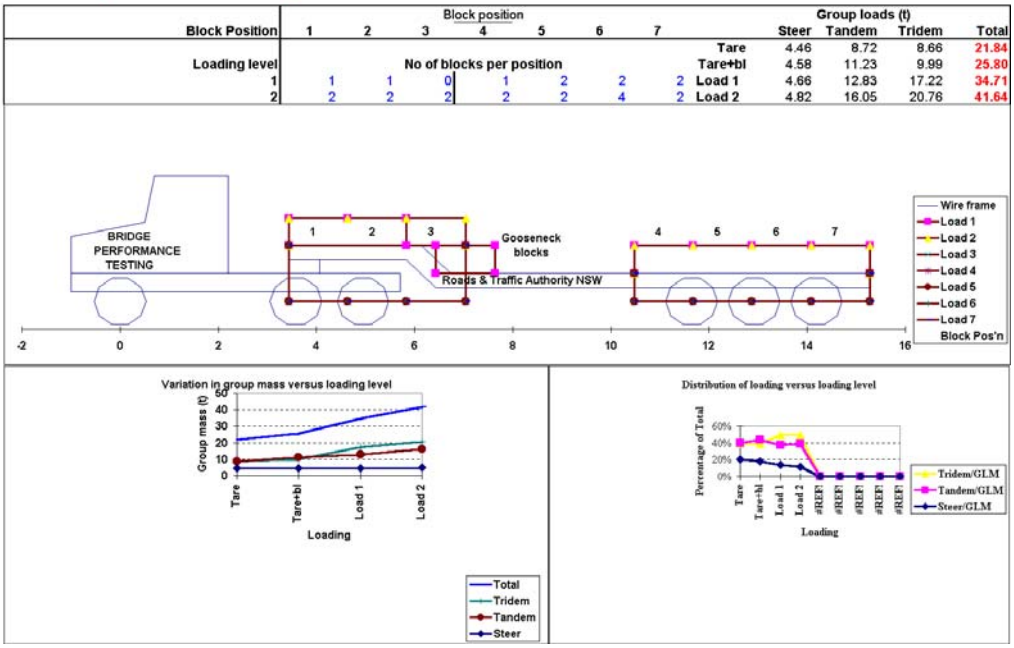

Figure 3.10 Test vehicle loading arrangement

Figure 3.11 presents a schematic elevation diagram of the modular expansion joint in relation to the nominal kerbside lane position and nominal test truck wheel positions.

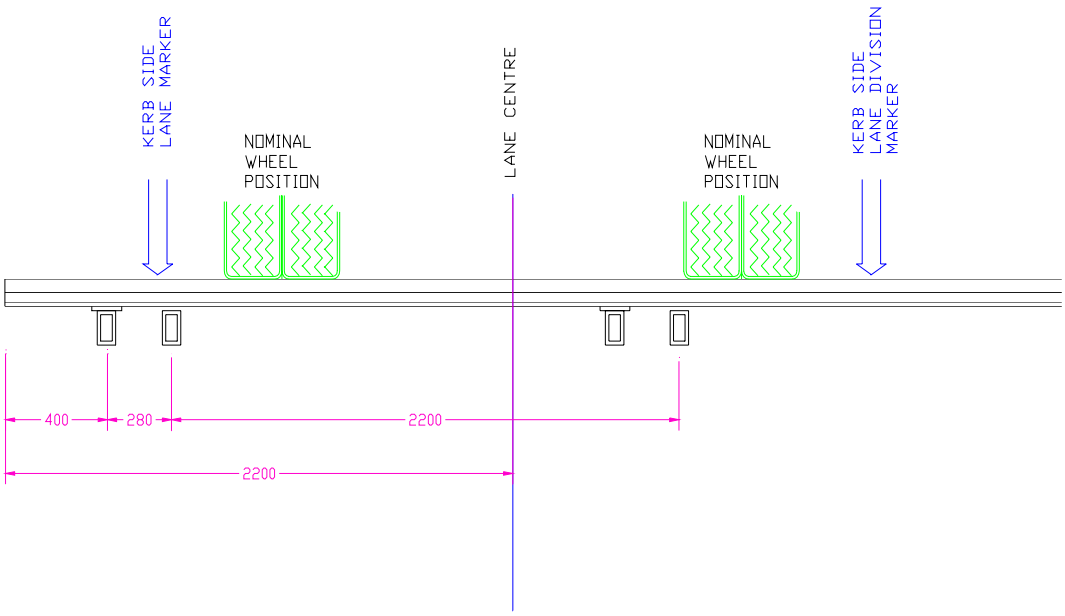

Figure 3.11 Elevation of modular expansion joint and nominal test truck position

3.5.3 Truck Slow Roll

In order to approximate true static strains and displacements, the truck was traversed over the joint at less than 3-km/hr producing negligible dynamic response of the truck or structure. All static and dynamic strains and displacements were recorded during this test.

3.5.4 Truck Pass-bys

Following as closely as possible to the same line as the slow roll test, the truck was used to traverse the test MBEJ at several speeds in the target speed range of 45-km/hr to 70-km/hr with the actual truck pass-by speeds measured using a radar speed gun.

The reproducible accuracy of the vehicle speed measurement is considered to be at least ± 2 km/hr. Table 3.3 presents the target pass-by speeds as well as the measured (actual) pass-by speeds.

Table 3.3 Target & actual test truck pass-by speeds

Run Number	Target Speed	Measured Actual Speed
1	40 kph	47 kph
2	50 kph	50 kph
3	60 kph	53 kph
4	60 kph	61 kph
5	65kph	63 kph
6	70 kph	68 kph

3.5.5 Strain and Displacement Measurements

The strain measurement system was calibrated using shunt resistors before and after each test. Strain and displacement signals were recorded on an 8-channel DAT-corder which was allowed to run for the entire test sequence. The recorded data were subsequently analysed to produce strain versus time and displacement versus time plots. In addition, Fast Fourier Transform (FFT) spectra of selected truck run and joint configuration strain measurement data were also prepared.

Further analysis included the extraction of the maximum and minimum strain and displacements resulting from the passage of the six individual test truck axles. These data were used to calculate dynamic amplification factors for each strain and displacement signal. Under conditions where a structure is well damped and static loads predominate, the peak-to-peak strain range may be approximated by the zero-to-peak strain. These conditions do not exist in modular joints and other vibration sensitive structures such as the Millennium Footbridge in London.

3.5.6 Strain Measurement Results

Table 3.4 presents a summary of the resulting maximum strains, stresses and dynamic amplification factors for each test.

Table 3.4 Summary of resulting strains, stresses and dynamic amplification factors

Test Truck Pass-by Speed	Transducer Location	Strain and Stress								
		Strain (με)			Stress (MPa)			DAF's		
		Max Tensile	Max Compress	Peak to Peak	Max Tensile	Max Compress	Peak to Peak	Max Tensile	Max Compress	Peak to Peak
Slow Roll	Support Bar	100	-1	101	20	0	20	0.0	0.0	0.0
	Centre Beams	154	-101	153	31	-20	31	0.0	0.0	0.0
47 kph	Support Bar	185	-30	215	37	-6	43	1.8	-0.4	2.2
	Centre Beams	167	-157	179	33	-31	36	1.9	-0.4	2.1
50 kph	Support Bar	226	-66	293	45	-13	59	2.3	-0.9	3.2
	Centre Beams	203	-113	234	41	-23	47	1.5	-0.3	1.8
53 kph	Support Bar	213	-54	268	43	-11	54	2.1	-0.6	2.7
	Centre Beams	136	-132	165	27	-26	33	2.0	-0.5	2.5
61 kph	Support Bar	270	-116	386	54	-23	77	2.7	-1.7	4.5
	Centre Beams	233	-141	308	47	-28	62	2.1	-0.6	2.6
63 kph	Support Bar	256	-114	370	51	-23	74	2.7	-1.9	4.6
	Centre Beams	225	-148	307	45	-30	61	1.9	-0.7	2.5
68 kph	Support Bar	218	-104	311	44	-21	62	2.4	-1.5	3.9
	Centre Beams	215	-137	280	43	-27	56	1.6	-0.7	2.2
Maximum	All	270	-157	386	54	-31	77	2.7	-1.9	4.6

The following DAF's are deduced from this investigation:

- The maximum beam stress total DAF measured was 4.6.
- The maximum beam stress positive DAF was 2.7.
- The maximum beam stress negative DAF was 1.9.

These DAF's are clearly well in excess of existing bridge codes and were a major influence with members of the committee producing the Australian Bridge Design Code, AS 5100-2004.

Preliminary fatigue analysis predicted support bar and centre beam failures after 2 x 10^7 and 3.8 x 10^6 pass-bys respectively of vehicles loaded similarly to the test truck, i.e. maximum legal axle loads. The maximum total dynamic amplification of support bar linear bearing displacement (i.e. compression) was 4.0. The maximum positive dynamic amplification of support bar linear bearing displacement was 2.2. The maximum negative dynamic amplification of support bar linear bearing displacement was 1.9. These higher than previously documented DAF's are most likely a major cause of both structural fatigue cracking as well as fracture and loss of linear bearing pads.

High negative support bar vertical displacement amplification, due to resonance of natural structural modes of the modular expansion joint and traffic forcing frequency is likely to cause uplift of the support bar and at times break contact with the lower linear bearing pad. This may allow the lower linear bearing pad to eventually dislodge. Alternatively, where the support bar is excessively restrained from uplift by elastomeric bearings, the high restraint forces may prevent proper sliding. This may distort and dislodge the upper compression spring allowing the lower linear bearing to ultimately dislodge (see Figure 3.12).

3.6 Vibration Induced Fatigue

The role of vibration in inducing fatigue in MBEJs is shown in Appendices C, H & J with the link to specific forcing frequencies (Beam Pass & Tyre Pulse frequencies) set out in Appendix C and Ghimire *et al.,* (2009). Additional vibration induced fatigue studies are shown in Appendices L, M & N. Heywood *et al.,* (2002) identified the link between road profile unevenness and bridge damage. More recently, Xie *et al.,* (2009) investigated the dynamic behaviour of a curved steel box girder bridge due to vehicle-induced vibration at a strip-seal expansion joint (essentially an MBEJ without a centre beam).

Whilst the dynamics of curved steel box girder bridges are reasonably well understood (Ancich & Brown, 2009, Huang, 2008, Okeil & El-Tawil, 2004 and Sennah & Kennedy, 2001), Xie *et al.,* (2009) do not appear to have been aware of this earlier work and largely limit their investigation to the roughness of the road profile. Ancich & Brown (2009) found the presence of a longitudinal profile with periodic corrugations of approximately 1.2 metres in length in the deck of a curved steel trough girder bridge. These corrugations were considered to explain results in which a 15 km/hr test vehicle pass-by speed produced the maximum dynamic strains. Whilst this vehicle speed was relatively low, the tested bridge was in a 50 km/hr speed zone and it was concluded that a 15km/hr speed differential between heavy vehicles passing on the bridge could produce the same dynamic response due to beating.

The importance of minimising height mismatches between the approach pavement and an expansion joint is clearly evident in the Karuah River Bridge MBEJ installation shown in Figure 2.6.

3.7 High Damping Bearings

A statistically based reliability analysis of the as-built Anzac Bridge MBEJ was undertaken by Reid & Ansourian (2004) and concluded that, without intervention, the joint would probably develop fatigue cracks approximately 13 years after the bridge was opened to traffic and that 8 of those fatigue years had already expired. As the critical MBEJ was cast into the western abutment of Anzac Bridge, there was no possibility of reducing the risk of premature fatigue failure either by decreasing the allowable loads, increasing the section properties of the structural steel members, or by reducing the unsupported spans. However, measurements of the structural dynamic properties of the joint indicated that the joint was lightly damped and this low level of damping was a major contribution to the measured dynamic amplification factor (DAF) of 4.6. The challenge was, therefore, how to add significant levels of damping to an existing structure without major modification.

Ancich & Chirgwin (2006) (see Appendix G) reported that modification of the structural dynamics of the Anzac Bridge MBEJ, by tuned mass dampers or damping coupled mass absorbers, was investigated and a trial of damping coupled mass absorbers was undertaken. Whilst the trial demonstrated that reductions in working stress of up to 30% were possible, the cost was very high and future maintenance access would be seriously impeded by the absorbers.

The damping coupled mass absorber trial confirmed that the provision of additional damping was a viable solution and that the most convenient and cost-effective locations for damping additions were the elastomeric bearings and springs installed at the ends of each support bar. Observation of the operation of the joint suggested that bearing failure resulted from the support bar bouncing on the lower bearing after the top bearing was dislodged.

Figure 3.12 shows a typically distorted top bearing prior to dislodgement.

Figure 3.12 Distorted upper support bar bearing

The joint manufacturer had used a very high preload on the top bearing to resist dynamic lift-off but this high preload prevented the PTFE surface from sliding on its mating stainless steel surface. Temperature related movement of the bridge deck eventually dislodged the '*frozen*' top bearing.

Arrangements were made to produce test bearings softer than the originals with the bottom bearing having a static stiffness double that of the top.

The net effect of this change was to decrease the preload and allow the prototype elastomeric bottom bearing to '*follow*' the support bar when it was rebounding. This modification may appear counter-intuitive to many involved in the specification or supply of MBEJs.

An initial trial was undertaken using steel/rubber laminated elastomeric bearings/springs modelled on the original top bearing (spring) and replacing the original two-piece POM bearing with a dimensionally similar laminated elastomeric bearing. These prototypes were produced using natural rubber and installed then tested in an identical manner to the original bearings using both experimental modal analysis and dynamic strain gauge measurements. This trial demonstrated that reductions in working stress of up to 30% were possible for support bars and up to 20% for centre beams. In addition, it was immediately apparent from the experimental modal analysis (EMA) results that the modal damping had also increased.

Some thought was directed at methods of increasing the non-linearity of the bearings. Davidson (2002) identified specialized synthetic polymer formulations offering very high levels of elastic-plastic hysteresis damping. As all damping converts kinetic energy to heat, a temperature rise in operational bearings was a potential problem, particularly if the temperature reached was high enough to cause pyrolysis of the synthetic polymer.

Two further trials were undertaken using the test prototype design but changing the elastomer to different formulations of synthetic high damping rubbers. One was medium damping to minimize heat build-up and the other full high damping.

The EMA and dynamic strain gauge measurements were repeated and Table 3.5 shows the comparative results obtained for the three prototypes and the original equipment manufacturer (OEM) bearings. Prototype #3 was clearly superior with around a 30% reduction in the peak-to-peak stress range for both centre beams and support bars. The peak DAF was also reduced by around 30%. Prototype #3 used the full high damping synthetic polymer. The anticipated heat build-up did not occur. Comparison measurements between modified and un-modified bearings showed that temperature increase was minimal.

Table 3.5 Comparison of prototype bearing test results

Component	OEM		Prototype #1		Prototype #2		Prototype #3	
	Stress Range, MPa	DAF	Stress Range, MPa	DAF	Stress Range, MPa	DAF	Stress Range, MPa	DAF
Centre beams	62	2.6	49	3.7	49	3.3	44	2.3
Support bars	77	4.6	67	4.1	61	4.0	53	3.1

Public tenders were called by the Roads & Traffic Authority for the manufacture and supply of production vulcanized bearings to match the static and dynamic properties of the hand-made prototypes and these were installed into the Anzac Bridge MBEJ in August 2004.

3.7.1 Post Installation Studies

Pre-and post-installation strain gauge measurements were undertaken over separate, but comparable two-week periods using ambient traffic as the loading source. Table 3.5 shows the results of those measurements. Figures 3.13 & 3.14 show the probability of failure for the welded connection between the centre beam and its yoke attachment to the support bar for the OEM condition and after fitting the Prototype #3 bearings.

The results in Table 3.6 show that the installation of these bearings has resulted in a 30% reduction in stress for both centre beams and support bars.

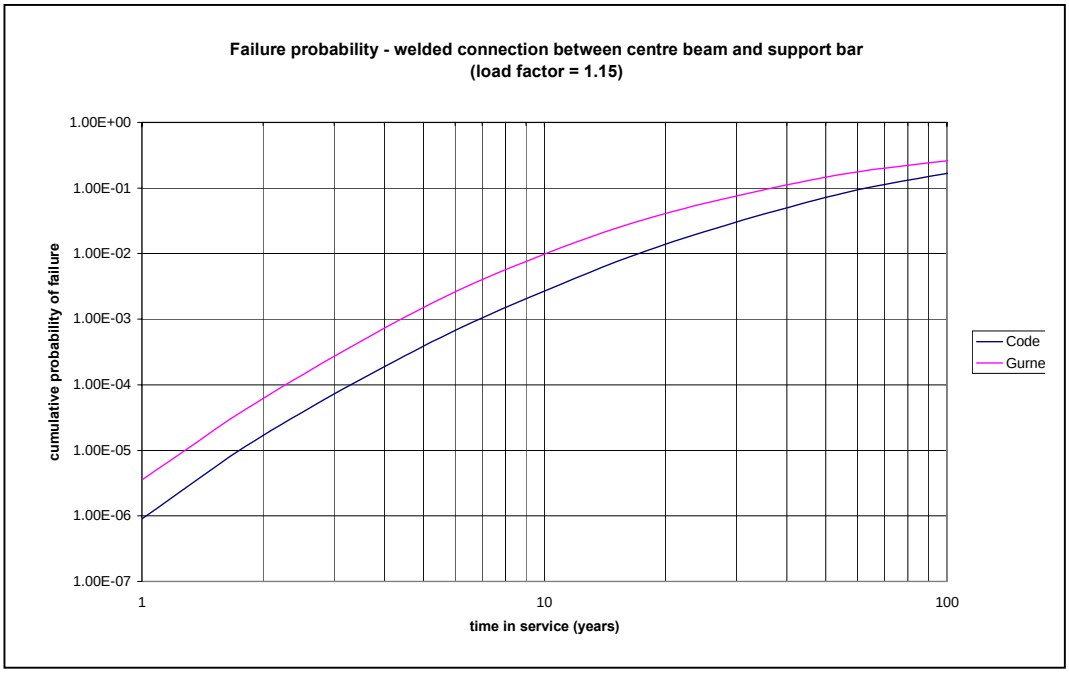

Figure 3.13 Time-dependent failure probability for a welded connection between centre beam and support bar – OEM condition
After Reid and Ansourian (2004)

Using Gurney line, probability of a single failure is 3% at 13 years => for 100 joints 95% probability of joint failure at 13 years.

In addition, there was the measured 98% reduction in stress events exceeding 15 MPa (the fatigue cut-off limit for the lowest detail category). The installation of high damping support bar bearings into the Anzac Bridge MBEJ has shown that a joint previously predicted to reach first fatigue failure within some 13 years from opening (2008) will now last in excess of 50 years (2045).

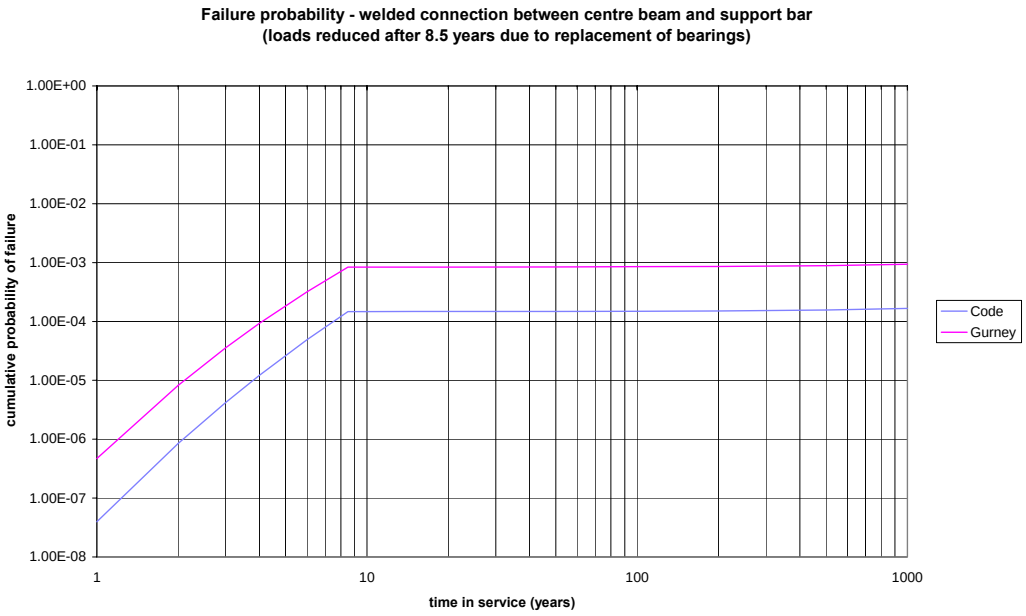

Figure 3.14 Time-dependent failure probability for a welded connection between centre beam and a support bar – prototype #3
After Reid and Ansourian (2004)
Using Gurney line, probability of a single failure is 0.1% at 50 years => for 100 connections, 10% probability of connection failure at 50 years.

Table 3.6 Annualised measurement results over comparable two-week periods

	Maximum Stress, MPa	**Significant Events, >15 MPa**
OEM	80	2,648,989
Prototype #3	55	45,630
Reduction	31.3%	98.3%

3.8 Summary

Experimental modal analysis and dynamic strain gauge studies were performed on the single support bar MBEJ installed in Anzac Bridge. The studies showed that for this joint (unmodified):

- The joint was very lightly damped (<2% of critical damping).
- The lowest frequency mode excited was a quasi-translational (bounce/bending) mode at 71 Hz.
- Due to access restrictions, horizontal modal data could not be acquired in sufficient detail to identify horizontal bending or torsional modes.
- The support bars and centre beams were acting dynamically as if simply supported.

It is considered that the dynamic response of this MBEJ is mainly due to coupled centre beam resonance and this is seen as a design characteristic of all single support bar designs. Static and dynamic strain gauge studies showed that for this joint (unmodified):

- The DAF is up to 4.6 for the fully laden test vehicle.
- This DAF is not necessarily the worst case as every possible vehicle speed and joint opening combination was not tested.
- Damping is important in the dynamic behaviour.
- The number of effective cycles of load due to vibration for each vehicle passage is very high.
- High uplift forces are generated within the joint under vehicle loading.

These results were used to develop high damping elastomeric support bar bearings and the installation of these bearings resulted in a 30% reduction in stress for both centre beams and support bars and reduce the uplift forces with consequent benefits on bearing retention.

A wholly unexpected benefit was the measured 98% reduction in stress events exceeding 15 MPa.

The installation of high damping support bar bearings into the Anzac Bridge MBEJ has ensured that a joint previously predicted to reach probable first fatigue failure within some 5 years from a 2004 study will now last in excess of 50 years. These results should be of interest to bridge asset owners and bridge designers as this approach offers a cost-effective alternative to total joint replacement provided fatigue cracking has not yet occurred. It should also be of interest to specifiers and suppliers, as they can now specify and supply joints that will last the lifetime of the bridge by using a dynamics approach to the design.

CHAPTER 4

Elliptical Loading Model

4.1 Introduction

There is by no means a universal acceptance of the most representative loading model. Steenbergen (2004) questioned the validity of the half sine wave input model but used an excitation pulse almost identical to that used in Appendix K. It is interesting to note that whilst most studies (including Appendix K) have used an essentially sinusoidal waveform input (half sine). Ostermann (1991) applied two axle transients to a single centre beam but there are no time waveforms to determine the phase relationship between these two transients and the structural response. By comparison, Medeot (2003) applied five axle transients (at 1.2m spacing) to a single centre beam and his time waveforms clearly indicate that successive axle pulses were almost perfectly out-of-phase with the dominant structural response, (i.e. not at resonance with any major natural modes of the structure). Whilst Roeder (1993) modelled an entire modular bridge expansion joint (MBEJ), it appears from the load duration data published that Roeder (1993) used a single triangular pulse excitation. Steenbergen (2004) also modelled an entire MBEJ but only considered a single axle excitation. The most common loading model for loads in the vertical direction is shown by Figure 4.1.

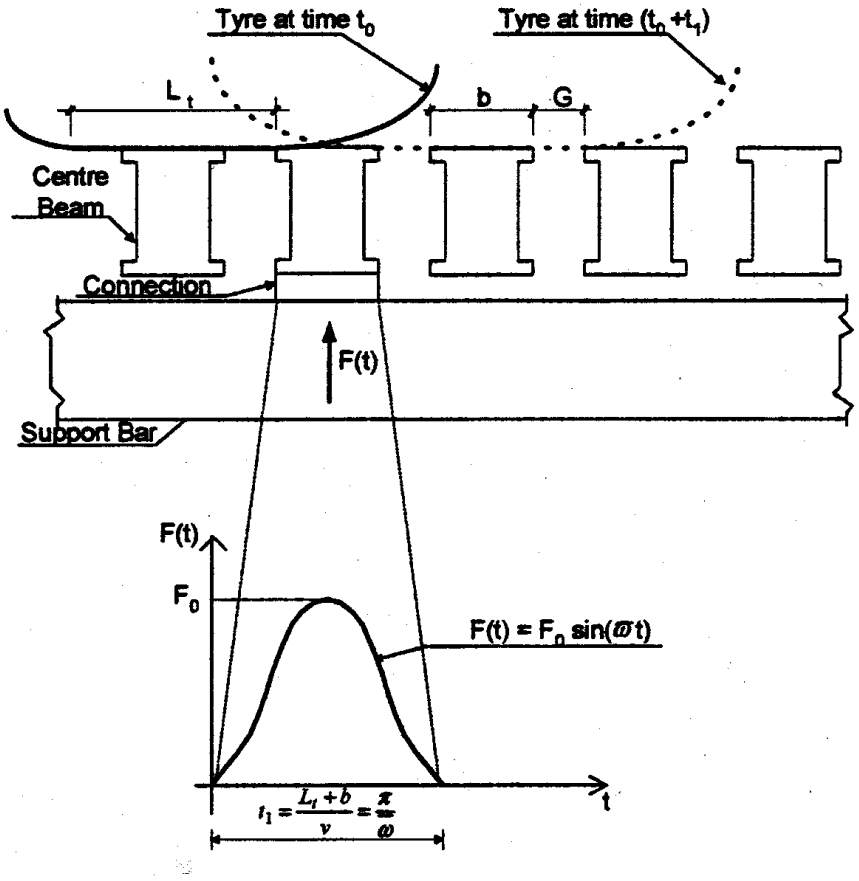

Figure 4.1 Characteristic half-sine wave impulsive load

4.2 An Elliptical Loading Model

Whilst most MBEJ design codes have provision for horizontal loading, this is normally to account for vehicle braking effects (see American Association of State Highway and Transportation Officials, 2004, Federal Ministry for Traffic, Construction & Urban Planning, 1992, Federal Ministry for Transport, Innovation and Technology, 1999, Roads & Traffic Authority, 2004).

Although sinusoidal (or quasi-sinusoidal) loading is the most common, it is proposed (based on observation) that an elliptical loading model is more appropriate as the locus of a point on the surface of a centre beam under dynamic loading appears to be a pro-grade ellipse. For multiple support bar designs, the elliptical loading model explains all three fatigue crack manifestations shown in Figure 3.3.

The position with respect to single support bar designs is unclear as there is very little in the literature about fatigue failure except for the 3rd Lake Washington Bridge in the US (Roeder, 1993 & 1995). Figure 3.2 shows fatigue cracking, in a swivel joist variant of the single support bar design, that may also be explained by the elliptical loading model. The observed cracking originated in the toe of the weld used to connect the one-sided stirrup to the centre beam.

Roeder (1993) considers that fatigue testing of a similar connection by Pattis & Tschemmernegg (1992) was not indicative of the fatigue behaviour of this joint because it did not develop the crack pattern and failure mode observed for the 3rd Lake Washington Bridge joint. He added that the test did not reflect the flexibility of the joint with respect to horizontal loads. Roeder does not report consideration of an elliptical loading model. However, such a model is considered to address the reported shortcomings of the Pattis & Tschemmernegg (1992) test.

4.2.1 Model Definition

The author has previously described the modes of vibration of MBEJ components (see Appendices A-E, H, J, & K). These modes of vibration (both analytical and experimental) are consistent with simple harmonic motion and include both horizontal and vertical modes. The general solution for a harmonic oscillator in two or more dimensions is an ellipse.

By definition, an ellipse is a smooth closed curve that is symmetric about its horizontal and vertical axes. The distance between antipodal points on the ellipse, or pairs of points whose midpoint is at the centre of the ellipse, is maximum along the major axis, and a minimum along the perpendicular minor axis.

Unlike the elliptical orbits of the planets as described by Kepler, however, these "*harmonic orbits*" have the centre of attraction at the geometric centre of the ellipse, and have fairly simple equations of motion.

By adapting the loading model illustrated in Figure 4.1, it can be shown that in the vertical direction, the loading may be expressed by Equation 4:

$$X(t) = \alpha \sin \omega t \qquad (4)$$

and in the horizontal direction by Equation 5:

$$Y(t) = \beta \sin \varpi t \qquad (5)$$

Where, α and β are the respective amplitudes.

By definition, an ellipse is a two dimensional closed curve that satisfies Equation 6:

$$\frac{x^2}{a^2} + \frac{y^2}{b^2} = 1 \qquad (6)$$

The ellipse is described by two lengths, a and b. The longer axis, a, is called the semi-major axis and the shorter, b, is called the semi-minor axis.

The parameters of an ellipse are also often given as the semi-major axis, a, and the eccentricity, e,

$$e = \sqrt{1 - \frac{b^2}{a^2}} \qquad (7)$$

and the flattening, f,

$$f = 1 - \frac{a}{b} \qquad (8)$$

In the above equations, two untested assumptions have been made. First, that the origin of the x-y co-ordinates is at the centre of the ellipse. Second, that the longer axis (major axis) of the ellipse is the x-axis. This assumption has been made because MBEJ centre beams are more flexible in the x-direction resulting in greater deflection relative to the y-direction. The assumption that the major axis is the x-axis needs additional research as the major axis may, after testing, be found to be inclined at an angle somewhere between 0^0 and 90^0 to the x-axis for a specific MBEJ or class of MBEJs.

McConnell (2010) reported dynamic measurements on a swivel joist variant of the single support bar design and noted that, in addition to the normally expected vertical loading, that there was also horizontal loading and horizontal mode excitation. However, the horizontal loading could not be quantified due to measurement limitations.

The elliptical loading model explains both the horizontal and vertical components from the reported accelerating and braking vehicles. Mc Connell (2010) appears to confirm the elliptical loading model experimentally as he notes "…*and appears as though the wheel was pushing the beam away as the wheels left the beam*…"

4.3 Summary

Whilst sinusoidal (or quasi-sinusoidal) loading models for the design of MBEJs are the most common, an elliptical loading model is proposed as being more appropriate as the locus of a point on the surface of an MBEJ centre beam under dynamic loading appears to be a pro-grade ellipse and the general solution for a harmonic oscillator in two or more dimensions is also an ellipse.

Although the generalised properties of the ellipse may be described, it is not yet possible to describe the properties of an ellipse as they apply to a specific MBEJ or class of MBEJs. This aspect of the elliptical loading model is clearly a fruitful area for further research.

CHAPTER 5

Conclusions and Suggestions for Future Work

5.1 Conclusions

It was shown in Chapter 2 that the noise produced by vehicles traversing modular bridge expansion joints (MBEJs) has a high frequency "above joint" component and a low frequency "below joint" component. The “above joint" noise was related to tyre/pavement noise generation and involved a combination of factors but was exacerbated by the roughness profile of the pavement, longitudinal discontinuities and a not un-common height mismatch between the expansion joint and the adjacent pavement. The “below joint” noise largely resulted from modal vibration frequencies of the MBEJ coupling with acoustic resonances in the chamber cast into the bridge abutment below the MBEJ. From an environmental perspective, low frequency noise is likely to be of more concern as the higher frequencies are more rapidly attenuated due to atmospheric and ground absorption, barriers, etc.

It was also shown that there were three basic engineering noise control methods available with the attachment of “*noise-reducing*” plates to the top surface of the edge and centre beams being the noise control method favoured by MBEJ manufacturers because this method could be fitted to the expansion joint at the place of manufacture. There is no information in the scientific literature relating to how the noise reducing plates are effective other than a small number of reports detailing the quantum of noise reduction.

In Chapter 3, experimental modal analysis and dynamic strain gauge studies were performed on the single support bar MBEJ installed in Anzac Bridge to understand the structural dynamics. It was considered that the dynamic response of this MBEJ was mainly due to coupled centre beam resonance and this was seen as a design characteristic of all single support bar designs. Static and dynamic strain gauge studies showed that for this joint (unmodified) the DAF was up to 4.6 for the fully laden test vehicle.

These results were used to develop high damping elastomeric support bar bearings and the installation of these bearings resulted in a 30% reduction in stress for both centre beams and support bars and reduced the uplift forces with consequent benefits on bearing retention. A wholly unexpected benefit was the measured 98% reduction in stress events exceeding 15 MPa. The installation of high damping support bar bearings into the Anzac Bridge MBEJ has ensured that a joint previously predicted to reach probable first fatigue failure within some 5 years from a 2004 study will now last in excess of 50 years. These results should be of interest to bridge asset owners and bridge designers as this approach offers a cost-effective alternative to total joint replacement provided fatigue cracking has not yet occurred.

In Chapter 4, the various loading models were outlined and discussed. Whilst sinusoidal (or quasi-sinusoidal) loading is the most common, it was proposed (based on observation) that an elliptical loading model is more appropriate as the locus of a point on the surface of a centre beam under dynamic loading is a pro-grade ellipse and the general solution for a harmonic oscillator in two or more dimensions is also an ellipse.

5.2 Suggestions for Future Work

5.2.1 MBEJ Noise Generation & Abatement

The hypothesis was offered in Chapter 2 that the various proprietary shapes of noise reducing plates all appear to work by minimising or reducing the discontinuity between adjacent centre beams so that the noise resulting from the tyre impact and resulting sidewall vibration (viz. Section 2.1) is reduced because there is no longer a longitudinal gap between adjacent centre beams for the vehicle tyre to cross. However, the action of the noise reducing plates appears to be limited to the "*above joint*" noise component. It is recommended that additional experimental and computational work needs to be undertaken in order to understand how noise reducing plates affect the "*below joint*" noise generation.

5.2.2 Elliptical Loading Model

The concept of an elliptical loading model for MBEJs is somewhat unique and has not previously been discussed in the scientific literature. It is recommended that additional experimental and computational work needs to be undertaken in order to fully develop the elliptical loading model into a form suitable for the MBEJ design process and to incorporate the model into the relevant national and international design codes. In formulating the elliptical loading model, it was assumed that the origin of the *x*-*y* co-ordinates is at the centre of the ellipse. And secondly, that the longer axis (major axis) of the ellipse is the *x*-axis. This second assumption was made because MBEJ centre beams are more flexible in the *x*-direction resulting in greater deflection relative to the *y*-direction. The assumption that the major axis is the *x*-axis needs additional research as the major axis may, after testing, be found to be inclined at an angle somewhere between 0^0 and 90^0 to the *x*-axis for a specific MBEJ or class of MBEJs.

REFERENCES

Agarwal A.C. (1991). Static And Dynamic Testing Of A Modular Expansion Joint In The Burlington Skyway*, Paper presented at the 3rd World Congress on Joint Sealing and Bearing Systems for Concrete Structures*, Toronto, Ontario, Canada, 1-22.

American Association of State Highway and Transportation Officials (1969). Standard Specification for Highway Bridges, AASHTO, 14th Edition, Washington, DC, USA.

American Association of State Highway and Transportation Officials (1973). Standard Specification for Highway Bridges, AASHTO, 15th Edition, Washington, DC, USA.

American Association of State Highway and Transportation Officials (2004). *AASHTO LRFD Bridge Design Specifications, SI Units*, 3rd Ed., Washington, DC, USA.

Ancich E.J. (2000). A Study of the Environmental Noise Generation & Propagation Mechanisms of Modular Bridge Expansion Joints, *RTA Environmental Technology Report No. 000203*, Roads & Traffic Authority of NSW, Sydney, NSW, Australia, 9 pp.

Ancich E.J., Brown S.C. & Chirgwin G.J. (2004). Modular Deck Joints – Investigations into structural behaviour and some implications for new joints, *Proc. 5th Austroads Bridge Conference*, Hobart, Tasmania, Australia.

Ancich E.J. & Brown S.C. (2004). Modular Bridge Joints – Reduction of noise emissions by use of Helmholtz Absorber, *Proc. 5th AUSTROADS Bridge Engineering Conference*, Hobart, Tasmania, Australia.

Ancich E.J., Brown S.C. & Chirgwin G.J. (2004). The Role of Modular Bridge Expansion Joint Vibration in Environmental Noise Emissions and Joint Fatigue Failure, *Proc. Acoustics 2004 Conference*, Surfers Paradise, Qld., Australia, 135-140.

Ancich E.J. and Brown S.C. (2004). Engineering Methods of Noise Control for Modular Bridge Expansion Joints, *Acoustics Australia*, 32(3), 101-107.

Ancich E. J. & Bhavnagri V. (2006). Fatigue Comparison of Modular Bridge Expansion Joints Using Multiple Bridge Design Code Approaches, *Proc. 6th World Congress on Joints, Bearings and Seismic Systems for Concrete Structures,* Halifax, Nova Scotia, Canada.

Ancich E.J. & Chirgwin G.J. (2006). Fatigue Proofing of an In-service Modular Bridge Expansion Joint, *Proc. 6th World Congress on Joints, Bearings & Seismic Systems for Concrete Structures*, Halifax, Nova Scotia, Canada.

Ancich E.J., Chirgwin G.J. and Brown S.C. (2006). Dynamic Anomalies in a Modular Bridge Expansion Joint, *Journal of Bridge Engineering*, 11(5), 541-554.

Ancich E.J. (2007). Dynamic Design of Modular Bridge Expansion Joints by the Finite Element Method, *Proc. International Association for Bridge & Structural Engineering (IABSE) Symposium,* Weimar, Germany.

Ancich E.J. and Brown S.C. (2009). Premature Fatigue Failure in a Horizontally Curved Steel Trough Girder Bridge, *Proc. International Association for Bridge & Structural Engineering (IABSE) Symposium,* Bangkok, Thailand.

Ancich E.J., Chirgwin G.J., Brown S.C. & Madrio H. (2009). Fatigue Implications of Growth in Heavy Vehicle Loads and Numbers on Steel Bridges, *Proc. International Association for Bridge & Structural Engineering (IABSE) Symposium,* Bangkok, Thailand.

Ancich E.J., Chirgwin G.J., Brown S.C. & Madrio H. (2009). Fatigue Sensitive Cope Details in Steel Bridges and Implications from Growth in Heavy Vehicle Loads and Numbers, *Proc. 7th Austroads Bridge Conference*, Auckland, New Zealand.

Anon. (1999). Microstran User Manual Version 7, Engineering Systems Pty Ltd, Sydney, NSW, Australia.

Anon. (2001). Geräuschminderung an Fahrbahnübergängen in Lamellenbauweise durch wellenförmigen Fugenverlauf, *Maurer Info Nr. 24*, Maurer Söhne, Munich, Germany, 10 pp (In German).

Barnard C.P. & Cuninghame J.R. (1997). Improving the Performance of Bridge Expansion Joints: Bridge Deck Expansion Joint Working Group Final Report, *TRL Report 236*, Transport Research Laboratory, Crowthorne, Berkshire, UK, 92 pp.

Bernhard, R. J. and Wayson R. L. (2005). An Introduction to Tire/Pavement Noise*, Publication SQDH 2005-1*, Institute for Safe, Quiet and Durable Highways, Purdue University, West Lafayette, Indiana, USA.

Brown S.C. (2005). Vibration and Fatigue Investigation Taree Bypass Modular Expansion Joint, *Report 10-1788-R4*, Richard Heggie Associates Pty Ltd (now SLR Consulting Australia Pty Ltd), Lane Cove, NSW, Australia. (Unpublished report prepared for the Roads & Traffic Authority of NSW).

Brown S.C. (2005). Measurement of Static and Dynamic Strains Taree Bypass Bridge Modular Expansion Joint, *Report 10-1788-R5*, Richard Heggie Associates Pty Ltd (now SLR Consulting Australia Pty Ltd), Lane Cove, NSW, Australia. (Unpublished report prepared for the Roads & Traffic Authority of NSW).

Brown S.C. (2005). Modal Analysis Karuah Bypass Bridge Modular Expansion Joint, *Report 10-1788-R21*, Richard Heggie Associates Pty Ltd (now SLR Consulting Australia Pty Ltd), Lane Cove, NSW, Australia. (Unpublished report prepared for the Roads & Traffic Authority of NSW).

Brown S. C. (2005). Measurement of Static and Dynamic Strains: Karuah Bypass Bridge, Karuah NSW Modular Expansion Joint, *Report 10-1788-R20*, Richard Heggie Associates Pty Ltd (now SLR Consulting Australia Pty Ltd), Lane Cove, NSW, Australia. (Unpublished report prepared for the Roads & Traffic Authority of NSW).

Boyd A.L., Schmidt B.R. & Thornton P.B. (1982). Loading and Impact Effects on Mine Haul Road Bridges, *MWP Technical Quarterly No. 4*, Macdonald Wagner & Priddle Pty Ltd (now Aurecon Pty Ltd), Sydney, NSW, Australia, 7-15.

Chaallal O., Sieprawski G. & Guizani L. (2006). Fatigue performance of modular expansion joints for bridges, Canadian Journal of Civil Engineering, Vol. 33, No. 8, 921-932.

Clough, R. and Penzien, J. (1975). *Dynamics of Structures*, McGraw-Hill.

Crocetti R. (2001). On some Fatigue Problems Related to Steel Bridges, *PhD Dissertation*, Chalmers University of Technology, Göteborg, Sweden.

Crocetti R. & Edlund B (2001). Fatigue Performance of Modular Bridge Expansion Joints, *Chalmers University of Technology*, Göteborg, Sweden.

Crocetti R. & Edlund B. (2003). Fatigue Performance of Modular Bridge Expansion Joints, *J. Perform. Constr. Facil.*, ASCE, 17(4), 167-176.

Davidson G. (2002). (Ludowici Ltd.). Personal Communication.

Deutsches Institut für Normung (1985). Road and foot bridges; design loads, *DIN 1072 -1985*, Berlin, Germany.

Dexter R.J., Connor R.J. & Kaczinski M.R., (1997). Fatigue Design of Modular Bridge Expansion Joints, *NCHRP Report 402,* Transportation Research Board, National Research Council, Washington, DC, USA.

Dexter R.J., Osberg C.B. & Mutziger M.J. (2001). Design, Specification, Installation, and Maintenance of Modular Bridge Expansion Joint Systems, *Journal of Bridge Engineering*, 6(6), 529-538.

Dexter R.J., Mutziger M.J. & Osberg C.B. (2002). Performance Testing for Modular Bridge Joint Systems, *NCHRP Report 467,* Transportation Research Board, National Research Council, Washington, DC, USA.

Edlund B. and Crocetti R. (2007). Bridge expansion joints – design for movements, performance and durability, *Proc. International Association for Bridge & Structural Engineering (IABSE) Symposium***,** Weimar, Germany.

Embleton T.F.W. (1988). Mufflers, *Noise and Vibration Control – Revised Edition* ed. L.L. Beranek, Institute of Noise Control Engineering, Indianapolis, Indiana, USA, 362-405.

European Commission (1992). Design of Steel Structures, *EN 1993 Eurocode 3 Section 9, Fatigue*, Brussels, Belgium.

European Patent Office (1993). Rollverschluss-Fahrbahnübergang, insbesondere für Dilationsfugen von Brücken, *EP 0 382 681 B1*, Paris, France.

Ewins D.J. (1999). Modal Testing: Theory, Practice & Application (2nd Edition), *Research Studies Press*, Hertfordshire, UK, 163-276.

Federal Ministry for Transport, Innovation and Technology (1999). Expansion Joints for Bridges, *Austrian Guideline RVS 15.45, Draft, version 1*, Vienna, Austria.

Federal Ministry for Traffic, Construction & Urban Planning (1992). Technical delivery and inspection specifications for watertight expansion joints of road and foot bridges, *TL/TP-FÜ 92*, Bonn, Germany. Non-revised translation (draft 1), provided by the German Association of Joint and Bearing Manufacturers [Vereinigung der Hersteller von Fahrbahnübergängen und (Brücken) Lagern].

Fobo W. (2004). Noisy Neighbours, *Bridge Design & Engineering*, 35, 75.

French S. (2005). Review of Cracking Remediation Reports and Recommended Remediation Scope, *Report 024-P1164-009-01*, Burns & Roe Worley Pty Ltd (now Worley Parsons Pty Ltd), Sydney, NSW, Australia, 10 pp. (Unpublished report prepared for the Roads & Traffic Authority of NSW).

Fritsche G. (2003). Dynamische Versuche zur Betriebstauglichkeit aufgeschraubter Fingerplatten Regelprüfung nach TL/TP-FÜ 92 für Fahrbahnübergänge mit geräushmindernder Oberfläche (Dynamic tests for operational integrity of screwed finger plates – Approval according to TL/TP-FÜ 92 for expansion joint with noise reducing surface), *Bericht Nr.: 38/2003; be38_03.doc*, University of Innsbruck, Innsbruck, Austria (Unpublished report prepared for Mageba SA) (in German).

Fu G., Feng J., Delelbab W., Moses F., Cohen H. & Mertz D. (2008). Impact of Commercial Vehicle Weight Change on Highway Bridge Infrastructure, *J. Bridge Engineering,* ASCE, 13(6), 556-564.

Gargett D., Hossain A & Cosgrove D. (2006). Interstate Freight on States' Roads, *Proc. 29th Australasian Transport Research Forum*, Surfers Paradise, Queensland, Australia, 2006.

Ghimire J.P. (2007). A Numerical Investigation of Noise Generation and Radiation from Bridge Modular Expansion Joint: Dependence on Frequency and Direction, *Proc. Of the Ninth International Summer Symposium*, JSCE, Yokohama, Japan.

Ghimire J.P., Matsumoto Y. and Yamaguchi H. (2007). Vibro-acoustic analysis of noise generation from a full-scale model of modular bridge expansion joint, *Proc. InterNoise 2007*, Istanbul, Turkey.

Ghimire J.P., Matsumoto Y. and Yamaguchi H. (2008). Vibro-acoustic analysis of noise generation from a full-scale model of modular bridge expansion joint, *Noise Control Eng. J.*, **56** (6), 442-450.

Ghimire J.P. (2008). Numerical investigation of noise generation and radiation from modular expansion joint, *PhD Thesis*, Saitama University, Tokyo, Japan.

Ghimire J.P., Matsumoto Y., Yamaguchi H. and Kurahashi I. (2009). Numerical investigation of noise generation and radiation from an existing modular expansion joint between prestressed concrete bridges, *Journal of Sound & Vibration, Vol 328, Issue 1-2*, 129-147 (DOI: 10.1016/j.jsv.2009.07.016).

Heywood R., Prem H. & McLean J. (2002). Guide to Road Profile Unevenness and Bridge Damage, *Report AP-T13*, Austroads, Sydney, NSW, Australia, 33 pp.

Heywood R., Brandis A. & Land K. (2004). Bridge over Darling River at Wilcannia: Design Review of Steel Trough Girder Web Crack Repairs, *Report 14024*, Texcel Pty Ltd, Brisbane, Qld., Australia, 40 pp (Unpublished report prepared for the Roads & Traffic Authority of NSW).

Huang D. (2008). Full-Scale Test and Analysis of a Curved Steel-Box Girder Bridges, *J. Bridge Engineering,* ASCE, 13(5), 492-500.

Imam B.M., Righiniotis T.D. & Chryssanthopoulos M.K (2008). Probabilistic Fatigue Evaluation of Riveted Railway Bridges, *J. Bridge Engineering,* ASCE, 13(3), 237-244.

Jones D.I.G. (1967). Effect of Isolated Tuned Dampers on Response of Multispan Structures. *J. Aircraft*, Vol. 4, No. 4, 343-346.

Kaczinski M.R. (2004). (D.S. Brown Co., Inc.). Personal Communication.

Köster, W. (1986). The Principle of Elasticity for Expansion Joints, *Joint Sealing and Bearing Systems for Concrete Structures*, *ACI SP-94*, American Concrete Institute, Detroit, Michigan, USA, 675-711.

Leendertz J., Weber F., Volk B. and Nagel O. (2007). Dynamic behaviour of modular expansion joints, *Proc. International Association for Bridge & Structural Engineering (IABSE) Symposium***,** Weimar, Germany.

MacDougall C., Green M. F. and Schillinglaw S. (2006). Fatigue Damage of Steel Bridges Due to Dynamic Vehicle Loads, *Journal of Bridge Engineering*, Vol. 11, No. 3, 320–328 [DOI: 10.1061/(ASCE)1084-0702(2006)11:3(320)].

Martner O. (1996). Noise Emission of Constructions for Bridge-To-Road Crossings, *Proc. Inter-Noise 96*, Liverpool, UK, 211-214.

Matsumoto Y., Yamaguchi H., Tomida N., Kato T., Uno Y., Hiromoto Y. & Ravshanovich K.A. (2007). Experimental investigation of noise generated by modular expansion joint and its control, *Journal of the Japan Society of Civil Engineers, Division A*, 63(1), 75-92 (In Japanese).

McConnell R. (2010). Insitu Dynamic Testing of Swivel Joist Modular Expansion Joints installed in the Go Between Bridge, *Report 86524*, Arup Pty Ltd, Brisbane, Qld., Australia, 41 pp (Unpublished report prepared for the Hale Street Link Alliance).

Medeot R. (2003). Impact Analysis of Maurer Expansion Joints: DS640 Swivel joist joint and D240 girder grid joint, Selvazzano, Italy, 38 pp (Unpublished report prepared for Maurer Söhne GmbH & Co. KG).

Metzger S. (2010). (Mageba SA). Personal Communication.

Morassi A. & Tonon S. (2008). Dynamic Testing for Structural Identification of a Bridge, *J. Bridge Engineering,* ASCE, 13(6), 573-585.

Mothe R.N. (2006). Partial Continuity in Prestressed Concrete Girder Bridges with Jointless Decks, *MSc Thesis*, Louisiana State University, Baton Rouge, Louisiana, USA.

NAASRA (1976). National Association of Australian State Road Authorities 1976 Bridge Design Specification, National Association of Australian State Road Authorities, Sydney, NSW Australia.

Okeil A.M. & El-Tawil S. (2004). Warping Stresses in Curved Box Girder Bridges: Case Study, *J. Bridge Engineering,* ASCE, 9(5), 487-496.

Ostermann M., (1991). Beanspruchung von elastisch gelagerten Fahrbahnübergängen unter Radstoßeinwirkung (Stresses in elastically supported modular expansion joints under wheel load impact), *Bauingenieur 66*, Springer-Verlag, 381-389 (In German).

Pattis A., & Tschemmernegg, F (1992). Fatigue Testing and Design of Modular Expansion Joints – The Brown/Maurer SWIVEL JOIST System – Repair Proposals for 3rd Lake Washington Bridge, Short version of an unpublished report, University of Innsbruck, Innsbruck, Austria.

Pritchard R.W. (2004). (Qld Dept of Transport & Main Roads). Personal Communication.

Purvis R. (2003). Bridge Deck Joint Performance – A Synthesis of Highway Practice, *NCHRP Synthesis 319,* Transportation Research Board, National Research Council, Washington, DC, USA.

Ramberger G., (2002). Structural Bearings and Expansion Joints for Bridges, *Structural Engineering Documents 6*, International Association for Bridge and Structural Engineering (IABSE), Zurich, Switzerland.

Ravshanovich K.A., Yamaguchi H., Matsumoto Y., Tomida N. & Uno S. (2007). Mechanism of noise generation from a modular expansion joint under vehicle passage, *Engineering Structures*, Elsevier Science Ltd, UK, 29(9), 2206–2218.

Ravshanovich K.A. (2007). Noise generation mechanism of modular expansion joints in highway bridges, *PhD Thesis*, Saitama University, Tokyo, Japan.

Reid S. & Ansourian P. (2004). Reliability Analysis of Expansion Joint in Anzac Bridge, *Investigation Report S1427*, Centre for Advanced Structural Engineering, University of Sydney, NSW, Australia, (Unpublished report prepared for the Roads & Traffic Authority of NSW).

Roads & Traffic Authority of NSW. (2004). *RTA QA Specification B316 – Modular Bridge Expansion Joints*. Sydney, NSW, Australia.

(http://www.rta.nsw.gov.au/doingbusinesswithus/specifications/bridgeworks.html)

Roads & Traffic Authority of NSW. (2008). Blueprint - RTA Corporate Plan 2008 to 2012, *RTA Publication 07.329*, Sydney, NSW, Australia.

Roeder C.W. (1993). Fatigue Cracking in Modular Expansion Joints, *Research Report WA-RD 306.1,* Washington State Transportation Center, Seattle, Washington, USA, 53 pp.

Roeder C.W. (1995). Field Measurements of Dynamic Wheel Loads on Modular Expansion Joints, *Research Report WA-RD 369.1*, Washington State Transportation Center, Seattle, Washington, USA, 66 pp.

Roeder C.W., Macrae G.A., Arima K., Crocker P.N. & Wong S.D. (1998). Fatigue Cracking of Riveted Steel Tied Arch and Truss Bridges, *Research Report WA-RD 447.1,* Washington State Transportation Center, Seattle, Washington, USA.

Roeder C.W., Macrae G.A., Kalogiros A.Y. & Leland A. (2001). Fatigue Cracking of Riveted, Coped, Stringer-to-Floorbeam Connections, *Research Report WA-RD 494.1,* Washington State Transportation Center, Seattle, Washington, USA.

Roeder C.W. (2004). (Uni. of Washington). Personal Communication.

Roeder C.W., Macrae G.A., Leland A. & Rospo A. (2005). Extending the Fatigue Life of Riveted Coped Stringer Connections, *J. Bridge Engineering,* ASCE, 10(1), 69-76.

Roberts W.S. and Heywood R.J. (2004). Fatigue-It Will Change Our Culture, *Proc. 5th Austroads Bridge Conference*, Hobart, Tasmania, Australia.

Schwammenhoefer F. (2001). (Min. of Transport, Austria). Personal Communication.

Sennah K.M. & Kennedy J.B. (2001). State-of-the-Art in Design of Curved Box-Girder Bridges, *J. Bridge Engineering,* ASCE, 6(3), 159-167.

Shigley J.E. & Mischke C.R. (1981). Mechanical Engineering Design (5th Edition), McGraw-Hill, New York, USA, 185.

Spuler T., Moor G. & Urich B. (2007). Expansion joints with noise reduction – will recent developments become widespread across Europe?, *Proc. International Association for Bridge & Structural Engineering (IABSE) Symposium***,** Weimar, Germany.

Standards Australia (2004). *Australian Standard AS5100.4 – 2004, Bridge Design Part 4: Bearings and deck joints,* Sydney, NSW, Australia.

Steenbergen M.J.M.M. (2004). Dynamic response of expansion joints to traffic loading, *Engineering Structures,* Elsevier Science Ltd, UK, 26(12), 1677-1690.

Tschemmernegg F. (1973). Messung von Vertikal- und Horizontallasten beim Anfahren, Bremsen und Überrollen von Fahrzeugen auf einem Fahrbahnübergang (Measurement of Vertical and Horizontal Loads due to Accelerating, Braking, and Rolling Vehicles on an Expansion Joint), *Der Bauingenieur*, 48, Heft 9, Springer-Verlag, 326-330 (In German).

Tschemmernegg F. (1991). The Design of Modular Expansion Joints, *Proc. 3rd World Congress on Joint Sealing and Bearing Systems for Concrete Structures*, Toronto, Ontario, Canada, 67-86.

Watson R.J. & Delattre X. (2008). A Low Noise, Large Movement Expansion Joint System for Concrete Bridges, *Proc. PCI-FHWA National Bridge Conference*, Precast/Prestressed Concrete Institute, Chicago, Illinois, USA.

Whitton R. J. (2003). Strengthening Options/Load Capacity – Bridge Over the Darling River at Wilcannia, *RTA Technical Services Report*, Roads & Traffic Authority, Sydney, NSW, Australia, 23 pp.

Xie X., Wu D.Y., Wang J.F., Zhang S.Q. and Zhou Y.J. (2009). Dynamical behaviour of steel box girder bridges due to vehicle-induced vibration at expansion joint, *J. Zhejiang University (Engineering Science)*, Vol 43, No 10, 1923-1930 (DOI: 10.3785/j.issn.1008-983X.2009.10.030) (In Chinese).

Journal Papers Based on This Thesis

The following Journal papers have been published based on the work in this thesis:

Journal Publications:

Ancich E.J., Chirgwin G.J. and Brown S.C. (2006). Dynamic Anomalies in a Modular Bridge Expansion Joint, *Journal of Bridge Engineering*, ASCE, 11 (5), 541-554.

Ancich E.J. and Brown S.C. (2004). Engineering Methods of Noise Control for Modular Bridge Expansion Joints, *Acoustics Australia*, 32 (3), 101-107.

Appendix A

Ancich E.J. (2000). A Study of the Environmental Noise Generation & Propagation Mechanisms of Modular Bridge Expansion Joints, *RTA Environmental Technology Report No. 000203*, Roads & Traffic Authority of NSW, Sydney, NSW, Australia.

Acoustical Assessment

A Study of the Environmental Noise Generation & Propagation Mechanisms of Modular Bridge Expansion Joints.

Prepared for:
RTA Operations, Technical Services – Bridge Section

Prepared by:
RTA Operations, Environmental Technology
Level 3, 52 Rothschild Avenue
Rosebery NSW 2018
Ph: 9662 5048
Fax: 9662 5045
email: Eric_Ancich@rta.nsw.gov.au
September 2000

Document Controls

Report No 001

Prepared For:	Prepared By:
Mr. Greg Forster **Operations Technical Services - Bridge** **52 Rothschild Avenue** **Rosebery NSW 2018**	**Environmental Technology Branch** **RTA Operations Directorate** **52 Rothschild Avenue** **Rosebery NSW 2018**

Business Unit	Environmental Technology			
Project No.	000203	NM Modular Bridge Expansion Joints		
Document description	A Study of the Environmental Noise Generation & Propagation Mechanisms of Modular Bridge Expansion Joints			
	Name		**Signed**	**Date**
Approving Manager	Eric Ancich			

Person managing this document	Person(s) writing this document
Eric Ancich	Eric Ancich

Location	CARMS File
G:\…\environ\projects\proj9900\0203\0203_2.doc	M1699

Client Reference	Status	Date
M1469	Final 1.0	8 September 2000

Quality System
Quality Endorsed Company

RTA Operations Directorate
AS/NZS ISO 9001
7443
Standards Australia

Table of Contents Page

1.0 Introduction

Whilst the use of expansion joints is common practice in bridge construction, modular bridge expansion joints are designed to accommodate large longitudinal expansion and contraction movements of bridge superstructures. In addition to supporting wheel loads, a properly designed modular joint will prevent rain water and road debris from entering into the underlying superstructure and substructure. Modular bridge expansion joints are subjected to more load cycles than other superstructure elements, but the load types, magnitudes and fatigue-stress ranges that are applied to these joints are not well defined (Dexter *et al* 1997).

It is known that an environmental noise nuisance occurs as motor vehicle wheels pass over the joint but the mechanism for the generation of the noise nuisance is not known. Environmental Technology Branch was engaged by Technical Services, Bridge Section to determine how the noise nuisance originates and is subsequently propagated into the surrounding environment. Modular bridge expansion joints built into the Georges River (Tom Ugly's) Bridge and Anzac Bridge were selected for the study due to their proximity and ease of access. Engineering measurements were made under operational conditions to determine how the noise nuisance originates and is subsequently propagated into the surrounding environment.

The study involved collaboration between RTA Operations, Environmental Technology, OLSAN Consulting (Dr. Stephen Samuels) and the University of NSW, School of Mechanical and Manufacturing Engineering (Assoc. Prof. Bob Randall and Mr. Russell Overhall).

2.0 Modular Bridge Expansion Joints & Environmental Noise

There is evidence from environmental noise nuisance complaints received by the RTA that the sound produced by the impact of a motor vehicle tyre with modular bridge expansion joints is audible at least 500 metres from the bridge. This observation suggests that the noise generation mechanism involves possibly both parts of the bridge structure and the joint itself as it is unlikely that there is sufficient acoustic power in the simple tyre impact to explain the persistence of the noise in the surrounding environment.

The hypothesis was developed by the writer (following an inspection of the southern abutment, South Channel bridge, Taree Bypass) that tyre impacts vibrationally excite modular bridge expansion joints thereby producing noise that is amplified within the bridge superstructure (due to resonance) and then propagated into the surrounding environment.

3.0 Measurement Procedure

To test the hypothesis described above, simultaneous noise and vibration measurements, at the Georges River (Tom Ugly's) and Anzac Bridges, were recorded and analysed.

Vibration data were obtained from an accelerometer attached to a transverse beam of the modular bridge expansion joint receiving primary wheel load impacts. Noise data were obtained from a precision (Type 1) Sound Level Meter located inside the void space within the bridge abutment beneath the modular bridge expansion joint and at external locations.

The simultaneous noise and vibration data were recorded using a DAT tape recorder and subsequently analysed using a Brüel & Kjaer dual channel Fast Fourier Transform (FFT) analyser in the University of NSW Noise & Vibration Laboratory.

4.0 Results & Discussion

Measurements were initially made at the Georges River (Tom Ugly's) Bridge and the narrow band frequency analysis of the vibration data indicated the presence of a small number of discrete frequencies generally in the range 50-150 Hz.

It was believed that these frequencies were likely to be the vertical and/or horizontal bending frequencies for the transverse beams (tyre contacting) of the modular expansion joint. **Figure 1** shows the ensemble average (50) of wheel load impacts on a transverse beam when viewed in the frequency domain. Examination of Figure 1 reveals the presence of three dominant peaks in the frequency spectrum (70 Hz, 82 Hz & 90 Hz). Consequently, simple natural frequency calculations (using MicroStran®) were undertaken and **Table 1** shows the measured and calculated vibration frequencies.

Figure 1 Transverse Beam Vibration Spectrum – Georges River (Tom Ugly's) Bridge

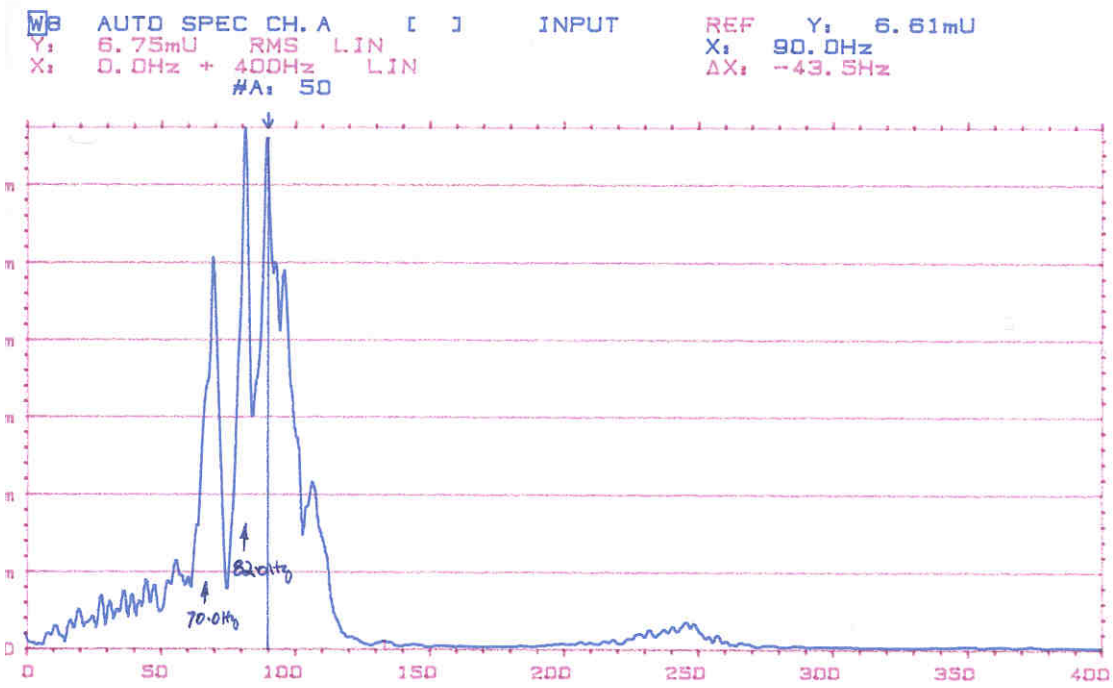

Table 1 Calculated and Measured Natural Frequencies - Georges River (Tom Ugly's) Bridge

Measured Frequency, Hz	Calculated Frequency, Hz[2]	Calculated Vibration Mode[1]
70	67.11	Vertical (1)
82	80.06, 80.78, 81.72, 82.91, 83.37, 83.45, 87.78, 88.97	Horizontal (4), Horizontal (2), Horizontal (3), Horizontal (5), Vertical (2 & 6), Vertical (1 & 4), Horizontal (4), Vertical (2 & 5)
90	88.97, 91.21, 97.36	Vertical (2 & 5), Horizontal (3), Vertical (3, 5 & 7)

Notes: (1) As the precise boundary conditions for the Georges River (Tom Ugly's) Bridge joint are not known, some assumptions were made. The Mode numbers associated with the various frequencies reflect the range of assumptions.
(2) Calculated frequencies are considered correct ± 10% due to assumption uncertainties.

Table 1 indicates a high degree of correlation between the calculated natural frequencies and the three dominant frequencies (70 Hz, 82 Hz & 90 Hz) measured at the Georges River (Tom Ugly's) Bridge.

A possible explanation for the high environmental noise nuisance is acoustic coupling between vibration of the modular joint and room acoustic modes inside the void space within the bridge abutment beneath the modular joint. This possible explanation was tested by calculating the frequencies of the various room acoustic modes encompassed by the vibration frequencies of interest. This comparison is shown as **Table 2**. Additional calculations were undertaken to determine the acoustic modal frequencies within the bridge box girders as these structures are acoustically connected to the void space within the bridge abutment beneath the modular joint. The calculated frequencies appear as **Table 2A**.

Figure 2 shows the acoustic excitation spectrum from measurements undertaken inside the void space within the bridge abutment beneath the modular bridge expansion joint. Examination of Figure 2 reveals the presence of two dominant peaks in the noise frequency spectrum (76 Hz & 82 Hz) and similar or matching frequencies also appear in Figure 1 and Table 2.

Figure 2 **Acoustic Excitation Spectrum – Georges River (Tom Ugly's) Bridge**

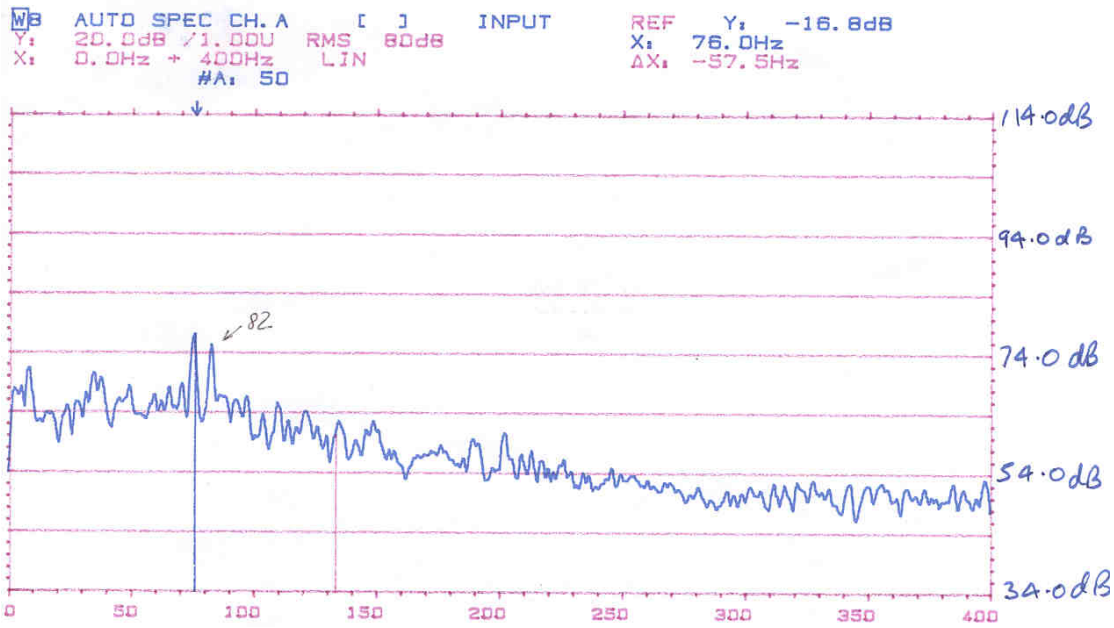

Table 2 **Calculated Room Acoustic Modal Frequencies compared with Measured Vibration Frequencies - Georges River (Tom Ugly's) Bridge**

Measured Frequency, Hz		Calculated Frequency, Hz[1]	Calculated Acoustic Mode
Noise	Vibration		
N.A	N.A	11.09	Transverse (1)
76	70	74.14	Vertical (1)
82	82	81.9	Vertical (1)
N.A	90	148.3; 163.8	Vertical (2)

Notes: (1) Calculation of multiple frequencies for some acoustic modes arises from varying dimensions within the void space.

Table 2A **Calculated Box Girder Acoustic Modal Frequencies compared with Measured Vibration Frequencies - Georges River (Tom Ugly's) Bridge**

Measured Frequency, Hz	Calculated Frequency, Hz[1]	Calculated Acoustic Mode
70	59, 73	Transverse (1), Vertical (1)
82	73, 86	Vertical (1), Transverse (1)
90	86	Transverse (1)

Notes: (1) Calculation of multiple frequencies for some acoustic modes arises from varying dimensions within the box girder.

Similar measurements to those undertaken at Georges River (Tom Ugly's) Bridge were repeated at the Anzac Bridge. **Figure 3** shows the corresponding ensemble average (30) of wheel load impacts on a transverse beam when viewed in the frequency domain. Examination of Figure 3 reveals the presence of six dominant peaks in the frequency spectrum (57 Hz, 65 Hz, 70.5 Hz, 84 Hz, 122 Hz & 189 Hz).

Consequently, simple natural frequency calculations (using MicroStran®) were undertaken and **Table 3** shows the measured and calculated vibration frequencies.

Figure 3 Transverse Beam Vibration Spectrum – Anzac Bridge

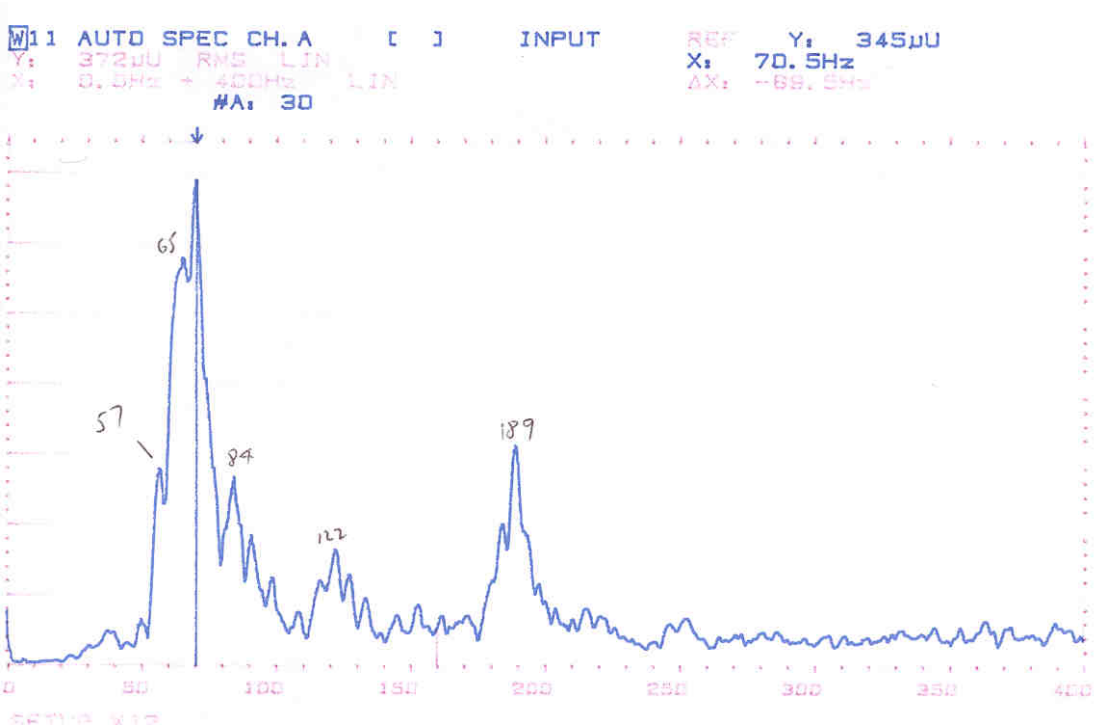

Table 3 Calculated and Measured Natural Frequencies (Anzac Bridge)

Measured Frequency, Hz	Calculated Frequency, Hz[2]	Calculated Vibration Mode[1]
57	34.49	Horizontal (1)
65	N.A	N.A
70.5	N.A	N.A
84	91.25, 94.94, 99.38	Vertical (2 & 3), Horizontal (4)
122	103.38, 108.42, 111.21, 118.75, 119.02, 124.27	Horizontal (5), Vertical (6), Horizontal (7), Vertical (8), Horizontal (9), Vertical (10)
189	N.A	N.A

Notes: (1) As the precise boundary conditions for the Anzac Bridge joint are not known, some assumptions were made. The Mode numbers associated with the various frequencies reflect the range of assumptions.
(2) Calculated frequencies are considered correct ± 10% due to assumption uncertainties.

Table 4 Calculated Room Acoustic Modal Frequencies compared with Measured Vibration Frequencies (Anzac Bridge)

Measured Frequency, Hz	Calculated Frequency, Hz[1]	Calculated Acoustic Mode
N.A	19.0	Transverse (3)
57	45.3, 47.8, 53.8	Axial (1), Vertical (1), Axial (1)
65	63.7	Vertical (1)
70.5	71.7	Vertical (1)
84	86.0	Vertical (1)
122	127.4, 135.8, 143.3	Vertical (2), Axial (3), Vertical (3)
189	172.0, 191.1	Vertical (2), Axial (2) & Vertical (3)

Notes: (1) Calculation of multiple frequencies for some acoustic modes arises from varying dimensions within the void space.

5.0 Noise Abatement Options

It is considered that effective noise abatement could be undertaken by:

- Modifying the dynamic behaviour of the joint to shift the natural frequencies so that they no longer co-incide with acoustic resonances. This option includes the trial use of tuned mass dampers.
- Providing acoustic absorption and limited screening, adjacent to the joint, to reduce noise propagation.
- Modify the acoustic absorption properties of the void space to eliminate or reduce the incidence of acoustic resonances.

The above strategies represent both "new construction" and "retro-fit" options. However, their efficacy and cost-effectiveness is still to be established by engineering measurement

A preliminary noise abatement trial was attempted at Georges River (Tom Ugly's) Bridge on 20 June 2000 by lining the floor of the void space within the bridge abutment beneath the modular joint with rockwool acoustic insulation batts. The batts were raised 75mm (nom.) above the concrete floor to improve the absorption at low frequencies. The principal outcome of this trial was the apparent reduction in extraneous noise that became evident in the Coherence Function analysis of the simultaneous noise and vibration measurements.

Figure 4 shows the Coherence (i.e. Correlation) between the noise and vibration spectra and it is clear that the noise and vibration are significantly coherent (i.e. related) at 79 Hz, 80.5 Hz, 91 Hz and 116 Hz. These data suggest that the acoustic noise (at these frequencies) is a direct result of excitation by the traffic-induced vibration of the modular bridge expansion joint.

Figure 4 Coherence Function between Noise & Vibration Spectra – Georges River (Tom Ugly's) Bridge

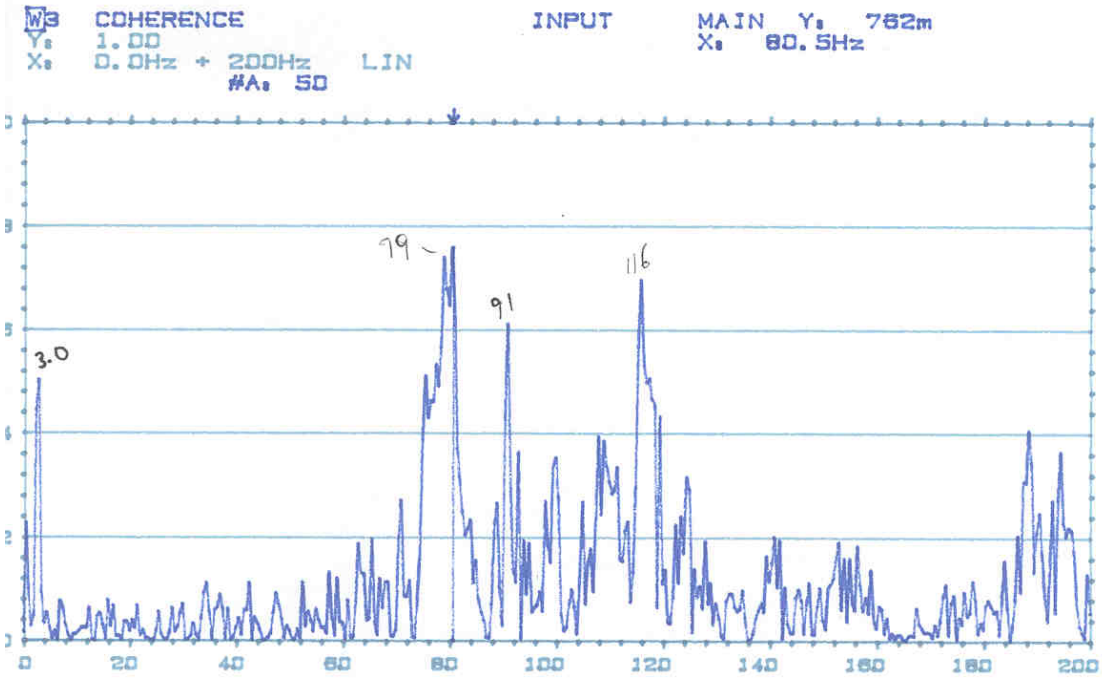

6.0 Conclusions and Recommendations

6.1 Conclusions

Noise and vibration measurements have been undertaken at Anzac and Georges River (Tom Ugly's) Bridges. The analysis of these measurements supports the hypothesis that an environmental noise nuisance results from the interaction of vibration of the modular bridge expansion joint with acoustic resonances produced inside the void space below the joint.

It is considered that effective noise abatement could be undertaken by:

- Modifying the dynamic behaviour of the joint to shift the natural frequencies so that they no longer co-incide with acoustic resonances. This option includes the trial use of tuned mass dampers.
- Providing acoustic absorption and limited screening, adjacent to the joint, to reduce noise propagation.
- Modify the acoustic absorption properties of the void space to eliminate or reduce the incidence of acoustic resonances.

The above strategies represent both "new construction" and "retro-fit" options. However, their efficacy and cost-effectiveness is still to be established. Accordingly, further R&D funding is required so that these options may be more fully tested and refined.

6.2 Recommendation

It is recommended that further funding be provided to enable testing and refinement of practical and effective noise abatement for acoustic amplified joint noise.

7.0 References & Further Reading

Beranek L.L. (Ed.) (1988): *Noise and Vibration Control*. Institute of Noise Control Engineering, Washington, DC, USA.

Dexter R.J., Connor R.J. & Kaczinski M.R. (1997): *Fatigue Design of Modular Bridge Expansion Joints*. Report 402, National Cooperative Highway Research Program, Transportation Research Board, Washington, DC, USA.

Jones D.I.G. (1967): *Effect of Isolated Tuned Dampers on Response of Multispan Structures*. J. Aircraft, Vol. 4, No. 4, pp343-346.

Martner O. (1996): *Noise Emission of Constructions for Bridge-To-Road Crossings*. Proc. Inter-Noise 96, pp211-214, Liverpool, UK.

Appendix B

Ancich E.J. and Brown S.C. (2004a). Modular Bridge Joints – Reduction of noise emissions by use of Helmholtz Absorber, *Proc. 5th Austroads Bridge Conference*, Hobart, Tasmania, Australia.

AustRoads

Fifth AustRoads Bridge Conference - May 2004

Bridges Another Dimension

-design - construction - procurement - maintenance -

Modular Bridge Joints – Reduction of noise emissions by use of Helmholtz Absorber

Eric J. Ancich, Senior Project Officer, Bridge Technology Section, Roads & Traffic Authority of NSW, PO Box 558 Blacktown 2148, Australia. E-mail: Eric_Ancich@rta.nsw.gov.au

Stephen C. Brown, Associate, Richard Heggie Associates Pty Ltd, PO Box 176 Lane Cove 1595, Australia. E-mail: steve.brown@heggies.com.au

SYNOPSIS

Modular bridge expansion joints are widely used throughout the world for the provision of controlled thermal expansion and contraction in bridges. Modular Bridge Joint Systems (MBJS) are considered to be the most modern design of waterproof bridge expans ion joint currently available. It was known that an environmental noise nuisance occurred as motor vehicle wheels passed over the joint but the mechanism for the generation of the noise nuisance was not previously known.

Observation suggested that the no ise generation mechanism involved possibly both parts of the bridge structure and the joint itself as it was unlikely that there was sufficient acoustic power in the simple tyre impact to explain the persistence of the noise in the surrounding environment. Engineering measurements were undertaken at Georges River (Tom Ugly's) Bridge and the analysis of these measurements indicated that an environmental noise nuisance resulted from the interaction of vibration of the modular bridge expansion joint with acoustic resonances produced within the void space of the abutment below the joint. A number of engineering methods of noise abatement were considered or investigated before a Helmholtz Absorber installation was adopted.

"Before" and "After" noise measuremen t results show a significant decrease of low frequency noise due to the Helmholtz Absorber installation. The benefit is most obvious in the frequency range of 50 to 200 Hz which encompasses all the natural vibration modes. The noise reduction provided by the Helmholtz Absorber installation is of the order of 10 dBA which is equivalent to a halving of the perceived loudness.

1 INTRODUCTION

Whilst the use of expansion joints is common practice in bridge construction, modular bridge expansion joints are d esigned to accommodate large longitudinal expansion and contraction movements of bridge superstructures. In addition to supporting wheel loads, a properly designed modular joint will prevent rainwater and road debris from entering into the underlying superstructure and substructure.

Modular bridge expansion joints are subjected to more load cycles than other superstructure elements, but the load types, magnitudes and fatigue -stress ranges that are applied to these joints are not well defined [Dexter *et al* (1)].

Modular bridge expansion joints are generally described as single or multiple support bar designs. In the single support bar design, the support bar (beam parallel to the direction of traffic) supports all the centre beams (beams transverse to the d irection of traffic). In the multiple support bar design, multiple support bars individually support each centre beam. **Figures 1 & 2** show typical single support bar and welded multiple support bar MBEJ's respectively.

The MBEJ installed into the Western abutment of Anzac Bridge is, in fact, a hybrid design having pairs of support bars in series across the full width of the joint. Each pair of support bars is attached to alternate groups of four centre beams [i.e. Centre beams 1, 3, 5 & 7 are attached to support bar #1 (and the other odd numbered support bars) and centre beams 2, 4, 6 & 8 attached to support bar #2 (and the other even numbered support bars)]. The support bar pairs are spaced at 2.25m centres across the full width of the bridge resulting in a total of 24 support bars (2 x 12).

The MBEJ installed into the southbound carriageway of the bridge over the Georges River at Tom Ugly's Point is a typical multiple support bar design as shown in **Figure 2**.

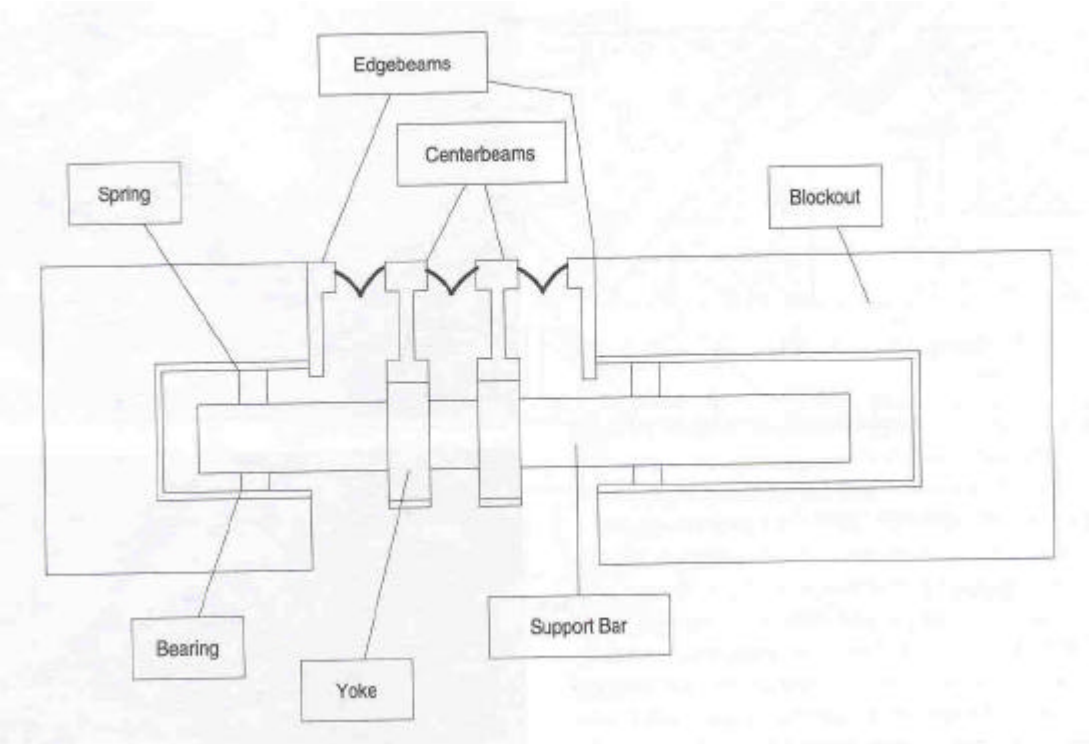

Figure 1: Typical Single Support Bar Design MBEJ

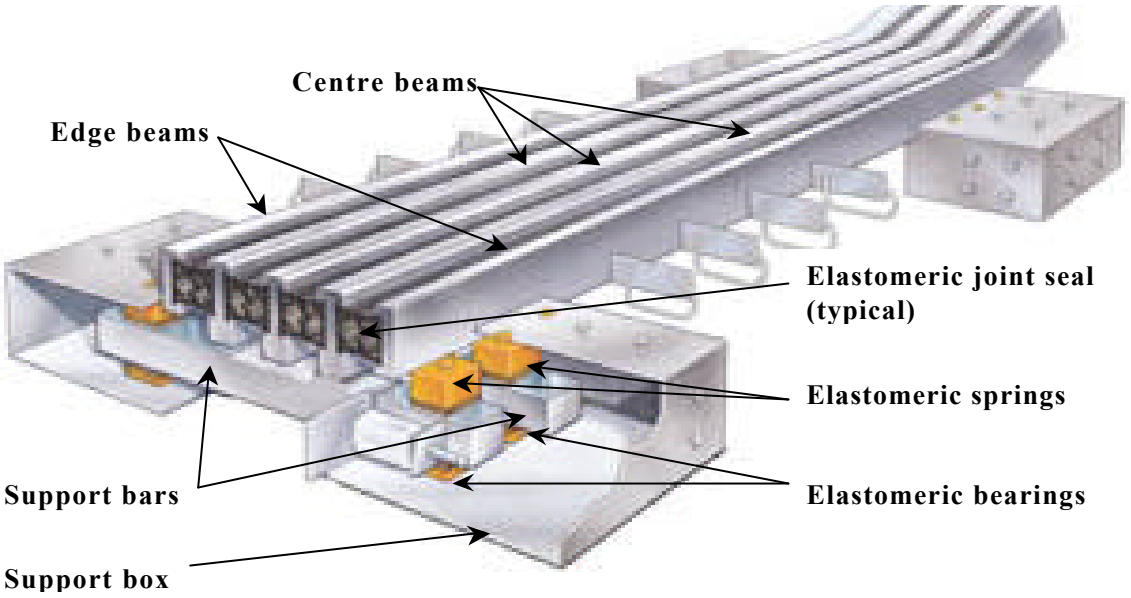

Figure 2: Typical Multiple Support Bar Design MBEJ

It is known that an environmental noise nuisance occurs as motor vehicle wheels pass over the joint but the mechanism for the generation of the noise nuisance is not widely known although Barnard & Cuninghame (2) do acknowledge the role of acoustic resonances. A study was undertaken and the modular bridge expansion joints built into the Georges River (Tom Ugly's) Bridge and Anzac Bridge were selected for the study due to their proximity and ease of access. Engineering measurements were made under operational conditions to determine how the noise nuisance originates and is subsequently propagated into the surrounding environment [Ancich (3)].

2 MODULAR BRIDGE EXPANSION JOINTS & ENVIRONMENTAL NOISE

There was evidence from environmental noise nuisance complaints received by the RTA that the sound produced by the impact of a motor vehicle tyre with modular bridge expansion joints was audible at least 500 metres from the bridge in a semi-rural environment. This observation suggests that the noise generation mechanism involves possibly both parts of the bridge structure and the joint itself as it is unlikely that there is sufficient acoustic power in the simple tyre impact to explain the persistence of the noise in the surrounding environment.

The hypothesis was developed by Ancich (3) that tyre impacts vibrationally excite modular bridge expansion joints thereby producing noise that is amplified within the bridge superstructure (due to resonance) and then propagated into the surrounding environment.

3 MEASUREMENT PROCEDURE

To test the hypothesis, simultaneous noise and vibration measurements, at the Georges River (Tom Ugly's) and Anzac Bridges, were recorded and a nalysed. Vibration data were obtained from an accelerometer attached to a transverse beam (centre beam) of the modular bridge expansion joint receiving primary wheel load impacts. Noise data were obtained from a precision Sound Level Meter located inside the void space within the bridge abutment beneath the modular bridge expansion joint and at external locations.

The simultaneous noise and vibration data were recorded using a DAT recorder and subsequently analysed using a dual channel FFT analyser.

4 RESULTS & DISCUSSION

Measurements were initially made at the Georges River (Tom Ugly's) Bridge and the narrow band frequency analysis of the vibration data indicated the presence of a small number of discrete frequencies generally in the range 50 -150 Hz.

It was believed that these frequencies were likely to be the vertical and/or horizontal bending frequencies for the transverse beams (tyre contacting) of the modular expansion joint. **Figure 3** shows the ensemble average (50) of wheel load impacts on a tran sverse beam when viewed in the frequency domain. Examination of Figure 3 reveals the presence of three dominant peaks in the frequency spectrum (70 Hz, 82 Hz & 90 Hz). Consequently, simple natural frequency calculations (using MicroStran®) were undertaken and **Table 1** shows the measured and calculated vibration frequencies.

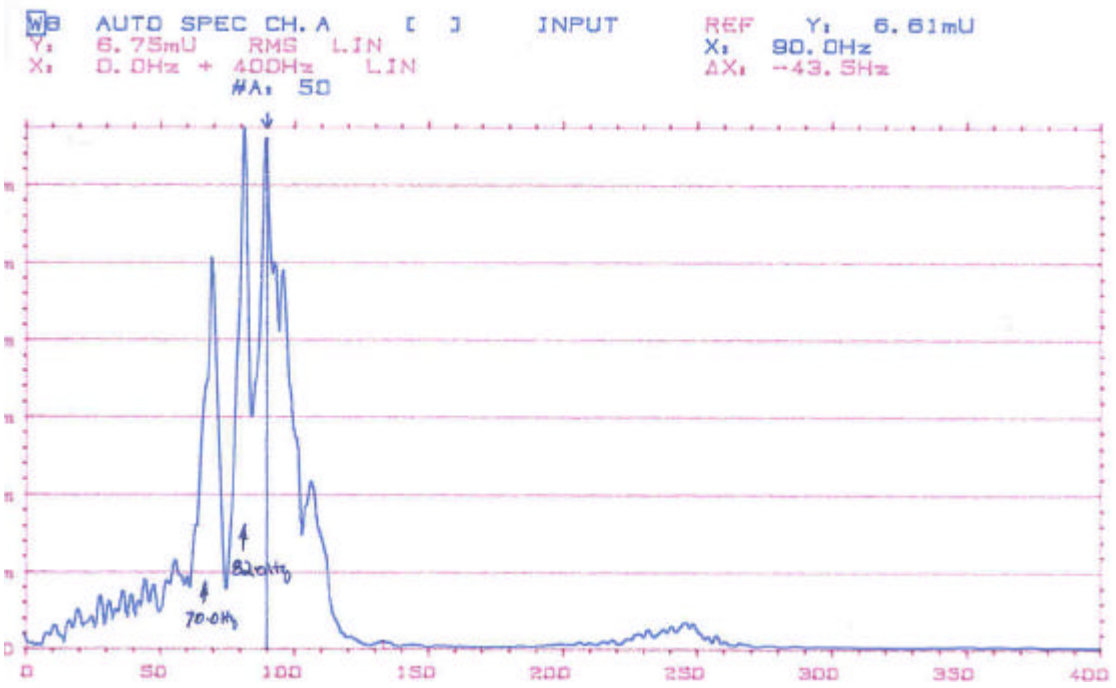

Figure 3: Transverse Beam Vibration Spectrum – Tom Ugly's Bridge

Table 1: Calculated and Measured Natural Frequencies - Georges River (Tom Ugly's) Bridge

Measured Frequency, Hz	Calculated Frequency, Hz[2]	Calculated Vibration Mode[1]
70	67.11	Vertical (1)
82	80.06, 80.78, 81.72, 82.91, 83.37, 83.45, 87.78, 88.97	Horizontal (4), Horizontal (2), Horizontal (3), Horizontal (5), Vertical (2 & 6), Vertical (1 & 4), Horizontal (4), Vertical (2 & 5)
90	88.97, 91.21, 97.36	Vertical (2 & 5), Horizontal (3), Vertical (3, 5 & 7)

Notes: (1) As the precise boundary conditions for the Georges River (Tom Ugly's) Bridge joint are not known, some assumptions were made. The Mode numbers associated with the various frequencies reflect the range of assumptions.
(2) Calculated frequencies are considered correct ± 10% due to assumption uncertainties.

Table 1 indicates a high degree of correlation between the calculated natural frequencies and the three dominant frequencies (70 Hz, 82 Hz & 90 Hz) measured at the Georges River (Tom Ugly's) Bridge.

A possible explanation for the high environmental noise nuisance is acoustic coupling between vibration of the modular joint and room acoustic modes inside the void space within the bridge abutment beneath the modular joint. This possible explanation was tested by calculating the frequencies of the various room acoustic modes encompassed by the vibration frequencies of interest [Beranek (4)]. This comparison is shown as **Table 2**.

Figure 4 shows the acoustic excitation spectrum from measurements undertaken inside the void space within the bridge abutment beneath the modular bridge expansion joint. Examination of Figure 2 reveals the presence of two dominant peaks in the noise frequency spectrum (76 Hz & 82 Hz) and similar or matching frequencies also appear in **Figure 3** and **Table 2**.

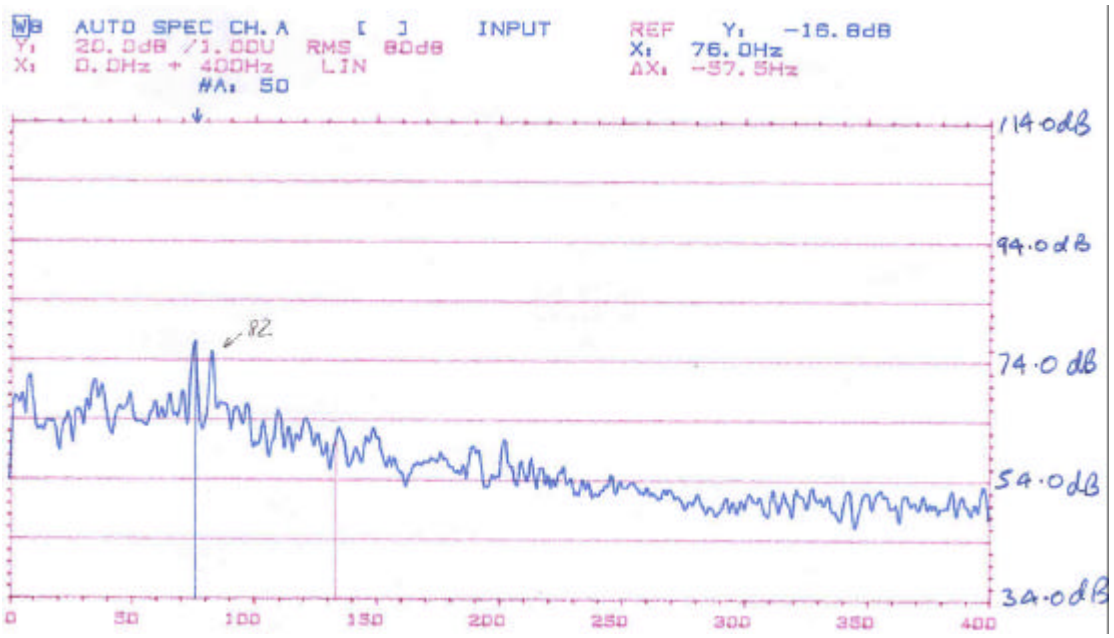

Figure 4: Acoustic Excitation Spectrum – Tom Ugly's Bridge

Table 2: Calculated Room Acoustic Modal Frequencies compared wit h Measured Vibration Frequencies - Georges River (Tom Ugly's) Bridge

Measured Frequency, Hz		Calculated Frequency, Hz[1]	Calculated Acoustic Mode
Noise	Vibration		
N.A	N.A	11.09	Transverse (1)
76	70	74.14	Vertical (1)
82	82	81.9	Vertical (1)
N.A	90	148.3; 163.8	Vertical (2)

Notes: (1) Calculation of multiple frequencies for some acoustic modes arises from varying dimensions within the void space.

Similar measurements to those undertaken at Georges River (Tom Ugly's) Bridge were repeated at the Anzac B ridge. **Figure 5** shows the corresponding ensemble average (30) of wheel load impacts on a transverse beam when viewed in the frequency domain. Examination of Figure 3 reveals the presence of six dominant peaks in the frequency spectrum (57 Hz, 65 Hz, 70.5 Hz, 84 Hz, 122 Hz & 189 Hz).

Consequently, simple natural frequency calculations (using MicroStran®) were undertaken and **Table 3** shows the measured and calculated vibration frequencies.

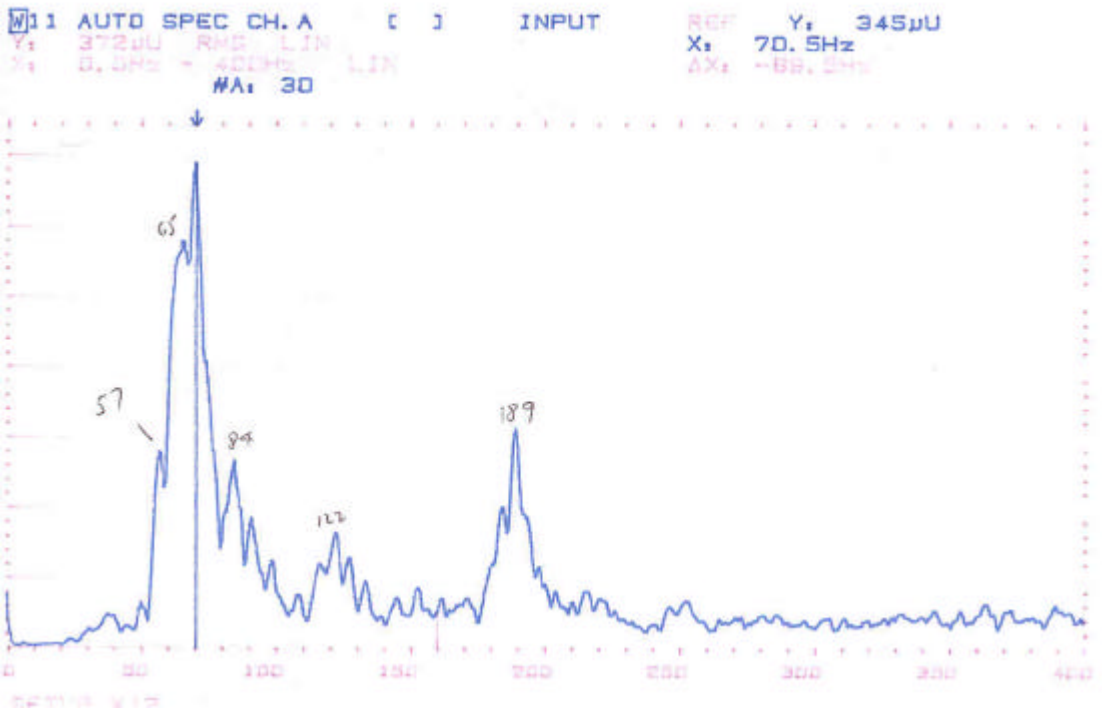

Figure 5: Transverse Beam Vibration Spectrum – Anzac Bridge

Table 3: Calculated and Measured Natural Frequencies (Anzac Bridge)

Measured Frequency, Hz	Calculated Frequency, Hz[2]	Calculated Vibration Mode[1]
57	34.49	Horizontal (1)
65	N.A	N.A
70.5	N.A	N.A
84	91.25, 94.94, 99.38	Vertical (2 & 3), Horizontal (4)
122	103.38, 108.42, 111.21, 118.75, 119.02, 124.27	Horizontal (5), Vertical (6), Horizontal (7), Vertical (8), Horizontal (9), Vertical (10)
189	N.A	N.A

Notes: (1) As the precise boundary conditions for the Anzac Bridge joint are not known, some assumptions were made. The Mode numbers associated with the various frequencies reflect the range of assumptions.
(2) Calculated frequencies are considered correct ± 10% due to assumption uncertainties.

Table 4: Calculated Room Acoustic Modal Frequencies compa red with Measured Vibration Frequencies (Anzac Bridge)

Measured Frequency, Hz	Calculated Frequency, Hz[1]	Calculated Acoustic Mode
N.A	19.0	Transverse (3)
57	45.3, 47.8, 53.8	Axial (1), Vertical (1), Axial (1)
65	63.7	Vertical (1)
70.5	71.7	Vertical (1)
84	86.0	Vertical (1)
122	127.4, 135.8, 143.3	Vertical (2), Axial (3), Vertical (3)
189	172.0, 191.1	Vertical (2), Axial (2) & Vertical (3)

Notes: (1) Calculation of multiple frequencies for some acoustic modes arises from varying dimensions within the void space.

5 NOISE ABATEMENT OPTIONS

Martner (5) reports the results of noise measurements of a number of different types of bridge expansion joints, including modular bridge expansion joints. Whilst he indicates that the installation of an acoustic enclosure beneath the expansion joint was very effective, it is not clear whether the enclosure was used with the modular design.

The analysis of measurements supported the hypothesis that an environmental noise nuisance resulted from the interaction of vibration of the modular bridge expansion joint with acoustic resonances produced inside the void space below the joint. The reverberant nature of the void space was considered to be the reason for the apparent amplification of the low frequency sound pre ssure within the void space. As true standing waves do not propagate, this highly reactive (long reverberation time characteristic) of the void is not apparent in the far field. Due to acoustic absorption (limited) in the void, some of this sound energy is absorbed within the void and some is radiated to the environment through openings. The build-up of acoustic energy is then radiated into the environment.

It was considered that effective noise abatement could be undertaken by:

- Modifying the dynamic behaviour of the joint to shift the natural frequencies so that they no longer co-incide with acoustic resonances. This option included the trial use of tuned mass dampers.
- Providing acoustic absorption and limited screening, adjacent to the joint, to reduce noise propagation.
- Modifying the acoustic absorption properties of the void space to eliminate or reduce the incidence of acoustic resonances.

The above strategies represent both "new construction" and "retro-fit" options. However, their efficacy and cost-effectiveness is still to be established by engineering measurement

A preliminary noise abatement trial was attempted at Georges River (Tom Ugly's) Bridge on 20 June 2000 by lining the floor of the void space within the bridge abutment beneath the modular joint with rockwool insulation batts. The batts were raised 75mm (nom.) above the concrete floor to improve the absorption at low frequencies. The principal outcome of this trial was the apparent reduction in extraneous noise that became evident in the Coherence Function analysis of the simultaneous noise and vibration measurements.

There were initial plans to design and test Option 1. However, this option was ultimately not pursued. Although tuned mass dampers (TMD) would likely provide an effective noise reduction, these devices were not strongly advocated due to the high number of natural modes present and hence a high number of TMD's needing to be fitted and tuned [Jones (6)]. An alternative to the TMD concept would be the use of broadband damping coupled mass absorbers.

The probable disadvantage of this approach being the requirement for a significant mass attachment to each centre beam.

Due to resonances within the void space, the use of acoustic absorption and limited screening, adjacent to the joint was not considered practical. Consequently, only Option 3 was investigated. This investigation was undertaken using two different approaches. Firstly, the simple addition of acoustic absorption into the void space was tested.

Noise measurements were conducted on 4 May 2001 at which time trial acoustical absorption material had been installed over the floor of the void below the expansion joint. The absorption was arranged in a 100 mm thick layer over the floor area of the void and raised 75 mm (nominally) above the floor surface (to optimise low frequency sound absorption).

Whilst the above deck (Locations 1 and 2 – Figure 3) and the side (Location 3) measurements show no significant change in the noise spectra, Locations 4 and 5 show a significant increase in the low frequency bands when the trial absorption was removed.

As the measurements at Location 5 (from within the void space) are the result of sound pressure due to both propagating sound energy as well as non-propagating standing waves, the results at Location 4 provide a better indication of the effect on the emitted (propagating) noise. The second approach involved the construction of a Helmholtz Absorber within the

void space. The internal dimensions of the Helmholtz chambers were calculated to co - incide with the dominant acoustic frequencies.
The Helmholtz Absorber panels were designed to target the critical frequencies shown in **Table 5**.

Table 5: Helmholtz Absorber Modules Target Frequencies

Segment	Design Centre Frequency of Helmholtz Absorber, Hz					
	1	2	3	4	5	6
Frequency (Hz)	64	80	90	105	110	120

The "Before" and "After" noise measurement results are provided graphically as **Figure 6**. It is clear from these measurement results that Location 4 (Refer Figure 8) shows a significant decrease of low frequency noise due to the Helmholtz Absorber installation. The benefit is most obvious in the frequency range of 50 to 200Hz. which encompasses all the natural vibration modes. The noise reduction provided by the Helmholtz Absorber installation is of the order of 10 dBA.

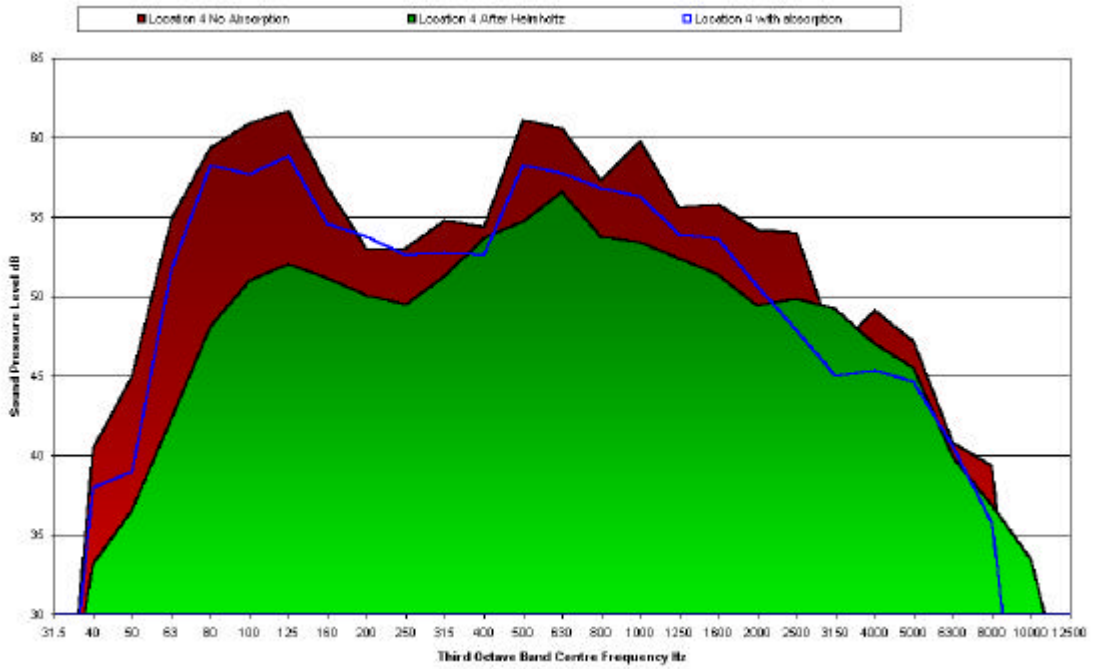

Figure 6: RMS Average Third Octave Band Noise Spectra at Location 4

Figure 6 shows a compa rison of RMS average ? octave band noise spectra at Location 4 before and after the Helmholtz absorber installation. Also shown are the ? octave band noise spectra with floor absorption only, for comparison.

These results clearly demonstrate the effectiv eness of the Helmholtz absorber modules in the target range of 60Hz to 160Hz.

Figure 7 shows the installed absorber modules.

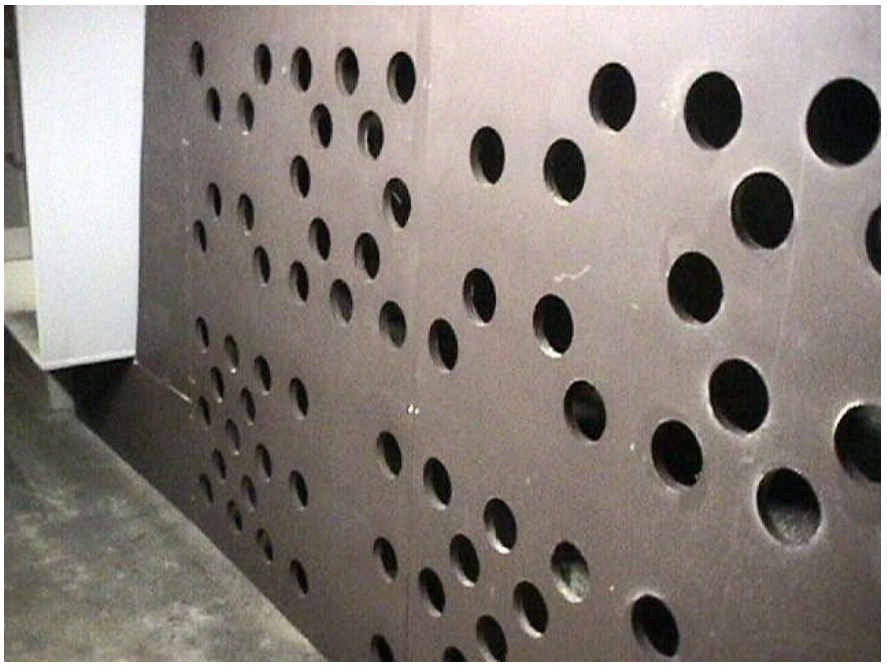

Figure 7: Helmholtz Absorber

6 NOISE MEASUREMENT LOCATIONS

Noise measurements were conducted at sever al locations in the vicinity of the expansion joint. **Figure 8** shows a site plan with noise measurement locations indicated.

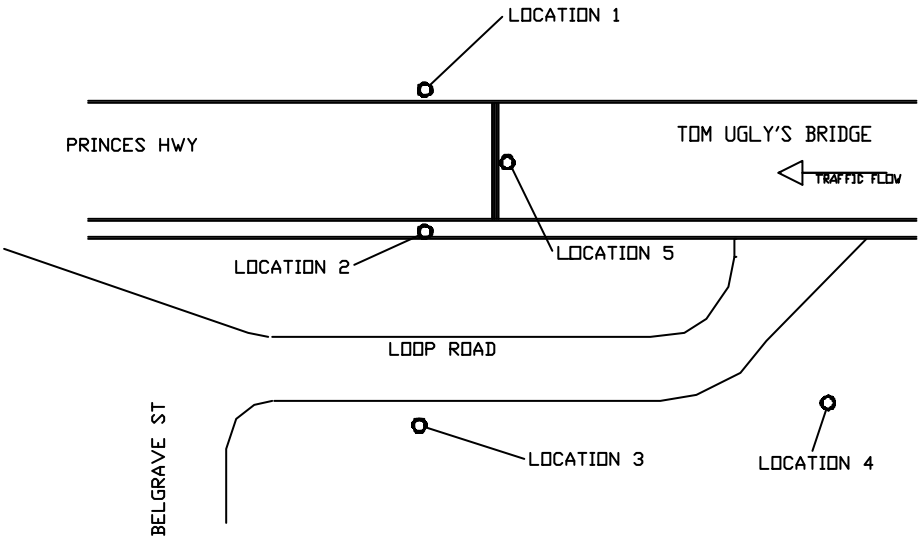

Figure 8: Site Plan Showing Noise Measurement Locations

7 CONCLUSION

Noise and vibration measurements have been undertaken at Anzac and Georges River (Tom Ugly's) Bridges. The analysis of these measurements supported the hypothesis that an environmental noise nuisance results from the interaction of vibration of the modular bridge expansion joint with acoustic resonances produced inside the void space below the joint.

The trial addition of acoustic absorption batts into the void space of Tom Ugly's Bridge was considered to be only marginally effective for noise control and was not pursued. However, the installed Helmholtz Absorber at Tom Ugly's Bridge has reduced the modular expansion joint induced low frequency "booming" noise emissions by up to 10 dB. The character of the noise emission from the underside of the bridge deck would no longer be classified as tonal and hence the likelihood of modular expansion joint related noise complaints has been significantly reduced.

The use of Helmholtz Absorbers at other bridges with modular expansion joints is considered to be viable as an engineering method of noise control.

ACKNOWLEDGEMENT

The authors wish to thank the Chief Executive of the Roads and Traffic Authority of NSW (RTA) for permission to publish this paper. The opinions and conclusions expressed in this paper do not necessarily reflect the views of the RTA.

REFERENCES

1. DEXTER R.J., CONNOR R.J. & KACZINSKI M.R.: "Fatigue Design of Modular Bridge Expansion Joints ". *NCHRP Report 402,* Transportation Research Board, National Research Council, 1997, 128 pp.
2. BARNARD C.P. & CUNINGHAME J.R. : "Improving the Performance of Bridge Expansion Joints: Bridge Deck Expansion Joint Working Group Final Report". *TRL Report 236*, Transport Research Laboratory, 1997, 92 pp.
3. ANCICH E.J.: "A Study of the Environmental Noise Generation & Propagation Mechanisms of Modular Bridge Expansion Joints" . *RTA Environmental Technology Report No. 000203*, Roads & Traffic Authority of NSW, September, 2000.
4. BERANEK L.L. (Ed.): " Noise and Vibration Control – Revised Edition" . *Institute of Noise Control Engineering*, 1988, 672 pp.
5. MARTNER O.: "Noise Emission of Constructions for Bridge-To-Road Crossings ". *Proc. Inter-Noise 96*, pp 211-214.
6. JONES D.I.G.: "Effect of Isolated Tuned Dampers on Response of Multispan

Structures". *J. Aircraft*, Vol. 4, No. 4, 1967, pp 343-346.

Appendix C

Ancich E.J., Brown S.C. and Chirgwin G.J. (2004). The Role of Modular Bridge Expansion Joint Vibration in Environmental Noise Emissions and Joint Fatigue Failure, *Proc. Acoustics 2004 Conference*, Surfers Paradise, QLD, Australia, 135-140.

Acoustics 2004

Transportation Noise and Vibration – The New Millennium

Proceedings of the Annual Conference of the Australian Acoustical Society

3–5 November 2004 ▪ Gold Coast, Australia

Hub Page | Search
Table of Contents | Support
Author Index | Install Software
Sponsors | Mac OS X Users Read This

Transportation Noise and Vibration
Underwater Acoustics
Architectural & Building Acoustics
Environmental & Occupational Noise
Industrial Noise & Vibration Control
Sound & Vibration Measurement

ISBN 0-909882-22-3. ISSN 1446-0998. Proceedings on CDROM of Acoustics 2004. Published by Australian Acoustical Society c/o Professional Centre, Private Bag 1, Darlinghurst NSW 2010, Australia.

THE ROLE OF MODULAR BRIDGE EXPANSION JOINT VIBRATION IN ENVIRONMENTAL NOISE EMISSIONS AND JOINT FATIGUE FAILURE

Eric J. Ancich(1), Stephen C. Brown(2) and Gordon J. Chirgwin(1)

(1) Bridge Technology Section, Roads & Traffic Authority of NSW, PO Box 558 Blacktown, Australia
(2) Richard Heggie Associates Pty Ltd, PO Box 176 Lane Cove, Australia

Abstract

Modular bridge expansion joints (MBEJ's) are widely used throughout the world for the provision of controlled pavement continuity during seismic, thermal expansion, contraction and long-term creep and shrinkage movements of bridge superstructures. Modular Bridge Joint Systems (MBJS) are considered to be the most modern design of waterproof bridge expansion joint currently available. It was generally known that an environmental noise nuisance occurred as motor vehicle wheels passed over the joint but the mechanism for the generation of the noise nuisance has only recently been described [1].

Observation suggested that the noise generation mechanism involved possibly both parts of the bridge structure and the joint itself as it was unlikely that there was sufficient acoustic power in the simple tyre impact to explain the persistence of the noise in the surrounding environment. Engineering measurements were undertaken at Anzac and Georges River (Tom Ugly's) Bridges and the analysis of these measurements indicated that an environmental noise nuisance resulted from modal vibration frequencies of the MBEJ coupling with acoustic resonances in the chamber cast into the bridge abutment below the MBEJ. This initial acoustic investigation was soon overtaken by observations of fatigue induced cracking in structural beams transverse to the direction of traffic. A literature search revealed little to describe the structural dynamics behaviour of MBEJ's but showed that there was an accepted belief amongst academic researchers dating from around 1973 that a significant part of the load history was dynamic. In spite of this knowledge it would appear that almost all designers use a static or quasi-static design with little consideration of the dynamic behaviour, either in the analysis or the detailing.

Principally, this paper identifies the role of vibration in the generation of environmental noise complaints and links this vibration to the now endemic occurrence of structural fatigue failures of MBEJ's throughout the world.

Nomenclature

f_t	tyre pulse frequency (Hz)
f_p	wheel/beam pass frequency (Hz)
V	Vehicle speed (m/s)
G	*S*pacing between centre beams (m)
L_t	Tyre patch length (m)
b	Width of the centre beam top flange (m)
ω	Forcing radian frequency (rads/s)
ω_n	Natural radian frequency (rads/s)

Introduction

Whilst the use of expansion joints is common practice in bridge construction, modular bridge expansion joints are designed to accommodate large longitudinal expansion and contraction movements of bridge superstructures. In addition to supporting wheel loads, a properly designed modular joint will prevent rainwater and road debris from entering into the underlying superstructure and substructure. Modular bridge expansion joints are subjected to more load cycles than other superstructure elements, but the load types, magnitudes and fatigue-stress ranges that are applied to these joints are not well defined [2]. Modular bridge expansion joints are generally described as single or multiple support bar designs.

In the single support bar design, the support bar (beam parallel to the direction of traffic) supports all the centre beams (beams transverse to the direction of traffic). In the multiple support bar design, multiple support bars individually support each centre beam. **Figures 1 & 2** show typical single support bar and multiple support bar MBEJ's respectively. In Figure 1, the term "*Blockout*" refers to the recess provided in the bridge superstructure to allow casting-in of an expansion joint.

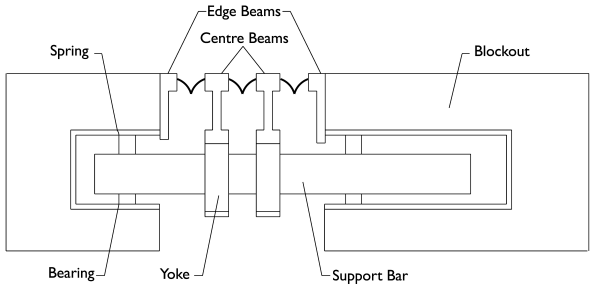

Figure 1 Typical Single Support Bar Design MBEJ

The MBEJ installed into the western abutment of Anzac Bridge consists of two interleaved single support bar structures that behave, in a dynamic sense, as independent structures. Previous experimental modal analysis studies [3] demonstrated only very light, almost negligible coupling between the two structures.

The MBEJ installed into the southbound carriageway of the bridge over the Georges River at Tom Ugly's Point is a typical multiple support bar design as shown in **Figure 2**.

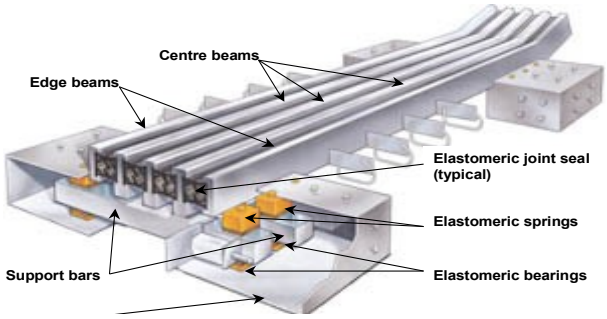

Figure 2 Typical Multiple Support Bar Design MBEJ

There was anecdotal evidence from environmental noise nuisance complaints received by the Roads and Traffic Authority of NSW (RTA) that the sound produced by the impact of a motor vehicle tyre with modular bridge expansion joints was audible at least 500 metres from the bridge in a semi-rural environment. This observation suggests that the noise generation mechanism involves possibly both parts of the bridge structure and the joint itself as it is unlikely that there is sufficient acoustic power in the simple tyre impact to explain the persistence of the noise in the surrounding environment.

Although it was generally known that an environmental noise nuisance occurred as motor vehicle wheels pass over the joint, the mechanism for the generation of the noise nuisance is not widely known. However, Barnard & Cuninghame [4] do point to the role of acoustic resonances. Studies were undertaken of the modular bridge expansion joints built into the Georges River (Tom Ugly's) Bridge and Anzac Bridge with engineering measurements made under operational conditions to determine how the noise nuisance originates and is subsequently propagated into the surrounding environment [1] [5] [6].

A literature search revealed little to describe the structural dynamics behaviour of MBEJ's but showed that there was an accepted belief amongst academic researchers from around 1973 that a significant part of the load history was dynamic [7].

Tschemmernegg [8] noted that "…*Although everybody knows that expansion joints of bridges are the heaviest dynamic-loaded components of bridges, the design calculations, if any, were of a static nature. The results are a lot of well-known problems of detail with high costs for repair, interruption of traffic, etc*…" Dexter *et al* [9] report that the poor performance of MBJS is in part due to the belief` that they are often procured with inadequate specifications. Whilst there is reasonable International agreement on the distribution factor (percentage of load carried by a single centre beam), there is no common view on the extent to which the nominal quasi-static axle load should be augmented to account for the dynamic response. Dexter *et al* [2] favour a dynamic amplification factor (DAF) of 1.75 regardless of whether the design is single or multiple support bar whereas Crocetti & Edlund [10] advocate a DAF of 1.7 for multiple support bar designs and 2.0 for single support bar designs. Ancich *et al* [11] suggest that the prudent asset owner or specifier should consider setting the DAF at a minimum value of 2.5 for both single and multiple support bar designs. There is also a lack of agreement on the method of calculating the DAF with some approaches only considering the zero-to-peak (positive) displacement or strain from a moving vehicle as the dynamic contribution.

Schwammenhoefer [12] reports that the Federal Ministry of Transport (Austria) has experienced premature fatigue failure of MBEJ's and has replaced joints for both serviceability (fatigue) and noise protection (excessive environmental noise generation) reasons. MBEJ are also known to have been replaced in recent years in both Canada and the USA for predominantly serviceability reasons. Possibly the highest profile in-service failure involved the 3rd Lake Washington Bridge in Seattle, USA. Approximately 6 months after the bridge was opened to traffic in 1989, the asset owner (Washington State Department of Transportation) received numerous noise complaints about the expansion joints. Some relatively minor shim adjustments of the elastomeric bearings were undertaken but within one year, cracks in the centre beams similar to **Figure 3** were observed.

Figure 3 Centre Beam Cracking – 3rd Lake Washington Bridge (After [14])

The MBEJ's in the 3rd Lake Washington Bridge were manufactured in the US under licence to the German patent holder. The design is known as the swivel joist design and is essentially a variant of the single support bar design shown as **Figure 1**. Because of the *Buy American* requirement for this US federally funded bridge construction project, the original German centre beam section was replaced with a fabricated section sourced from a local hollow section and an extruded rail cap. Roeder [13] notes that "…*The tubular center beams clearly contribute to the fatigue problem because they cause local deformation and through-thickness plate bending stress…Despite the local deformation, fatigue would almost certainly have been a problem even if another section had been used for the center beams*…"

Kaczinski [15] believes that the 3rd Lake Washington Bridge joint failure was the result of very poor fatigue detail and the perception that no one even considered fatigue in the design.

The RTA has experienced premature fatigue failure of MBEJ's in two bridges. Fatigue cracks were observed in Pheasant's Nest Bridge on the Hume Highway (opened December 1980) and Mooney Mooney Creek Bridge on the F3 Freeway (opened December 1986). The MBEJ's installed into both bridges are multiple support bar designs and are essentially identical having been supplied by the same European manufacturer. **Figure 4** shows the typical locations for fatigue cracks in multiple support bar designs. Type A, B, & C cracks were observed at Pheasant's Nest and many developed into complete member failure. At Mooney Mooney, only Type B cracks were observed of which some developed into complete member failure. Several weld repair exercises were attempted at both bridges but these proved to be only stopgap solutions as fatigue cracks continued to develop. The Pheasant's Nest joints were replaced in 2003 and the Mooney Mooney joints are scheduled for replacement in 2004.

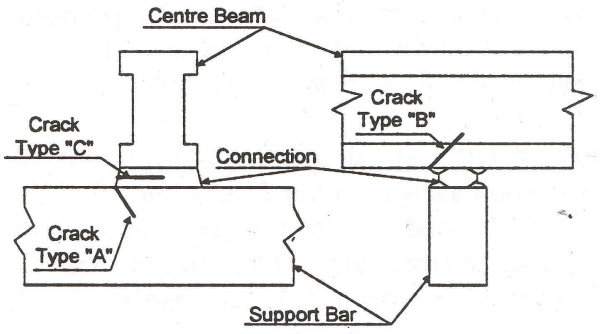

Figure 4 Established Fatigue Crack Patterns – Multiple Support Bar Designs

The Noise Issue

Noise measurements and analysis [1] [6] confirmed the hypothesis that an environmental noise nuisance resulted from the interaction of vibration of the modular bridge expansion joint with acoustic resonances produced inside the abutment void space below the joint. It was considered that cost-effective noise abatement could be undertaken by:

1. Modifying the dynamic behaviour of the joint to shift the natural frequencies so that they no longer co-incide with acoustic resonances.
2. Reducing the overall dynamic response by additional modal damping. This option included the trial use of tuned mass dampers (TMD's).
3. Providing acoustic absorption and limited screening, adjacent to the joint, to reduce noise propagation.
4. Modifying the acoustic absorption properties of the void space to eliminate or reduce the incidence of acoustic resonances.

The above strategies represented both "*new construction*" and "*retro-fit*" options. However, their efficacy and cost-effectiveness was still to be established by engineering measurement.

There were initial plans to design and test Option 2. However, this option was ultimately not pursued. Although TMD's would likely provide an effective noise reduction, these devices were not strongly advocated due to the high number of natural modes present and hence a high number of TMD's needing to be fitted and tuned. An alternative to the TMD concept would be the use of broadband damping coupled mass absorbers.

The perceived disadvantage of this approach being the requirement for a significant mass attachment to each centre beam. An array of damping coupled mass absorbers was subsequently trialled at Anzac Bridge to reduce the risk of fatigue failure but elaboration of that work is beyond the present discussion.

Due to resonances within the void space, the use of acoustic absorption and limited screening, adjacent to the joint was not considered practical. Consequently, only Option 4 was investigated. The chosen approach involved the construction of a Helmholtz Absorber within the void space of Tom Ugly's Bridge. The internal dimensions of the Helmholtz chambers were calculated to co-incide with the dominant acoustic frequencies. The Helmholtz Absorber panels were

designed to target the critical frequencies shown in **Table 1**.

Table 1. Helmholtz Absorber Modules Target Frequencies

Segment	Design Centre Frequency of Helmholtz Chambers, Hz					
	1	2	3	4	5	6
Frequency	64	80	90	105	110	120

The "*Before*" and "*After*" noise measurement results showed that the benefit is most obvious in the frequency range of 50 to 200 Hz that encompasses all the natural vibration modes. The noise reduction provided by the Helmholtz Absorber installation is of the order of 10 dBA.

Vibration Induced Fatigue

In an almost universal approach to the design of modular bridge expansion joints, the various national bridge design codes do not envisage that the embedded joint may be lightly damped and could vibrate as a result of traffic excitation.

These codes only consider an amplification of the static load to cover sub-optimal installation impact, poor road approach and the dynamic component of load. The codes do not consider the possibility of free vibration after the passage of a vehicle axle. Codes also ignore the possibilities of vibration transmission and response reinforcement through either following axles or loading of subsequent components by a single axle. Ancich *et al* [3] showed that, for the measured MBEJ, the number of effective cycles of load, due to vibration, for each vehicle passage was quite high. It was found that each heavy vehicle passage, of the load configuration of the 42t GVM test vehicle, produced around 30 vibration cycles where the dynamic strain equalled or exceeded the quasi-static strain of 100 με (0-Pk). Whilst these measurements relate to one particular MBEJ, they are considered to be generally representative of the single support bar design. The data must surely be of concern to MBEJ designers and specifiers who assume a single quasi-static load calculated from their national maximum permissible axle loading.

Heywood *et al* [17] identify the role of road profile unevenness in bridge damage. The unevenness of the approach pavement to a MBEJ will determine the quantum of the peak dynamic wheel force applied to the joint and this may be controlled to some extent by maintaining the road profile within predetermined International Roughness Indices (IRI) or NAASRA Roughness Counts.

However, the quantum of the peak dynamic wheel force applied to the joint will only determine the amplitude of the initial displacement. The response of the MBEJ to this dynamic force input will be principally determined by the structural dynamics behaviour of the joint.
It is likely, however, that the dynamic response of the joint is "*moderated*" by the presence of the tyre.

Figure 5 shows a typical heavy vehicle response to a deliberately introduced 40mm high vertical discontinuity in the pavement. It should be noted that the vertical scale for the road profile, axle movement (axle-hop), and body movement (body-bounce), is distorted for illustration. The abbreviations SWF and PDWF refer to the static wheel force and peak dynamic wheel force respectively.

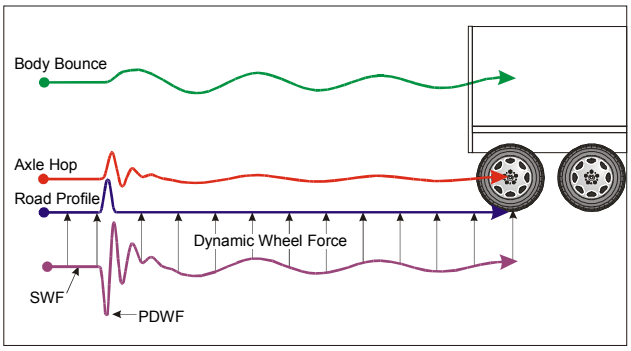

Figure 5 Axle-hop, body-bounce movements and tyre forces induced by a 1.5 m long 40 mm high hump – quarter truck simulation at 80 km/h (After [17])

Heywood *et al* [17] measured axle movement (axle-hop) frequencies generally in the range 8 – 12 Hz, and body movement (body-bounce) in the range 1.2 – 4 Hz. Consequently, if both the MBEJ and vehicle were lightly damped, vibration resonance between the two systems could potentially lead to very large vibration amplitudes. Work by Boyd *et al* [18] suggests that provided the forcing frequency is less than one quarter of the natural frequency of the lowest mode of the MBEJ then resonance effects may be ignored ($\omega/\omega_n << 1$). In the present study, the highest vehicle related frequency of 12 Hz is considerably less than one quarter of the lowest measured modal frequency (either bending or translational). However, resonance effects may not be totally ignored. If the beam pass frequency (f_p) is examined, it is obvious that some vehicle speed ranges will co-incide with modal frequencies. The beam pass frequency (f_p) is calculated as follows:

$$f_p = \frac{V}{G + b} \qquad (1)$$

Figure 6 shows the calculated resonance speeds for the single support bar MBEJ at Anzac Bridge over a range of centre beam spacings. Resonance effects are further complicated by a second, speed related, frequency described as the tyre pulse frequency (f_t).

The impact time or duration of loading for a wheel impact load may be expressed as a function of the vehicle speed, tyre patch length and the width of the centre beam top flange. The shape of the loading function may also be conveniently approximated by a half-sine wave (see **Figure 7**).

$$f_t = \frac{V}{L_t + b} \qquad (2)$$

For the legal speed limit at Anzac Bridge of 70 km/hr, a heavy vehicle tyre patch length of 200mm and a centre beam width of 75mm, the tyre pulse frequency f_t = 71 Hz. This is precisely the frequency identified by Ancich *et al* [3] [19] for a predominantly translational mode in the Anzac MBEJ. As **Figure 8** shows, 71 Hz is also the frequency at which most traffic induced vibration occurs.

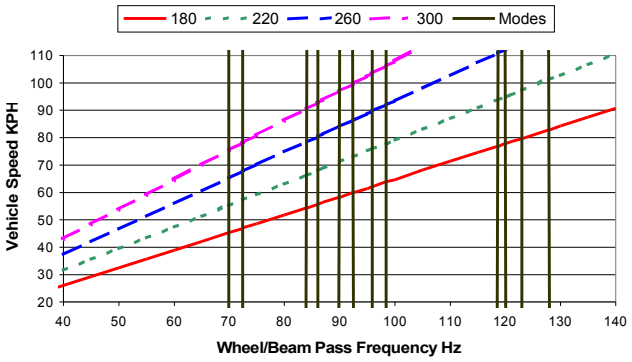

Figure 6 Calculated Beam Pass Frequencies for a Range of Expansion Joint Spacings

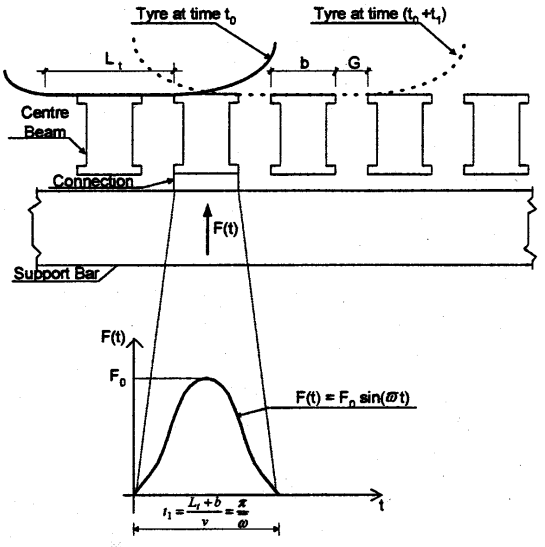

Figure 7 Characteristic Half-Sine Wave Impulsive Load

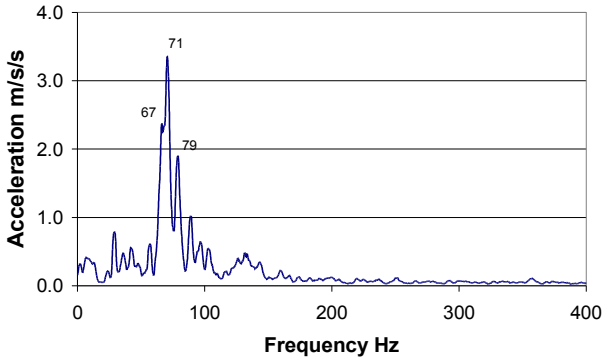

Figure 8 Centre Beam Vibration Spectrum – Anzac Bridge

Conclusions

Noise and vibration measurements have been undertaken at Anzac and Georges River (Tom Ugly's) Bridges. The analysis of these measurements supported the hypothesis that an environmental noise nuisance results from the interaction of vibration of the modular bridge expansion joint with acoustic resonances produced inside the void space below the joint. The trial installation of a Helmholtz Absorber at Tom Ugly's Bridge reduced the modular expansion joint induced low frequency "*booming*" noise emissions by up to 10 dBA. The character of the noise emission from the underside of the bridge deck would no longer be characterised as tonal and hence the likelihood of modular expansion joint related noise complaints has been significantly reduced. The use of Helmholtz Absorbers at other bridges with modular expansion

joints is considered to be viable as an engineering method of noise control.

High vibration levels were also considered largely responsible for premature fatigue failure. Experimental modal analysis and operational response shape studies were performed on a hybrid MBEJ installed in Anzac Bridge. The studies showed that for this joint:

- The joint is very lightly damped (<2% of critical damping).
- The lowest frequency mode excited was a quasi-translational (bounce/bending) mode at 71 Hz.
- Due to access restrictions, horizontal modal data could not be acquired in sufficient detail to identify horizontal bending or torsional modes.
- The support bars and centre beams were acting dynamically as if simply supported.
- There was good agreement between the experimental modal analysis and the operational response shape studies.

It is considered that the dynamic response of this MBEJ is mainly due to coupled centre beam resonance and this is seen as a design characteristic of all single support bar designs. Static and dynamic strain gauge studies showed that for this joint:

- The DAF is up to 4.6 for the fully laden test vehicle
- This DAF is not necessarily the worst case as every possible vehicle speed and joint opening combination was not tested
- Damping is important in the dynamic behaviour
- The number of effective cycles of load, due to vibration, for each vehicle passage is very high
- High uplift forces are generated within the joint under vehicle loading

These results should be of concern to bridge asset owners, bridge designers and modular joint suppliers. The normal assumption of quasi-static behaviour for both the single and multiple support bar design MBEJ's (and variants thereof) is not sustainable and both bridge designers and modular joint suppliers must think in terms of a fully dynamic system. The lack of International agreement for the method of calculating and assessing the dynamic amplification of load is seen as an impediment to this process.

Acknowledgement

The authors wish to thank the Chief Executive of the Roads and Traffic Authority of NSW (RTA) for permission to publish this paper. The opinions and conclusions expressed in this paper do not necessarily reflect the views of the RTA.

References

[1] Ancich E.J. & Brown S.C.: "Modular Bridge Joints – Reduction of noise emissions by use of Helmholtz Absorber", *Proc. 5th Austroads Bridge Conference*, Hobart, Tasmania, Australia (2004).

[2] Dexter R.J., Connor R.J. & Kaczinski M.R.: "Fatigue Design of Modular Bridge Expansion Joints", *NCHRP Report 402,* Transportation Research Board, National Research Council, Washington, DC, USA (1997) 128 pp.

[3] Ancich E.J., Chirgwin G.J. & Brown S.C.: "Dynamic Anomalies in a Modular Bridge Expansion Joint", *J. Bridge Engrg*., ASCE, (Submitted).

[4] Barnard C.P. & Cuninghame J.R.: "Improving the Performance of Bridge Expansion Joints: Bridge Deck Expansion Joint Working Group Final Report", *TRL Report 236*, Transport Research Laboratory, Crowthorne, Berkshire, UK (1997) 92 pp.

[5] Ancich E.J.: "A Study of the Environmental Noise Generation & Propagation Mechanisms of Modular Bridge Expansion Joints", RTA *Environmental Technology Report No. 000203*, Roads & Traffic Authority, Sydney, NSW, Australia (2000) 9 pp.

[6] Ancich E.J. & Brown S.C.: "Engineering Methods of Noise Control for Modular Bridge Expansion Joints", *Acoustics Australia*, (2004), 32 (4). 97-103.

[7] Tschemmernegg F.: "Messung von Vertikal- und Horizontallasten beim Anfahren, Bremsen und Überrollen von Fahrzeugen auf einem Fahrbahnübergang (Measurement of Vertical and Horizontal Loads due to Accelerating, Braking, and Rolling Vehicles on an Expansion Joint)", *Der Bauingenieur*, 48, Heft 9, Springer-Verlag, (1973) 326-330 (In German).

[8] Tschemmernegg F.: "The Design of Modular Expansion Joints", *Proc. 3rd World Congress on Joint Sealing and Bearing Systems for Concrete Structures*, Toronto, Ontario, Canada, (1991) 67-86.

[9] Dexter R.J., Osberg C.B. & Mutziger M.J.: "Design, Specification, Installation, and Maintenance of Modular Bridge Expansion Joint Systems", *J. Bridge Engrg*., ASCE, (2001), 6(6), 529-538.

[10] Crocetti R. & Edlund B.: "Fatigue Performance of Modular Bridge Expansion Joints", *J. Perform. Constr. Facil.*, ASCE, (2003) 17(4), 167-176.

[11] Ancich E.J., Brown S.C. & Chirgwin G.J.: "Dynamic Design of Modular Bridge Expansion Joints by the Finite Element Method", *J. Bridge Engrg*., ASCE, (In Preparation).

[12] Schwammenhoefer F.: Personal Communication (2001).

[13] Roeder C.W.: "Fatigue Cracking in Modular Expansion Joints", *Research Report WA-RD 306.1*,

Washington State Transportation Center, Seattle, Washington, USA (1993) 53 pp.
[14] Roeder C.W.: Personal Communication (2004).
[15] Kaczinski M.R.: Personal Communication (2004).
[16] Roeder C.W.: "Field Measurements of Dynamic Wheel Loads on Modular Expansion Joints", *Research Report WA-RD 369.1*, Washington State Transportation Center, Seattle, Washington, USA (1995) 66 pp.
[17] Heywood R., Prem H. & McLean J.: "Guide to Road Profile Unevenness and Bridge Damage", *Report AP-T13*, Austroads Inc., Sydney, NSW, Australia (2002) 33 pp.
[18] Boyd A.L., Schmidt B.R. & Thornton P.B.: "Loading and Impact Effects on Mine Haul Road Bridges" *MWP Technical Quarterly No. 4*, Macdonald Wagner & Priddle Pty Ltd (now Connell Wagner Pty Ltd), Sydney, NSW, Australia (1982) 7-15.
[19] Ancich E.J., Brown S.C. & Chirgwin G.J.: "Modular Deck Joints – Investigations into structural behaviour and some implications for new joints", *Proc. 5th Austroads Bridge Conference*, Hobart, Tasmania, Australia (2004).

Appendix D

Ancich E.J. and Brown S.C. (2004b). Engineering Methods of Noise Control for Modular Bridge Expansion Joints, *Acoustics Australia*, Vol. 32, No. 3, 101-107.

Acoustics Australia

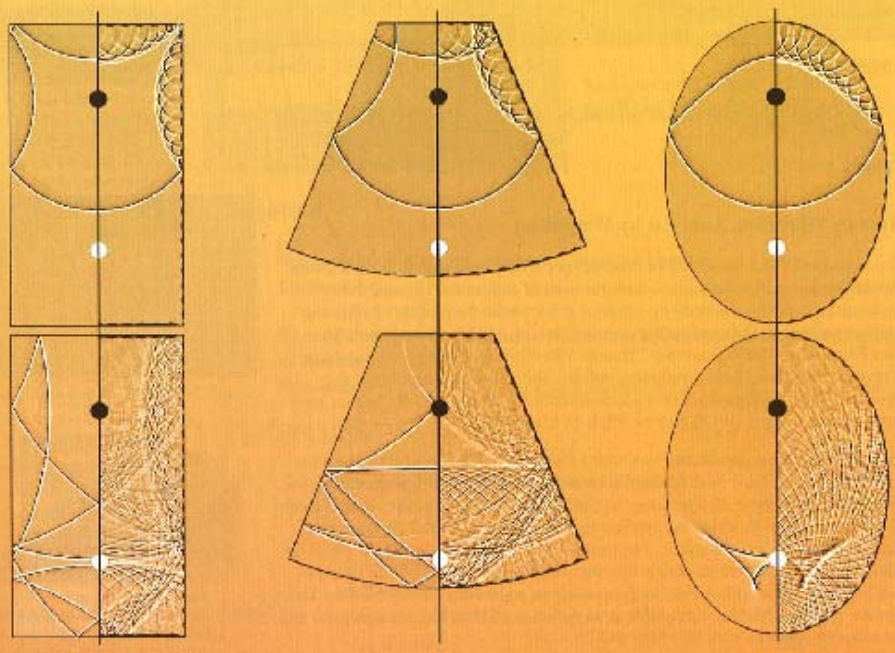

- Visualization of Sound Fields
- Resonance Theories of Hearing
- Noise Control in Bridge Joints
- Noise from Seasonal Industry
- Building Code Revisions

Australian Acoustical Society Vol. 32 No. 3 December 2004

ENGINEERING METHODS OF NOISE CONTROL FOR MODULAR BRIDGE EXPANSION JOINTS

Eric J. Ancich,
Bridge Technology Section, Roads & Traffic Authority of NSW, PO Box 558 Blacktown 2148.

Stephen C. Brown,
Richard Heggie Associates Pty Ltd, PO Box 176 Lane Cove 1595.

ABSTRACT Modular bridge expansion joints are widely used throughout the world for the provision of controlled pavement continuity during seismic, thermal expansion, contraction and long-term creep and shrinkage movements of bridge superstructures. It was known that an environmental noise nuisance occurred as motor vehicle wheels passed over the joint but the mechanism for the generation of the noise nuisance was not previously known. Noise abatement options were investigated before settling on a Helmholtz Absorber installation. The benefit is most obvious in the frequency range of 50 to 200 Hz. The noise reduction provided by the Helmholtz Absorber installation is of the order of 10 dBA.

INTRODUCTION

Whilst the use of expansion joints is common practice in bridge construction, modular bridge expansion joints are designed to accommodate large longitudinal expansion and contraction movements of bridge superstructures. In addition to supporting wheel loads, a properly designed modular joint will prevent rainwater and road debris from entering into the underlying superstructure and substructure. Modular bridge expansion joints are subjected to more load cycles than other superstructure elements, but the load types, magnitudes and fatigue-stress ranges that are applied to these joints are not well defined [1].

The basic modular joint design appears to have been patented around 1960 but the original patent has now expired and approximately a dozen manufacturers now exist throughout the world.

Modular bridge expansion joints are generally described as single or multiple support bar designs. In the single support bar design, the support bar (beam parallel to the direction of traffic) supports all the centre beams (beams transverse to the direction of traffic). In the multiple support bar design, multiple support bars individually support each centre beam. **Figures 1 & 2** show typical single support bar and welded multiple support bar design MBEJ's respectively. In Figure 1, the term "blockout" refers to the recess provided in the bridge superstructure to accommodate the casting-in of an expansion joint.

The MBEJ installed into the Western abutment of Anzac Bridge is, in fact, a hybrid design having pairs of support bars in series across the full width of the joint. Each pair of support bars is attached to alternate groups of four centre beams (i.e. Centre beams 1, 3, 5 & 7 are attached to the odd numbered support bars and centre beams 2, 4, 6 & 8 attached to the even numbered support bars). The support bar pairs are spaced at 2.25m centres across the full width of the bridge resulting in a total of 24 support bars.

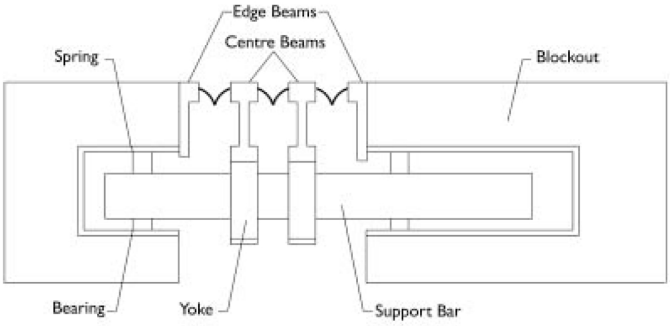

Figure 1 Typical Single Support Bar Design MBEJ

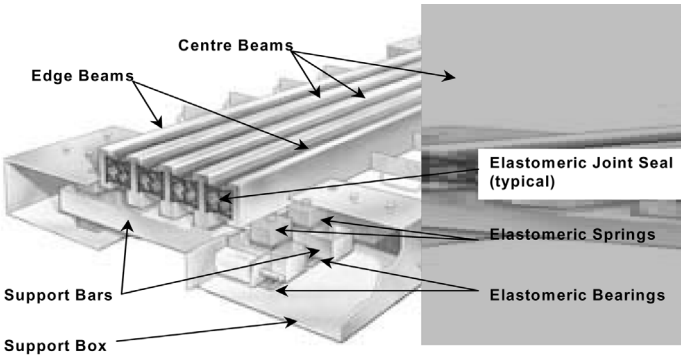

Figure 2 Typical Multiple Support Bar Design MBEJ

The MBEJ installed into the southbound carriageway of the bridge over the Georges River at Tom Ugly's Point is a typical welded multiple support bar design as shown in **Figure 2**.

It is known that an environmental noise nuisance occurs as motor vehicle wheels pass over the joint but the mechanism for the generation of the noise nuisance is not widely understood although Barnard & Cuninghame [2] do confirm the role of acoustic resonances.

A study was undertaken and the modular bridge expansion joints built into the Georges River (Tom Ugly's) Bridge and Anzac Bridge were selected for the study due to their proximity and ease of access. Engineering measurements were made under operational conditions to determine how the noise nuisance originated and was subsequently propagated into the surrounding environment [3].

2.0 NOISE GENERATION HYPOTHESIS

There was anecdotal evidence from environmental noise nuisance complaints received by the Roads & Traffic Authority of NSW (RTA) that the sound produced by the impact of a motor vehicle tyre with modular bridge expansion joints was audible at least 500 metres from the bridge in a semi-rural environment. Site inspection suggested that the noise generation mechanism involved possibly both parts of the bridge structure and the joint itself as there was distinct difference between the subjective character of the noise above and below the bridge deck.

The hypothesis was developed by Ancich [3] that motor vehicle tyre impacts vibrationally excite modular bridge expansion joints thereby producing noise that is amplified within the bridge superstructure (due to acoustic resonances) and then propagated into the surrounding environment.

As **Figures 1 & 2** show, each transverse centre beam is connected (at the tyre contact level) to the adjoining centre beam or edge beam by a thick rubber strip seal. It is this combination of the rubber strip seals with the steel beams that acts as a continuous membrane and affords MBJS their unique water proofing properties. However, when the MBEJ vibrates, this membrane behaves in much the same way as the skin of a drum or the diaphragm of a loudspeaker. Experimental modal analysis studies [4] [5] indicated that typical MBEJ's have both flexural and translational modes. The most significant translational mode was a vertical bounce/bending mode where all parts of the MBEJ were vibrating essentially in phase at the same frequency and in combination with some vertical bending of centre beams and support bars.

Ancich *et al* [6] confirmed with finite element modelling the measured natural modes and indicated that MBEJ's were very sensitive to damping and operational conditions where motor vehicle tyre impacts to successive centre beams were in-phase or notionally in-phase. In the worst combination of low damping (<5% of critical) and in-phase excitation, the modelled dynamic amplification factor was as high as 11.

3.0 MEASUREMENT PROCEDURE

To test the hypothesis, simultaneous noise and vibration measurements, at the Georges River (Tom Ugly's) and Anzac Bridges, were recorded and analysed. Vibration data were obtained from an accelerometer attached to a transverse beam (centre beam) of the MBEJ. Noise data were obtained from a precision Sound Level Meter located inside the void space within the bridge abutment directly beneath the MBEJ and at external locations.

The simultaneous noise and vibration data were recorded onto a Sony Model PC 208A DAT recorder using a Bruel & Kjaer Type 2260 (Investigator) Sound Level Meter, Type 4370 Accelerometer and Type 2635 Charge Amplifier and subsequently analysed using a OROS Type OR25 FFT analyser.

4.0 RESULTS & DISCUSSION

Measurements were initially made at the Georges River (Tom Ugly's) Bridge and the narrow band frequency analysis of the vibration data indicated the presence of a small number of discrete frequencies generally in the range 50-150 Hz.

It was believed that these frequencies were likely to be the vertical and/or horizontal bending frequencies for the transverse beams (tyre contacting) of the modular expansion joint. **Figure 3** shows the vibration spectrum of a typical

Table 1 Calculated and Measured Natural Frequencies - Georges River (Tom Ugly's) Bridge

Measured Frequency, Hz	Calculated Frequency, Hz[2]	Calculated Vibration Mode[1]
70	67.11	Vertical (1)
82	80.1, 80.8, 81.7, 82.9, 83.4, 83.5, 87.8, 89	Horizontal (4), Horizontal (2), Horizontal (3), Horizontal (5), Vertical (2 & 6), Vertical (1 & 4), Horizontal (4), Vertical (2 & 5)
90	89, 91.2, 97.4	Vertical (2 & 5), Horizontal (3), Vertical (3, 5 & 7)

Notes: (1) As the precise boundary conditions for the Georges River (Tom Ugly's) Bridge joint are not known, some assumptions were made. The Mode numbers associated with the various frequencies reflect the range of assumptions. Numbers in brackets refer to the calculated mode number.

(2) Calculated frequencies are considered correct ± 10% due to assumption uncertainties.

(3) Bracketed numbers following mode type refer to the calculated mode number.

Table 2 Calculated Room Acoustic Modal Frequencies compared with Measured Vibration Frequencies - Georges River (Tom Ugly's) Bridge

Measured Frequency, Hz		Calculated Frequency, Hz[1]	Calculated Acoustic Mode
Noise	Vibration		
N.A	N.A	11.1	Transverse (1)
76	70	74.1	Vertical (1)
82	82	81.9	Vertical (1)
N.A	90	148.3; 163.8	Vertical (2)

Notes: (1) Calculation of multiple frequencies for some acoustic modes arises from varying dimensions within the void space.
(2) Bracketed numbers following mode type refer to the calculated mode number.
(3) N.A indicates that the calculated frequency was not identified in the measurements.

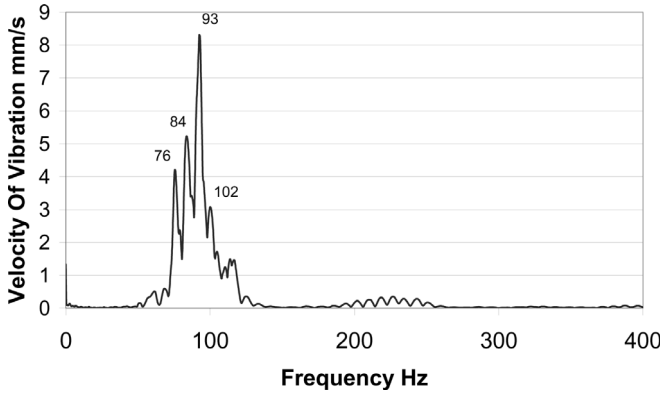

Figure 3 Centre Beam Vibration Spectrum – Tom Ugly's Bridge

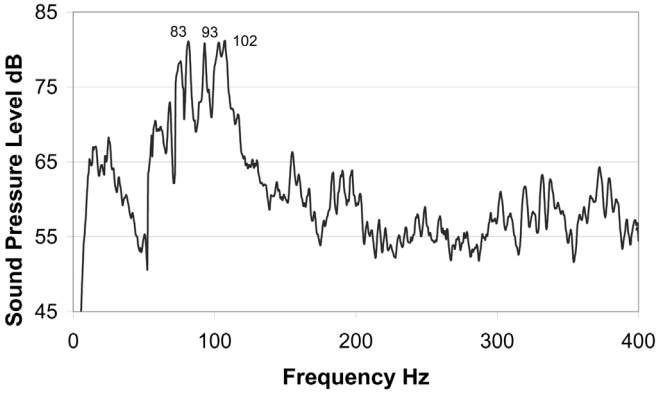

Figure 4 Acoustic Excitation Spectrum – Tom Ugly's Bridge

Georges River (Tom Ugly's) Bridge centre beam. Examination of **Figure 3** reveals the presence of three dominant peaks in the frequency spectrum (70 Hz, 82 Hz & 90 Hz). Consequently, a grillage analysis of the joint was undertaken using Microstran® [7]. This analysis was used to calculate natural modal frequencies and **Table 1** shows the measured and calculated vibration frequencies.

Table 1 indicates a high degree of correlation between the calculated natural frequencies and the three dominant

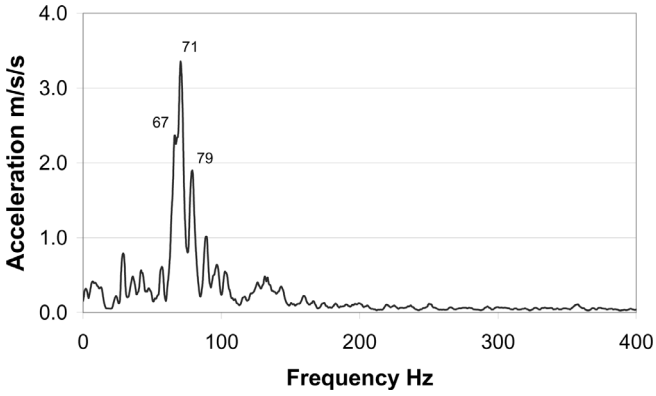

Figure 5 Centre Beam Vibration Spectrum – Anzac Bridge

frequencies (70 Hz, 82 Hz & 90 Hz) measured at the Georges River (Tom Ugly's) Bridge.

A possible explanation for the high environmental noise nuisance is acoustic coupling between vibration of the modular joint and room acoustic modes inside the void space within the bridge abutment beneath the modular joint. This possible explanation was tested by calculating the frequencies of the various room acoustic modes encompassed by the vibration frequencies of interest [8]. This comparison is shown as **Table 2**.

Additional calculations were undertaken to determine the acoustic modal frequencies within the bridge box girders as these structures are acoustically connected to the void space within the bridge abutment beneath the modular joint. The calculated frequencies appear as **Table 3**.

Figure 4 shows the acoustic excitation spectrum from measurements undertaken inside the void space within the bridge abutment beneath the modular bridge expansion joint. Examination of **Figure 4** reveals the presence of two dominant peaks in the noise frequency spectrum (76 Hz & 82 Hz) and similar or matching frequencies also appear in **Figure 3** and **Table 2**.

Similar measurements to those undertaken at Georges River (Tom Ugly's) Bridge were repeated at the Anzac Bridge. **Figure 5** shows the corresponding vibration spectrum of a

Table 3 Calculated Box Girder Acoustic Modal Frequencies compared with Measured Vibration Frequencies - Georges River (Tom Ugly's) Bridge

Measured Frequency, Hz	Calculated Frequency, Hz[1]	Calculated Acoustic Mode
70	59, 73	Transverse (1), Vertical (1)
82	73, 86	Vertical (1), Transverse (1)
90	86	Transverse (1)

Notes: (1) Calculation of multiple frequencies for some acoustic modes arises from varying dimensions within the box girder.
(2) Bracketed numbers following mode type refer to the calculated mode number.

Table 4 Calculated and Measured Natural Frequencies (Anzac Bridge)

Measured Frequency, Hz	Calculated Frequency, Hz[2]	Calculated Vibration Mode[1]
57	34.5	Horizontal (1)[3]
65	N.A[4]	N.A
70.5	N.A	N.A
84	91.3, 94.9, 99.4	Vertical (2 & 3), Horizontal (4)
122	103.4, 108.4, 111.2, 118.8, 119, 124.3	Horizontal (5), Vertical (6), Horizontal (7), Vertical (8), Horizontal (9), Vertical (10)
189	N.A	N.A

Notes: (1) As the precise boundary conditions for the Anzac Bridge joint are not known, some assumptions were made. The Mode numbers associated with the various frequencies reflect the range of assumptions.
(2) Calculated frequencies are considered correct ± 10% due to assumption uncertainties.
(3) Bracketed numbers following mode type refer to the calculated mode number.
(4) "N.A" indicates that no calculated frequency was found to correspond with the measured frequency.

typical Anzac Bridge centre beam. Examination of **Figure 5** reveals the presence of six dominant peaks in the frequency spectrum (57 Hz, 65 Hz, 70.5 Hz, 84 Hz, 122 Hz & 189 Hz).

Consequently, a grillage analysis of the joint was undertaken using Microstran®. This analysis was used to calculate natural modal frequencies and **Table 4** shows the measured and calculated vibration frequencies. The possibility of acoustic coupling to room modes in the Anzac Bridge abutment void space was also tested by calculating the frequencies of the various room acoustic modes encompassed by the vibration frequencies of interest. This comparison is shown as **Table 5**.

5.0 NOISE ABATEMENT OPTIONS

The analysis of measurements supported the hypothesis that an environmental noise nuisance resulted from the interaction of vibration of the modular bridge expansion joint with acoustic resonances produced inside the abutment void space below the joint.

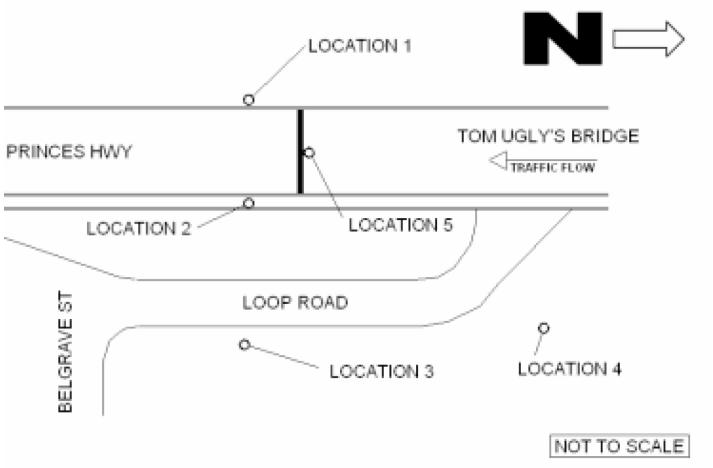

Figure 6 Site Plan Showing Noise Measurement Locations

Table 5 Calculated Room Acoustic Modal Frequencies compared with Measured Vibration Frequencies (Anzac Bridge)

Measured Frequency, Hz	Calculated Frequency, Hz[1]	Calculated Acoustic Mode
N.A	19.0	Transverse (3)
57	45.3, 47.8, 53.8	Axial (1), Vertical (1), Axial (1)
65	63.7	Vertical (1)
70.5	71.7	Vertical (1)
84	86.0	Vertical (1)
122	127.4, 135.8, 143.3	Vertical (2), Axial (3), Vertical (3)
189	172.0, 191.1	Vertical (2), Axial (2) & Vertical (3)

Notes: (1) Calculation of multiple frequencies for some acoustic modes arises from varying dimensions within the void space.
(2) Bracketed numbers following mode type refer to the calculated mode number.
(3) N.A indicates that the calculated frequency was not identified in the measurements.

Table 6 Helmholtz Absorber Modules Target Frequencies

Segment	Design Centre Frequency of Helmholtz Absorber, Hz					
	1	2	3	4	5	6
Frequency (Hz)	64	80	90	105	110	120

The reverberant nature of the void space was considered to be the reason for the apparent amplification of the low frequency sound pressure within the void space. As true standing waves do not propagate, this highly reactive (long reverberation time characteristic) of the void is not apparent in the far field. Due to the small amount of acoustic absorption in the void, some of this sound energy is absorbed within the void and some is radiated to the environment through openings. The build-up of acoustic energy is then radiated into the environment.

Martner [9] reports the results of noise measurements of a number of different types of bridge expansion joints, including modular bridge expansion joints. Whilst he indicates that the installation of an acoustic enclosure beneath the expansion joint was very effective, it is not clear whether the enclosure was used with the modular design. Rhombic plates welded onto the top surface of the edge and centre beams are reported to offer noise reductions of up to 9 dBA below the bridge deck [10]. However, these engineering methods of noise control were considered to be either too expensive or, in the case of the rhombic plates, largely developed for a particular proprietary design MBEJ. In addition, whilst these noise control measures are undoubtedly effective, their use may have an adverse impact on the ability of the asset owner to routinely inspect and maintain the joint.

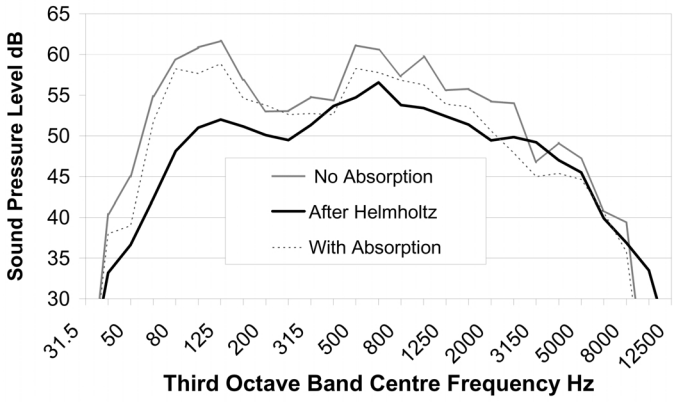

Figure 7 RMS Average Third Octave Band Noise Spectra at Location 4

It was considered that cost-effective noise abatement could be undertaken by:

1. Modifying the dynamic behaviour of the joint to shift the natural frequencies so that they no longer co-incide with acoustic resonances.

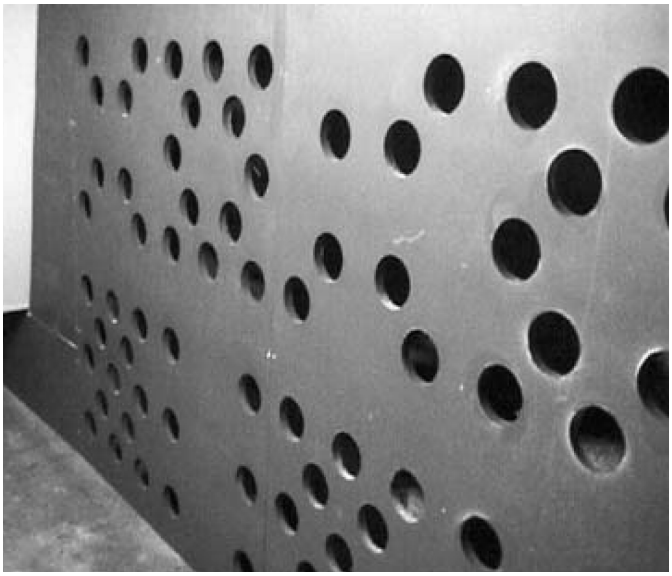

Figure 8 Helmholtz Absorber

2. Reducing the overall dynamic response by additional modal damping. This option included the trial use of tuned mass dampers.
3. Providing acoustic absorption and limited screening, adjacent to the joint, to reduce noise propagation.
4. Modifying the acoustic absorption properties of the void space to eliminate or reduce the incidence of acoustic resonances.

The above strategies represent both "new construction" and "retro-fit" options. However, their efficacy and cost-effectiveness was still to be established by engineering measurement

There were initial plans to design and test Option 2. However, this option was ultimately not pursued. Although tuned mass dampers (TMD) would likely provide an effective noise reduction, these devices were not strongly advocated due to the high number of natural modes present and hence a high number of TMD's needing to be fitted and tuned [11]. An alternative to the TMD concept would be the use of broadband damping coupled mass absorbers.

The perceived disadvantage of this approach being the requirement for a significant mass attachment to each centre beam. An array of damping coupled mass absorbers was subsequently trialled at Anzac Bridge to reduce the risk of fatigue failure but elaboration of that work is beyond the present discussion.

Due to resonances within the void space, the use of acoustic absorption and limited screening, adjacent to the joint was not considered practical. Consequently, only Option 4 was investigated. This investigation was undertaken using two different approaches. Firstly, the simple addition of acoustic absorption into the void space was tested.

Noise measurements were conducted on 4 May 2001 at which time trial acoustical absorption material had been installed over the floor of the void below the expansion joint. The absorption was arranged in a 100 mm thick layer over the floor area of the void and raised 75 mm (nominally) above the floor surface (to optimise low frequency sound absorption). Noise measurement locations are shown as **Figure 6**.

Whilst the above deck (Locations 1 and 2) and the side (Location 3) measurements show no significant change in the noise spectra, the below deck Locations 4 and 5 show a significant increase in the low frequency bands when the trial absorption was removed.

As the measurements at Location 5 (from within the void space) are the result of sound pressure due to both propagating sound energy as well as non-propagating standing waves, the results at Location 4 provide a better indication of the effect on the emitted (propagating) noise.

The second approach involved the construction of a Helmholtz Absorber within the void space. The internal dimensions of the Helmholtz chambers were calculated to co-incide with the dominant acoustic frequencies. The Helmholtz Absorber panels were designed to target the critical frequencies shown in **Table 6**.

Figure 7 shows a comparison of RMS average one-third octave band noise spectra at Location 4 before and after the Helmholtz absorber installation. Also shown are the one-third octave band noise spectra with floor absorption only, for comparison.

These results clearly demonstrate the effectiveness of the Helmholtz absorber modules in the target range of 60 Hz to 160 Hz.

Figure 8 shows the installed absorber modules.

6.0 CONCLUSION

Noise and vibration measurements have been undertaken at Anzac and Georges River (Tom Ugly's) Bridges. The analysis of these measurements supported the hypothesis that an environmental noise nuisance results from the interaction of vibration of the modular bridge expansion joint with acoustic resonances produced inside the void space below the joint.

The trial addition of acoustic absorption batts into the void space of Tom Ugly's Bridge was considered to be only marginally effective for noise control and was not pursued. However, the installed Helmholtz Absorber at Tom Ugly's Bridge has reduced the modular expansion joint induced low frequency "booming" noise emissions by up to 10 dB. The character of the noise emission from the underside of the bridge deck would no longer be classified as tonal and hence the likelihood of modular expansion joint related noise complaints has been significantly reduced.

The use of Helmholtz Absorbers at other bridges with modular expansion joints is considered to be viable as an engineering method of noise control.

ACKNOWLEDGEMENT

The authors wish to thank the Chief Executive of the Roads and Traffic Authority of NSW (RTA) for permission to publish this paper. The opinions and conclusions expressed in this paper do not necessarily reflect the views of the RTA.

REFERENCES

1. R.J. Dexter, R.J. Connor & M.R. Kaczinski, "Fatigue Design of Modular Bridge Expansion Joints" *NCHRP Report 402,* Transportation Research Board, National Research Council, Washington, DC, USA (1997) 128 pp.
2. C.P. Barnard & J.R. Cuninghame, "Improving the Performance of Bridge Expansion Joints: Bridge Deck Expansion Joint Working Group Final Report" *TRL Report 236*, Transport Research Laboratory, Crowthorne, Berkshire, UK (1997) 92 pp.
3. E.J. Ancich, "A Study of the Environmental Noise Generation & Propagation Mechanisms of Modular Bridge Expansion Joints" *RTA Environmental Technology Report No. 000203*, Roads & Traffic Authority of NSW, Sydney (2000) 9 pp.
4. E.J. Ancich, G.J. Chirgwin & S.C. Brown, "Dynamic Anomalies in a Modular Bridge Expansion Joint" *J. Bridge Engrg*., ASCE, (Submitted).
5. E.J. Ancich, S.C. Brown & G.J. Chirgwin, "Modular Deck Joints – Investigations into structural behavior and some implications for new joints" *Proc. 5th AUSTROADS Bridge Conference*, Hobart, Tasmania (2004) 15 pp.
6. E.J. Ancich, S.C. Brown & G.J. Chirgwin, "Dynamic Design of Modular Bridge Expansion Joints by the Finite Element Method" *J. Bridge Engrg*., ASCE, (In Preparation).
7. Anon., "Microstran User Manual Version 7", Engineering Systems Pty Ltd, Sydney (1999).
8. T.F.W. Embleton, "Mufflers" in *Noise and Vibration Control – Revised Edition* ed. L.L. Beranek, Institute of Noise Control Engineering, Washington (1988) pp 362-405.
9. O. Martner, "Noise Emission of Constructions for Bridge-To-Road Crossings" *Proc. Inter-Noise 96*, Liverpool, UK, 211-214 (1996).
10. Anon., "Geräuschminderung an Fahrbahnübergängen in Lamellenbauweise durch wellenförmigen Fugenverlauf" *Maurer Info Nr. 24*, Maurer Söhne, Munich, Germany (2001) 10 pp (In German).
11. D.I.G. Jones, "Effect of Isolated Tuned Dampers on Response of Multispan Structures" *J. Aircraft*, Vol. 4, No. 4, 343-346 (1967).

Appendix E

Ancich E.J., Brown S.C. and Chirgwin G.J. (2004). Modular Deck Joints – Investigations into structural behaviour and some implications for new joints, *Proc. 5th Austroads Bridge Conference*, Hobart, Tasmania, Australia.

AustRoads

Fifth AustRoads Bridge Conference - May 2004

Bridges Another Dimension

-design - construction - procurement - maintenance -

Modular Deck Joints – Investigations into structural behaviour and some implications for new joints

Eric J. Ancich, Senior Project Officer, Bridge Technology Section, Roads & Traffic Authority of NSW, PO Box 558 Blacktown 2148, Australia. E-mail: Eric_Ancich@rta.nsw.gov.au

Stephen C. Brown, Associate, Richard Heggie Associates Pty Ltd, PO Box 176 Lane Cove 1595, Australia. E-mail: steve.brown@heggies.com.au

Gordon J. Chirgwin, Manager, Bridge Policies Standards & Records, Roads & Traffic Authority of NSW, PO Box 558 Blacktown 2148, Australia. E-mail: Gordon_Chirgwin@rta.nsw.gov.au

SYNOPSIS

Environmental noise complaints from homeowners near bridges with modular expansion joints (MBEJ) led to an engineering investigation into the noise production mechanism. The investigation identified modal vibration frequencies in the MBEJ coupling with acoustic resonances in the chamber cast into the bridge abutment below the MBEJ. This initial acoustic investigation was soon overtaken by observations of fatigue induced cracking in structural beams transverse to the direction of traffic. These beams are, in the English-speaking world, universally referred to as centre beams. However, in Europe the use of *lamella* to describe these beams is equally common. A literature search revealed little to describe the structural dynamics behaviour of MBEJ's but showed that there was an accepted belief amongst academic researchers dating from around 1973 that the loading was dynamic. In spite of this knowledge almost all designers use a static or quasi-static design with little consideration of the dynamic behaviour, either in the analysis or the detailing.

Principally, this paper identifies the natural modes of vibration of the single support bar design MBEJ installed into Sydney's Anzac Bridge and the welded multiple support bar design MBEJ installed into the southern abutment of the southbound carriageway of the bridge over the south channel of the Manning River (Taree By-pass). Secondly, the paper will report the dynamic amplification factors (DAF) obtained after extensive static and dynamic strain gauge measurements of both MBEJ's.

1 INTRODUCTION

Whilst the use of expansion joints is common practice in bridge construction, modular bridge expansion joints are designed to accommodate large longitudinal expansion and contraction movements of bridge superstructures. In addition to supporting wheel loads, a properly designed modular joint will prevent rainwater and road debris from entering into the underlying superstructure and substructure. Modular bridge expansion joints are subjected to more load cycles than other superstructure elements, but the load types, magnitudes and fatigue-stress ranges that are applied to these joints are not well defined [Dexter *et al* (1)].

A literature search revealed little to describe the structural dynamics behaviour of MBEJ's but showed that there was an accepted belief amongst academic researchers from around 1973 that the loading was dynamic [Tschemmernegg (2)]. Subsequently, Tschemmernegg (3) noted that "… *Although everybody knows that expansion joints of bridges are the heaviest dynamic-loaded components of bridges, the design calculations, if any, were of a static nature. The results are a lot of well-known problems of detail with high costs for repair, interruption of traffic, etc…*"

2 DESCRIPTION OF MODULAR BRIDGE EXPANSION JOINTS

Modular bridge expansion joints are generally described as single or multiple support bar designs. In the *single* support bar design, the support bar (beam parallel to the direction of traffic) supports all the centre beams (beams transverse to the direction of traffic). In the *multiple* support bar design, multiple support bars individually support each centre beam. **Figures 1 & 2** show typical single support bar and welded multiple support bar MBEJ's respectively.

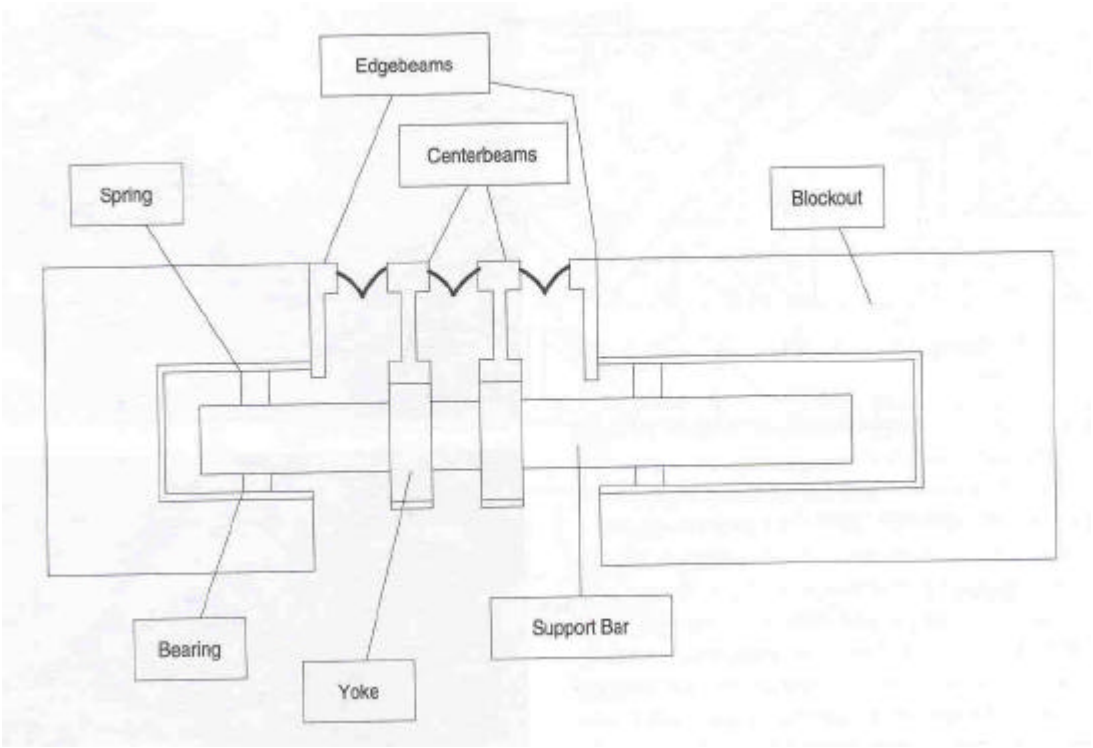

Figure 1: Typical Single Support Bar Design MBEJ

The MBEJ installed into the Western abutment of Anzac Bridge is, in fact, a hybrid design having pairs of support bars in series across the full width of the joint. Each pair of support bars is attached to alternate groups of four centre beams [i.e. Centre beams 1, 3, 5 & 7 are attached to support bar #1 (and the other odd numbered support bars) and centre beams 2, 4, 6 & 8 attached to support bar #2 (and the other even numbered support bars)]. The support bar pairs are spaced at 2.25m centres across the full width of the bridge resulting in a total of 24 support bars (2 x 12).

The MBEJ installed into the southern abutment of the southbound carriageway of the bridge over the south channel of the Manning River (Taree By -pass) is a typical mu ltiple support bar design as shown in **Figure 2**. MBEJ's typically employ mechanisms to maintain equidistant centre beam spacing over the full range of joint movement. Equidistant devices include elastomeric springs and mechanical linkages such as pantogra phs or the so -called "*lazy tong*". The MBEJ installed into the Western Abutment of Anzac Bridge employs a mechanical linkage system and the Taree By-pass MBEJ utilises elastomeric control springs.

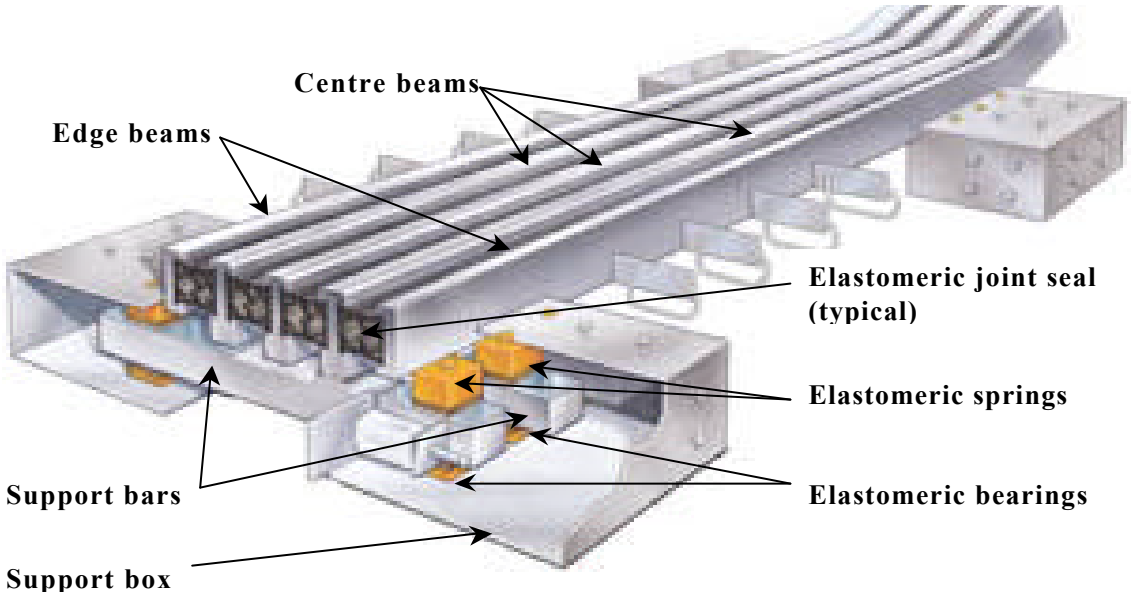

Figure 2: Typical Multiple Support Bar Design MBEJ

3 STRUCTURAL DYNAMICS STUDIES

3.1 Initial Noise Investigation

There was anecdotal evidence from environmental noise nuisance complaints received by the Roads & Traffic Authority of NSW (RTA) that the sound produced by the impact of a motor vehicle tyre with modular bridge expansion joints was audible up to 500 metres from a bridge in a semi -rural environment. This observation suggested that the noise generation mechanism involved possibly both parts of the bridge structure and the j oint itself as it is unlikely that there is sufficient acoustic power in the simple tyre impact to explain the persistence of the noise in the surrounding environment [Ancich & Brown (4)].

The analysis of simple vibration measurements of the 9 -seal MBEJ installed into the Anzac Bridge [Ancich *et al* (5)] revealed that most of the traffic -induced vibration was at a frequency of 71 Hz. An FFT spectrum is shown as **Figure 3**.

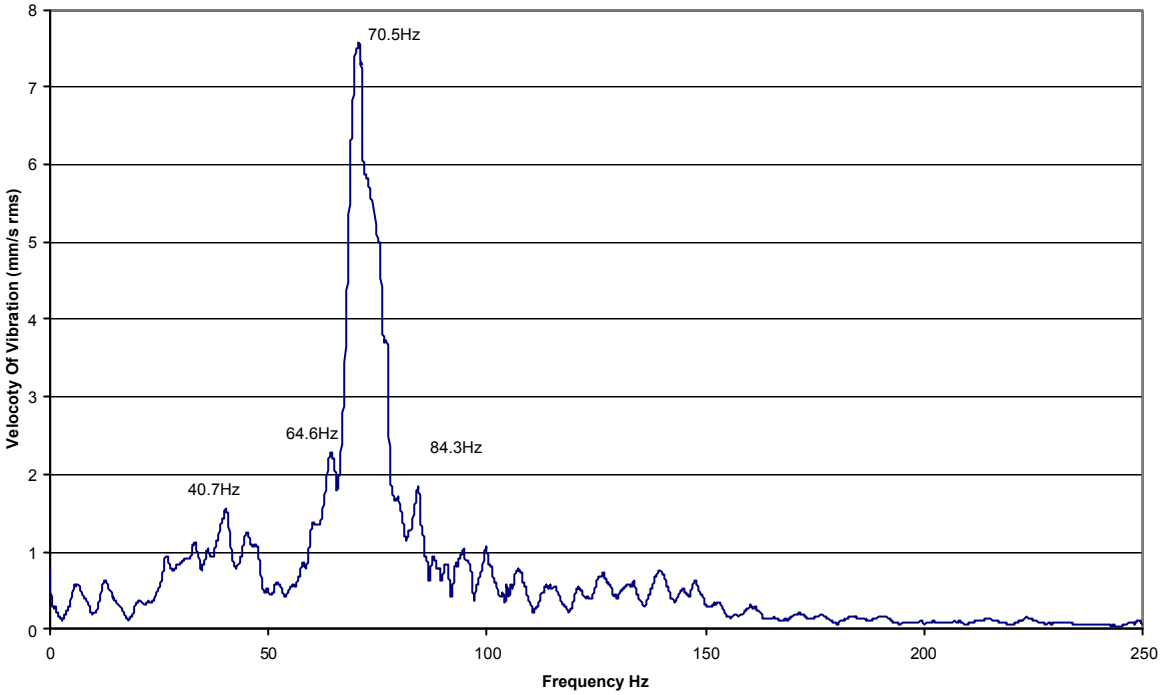

Figure 3: Centre Beam Vibration Spectrum – Anzac Bridge

A preliminary analytical study failed to identify the vibrational mode responsible for this frequency and an experimental modal analysis study was subsequently undertaken. The modal analysis study revealed that the 71 Hz frequency was predominantly due to a quasi-rigid body mode where the MBEJ was essentially bouncing on its bearing supports in combination with some support bar and centre beam vertical bending. It was deduced that at least 90% of the MBEJ mass was mobilised at this frequency.

Classical first and second order centre beam vertical bending modes were found at 85 Hz, 91 Hz and 97 Hz. Due to access restrictions, horizontal modal data could not be acquired in sufficient detail to identify horizontal bending or torsional modes. It should be noted that Ostermann (6) also shows an analytically determined vertical mode at 87 Hz that exhibits elements of the quasi-rigid body (bounce/bending) mode.

It is also interesting to note that experimental modal analysis results [Ancich *et al* (5)] indicated that the support bars and centre beams were acting dynamically as if simply supported. This observation is somewhat counter-intuitive.

Roeder (7) postulated that the dynamic response of MBEJ's is complicated because hundreds of modes of vibration may contribute to the response. The present data do not support that view.

To the contrary, the predominant dynamic response responsible for peak dynamic strains is attributed to the participation of the first three or four vertical modes. Horizontal bending and torsional modes were not identified due to experimental limitations.

However, the presence of the quasi-rigid body (bounce/bending) mode at 71 Hz was unexpected. Although this mode was implied by Köster (8), it does not appear to have been previously reported.

It is noted that modal analysis measurements at Taree also revealed the presence of this quasi-rigid body (bounce/bending) mode. In all cases measured, the "bounce/bending" mode occurred at lower frequencies than the respective centre beam fundamental (vertical) bending modes. The experimental modal analysis results revealed that all the Anzac modes were very lightly damped (<2% of critical) and consequently likely to contribute to free un - damped vibration of structural members of the MBEJ.

Under some operating conditions, lightly damped single support bar systems may experience dynamic amplification of loads up to 5 times the nominal static load. It is considered that this dynamic response is a direct result of the phenomenon of coupled centre beam resonance [Ancich *et al* (5)].

The modal analysis data were subsequently used to optimise the placement of strain gauges as part of the fatigue life assessment of the Anzac and Taree MBEJ's. Details of the methodology employed in the strain gauge testing are given in Ancich *et al* (5).

4 STATIC & DYNAMIC STRAIN MEASUREMENT

Figure 4 represents a plan view diagram of the eastbound kerbside lane of Anzac Bridge and shows the six strain gauge locations (SG1 to SG6) and **Figure 5** represents a plan view diagram of the southbound ker bside lane of the Taree By -pass Bridge and shows the six strain gauge locations (SG1 to SG6). All gauges were of a linear type and orientated in the anticipated principal stress direction (i.e. parallel to the long axis of the respective structural members).

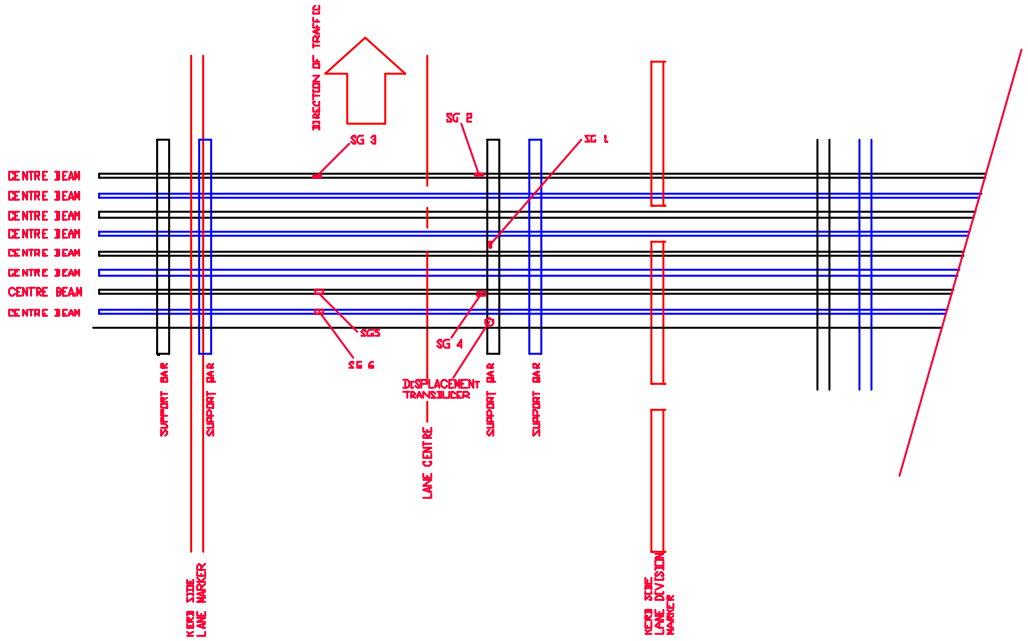

Figure 4: Anzac Eastbound Carriageway - Strain Gauge Locations (SG1 to SG6)

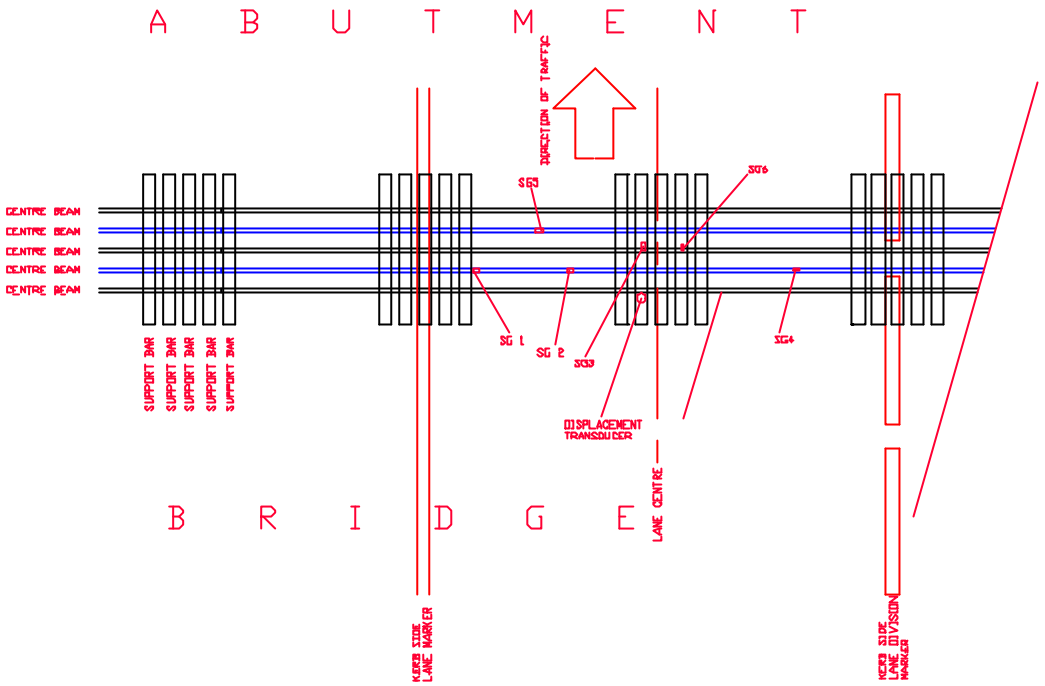

Figure 5: Taree Southbound Carriageway - Strain Gauge Locations (SG1 to SG6)

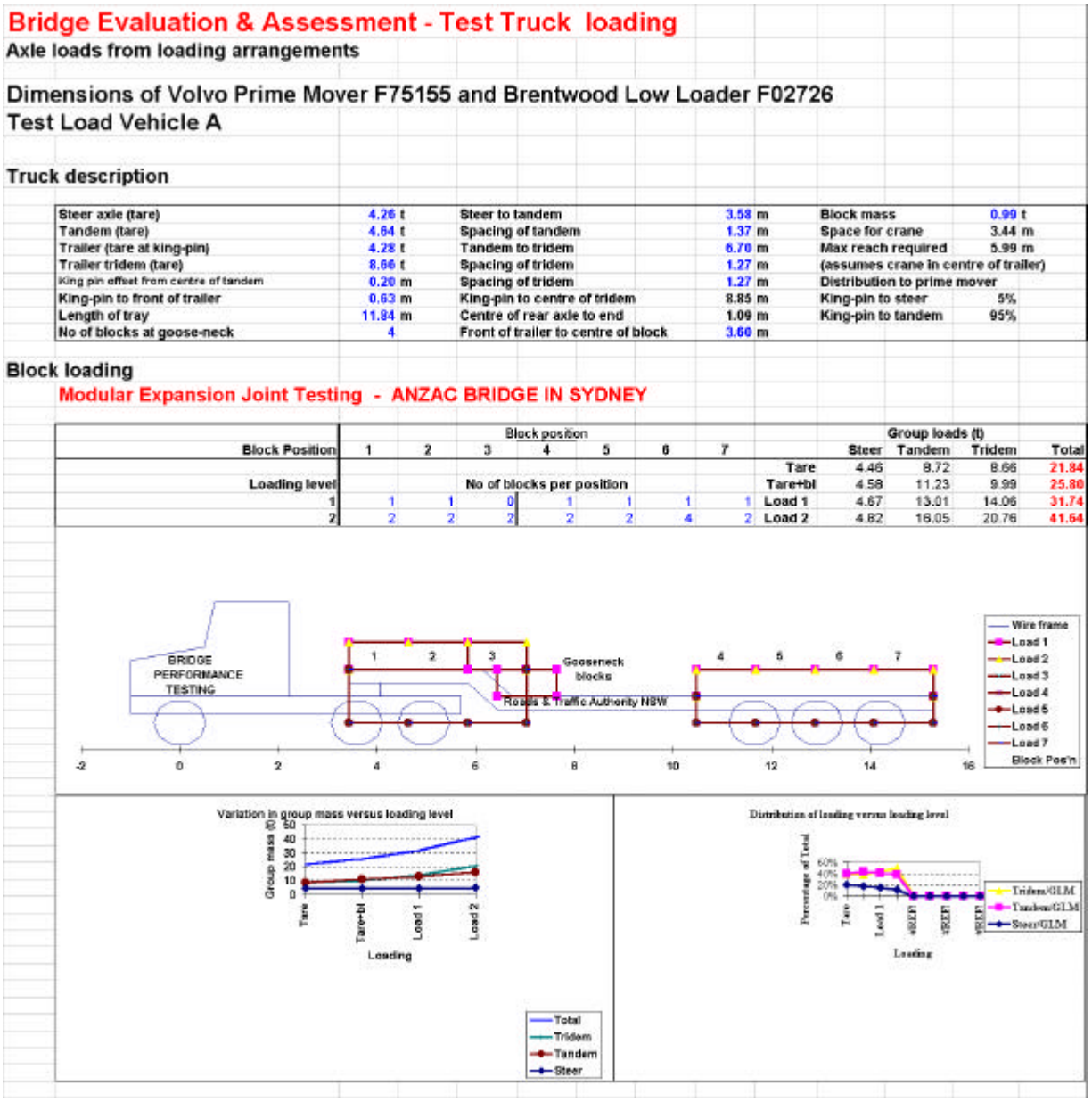

Figure 6: Test Truck Load Profile used in Dynamic Testing at Anzac & Taree

Figure 6 shows the test vehicle loading arrangement used for both series of tests. The test truck was loaded to the maximum legal axle load for Australia and had a gross vehicle mass (GVM) of 42 tonnes.

Figures 7 & 8 present a schematic elevation diagram of each modular expansion joint in relation to the nominal kerbside lane position and nominal test truck wheel positions. In order to approximate true static strains and displacements, the truck was tr aversed over the joints at less than 3 -km/hr producing negligible dynamic response of the truck or structure. All static and dynamic strains and displacements were recorded during this test.

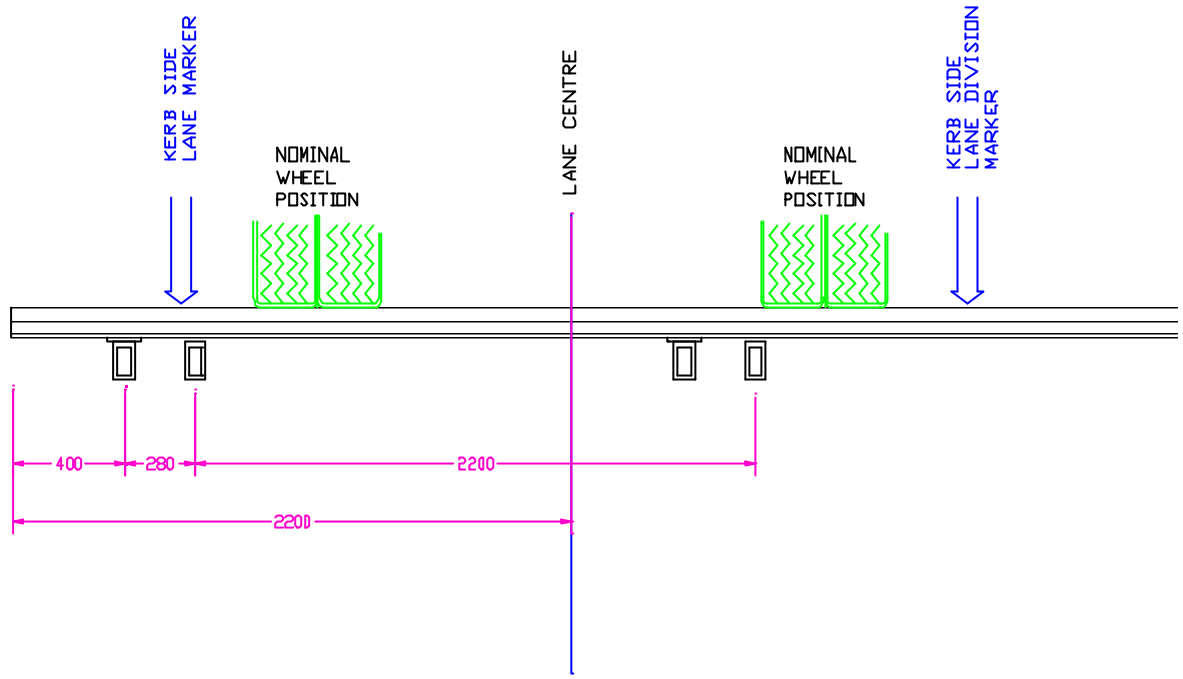

Figure 7: Elevation of MBEJ and Nominal Test Truck Position (Anzac)

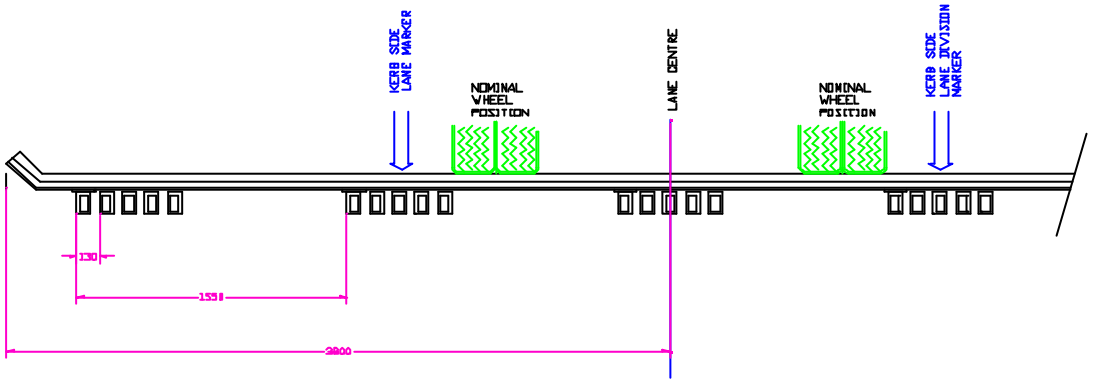

Figure 8: Elevation of MBEJ and Nominal Test Truck Position (Taree)

Following as closely as possible to the same line as the slow roll test, the truck was traversed at several speeds in the target speed range of 45 -km/hr to 70 -km/hr (Anzac) and 39 -km/hr to 105-km/hr (Taree) with the actual truck pass -by speeds measured using a radar speed gun. The reproducible accuracy of the vehicle speed measurement is considered to be at least ± 2-km/hr.

Table 1 presents the target pass-by speeds as well as the measured (actual) pass -by speeds.

Table 1 Target & Actual Test Truck Pass-by Speeds

Run Number	Anzac		Taree	
	Target	Actual	Target	Actual
1	40 km/hr	47 km/hr	39 km/hr	39 km/hr
2	50 km/hr	50km/hr	57km/hr	57 km/hr
3	60 km/hr	53 km/hr	73 km/hr	70 km/hr
4	60 km/hr	61 km/hr	78 km/hr	82 km/hr
5	65 km/hr	63 km/hr	97 km/hr	98 km/hr
6	70 km/hr	68 km/hr	105 km/hr	104 km/hr

Further analysis included the extraction of the maximum and min imum strain and displacements resulting from the passage of the six individual test truck axles. These data were used to calculate dynamic amplification factors for each strain and displacement signal.

The positive dynamic amplification factor was calcul ated as follows:

$$\textbf{Dynamic Amplification Factor (Positive)} = \frac{\text{Max. Dynamic Strain (same sense as static strain)}}{\text{Maximum Static Strain}}$$

The negative dynamic amplification factor was calculated as follows:

$$\textbf{Dynamic Amplification Factor (Negative)} = \frac{\text{Max. Dynamic Strain (opposite sense to static strain)}}{\text{Minimum Static Strain}}$$

The total dynamic amplificatio n factor was calculated as follows:

$$\textbf{Dynamic Amplification Factor (Total)} = \frac{\text{Max.+ve Dynamic Strain - Max.-ve Dynamic Strain}}{\text{Maximum Static Strain}}$$

5 STRAIN MEASUREMENT RESULTS

Tables 2 & 3 present summaries of the resulting maximum strains, stresses and dynamic amplification factors for each bridge test.

Table 2: Summary of Resulting Strains, Stresses and Dynamic Amplification Factors (Anzac)

Test Truck Pass-by Speed	Transducer Location	Strain and Stress								
		Strain (με)			Stress (MPa)			Dynamic Amplification Factors		
		Max Tensile	Max Compressive	Peak to Peak	Max Tensile	Max Compressive	Peak to Peak	Max Tensile	Max Compressive	Peak to Peak
Slow Roll	Support Bar	100	-1	101	20	0	20	0.0	0.0	0.0
	Centre Beam	154	-101	153	31	-20	31	0.0	0.0	0.0
47 km/hr	Support Bar	185	-30	215	37	-6	43	1.8	-0.4	2.2
	Centre Beam	167	-157	179	33	-31	36	1.9	-0.4	2.1
50 km/hr	Support Bar	226	-66	293	45	-13	59	2.3	-0.9	3.2
	Centre Beam	203	-113	234	41	-23	47	1.5	-0.3	1.8
53 km/hr	Support Bar	213	-54	268	43	-11	54	2.1	-0.6	2.7
	Centre Beam	136	-132	165	27	-26	33	2.0	-0.5	2.5
61 km/hr	Support Bar	270	-116	386	54	-23	77	2.7	-1.7	4.5
	Centre Beam	233	-141	308	47	-28	62	2.1	-0.6	2.6
63 km/hr	Support Bar	256	-114	370	51	-23	74	2.7	-1.9	4.6
	Centre Beam	225	-148	307	45	-30	61	1.9	-0.7	2.5
68 km/hr	Support Bar	218	-104	311	44	-21	62	2.4	-1.5	3.9
	Centre Beam	215	-137	280	43	-27	56	1.6	-0.7	2.2
Maximum	All	270	-157	386	54	-31	77	2.7	-1.9	4.6

Table 3: Summary of Resulting Strains, Stresses and Dynamic Amplification Factors (Taree)

Test Truck Pass-by Speed	Transducer Location	Strain and Stress								
		Strain (με)			Stress (MPa)			Dynamic Amplification Factors		
		Max Tensile	Max Compressive	Peak to Peak	Max Tensile	Max Compressive	Peak to Peak	Max Tensile	Max Compressive	Peak to Peak
Slow Roll	Support Bar	85	0	85	17	0	17	0.0	0.0	0.0
	Centre Beam	161	0	161	32	0	32	0.0	0.0	0.0
39 km/hr	Support Bar	97	-10	104	19	-2	21	1.5	-0.3	1.8
	Centre Beam	183	-9	192	37	-2	38	1.3	-0.1	1.4
57 km/hr	Support Bar	121	-21	139	24	-4	28	1.7	-0.3	1.9
	Centre Beam	185	-23	199	37	-5	40	1.3	-0.3	1.6
70 km/hr	Support Bar	133	-25	153	27	-5	31	1.9	-0.5	2.3
	Centre Beam	186	-33	202	37	-7	40	1.3	-0.5	2.1
80 km/hr	Support Bar	151	-43	177	30	-9	35	2.2	-0.6	2.6
	Centre Beam	203	-45	239	41	-9	48	1.8	-0.6	2.5
98 km/hr	Support Bar	177	-49	226	35	-10	45	2.3	-0.8	3.1
	Centre Beam	233	-56	265	47	-11	53	1.6	-0.7	2.7
104 km/hr	Support Bar	165	-54	219	33	-11	44	2.3	-0.9	3.1
	Centre Beam	219	-46	255	44	-9	51	1.6	-0.6	2.6
Maximum	All	233	-56	265	47	-11	53	2.3	-0.9	3.1

The following amplification factors are deduced from this investigation:

- The maximum beam stress total dynamic amplification factors measured were 4.6 (Anzac) and 3.1 (Taree).
- The maximum beam stress positive dynamic amplification factors were 2.7 (Anzac) and 2.3 (Taree).
- The maximum beam stress negative dynamic amplification factor s were 1.9 (Anzac) and 0.9 (Taree).

These dynamic amplification factors are clearly well in excess of existing bridge codes. From a fatigue analysis perspective, the dynamic response of a structure may lead to higher than expected strain levels due to dy namic amplification.

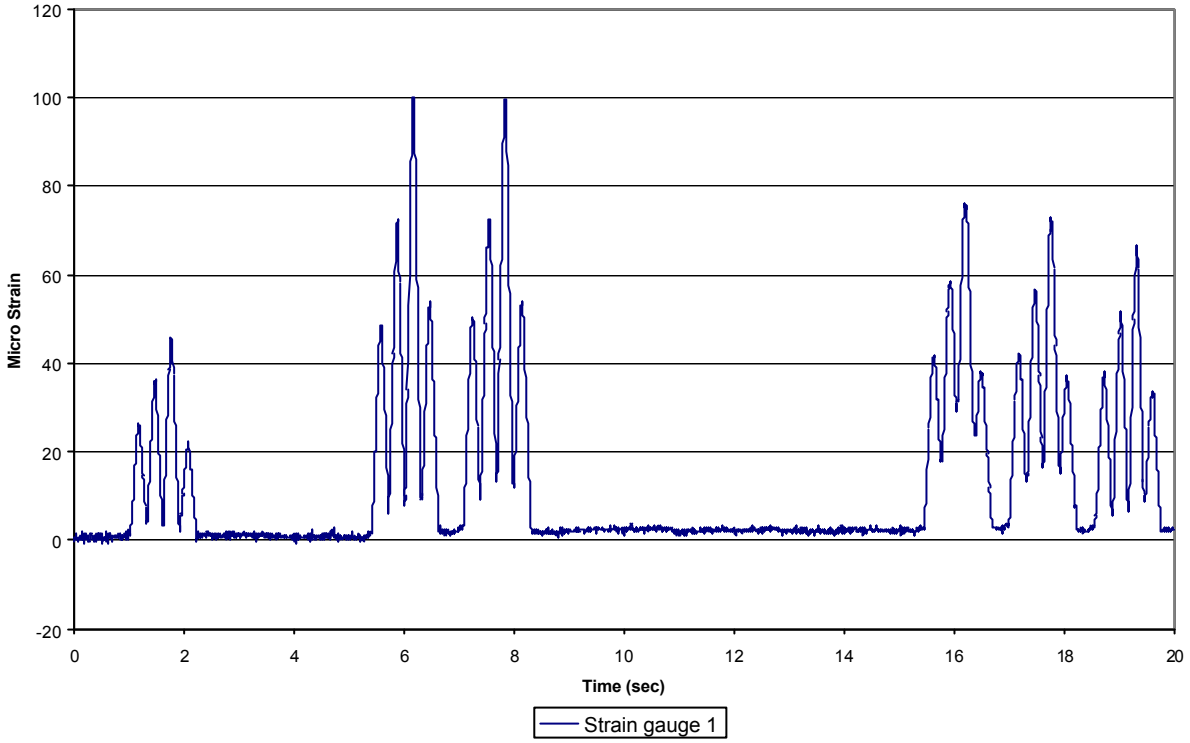

Figure 9: Quasi-static response due to test vehicle pass-by (Anzac)

Figure 9 shows the quasi-static response of a strain gauge (SG1) located in the middle of an Anzac support bar and the impact of each of the test vehicle's six axles with each of the centre beams connected to this support bar is clearly evident.

The dynamic behaviour of the Anzac Bridge MBEJ may be considered as two independent structures (i.e. one structure with one set of odd numbered centre beams with associated support bars, and a second structure with one set of even numbered centre beams and support bars). The coupled nature of the "*odd*" and "*even*" structures is further demonstrated in **Figure 10**.

The dynamic response here is demonstrated by the impact of the tandem axles of the prime mover and the tri-axles of the trailer where the vibration is in phase and virtually continuous. An independent centre beam structure responding to a single impulse would, of course, be expected to display an initial maximum amplitude followed by an exponential decay.

The build-up in centre beam response may be attributed to the phase relationship of each wheel to centre beam impact. This phenomenon is described as coupled centre beam resonance [Ancich *et al* (8)].

A simple comparison between **Figures 9 & 10** shows that the quasi-static slow roll produced 100 με (Peak-Peak) and the 61-km/hr pass-by produced 386 με (Peak-Peak). This comparison indicates a dynamic amplification factor (DAF) of, at least, 3.86 times static.

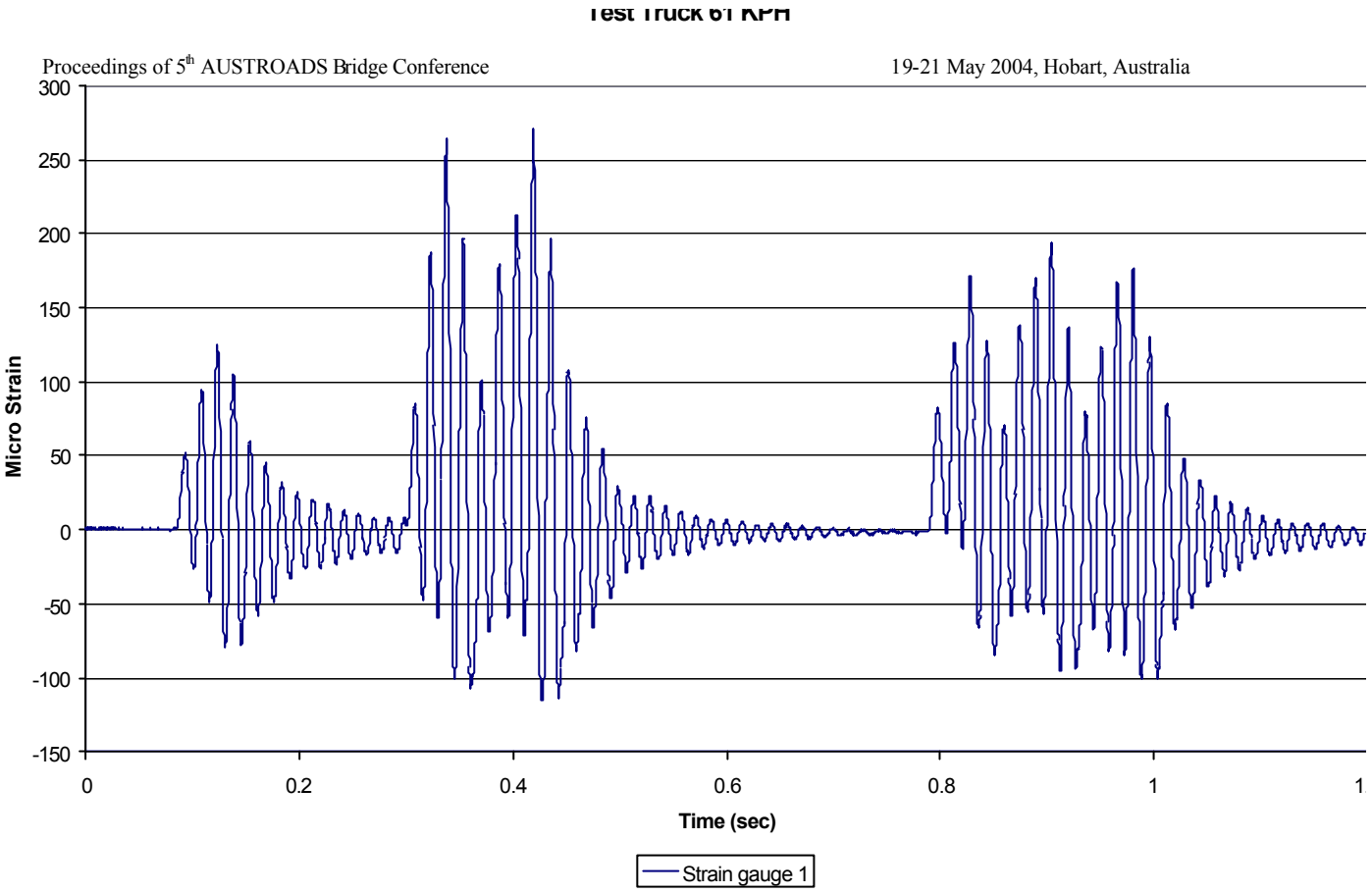

Figure 10: Dynamic response induced by heavy vehicle pass-by (Anzac)

Furthermore, not only are the peak dynamic strains at least 3.86 times the quasi-static but further observation of **Figure 10** shows that the steer and tandem axles of the prime mover produced at least 16 cycles of vibration (per vehicle passage) where the dynamic strain equalled or exceeded the quasi-static strain of 100 με (Peak-Peak).

Similarly, the tri-axle group of the trailer produced at least 14 cycles of vibration (per vehicle passage) where the dynamic strain equalled or exceeded the quasi-static strain of 100 με (Peak-Peak). The simple addition of these events shows that each heavy vehicle passage, of the load configuration of the test vehicle, produced around 30 vibration cycles where the dynamic strain equalled or exceeded the quasi-static strain of 100 με (Peak-Peak).

6 CONCLUSION

Structural dynamics studies were performed on a single support bar design MBEJ installed in the western abutment of Anzac Bridge and a multiple support bar design MBEJ installed into the southern abutment of the southbound carriageway of the bridge over the south channel of the Manning River (Taree By-pass). The studies showed that for these joints:

- The response of MBEJ's, responsible for peak strains, is predominantly dynamic.
- Depending on the components of construction, configuration and loading, MBEJ's may exhibit a non-linear dynamic response.
- The DAF cannot be adequately prescribed in a Code-of-Practice.
- Notionally in-phase or partially in-phase excitation is common. Notionally out-of-phase excitation is less common.

- The DAF for single support bar design MBEJ's (and variants thereof) is damping dependent and has a lower limit of 2.5 and an upper limit exceeding 5.
- The DAF for multiple support b ar design MBEJ's is also damping dependent (but to a lesser extent) and has a lower limit of 2 and an upper limit exceeding 3.
- However, for any joint (both single & multiple support bar designs) the DAF achieved in service will depend on a number of factor s including, joint configuration, number of exciting axles and the extent to which the manufacturer is able to incorporate damping into the design.
- Dynamic Finite Element Models must be used in design. The calibration must be to real loads operating at speeds that will give rise to notionally in -phase excitation.
- Steel components should be designed for infinite fatigue cycles.
- It is easier to estimate the extreme values of dynamic load response than to estimate the weighted mean value of dynamic load respo nse. Hence, design should be done using extreme values coupled with CAFL properties of steel.

The widely held assumption of quasi -static behaviour for single and multiple support bar design MBEJ's (and variants thereof) is not sustainable and both bridge designers and modular joint suppliers must think in terms of a fully dynamic system.

ACKNOWLEDGEMENT

The authors wish to thank the Chief Executive of the Roads and Traffic Authority of NSW (RTA) for permission to publish this paper. The opinions and c onclusions expressed in this paper do not necessarily reflect the views of the RTA.

REFERENCES

1. DEXTER R.J., CONNOR R.J. & KACZINSKI M.R.: "Fatigue Design of Modular Bri dge Expansion Joints ", *NCHRP Report 402,* Transportation Research Board, National Research Council, 1997, 128 pp.
2. TSCHEMMERNEGG F.: " Messung von Vertikal - und Horizontallasten beim Anfahren, Bremsen und Überrollen von Fahrzeugen auf einem Fahrbahnübergäng (Measurement of Vertical and Horizontal Loads due to Accelerating, Braking, and Rolling Vehicles on an Expansion Joint)", *Der Bauingenieur*, 48, Heft 9, Springer -Verlag, 1973, pp 326 -330 (In German).
3. TSCHEMMERNEGG F.: " The Design of Modular Expansion Joints ". *Proc. 3rd World Congress on Joint Sealing and Bearing Systems for Concret e Structures* , American Concrete Institute, 1991, pp 67-86.
4. ANCICH E.J. & BROWN S.C.: "Modular Bridge Joints – Reduction of noise emissions by use of Helmholtz Absorber". *Proc. 5th AUSTROADS Bridge Conference*, May, 2004.
5. ANCICH E.J., CHIRGWIN G.J. & BROWN S.C.: "Dynamic Anomalies in a Modular Bridge Expansion Joint", *J. Bridge Engrg*., ASCE, (Submitted), 2004.
6. OSTERMANN M. (1991): "Beanspruchung von elastisch gelagerten Fahrbahnübergängen unter Radstoßeinwirkung (Stresses in elastically supported mod ular expansion joints under wheel load impact)", *Bauingenieur*, 66, Springer-Verlag, 1991, pp 381-389 (In German).
7. ROEDER C.W.: "Fatigue Cracking in Modular Expansion Joints", *Research Report WA - RD 306.1*, Washington State Transportation Commission, 1993, 53 pp.

8. KÖSTER W. (1986): " The Principle of Elasticity for Expansion Joints ", *Proc. 2nd World Congress on Joint Sealing and Bearing Systems for Concrete Structures* , ACI SP -94, American Concrete Institute, 1986, pp 675-711.

Appendix F

Ancich E.J. and Bhavnagri V. (2006). Fatigue Comparison of Modular Bridge Expansion Joints Using Multiple Bridge Design Code Approaches, *Proc. 6th World Congress on Joints, Bearings, and Seismic Systems for Concrete Structures*, Halifax, Nova Scotia, Canada.

6th World Congress

on Joints, Bearings, and Seismic Systems for Concrete Structures

September 17-21, 2006 – Halifax, Nova Scotia, Canada

FATIGUE COMPARISON OF MODULAR BRIDGE EXPANSION JOINTS USING MULTIPLE BRIDGE DESIGN CODE APPROACHES

Eric J. Ancich and Viraf Bhavnagri

Engineering Technology Branch, Roads & Traffic Authority of NSW, PO Box 3035, Parramatta NSW 2124 Australia.

BIOGRAPHY

Eric Ancich is a Senior Project Engineer with the Roads & Traffic Authority (RTA) of NSW (Australia). He has over 20 years experience in acoustics, vibration and structural dynamics. For the last six years he has directed the structural dynamics studies of six RTA road bridges to determine the mechanism causing environmental noise emissions and the premature fatigue induced failure of modular expansion joints.

Viraf Bhavnagri is a Contract Project Engineer who has been working in the Bridge Specification and Rehabilitation Unit of the Roads and Traffic Authority of NSW (RTA) since March 2002. Prior to that he has worked for 20 years in a number of consulting engineering firms on the design of road and rail bridges in Australia.

ABSTRACT

Modular bridge expansion joints (MBEJ's) are considered to be the most modern design of waterproof bridge expansion joint currently available; nevertheless, there have been endemic occurrences of structural fatigue failures of MBEJ's throughout the world. Whilst there was an accepted belief amongst academic researchers from around 1973 that a significant part of the load history of the MBEJ was dynamic, international bridge design codes continued to base the design requirements around quasi-static principles without fully embracing the highly dynamic response of the MBEJ to transient traffic loading until 2004.

Similarly, it would appear that almost all MBEJ designers use a static or quasi-static design with little consideration of the dynamic behavior, either in the analysis or the detailing. Work done in the RTA over the past six years work has identified a major defect in the quasi-static load case assumption used universally in bridge design codes. The defect has now been recognized in Australian Standard AS5100:2004[1] and the RTA has recently produced a specification (RTA QA Specification B316)[2] for modular expansion joints, which includes a number of design requirements based on dynamic analysis for these joints. Subsequent to the installation of MBEJ's designed in accordance with this specification in bridges on the Karuah Bypass, the RTA conducted an experimental study of the dynamic response of the joint to the passage of a truck at different speeds. The results showed that the dynamic amplification factor (DAF) specified in RTA B316 was in good agreement with measured values.

The RTA also made a comparative study of the design of the MBEJ in accordance with design codes of different countries that had tendered for the design. Calculations showed that there are quite significant differences in the results obtained in accordance with different codes, based on the DAF and other requirements prescribed by these specifications. Most international codes also leave a number of factors un-specified; hence, tendered designs cannot be evaluated on a uniform basis. RTA B316 has incorporated several design requirements to eliminate this lacuna.

Keywords: Bridges; expansion joints; fatigue; vibration; structural dynamics; AASTHO; Austrian Code; German Code

1.0 INTRODUCTION

The Roads and Traffic Authority of NSW (RTA) designs and maintains a number of bridges in the State of New South Wales in Australia. During recent work on the rehabilitation or new installations of MBEJ's on some of their bridges, the design and construction requirements for these joints have been reviewed and a specification has been developed for the design, production, and installation of these joints. The Australian Bridge Design Code[1] (AS 5100:2004) has also recently been revised and some clauses on design of modular expansion joints have been added. The strength, serviceability and fatigue limit state requirements of the design have to conform to this code. For the installation of modular expansion joints on two of RTA's bridges recently, tenders were received from a number of international manufacturers. This opportunity was taken to review the designs of the joints done in accordance with the codes of the respective countries and a comparative study of the code requirements was made, while formulating the RTA B316 specification[2]. However, as different international specifications prescribe different design loads, dynamic amplification factors, wheel load distribution factors, acceptance criteria for fatigue stresses, etc, the end results of these variables acting in combination are not directly evident. For the comparative study, one of the above-mentioned modular joints was chosen as a typical example for analysis in accordance with the requirements of the international specifications of each of the tendered designs and the end results were compared by means of the following two ratios:

(a) The fatigue stress ratio, $f^*_f / (\phi_f f_{lim})$, which compares the fatigue design stress with the limit state stress, and

(b) The strength ratio, $f^*_u / (\phi_u f_y)$, which compares the ultimate design stress with the yield strength.

If either ratio is greater than 1.0, the component is inadequate. A small ratio indicates that the member size is adequate in accordance with the specification for which it is designed. However, if the member size is reduced and/or the specification under estimates the true load or dynamic response of the structure, then this would probably result in eventual fatigue failure.

The typical example is analysed in accordance with the following documents:

1. RTA QA Specification B316 (December, 2004) / AS 5100.4
2. AASHTO LRFD, 2004[4]
3. Austrian Guideline RVS 15.45[5]
4. German Specification TL/TP-FÜ 92[6]

Calculations are based on the versions that were current in 2004. The American specifications are based on the work done by Dexter *et al*[3] and were subsequently incorporated into AASHTO LRFD[4].

2 DESIGN REQUIREMENTS

The structure selected for the analysis is a single support bar system shown in Figure 1. The support bars are placed on elastomeric bearings for which the spring stiffness values were given by the supplier. For the comparative study the center beams are analyzed as continuous beams on rigid supports, in accordance with the recommendations of AASHTO. Subsequently it was decided to investigate the effect of elastic supports on the bending moments in the center beams. The difference in bending moments due to elastic supports and rigid supports was found to be quite significant. This is discussed further in the Section 4 of this paper. The axle load is placed in the most adverse position for each effect. A minimum distance from the curb is specified but other lane markings are ignored.

As the wheel contact area is generally large enough to load three center beams, the combined stiffness of three center beams is considered.

The joint is analyzed in accordance with the four above-mentioned specifications. Salient items of these specifications are summarized in Table 1 in a consistent format.

The important issues are as follows:

(a) The axle load (W_x) is applied in accordance with the appropriate specifications. Results are factored by a dynamic amplification factor (DAF) (χ); hence the dynamic design axle load is given by

$$W^*_x = \chi W_x \quad (1)$$

For the strength limit state, W_x is factored by γ_u and for the fatigue limit state, by γ_f.

(b) In RTA B316 it is recognised that the dynamic effects on modular joints result in upward as well downward amplification; hence both values are defined separately and it is specified that

$$\chi_{dn} = 0.67\chi \quad \text{and} \quad \chi_{up} = 0.33\chi \quad (2)$$

For strength design, only χ_{dn} is considered whereas for fatigue design χ is considered.

A major requirement of RTA B316 is that the DAF be based on a dynamic analysis. Three options are specified:

(i) Use the simplified design method in accordance with AASHTO[4], with $\chi = 2.0$ for multiple support bar systems and $\chi = 2.5$ for single support bar systems.

(ii) Perform an experimental modal analysis to determine χ.

(iii) Perform a dynamic analysis using a three-dimensional finite element model, previously calibrated by experimental modal analysis and strain gauge data for a similar MBEJ, to compute χ_{up} and χ_{dn} .

Therefore a quasi-static analysis is not ruled out but the penalty is a higher value of DAF.

(c) The axle load applied to one center beam is given by

$$W_{1x} = \beta W_x \quad (3)$$

where β is termed "The Distribution Factor".

In RTA B316, β is given by

$$\beta = (B_c + g_c)/L_w \quad (4)$$

with notation as defined in the Appendix. The justification for this formula is presented in Item 3.2.3.

(d) The longitudinal load due to acceleration or braking is specified as a fraction (η) of the axle load. AASHTO specifies a value of $\eta = 0.2$ in general, based on measurements made by Dexter *et al*[3], with appropriate modifications for steeper gradients, and/or unusual braking situations. AS5100 specifies a rather conservative value of 0.35 for all situations and RTA B316 has to comply with that requirement. However, observations have shown that dynamic effects in the horizontal direction are effectively damped and the vertical and horizontal peak effects do not always occur simultaneously. Therefore, whereas in the other specifications the dynamic longitudinal load due to tractive forces must be taken equal to $\eta\chi W_{x.,}$ in RTA B316 it is specified as only $\eta W_{x.}$ for fatigue analysis and $\eta\chi_{dn}W_{x.,}$ for strength design.

(e) The fatigue stress range limit (f_{lim}) is specified by Codes for certain standard types of connections. Several types of welded connections in MBEJs cannot be readily classified into these standard types. The welded connection between center beams and support bars in multiple support bar systems has been treated in detail in AASHTO LRFD and the type of cracking to which the welds are susceptible has been categorised

as Types A, B and C cracking. Other Codes have not dealt with this subject. To avoid ambiguities in the interpretation of Code recommendations of unclassified details by different designers, the values of f_{lim} have been specified in RTA B316 for different types of welded connections provided in MBEJs, as shown in Table 2. Comparison has also been attempted with the AASHTO recommendations in Table 2. The comparison is not straightforward, as the approach to fatigue design is slightly different in AASHTO and AS5100. The AASHTO LRFD detail categories are based on the "fatigue threshold limit" (f_{TH}); for infinite cycles of the design load, it is recommended that $f_{lim}= f_{TH}/2$. In accordance with AS 5100 for infinite cycles of the design load, it is specified that $f_{lim}= f_{5,}$ the stress at the cut-off limit. Moreover, the stress range-load cycle curves are not identical in the two documents and f_{TH} in AASHTO does not occur at the same number of stress cycles for all categories. Meaningful comparison is only possible at stresses corresponding to 2×10^6 stress cycles (f_2), beyond which the curves diverge. This stress is termed the Detail Category Number in AS 5100.

(f) The span of the support bar varies with the joint opening and it is accepted that the joint openings for the limit states of strength, serviceability, and fatigue should be different. In AS 5100 the temperature movements are calculated for the serviceability limit state, based on specified extreme temperature ranges. For the ultimate limit state, these values have to be factored by 1.25. Movements due to creep and shrinkage also have to be appropriately factored. For the limit state of fatigue, the recommendation by Dexter *et al*[3] is to take the fatigue joint opening as the average of the maximum and minimum values. In the German and Austrian specifications the opening is left undefined. In RTA B316 the concept of the root-mean-cubed value for the fatigue design joint opening is introduced and the joint opening for the fatigue limit state is given by

$$J_f = \sqrt[3]{\left(J_{s,\min}^3 + J_{s,\max}^3\right)} \qquad (5)$$

where $J_{s,max}$ and $J_{s,min}$ are the maximum and minimum joint openings for the serviceability limit state.

This recommendation is based on the logic that fatigue damage varies as the 3rd to 5th power of the stress and stress varies linearly with the span for a concentrated load. Hence the root-mean-cubed value should give a better approximation than the arithmetic mean. Note that in accordance with Equation 2, the distribution factor also varies with the joint opening.

All the above requirements have been interpreted for the three international specifications and expressed in the same format as RTA B316, for ready comparison, in Table 1.

3 EXAMPLE

3.1 Data

A modular joint comprising a single support bar system with five center beams was recently installed on the twin bridges over Mooney Mooney Creek and was analyzed for the comparative study. Details of the joint are shown in Figure 1. Data used for the analyses is summarised in Table 3. The parameters that vary when applying the provisions of the different specifications are listed and compared in Table 4.

3.2 Results

Results for each member of the modular joint and critical connections are summarized in Table 5. The stress ratios and strength ratios are the highest in almost all cases for design in accordance with the RTA B316 specification and the lowest for the AASHTO specification. This indicates that the RTA specification is the most demanding whereas if member sizes are reduced to bring stress ratios closer to unity and the assumptions on which the factors are based are not met, there is risk of fatigue failure. Comments on some of the items follow.

3.2.1 Axle loads

The AASHTO specification uses not only a reduced axle load for fatigue but further factors it down for fatigue stress calculations. However, values cannot be compared directly because the limiting criteria for fatigue are also different. The axle loads in the German specification[6] are based on DIN1072[7]. For bridge Class 60/30, a heavy lorry (SLW) with 3 axles of 200 kN each is specified. The factors applicable to this axle load in accordance with DIN 1072 and TL/TP-FÜ, are given in Table 1. The stress range limit is $0.8f_3$, which is much higher than f_5. In the Austrian guideline[5] the stress range limit is f_5, like the Australian standard, but the axle load is slightly less. Measurements of axle loads on Australian roads[8] indicates a consistent trend of increasing axle loads with time and a reasonably conservative value should be used to comply with projected increases over a 100 year service life. The fatigue stress ratio $f^*_f/\phi f_{lim}$ enables comparison of the overall effect of the axle load, DAF and stress range limit for the example in Table 5 and shows that RTA B316 is the most demanding and the Austrian specification is a close second.

3.2.2 Dynamic Amplification

For the Mooney Mooney Creek Bridge MBEJ, the successful tenderer submitted a dynamic finite element analysis giving a value of $\chi = 2.5$, which was accepted as it was equivalent to the default DAF value.

3.2.3 Distribution Factor

The axle load (W_x) acts on more than one center beam and the maximum load carried by one center beam is βW_x. Dexter *et al*[3] have assessed β by means of measurements on four bridges (refer Table 6) and compared measured values with values calculated by Tschemmernegg's method and their proposed method, which is incorporated in AASHTO. The values of β recommended by AASHTO are based only on the top width of the centerbeams. Values recommended by Tschemmernegg are presented as a set of curves

based on the width of the centerbeams as well as the gaps. Equation 4 is based on the simplified assumption that the tyre pressure is uniform and the tyre spans as a beam across the gap between the centerbeams. The wheel load per unit length of tyre contact area is W/L_w and the load applied to a center beam is therefore $(B_c+g_c)W/L_w$. It is reasonable to expect that although the bending stiffness of a tyre tread is negligible, its resistance to shear deformation will enable it to span across a small gap. None of the three methods appear to give fully satisfactory results for all four of the bridges tested, as apparent from Table 6. However, inclusion of B_c as well as g_c in the formula for β allows the designer to introduce more center beams to carry the load if the center beam section is found to be inadequate, whereas this is not possible with the AASHTO recommendation. Equation 4 is much more easily incorporated into a spreadsheet than Tschemmernegg's non-linear graphs, hence it is preferred. In any case, upper and lower bounds are prescribed for β (0.8 and 0.5 respectively) in RTA B316, in accordance with AASHTO, hence excessive discrepancies between the recommendations are avoided.

In the German specification a constant value of 0.6 is specified and the Austrian specification refers to Tschemmernegg's recommendations.

3.2.4 Yoke

The method of designing the yoke and connections is specified in AASHTO and has been followed for this example. There are no requirements in the German and Austrian specifications.

3.2.5 Connections

The method of designing welded connections of center beam to support bars in multiple support bar systems is specified in detail in AASHTO and has been adopted in RTA B316.

For this MBEJ, the yoke provides a sliding connection between the center beam and the support bar. Slider plates are welded to the support bars and the welds should be carefully

prepared and fatigue stresses checked. Center beams are kept at equidistant spacing by some type of spring-buffer system. There may be cleats welded to the center beams to connect the buffers and the welding degrades the fatigue resistance of the center beam. The force transmission system in the buffers should be considered and additional stresses due to these forces combined with the flexural stress in the center beam. These aspects are not dealt with in any of the specifications other than RTA B316. Results in Table 2 indicate that some of the welded connection details as originally proposed did not satisfy fatigue stress range limitations and had to be modified. Another critical item is the strength of the top plate of the box housing the support bar bearings, which is directly subjected to wheel load with very limited concrete cover above it. None of the specifications draw attention to this item.

4 TESTING

An MBEJ similar to the one in the example was tested to measure the dynamic response to a loaded truck run at different speeds over the joint. Details of the joint are identical to those shown in Figures 1a and 1c and only the spans of the center beams are slightly different, as shown in Figure 2. The joint was installed in a 594 meter long concrete box girder bridge forming part of the as then unopened Karuah Bypass on the Pacific Highway linking the state capitals of Sydney and Brisbane.

4.1 Experimental Modal Analysis

An experimental modal analysis study[9,10] (EMA) was undertaken to gain a better understanding of the structural dynamics behavior of the Karuah River MBEJ. The EMA measurement defines the natural frequencies and mode shapes of a structure and allows an estimate of the energy involved in each mode.

These measurements involved the simultaneous measurement of the input force and the vibration response. In the Karuah River Bridge tests[11], force over the frequency range of interest was imparted to the structure using a force hammer. The vibration response was measured at selected locations using accelerometers attached to the structure by a magnetic base. The input force and vibration response at each location were measured simultaneously using the two-channel Fast Fourier Transform (FFT) analyzer. Frequency Response Functions (FRF's) for each measurement were stored on the hard disk drive of a personal computer. This study identified eight natural modes with frequencies ranging from 44 Hz to 183 Hz. The vibrational modes identified include a translational (bounce/bending) mode where all parts of the MBEJ are vibrating in phase at the same frequency. Roeder[12] reports theoretical translational modes and Ostermann[13] shows an analytically determined (FEM) vertical mode at 87 Hz that exhibits elements of the whole body (bounce/bending) mode. Table 7 presents a summary of the experimentally determined frequency and associated damping for each natural mode identified in the EMA. Figure 2 shows a sample plot depicting the characteristic shape of Mode 1 at 44 Hz. Mode 1 was characterized by in-phase displacement of all structural beams. This translational mode is best described as fundamental bounce of the MBEJ on the linear bearing pads. Significant translation and bending of the center beams and support bars is also evident up to Mode 5 at 133 Hz. The first true vertical bending mode occurs at 149 Hz (Mode 6).

4.2 Dynamic Strain Gage Measurements

The modal analysis data were used to optimize the placement of strain gages as part of the fatigue life assessment of the Karuah MBEJ[14]. Figure 4 presents a plan view diagram of the southbound curbside lane of Karuah River Bridge and shows the six strain gauge locations (SG1 to SG6). All gauges were of a linear type and orientated in the anticipated principal stress direction (i.e. parallel to the long axis of the respective structural members).

The measurement instrumentation was selected with a data sampling rate of 25 kHz. This was sufficient to ensure that frequencies up to 10 kHz were sampled accurately. The test truck was loaded to the maximum legal axle load for Australia and had a gross vehicle mass (GVM) of 42 tonnes (92,400 lbs). Figure 5 presents a schematic elevation diagram of the modular expansion joint in relation to the nominal curbside lane position and the nominal test truck wheel positions. In order to approximate true static strains and displacements, the truck was traversed over the joints at less than 3 km/hr thereby producing negligible dynamic response of the truck or structure. All static and dynamic strains and displacements were recorded during this test. Following as closely as possible to the same line as the slow roll test, the truck was traversed at several speeds in the target speed range of 45 km/hr to 70 km/hr with the actual truck pass-by speeds measured using a Laser speed gun. The reproducible accuracy of the vehicle speed measurement is considered to be better than ± 2 km/hr. As the position of the test vehicle on the joint was critical for the reliability and reproducibility of the test results, a procedure was developed using a bead of water dispersible paste (standard toothpaste) on the top surface of the first center beam to mark the vehicle passage. Figure 6 shows a typical application. Table 8 presents the target pass-by speeds as well as the measured (actual) pass-by speeds.

The results of strain gage testing are shown a Table 9. It is interesting to note that the peak DAF shown in Table 9 is 3.2. For this table, the DAF is defined as follows:

$$\text{DAF} = \frac{\varepsilon_{\text{dyn}}}{\varepsilon_{stat}} \qquad (3)$$

where

DAF = dynamic amplification factor

ε_{dyn} = Strain range due to the vehicle traveling at designated speed (peak-to-peak)

ε_{stat} = Strain range due to vehicle traveling at crawl (slow roll) speed (zero-to-peak).

It is noted that a DAF of this magnitude is significantly higher than any current design code requirement, except B316[2]. It is recommended that designers should use 80% of the peak empirical DAF. For the Karuah By-pass MBEJ, this would equate to a design DAF of 2.56. The design calculations for this joint used a DAF of 2.5.

4.3 Static Analysis

As dynamic amplification factors are applied to the static analysis, validating the static analysis beam model is important. The slow roll test results for Runs 1, 2 and 3 enable comparison of test results with static analysis. An average value of 3.0 m is adopted in the analysis for the measured distance of the wheel from the curb, which varies from 2.9 m to 3.1 m (Table 8). The modeled beam represents the combined stiffness of 3 center beams and the distribution factor was estimated from gap measurements to be 0.37. Figure 3 shows the continuous beam model and truck loading.

Computed stresses at mid spans are correlated with stresses calculated from strains measured by gauges SG1 at support and SG6 at mid span (Figure 5) assuming E = 200 GPa. Results are shown in Table 10. Due to the short spans involved, the bending moment gradients are steep and discrepancies in the locations of the strain gauge and the computed stress location could account for the inaccuracies in the results. Computations were carried out for rigid as well as elastic supports. The spring support stiffness of 49 MN/m results in a maximum support deflection of only 0.5 mm but the elastic deflection of supports causes very significant changes in the longitudinal variation of stresses in the center beams. This aspect has not received adequate attention in any of the specifications. The worked examples by Dexter *et al*[3] are based on analysis of continuous beams on rigid supports. Comparison of the limited results in Table 10 indicates that the analysis based on elastic supports gives better agreement with the measured values. The current load test was primarily aimed at assessing dynamic effects and this aspect needs to be given more attention in future tests.

CONCLUSION

The Roads and Traffic Authority NSW has recently formulated a specification (RTA B316) for design of modular bridge expansion joints (MBEJs). In this paper the specification has been compared with three other specifications-AASHTO LRFD, the German and Austrian specifications. Detailed requirements of these specifications have been interpreted and concisely presented, item by item, in Table 1 in consistent format and notation, for ready comparison. Salient features and differences have been discussed in Section 2. Limiting stress ranges for details critical in fatigue have been specified and compared with AASHTO recommendations.

RTA B316 requires that the dynamic amplification factors used for design be based on dynamic analysis, which has been formerly validated by test measurements on another similar joint. Measurements carried out by the RTA over the past few years have consistently found that the DAF's prescribed by most codes are frequently exceeded. Calculations required by RTA B316 are more complex than those illustrated in the design examples presented by Dexter *et al*[3] but with modern electronic computing facilities, this does not present any problem. Using the most appropriate model for each effect is the primary consideration. Where the support bars rest on compressible bearings, analysis of the center beam as a continuous beam on elastic supports gives substantially different results from the assumption of rigid supports. Different joint openings for the three limit states of serviceability, fatigue and ultimate strength are considered in the analysis. Attention must be given to all connection details as these can often be more critical for fatigue than the main members.

In RTA B316 the limiting stress ranges for connections of slider plates, yoke members, cleats for buffers provided for maintaining equidistant spacing of center beams, etc, have been

specified. Strength of the top plate of the support box housing, which is directly subjected to wheel loads, is another critical item. Design of an MBEJ provided for the twin bridges over Mooney Mooney Creek has been carried out in accordance with the four specifications and results compared with the help of a stress ratio equal to the ratio of the computed stress to the stress at the corresponding limit state. Ratios exceeding 1.0 indicate that the member or detail is inadequate. However, an unduly small ratio for any item resulting from one specification compared to another may indicate a shortcoming in the specification rather than a license to reduce the member size. The RTA B316 specification demanded the most conservative design for the example of the joint at Mooney Mooney. The Austrian specification was next, whereas AASHTO was the least demanding.

A dynamic load test was conducted for an MBEJ installed for the Karuah By-pass, which is very similar to the one analyzed at Mooney Mooney. The test demonstrated the high values of DAF's obtained, which were close to those required by RTA B316 and substantially greater than those recommended by the other specifications. Although peak values of DAF's may be discounted (use 80%) for fatigue analysis, factoring down the axle load as well as the DAF for fatigue design may result in designs prone to fatigue failure. The cost of using larger section members is trivial compared to the cost of rehabilitating a failed MBEJ. The comparison between computed and measured stresses for the Karuah By-pass MBEJ (quasi-static analysis) indicated a very close level of agreement, particularly when center beams were modeled on elastic supports.

ACKNOWLEDGEMENT

The authors wish to thank the Chief Executive of the Roads and Traffic Authority of NSW (RTA) for permission to publish this paper. The opinions and conclusions expressed in this paper do not necessarily reflect the views of the RTA.

REFERENCES

1. Standards Australia, Australian Standard AS5100.4 – 2004, Bridge Design Part 4: Bearings and deck joints, Sydney, Australia, 2004.
2. Roads & Traffic Authority of NSW. *RTA QA Specification B316 – Modular Bridge Expansion Joints*. Sydney, Australia, 2004. (http://www.rta.nsw.gov.au/doingbusinesswithus/specifications/bridgeworks/)
3. Dexter R.J., Connor R.J. & Kaczinski M.R., "Fatigue Design of Modular Bridge Expansion Joints", *NCHRP Report 402,* Transportation Research Board, National Research Council, Washington, DC, USA, 1997, 128 pp.
4. American Association of State Highway and Transportation Officials (AASHTO) *AASHTO LRFD Bridge Design Specifications, SI Units*, 3rd Ed., Washington, DC, USA, 2004.
5. "Expansion Joints for Bridges", *Austrian Guideline RVS 15.45*, Draft, version 1, Vienna, Austria, 1999.
6. TL/TP-FÜ 92, "Technical delivery and inspection specifications for watertight expansion joints of road and foot bridges", Federal Ministry of Transport (BMV), Bonn, Germany, 1992. Non-revised translation (draft 1), provided by the German Association of Joint and Bearing Manufacturers [Vereinigung der Hersteller von Fahrbahnübergängen und (Brücken) Lagern].
7. DIN 1072 (1985) "Road and foot bridges; design loads", German Standards Institution.
8. Roberts W.S. and Heywood R.J., "Fatigue-It Will Change Our Culture", *Proc. 5th Austroads Bridge Conference*, Hobart, Tasmania, Australia, May 2004.
9. Ewins D.J., "Modal Testing: Theory, Practice & Application (2nd Edition)", *Research Studies Press*, Hertfordshire, UK, 1999, pp.163-276.

10. Ancich E.J., Brown S.C. & Chirgwin G.J., "The Role of Modular Bridge Expansion Joint Vibration in Environmental Noise Emissions and Joint Fatigue Failure", *Proc. Acoustics 2004 Conference*, Surfers Paradise, Qld., Australia, 2004, pp 135-140.

11. Brown S.C., "Modal Analysis Karuah Bypass Bridge Modular Expansion Joint", *Report 10-1788-R21*, Richard Heggie Associates Pty Ltd (now Heggies Australia Pty Ltd), Lane Cove, Australia, 2005 (Unpublished report prepared for the Roads & Traffic Authority of NSW).

12. Roeder C.W., "Fatigue Cracking in Modular Expansion Joints", *Research Report WA-RD 306.1,* Washington State Transportation Center, Seattle, WA, USA, 1993, 53 pp.

13. Ostermann M., "Beanspruchung von elastisch gelagerten Fahrbahnübergängen unter Radstoßeinwirkung (Stresses in elastically supported modular expansion joints under wheel load impact)", *Bauingenieur* 66, Springer-Verlag, 1991, pp 381-389 (In German).

14. Brown S.C., "Measurement of Static and Dynamic Strains: Karuah Bypass Bridge, Karuah NSW Modular Expansion Joint", *Report 10-1788-R20*, Richard Heggie Associates Pty Ltd (now Heggies Australia Pty Ltd), Lane Cove, Australia, 2005 (Unpublished report prepared for the Roads & Traffic Authority of NSW).

15. Ancich E.J. & Chirgwin G.J. "Fatigue Proofing of an In-service Modular Bridge Expansion Joint", *Proc. 6th World Congress on Joints, Bearings & Seismic Systems for Concrete Structures*, Halifax, Nova Scotia, Canada, 2006.

APPENDIX: NOTATION

a_x = width of axle, center to center of tyre footprint

d_{cs} = depth from road surface to mid-depth of support bar

f^* = computed stress for design load

f_3 = constant stress range fatigue limit

f_5 = stress at cut-off limit

f_{lim} = stress at limit state for fatigue

f_{TH} = fatigue threshold stress as per AASHTO LRFD

g_c = gap between center beams at appropriate joint opening

n_f = number of cycles to limit state for fatigue

B_s = width of support bar

B_c = width of center beam

B_w = width of tyre footprint in direction perpendicular to traffic

D_s = depth of support bar

D_c = depth of center beam

E = modulus of elasticity

H = Horizontal force due to acceleration or braking of vehicle

J = joint opening at top (clear gap between edge beams)

K_s = spring stiffness of each support in continuous beam model

L_b = span of support bar c/c bearings

L_w = length of tyre footprint in direction parallel to traffic

W_x = static axle load

W_{1x} = static axle load applied to one center beam

W^*_x = dynamic design axle load

α = dynamic load allowance (DLA) as a fraction of static load

β = distribution factor (fraction of wheel load carried by one center beam)

χ = dynamic amplification factor (DAF)

χ_{up} = upward component of DAF

χ_{dn} = downward component of DAF

χ_{mod} = DAF obtained by experimental modal analysis

η = ratio of horizontal load to vertical load

ϕ = capacity reduction factor

γ = load factor

σ = stress due to static loads

Subscripts:

avg = average

max = maximum

min = minimum

f = value for fatigue design

u = value for ultimate strength design

s = value at serviceability

Abbreviation

DAF dynamic amplification factor

MBEJ modular bridge expansion joint

RTA Roads and Traffic Authority NSW

Table 1 - Comparison of Requirements of Different Standards

ITEM	NOTA-TION	RTA B316	AASHTO LRFD	German TL/TP-FÜ	Austrian RVS 15.45
Axle load for strength design	W_{xu}	160 kN	111 kN (25 kips)	200 kN	280 kN
Axle load for fatigue design	W_{xf}	160 kN	71 kN (16 kips)	200 kN	130 kN
Load factor for strength design	γ_u	1.8	1.75	1.3	1.0
Load factor for fatigue design	γ_f	0.6	0.75	0.6	1.0
Fatigue stress range limit	f_{lim}	f_5	f_{TH} /2	f_3	f_5
Capacity factor for fatigue	ϕ_f	1	1	0.8	1
Axle width, c/c wheels [mm]	a_x	2000 mm	1830 mm (6'-0")		1600 ultimate 1800 fatigue
Length of tyre footprint [mm]	L_w	250 mm	variable	200	variable
Width of tyre footprint [mm]	B_w	400 mm	508 (20")	600	500 mm
Maximum span of centerbeam		1500 mm	1220 mm		
Maximum gap betw. C'beams		85 mm		max 70 min 5	
Joint opening for fatigue	J_f	Eq.2	$J_{s,avg}$	$[J_{s,max}]$	$[J_{s,max}]$
Distribution factor	β	$(B_c+g_c)/ L_w$	AASHTO Table 3.1	0.6	Tschem-merneg's
Dynamic Amplification Factor	χ_{up} χ_{dn} χ	$\chi_{up}=0.33\chi$ $\chi_{dn}=0.67\chi$ $\chi=0.67\chi_{mod}$	$\chi=1.75$	$\chi=1.4$	$\chi=1.4$
Longitudinal live load factor	η	0.35	0.2	0.25	0.3 ult 0.2 fatigue
Longitudinal axle loading		ηW_x	$\eta \chi W_x$	ηW_x	$\eta \chi W_x$
Yoke loading factor	ψ	0.3	0.3	[0.3]	[0.3]
Transverse force factor	τ			0.15 η	
Minimum anchorage		19 Ø @ 300		20 Ø @ 250	

NOTE: 1 kip = 4.448 kN 1 kip/in^2 = 6.894 MPa

[ ] value assumed for the Example as it is not available in the Standard.

Table 2 - Detail Classifications for Fatigue

Member or Connection	Detail	AS 5100			AASHTO / LRFD		
		Refer Illus-tration	Detail Category $f_{rn} = f_2$ @ 2×10^6 cycles	Cut off limit f_5 MPa	Cate-gory	f_2 (MPa) @ 2×10^6 cycles	Fatigue thresh-old f_{TH} (MPa)
C'beam or S'bar	Polished steel bar		180	73	A	165	165
Flats for yokes	Rolled products	(1)	160	65	A	130	165
C'beam at bolt hole for yoke	Bolted connection 8.8 / TF	(5)	140	57	D	70	48
Sliding plate welded to S'bar	Cover plate, full weld both sides	(9)	125	51	E	55	31
C'beam splice	Butt weld 100% NDT	(16)	112	45	B	110	110
C'beam to S'bar	Butt weld with extra fillets		90	36	C	90	69
Yoke to C'beam	Transverse butt weld		90	36	C	90	69
Connections of yoke members	Shear stress in FW	(39)	80	32	E	55	31
Sliding joint between C'beam and S'bar	Longitudinal weld of teflon disc housing to C'beam: • intermittent • continuous	 (14) (9)	 80 125	 32 51	 B' E	 103 55	 82 31
Attachment for spring buffer	Cleat attachments: • $t \le 12$ mm • $t > 12$ mm	 (35) (36)	 80 71	 32 29	C	90	69

Table 3 – Common Data for Joint in Example

ITEM	NOTATION	VALUE
Width of center beam	B_c	64 mm
Depth of center beam	D_c	152 mm
Width of support bar	B_s	125 mm
Depth of support bar	D_s	130 mm
Top to mid-depth of support bar	d_{cs}	240 mm
Span of support bar	L_b	(J + 100) mm
Maximum joint opening at serviceability	$J_{s,max}$	750 mm
Minimum joint opening at serviceability	$J_{s,min}$	458 mm
Maximum joint opening at ultimate	$J_{u,max}$	780 mm
Minimum joint opening at ultimate	$J_{u,min}$	420 mm
Average joint opening at serviceability	$J_{s,avg}$	604 mm
Ultimate strength of center beam & support bar	f_y	290 MPa
Spring stiffness of each center beam support	K_s	44 kN/mm

Table 4 – Parameters Computed/ Adopted for Alternative Designs

ITEM	NOTA-TION	Design by RTA B316	Design by AASHTO LRFD	Design by German Specs	Design by Austrian Specs
Joint opening for fatigue design	J_f	RMC = 637	$J_{s,avg}$ = 605	$J_{s,max}$ = 750	$J_{s,max}$ = 750
Distribution factor for fatigue	β_f	0.5	0.50	0.60	0.50
Distribution factor for strength	β_u	0.564	0.50	0.60	0.53
DAF adopted for fatigue design	χ_{up} χ	χ_{up}=0.825 χ=2.5	χ_{up}=0 χ=1.75	χ_{up}=0 χ=1.4	χ_{up}=0 χ=1.4
DAF adopted for strength design	$\chi_u=\chi_{dn}$	1.675	1.75	1.4	1.4

Table 5 – Results for Example of Modular Joint in Figure 1

ELEMENT	ITEM	NOTA-TION	Design by RTA B316	Design by AASHTO LRFD	Design by German Specs	Design by Austrian Specs
Centerbeam	Maximum stress due to fatigue	f^*_f	70	29	58	66
	Limiting stress due to fatigue	ϕf_{lim}	73	83	106	73
	Fatigue stress ratio	$f^*_f / \phi f_{lim}$	**0.96**	**0.35**	**0.55**	**0.90**
	Ultimate stress	f^*_u	184	105	107	125
	Strength ratio	$f^*_u / \phi f_y$	**0.70**	**0.40**	**0.41**	**0.48**
Support Bar	Maximum stress due to fatigue	f^*_f	39	16	33	36
	Limiting stress due to fatigue	ϕf_{lim}	73	83	106	73
	Stress ratio	$f^*_f / \phi f_{lim}$	**0.53**	**0.19**	**0.31**	**0.49**
	Ultimate stress	f^*_u	67	46	52	55
	Strength ratio	$f^*_u / \phi f_y$	**0.26**	**0.18**	**0.20**	**0.21**
Weld	Longitudinal weld of PTFE disc housing to center beam	$f^*_f / \phi f_{lim}$	**1.33**	0.40	0.65	**1.04**
Yoke	Stress range in vertical yoke members	$f^*_f / \phi f_{lim}$	0.19	0.07	0.09	0.11
	Lap joints in yoke members	$f^*_f / \phi f_{lim}$	0.58	0.44	0.31	0.37
	Welding of yoke vertical to center beam	$f^*_f / \phi f_{lim}$	**1.23**	0.48	0.60	0.94
Weld	Attachments for control spring buffers	$f^*_f / \phi f_{lim}$	**1.39**	0.47	0.68	**1.02**

Table 6 – Comparison of NCHRP-Measured and Computed Distribution Factors

MBEJ Location	Center beam width B_c mm	Gap width g_c mm	Measured static DF	Computed Distribution Factor, β		
				$(B_c+g_c)/L_w$ with L_w=250	Tschemmer-negg Method	AASHTO
Charter Oak Bridge	57	51.1	**0.37**	0.43	0.49	0.50
Lacey V. Murrow Bridge	114	38.3	**0.69**	0.61	0.62	0.77
I-90/5 HOV Bridge	64	35	**0.34**	0.40	0.37	0.50
I-70/I-25 Flyover Ramp	80	32	**0.51**	0.45	0.48	0.60

Table 7 - Summary of Natural Modes and Damping

Mode Number	Center Frequency Hz	Damping %
1	44	13
2	75	10
3	92	9
4	119	3
5	133	9
6	149	3
7	168	4
8	183	3

Table 8 Target and Actual Test Truck Pass-by Speeds

Run Number	Target Speed, km/hr	Actual Speed, km/hr	Measured Distance From Curb To Nearest Wheel (m)
1	Slow Roll 1	-	3.1
2	Slow Roll 2	-	2.9
3	Slow Roll 3	-	2.97
3	26	26	3.1
4	30	29	3.0
5	41	41	3.1
6	52	51	3.1
7	69	69	3.03
8	83	82	3.01
9	90	88	3.03
10	90	89	3.06
11	95	92	3.03
12	95	93	3.06
13	103	104	2.99

Table 9 Summary of Resulting Strains, Stresses and Dynamic Amplification Factors for SG5 – Center Beam (After Brown[14])

Test Truck Passby Speed	Transducer Location	Strain and Stress								
		Strain (micro strain)			Stress (MPa)			Dynamic Amplification Factors		
		Max Tensile	Max Compressive	Peak to Peak	Max Tensile	Max Compressive	Peak to Peak	Max Tensile	Max Compressive	Peak to Peak
Slow Roll-1	SG5	55	-2	57	11	0	11			
Slow Roll-2	SG5	58	0	58	12	0	12			
Slow Roll-3	SG5	56	0	56	11	0	11			
26 kph	SG5	46	-2	44	9	0	9	0.8	-0.1	0.9
29 kph	SG5	47	-2	47	9	0	9	0.9	-0.1	1.0
41 kph	SG5	67	-5	69	13	-1	14	1.2	-0.2	1.3
51 kph	SG5	74	-6	80	15	-1	16	1.4	-0.3	1.5
69 kph	SG5	94	-7	100	19	-1	20	1.7	-0.3	1.8
80 kph	SG5	112	-20	133	22	-4	27	2.1	-0.4	2.4
82 kph	SG5	112	-26	139	22	-5	28	2.1	-0.5	2.5
88 kph	SG5	119	-30	149	24	-6	30	2.2	-0.6	2.7
89 kph	SG5	124	-29	153	25	-6	31	2.2	-0.5	2.7
92 kph	SG5	116	-34	148	23	-7	30	2.0	-0.6	2.6
93 kph	SG5	75	-9	80	15	-2	16	1.4	-0.3	1.5
104 kph	SG5	133	-45	179	27	-9	36	2.4	-0.8	3.2
Maximum	**SG5**	**133**	**-45**	**179**	**27**	**-9**	**36**	**2.4**	**-0.8**	**3.2**

Table 10 - Comparison of Measured and Computed Static Load Stresses

MEMBER	SUPPORTS MODELLED AS	ITEM	STRESS (MPa)			
			RUN 1	RUN 2	RUN 3	AVERAGE
Center beam (Strain gauge SG1 at support)	Elastic	Computed	13.5			
		Measured	16.0	18.0	18.0	17.3
		Difference	-15.4%	-24.8%	-24.8%	-21.7%
	Rigid	Computed	9.3			
		Measured	16.0	18.0	18.0	17.3
		Difference	-42.1%	-48.5%	-48.5%	-46.4%
Center beam (Strain gauge SG6 at mid span 5)	Elastic	Computed	9.5			
		Measured	9.6	10.0	11.2	10.3
		Difference	-0.6%	-4.5%	-14.8%	-6.6%
	Rigid	Computed	4.6			
		Measured	9.6	10.1	11.2	10.3
		Difference	-52.1%	-54%	-58.9%	-55%
Support Bar	No effect	Computed	15.5			
		Measured	16.0	18.0	18.0	17.3
		Difference	-3.1%	-13.8%	-13.8%	-10.4%

NOTE: % Difference = (Computed – Measured)/(Measured value) × 100

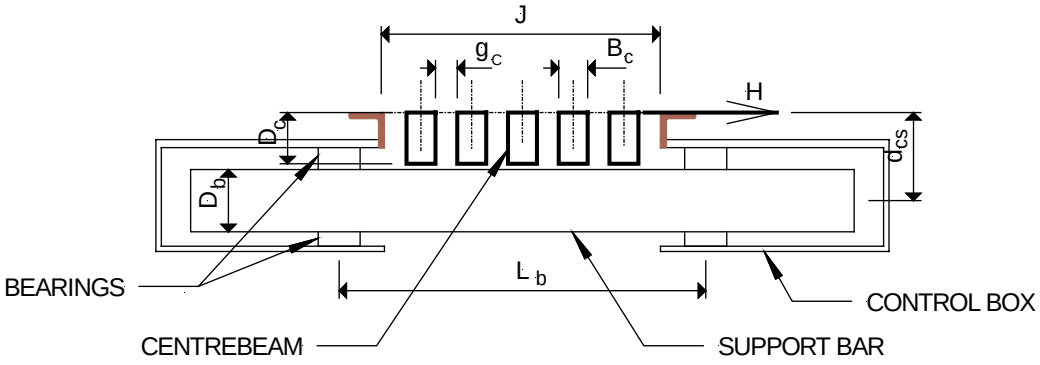

(a) CROSS SECTION THROUGH JOINT

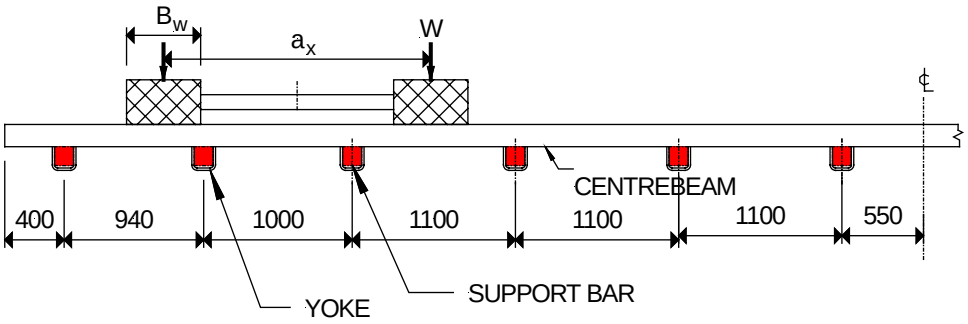

(b) SPANS AND LOADING OF CENTREBEAM

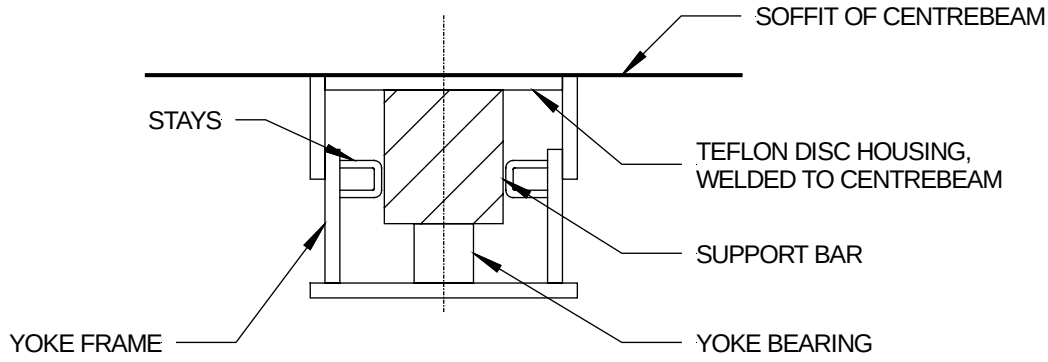

(c) YOKE DETAIL

Figure 1 Modular Joint Example Used for Comparing the Specifications

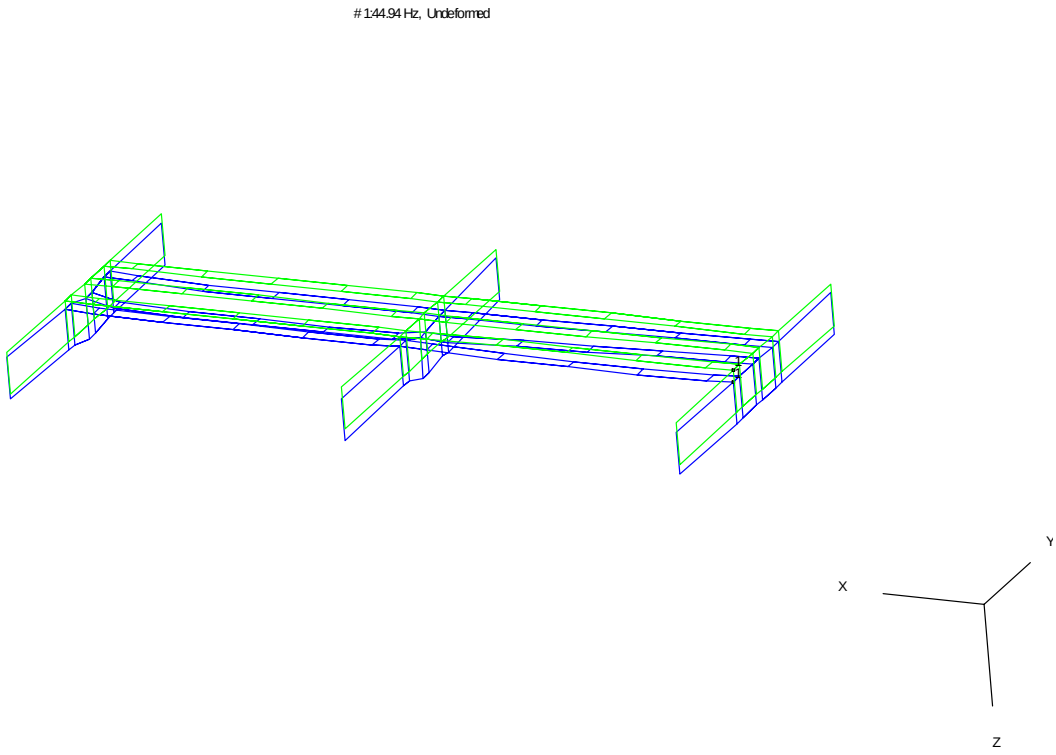

Figure 2 Experimental Mode 1 @ 44 Hz

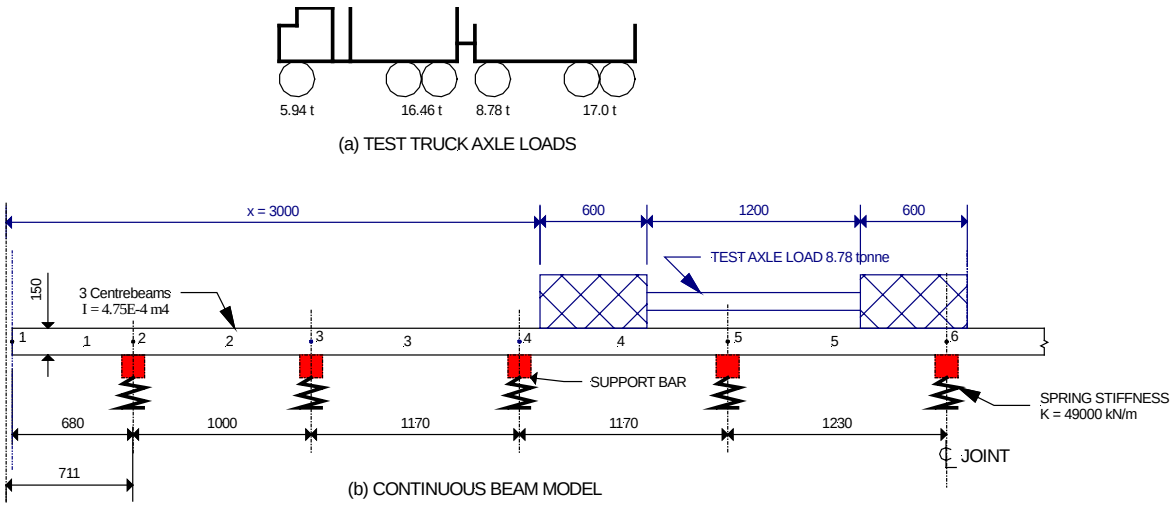

Figure 3 Center beam and Truck Used for the Load Test

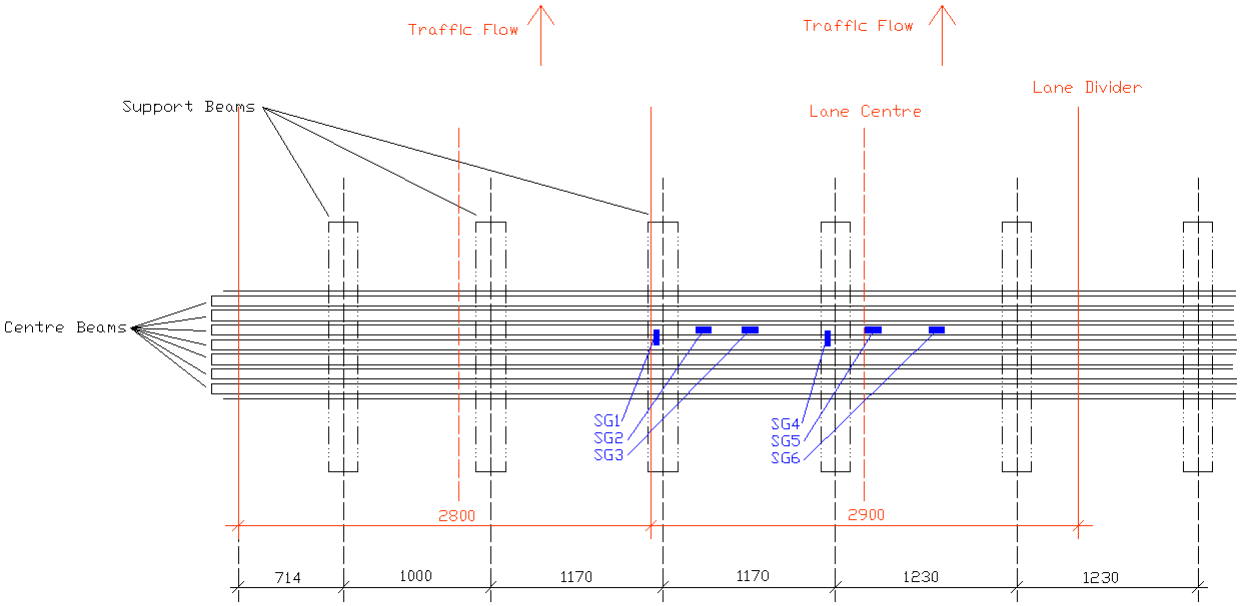

Figure 4 Plan View Southbound Curbside Lane - Six Strain Gage Locations (SG1 to SG6)

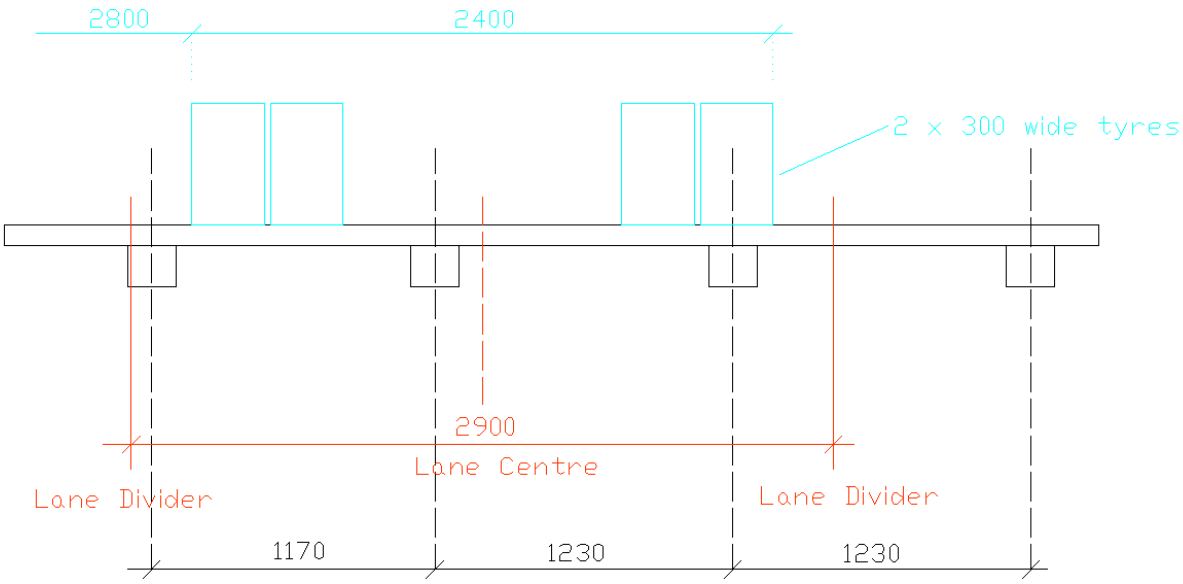

Figure 5 Elevation of Modular Expansion Joint and Nominal Test Truck Position

Figure 6 Tracking Check Paste

Figure 7 Photograph - Test Truck

Appendix G

Ancich E.J. and Chirgwin G.J. (2006). Fatigue Proofing of an In-service Modular Bridge Expansion Joint, *Proc. 6th World Congress on Joints, Bearings, and Seismic Systems for Concrete Structures*, Halifax, Nova Scotia, Canada.

6th World Congress

on Joints, Bearings, and Seismic Systems for Concrete Structures

September 17-21, 2006 – Halifax, Nova Scotia, Canada

Fatigue Proofing of an In-service Modular Bridge Expansion Joint

Eric J. Ancich and Gordon J. Chirgwin

BIOGRAPHY

Eric Ancich is a Senior Project Engineer with the Roads & Traffic Authority (RTA) of NSW (Australia). He has over 20 years experience in acoustics, vibration, and structural dynamics. For the last six years he has managed the structural dynamics studies of six RTA road bridges to determine the mechanism causing environmental noise emissions and the premature fatigue induced failure of modular expansion joints. It is considered that this work has identified a major defect in the quasi-static load case assumption used universally in bridge design codes.

Gordon Chirgwin is the Manager Bridge Policy, Standards and Records with the Road and Traffic Authority of NSW (Australia). He holds a Masters Degree in Engineering Science and has over thirty years experience encompassing all facets of professional engineering in roads and bridges, including twelve years in his current role. He represents the Authority in a number of forums. He has managed research into a number of facets of bridge engineering, and has authored over thirty technical papers.

ABSTRACT

In an almost universal approach to the design of the modular bridge expansion joint (MBEJ), the various national bridge design codes do not envisage that the embedded joint may be lightly damped and could vibrate as a result of traffic excitation. These codes consider only an amplification of the static load to cover sub-optimal installation impact, poor road approach, and the dynamic component of load. The codes do not consider the possibility of free vibration after the passage of a vehicle axle. Codes also ignore the possibilities of vibration transmission and response reinforcement through either following axles or loading

of subsequent components by a single axle. Dynamic strain gauge measurements were made on a 9-seal MBEJ installed in Sydney's Anzac Bridge using a 42t GVM test vehicle. At some speeds it was found that each vehicle passage produced around 30 vibration cycles where the peak-to-peak strain equalled or exceeded the quasi-static strain of 100 με and that the dynamic strain maxima were 4-5 times greater than the quasi-static strain.

A series of trials were conducted using a range of prototype support bar bearings and compression springs before a design was selected for installation. Post-installation measurements confirmed stress reductions such that the fatigue damage that would have occurred in any pre-modification year would now take well over 50 years to occur.

Keywords: Bridges; expansion joints; fatigue; vibration; structural dynamics; dynamic strain

INTRODUCTION

Whilst the use of expansion joints is common practice in bridge construction, modular bridge expansion joints (MBEJs) are designed to accommodate large longitudinal expansion and contraction movements of bridge superstructures. In addition to supporting wheel loads, a properly designed modular joint will prevent rainwater and road debris from entering into the underlying superstructure and substructure. Modular bridge expansion joints are generally described as single or multiple support bar designs. In the single support bar design, the support bar (beam parallel to the direction of traffic) supports all the center beams (beams transverse to the direction of traffic). In the multiple support bar design, multiple support bars individually support each center beam. Figure 1 shows a typical single support bar design MBEJ similar to the one installed in Sydney's Anzac Bridge. In Figure 1, the term '*Blockout'* refers to the recess provided in the bridge superstructure to allow casting-in of an expansion joint. The MBEJ installed into the western abutment of Anzac Bridge consists of two interleaved single support bar structures that behave, in a dynamic sense, as independent

structures. Previous experimental modal analysis studies[1] demonstrated only very light, almost negligible coupling between the two structures.

Sydney's Anzac Bridge was opened to traffic on 4th December 1995. The name Anzac is an acronym derived from Australian and New Zealand Army Corps and it was by this name that Australian troops participating in the First World War were known.

Anzac Bridge is a cable-stayed bridge spanning a portion of Sydney Harbor on the western approach to the central business district and is of reinforced concrete construction carrying 8 lanes of traffic and a combined pedestrian/bicycle way. The 805 meter long concrete structure comprises six spans with three cable-stayed central spans. With a main span of 345 meters, the bridge is the longest span cable-stayed bridge in Australia. There are two MBEJ's installed into Anzac Bridge, a small 3-seal joint in the deck (Pier 1) and a larger 9-seal joint located in the western abutment. The fatigue proofing studies reported here relate to this latter joint. Anzac Bridge currently carries 130,000 vehicles each day including some 800 commuter bus journeys carrying approximately 25,000 passengers. By 2011, when the joint would probably otherwise have been due for major repair or replacement, daily traffic volumes are predicted to have risen to 170,000. Should this joint fail and require total replacement, the direct cost to the RTA is conservatively estimated at $AU5 million. There are also large community costs associated with the full replacement of this joint, such as traffic disruption, increased travel times, increased pollution, etc. Community savings by avoiding replacement are estimated at a further $AU10 million. The RTA currently has over 25 MBEJs in its inventory. The cost of replacing the RTA's inventory of MBEJs following premature fatigue failure is estimated at $AU50 million. The lessons learnt have been incorporated into new projects to ensure that the problem of fatigue failure of modular bridge expansion joints has been eliminated effectively.

FATIGUE FAILURE

In an almost universal approach to the design of modular bridge expansion joints, the various national bridge design codes do not envisage that the embedded joint may be lightly damped and could vibrate as a result of traffic excitation. These codes consider only an amplification of the static load to cover sub-optimal installation impact, poor road approach, and the dynamic component of load. The codes do not consider the possibility of free vibration after the passage of a vehicle axle.

Codes also ignore the possibilities of vibration transmission and response reinforcement through either following axles or loading of subsequent components by a single axle. The possibility of premature fatigue failure in MBEJ's was identified by Dexter *et al*[2]. Observations of fatigue cracking in the MBEJ's at Pheasant's Nest Bridge (opened December 1980) on the Hume Highway and on the Mooney Mooney Creek Bridge (opened December 1986) on the Sydney-Newcastle (F3) Freeway confirmed the U.S. study. The MBEJ's installed into both bridges are multiple support bar designs and are essentially identical, having been supplied by the same European manufacturer. Figure 2 shows the typical locations for fatigue cracks in multiple support bar designs. Type A, B, & C[2] cracks were observed at Pheasant's Nest and many developed into complete member failure. At Mooney Mooney, only Type B cracks were observed of which some developed into complete member failure. Several weld repair exercises were attempted at both bridges but these proved to be only stopgap solutions as fatigue cracks continued to develop. The Pheasant's Nest joints were replaced in 2003 and the Mooney Mooney joints were replaced in 2004/5.

STRUCTURAL DYNAMICS STUDIES

(a) Experimental Modal Analysis

During the first few years of operation of Anzac Bridge, the fractured remains of a number of the lower anti-friction bearings from the MBEJ were observed on the floor of the western abutment void space. The lower anti-friction bearings supplied with the joint were not elastomeric but rather a two-piece '*cup & cone*' design machined from polyoxymethylene (POM)**.** The absence of these lower anti-friction bearings, which were discovered during a routine inspection, would cause bending moments in the supported center beams to be at least doubled due to the increased unsupported span. It was considered that the simple replacement of the failed components would not identify the failure mechanism or assist with a remaining fatigue life assessment. Clearly, an engineering investigation was necessary. There was little in the published literature to describe the structural dynamics behavior of MBEJ's. However, Ostermann[3] reported the theoretical and empirical dynamic response of a MBEJ and Roeder[4] reported the results of an analytical modal analysis study (FEM) of a swivel joist design MBEJ. Roeder noted that "*…the modes were closely spaced, and many hundreds (of modes) would be needed to include the predominate portion of the mass in three-dimensional vibration…"* However, this observation is considered to only apply to the swivel joist design.

Roeder[4] noted that the dynamic response of MBEJ's was complex and field measurements of the dynamic response would assist in evaluating the dynamic behavior. Accordingly, an experimental modal analysis study[5] (EMA) was undertaken to gain a better understanding of the structural dynamics behavior of the critical Anzac MBEJ. The EMA measurement defines the natural frequencies and mode shapes of a structure and allows an estimate of the energy involved in each mode. These measurements involve the simultaneous measurement of input force and vibration response. In the Anzac Bridge tests, force over the frequency range of interest was imparted to the structure using a force hammer.

The vibration response was measured at selected locations using accelerometers attached to the structure by a magnetic base. The input force and vibration response at each location were measured simultaneously using a two-channel Fast Fourier Transform (FFT) analyzer. Frequency Response Functions (FRF's) for each measurement were stored on the hard disk drive of a personal computer. This study identified the major natural modal frequencies (all lightly damped) and, importantly, provided an insight into the source of a previously unidentified dominant frequency at 71 Hz observed during an initial noise investigation[6]. The vibrational modes identified include a translational (bounce/bending) mode where all parts of the MBEJ are vibrating in phase at the same frequency, and vertical bending modes for the center beams where the first three bending modes are strongly excited. Reid & Ansourian[7] undertook FEM analysis of the Anzac Bridge MBEJ; their predicted modes are remarkably similar to the experimentally observed modes. The experimentally observed bounce/bending mode at 71 Hz actually appears to be two very closely spaced modes. The FEM Mode 1 at 71 Hz is predominantly bending with some translation whereas Mode 2 at 72 Hz is predominantly translation with some bending.

Roeder[4] reports theoretical translational modes and Ostermann[3] shows an analytically determined (FEM) vertical mode at 87 Hz that exhibits elements of the whole body (bounce/bending) mode. Table 1 presents a summary of frequency and associated damping for each natural mode identified in the EMA. Figure 3 shows a sample plot depicting the characteristic shape of Mode 1 at 71 Hz. Mode 1 was characterized by in-phase displacement of all structural beams. This translational mode is best described as fundamental bounce of the MBEJ on the linear bearing pads. Significant bending of the center beams and support bars is also evident. Mode 2 at 85 Hz was defined as the first vertical bending mode of center beams. Mode 3a at 91 Hz - 2nd bending mode of center beams. Mode 3b at 97 Hz - similar to Mode 3. Mode 4 at 119 Hz - 3rd bending mode of center beams. Mode 5 at 125 Hz - 4th bending mode of center beams.

It is particularly interesting to note that the translational mode and first bending modes of center beams are the predominant modes excited by typical traffic flow.

(b) Dynamic Strain Gage Measurements

The modal analysis data were used to optimize the placement of strain gages as part of the fatigue life assessment of the Anzac MBEJ. Figure 4 presents a plan view diagram of the eastbound curbside lane of Anzac Bridge and shows the six strain gauge locations (SG1 to SG6). All gauges were of a linear type and were orientated in the anticipated principal stress direction (i.e. parallel to the long axis of the respective structural members). The measurement instrumentation was selected with a data sampling rate of 25 kHz. This was sufficient to ensure that frequencies up to 10 kHz were sampled accurately. Figure 5 shows the test vehicle loading arrangement used for both series of tests. The test truck was loaded to the maximum legal axle load for Australia and had a gross vehicle mass (GVM) of 42 tonnes.

Figure 6 presents a schematic elevation diagram of the modular expansion joint in relation to the nominal curbside lane position and nominal test truck wheel positions. In order to approximate true static strains and displacements, the truck was traversed over the joints at less than 3-km/hr in order to induce negligible dynamic response of the truck or structure. All static and dynamic strains and displacements were recorded during this test. Following as closely as possible to the same line as the slow roll test, the truck was traversed at several speeds in the target speed range of 45-km/hr to 70-km/hr with the actual truck pass-by speeds measured using a radar speed gun. The reproducible accuracy of the vehicle speed measurement is considered to be better than ± 2-km/hr. As the position of the test vehicle on the joint was critical for the reliability and reproducibility of the test results, a procedure was developed using a bead of water dispersible paste (standard toothpaste) on the top surface of

the first center beam to mark the vehicle passage. Figure 7 shows a typical application. Table 2 presents the target pass-by speeds as well as the measured (actual) pass-by speeds.

Further analysis included the extraction of the maximum and minimum strain and displacements resulting from the passage of the six individual test truck axles. These data were used to calculate dynamic range factors for each strain and displacement signal. The dynamic range factor, which is discussed below, should not be confused with the live load factor often used to account for variability in the magnitude of the live load. It is also different from the dynamic amplification factor normally defined as

$$\text{DAF} = 1 + \left(\frac{\delta_{dyn} - \delta_{stat}}{\delta_{stat}} \right) \tag{1}$$

where

DAF = dynamic amplification factor,

δ_{dyn} = Maximum displacement due to the vehicle traveling at designated speed, and

δ_{stat} = Maximum displacement due to vehicle traveling at crawl (slow roll) speed.

It is also different from the dynamic load allowance used in Australian Codes[8], normally defined as

$$\text{DLA} = \left(\frac{\delta_{dyn} - \delta_{stat}}{\delta_{stat}} \right) = \text{DAF} - 1 \tag{2}$$

The dynamic load allowance is usually applied to anticipated static loads in an attempt to predict maximum dynamic loads due, in the case of MBEJ's, to additional acceleration of vehicle components as a vehicle traverses the MBEJ. It is understood that MBEJ designers typically use a dynamic amplification factor of about 1.7, which appears to be based on testing of multiple support bar systems. The measured dynamic range factor proposed here is

the peak-to-peak dynamic response divided by the quasi-static response. The dynamic range factor is defined as

$$\text{DRF} = \frac{\varepsilon_{\text{dyn}}}{\varepsilon_{stat}} \tag{3}$$

where

DRF = dynamic range factor,

ε_{dyn} = Strain range due to the vehicle traveling at designated speed (peak-to-peak), and

ε_{stat} = Strain range due to vehicle traveling at crawl (slow roll) speed (zero-to-peak).

The results demonstrate measured peak dynamic range factors of at least 3.0. It is important to note that this response factor of 3 would not apply to all vehicle pass-bys but selectively depending on vehicle speed, center beam spacing, and positions of natural MBEJ modes. It is important also to note that the apparent dynamic range factors reported here were at relatively low response amplitudes. The probable non-linear effects of the structural response have yet to be understood. Strain measurement of center beams and support bars under static and dynamic load cases is considered to be essential to quantify the dynamic range factors more accurately. Table 3 presents a summary of the resulting maximum strains, stresses and dynamic range factors for each test. The following amplification factors are deduced from this investigation:

- The maximum beam stress total dynamic range factors measured was 4.6.
- The maximum beam stress positive dynamic range factor was 2.7.
- The maximum beam stress negative dynamic range factor was 1.9.

In this context, “positive” is the direction of gravity and “negative” is the opposite or rebound direction.

These dynamic range factors are clearly well in excess of existing bridge codes. From a fatigue analysis perspective, the dynamic response of a structure may lead to higher than expected strain levels due to dynamic amplification.

Figure 8 shows the quasi-static response of a strain gauge (SG1) located in the middle of an Anzac support bar. The impact of each of the test vehicle's six axles with each of the centre beams connected to this support bar is clearly evident. The dynamic behavior of the Anzac Bridge MBEJ may be considered as two independent structures (i.e. one structure with one set of odd numbered centre beams with associated support bars, and a second structure with one set of even numbered centre beams and support bars). The coupled nature of the '*odd*' and '*even*' structures is further demonstrated in Figure 9. The dynamic response here is demonstrated by the impact of the steer and tandem axles of the prime mover (truck-tractor) and the tri-axles of the trailer where the vibration is in phase and virtually continuous. An independent center beam structure responding to a single impulse would, of course, be expected to display an initial maximum amplitude followed by an exponential decay. The build-up in center beam response is attributed to the phase relationship of each wheel to center beam impact. This phenomenon is described as coupled center beam resonance[1].

A simple comparison between Figures 8 & 9 shows that the quasi-static slow roll produced 100 με (Peak-Peak) and the 61-km/hr pass-by produced 386 με (Peak-Peak). This comparison indicates a dynamic range factor (DRF) of, at least, 3.86 times static. Furthermore, not only are the peak dynamic strains at least 3.86 times the quasi-static but further observation of Figure 9 shows that the steer and tandem axles of the prime mover (truck-tractor) produced at least 16 cycles of vibration (per vehicle passage) where the dynamic strain equalled or exceeded the quasi-static strain of 100 με (Peak-Peak). Similarly, the tri-axle group of the trailer produced at least 14 cycles of vibration (per vehicle passage) where the dynamic strain equalled or exceeded the quasi-static strain of 100 με (Peak-Peak).

The simple addition of these events shows that each passage of the test vehicle, produced around 30 vibration cycles where the dynamic strain equalled or exceeded the quasi-static strain of 100 με (Peak-Peak). Tables 3 and 4 show that for the OEM condition, center beam stresses of 62 MPa exceed the fatigue cut-off limit for all detail categories except 160 and 180 (Figure 13.6.1, Australian Bridge Design Code[8]). Inspection of the weld quality in the Anzac Bridge MBEJ had shown that whilst the welds were of '*general purpose*' standard and conformed to the tender specification, they were not now considered suitable for fatigue critical applications. The detailing of the yoke to center beam weld is not satisfactory and the execution is poor, with welds containing lack of penetration and lack of parent metal fusion. With these faults, the assessment of the detail category is somewhat subjective, with estimates ranging from 36 (present authors) to 71 (Reid & Ansourian[7]) of AS5100[8]. Were the detail category below 36, it may be inferred from Reid & Ansourian[7] that fatigue cracking would probably have commenced by 2003. Similarly, reference to Tables 3 and 4 shows that for the as-built condition, support bar stresses of 77 MPa exceed the fatigue cut-off limit for all detail categories.

DYNAMIC MODIFICATION

The reliability analysis of the as-built MBEJ was undertaken by Reid & Ansourian[7] and concluded that, without intervention, the as-built MBEJ would probably develop fatigue cracks approximately 13 years after the bridge was opened to traffic and that 8 of those fatigue years had already expired. As the critical MBEJ was cast into the western abutment of Anzac Bridge, there was no possibility of reducing the risk of premature fatigue failure either by decreasing the allowable loads, increasing the section properties of the structural steel members, or by reducing the unsupported spans. However, measurements of the structural dynamic properties of the joint indicated that the joint was lightly damped and this low level of damping was a major contribution to the measured dynamic range factor (DRF)

of 4.6. The challenge was, therefore, how to add significant levels of damping to an existing structure without major modification.

Modification of the structural dynamics of the joint by tuned mass dampers or damping coupled mass absorbers was investigated and a trial of damping coupled mass absorbers was undertaken. Whilst the trial demonstrated that reductions in working stress of up to 30% were possible, the cost was very high and future maintenance access would be seriously impeded by the absorbers. The damping coupled mass absorber trial confirmed that the provision of additional damping was a viable solution and that the most convenient and cost-effective locations for damping addition were the elastomeric bearings and springs installed at the ends of each support bar.

Observation of the operation of the joint suggested that bearing failure resulted from the support bar bouncing on the lower bearing after the top bearing was dislodged. The joint manufacturer had used a very high preload on the top bearing to resist dynamic lift-off but this high preload prevented the PTFE surface from sliding on its mating stainless steel surface. Temperature related movement of the bridge deck eventually dislodged the '*frozen*' top bearing. A decision was taken to produce test bearings softer than the originals with the bottom bearing having a static stiffness double that of the top. The net effect of this change was to decrease the preload and allow the prototype elastomeric bottom bearing to '*follow*' the support bar when it was rebounding. This decision may appear counter-intuitive to many involved in the specification or supply of MBEJ's.

An initial trial was undertaken using steel/rubber laminated elastomeric bearings/springs modeled on the original top bearing (spring) and replacing the original two-piece POM bearing with a dimensionally similar laminated elastomeric bearing. These prototypes were produced using natural rubber and tested identically to the original bearings using both experimental modal analysis and dynamic strain gage measurements. This trial demonstrated

that reductions in working stress of up to 30% were possible for support bars and up to 20% for center beams. In addition, it was immediately apparent from the EMA results that the modal damping had also increased.

Some thought was directed at methods of increasing the non-linearity of the bearings. Davidson[9] identified specialized synthetic polymer formulations offering very high levels of Elastic-Plastic Hysteresis Damping. As all damping converts kinetic energy to heat, temperature rise in operational bearings was a potential problem, particularly if the temperature reached caused pyrolysis of the synthetic polymer.

Two further trials were undertaken using the test prototype design but changing the elastomer to different formulations of synthetic high damping rubbers. One was medium damping to minimize heat build-up and the other full high damping. The EMA and dynamic strain gage measurements were repeated and Table 4 shows the comparative results obtained for the three prototypes and the original equipment manufacturer (OEM) bearings. Prototype #3 was clearly superior with around a 30% reduction in the peak-to-peak stress range for both center beams and support bars. The peak DRF was also reduced by around 30%. Prototype #3 used the full high damping synthetic polymer and the anticipated heat build-up did not occur. Comparison measurements between modified and un-modified bearings showed that temperature increase was minimal.

Public tenders were called for the manufacture and supply of production vulcanized bearings to match the static and dynamic properties of the hand-made prototypes and these were installed into the Anzac Bridge MBEJ in August 2004.

(a) Post Installation Studies

Pre-and post-installation strain gauge measurements were undertaken over separate, but comparable two-week periods using ambient traffic as the loading source. Table 4 shows the results of those measurements. However, for these measurements, the data sampling rate was

reduced to 2.5 kHz to conserve hard disk space. Nonetheless, the sampling rate was sufficient to record transients up to 1 kHz. Figures 10 & 11 show the probability of failure for the welded connection between the center beam and its yoke attachment to the support bar for the OEM condition and after fitting the Prototype #3 bearings. The results in Table 5 show that the installation of these bearings has resulted in a 30% reduction in stress for both center beams and support bars. In addition, there was the measured 98% reduction in stress events exceeding 15 MPa (the fatigue cut-off limit for the lowest detail category). The installation of high damping support bar bearings into the Anzac Bridge MBEJ has shown that a joint previously predicted to reach first fatigue failure within some 13 years from opening (5 years from this study) will now last in excess of 50 years.

CONCLUSION

Experimental Modal Analysis and dynamic strain gage studies were performed on the single support bar MBEJ installed in Anzac Bridge. The studies showed that for this joint (unmodified):

- The joint is very lightly damped (<2% of critical damping).
- The lowest frequency mode excited was a quasi-translational (bounce/bending) mode at 71 Hz.
- Due to access restrictions, horizontal modal data could not be acquired in sufficient detail to identify horizontal bending or torsional modes.
- The support bars and centre beams were acting dynamically as if simply supported.

It is considered that the dynamic response of this MBEJ is mainly due to coupled centre beam resonance and this is seen as a design characteristic of all single support bar designs. Static and dynamic strain gauge studies showed that for this joint (unmodified):

- The DRF is up to 4.6 for the fully laden test vehicle

- This DRF is not necessarily the worst case as every possible vehicle speed and joint opening combination was not tested
- Damping is important in the dynamic behavior
- The number of effective cycles of load due to vibration for each vehicle passage is very high
- High uplift forces are generated within the joint under vehicle loading.

These results were used to develop high damping elastomeric support bar bearings and the installation of these bearings resulted in a 30% reduction in stress for both center beams and support bars and reduce the uplift forces with consequent benefits on bearing retention.

A wholly unexpected benefit was the measured 98% reduction in stress events exceeding 15 MPa. The installation of high damping support bar bearings into the Anzac Bridge MBEJ has ensured that a joint previously predicted to reach probable first fatigue failure within some 5 years from this study will now last in excess of 50 years. These results should be of interest to bridge asset owners and bridge designers as this approach offers a cost-effective alternative to total joint replacement provided fatigue cracking has not yet occurred. It should also be of interest to specifiers and suppliers, as they can now specify and supply joints that will last the lifetime of the bridge by using a dynamics approach to the design.

ACKNOWLEDGEMENT

The authors wish to thank the Chief Executive of the Roads and Traffic Authority of NSW (RTA) for permission to publish this paper. The opinions and conclusions expressed in this paper do not necessarily reflect the views of the RTA.

REFERENCES

1. Ancich E.J., Brown S.C. & Chirgwin G.J., "Modular Deck Joints – Investigations into structural behavior and some implications for new joints", *Proc. 5th Austroads Bridge Conference*, Hobart, Tasmania, Australia, 2004.
2. Dexter R.J., Connor R.J. & Kaczinski M.R., "Fatigue Design of Modular Bridge Expansion Joints", *NCHRP Report 402,* Transportation Research Board, National Research Council, Washington, DC, USA, 1997, 128 pp.
3. Ostermann M., "Beanspruchung von elastisch gelagerten Fahrbahnübergängen unter Radstoßeinwirkung (Stresses in elastically supported modular expansion joints under wheel load impact)", *Bauingenieur* 66, Springer-Verlag, 1991, pp 381-389 (In German).
4. Roeder C.W., "Fatigue Cracking in Modular Expansion Joints", *Research Report WA-RD 306.1,* Washington State Transportation Center, Seattle, WA, USA, 1993, 53 pp.
5. Ewins D.J., "Modal Testing: Theory, Practice & Application (2nd Edition)", *Research Studies Press*, Hertfordshire, UK, 1999, pp.163-276.
6. Ancich E.J., Brown S.C. & Chirgwin G.J., "The Role of Modular Bridge Expansion Joint Vibration in Environmental Noise Emissions and Joint Fatigue Failure", *Proc. Acoustics 2004 Conference*, Surfers Paradise, Qld., Australia, 2004, pp 135-140.
7. Reid S. & Ansourian P., "Reliability Analysis of Expansion Joint in Anzac Bridge", *Investigation Report S1427*, Centre for Advanced Structural Engineering, University of Sydney, Australia, 2004 (Unpublished report prepared for the Roads & Traffic Authority of NSW).
8. Standards Australia, Australian Standard AS5100.4 – 2004, Bridge Design Part 4: Bearings and deck joints, Sydney, Australia, 2004
9. Davidson G. (Ludowici Ltd.), Personal Communication, 2002.

Table 1 Summary of Modal Frequencies and Damping (% of Critical)

Mode Number	Mode Type	Center Frequency, Hz	Damping, %
1	Whole body bounce	71	1.7
2	1st Bending	85	1.3
3a	2nd Bending	91	1.4
3b	Similar to Mode 3	97	1.3
4	3rd Bending	119	1.1
5	4th Bending	126	2.1

Table 2 Target & Actual Test Truck Pass-by Speeds (km/hr)

Run Number	OEM		Prototype #1		Prototype #2		Prototype #3	
	Target	Actual	Target	Actual	Target	Actual	Target	Actual
1	40	47	41	38	35	35	37	36
2	50	50	54	46	42	42	47	47
3	60	53	54	54	42	42	51	50
4	60	61	63	63	51	51	57	57
5	65	63	63	67	59	58	61	60
6	70	68	70	72	59	58	66	64
7	-	-	-	-	64	65	-	-

Table 3 Summary of Resulting Strains, Stresses and Dynamic Range Factors

Test Truck Pass-by Speed	Transducer Location	Strain and Stress								
		Strain (με)			Stress (MPa)			Dynamic Range Factors		
		Max Tensile	Max Compressive	Peak to Peak	Max Tensile	Max Compressive	Peak to Peak	Max Tensile	Max Compressive	Peak to Peak
Slow Roll	Support Bar	100	-1	101	20	0	20	0.0	0.0	0.0
	Centre Beam	154	-101	153	31	-20	31	0.0	0.0	0.0
47 km/hr	Support Bar	185	-30	215	37	-6	43	1.8	-0.4	2.2
	Centre Beam	167	-157	179	33	-31	36	1.9	-0.4	2.1
50 km/hr	Support Bar	226	-66	293	45	-13	59	2.3	-0.9	3.2
	Centre Beam	203	-113	234	41	-23	47	1.5	-0.3	1.8
53 km/hr	Support Bar	213	-54	268	43	-11	54	2.1	-0.6	2.7
	Centre Beam	136	-132	165	27	-26	33	2.0	-0.5	2.5
61 km/hr	Support Bar	270	-116	386	54	-23	77	2.7	-1.7	4.5
	Centre Beam	233	-141	308	47	-28	62	2.1	-0.6	2.6
63 km/hr	Support Bar	256	-114	370	51	-23	74	2.7	-1.9	4.6
	Centre Beam	225	-148	307	45	-30	61	1.9	-0.7	2.5
68 km/hr	Support Bar	218	-104	311	44	-21	62	2.4	-1.5	3.9
	Centre Beam	215	-137	280	43	-27	56	1.6	-0.7	2.2
Maximum	All	270	-157	386	54	-31	77	2.7	-1.9	4.6

Table 4 Comparison of Prototype Bearing Test Results

Component	OEM		Prototype #1		Prototype #2		Prototype #3	
	Stress Range, MPa	DRF	Stress Range, MPa	DRF	Stress Range, MPa	DRF	Stress Range, MPa	DRF
Center beams	62	2.6	49	3.7	49	3.3	44	2.3
Support bars	77	4.6	67	4.1	61	4.0	53	3.1

Table 5 Annualized measurement results over comparable two-week periods

	Maximum Stress, MPa	Significant Events, >15 MPa
OEM	80	2,648,989
Prototype #3	55	45,630
Reduction	31.3%	98.3%

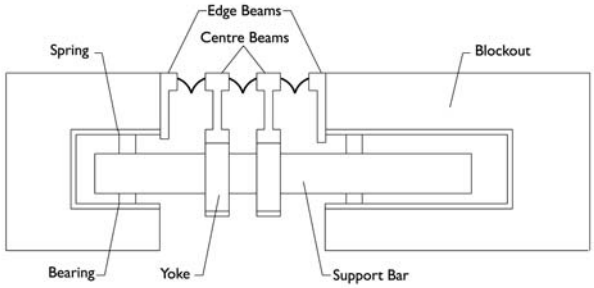

Figure 1 Typical Single Support Bar Design MBEJ

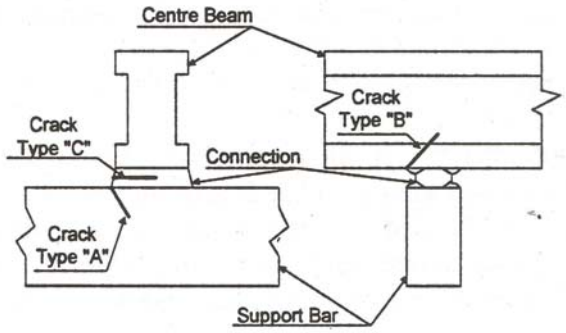

Figure 2 Established Fatigue Crack Patterns – Multiple Support Bar Designs
(After Dexter *et al*)

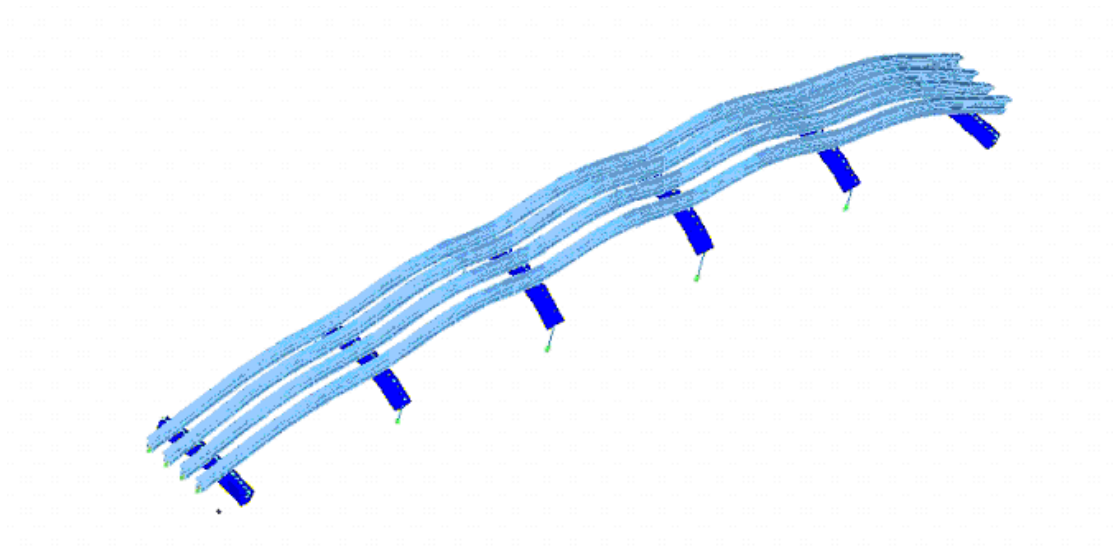

Figure 3 Quasi-translational Mode 1 @ 71 Hz

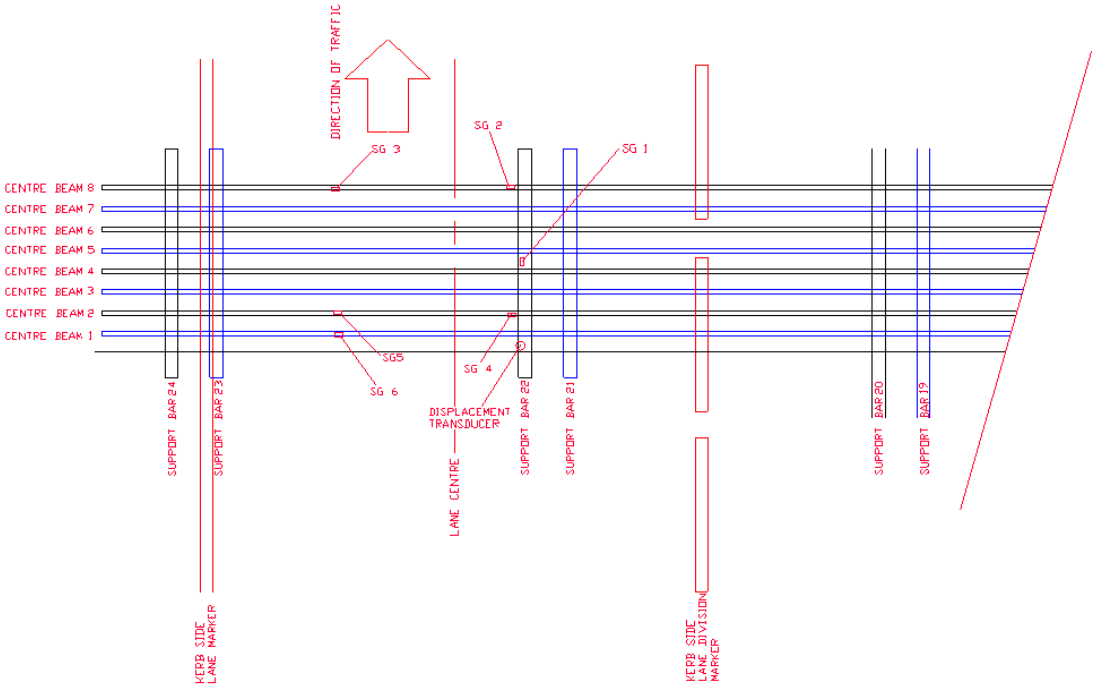

Figure 4 Eastbound Carriageway - Strain Gage Locations (SG1 to SG6)

Bridge Evaluation & Assessment - Test Truck loading

Axle loads from loading arrangements

Dimensions of Volvo Prime Mover F75155 and Brentwood Low Loader F02726
Test Load Vehicle A

Truck description

Steer axle (tare)	4.26 t	Steer to tandem	3.58 m	Block mass	0.99 t
Tandem (tare)	4.64 t	Spacing of tandem	1.37 m	Space for crane	3.44 m
Trailer (tare at king-pin)	4.28 t	Tandem to tridem	6.70 m	Max reach required	5.99 m
Trailer tridem (tare)	8.66 t	Spacing of tridem	1.27 m	(assumes crane in centre of trailer)	
King pin offset from centre of tandem	0.20 m	Spacing of tridem	1.27 m	Distribution to prime mover	
King-pin to front of trailer	0.63 m	King-pin to centre of tridem	8.85 m	King-pin to steer	5%
Length of tray	11.84 m	Centre of rear axle to end	1.09 m	King-pin to tandem	95%
No of blocks at goose-neck	4	Front of trailer to centre of block	3.60 m		

Block loading

Modular Expansion Joint Testing - ANZAC BRIDGE, WESTERN ABUTMENT

Block Position	Block position 1	2	3	4	5	6	7		Group loads (t) Steer	Tandem	Tridem	Total
								Tare	4.46	8.72	8.66	21.84
Loading level	No of blocks per position							Tare+bl	4.58	11.23	9.99	25.80
1	1	1	0	1	2	2	2	Load 1	4.66	12.83	17.22	34.71
2	2	2	2	2	2	4	2	Load 2	4.82	16.05	20.76	41.64

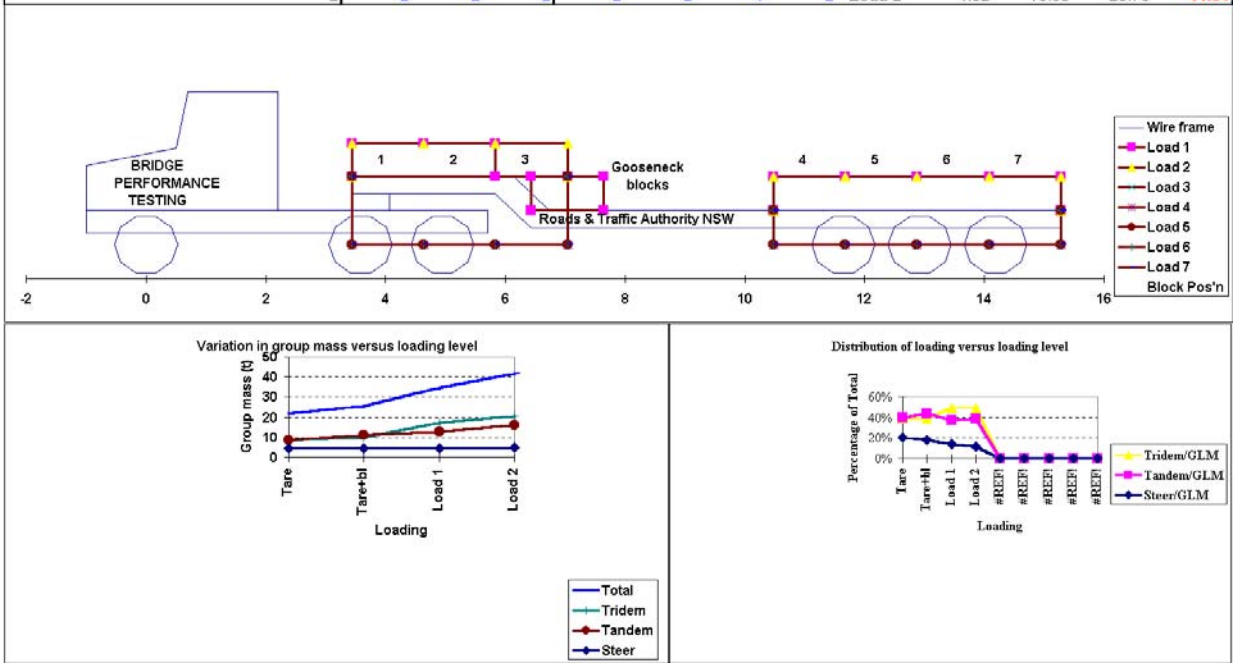

Figure 5 Test Vehicle Loading Arrangement

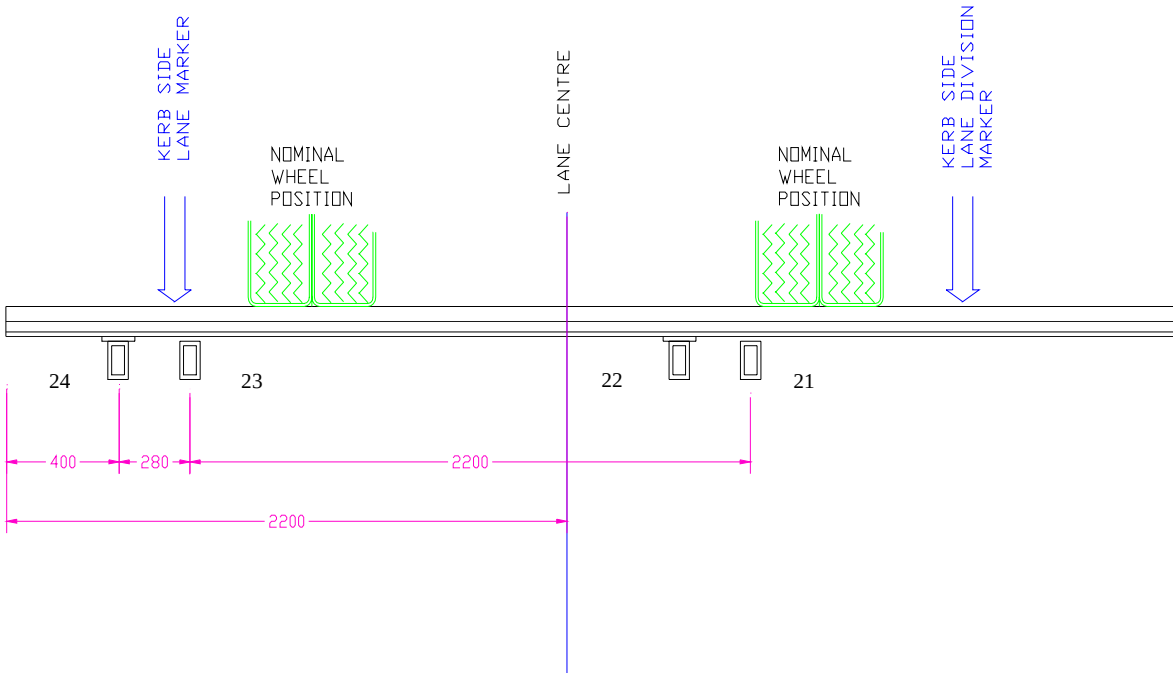

Figure 6 Elevation of Joint and Nominal Pass-by Locations
(Support bars shown numbered)

Figure 7 Tracking Check Paste

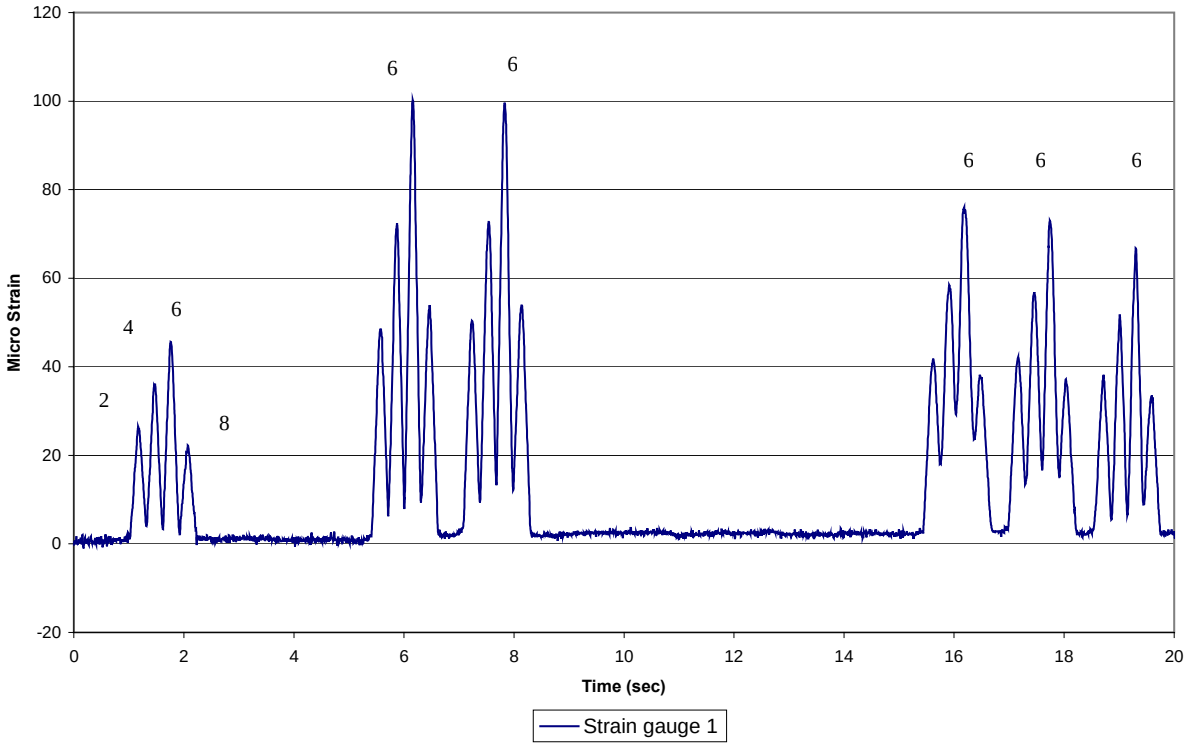

Figure 8 Quasi-static response due to test vehicle pass-by
(Contacted center beams shown numbered)

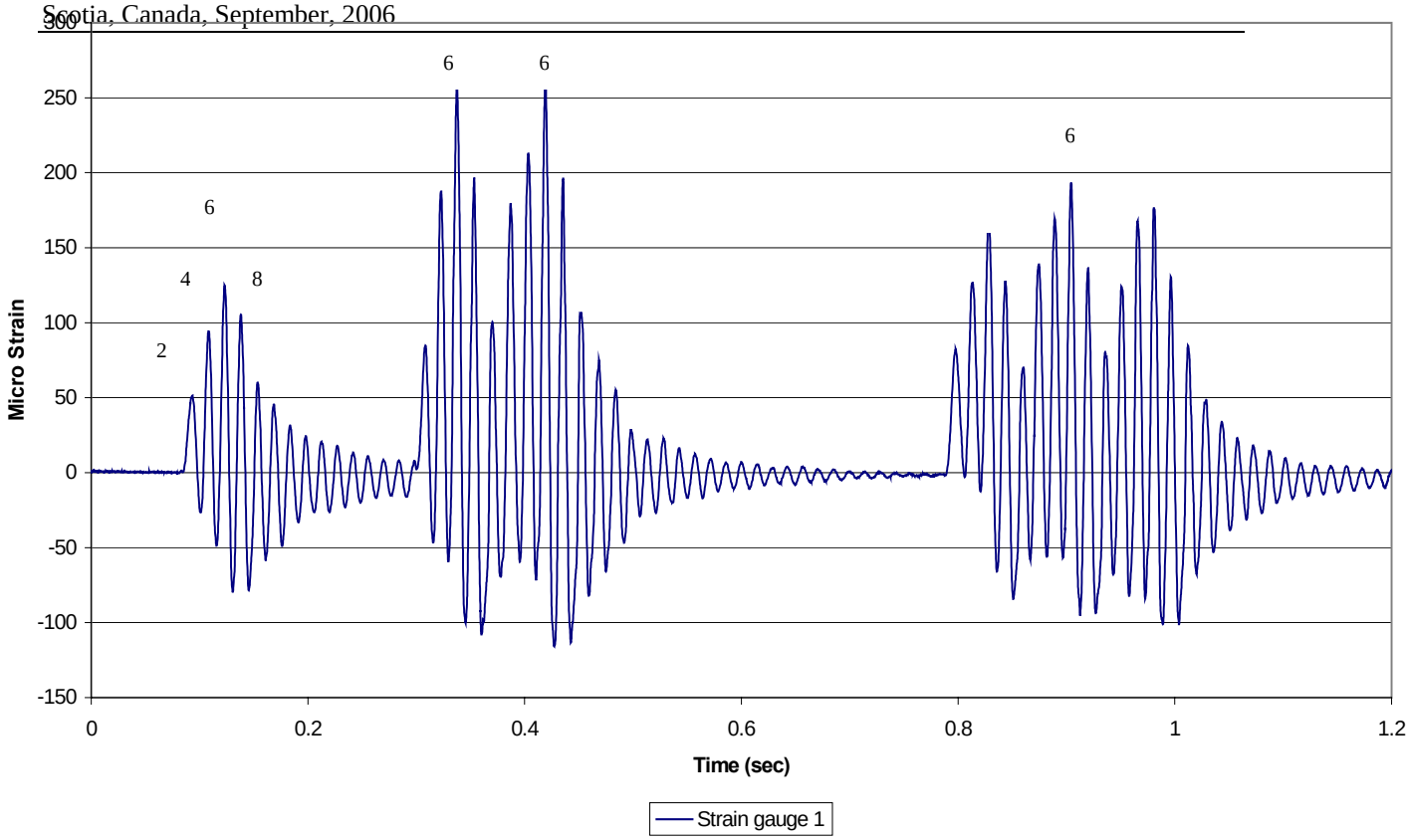

Figure 9 Dynamic response induced by heavy vehicle pass-by at 61 km/hr
(Contacted center beams shown numbered)

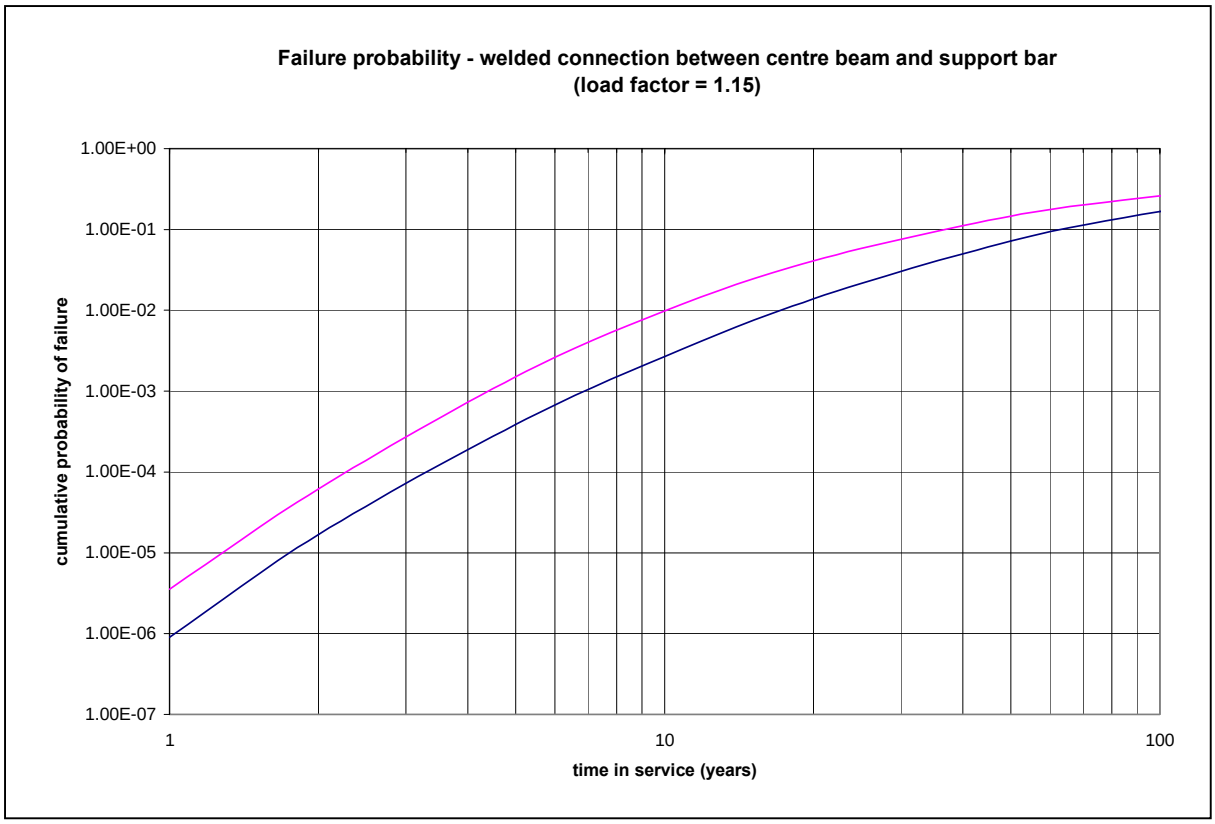

Figure 10 Time-dependent failure probability for a welded connection between center beam and support bar – OEM Condition
(After Reid and Ansourian)

Using Gurney line, probability of a single failure is 3% at 13 years => for 100 joints 95% probability of joint failure at 13 years.

Figure 11 Time-dependent failure probability for a welded connection between center beam and a support bar – Prototype #3
(After Reid and Ansourian)

Using Gurney line, probability of a single failure is 0.1% at 50 years => for 100 joints 10% probability of joint failure at 50 years.

Appendix H

Ancich E.J. and Bradford P. (2006). Modular Bridge Expansion Joint Dynamics, *Proc. 6th World Congress on Joints, Bearings, and Seismic Systems for Concrete Structures*, Halifax, Nova Scotia, Canada.

6th World Congress

on Joints, Bearings, and Seismic Systems for Concrete Structures

September 17-21, 2006 – Halifax, Nova Scotia, Canada

MODULAR BRIDGE EXPANSION JOINT DYNAMICS

Eric J. Ancich[1] and Paul Bradford[2]

(1) Technology & Technical Services Branch, Roads & Traffic Authority of NSW, PO Box 3035, Parramatta NSW 2124 Australia.

(2) Watson Bowman Acme Corp., 95 Pineview Drive, Amherst, NY 14068

BIOGRAPHY

Eric Ancich is a Senior Project Engineer with the Roads & Traffic Authority (RTA) of NSW (Australia). He has over 20 years experience in acoustics, vibration and structural dynamics. For the last six years he has managed the structural dynamics studies of six RTA road bridges to determine the mechanism causing environmental noise emissions and the premature fatigue induced failure of modular expansion joints. It is considered that this work has identified a major defect in the quasi-static load case assumption used universally in bridge design codes.

Paul Bradford is a product development engineer with 17 years experience in the design and analysis of bridge bearings and bridge expansion joints.

ABSTRACT

Recent experimental modal analysis (EMA) work by an Australian State Government Road Agency [Roads and Traffic Authority of NSW (RTA)] has enabled the development of calibrated FEA modular bridge expansion joint (MBEJ) models. Previously a relatively unexplored topic, this combination of FEA/EMA transient analyses helps reveal the underlying dynamic structure applicable to general classes of MBEJs.

Such dynamic characteristics as fundamental mode shapes, energy storage, damping effects, resonance, dynamic amplification factors, and dynamic stiffness in elastomeric support elements can be parametrically studied for design guidance. Many questions, such as why large joints have higher failure rates, how the dynamic amplification factor is affected by box spacing and bearing stiffness, what causes joint resonance, how it is prevented, what is the tire impact factor due to increased momentum, why joints do not move significantly in a horizontal sense when impacted, etc., can be derived and answered. The paper summarizes recent advances in the area of modular bridge expansion joint dynamics, focusing on FEA and EMA analyses. The experimental and theoretical confirmation of the single support bar phenomenon of coupled center beam resonance is also discussed.

Keywords: Bridges; expansion joints; fatigue; vibration; structural dynamics; dynamic strain

INTRODUCTION

Experimental Modal Analysis[1] (EMA) field tests have been performed on several modular joints located in the State of New South Wales, Australia, under the supervision of the Roads and Traffic Authority (RTA). Modulars were of the single support bar and multiple support bar designs. The motivation for undertaking field testing had its roots in the failure of three joints, including the dual support bar design of the Anzac Bridge modulars, in Sydney Australia. Significant component damage on this structure suggested a failure mode of high cycle fatigue. Subsequent EMA testing confirmed this hypothesis, that the root of failure lay with the joint's poor dynamic characteristics, namely low damping (1.2%) and near resonance dynamic amplifications. The Anzac Bridge modulars, along with several other joints in the region, were characterized dynamically through the use of field testing using a calibrated truck.

This paper focuses on two of these installations, the Anzac Bridge in Sydney (Figure 1) and the Taree Bypass located just outside the township of Taree, north of Newcastle (Figure 2). There are four bridges in the Taree Bypass, each with two MBEJ's. The subject joint is in the southern abutment of the southbound bridge over the south channel of the Manning River.

Geometry for the six axle RTA calibrated truck is shown in Figure 3. As can be seen, the truck is of the single-dual-tri axle configuration, allowing researchers to gain a better insight into multiple excitation joint dynamics. The 16.05 metric ton (35.4 kip) dual and 20.76 metric ton (45.8 kip) tri-axle loads correspond roughly to AASHTO[2] HS16 tandem axle and tri-axle loads, respectively. The modular expansion joint for the Taree Bypass testing was a 6 cell multiple support bar design. In the multiple support bar (MSB) design, each centerbeam is welded to a separate support bar, which in turn is supported on flexible bearings housed within steel boxes embedded within the deck slabs. The function of the centerbeam is to support vehicular loading with an elastomeric seal used to prevent water/debris intrusion to the structure. Equidistance springs are used to keep the seal gaps evenly spaced as the structure expands and contracts. The support bar bearings perform a variety of functions, not the least important of which are to add damping essential in mitigating resonance effects and absorbing vehicular impact. Bearings can have a significant effect on a joint's dynamic characteristics, as detailed further in this paper.

Dynamic Strain Gage Study

The MSB strain gage layout is shown in Figures 4 and 5, positioned at locations just under the truck wheel excitations. Continuous beam analyses show that peak moments often occur in the exterior support box regions, since many MSB designs utilize equal (or nearly so) box spacing. The measurement instrumentation was selected with a data sampling rate of 25 kHz and this was sufficient to ensure that frequencies up to 10 kHz were sampled accurately.

Transient response for two different truck passes at strain gage #6 (support bar) are shown in Figures 7 and 8. The single-dual-tri axle tire pulse set is clearly evident, as is the increasing dynamic character with increasing velocity. The 104 km/hr trace shows the most dynamic behavior, for two reasons, increased vehicle momentum and proximity of the tire pulses to the joint's natural frequencies. Negative strain values indicate that the bottom of the centerbeam enters compression after being loaded in tension, i.e. the centerbeam is rebounding dynamically. Examination of Figure 8, for gage #6 (support bar), shows a peak-to-peak value of 155.7 microstrain (με) for axle #6 compared with a quasi-static (slow roll) value of 51.6 με. This is equivalent to a DAF of 3.02, where the DAF is defined as the peak-to-peak strain range at the designated vehicle speed (104 km/hr) divided by the zero-to-peak strain range at slow roll. Further examination of Figure 8 shows the effect of in-phase (or notionally in-phase) excitation where the joint vibration has not fully decayed before subsequent axle excitation. The DAF values for each axle of the tri-axle set are 2.1, 2.7 and 3.02. Similar, but lower values were obtained for centerbeams. Strain gage #4 (centerbeam) showed a peak DAF of 1.94 (191.7 με/98.8 με) at axle #6, significantly greater than the DAF of 1.4 at axle #4. It should be noted that the tested MBEJ is in a long section of controlled access road where the legal speed limit is 110 km/hr. These dynamic amplification factors are clearly not in agreement with the 1.75 value recommended in AASHTO[2]. However, even higher values were measured at Anzac Bridge. The MBEJ installed into the western abutment of Anzac Bridge consists of two interleaved single support bar structures that behave, in a dynamic sense, as independent structures. Previous EMA studies demonstrated only very light, almost negligible coupling between the two structures.

Figure 9 shows the quasi-static response of a strain gauge (SG1) located in the middle of an Anzac support bar and the impact of each of the test vehicle's six axles with each of the centre beams connected to this support bar is clearly evident. The dynamic behaviour of the Anzac Bridge MBEJ may be considered as two independent structures (i.e. one structure with one set of odd numbered centerbeams with associated support bars, and a second structure with one set of even numbered centerbeams and support bars). The coupled nature of the "*odd*" and "*even*" structures is further demonstrated in Figure 10. The dynamic response here is demonstrated by the impact of the tandem axles of the tractor and the tri-axles of the trailer where the vibration is in phase and virtually continuous. An independent centerbeam structure responding to a single impulse would, of course, be expected to display an initial maximum amplitude followed by an exponential decay. The build-up in centerbeam response may be attributed to the phase relationship of each wheel to centerbeam impact. This phenomenon is described as coupled centerbeam resonance[3]. A simple comparison between Figures 9 & 10 shows that the quasi-static slow roll produced 100 με (Peak-Peak) and the 61-km/hr pass-by produced 386 με (Peak-Peak). This comparison indicates a dynamic amplification factor (DAF) of at least 3.86 times static.

Furthermore, not only are the peak dynamic strains at least 3.86 times the quasi-static but further observation of Figure 10 shows that the steer and tandem axles of the tractor produced at least 16 cycles of vibration (per vehicle passage) where the dynamic strain equalled or exceeded the quasi-static strain of 100 με (Peak-Peak). Similarly, the tri-axle group of the trailer produced at least 14 cycles of vibration (per vehicle passage) where the dynamic strain equalled or exceeded the quasi-static strain of 100 με (Peak-Peak).

The Coupled Centerbeam Resonance phenomenon occurs in the single support bar design when all centerbeams attached to a support bar vibrate virtually simultaneously when the excitation is in-phase or notionally in-phase.

The simple addition of these events shows that each passage of the load configuration of the test vehicle, produced around 30 vibration cycles where the dynamic strain equalled or exceeded the quasi-static strain of 100 με (Peak-Peak). A peak DAF of 4.6 was measured on a support bar of the Anzac Bridge MBEJ at a test vehicle speed of 63 km/hr (The legal maximum for this bridge is 70 km/hr).

Current RTA practice[7] is to use 80% of the peak DAF in design calculations or a default value of 2.5, which ever is the highest. Ancich & Bhavnagri[8] demonstrate a very high level of agreement between measured and calculated stress using this approach.

Tire Pulse Frequencies

Both field data and FEA/EMA correlations suggest that tire pulses, i.e. tire excitation to the centerbeam, can be modeled as half sine wave pulses. The question at hand is what frequency should these half sine waves be?[1]. Scaling the (tire) pulse width from the 39 km/hr (24.2 MPH) test, one arrives at a tire pulse frequency of 21.8 Hz. Using a standard tire patch length of 200 mm (7.87") and a beam width of 63.5 mm (2.5"), and noting that a simple model for pulse duration is based upon a load length of one tire length plus one beam width, one calculates a pulse frequency of 20.5 Hz.

$$f_t = \frac{V}{2\times(L+b)} + O(\varepsilon) \qquad (1)$$

where second order effects are represented by the $O(\varepsilon)$ term. Tests show, however that the agreement is much less, i.e. the $O(\varepsilon)$ term is much larger at higher velocities. Calculating this higher order appears to be a fairly complex study, involving both the joint and tire dynamics. For example, by examining the 39 km/hr plot (not shown), one observes both an asymmetry in the pulse and an out of phase component that causes a kink in the pulse. The

[1] The problem is further complicated by the fact that the time domain traces used to estimate tire pulses are the structure's response to the pulse, not the pulse itself. Estimating tire pulse amplitude is another complication addressed later.

kink is probably caused by the fact that at this low tire pulse frequency, the natural frequency of the joint in this mode of bending is higher than that of the tire pulse, and hence rebounds faster than the joint is being unloaded. This is similar to the transient response of a single degree of freedom system (SDOF) whose excitation-to-natural frequency ratio is less than 1.0. At higher tire pulse frequencies, this characteristic disappears.

Tire pulse asymmetry is at least partially due to the fact that the problem is in essence is a Floquet theory problem, i.e. a non-constant parameter problem. The downward motion of the beam is not driven harmonically by a force, but rather by the loading and unloading of vehicular mass, i.e. the mass on the beam is not constant. To be more exact, it is a coupled spring-mass-damper system. A SDOF simplification of this coupled system would be as in Equation 2. The tire pulse is often modeled instead by a force driven, half period sine wave; the equivalent SDOF simplification is equation,

$$\left(m_V \times P(t) + m_B\right) \times \ddot{x} + c \times \dot{x} + k \times x = 0 \tag{2}$$

$$m_B \times \ddot{x} + c \times \dot{x} + k \times x = -m_V \times g \times P(t) \tag{3}$$

where m_B and m_V represent the effective mass of the centerbeam and vehicle respectively, and $P(t)$ the unit vehicle (pulse) excitation with a maximum value of 1. Previous numerical simulations by the authors of (2) replicated this pulse asymmetry.

Modeling in FEA requires that the vehicle tire pulse excitation be applied to the beam nodes. This can be done using a half-sine wave pulse with a delay according to the beam position (see Figure 11).

$$P(t) = A \times \sin(2\pi f_T \times t) U\left(t - \frac{x - x_0}{v}\right) U\left(\frac{x - x_0}{v} + \Delta t_T - t\right) \quad (4)$$

x_0 is the coordinate of the first beam node, v vehicle velocity, f_T the tire passing frequency, and Δt_T the tire pulse duration. The tire pulse duration and tire passing frequency can be calculated using the tire patch length (L) and the vehicle's velocity;

$$\Delta t_T = \frac{L}{v} \quad (5)$$

$$f_T = \frac{1}{2 \times \Delta t_T} = \frac{v}{2L} \quad (6)$$

For beam node row *i*, equally spaced at Δx across the joint,

$$P_i(t) = A \times \sin(2\pi f_T \times t) U\left(t - \frac{\Delta x \times i - x_0}{v}\right) U\left(\frac{\Delta x \times i - x_0}{v} + \Delta t_T - t\right) \quad (7)$$

Equation 7 synchronizes the beam excitations, forming a tire pulse train that replicates a tire moving across a joint (Figure 12). When the joint is fully loaded, the summation of the pulses must equal the tire load, i.e. a constant. As Figure 12 shows, this is clearly not the case if unit pulses of unit magnitude are used.

Also, Figure 12 shows that that although the load is close to constant, it is not exact. This shows that the sine pulse model for vehicle excitation is an approximation that can be improved upon if so desired. For the purposes of FEA modeling however, it is usually close

enough. It should be noted that as the beam node spacing becomes smaller and smaller, the variation in total load decreases, such that at very small spacings the load is essentially constant. This characteristic suggests that the shape of the tire pulse changes somewhat with beam spacing. The constant A in Equation 7 is used to scale the individual beam pulses such that the total load on the joint equals that of the tire. This can be found by evaluating the series expression for the total tire loading;

$$P_T(t) = A \times \sum_{i=1}^{N} \sin(2\pi f_T \times t) U\left(t - \frac{\Delta x \times i - x_0}{v}\right) U\left(\frac{\Delta x \times i - x_0}{v} + \Delta t_T - t\right) \tag{8}$$

where N is the total number of beams. Noting that the joint is fully loaded when the first tire has completely passed over the first beam, i.e. after Δt_T means that,

$$P_T(\Delta t_T) = 1 \tag{9}$$

Evaluating Equation 8 at $t = \Delta t_T$ gives,

$$1 = A \times \sum_{i=1}^{p} \sin\left(2\pi f_T \frac{\Delta x}{v}(p - i)\right) \tag{10}$$

where p is the total number of pulses in the tire passing time Δt_T.

$$p = \frac{L}{\Delta x} \tag{11}$$

The finite series in Equation 10 can be evaluated; solving for A gives,

$$A = \sin\left(\frac{\pi}{2}\frac{\Delta x}{L}\right) \tag{12}$$

The significance of Equation 12 is that for, Δx equal to the beam spacing, the beam distribution factor A, shows good correlation with the Dexter *et al*[3] test results.

Modal Damping

Damping ratios for the various modes were estimated using hammer pulse testing, with resulting values of 0.064, 0.129, 0.025, 0.025, and 0.030 for the first five modes (69, 91, 122, 139, and 155 Hz respectively). These will in general be smaller than those found via field testing, namely because the bearings contribute more to the response at higher loads; they serve to add a significant amount of damping to the system. Damping can also be estimated directly from the time history trace by a variety of methods, e.g. the logarithmic decrement method. Damping ratios, which can be position, vehicle speed, and load dependent, are typically in the 5% - 20% range. It should be noted that the damping ratio should not be measured using the tire pulse peak as a baseline, as the system is not in a state of free vibration. An EMA damping ratio of 0.164 is calculated at strain gage 2 at 104 km/hr, and 0.146 as calculated at the bearing transducer.

Through FEA analysis, it was found that a system damping ratio of 0.10 produced the best correlation with field data for the joint type used in the Taree Bypass testing.

This appears to be in agreement with damping trends, which showed larger damping ratios for lower modes; the influence of higher modes brings the system (average) damping ratio down somewhat, in this case from the 15% measured at the strain gage and bearing to 10% overall. Of critical concern to the RTA was the case of a system that has very low damping, as displayed by the Anzac Bridge modular. This bridge stands at the gateway to the Sydney

CBD. The joint's problems not only slowed traffic, but also produced an explosive type noise upon vehicular loading that reverberated across the area. The RTA suspected that high cycle fatigue was the cause of component damage (welds, bearings, steel members, etc.). Suspicions were confirmed when measurements showed that the very low damping ratio (1.2%) led to very high dynamic amplification factors,(up to 4.6 at support bars) producing stress ranges that lay within the finite stress range for fatigue life. Lack of resilience and damping in the support box bearings was found to be the root cause of all this damage. The lower support box bearings were essentially rigid in the vertical direction with little or no impact absorption capability. Support bar "hopping", the characteristic in which the support bar rebounds so strongly that it comes off its supports, was observed. Increasing the downward force applied by the retention springs was counter-productive, as the resulting increased friction caused spring distortion and eventual dislodgement.

EMA Vertical Mode Shapes and Modal Frequencies for Taree

The first few mode shapes can be categorized generally as vertical, horizontal, axial, or torsional. Figure 13 shows the extracted vertical mode shapes and frequencies from the experimental modal analysis, with a controlled input using a 2 kg hammer pulse. Figure 14 shows mode shapes and frequencies for vehicular loading. Frequency correlation is good between the two, though some differences are observed between the shapes.

The first mode is a cantilever wagging type mode. Its frequency reflects the length of the cantilever, the flexibility of the centerbeam, and to some extent the flexibility of the support bearings. The authors have found excellent agreement using the lumped parameter equation for the first mode frequency of a fixed end cantilever beam,

$$f_C = \frac{0.56}{(L+\Delta)^2}\sqrt{\frac{E \times I}{A \times \rho}} \tag{13}$$

L is the length of the cantilever, Δ is the length beyond the bearing at which the beam rotation is zero. Together they make up a dynamic length of the cantilever. This length can be easily extracted from FEA, or estimated using the bearing stiffness - the stiffer the bearing the smaller the Δ. Since this mode often lies in the tire pulse frequency range, it has the potential to produce large DAFs. Although the cantilever region is oft neglected in design based on the assumption that the ADT (average daily traffic) will be low in this region, it's dynamic susceptibility points to the use of short cantilevers as good design practice.

The second RTA mode is described by the RTA as a "vertical bounce" or "whole body" mode, is essentially the fundamental mode of the joint (in the vertical direction). If the centerbeam and support bar were perfectly rigid, this would be a purely translational rigid body mode. This a little difficult to see from the impact testing, a little easier to see in the tire pulse testing, but becomes very clear in the FEA analysis. Its frequency can be estimated using the mass of the centerbeam and support bars along with the total bearing dynamic stiffness in simple SDOF equation form,

$$f = \frac{1}{2 \times \pi}\sqrt{\frac{n_b \times k_{bear}}{m_{Tot}}} \tag{14}$$

where k_{bear} is the dynamic stiffness of the bearing, and n_b is the number of the support bars and m_{Tot} is the total mass of the centerbeam and support bars. If the joint is large and/or the support bars are flexible, support bar dynamics needs to be considered as well. The system can be modeled as a 2 DOF series combination of the bar/bearing mass and the centerbeam

mass. Using structural dynamics methods for distributed systems, the frequency equations for the two components of the 2 DOF system can be derived. The fundamental frequency for a continuous beam with rigid supports (f_{cb}) is;

$$f_{cb} = 317300 \times \frac{\rho_{cb}}{S^2} \tag{15}$$

The natural frequency of the bar/bearing system (f_{bb}) can be found using the method of generalized coordinates and an assumed mode shape:

$$\psi(x) = \frac{y(x)}{y_{max}} = \frac{L^2 \times x - 2 \times x^3 + x^4 / L + 12EI / k_{bear}}{5/16\, L^3 + 12EI / k_{bear}} \tag{16}$$

with a generalized mass and stiffness,

$$M = \int_0^L m_u \times \psi(x)^2 dx \tag{17}$$

$$K = \int_0^L EI \times [\psi''(x)]^2 dx + 2 \times k_{bear} \times \psi(0)^2 \tag{18}$$

with $f_{bb} = 1/2\pi \sqrt{K/M}$. The integrations are simple but algebraically messy. Using canonical transformations for a two degree of freedom system and the first term of its binomial expansion, it can be shown that the first mode of the bar/bearing/centerbeam system can be approximated as Equation 19. Figure 15 shows a plot of the system's first mode frequency as a function of the support bar bearing stiffness for a typical 8 seal system.

$$f = \alpha \times f_{cb} \tag{19}$$

when

$$\alpha = \left(1 + \left(\frac{f_{cb}}{f_{bb}} \right)^2 \times \left(1 + \frac{W_{cb}}{W_{sb}} \right) \right)^{-1/2} \tag{20}$$

where W_{cb} and W_{sb} are the weight of one centerbeam span length or one support bar, respectively. This frequency is an important dynamic characteristic of the joint. It establishes a dynamic baseline that supplies a big piece of the qualitative behavior puzzle. One recipe for a well performing joint is a high first mode frequency (e.g. above 100 Hz) together with good separation between the first and second modes (e.g. 30%). The joint configuration that produces these modal characteristics is one of a stiff steel member network in conjunction with resilient bearings. Examination of time history traces indicates that there is significant first mode participation in the total response.

Mode shapes of two adjacent bars are shown in Figure 14. Light coupling is observed, as should be probably expected; the tremendous impulse load applied to one beam will be transferred to a much lesser extent in the others. Loads are transferred from one centerbeam to the next via the following load path: support bar 1> bearing 1>support box 1>bearing 2>support bar 2>beam 2. As the means of communication between bars is through the bearings and support box, stiffer bearings and mode flexible support boxes will increase this coupling. Figure 16 gives another perspective of this coupling, a simultaneous time history trace of two centerbeams.

CONCLUSIONS

The dynamics of MBEJs are not clearly understood at this time. EMA lends many insights that help guide design and FEA modeling. Accurate correlation is difficult because of several reasons, not the least being that the problem is in essence a variable mass problem of more

than one degree of freedom. Common mode shapes for multiple support bar expansion joints are identified, as well as methods to predict the first mode frequencies and tire pulse parameters. The negative effects of hard support box bearings are seen to exacerbate dynamic effects in lack of damping and in promoting proximity to resonance. Cross coupling in multiple support bar configurations is in general minimal, but does have the potential to be problematic (depending upon the support box transfer function and bearing response).

The issue of appropriate design DAF values clearly needs more work and there is a gaping need for a universal DAF definition, particularly in fatigue prone situations where full stress reversals need to be addressed.

ACKNOWLEDGEMENT

The authors wish to thank the Chief Executive of the Roads and Traffic Authority of NSW (RTA) for permission to publish this paper. The opinions and conclusions expressed in this paper do not necessarily reflect the views of the RTA.

REFERENCES

1. Ewins D.J., "Modal Testing: Theory, Practice & Application (2nd Edition)", *Research Studies Press*, Hertfordshire, UK, 1999, pp.163-276.
2. American Association of State Highway and Transportation Officials (AASHTO) *AASHTO LRFD Bridge Design Specifications, SI Units*, 3rd Ed., Washington, DC, USA, 2004.
3. Ancich E.J., Brown S.C. & Chirgwin G.J., "Modular Deck Joints – Investigations into structural behavior and some implications for new joints", *Proc. 5th Austroads Bridge Conference*, Hobart, Tasmania, Australia, 2004.

3. Dexter R.J., Connor R.J. & Kaczinski M.R., "Fatigue Design of Modular Bridge Expansion Joints", *NCHRP Report 402,* Transportation Research Board, National Research Council, Washington, DC, USA, 1997, 128 pp.

4. Ostermann M., "Beanspruchung von elastisch gelagerten Fahrbahnübergängen unter Radstoßeinwirkung (Stresses in elastically supported modular expansion joints under wheel load impact)", *Bauingenieur* 66, Springer-Verlag, 1991, pp 381-389 (In German).

5. Roeder C.W., "Fatigue Cracking in Modular Expansion Joints", *Research Report WA-RD 306.1,* Washington State Transportation Center, Seattle, WA, USA, 1993, 53 pp.

6. Ancich E.J., Brown S.C. & Chirgwin G.J., "The Role of Modular Bridge Expansion Joint Vibration in Environmental Noise Emissions and Joint Fatigue Failure", *Proc. Acoustics 2004 Conference*, Surfers Paradise, Qld., Australia, 2004, pp 135-140.

7. Roads & Traffic Authority of NSW. *RTA QA Specification B316 – Modular Bridge Expansion Joints*. Sydney, Australia, 2004.

8. Ancich E. J. & Bhavnagri V., "Fatigue Comparison of Modular Bridge Expansion Joints Using Multiple Bridge Design Code Approaches", *Proc. 6th World Congress on Joints, Bearings and Seismic Systems for Concrete Structures,* Halifax, Nova Scotia, Canada, 2006.

9. Standards Australia, Australian Standard AS5100.4 – 2004, Bridge Design Part 4: Bearings and deck joints, Sydney, Australia, 2004

10. Clough, R. and Penzien, J., *Dynamics of Structures*, McGraw-Hill, 1975.

11. Brown S.C., "Vibration and Fatigue Investigation Taree Bypass Modular Expansion Joint", *Report 10-1788-R4*, Richard Heggie Associates Pty Ltd, Lane Cove, Australia, 2005 (Unpublished report prepared for the Roads & Traffic Authority of NSW).

12. Brown S.C., "Measurement of Static and Dynamic Strains Taree Bypass Bridge Modular Expansion Joint", *Report 10-1788-R5*, Richard Heggie Associates Pty Ltd, Lane Cove,

Australia, 2005 (Unpublished report prepared for the Roads & Traffic Authority of NSW).

Figure 1 - Anzac Bridge, Sydney **Figure 2 - Taree Bypass, Taree**

Bridge Evaluation & Assessment - Test Truck loading

Axle loads from loading arrangements

Dimensions of Volvo Prime Mover F75155 and Brentwood Low Loader F02726
Test Load Vehicle A

Truck description

Steer axle (tare)	4.26 t	Steer to tandem	3.58 m	Block mass	0.99 t
Tandem (tare)	4.64 t	Spacing of tandem	1.37 m	Space for crane	3.44 m
Trailer (tare at king-pin)	4.28 t	Tandem to tridem	6.70 m	Max reach required	5.99 m
Trailer tridem (tare)	8.66 t	Spacing of tridem	1.27 m	(assumes crane in centre of trailer)	
King pin offset from centre of tandem	0.20 m	Spacing of tridem	1.27 m	Distribution to prime mover	
King-pin to front of trailer	0.63 m	King-pin to centre of tridem	8.85 m	King-pin to steer	5%
Length of tray	11.84 m	Centre of rear axle to end	1.09 m	King-pin to tandem	95%
No of blocks at goose-neck	4	Front of trailer to centre of block	3.60 m		

Block loading

Modular Expansion Joint Testing - ANZAC BRIDGE IN SYDNEY

	Block position								Group loads (t)			
Block Position	1	2	3	4	5	6	7		Steer	Tandem	Tridem	Total
								Tare	4.46	8.72	8.66	21.84
Loading level			No of blocks per position					Tare+bl	4.58	11.23	9.99	25.80
1	1	1	0	1	1	1	1	Load 1	4.67	13.01	14.06	31.74
2	2	2	2	2	2	4	2	Load 2	4.82	16.05	20.76	41.64

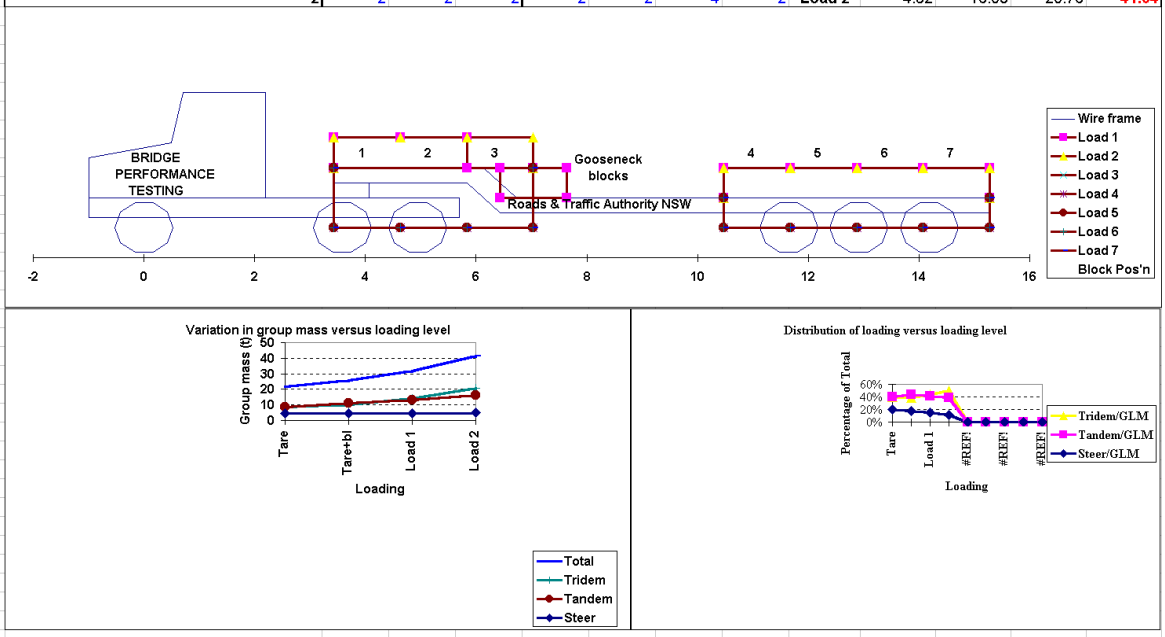

Figure 3 - RTA calibrated truck (Anzac & Taree)

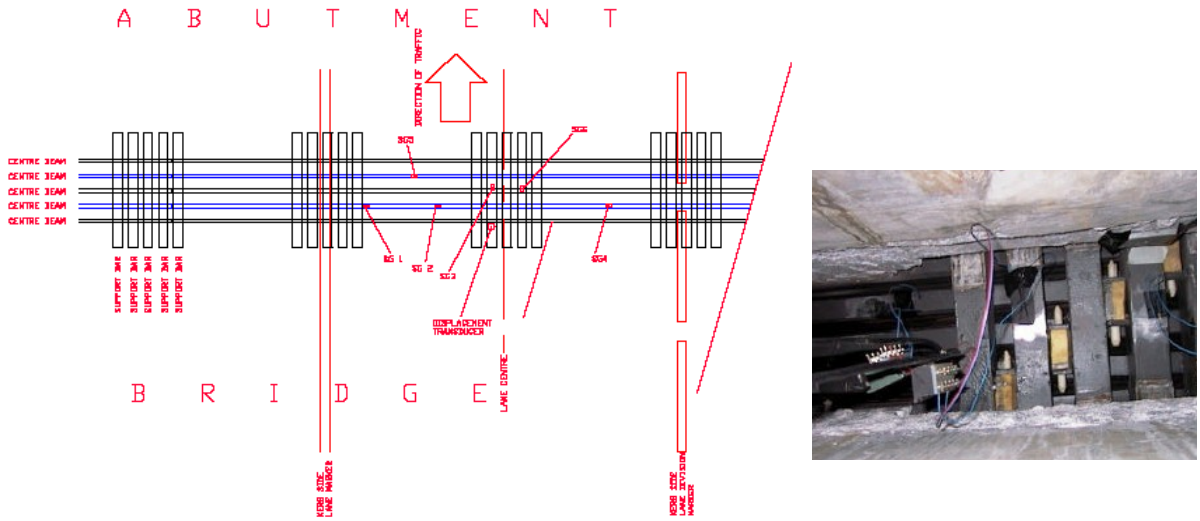

Figures 4 and 5 - Strain gage layout on the Taree Bypass structure

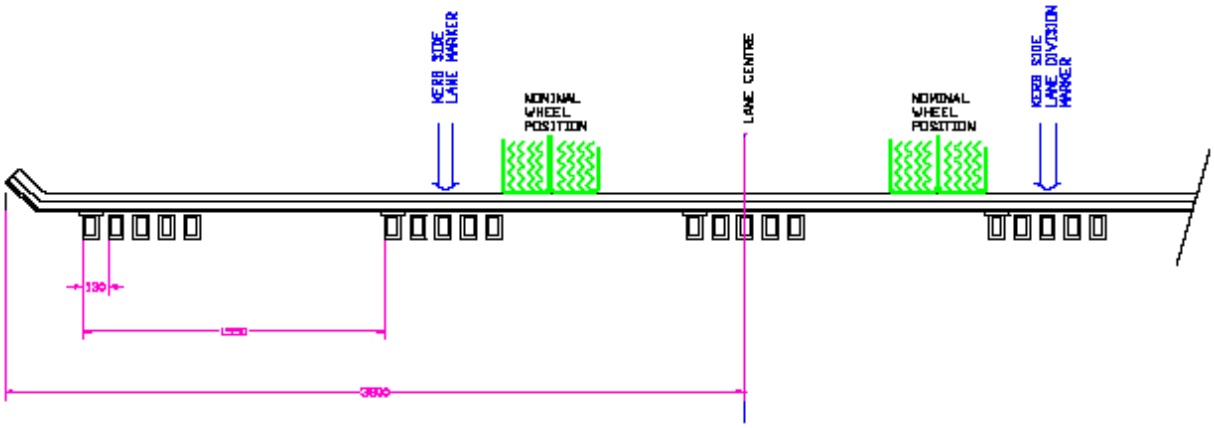

Figure 6 - Truck position on joint, Taree Bypass - Strain Gage Testing

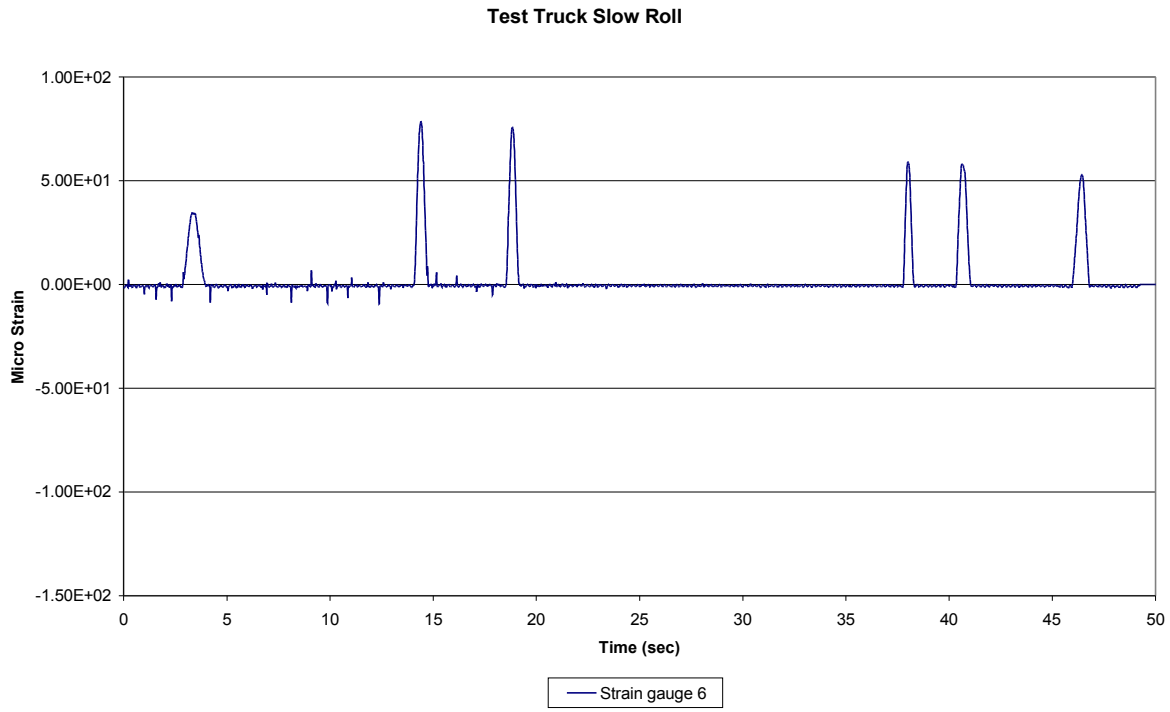

Figure 7 - Time domain response of a support bar at slow roll (Taree)

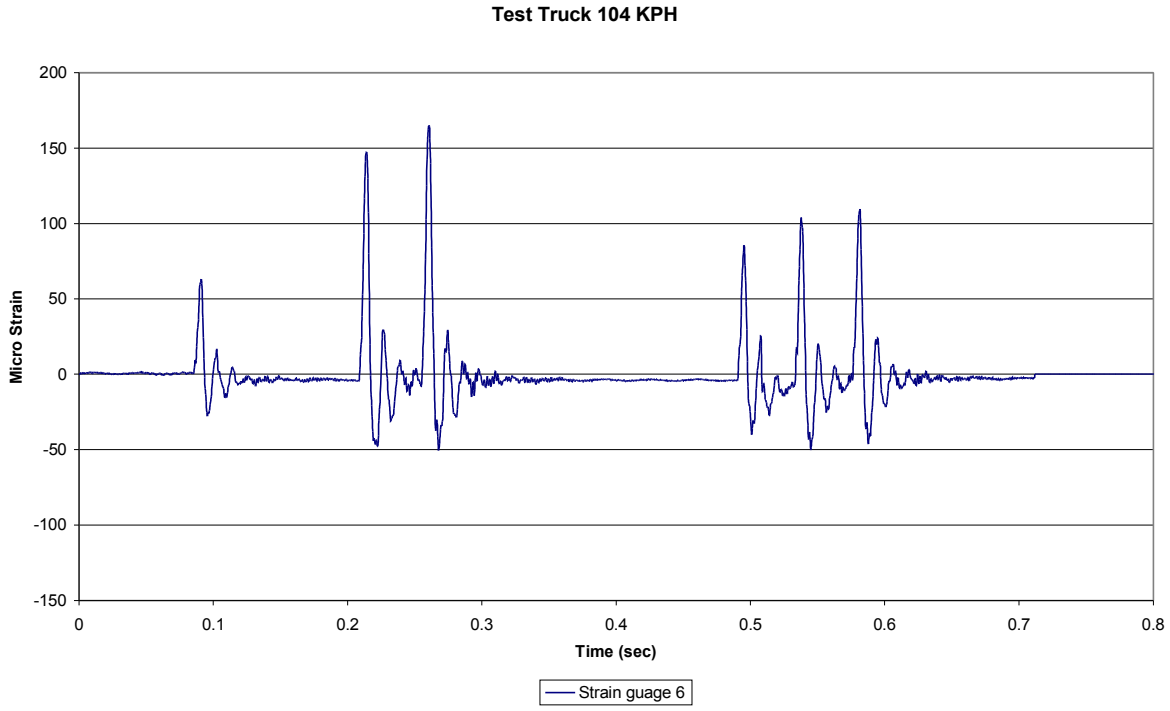

Figure 8 - Time domain response of a support bar at 104 km/hr (Taree)

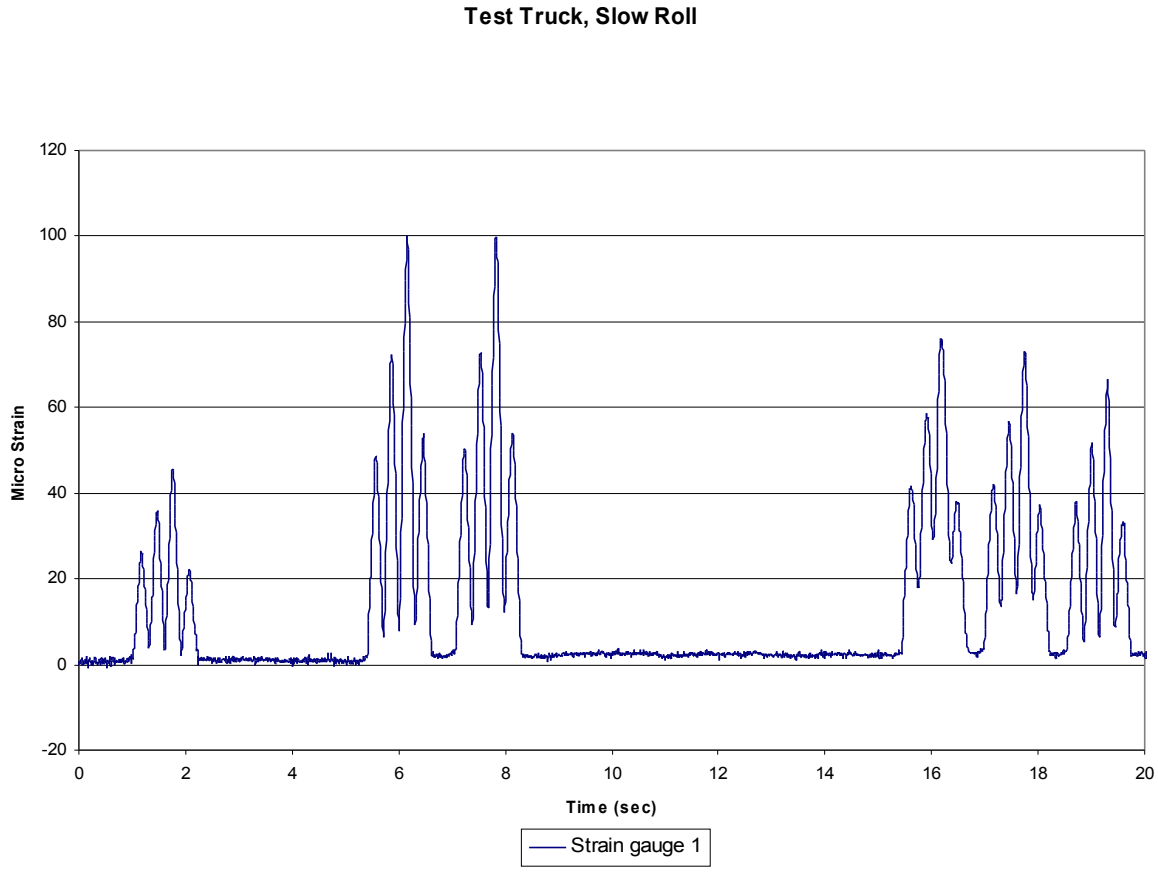

Figure 9 – Static response induced by heavy vehicle slow roll (Anzac)

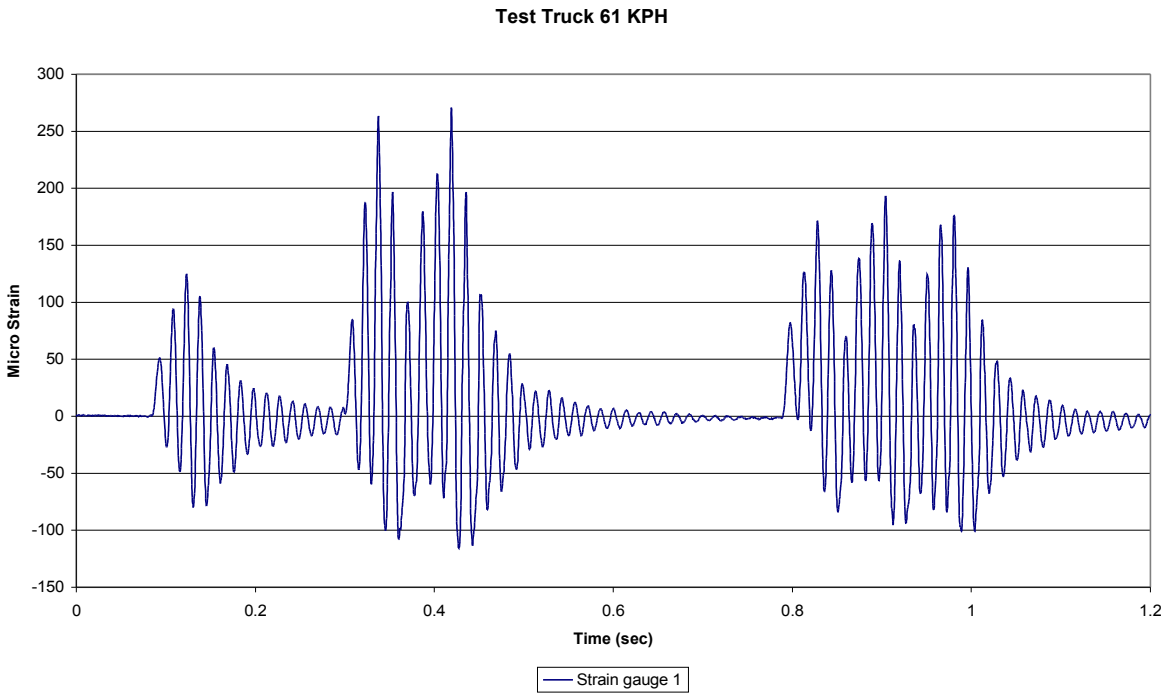

Figure 10 - Dynamic response induced by heavy vehicle pass-by (Anzac)

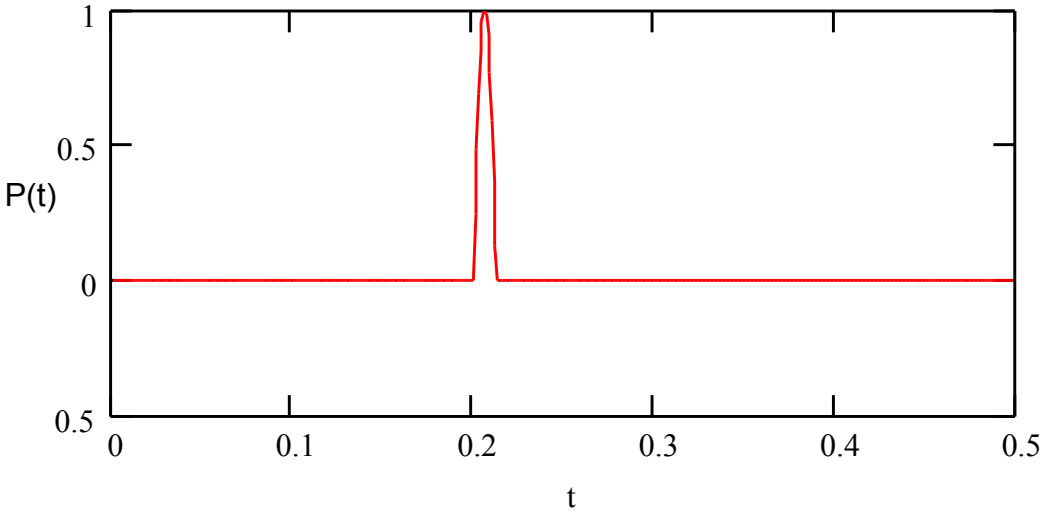

Figure 11 – FEA model function of a tire pulse

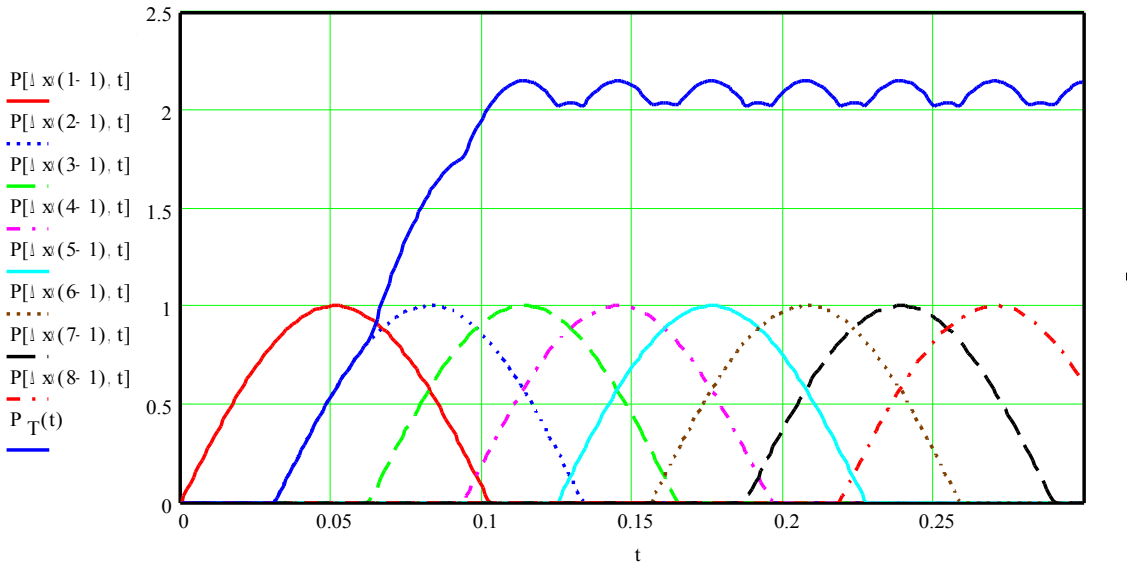

Figure 12 – Pulse train for FEA modeling. Note the pulses should add to 1.0 when the joint is fully loaded, hence the need for the pulse scale factor, A.

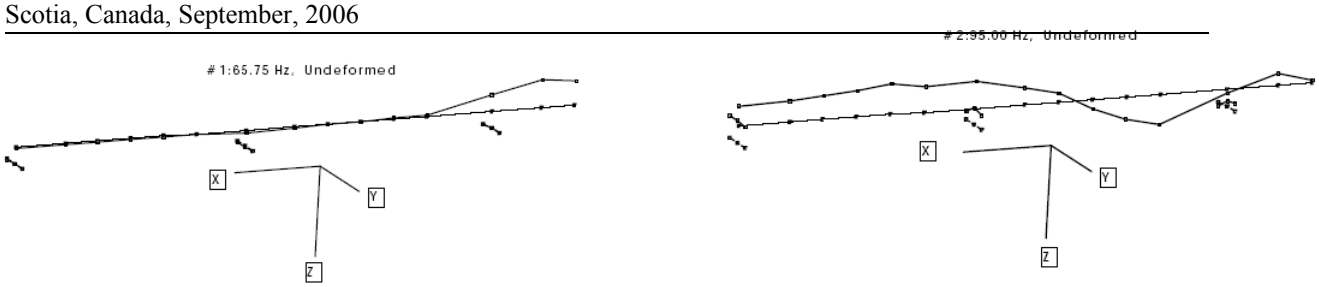

Figure 13 - Mode shapes of one centerbeam & support bars for hammer pulse excitation.

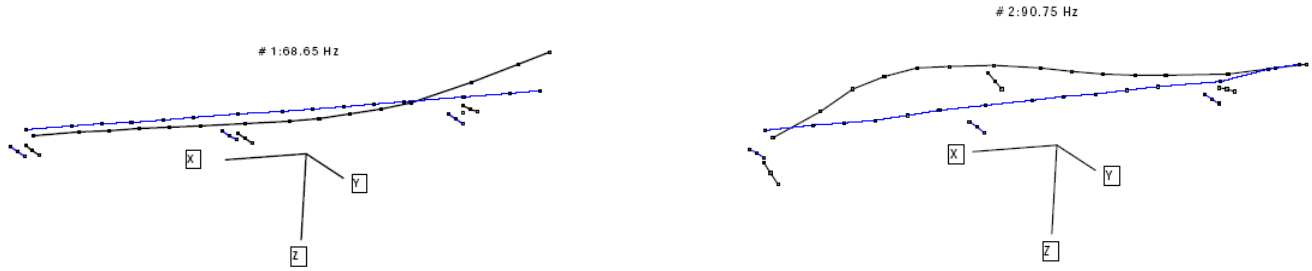

Figure 14 - - Mode shapes of one centerbeam & support bars for truck tire excitation.

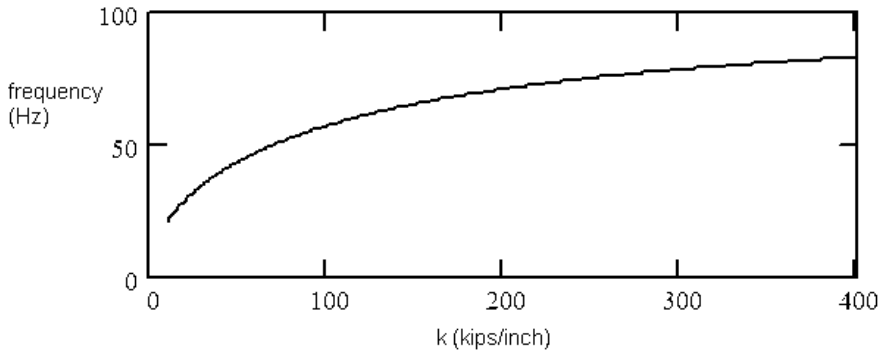

Figure 15 - Plot showing the vertical fundamental joint frequency versus bearing stiffness (Eq. 19)

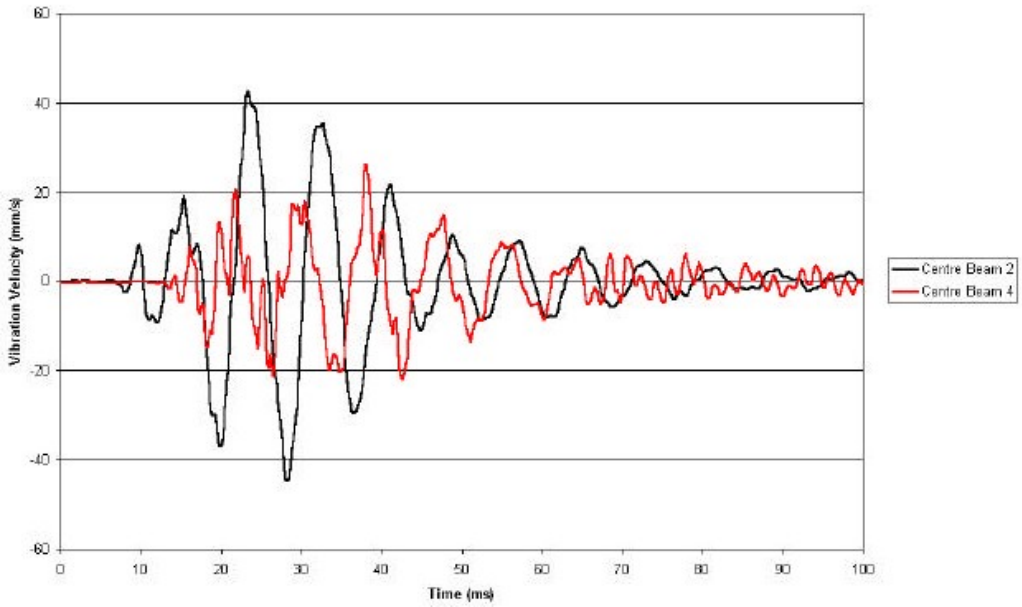

Figure 16 - Time domain plot characterizing centerbeam cross coupling

Appendix I

Ancich E.J., Forster G. and Bhavnagri V. (2006). Modular Bridge Expansion Joint Specifications and Load Testing, *Proc. 6th Austroads Bridge Conference*, Perth, WA, Australia.

AUSTROADS 6TH BRIDGE Conference

BRIDGING THE GAP

12-15 SEPT

06

PERTH
WESTERN
AUSTRALIA

Introduction

Austroads' Bridge Conferences are held every two years, bringing together professionals i engineering and management to further develop their knowledge and expertise.

The 6th Bridge Conference was held in 2006 and hosted by Main Roads Western Australia

Conference theme

The theme of the 2006 conference was on "Bridging the Gap" through knowledge, techno development as well as needs versus delivery across generations and communities.

The conference also investigated progress and future directions, both nationally and inter engineering and management and identify opportunities to contribute to the success of in

Government of Western Australia | MAIN ROADS Western Australia | Austroads | The University of Western Australia | online WA

Modular Bridge Expansion Joint Specifications and Load Testing

Eric Ancich, Greg Forster and Viraf Bhavnagri

Bridge Engineering, Roads & Traffic Authority of NSW

SYNOPSIS

The Roads and Traffic Authority of NSW (RTA) B316 specification covers the design, fabrication, testing, supply and installation of modular bridge expansion joints (MBEJs). It specifies dynamic analysis and testing of MBEJs and allows lower dynamic amplification factors (DAFs) for such analyses than for designs carried out using quasi-static analysis. RTA B316 specifies detailed checking of fatigue stress ranges for connections, which can be more critical than the main joint elements.

In this paper, features of the RTA B316 specification are compared to those of the AASHTO LRFD, German and Austrian specifications, using as case studies MBEJ designs submitted to RTA in tenders for its bridgeworks contracts. Analysis of the MBEJ in accordance with these four specifications showed that RTA B316 was the most demanding and the AASHTO LRFD specification was the least conservative.

One of the installed MBEJs was subsequently tested by running a truck over it at different speeds. The test results showed that the higher DAFs prescribed by the RTA specification are realistic. Where support bars rest on elastomeric bearings, it is critical to model the stiffnesses of the spring supports correctly as this significantly affects the bending moments in the centre beams.

INTRODUCTION

The Roads and Traffic Authority of NSW maintains all bridges on the classified road network in New South Wales, and has recently replaced deficient modular bridge expansion joints (MBEJs) on two sets of twin bridges (at Mooney Mooney Creek on the F3 Sydney-Newcastle Freeway and Pheasants Nest on the F5 South-Western Freeway) and installed new MBEJs on the Mooney Mooney Creek bridges and on four newly constructed bridges on the Karuah Bypass on the Pacific Highway. During this work the design and fabrication requirements for these joints were reviewed and the RTA's specification (RTA B316[1]) for the design, fabrication, testing, supply and installation of these joints was revised.

Strength, serviceability and fatigue limit state designs for bridge expansion joints must conform to the Australian Bridge Design Code[2] (AS 5100:2004), but RTA B316 specifies the design of MBEJ in greater detail.

Tenders were received from some international manufacturers for the supply of MBEJs on RTA bridges over Mooney Mooney Creek and on the Karuah Bypass recently.

The opportunity was taken to review the joint designs in accordance with the design codes of the countries from which the joints would be supplied and a comparative study of the code requirements made whilst considering revisions necessary to RTA B316.

These specifications were compared:

- RTA B316 (Draft Ed2/Rev0)[1]
- AASHTO LRFD, 2004[3]
- Austrian Guideline RVS 15.45[4]
- German Specification TL/TP-FÜ 92[5]

As the dynamic amplification factor (DAF) is one of the major unknowns in the behaviour of MBEJs (the current version of AS5100.4 specifies for MBEJs that this should be determined from specialist studies) this aspect has received special attention in RTA B316. To assess the DAF of the MBEJs installed on the Karuah Bypass bridges a load test was conducted. Salient test results are described in this paper, and have generally confirmed that the DAFs specified by the other specifications are on the low side whereas the values and procedures specified in RTA B316 for evaluating the DAF are justified.

In the quasi-static analyses commonly used for MBEJ design that model the centre beam spanning over the support bars, the results are factored by the DAF to obtain the design values. It is therefore important to model the continuous beam correctly. Where the support bars rest on elastomeric bearings, the stiffness of the supports has a significant effect on the bending moments in the centre beam. This is demonstrated by analysis of the MBEJ studied and compared with results of strain gauging during joint testing.

1 COMPARISON OF SPECIFICATIONS

Aspects of the specifications compared are given in Table 1. RTA B316 complies with AS5100 requirements where these aspects have been specified. Some comments on the compared aspects follow.

1.1 AXLE LOADS AND FATIGUE STRESS RANGES

The greatest discrepancy in the four specifications is in the axle loads and the associated load factors for strength and fatigue.

The factored axle loads for fatigue design vary widely but cannot be compared directly as the limiting fatigue stress ranges are different. To enable direct comparison, the studied MBEJ was analysed in accordance with the four specifications and the ratio of the calculated fatigue stress range to the limiting stress range (f^*_f / f_{lim}) compared.

The limiting stress range depends on the fatigue detail classification. This is not straightforward, as several of the connections in MBEJs cannot be readily classified in accordance with the fatigue detail categories given in AS 5100.6.

After consideration of several factors, the values of f_{lim} shown in Table 2 were arrived at and specified in RTA B316 to avoid different interpretations by different designers for tendered designs.

For multiple support bar systems, AASHTO LRFD specifies in considerable detail the design of the welded connection between the support bar and the centre beam. The stress at 2×10^6 cycles was used for comparison between the S-N curves of AASHTO and AS 5100.6.

A yoke connection which allows the centre beams to slide over the support bars is provided for the single support bar MBEJ studied. Stainless steel plates are welded to the centre beams and support bars on which PTFE surfaces slide. A system of elastomeric buffers which require cleat connections is used to maintain the centre beams at equidistant spacings. The fatigue stresses at the welded cleat connections can often be more critical than the main elements and requires careful consideration in design as well as fabrication. Most of the specifications do not adequately consider these details.

Table 1 - Comparison of Requirements of Different Specifications

ITEM	NOTATION	RTA B316	AASHTO LRFD	German TL/TP-FÜ	Austrian RVS 15.45
Specified axle load	W_x	160 kN	Strength:111kN Fatigue: 71 kN	200 kN	Strength:280kN Fatigue:130 kN
Factored axle load for strength design	W_{xu}	288 kN	194 kN	260 kN	280 kN
Factored axle load for fatigue design	W_{xf}	96 kN	53 kN	120 kN	130 kN
Fatigue stress range limit	f_{lim}	f_5	f_{TH} /2	$0.8f_3$	f_5
Joint opening for fatigue	J_f	Equation 1	$J_{s,avg}$	Not specified	Not specified
Distribution factor	β	$(B_c+g_c)/ L_w$	AASHTO Table 3.1	0.6	Tschemmerneg's
Dynamic Amplification Factor	χ_{up} χ_{dn} χ	$\chi_{up}=0.33\chi$ $\chi_{dn}=0.67\chi$ $\chi=0.67\chi_{mod}$	$\chi=1.75$	$\chi=1.4$	$\chi=1.4$
Longitudinal live load	H	0.35 W_x	0.2 χ W_x	0.25 W_x	Strength:$0.3\chi W$ Fatigue:$0.2\chi W_x$

1.2 DYNAMIC AMPLIFICATION

A significant difference between the specifications is the DAF defined as $\chi = 1 + \alpha$, where α is the dynamic load allowance in AS 5100. In RTA B316 the upward and downward components are specified separately, as only the downward component needs be considered for strength design whereas the overall stress range is considered for fatigue design. Where other specifications give a single DAF value (refer to Table 1), RTA B316 specifies that χ be determined from a dynamic modal analysis.

Three options are specified in RTA B316:

(i) Use the simplified design method in accordance with AASHTO LRFD, with $\chi = 2.0$ for multiple support bar systems and $\chi = 2.5$ for single support bar systems.

(ii) Perform an experimental modal analysis to determine χ_{mod}.

(iii) Perform dynamic analysis using a three-dimensional finite element model which has been previously calibrated by experimental modal analysis and strain gauge test data for a similar MBEJ to compute χ_{up} and χ_{dn}.

In RTA B316, quasi-static analysis is not ruled out but is penalised with a higher DAF value.

1.3 LONGITUDINAL LOADS

Longitudinal loads due to traction and braking are expressed as a factor (η) of the vertical loads. Measurements by Dexter ***et al***[6] indicate $\eta = 0.2$ in normal situations, increasing to $\eta = 0.35$ in locations where hard braking is expected. RTA B316 complies with the conservative value of 0.35 specified in AS 5100 for all situations. The DAF is not applied to the longitudinal loads because peaks due to transverse and vertical vibrations seldom occur simultaneously and transverse vibrations are quickly damped out.

1.4 JOINT OPENING

The joint opening affects the stresses in the support bars. AASHTO LRFD specifies an average joint opening for fatigue design whereas the German and Austrian specifications leave it unspecified. RTA B316 specifies that the joint opening for fatigue design (J_f) be given by

$$J_f = \sqrt[3]{\frac{1}{2}\left(J_{s,\min}^3 + J_{s,\max}^3\right)} \qquad (1)$$

where $J_{s,min}$ and $J_{s,max}$ are the minimum and maximum joint openings, respectively, for the serviceability limit state. Equation 1 is based on the concept that fatigue damage varies as the 3rd (to 5th) power of the stress whereas stress due to a concentrated wheel load varies linearly as the span.

Table 2 - Detail Classifications for Fatigue

Member or Connection	Detail	Refer Illustration in AS 5100.6	Detail Category f_{rn}	Cut off limit f_5 MPa
Centre beam or support bar	Polished steel bar		180	73
Flats for yokes	Rolled products	(1)	160	65
Centre beam at bolt hole for yoke	Bolted connection 8.8 / TF	(5)	140	57
Sliding plate welded to support bar	Cover plate, full weld both sides	(9)	125	51
Centre beam splice	Butt weld 100% NDT	(16)	112	45
Centre beam to support bar	Butt weld with extra fillets	(Type A, B or C cracking)	90	36
Yoke to centre beam	Transverse butt weld		90	36
Connections of yoke members	Shear stress in fillet welds	(39)	80	32
Sliding joint between centre beam and support bar	Longitudinal weld of Teflon disc housing to centre beam • intermittent • continuous	 (14) (9)	 80 125	 32 51
Attachment for spring buffer	Cleat attachments: • t ≤ 12 mm • t > 12 mm	 (35) (36)	 80 71	 32 29

1.5 DISTRIBUTION FACTOR

The wheel load (W_x) is generally applied to more than one centre beam and the maximum load on one centre beam (W_{1x}) is given by

$$W_{1x} = \beta W_x \qquad (2)$$

where β is defined as the "Distribution Factor". In RTA B316 this is given by

$$\beta = \frac{B_c + g_c}{L_w} \qquad 0.5 \leq \beta \leq 0.8 \qquad (3)$$

where

B_c = width of centre beam at top

g_c = gap between centre beams at appropriate joint opening

L_w = length of tyre footprint in direction parallel to traffic

There is considerable uncertainty in the assessment of the distribution factor and apart from the proposed formula, which is based on the concept of tributary area, other methods have been proposed by Dexter *et al*[6], who compared these with those of Tschemmernegg[7]. A comparison of the different methods was made by

Ancich & Bhavnagri[8] and they justified adoption of the above formula. An upper limit of 0.8 and a lower limit of 0.5 are applied to β as recommended by Dexter *et al*.

1.6 TYPICAL EXAMPLE

The MBEJ proposed for the Mooney Mooney Creek was analysed to compare the four specifications, and the results are summarised in Table 3. Generally the stress ratios are highest for RTA B316 and lowest for AASHTO LRFD, implying that RTA B316 is the most conservative and AASHTO LRFD the least conservative of the specifications compared.

Table 3 - Results for Example

ELEMENT	ITEM	NOTA-TION	Design by RTA B316	Design by Austrian Specs	Design by German Specs	Design by AASHTO LRFD
Centre beam	Maximum stress due to fatigue	f^*_f	70	66	58	29
	Limiting stress due to fatigue	f_{lim}	73	73	106	83
	Fatigue stress ratio	f^*_f / f_{lim}	**0.96**	**0.90**	**0.55**	**0.35**
Support Bar	Maximum stress due to fatigue	f^*_f	39	36	33	16
	Limiting stress due to fatigue	f_{lim}	73	73	106	83
	Stress ratio	f^*_f / f_{lim}	**0.53**	**0.49**	**0.31**	**0.19**
Welded connections	Longitudinal weld of PTFE disc housing to centre beam	f^*_f / f_{lim}	**1.33**	**1.04**	0.65	0.40
	Welding of yoke vertical to centre beam	f^*_f / f_{lim}	**1.23**	0.94	0.60	0.48
	Attachments for control spring buffers	f^*_f / f_{lim}	**1.39**	**1.02**	0.68	0.47

2 LOAD TESTING

An experimental modal analysis study[9] [10] (EMA) was undertaken to better understand the structural dynamics behaviour of the Karuah River MBEJ. The EMA measurement provides definition of the natural frequencies and mode shapes of a structure and allows an estimate of the energy involved in each mode. The modal analysis data were used to optimize the placement of strain gauges as part of the

fatigue life assessment of the Karuah River MBEJ[11]. Figure 1 presents a plan view diagram of the southbound kerbside lane showing the six strain gauge locations (SG1 to SG6). All gauges were the linear type and orientated in the anticipated principal stress direction (i.e. parallel to the long axis of the respective structural elements). The instrumentation was selected with a data sampling rate of 25 kHz, sufficient to ensure that frequencies up to 10 kHz were accurately sampled.

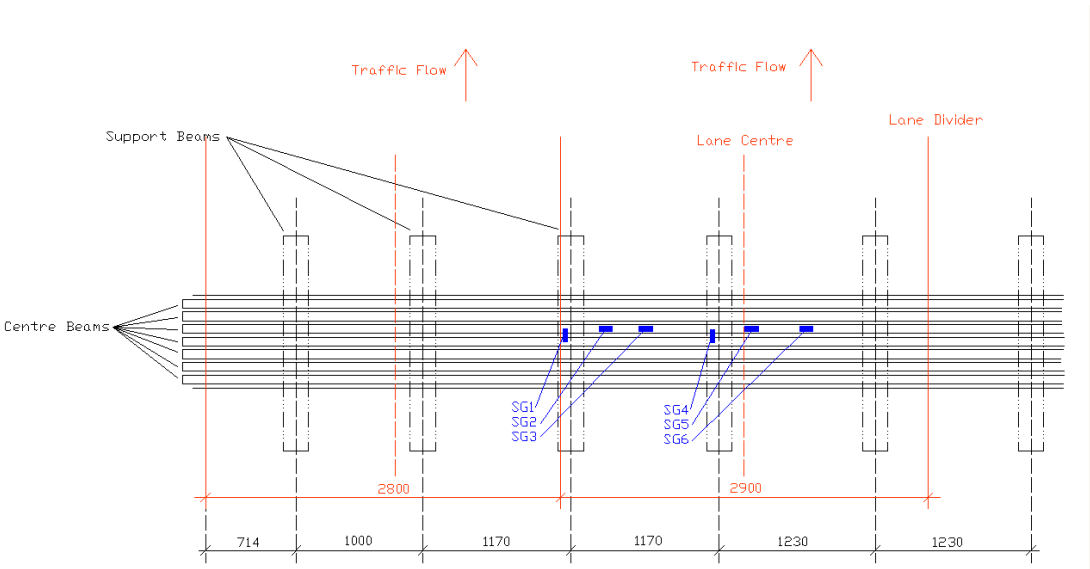

Figure 1 - Plan View Southbound Kerbside Lane - Six Strain Gauge Locations (SG1 to SG6)

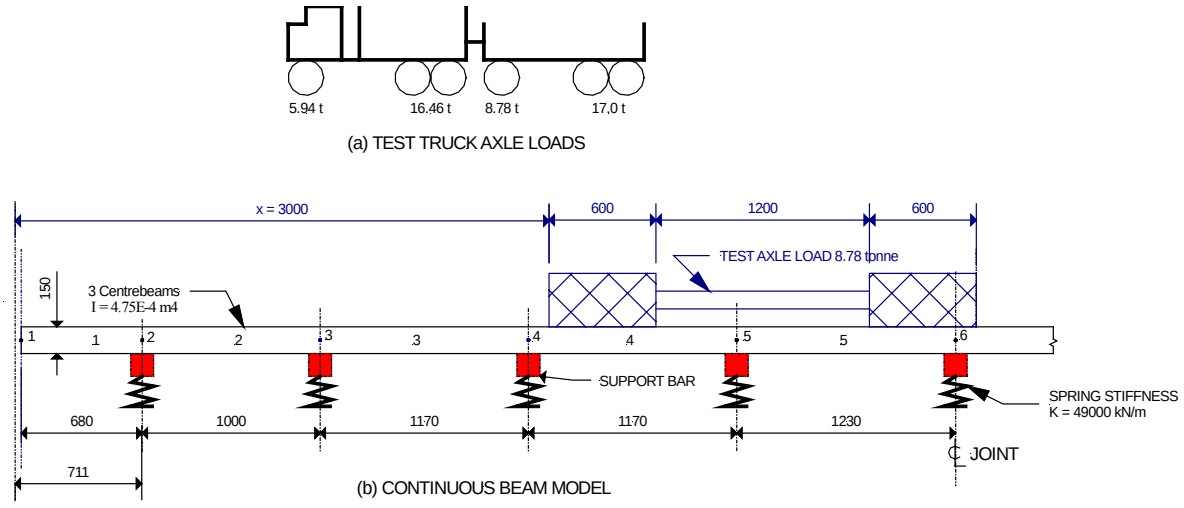

Figure 2 - Centre beam and Truck Used for the Load Test

Figure 3 shows the test vehicle used for the tests, with axle loads as shown in Fig.2a. The test truck was loaded to the maximum Australian legal axle load with a gross vehicle mass of 42 tonnes. Figure 2b shows the continuous beam model used for the analyses with the axle in the test position.

To approximate true static strains and displacements, the truck was made to traverse the MBEJ at less than 3 km/hr to produce negligible dynamic response of the truck or structure, with all static and dynamic strains and displacements recorded. As closely as possible to the same line as the slow roll test, the truck traversed the MBEJ at several speeds in the target speed range of 26 km/hr to 104 km/hr with actual truck pass-by speeds measured using a laser speed gun. The reproducible accuracy of the vehicle speed measurement is better than ± 2 km/hr. Figure 3 shows the test truck positioned on the joint.

Figure 3 - Test Truck in Position on the Joint

Figure 4 - Tracking Check Paste

As the position of the test vehicle on the joint was critical for the reliability and reproducibility of the test results, a procedure was developed using a bead of water dispersible toothpaste on the top surface of the first centre beam to mark the vehicle passage and Figure 4 shows a typical application. Vehicle speeds were chosen to closely match the beam pass and tyre pulse frequencies[9] to the experimentally determined modes for the centre beam spacing at the time of testing.

2.1 STATIC LOAD TEST AND ANALYSIS

The static analysis of the centre beam using continuous beam theory was compared with the slow roll test results for Runs 1, 2 and 3.

The centre beam was modelled using a stiffness equivalent to that of 3 centre beams. The axle load analysed is the fourth axle of the truck, placed at an average distance of 3.0 m from the end, as shown in Figure 2b.

Two models were analysed:

(a) Continuous beam on rigid supports.

(b) Continuous beam on elastic supports. The spring stiffness of each support (49 kN/mm) is based on the combined stiffnesses of the elastomeric bearings supporting both ends of each support bar. Bearing stiffnesses were given by the supplier and were not evaluated during the load test.

Results are compared using the bending moments computed from the strain gauge measurements and plotting the values on the bending moment diagrams obtained from the static analysis. The bending moment based on the strain gauge measurement (M_g) is given by

$$M_g = \varepsilon E Z / \beta \qquad (4)$$

where

ε = measured strain

E = modulus of elasticity, assumed = 200,000 MPa

Z = section modulus of the centre beam

β = distribution factor

The distribution factor was not measured accurately, as this required simultaneous measurements on 3 adjacent centre beams and accurate measurements of the gap width and tyre contact length, which was not done. In accordance with AASHTO LRFD, for a top width of centre beam of 64 mm, β = 0.5 was used in Equation 4.

The bending moment diagrams obtained for Cases (a) and (b) differ very significantly, as shown in Figure 5 and neither result appears to fit the observations well. A possible reason may be that the support bar bearings do not function as expected. By arbitrarily increasing the stiffnesses of Supports 4 and 5 to 300 MN/m and factoring the bending moments by 1.4, a closer fit to the observations can be

achieved, as indicated by Curve (c) in Figure 3. The 1.4 factor is probably due to the distribution factor being higher than 0.5 assumed and some impact effect being experienced even at slow roll.

This test was primarily aimed at assessing dynamic amplification factors and the lack of correlation with static analysis does not affect the stress ratios at different speeds on the same gauges. It is obvious from this study that the aspect of elastic *vs* rigid supports deserves greater attention, as the DAFs are usually applied to the results of static analysis. The worked examples by Dexter *et al*[6] are based on rigid supports but significant errors could result from neglecting the elasticity of the supports.

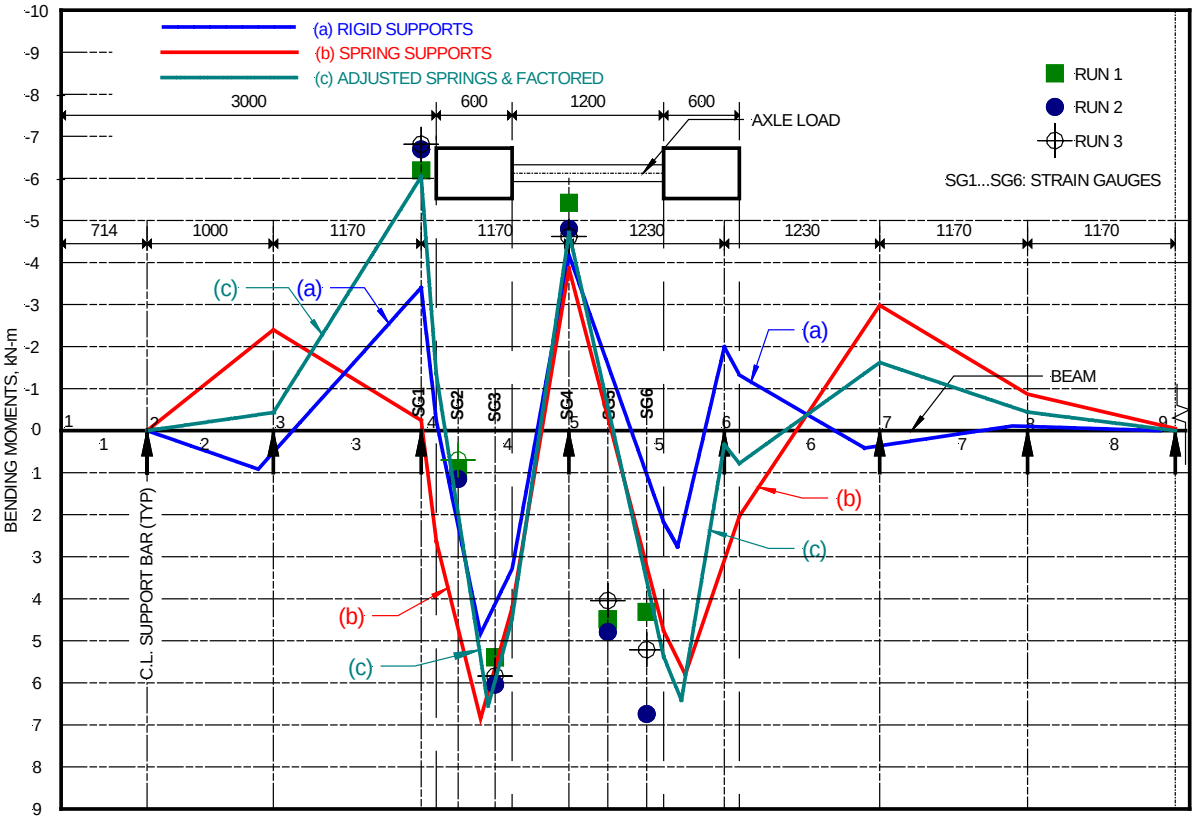

Figure 5 – Bending Moment Diagrams based on Static Analysis

2.2 DYNAMIC AMPLIFICATION MEASUREMENTS

The results of strain gauge testing are shown in Table 4. It is interesting to note that the peak DAF shown in Table 4 is 3.2. For this table, the DAF is defined as

$$\text{DAF} = \frac{\varepsilon_{\text{dyn}}}{\varepsilon_{stat}} \qquad (5)$$

where

DAF = dynamic amplification factor,

ε_{dyn} = Strain range due to the vehicle travelling at designated speed (peak-to-peak)

ε_{stat} = Strain range due to vehicle travelling at crawl (slow roll) speed (zero-to-peak).

Table 4 - Summary of Resulting Strains, Stresses and Dynamic Amplification Factors for Centre beam at SG5 (after Brown[11])

Test Truck Passby Speed	Trans-ducer Location	Strain and Stress								
		Strain (micro strain)			Stress (MPa)			Dynamic Amplification Factors χ_{mod}		
		Maximum Tensile	Maximum Compre-ssive	Peak to Peak	Maximum Tensile	Maximum Compre-ssive	Peak to Peak	Maximum Tensile	Maximum Compre-ssive	Peak to Peak
Slow Roll-1	SG5	55	-2	57	11	0	11	0	0	0
Slow Roll-2	SG5	58	0	58	12	0	12	0	0	0
Slow Roll-3	SG5	56	0	56	11	0	11	0	0	0
26 km/h	SG5	46	-2	44	9	0	9	0.8	-0.1	0.9
29 km/h	SG5	47	-2	47	9	0	9	0.9	-0.1	1.0
41 km/h	SG5	67	-5	69	13	-1	14	1.2	-0.2	1.3
51 km/h	SG5	74	-6	80	15	-1	16	1.4	-0.3	1.5
69 km/h	SG5	94	-7	100	19	-1	20	1.7	-0.3	1.8
80 km/h	SG5	112	-20	133	22	-4	27	2.1	-0.4	2.4
82 km/h	SG5	112	-26	139	22	-5	28	2.1	-0.5	2.5
88 km/h	SG5	119	-30	149	24	-6	30	2.2	-0.6	2.7
89 km/h	SG5	124	-29	153	25	-6	31	2.2	-0.5	2.7
92 km/h	SG5	116	-34	148	23	-7	30	2.0	-0.6	2.6
93 km/h	SG5	75	-9	80	15	-2	16	1.4	-0.3	1.5
104 km/h	SG5	133	-45	179	27	-9	36	2.4	-0.8	3.2
Maximum	**SG5**	**133**	**-45**	**179**	**27**	**-9**	**36**	**2.4**	**-0.8**	**3.2**

A DAF of 3.2 is significantly higher than any current bridge design code requirements, except RTA B316. It is recommended that designers use 80% of the peak empirical DAF to approximate Method (iii) of RTA B316. For the Karuah Bypass MBEJ, this would equate to a design DAF of 2.56 and the design calculations for this joint used a DAF of 2.5. The sensitivity of the tested joint to dynamic effects is well demonstrated in Table 4. At a vehicle speed of 92 km/h, we see a DAF of 2.6, whereas at a speed of 93 km/h, the DAF is only 1.5.

CONCLUSION

The Roads and Traffic Authority of NSW has recently revised its specification RTA B316 for the design, fabrication, testing, supply and installation of modular bridge expansion joints (MBEJs). Comparisons were made during the revision with the AASHTO LRFD, German and Austrian specifications. Salient aspects of all four specifications are briefly compared in this paper. The RTA B316 specification is the

most conservative whereas the AASHTO LRFD specification is the least conservative.

Dynamic load testing conducted by the RTA on the MBEJ treated in this paper and on other MBEJs indicates that the higher dynamic amplification factors specified in RTA B316 are justified.

The Mooney Mooney Creek MBEJ studied indicates that fatigue stresses at welded connections and details could be more critical than for the main elements. RTA B316 requires analysis of all MBEJ details and specifies limiting fatigue stress ranges for typical connections.

A dynamic load test was conducted on an MBEJ installed for the Karuah Bypass, which is very similar to the one analysed for Mooney Mooney Creek. The test demonstrated that high DAF values obtained are close to those required by RTA B316 and are substantially greater than those specified by the other specifications compared. Although the peak values of DAF used for design may be discounted to 80% of the measured values for fatigue design, factoring down the axle loads as well as the DAF may result in designs prone to fatigue failure.

Static analysis of the load tested centre beam indicates that continuous beam analyses of centre beams assuming rigid supports could yield significant errors if the supports are elastic. Elasticity of the supports for a single support bar system is due to the support bars resting on elastomeric bearings.

It is considered that the conservatism in MBEJ designs conforming to the RTA B316 specification is justified considering the enormous cost of replacing failed MBEJs compared to the marginal increase in costs of MBEJs supplied with larger sized elements and higher quality fabrication.

ACKNOWLEDGEMENT

The authors wish to thank the Chief Executive of the Roads and Traffic Authority NSW for permission to publish this paper. The opinions and conclusions expressed in this paper do not necessarily reflect the views of the RTA.

REFERENCES

1. Roads & Traffic Authority of NSW., *RTA QA Specification B316 – Modular Bridge Expansion Joints Ed2/Rev0,* Sydney, Australia, December 2004.

2. Standards Australia, *Australian Standard AS5100 – 2004, Part 2: Design loads, Part 4: Bearings and deck joints, Part 6: Steel and composite construction*, Sydney, Australia, 2004

3. American Association of State Highway and Transportation Officials (AASHTO) *AASHTO LRFD Bridge Design Specifications, SI Units*, 3rd Ed., Washington, DC, USA, 2004.

4. "Expansion Joints for Bridges", *Austrian Guideline RVS 15.45, Draft, version 1*, Vienna, Austria, 1999.

5. TL/TP-FÜ 92, "Technical delivery and inspection specifications for watertight expansion joints of road and foot bridges", *Federal Ministry of Transport (BMV), Bonn, Germany, 1992.* Non-revised translation (draft 1), provided by the German Association of Joint and Bearing Manufacturers [Vereinigung der Hersteller von Fahrbahnübergängen und (Brücken) Lagern].

6. DEXTER R.J., CONNOR R.J. & KACZINSKI M.R., "Fatigue Design of Modular Bridge Expansion Joints", *NCHRP Report 402,* Transportation Research Board, National Research Council, Washington, DC, USA, 1997, 128 pp.

7. TSCHEMMERNEGG F., "The Design of Modular Expansion Joints", *Proc. 3rd World Congress on Joint Sealing and Bearing Systems for Concrete Structures (Toronto, Canada)*, American Concrete Institute, Detroit, Michigan, USA, 67-86, 1991.

8. ANCICH E.J., & BHAVNAGRI V.S., "A Case Study Comparison of Fatigue in Modular Bridge Expansion Joints Using Multiple Bridge Design Code Approaches and Empirical Data", *Proc. 6th World Congress on Joints, Bearings & Seismic Systems for Concrete Structures*, Halifax, Nova Scotia, Canada, 2006.

9. ANCICH E.J., BROWN S.C. & CHIRGWIN G.J., "The Role of Modular Bridge Expansion Joint Vibration in Environmental Noise Emissions and Joint Fatigue Failure", *Proc. Acoustics 2004 Conference*, Surfers Paradise, Qld, Australia, 2004, pp 135-140.

10. EWINS D.J., "Modal Testing: Theory, Practice & Application (2nd Edition)", *Research Studies Press*, Hertfordshire, UK, 1999, pp.163-276.

11. BROWN S.C., "Measurement of Static and Dynamic Strains: Karuah Bypass Bridge, Karuah NSW Modular Expansion Joint", *Report 10-1788-R20*, Richard Heggie Associates Pty Ltd (now Heggies Australia Pty Ltd), Lane Cove, NSW, Australia, 2005 (Unpublished report prepared for the Roads & Traffic Authority of NSW).

Appendix J

Ancich E.J., Chirgwin G.J. and Brown S.C. (2006). Dynamic Anomalies in a Modular Bridge Expansion Joint, *Journal of Bridge Engineering*, Vol. 11, No. 5, 541-554 (With permission from ASCE).

ASCE
American Society of Civil Engineers

September / October 2006
Volume 11, Number 5

ISSN 1084-0702
CODEN: JBENF2

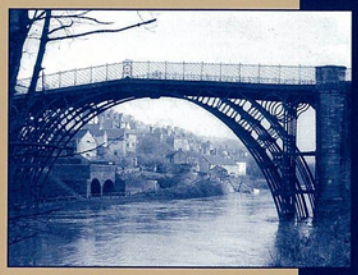

Journal of Bridge Engineering

contents continue on back cover

SEI
Technical Activities Division of the Structural Engineering Institute

Dynamic Anomalies in a Modular Bridge Expansion Joint

Eric J. Ancich[1]; Gordon J. Chirgwin[2]; and Stephen C. Brown[3]

Abstract: Environmental noise complaints from homeowners near bridges with modular bridge expansion joints (MBEJs) led to an engineering investigation into the noise production mechanism. The investigation identified modal vibration frequencies in the MBEJ coupling with acoustic resonances in the chamber cast into the bridge abutment below the MBEJ. This initial acoustic investigation was soon overtaken by observations of fatigue induced cracking in structural beams transverse to the direction of traffic. These beams are, in the English-speaking world, universally referred to as center beams. However, in Europe the term *lamellae* is equally common. A literature search revealed little to describe the structural dynamics behavior of MBEJs but showed that there was an accepted belief dating from around 1973 that the loading was dynamic. In spite of this knowledge many bridge design codes used throughout the world specify a static or quasi-static load case with no mention of the dynamic behavior. This paper identifies the natural modes and operational response modes of vibration of the MBEJ installed into Sydney's Anzac Bridge. In addition, the paper will introduce the dynamic range factor (DRF) and report a DRF of 4.6 obtained after extensive static and dynamic strain gage measurements. The studies indicated that the Anzac Bridge MBEJ was very lightly damped (<2% of critical) and a reduction in the measured DRF through the introduction of additional damping was an option.

DOI: 10.1061/(ASCE)1084-0702(2006)11:5(541)

CE Database subject headings: Australia; Absorption; Acoustics; Bridge decks; Bridges; cable; Damping; Joints; Modal analysis.

Introduction

While the use of expansion joints is common practice in bridge construction, modular bridge expansion joints (MBEJs) are designed to accommodate large longitudinal expansion and contraction movements of bridge superstructures. In addition to supporting wheel loads, a properly designed modular joint will prevent rainwater and road debris from entering into the underlying superstructure and substructure. Modular bridge expansion joints are subjected to more load cycles than other superstructure elements, but the load types, magnitudes, and fatigue–stress ranges that are applied to these joints are not well defined (Dexter et al. 1997).

MBEJs are considered to be the most modern design of waterproof bridge expansion joint currently available. The basic joint design appears to have been patented around 1960, but the original patent has now expired and approximately one dozen manufacturers now exist throughout the world.

Sydney's Anzac Bridge was opened to traffic on December 4, 1995. The name Anzac is an acronym derived from Australian and New Zealand Army Corps, and it was by this name that Australian troops participating in the First World War were known. The Anzac Bridge is a cable-stayed bridge spanning a portion of Sydney Harbor on the western approach to the central business district and is of reinforced concrete construction carrying seven lanes of traffic and a combined pedestrian/bicycle way.

The 805-m-long concrete structure comprises six spans with three cable-stayed central spans. With a main span of 345 m, the bridge is the longest span cable-stayed bridge in Australia. There are two MBEJs installed into Anzac Bridge. A small three-seal joint is located in the deck (Pier 1) and a larger nine-seal joint is located in the western abutment. The structural dynamics studies reported here relate to this latter joint.

Description of Modular Bridge Expansion Joints

MBEJs are generally described as single- or multiple-support bar designs. In the *single*-support bar design, the support bar (beam

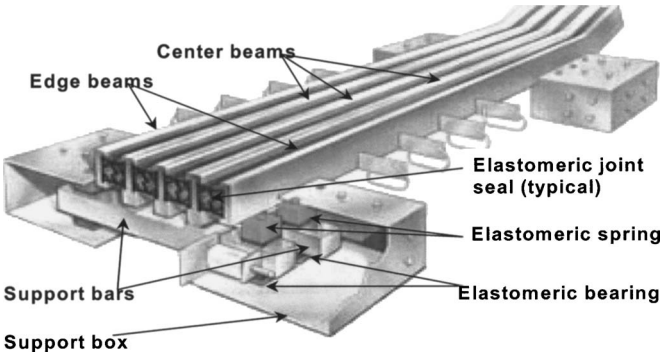

Fig. 1. Example of a multiple-support bar MBEJ system

[1]Senior Project Engineer, Bridge Technology Section, Roads and Traffic Authority of NSW, PO Box 558, Blacktown 2148, Australia. E-mail: Eric_Ancich@rta.nsw.gov.au

[2]Manager, Bridge Policies Standards & Records, Roads and Traffic Authority of NSW, PO Box 558, Blacktown 2148, Australia. E-mail: Gordon_Chirgwin@rta.nsw.gov.au

[3]Associate, Heggies Australia Pty Ltd, PO Box 176, Lane Cove 1595, Australia. E-mail: steve.brown@heggies.com.au

Note. Discussion open until February 1, 2007. Separate discussions must be submitted for individual papers. To extend the closing date by one month, a written request must be filed with the ASCE Managing Editor. The manuscript for this paper was submitted for review and possible publication on October 28, 2003; approved on June 14, 2005. This paper is part of the ***Journal of Bridge Engineering***, Vol. 11, No. 5, September 1, 2006. ©ASCE, ISSN 1084-0702/2006/5-541–554/$25.00.

Fig. 2. View of Anzac Bridge MBEJ, western abutment

parallel to the direction of traffic) supports all the center beams (beams transverse to the direction of traffic). In the *multiple*-support bar design, multiple support bars individually support each center beam. Fig. 1 shows a typical welded multiple support bar MBEJ.

The MBEJ installed into the western abutment of Anzac Bridge is a hybrid design having pairs of support bars in series across the full width of the joint. Each pair of support bars is attached to alternate groups of four center beams [i.e., center beams 1, 3, 5, and 7 are attached to support bar 1 (and the other odd numbered support bars) and center beams 2, 4, 6, and 8 are attached to support bar 2 (and the other even numbered support bars)] The support bar pairs are spaced at 2.25 m centers across the full width of the bridge, resulting in a total of 24 support bars (2×12).

MBEJs typically employ mechanisms to maintain equidistant center beam spacing over the full range of joint movement.

Equidistant devices include elastomeric springs and mechanical linkages such as pantographs or the so-called "*lazy tong*." The MBEJ installed into the western abutment of Anzac Bridge employs a mechanical linkage system and the sliding yokes welded to the soffit of each center beam are clearly visible in Fig. 2. The principal components of the mechanical linkage system are also to be seen in Fig. 3.

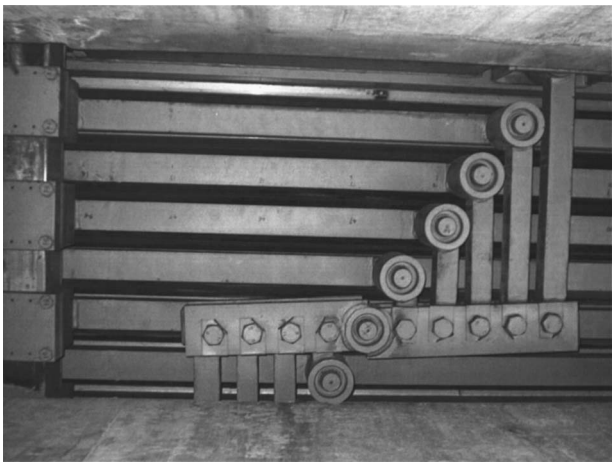

Fig. 3. View of underside of Anzac Bridge modular joint

Structural Dynamics Studies

Initial Noise Investigation

There was anecdotal evidence from environmental noise nuisance complaints received by the Roads & Traffic Authority (RTA) of New South Wales (NSW) that the sound produced by the impact of a motor vehicle tire with MBEJs was audible up to 500 m from a bridge in a semirural environment. This observation suggested that the noise generation mechanism involved possibly both parts of the bridge structure and the joint itself as it is unlikely that there is sufficient acoustic power in the simple tire impact to explain the persistence of the noise in the surrounding environment. Vibration measurements during the initial environmental noise investigation indicated that most of the measured vibration

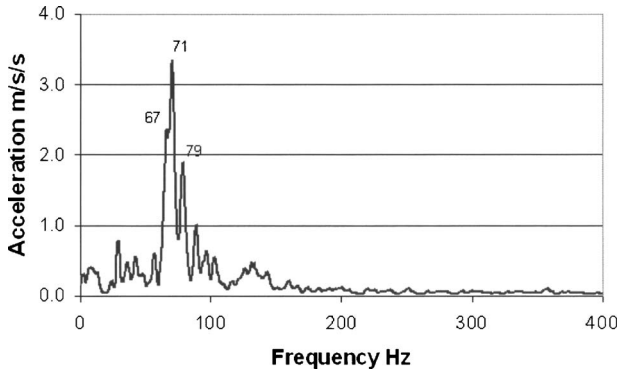

Fig. 4. Center beam vibration spectrum, Anzac Bridge

Table 1. Calculated and Measured Natural Frequencies

Measured frequency (Hz)	Calculated frequency (Hz)[a]	Calculated vibration mode[b]
41	35	Horizontal (1)
65	—[c]	—[c]
71	—[c]	—[c]
84	91, 96, 99	Vertical (2 and 3), Horizontal (4)
122	103, 108, 111, 119, 119, 124	Horizontal (5), Vertical (6), Horizontal (7), Vertical (8), Horizontal (9), Vertical (10)
189	—[c]	—[c]

[a]Calculated frequencies are considered correct ±10% due to assumption uncertainties.

[b]As the precise boundary conditions for the Anzac Bridge joint were not known, some assumptions were made. The mode numbers associated with the various frequencies reflect the range of assumptions. Bracketed numbers following mode type refer to the calculated mode number.

[c]Not identified.

was in a narrow range of frequencies between 50 and 120 Hz, with a pronounced peak at 71 Hz. An FFT frequency spectrum is presented as Fig. 4.

In order to identify the possible sources for these frequencies, simple natural frequency calculations (using Microstran®) were undertaken and Table 1 shows the measured and calculated vibration frequencies.

In addition, acceleration measurements were undertaken on a support bar, adjacent to the bearing locations. These measurements indicated that acceleration levels were of the order of 3 g.

Experimental Modal Analysis

During the first few years of operation of the Anzac Bridge, the fractured remains of a number of the lower antifriction bearings from the MBEJ were observed on the floor of the western abutment void space. Generic design examples are shown as *elastomeric bearings* in Fig. 1. The absence of these lower antifriction bearings, which were discovered during a routine inspection, would cause bending moments in the supported center beams to be at least doubled due to the increased unsupported span. It was considered that the simple replacement of the failed components would not identify the failure mechanism or assist with a remaining fatigue life assessment. Clearly, an engineering investigation was necessary. There was little in the published literature to describe the structural dynamics behavior of MBEJs; however, Ostermann (1991) reported the theoretical and practical dynamic response of an MBEJ, and Roeder (1993) reported the results of an analytical modal analysis study (FEM) of a swivel joist design MBEJ. Roeder noted that "*the modes were closely spaced, and many hundreds would be needed to include the predominate portion of the mass in three-dimensional vibration*." However, this observation is considered to only apply to the swivel joist design.

Earlier, Köster (1986) had set out the principal dynamic aspects of good design and argued against the prevailing static design philosophy, stating: "*Static calculations often lead to contrary solutions when trying to reach a higher level of security for a bridge by assuming fictitious and higher loads. The reason is that stiffer constructions are less elastic which causes them to react harder to wheel impacts than an elastic construction would*." Subsequent researchers (Tschemmernegg 1973, 1991; Agarwal 1991; Roeder 1995; Dexter et al. 1997; Crocetti 2001; Crocetti and Edlund 2001) have repeatedly noted that the loading was dynamic in spite of many bridge design codes used throughout the world still specifying a static or quasi-static load case. The possibility of premature fatigue failure in MBEJs was clearly identified by Dexter et al. (1997) and observations of fatigue cracking in the MBEJ at Pheasant's Nest Bridge (built 1980) on the Hume Highway (State Highway 2) linking Sydney and Melbourne confirmed the U.S. study. Roeder (1993) noted that the dynamic response of MBEJs was complex and field measurements of the dynamic response would assist in evaluating the dynamic behavior. Accordingly, an experimental modal analysis study was undertaken (Ewins 1999) to gain a better understanding of the structural dynamics behavior of the critical Anzac MBEJ.

Experimental Modal Analysis Test Procedure

The measurement and definition of the natural frequencies and mode shapes of a structure is referred to as experimental modal analysis. These measurements involved the simultaneous measurement of input force and vibration response. In these tests, force over the frequency range of interest was imparted to the structure using a force hammer.

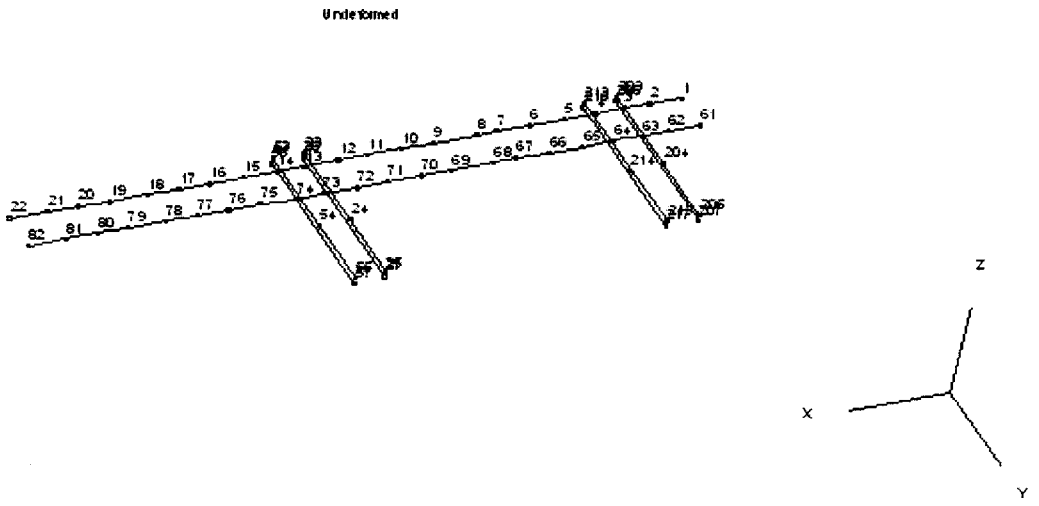

Fig. 5. Undeformed line diagram of structure

Table 2. Summary of Modal Frequencies and Damping (Percentage of Critical)

Mode Number	Mode Type	Center Frequency (Hz)	Damping (%)
1	Whole body bounce	71	1.7
2	1st bending	85	1.3
3a	2nd bending	91	1.4
3b	Similar to Mode 3	97	1.3
4	3rd bending	119	1.1
5	4th bending	126	2.1

The vibration response was measured at selected locations using accelerometers attached to the structure by a magnetic base. The input force and vibration response at each location was simultaneously measured using the two-channel fast Fourier transform (FFT) analyzer. Frequency response functions (FRFs) for each measurement were stored on the hard disk drive of a personal computer. This type of modal test is referred to as a fixed excitation test as the force is input at the same location for all measurements.

Extraction of Modal Parameters

This step in the modal analysis process is to reduce the large amount of data (FRF measurements) and produce the more important modal parameters [i.e., natural frequencies (eigenvalues), damping (% of critical), and mode shapes (eigenvectors)]. This was achieved by processing the FRF measurements with modal analysis software (SMS STARStruct®).

The stages in this process were:

- Identify natural modes; and
- Curve fit FRF measurements and produce modal parameters (frequency and damping tables, mode shape tables).

Animate and Display Mode Shapes

Animation and display of mode shapes was achieved again within the modal software by entering the three-dimensional coordinates of all measurement points to produce a line drawing of the structure (see **Experimental Modal Analysis Results**). The resulting residues were superimposed on the line drawing of the test specimen and animated for viewing.

Measurement Locations

A total of 90 measurement locations were selected on center beam 2, center beam 3, and center beam 4 of the joint, beginning on the LHS of each center beam and extending to the third support bar. Additional locations were also selected on the first four support bars. Fig. 5 shows the undeformed line diagram of center beams 2, 3, and 4, as well as the measurement point numbers and coordinate system.

Measurement Procedure

Vibration measurements were recorded at a fixed *reference* location (8z) and varying *roving* locations in the *x*-, *y*-, and *z*-axes. These recordings were later analyzed to produce frequency response (transfer) functions for each measured location and degree of freedom. The SMS STARStruct® modal analysis software was subsequently used to extract the mode shapes at the dominant modal frequencies.

Table 3. Comparison of Natural and Operational Response Modal Frequencies

Mode number	Natural modes (Hz)	Operational response modes (Hz)
1	71	71
2	85	85
3a	91	91
3b	97	—[a]
4	119	119
5	126	127

[a]Not identified.

Experimental Modal Analysis Results

This study identified the major natural modal frequencies (all lightly damped) and, importantly, provided an insight into the source of the previously unidentified dominant frequency at 71 Hz observed during the initial noise investigation. The vibrational modes identified include a translational (bounce/bending) mode where all parts of the MBEJ are vibrating in phase at the same frequency and vertical bending modes for the center beams where the first three bending modes are strongly excited.

Roeder (1993) reports theoretical translational modes and Ostermann (1991) shows an analytically determined (FEM) vertical mode at 87 Hz that exhibits elements of the whole body (bounce/bending) mode. Table 2 presents a summary of the resulting frequency and associated damping for each natural mode identified. Fig. 6 shows sample plots depicting the characteristic shape of mode 1 at 71 Hz. Mode 1 was characterized by in-phase displacement of all structural beams. This translational mode is best described as fundamental bounce of the MBEJ on the linear bearing pads. Significant bending of the center beams and support bars is also evident. Mode 2 at 85 Hz was defined as the first vertical bending mode of center beams. Mode 3a at 91 Hz is the second bending mode of center beams. Mode 3b at 97 Hz is similar to mode 3. Mode 4 at 119 Hz is the third bending mode of center beams. Mode 5 at 125 Hz is the fourth bending mode of center beams.

It is particularly interesting to note that the translational mode and the first center beam bending mode are predominantly excited by typical traffic flow. Furthermore, Table 3 confirms that typical traffic across the MBEJ excites the joint at the identified natural modes.

Response Shape Analysis (Ambient Traffic Excitation)

Response shape analysis is a measurement and analysis technique that enables the dynamic response or deflection shape at particular frequencies of interest to be defined. Response shape analysis differs from true experimental modal analysis as an input force is not applied and measured in a controlled manner, but rather supplied by the actual forces due to normal operation of the structure—in this case the input force is supplied by the passage of vehicles over the expansion joint. In all other respects, the analysis method, instrumentation, and transducer locations are the same as for the experimental modal analysis. Table 3 presents a comparison between the natural and operational response modes.

Resulting Response Shapes

The identified operational response mode shapes were characterized as follows:

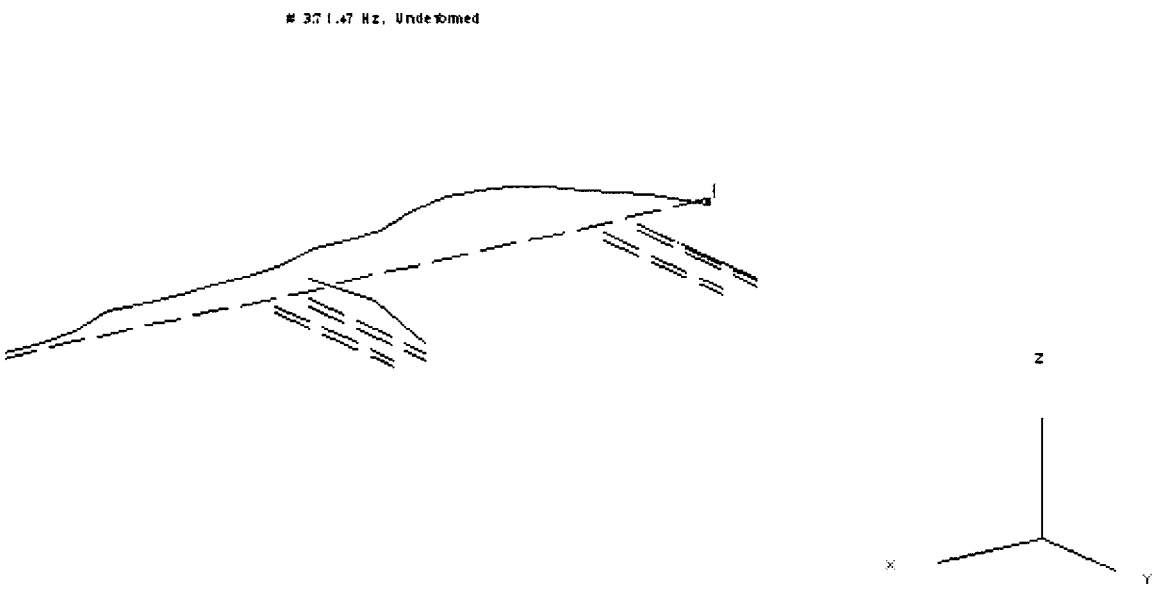

Fig. 6. Mode 1 at 71 Hz

- Mode 1 at 71 Hz: fundamental bounce/bending mode of the MBEJ
- Mode 2 at 85 Hz: fundamental bending mode of center beams
- Mode 3 at 91 Hz: second bending mode of center beams
- Mode 4 at 119 Hz: third bending mode of center beams
- Mode 5 at 126 Hz: fourth bending mode of center beams

Discussion of Operational Response Shapes

The operational response shape results revealed poor correlation of the response of center beam 2 and center beam 3 (i.e., indicative of relatively lightly coupled modes of vibration). The response of center beam 2 and center beam 4 showed good correlation, indicative of more highly coupled modes. The difference in coupling effects is explained by the relation of each center beam to the respective support bar. Center beams 2 and 4 (even beam numbers) share the same support bars, while odd center beam numbers share different support bars. It was concluded that the dynamic behavior of this MBEJ design should be considered as two similar but independent structures.

Vibration Response of MBEJ and Relation to Force Input

The dynamic behavior of this MBEJ may be considered as two independent structures (i.e., one structure with one set of odd numbered center beams with associated support bars, and a second structure with one set of even numbered center beams and support bars). The build-up in beam response may be attributed to the phase relationship of each wheel beam impact.

For example, reinforcement of the fundamental bounce mode (at 71 Hz) will occur when the wheel/beam impact occurs in phase with the center beam structure response from previous wheel/beam impacts. In the "*as-measured*" condition, the even center beam spacing was 260 mm. A perfectly in-phase reinforcement would occur at a wheel passage speed of 66.5 km/hr (i.e., the speed at which even center beam impacts occur every 14 ms, the time for one cycle of center beam response at 71 Hz). Fig. 7 shows a graph of calculated wheel/center beam pass frequencies for a range of expansion joint center beam spacings and vehicle speeds. Also marked in this graph are the spectral regions where natural structural modes were identified.

The bandwidth of each mode displayed is the approximate 3 dB down-point (i.e., marked bands are narrow spectral regions within 3 dB of maximum amplification for each mode). It should be noted that the frequencies of these modes may also be affected by the joint expansion/contraction.

This variable is not indicated in Fig. 7 where the center beam spacings (180, 220, 260, and 300 mm) refer to the spacing between successive odd (or even) numbered center beams, not simply adjacent center beams. Assuming a random distribution of vehicle speeds around the legal speed limit 70 km/hr, it is estimated that 10% of all vehicle pass-bys between 60 km/hr and 80 km/hr would fall into these regions of amplified response. It is therefore clear that for operational speeds on Anzac Bridge, a significant proportion of all vehicle pass-bys would result in reinforcement or amplification of modal response.

Dynamic Amplification of Load

The dynamic range factor (DRF), which is discussed below, should not be confused with the live load factor often used to

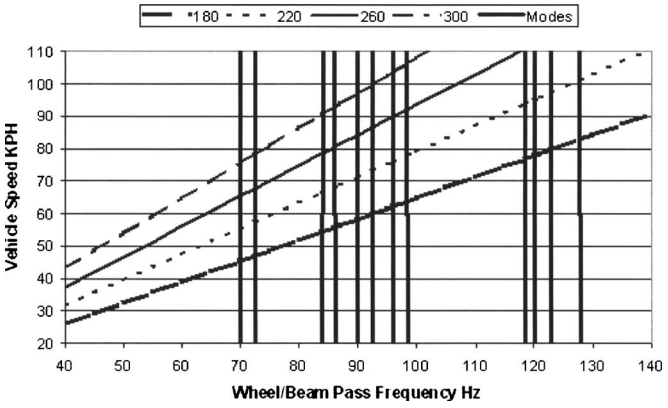

Fig. 7. Calculated wheel beam pass frequency for a range of expansion joint spacings

account for variability in the magnitude of the live load. It is also different from the dynamic amplification factor (DAF), normally defined as

$$\text{DAF} = 1 + \left(\frac{\delta_{dyn} - \delta_{stat}}{\delta_{stat}} \right) \tag{1}$$

where δ_{dyn}= maximum displacement due to the vehicle traveling at designated speed; and δ_{stat}= maximum displacement due to vehicle traveling at crawl (slow roll) speed.

It is also different from the dynamic load allowance (DLA), used in Australian codes, normally defined as

$$\text{DLA} = \left(\frac{\delta_{dyn} - \delta_{stat}}{\delta_{stat}} \right) = \text{DAF} - 1 \tag{2}$$

The DLA is usually applied to anticipated static loads in an attempt to predict maximum dynamic loads due, in the case of MBEJs, to additional acceleration of vehicle components as a vehicle traverses the MBEJ. It is understood that MBEJ designers typically use a DAF of about 1.7, which appears to be based on testing of multiple-support bar systems. The measured DRF proposed here is the peak-to-peak dynamic response divided by the quasi-static response (i.e., a measure of the reinforced response due to multiple wheel/beam impacts, as discussed earlier). The DRF is defined as follows

$$\text{DRF} = \frac{\varepsilon_{dyn}}{\varepsilon_{stat}} \tag{3a}$$

where ε_{dyn}= strain range due to the vehicle traveling at designated speed (peak-to-peak); and ε_{stat}= strain range due to vehicle traveling at crawl (slow roll) speed (zero-to-peak).

The results demonstrate measured DRFs of at least 3.0. It is important to note that this response factor of 3 would not apply to all vehicle pass-bys, but would apply selectively depending on vehicle speed, center beam spacing, and positions of natural MBEJ modes. It is important also to note that the apparent DRFs reported here were at relatively low response amplitudes.

The probable nonlinear effects of the structural response have yet to be understood. Strain measurement of center beams and support bars, under static and dynamic load cases, is considered to be essential to more accurately quantify the DRFs.

Discussion of Experimental Modes

The modal analysis study revealed that the 71-Hz frequency was predominantly due to a quasi-rigid body mode where the MBEJ was essentially bouncing on its bearing supports in combination with some support bar and center beam vertical bending. It is considered that at least 90% of the MBEJ mass was mobilized at this frequency.

Classical first- and second-order center beam vertical bending modes were found at 85, 91, and 97 Hz. Although Ostermann (1991) reported theoretical horizontal bending modes from an FEM study, these modes were not identified in this study due to access restrictions that limited the precision of horizontal data acquisition.

In addition to the experimental modal analysis study, an operational response shape analysis was undertaken using ambient road traffic excitation. This analysis revealed that ambient road traffic excited all the major natural modes identified.

Roeder (1993) postulated that the dynamic response of MBEJs is complicated because hundreds of modes of vibration may contribute to the response. The present data do not support that view except for the swivel joist design due to the greater variation of center beam spans in that design. With respect to the tested joint, only the first-, second-, and third-order center beam vertical bending modes are strongly excited by ambient traffic.

Horizontal modal data could not be acquired in sufficient detail to identify horizontal bending or torsional modes. However, the presence of the quasi-rigid body (bounce/bending) mode at 7.1 Hz was unexpected. Although this mode was implied by Köster (1986), it appears to have been unrecognized by Ostermann (1991), but apparently identified by Roeder (1993), who reported theoretical translational modes. It is noted that identical modal analysis measurements at two other MBEJs (both welded multiple-support bar systems by different manufacturers) revealed the presence of this quasi-rigid body (bounce/bending) mode. Because of the unusual "*hybrid*" design of this nominal single-support bar system, less than full motorway traffic speeds are capable of exciting this MBEJ at, or near, the 71-Hz modal resonance. This is due to the joint design wherein only even numbered center beams are attached to one support bar and odd numbered center beams are attached to the other.

This arrangement provides double the apparent center beam spacing (but load distribution between adjacent center beams is unaffected). This dynamic behavior is considered to be *coupled center beam resonance*. As Fig. 7 shows, all of the measured modes can be excited at traffic speeds between 60 km/hr and 80 km/hr (the legal speed limit for this bridge is 70 km/hr).

The experimental modal analysis results revealed that all modes were very lightly damped (<2% of critical) and consequently likely to contribute to free un-damped vibration of structural members of the MBEJ. It is also interesting to note that the experimental modal analysis results indicate that the support bars and center beams are acting dynamically as if simply supported. This observation is somewhat counterintuitive. Under some operating conditions, lightly damped single-support bar systems may experience dynamic amplification of load effects up to five times the nominal static load. It is considered that this dynamic response is a direct result of coupled center beam resonance. The modal analysis data were subsequently used to optimize the placement of strain gages as part of the fatigue life assessment of this MBEJ.

Fatigue Investigation

In an almost universal approach to the design of MBEJs the various national bridge design codes do not envisage that the embedded joint may be lightly damped and could vibrate as a result of traffic excitation. These codes only consider an amplification of the static load to cover suboptimal installation impact, poor road approach, and the dynamic component of load. The codes do not consider the possibility of free vibration after the passage of a vehicle axle.

Codes also ignore the possibilities of vibration transmission and response reinforcement through either following axles or loading of subsequent components by a single axle. What the codes normally consider is that any dynamic loading of the expansion joint is most likely to result from a sudden impact of the type produced by a moving vehicle "*dropping*" onto the joint due to a difference in height between the expansion joint and the approach pavement.

In climates where snow ploughs are required for winter maintenance, the expansion joint is always installed below the sur-

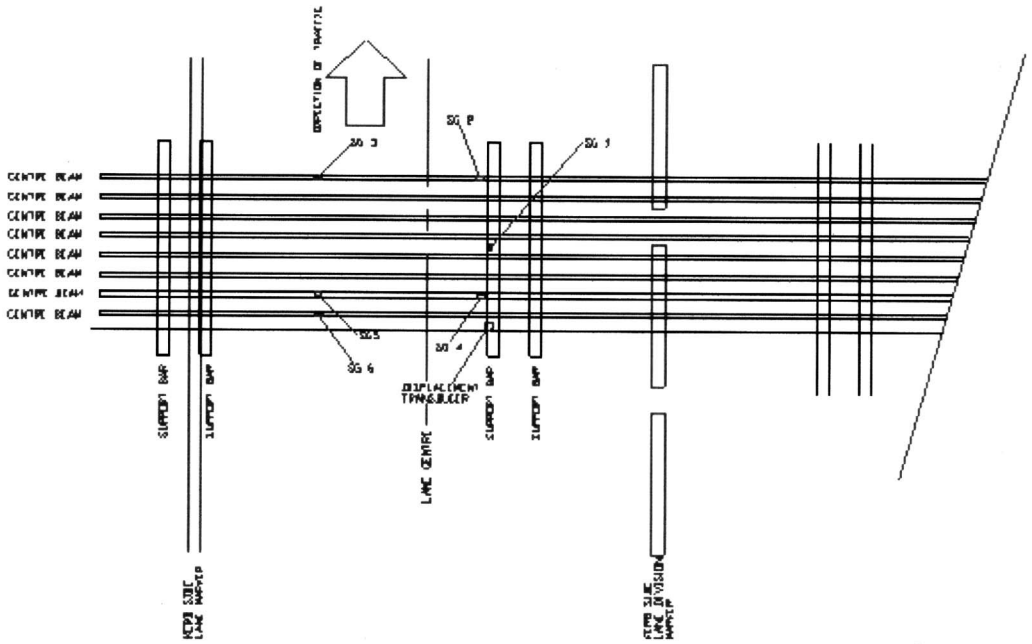

Fig. 8. Plan view eastbound curbside lane—six strain gage locations (SG1 to SG6)

rounding pavement to prevent possible damage from snow plough blades. In other cases, height mismatches may occur due to suboptimal installation. However, there are some major exceptions, with Standards Australia (2004) noting that for modular deck joints "*the dynamic load allowance shall be determined from specialist studies, taking account of the dynamic characteristics of the joint*." Whilst this code recognizes the dynamic behavior of MBEJs, there is no guidance given to the designer on the interpretation of the specialist study data. AASHTO (2004) is a major advancement as infinite fatigue cycles are now specified and braking forces considered but there is an incomplete recognition of the dynamic response phenomenon described earlier.

Based upon the experimental modal analysis data, a series of static and dynamic strain gage tests were undertaken to clarify modular expansion joint strains and dynamic response.

The main aims of the strain gage tests were to:

1. Measure strains in critical modular expansion joint elements at potential areas of high stress, as indicated by the experimental modal analysis;
2. Measure static strains for a test vehicle loaded to the maximum legal axle load for Australia;
3. Measure dynamic strains for the same test vehicle over a range of vehicle speeds;
4. Determine maximum measured dynamic range factors; and
5. Determine maximum measured dynamic stress, both positive (same sense as static) and negative (opposite sense to static).

Strain Gage Locations

Fig. 8 represents a plan view diagram of the eastbound curbside lane of Anzac Bridge and shows the six strain gage locations (SG1 to SG6). All gages were of a linear type and orientated in the anticipated principal stress direction (i.e., parallel to the long axis of the respective structural members).

Support Bar—Vertical Displacement

The laser displacement transducer was mounted to record the relative vertical displacement of the selected center beam and indicate vertical compression and extension of the support bar linear bearings.

Test Vehicle Loading

Fig. 9 shows the test vehicle loading arrangement used. The test truck was loaded to the maximum legal axle load for Australia and had a gross vehicle mass (GVM) of 42 t.

Fig. 10 presents a schematic elevation diagram of the modular expansion joint in relation to the nominal curbside lane position and nominal test truck wheel positions.

Truck Slow Roll

In order to approximate true static strains and displacements, the truck was traversed over the joint at less than 3 km/hr, producing negligible dynamic response of the truck or structure. All static and dynamic strains and displacements were recorded during this test.

Truck Pass-bys

Following as closely as possible to the same line as the slow, roll test. The truck was traversed at several speeds in the target speed range of 45–70 km/hr with the actual truck pass-by speeds measured using a radar speed gun.

The reproducible accuracy of the vehicle speed measurement is considered to be at least ±2 km/hr. Table 4 presents the target pass-by speeds as well as the measured (actual) pass-by speeds.

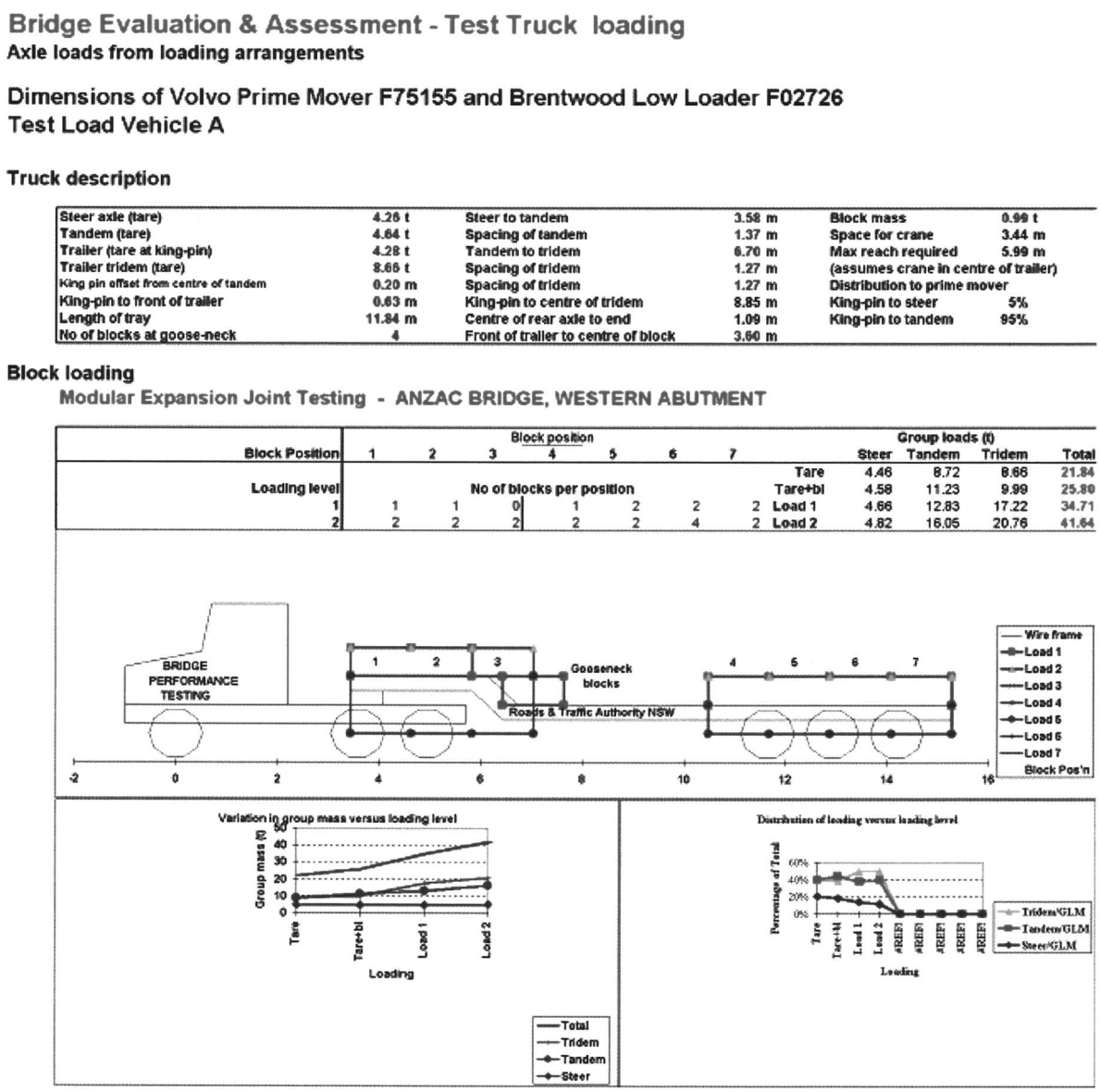

Fig. 9. Test vehicle loading arrangement

Strain and Displacement Measurements

The strain measurement system was calibrated using the shunt resistors before and after each test. Strain and displacement signals were recorded on the eight-channel DAT-corder, which was allowed to run for the entire test sequence. The recorded data were subsequently analyzed to produce strain versus time and displacement versus time plots. In addition, FFT spectra of selected truck run and joint configuration strain measurement data were also prepared.

Further analysis included the extraction of the maximum and minimum strain and displacements resulting from the passage of the six individual test truck axles. These data were used to calculate DRFs for each strain and displacement signal. Under conditions where a structure is well damped and static loads predominate, the peak-to-peak strain range may be approximated by the zero-to-peak strain. These conditions do not exist in modular joints and other vibration-sensitive structures such as the Millennium Footbridge in London.

Strain Measurement Results

Table 5 presents a summary of the resulting maximum strains, stresses, and dynamic range factors for each test. Table 6 presents a summary of the resulting displacements and DRFs for each test.

Table 4. Target and Actual Test Truck Pass-by Speeds

Run number	Target speed (kph)	Measured actual speed (kph)
1	40	47
2	50	50
3	60	53
4	60	61
5	65	63
6	70	68

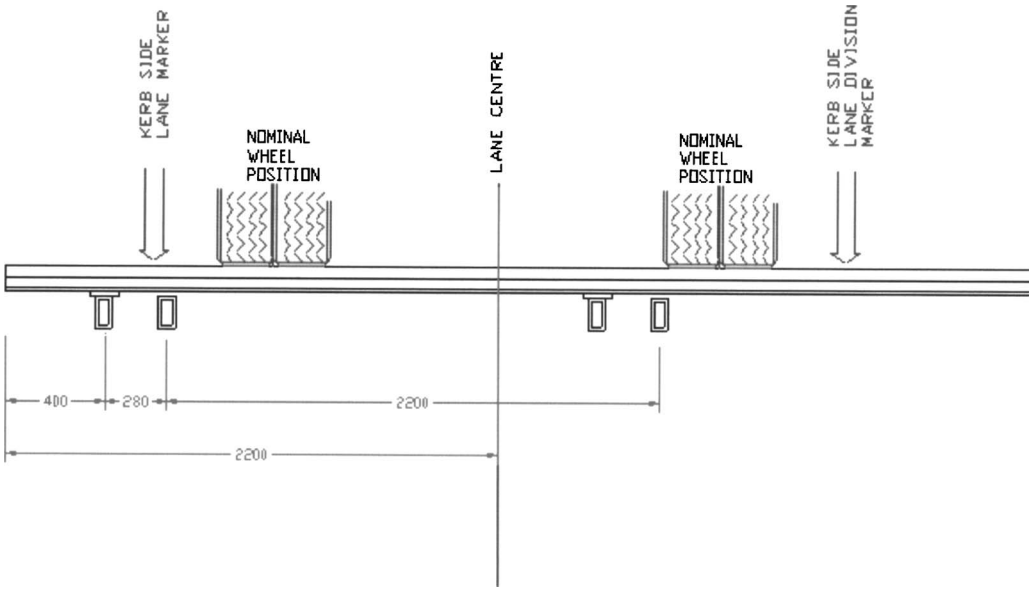

Fig. 10. Elevation of modular expansion joint and nominal test truck position

The following dynamic response factors are deduced from this investigation:

- The maximum beam stress total dynamic range factor measured was 4.6;
- The maximum beam stress positive dynamic range factor was 2.7; and
- The maximum beam stress negative dynamic range factor was 1.9.

These DRFs are clearly well in excess of existing bridge codes. Preliminary fatigue analysis predicts support bar and center beam failures after 2 E7 and 3.8 E6 pass-bys respectively of vehicles loaded similarly to the test truck (i.e., maximum legal axle loads). The maximum total dynamic amplification of support bar linear bearing displacement (compression) was 4.0.

The maximum positive dynamic amplification of support bar linear bearing displacement was 2.2. The maximum negative dynamic amplification of support bar linear bearing displacement was 1.9. These higher than previously documented DRFs are most likely a major cause of both structural fatigue cracking as well as fracture and loss of linear bearing pads.

High negative support bar vertical displacement amplification due to resonance of natural structural modes of the modular expansion joint and traffic forcing frequency is likely to cause uplift of the support bar and at times break contact with the lower linear bearing pad. This may allow the lower linear bearing pad to eventually dislodge. Alternatively, where the support bar is excessively restrained from uplift by elastomeric bearings, the high restraint forces may prevent proper sliding. This may distort and

Table 5. Summary of Resulting Strains, Stresses, and Dynamic Range Factors

		Strain and Stress								
		Strain ($\mu\epsilon$)			Stress (MPa)			Dynamic Range Factors		
Test truck pass-by speed	Transducer location	Maximum tensile	Maximum compressive	Peak to peak	Maximum tensile	Maximum compressive	Peak to peak	Maximum tensile	Maximum compressive	Peak to peak
Slow roll	Support bar	100	−1	101	20	0	20	0.0	0.0	0.0
	Center beams	154	−101	153	31	−20	31	0.0	0.0	0.0
47 kph	Support bar	185	−30	215	37	−6	43	1.8	−0.4	2.2
	Center beams	167	−157	179	33	−31	36	1.9	−0.4	2.1
50 kph	Support bar	226	−66	293	45	−13	59	2.3	−0.9	3.2
	Center beams	203	−113	234	41	−23	47	1.5	−0.3	1.8
53 kph	Support bar	213	−54	268	43	−11	54	2.1	−0.6	2.7
	Center beams	136	−132	165	27	−26	33	2.0	−0.5	2.5
61 kph	Support bar	270	−116	386	54	−23	77	2.7	−1.7	4.5
	Center beams	233	−141	308	47	−28	62	2.1	−0.6	2.6
63 kph	Support bar	256	−114	370	51	−23	74	2.7	−1.9	4.6
	Center beams	225	−148	307	45	−30	61	1.9	−0.7	2.5
68 kph	Support bar	218	−104	311	44	−21	62	2.4	−1.5	3.9
	Center beams	215	−137	280	43	−27	56	1.6	−0.7	2.2
Maximum	All	270	−157	386	54	−31	77	2.7	−1.9	4.6

Table 6. Summary of Displacements and Dynamic Range Factors

Test truck pass-by speed	Transducer location	Displacement (mm)			Dynamic Range Factors		
		Maximum tensile	Maximum compressive	Peak to peak	Maximum tensile	Maximum compressive	Peak to peak
Slow roll	Support bar	0.01	−0.22	0.22	0.0	0.0	0.0
47 kph	Support bar	0.05	−0.32	0.37	1.8	−0.4	2.2
50 kph	Support bar	0.10	−0.37	0.47	2.3	−0.9	3.2
53 kph	Support bar	0.10	−0.32	0.43	2.1	−0.6	2.7
61 kph	Support bar	0.41	−0.43	0.84	2.7	−1.7	4.5
63 kph	Support bar	0.39	−0.50	0.89	2.7	−1.9	4.6
68 kph	Support bar	0.20	−0.48	0.65	2.4	−1.5	3.9
Maximum	Support bar	**0.41**	**−0.50**	**0.89**	**2.7**	**−1.9**	**4.6**

dislodge the upper compression spring allowing the lower linear bearing to ultimately dislodge.

Dynamic Implications

Impact on the Anzac Bridge Joint

The DRF introduced earlier utilizes the full measured strain range in the fatigue assessment. As part of this study, knowledge of the frequency associated with the dynamic strains was considered important.

An FFT frequency spectrum of the dynamic strain data from SG 1 (support bar) is presented as Fig. 11. It should be noted that due to the ensemble averaging process used in FFT analysis, the peak strain frequency at 64.8 Hz is not the absolute strain value but rather the value relative to other spectral peaks. It is clear that the peak strain frequency was coincident with the wheel/beam pass frequency for the respective truck pass-by speed (i.e., the input forcing frequency). It was also clear that this input force was amplified by the dynamic response of the MBEJ structure—the input forcing frequency was in close proximity to a major natural structural mode (nominally at resonance). For the joint opening position at the time of testing, the peak strain frequencies were encompassed by traffic speeds in the 60–65 km/hr range.

The dynamic behavior of the Anzac Bridge MBEJ may be considered as two independent structures—one structure with one set of odd-numbered center beams with associated support bars, and a second structure with one set of even-numbered center beams and support bars. The coupled nature of the *odd* and *even* structures is demonstrated in Fig. 12. For this measurement, the strain gage (SG1) was located in the middle of a support bar and the impact of each of the test vehicles' six axles with each of the center beams connected to this support bar is clearly evident.

The dynamic response is also demonstrated by the impact of the tandem axles of the prime mover (tractor) and the tri-axles of the trailer where the vibration is in phase and virtually continuous.

An independent center beam structure responding to a single impulse would, of course, be expected to display an initial maxi-

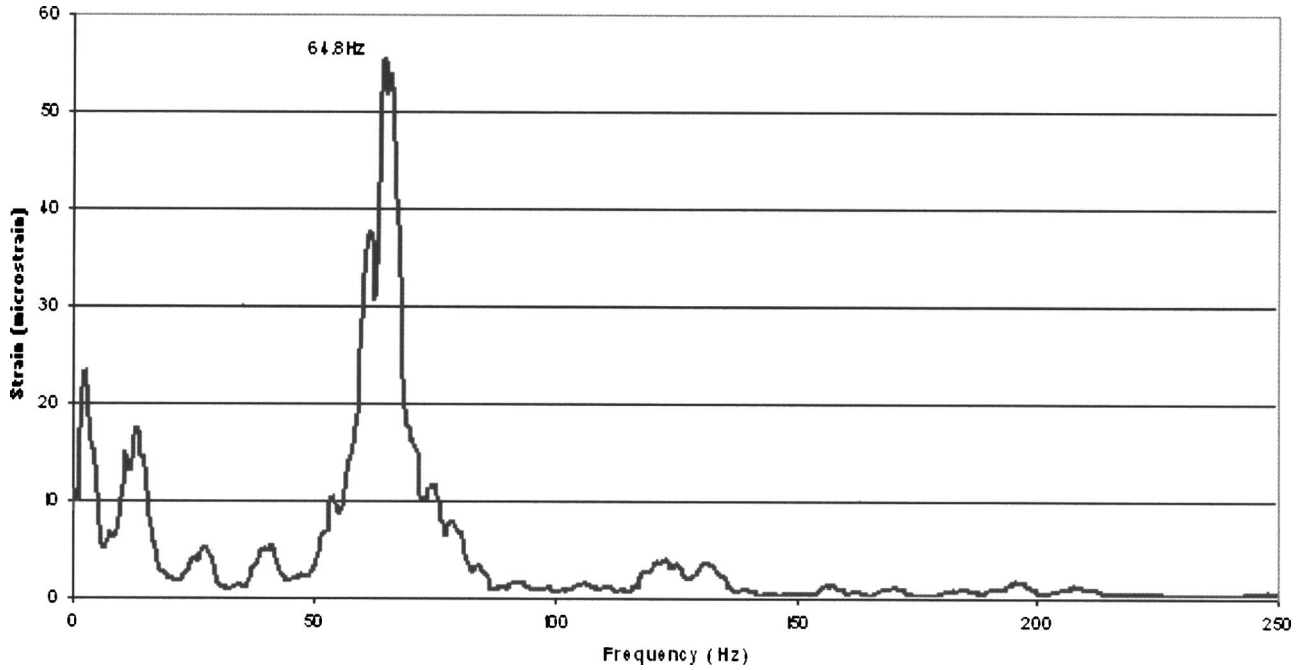

Fig. 11. Strain frequency spectrum (SG 1)

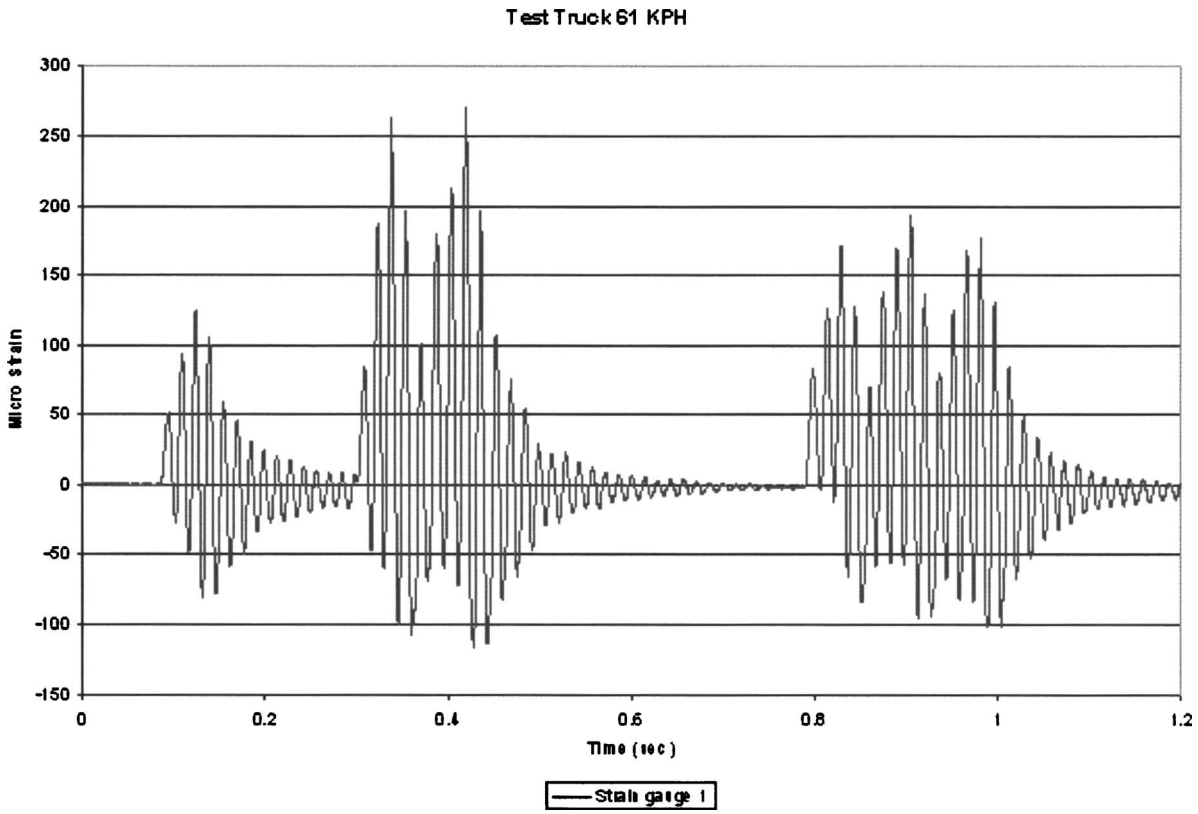

Fig. 12. Response induced by heavy vehicle pass-by

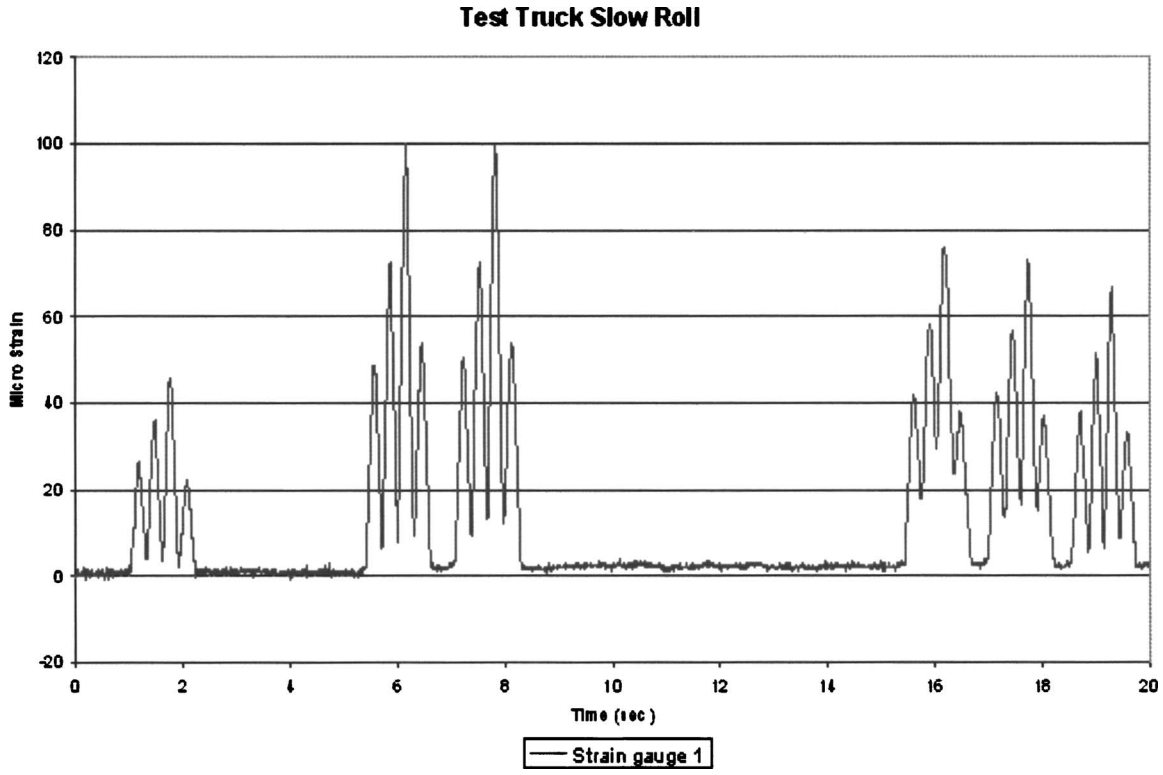

Fig. 13. Quasi-static response due to test vehicle pass-by

mum amplitude followed by an exponential decay. The build-up in center beam response may be attributed to the phase relationship of each wheel center beam impact.

For example, reinforcement of the fundamental bounce/bending mode (at 71 Hz) will occur when the wheel/beam impact occurs in phase with the center beam structure response from previous wheel/center beam impacts. In the *as-measured* condition, the even center beam spacing was 260 mm. A perfectly in-phase reinforcement would occur at a wheel passage speed of 66.5 kph (i.e., the speed at which even center beam impacts occur every 14 ms, the time for one cycle of center beam response at 71 Hz).

Implications of Dynamic Response

From a fatigue analysis perspective, the dynamic response of a structure may lead to higher than expected strain levels due to dynamic amplification. Fig. 13 shows the quasi-static response of a strain gage (SG1) located in the middle of a support bar, and the impact of each of the test vehicle's six axles with each of the center beams connected to this support bar is clearly evident. A simple comparison between Figs. 12 and 13 shows that the quasi-static slow roll produced 100 $\mu\epsilon$ (Pk-Pk) and the 61-km/hr pass-by produced 385 $\mu\epsilon$ (Pk-Pk). This simple comparison indicates a DRF of at least 3.8 times static.

Furthermore, not only are the peak dynamic strains at least 3.8 times the quasi-static, but further observation of Fig. 12 shows that the steer and tandem axles of the prime mover (tractor) produce at least 16 cycles of vibration (per vehicle passage) where the dynamic strain equals or exceeds the quasi-static strain of 100 $\mu\epsilon$ (Pk-Pk). Similarly, the tridem axles of the trailer produce at least 14 cycles of vibration (per vehicle passage) where the dynamic strain equals or exceeds the quasi-static strain of 100 $\mu\epsilon$ (Pk-Pk). The simple addition of these events shows that each heavy vehicle passage (of the load configuration of the test vehicle) produces around 30 vibration cycles where the dynamic strain equals or exceeds the quasi-static strain of 100 $\mu\epsilon$ (Pk-Pk). These data must surely be of concern to MBEJ designers and specifiers who assume a single quasi-static load calculated from their national maximum permissible axle loading.

Roeder (1993) reported the results of an analytical modal analysis on a swivel joist design and noted that, as the actual system damping was unknown, the analytical model assumed no damping. Roeder concluded from this study that the model was relatively insensitive to damping and that "*damping must be relatively large (20% of critical or more) before significant changes in the dynamic periods are noted*." The present data suggest that the contrary may be the case as the tested MBEJ is very sensitive to changes in the system damping. Indeed, the very high dynamic range factor of 4.6 is considered to relate directly to the measured damping of $<2\%$ of critical.

Tschemmernegg (1973) first reported the dynamic nature of MBEJs and later, (Tschemmernegg 1991) noted: "*Although everybody knows that expansion joints of bridges are the heaviest dynamic-loaded components of bridges, the design calculations, if any, were of a static nature. The results are a lot of well-known problems of detail with high costs for repair, interruption of traffic, etc.*"

Fatigue Assessment

A preliminary fatigue life analysis was carried out based on the results presented. The fatigue lives of components were estimated from the S-N curves presented in *Eurocode 3* (CEN 1992). A worst-case stress profile for each structural component assessed was derived from the maximum stress range measured (i.e., support bars at 77 MPa and center beams at 62 MPa).

Table 7. Nominal Stress Profile of Test Truck Passage

Transducer location	Stress range (σ) (MPa)	Number of cycles per truck passage
Support bar	77	2
	60	10
	40	12
Center beam	62	2
	34	4
	20	16

The number of stress cycles per year was estimated as follows:

- Support bars: (number of trucks per year)$\times$(number of axles) $\times 4$
- Center beams: (number of trucks per year)$\times$(number of axles)

This stress profile assumes that all trucks would produce similar axle loads. A less conservative approach would be to reduce the maximum axle load case by a fatigue load factor of 0.75 and apply this to all heavy vehicles, as proposed in AASHTO (2004). A factor of 4 is used above for support bars because each support bar experiences 4 load cycles for each axle pass whereas the center beams only experience a single load cycle per axle.

A further proposed best estimate stress profile would be to apply the Palmgren Miner cycle ratio summation theory (also called Miner's rule) to the stress profile for the worst-case test truck pass-by. Cumulative fatigue damage is an assessment of the fatigue life for elements that may be subjected to n_1, cycles at a stress range of σ_1, and n_2 cycles at a stress range of σ_2, etc. The preferred theory in use at the present time to explain cumulative fatigue damage is Miner's rule.

Mathematically, the theory is stated as

$$\frac{n_1}{N_1} + \frac{n_2}{N_2} + \cdots + \frac{n_i}{N_i} = C \tag{3b}$$

where n=number of cycles of stress δ applied to the specimen; and N=life corresponding to σ. The constant C is determined experimentally and is usually found in the range $0.7 \leqslant C \leqslant 2.2$.

Shigley and Mischke (1981) recommend using $C=1$, so that

$$\sum \frac{n}{N} = 1 \tag{4}$$

Table 7 presents the resulting stress ranges and number of cycles per truck passage, extracted from strain measurements. Table 8 shows a summary of the resulting fatigue life predictions based on the test truck pass-bys.

Discussion

The analysis of simple vibration measurements of the nine-seal MBEJ installed into the Anzac Bridge revealed that most of the traffic-induced vibration was at a frequency of 71 Hz. A preliminary analytical study failed to identify the vibrational mode responsible for this frequency and an experimental modal analysis study was subsequently undertaken. The modal analysis study revealed that the 71 Hz frequency was predominantly due to a

Table 8. Fatigue Life Predictions of Test Truck Passage

	Stress range (σ) (MPa)	Number of cycles to failure (N)	Number of cycles per truck passages (n)	n/N per truck
	77	4 E7 (Euro 160)	2	5 E-8
	60	No Limit (Euro 160)	10	0
Support bar	40	No Limit (Euro 160)	12	0
			$\Sigma n/N$	5 E-8
		Number of trucks passages to failure		**2E7**
	62	9 E5 (Euro 36)	2	2.2 E-7
	34	1 E8 (Euro 36)	4	4 E-8
Center beam	20	No Limit (Euro 36)	16	0
			$\Sigma n/N$	2.6 E-7
		Number of truck passages to failure		**3.8 E6**

quasi-rigid body mode where the MBEJ was essentially bouncing on its bearing supports in combination with some support bar and center beam vertical bending.

It is considered that at least 90% of the MBEJ mass was mobilized at this frequency. Classical first- and second-order center beam vertical bending modes were found at 85 , 91, and 97 Hz. Due to access restrictions, horizontal modal data could not be acquired in sufficient detail to identify horizontal bending or torsional modes. It is interesting to note that the experimental modal analysis results reported earlier indicated that the support bars and center beams were acting dynamically as if simply supported. This observation may be considered counterintuitive. In addition to the experimental modal analysis study, an operational response shape analysis was undertaken using ambient road traffic excitation. This analysis revealed that ambient road traffic excited all the major natural modes identified. It is noted that identical modal analysis measurements at two other MBEJs (both welded multiple-support bar systems by different manufacturers) revealed the presence of this quasi-rigid body (bounce/bending) mode. In all cases measured, the bounce/bending mode occurred at lower frequencies than the respective center beam fundamental (vertical) bending modes.

Because of the unusual hybrid design of this nominal single-support bar system, less than full motorway traffic speeds are capable of exciting this MBEJ at or near the 71-Hz modal resonance. This is due to the joint design wherein only even-numbered center beams are attached to one support bar and odd-numbered center beams are attached to the other. This arrangement provides double the apparent center beam spacing (but load distribution between adjacent center beams is unaffected). This dynamic behavior is considered to be *coupled center beam resonance*.

As Fig. 7 shows, all of the measured modes can be excited at traffic speeds between 60 km/hr and 80 km/hr (the legal speed limit for this bridge is 70 km/hr). The experimental modal analysis results revealed that all modes were very lightly damped ($<2\%$ of critical) and consequently likely to contribute to free un-damped vibration of structural members of the MBEJ. Under some operating conditions, lightly damped single-support bar systems may experience dynamic range amplification of loads up to five times the nominal static load. It is considered that this dynamic response is a direct result of coupled center beam resonance. However, it is not recommended that the peak value of the DRF should be used for design purposes. Rather, the peak DRF multiplied by 0.8 would be more appropriate. Alternatively, the RMS dynamic range factor could be used but more study is needed to determine whether an RMS calculation should be over the full axle/axle train strain range or just the maximum peak positive and negative strains.

The experimental modal analysis data were subsequently used to optimize the placement of strain gages as part of the fatigue life assessment of this MBEJ.

The following DRFs were deduced from the strain gage investigation:

- The maximum total dynamic range factor measured was 4.6;
- The maximum positive dynamic range factor was 2.7; and
- The maximum negative dynamic range factor was 1.9.

Conclusion

Experimental modal analysis and operational response shape studies were performed on a hybrid MBEJ installed in the Anzac Bridge. The studies showed that for this joint:

- The joint is very lightly damped ($<2\%$ of critical damping);
- The lowest frequency mode excited was a quasi-rigid body (bounce/bending) mode at 71 Hz;
- In contrast with reported theoretical studies, only the first four fundamental vertical bending modes were excited;
- Due to access restrictions, horizontal modal data could not be acquired in sufficient detail to identify horizontal bending or torsional modes;
- The support bars and center beams were acting dynamically as if simply supported; and
- There was good agreement between the experimental modal analysis and the operational response shape studies.

It is considered that the dynamic response of this MBEJ is mainly due to coupled center beam resonance and this is seen as a design characteristic of all single support bar design systems. Static and dynamic strain gage studies were also performed on this MBEJ.

The studies showed that for this joint:

- The DRF is up to 4.6 for the fully laden test vehicle;
- This DRF is not necessarily the worst case, as every possible vehicle speed and joint opening combination was not tested;
- Coupled center beam resonance is the basis of the dynamic behavior;
- Damping is important in the dynamic behavior;
- The number of effective cycles of load, due to vibration, for each vehicle passage is very high; and

- High uplift forces are generated within the joint under vehicle loading.

These results should be of concern to bridge asset owners, bridge designers, and modular joint suppliers. The normal assumption of quasi-static behavior for the single-support bar design MBEJ (and variants thereof) is not sustainable and both bridge designers and modular joint suppliers must think in terms of a fully dynamic system.

Acknowledgment

The writers wish to thank the Chief Executive of the Roads and Traffic Authority of NSW (RTA) for permission to publish this paper. The opinions and conclusions expressed in this paper do not necessarily reflect the views of the RTA.

References

AASHTO. (2004). *AASHTO LRDF Bridge Design Specifications, Sl Units*, 3rd Ed., Washington, D.C.

Agarwal, A. C. (1991). "Static and dynamic testing of a modular expansion joint in the Burlington Skyway," *Proc., 3rd World Congress on Joint Sealing and Bearing Systems for Concrete Structures*, American Concrete Institute, Detroit.

Crocetti, R. (2001). "On some fatigue problems related to steel bridges," Ph.D. thesis, Chalmers Univ. of Technology, Göteborg, Sweden.

Crocetti, R., and Edlund, B. (2001). "Fatigue performance of modular bridge expansion joints," Chalmers Univ. of Technology, Göteborg, Sweden.

Dexter, R. J., Connor, R. J., and Kaczinski, M. R. (1997). "Fatigue design in modular bridge expansion joints," *Report 402*, National Cooperative Highway Research Program, Transportation Research Board, Washington, D.C.

European Committee for Standardization (CEN). (1992). "Design of steel structures, section 9". *Eurocode 3*, Brussels.

Ewins, D. J. (1999). *Modal testing: Theory, practice & application*, 2nd Ed., Research Studies Press, Hertfordshire, UK, 163–276.

Köster, W. (1986). "The principle of elasticity for expansion joints," *Joint Sealing and Bearing Systems for Concrete Structures, ACI SP-94*, American Concrete Institute, Detroit, 675–711.

Ostermann, M. (1991). "Beanspruchung von elastisch gelagerten Fahrbahnübergängen unter Radstoßeinwirkung ("Stresses in elastically supported modular expansion joints under wheel load impact")." *Bauingenieur*, Springer-Verlag, 381–389 (in German).

Roeder, C. W. (1993). "Fatigue cracking in modular expansion joints," *Research Report WA-RD 306.1*, Washington State Transportation Center, Seattle.

Roeder, C. W. (1995). "Field measurements of dynamic wheel loads on modular expansion joints," *Research Report WA-RD 369.1*, Washington State Transportation Center, Seattle.

Shigley, J. E., and Mischke, C. R. (1981). "*Mechanical engineering design*," 5th Ed., McGraw-Hill, New York.

Standards Australia. (2004). *Australian standard AS5100.4–2004, Bridge Design Part 4: Bearing and deck joints*, Sydney, NSW, Australia.

Tschemmernegg, F. (1973). "Messung von Vertikal und Horizontallasten beim Anfahren, Bremsen und Überrollen von Fahrzeugen auf einem Fahrbahnübergang ("Measurement of vertical and horizontal loads due to accelerating, braking, and rolling vehicles on an expansion joint")." *Bauingenieur*, 48, Heft 9, Springer-Verlag, 326–330 (in German).

Tschemmernegg, F. (1991). "The design of modular expansion joints," *Proc., 3rd World Congress on Joint Sealing and Bearing Systems for Concrete Structures*, American Concrete Institute, Detroit, 67–86.

Appendix K

Ancich E.J. (2007). Dynamic Design of Modular Bridge Expansion Joints by the Finite Element Method, *Proc. International Association for Bridge & Structural Engineering (IABSE) Symposium*, Weimar, Germany.

IABSE

International Association for Bridge and Structural Engineering

Annual Meetings and Symposium 2007
Weimar, Germany

Dynamic Design of Modular Bridge Expansion Joints by the Finite Element Method

Eric Ancich
Senior Project Engineer
Roads & Traffic Authority
PO Box 3035
Parramatta NSW 2124
Australia

Eric_Ancich@rta.nsw.gov.au

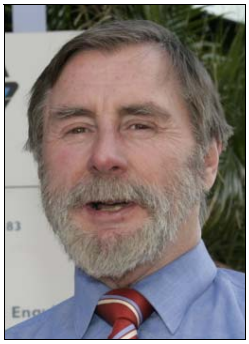

Eric Ancich, born 1941, is a senior project engineer with the Roads & Traffic Authority (NSW). He has over 20 years experience in acoustics, vibration and structural dynamics and manages the delivery of engineering consultant services for bridge rehabilitation and technically unique bridge projects.

Summary

Although it is not unusual for modular bridge expansion joints (MBEJ's) to be designed using the Finite Element Method, it appears that designers have been more concerned with quasi-static modelling rather than the development of a fully dynamic model that reproduces all of the characteristics of an operational MBEJ. The paper reports the calibration of a finite element model of both single support bar and multiple support bar design MBEJ's using experimental modal analysis and strain gauge data. Once calibrated, the models accurately reproduce the empirical vibrational modes and dynamic strains of the operational joints. Modelled results display acceptable variation with the measured data. As motor vehicle excitation is transient, a unique procedure was developed that utilised measured strain data to simulate the force-time history of a vehicle pass-by. This is described as a '*virtual dynamic truck pass-by*' and its application to the models permitted the accurate reproduction of all the dynamic characteristics including the dynamic amplification factor. The experimental modal analysis results of the single support bar MBEJ strongly suggested that in some regions, the dynamic response was linear and in other regions, non-linear. A moderately successful attempt was made to reproduce this effect by introducing non-linear stiffness into the model by way of the elastomeric bearings.

Keywords: Bridge decks; Bridges, cable-stayed; Damping; Expansion joints; Finite element method; Modal analysis; Strain measurement.

1. Introduction

Modular bridge expansion joints (MBEJ's) are widely used throughout the world for the provision of controlled pavement continuity during seismic, thermal expansion, contraction and long-term creep and shrinkage movements of bridge superstructures. Modular Bridge Joint Systems (MBJS) are considered to be the most modern design of waterproof bridge expansion joint currently available. The Roads and Traffic Authority of NSW (RTA) has experienced premature fatigue failure of MBEJ's in two bridges. Fatigue cracks were observed in Pheasant's Nest Bridge on the Hume Highway (opened December 1980) and Mooney Mooney Creek Bridge on the F3 Freeway (opened December 1986). The MBEJ's installed into both bridges are multiple support bar designs and are essentially identical having been supplied by the same European manufacturer. In addition, the RTA has a '*hybrid*' single support bar MBEJ in the western abutment of Sydney's Anzac Bridge. Whilst termed '*hybrid*', the Anzac joint consists of two interleaved single support bar structures that behave, in a dynamic sense, as quite independent structures. Although the Anzac MBEJ did not exhibit any evidence of fatigue induced cracking, a routine non-destructive examination of all accessible welds identified a number of manufacturing irregularities that were of concern.

The RTA also has a large inventory of U.S. designed welded multiple support bar joints and, as a result of the Pheasant's Nest and Mooney Mooney failures, all welded multiple support bar joints were considered potentially vulnerable to fatigue induced cracking. A literature search revealed little to describe the structural dynamics behavior of MBEJ's but showed that there was an accepted belief dating from around 1973 that the loading was dynamic [1]. There appear to be relatively few published accounts of the dynamic analysis of MBEJ's. Ostermann [2], Medeot [3] and Steenbergen [4] undertook the computational analysis of MBEJ's but only modelled one centre beam. Roeder [5] modelled a full single support bar design MBEJ (swivel joist variant) but the initial analyses did not include any dynamic response or impact. Subsequent dynamic analyses were performed assuming zero damping with Roeder concluding that "…*damping must be relatively large (20% of critical or more) before significant changes in the dynamic periods are noted*…" This observation is undoubtedly correct with respect to frequency (reciprocal of period) but does not recognize the role of damping in the dynamic response factor (DAF). Roeder also noted from this study that the dynamics of MBEJ's were complex and field measurements of the dynamic response would assist in evaluating the dynamic behavior. Accordingly, experimental modal analysis studies of the Anzac Bridge MBEJ [6] and a typical welded multiple support bar joint [7] were undertaken and these data were used to '*calibrate*' separate finite element models.

As the present study will show, the DAF is substantially dependent on damping and the previously reported phenomenon of coupled centre beam resonance [6] and this requires multiple axle excitation of multiple centre beams for the phenomenon to manifest. The principal aims of the current study were to:

- Develop a dynamic finite element model (FEM) of the Anzac Bridge Single Support Bar Modular Expansion Joint in the '*As Built*' condition.
- Develop a dynamic finite element model (FEM) of a representative U.S. Design Multiple Support Bar Modular Expansion Joint in the '*As Built*' condition.
- Apply a static load case to simulate the maximum legal axle load, as measured in previous tests.
- Determine relevant natural modes and mode shapes and correlate with the results of experimental modal analysis, and tune the FEM to match where possible.
- Modify the FEM to simulate replacement of the '*As Built*' springs and bearings with high damping springs and bearings (Anzac MBEJ only).

In addition to the above aims, an analysis technique was developed that enabled the application of a virtual dynamic truck pass-by at critical speeds. This transient analysis also enabled the calculation and prediction of the DAF. The technique also offered the potential to study the DAF sensitivity to damping, mount stiffness, etc.

2. The Finite Element Models

2.1 Anzac Bridge Model

The finite element model was formulated using NASTRAN (MSC Visual Nastran for Windows 2003). The Anzac Bridge MBEJ consists of two interleaved single support bar structures and previous experimental modal analysis studies [6] had demonstrated only very light, almost negligible coupling between the two structures. The FE model developed was a representation of one complete single support bar structure, comprising six support bars and four centre beams. Support bars and centre beams were represented by beam elements. The precise centre beam and support bar cross sections were mapped and section properties developed by NASTRAN. The centre beam-to-support bar yoke connection was represented by a MDOF spring/damper element. Support bar springs and bearings were also represented by MDOF spring/damper elements.

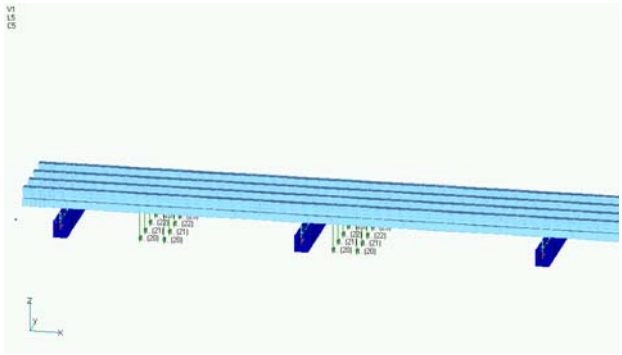

Figure 1 *View of Base Anzac Mode showing load points*

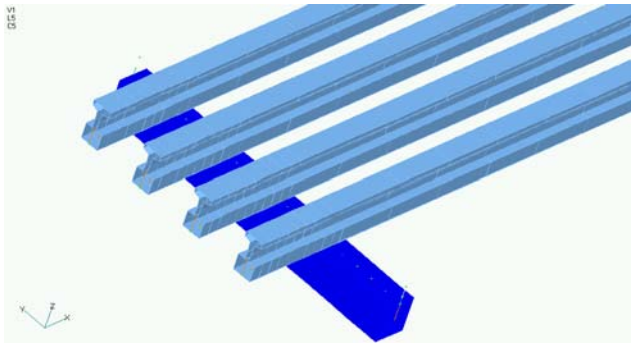

Figure 2 *Zoomed View of Base Anza Model*

Figures 1 and 2 show a perspective view including wheel load points and a zoomed view of the base model. It is important to note that the emphasis of dynamic analysis was on the vertical response of the structure (i.e. any resulting horizontal centre beam bending modes have not been reported). Based on the results of investigations to date, horizontal modes were not found to be particularly relevant to the major dynamic loads developed during traffic excitation.

2.2 Taree By-Pass Model

This finite element model was also formulated using NASTRAN. The Taree Bypass MBEJ was chosen as representative of the RTA's inventory of the U.S. multiple support bar design. The centre beams are 63.5mm by 127mm and the 80mm by 110mm support bars are at nominal 1.5m centres (except outermost support bars and end cantilevers). The Taree Bypass MBEJ consists of a 6-seal welded multiple support bar structure that behaves in a dynamic sense as five independent single support bar structures but with fixed, rather than sliding, connections between centre beam and support bars. Previous experimental modal studies [7] had demonstrated only very light, almost negligible coupling between the separate structures. The FE model developed was a representation of the full multiple support bar structure, including seven support bars and five centre beams. Support bars and centre beams were represented by beam elements. The precise centre beam and support bar cross sections were mapped and section properties developed by NASTRAN. Centre Beam-to-Support Bar connections were represented by rigid elements.

Support bar springs and bearings were represented by MDOF spring/damper elements. **Figures 3 and 4** show a perspective view including wheel load points and a zoomed view of the base model. It is again important to note that the emphasis of dynamic analysis was on the vertical response of the structure (i.e. any resulting horizontal centre beam bending modes have not been reported). Based on the results of investigations to date, horizontal modes were not found to be particularly relevant to the major dynamic loads developed during traffic excitation.

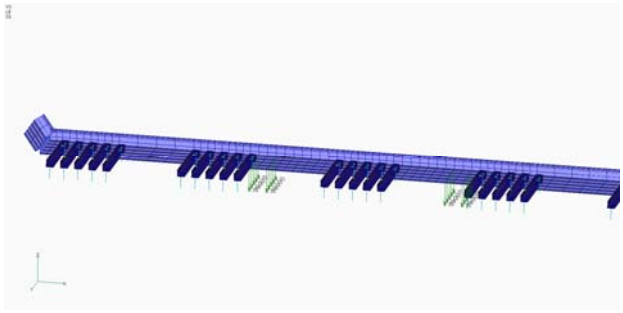

Figure 3 *View of Base Taree Model showing load points*

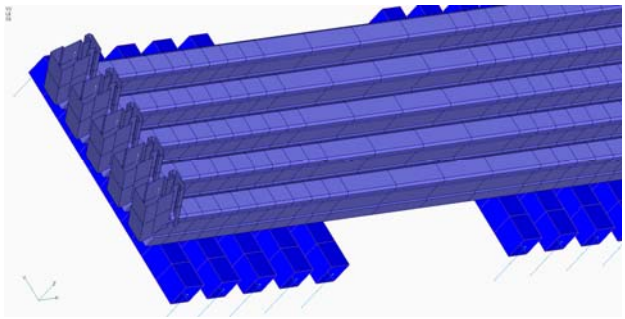

Figure 4 *Zoomed View of Base Taree Model*

3. Static Analysis

3.1 The '*As Built*' Models

Reference [7] shows the load profile for the test truck used in static and dynamic testing. A proportion of the maximum tandem axle load was used in the static analysis (i.e. a wheel load of 32 kN was applied split over two nodes).

3.2 Static Stress Results

Reference [7] shows the location of strain gauges for the Anzac and Taree static load case measurements. **Table 1** shows a summary of the resulting predicted maximum stress and strain for centre beams and support bars. This table also presents a comparison with typical measured results from the slow roll tests. These results demonstrate very good correlation between measured and FEM predicted results.

Table 1 *Summary of the Resulting Maximum Stress and Strain*

Study MBEJ	Component Description	Strain Gauge Location [7]	Maximum Strain Predicted by FEM	Maximum Strain Measured	Maximum Stress Predicted by FEM	Maximum Stress Measured
Anzac	Centre beam	SG3, SG5	136 με	145 με	26 MPa	29 MPa
	Support bar	SG1	95 με	100 με	19 MPa	20 MPa
Taree	Centre beam	SG5 SG2	120 με	160 με	24 MPa	32 MPa
	Support bar	SG3 SG6	100 με	85 με	20 MPa	17 MPa

4. Normal Mode Analysis Results

For this analysis, the predicted mode shapes and modal frequencies were compared with the previously reported experimental modal analysis data [6] for the original condition or '*As Built*' MBEJ.

4.1 Normal Mode Analysis Results – '*As Built*' Model (Anzac)

Table 2 shows a summary of the resulting natural modal frequencies with a description of the associated mode shapes. The predicted modes are remarkably similar to the experimentally observed modes [6]. However, there are some interesting differences. For instance, the experimentally observed bounce/bending mode at 71 Hz actually appears to be two very closely spaced modes. The FEM Mode 1 at 71 Hz is predominantly bending with some in-phase support bar bounce whereas Mode 2 at 72 Hz is predominantly in-phase support bar bounce with some bending. Mode 3 at 85 Hz is virtually identical to the experimental mode at the same frequency. Mode 4 at 98 Hz is also virtually identical to the two similar experimental modes at 91 Hz and 97 Hz respectively. Finally,

Mode 5 at 101 Hz appears to combine the major elements of the separate experimental modes at 119 Hz and 125 Hz respectively.

Table 2 *Summary of Natural Modal Frequencies- "As Built" Condition (Anzac)*

Mode No	Mode Shape Description	Natural frequency from FEM	Natural frequency of similar mode from EMA
1	Fundamental Bounce/Bending	71 Hz	71 Hz
2	Fundamental Bounce/Bending	72 Hz	Not Identified
3	First Centre Beam Vertical Bending Mode	85 Hz	85 Hz
4	Second Vertical Centre Beam Bending	98 Hz	91 Hz
5	Third Vertical Centre Beam Bending	101 Hz	97 Hz

4.2 Normal Mode Analysis Results – '*As Built*' Model (Taree)

Table 2 shows a summary of the resulting natural modal frequencies with a description of the associated mode shapes. The predicted modes are remarkably similar to the experimentally observed modes [5]. These modes relate to beam 4 only and also shown is a comparison with the experimentally observed modes. It is interesting to note that modes 2 and 3 were not identified by Ancich *et al* [7] and possibly require more extensive measurement for complete definition.

The mode shapes for each beam may be readily grouped with generally little difference in frequency and mode shape. However, the experimentally observed bounce/bending mode at 91 Hz actually appears to be three closely spaced modes. The FEM Mode 1 at 71 Hz is predominantly bending with some in-phase support bar bounce whereas Mode 2 at 72 Hz is predominantly in-phase support bar bounce with some bending. Mode 3 at 85 Hz is virtually identical to the experimental mode at the same frequency. Mode 4 at 98 Hz is also virtually identical to the two similar experimental modes at 91 Hz and 97 Hz respectively. Finally, Mode 5 at 101 Hz appears to combine the major elements of the separate experimental modes at 119 Hz and 125 Hz respectively.

Table 3 *Summary of Natural Modal Frequencies - Centre Beam 4 Only (Taree)*

Mode No	Mode Shape Description	Natural frequency from FEM	Natural frequency of similar mode from EMA
1	Centre Beam End-Cantilever Bending	69 Hz	69 Hz
2	Fundamental Bounce/Bending	79 Hz	Not Identified
3	Bounce/Bending	81 Hz	Not Identified
4	Bounce/Bending	91 Hz	91 Hz
5	First Vertical Centre Beam Bending	118 Hz	122 Hz
6	Second Vertical Centre Beam Bending	130 Hz	130 Hz

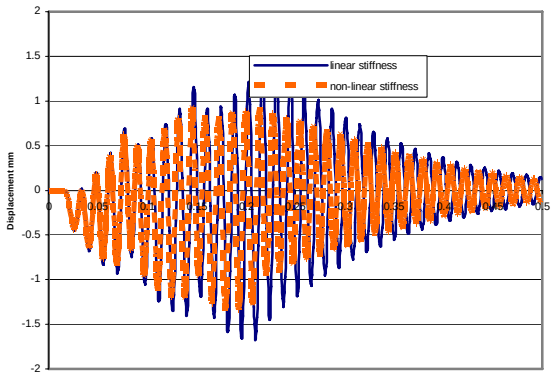

iFigure 5 *Non-linear Stiffness (Anzac)*

4.3 Structural Non–Linearity

It was suspected that there are structural non-linearity's in the dynamic response of MBEJ's but there was nothing in the published literature to support this hypothesis. However, the experimental modal analysis results of the Anzac MBEJ [7] in particular were strongly suggestive that in some regions, the dynamic response is linear and in other regions, non-linear.

An attempt was made to reproduce this effect by introducing non-linear stiffness into the system by way of the elastomeric bearings. As **Figure 5** shows, the dynamic response of the system is significantly moderated by the incorporation of a measure of non-linearity into the elastomeric bearing stiffness.

5. Transient Dynamic Response

5.1 Virtual Dynamic Truck Pass-by

In order to more confidently predict the dynamic amplification factors associated with modular joint structures, a procedure was developed that utilized measured strain data to simulate the force time history of a vehicle pass-by. A typical slow roll strain time history was '*calibrated*' to simulate a force time history. This single time history was replicated at time spacings to match the approximate tridem axle spacing of 1.2m. **Figure 6** shows a plot of this virtual wheel load force profile and **Figure 7** shows a sample force time history for a 62-km/hr pass-by. A time delay was applied to the time history for each centre beam to represent the appropriate pass-by speed and nominal 1.2m axle spacing. It is interesting to note that whilst most studies (including this one) have used an essentially sinusoidal waveform input (half sine), Roeder [5] used a triangular waveform. At the present time, there is insufficient data upon which to make an informed recommendation but a sinusoidal waveform would seem to be more appropriate. However, Steenbergen [4] questions the validity of the half sine wave input model but used an excitation pulse almost identical to that used for the present study. It is considered that the present study is distinguished from previously referenced studies by this '*virtual dynamic truck pass-by*'.

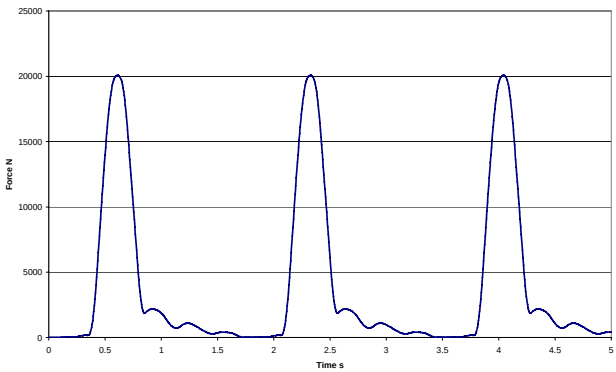

Figure 6 *Plot of Virtual Wheel Load Force Profile*

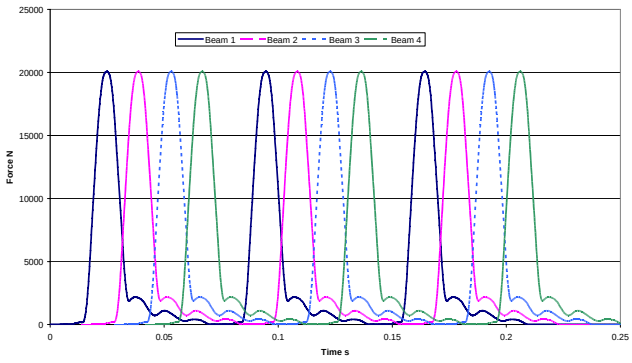

Figure 7 *Sample Force Time History for a 62 km/h Pass-By (Anzac)*

Ostermann [2] applied two axle transients to a single centre beam but there are no time waveforms to determine the phase relationship between these two transients and the structural response. By comparison, Medeot [3] applied five axle transients (at 1.2m spacing) to a single centre beam and his time waveforms clearly indicate that successive axle pulses were almost perfectly out-of-phase with the dominant structural response, (i.e. not at resonance with any major natural modes of the structure). Whilst Roeder [5] modelled an entire MBEJ, it appears from the load duration data published that he used a single triangular pulse excitation. Steenbergen [4] also modelled an entire MBEJ but only considered a single axle excitation. For the phenomenon of coupled centre beam resonance to manifest, it is considered that multiple in-phase axle pulses need to be applied to the full joint.

Whilst some in-service load configurations may result in notionally out-of-phase excitation, notionally in-phase excitation will frequently occur and it is clearly a worst-case for fatigue assessment. Furthermore, it is considered that at least 1 in every 10,000 heavy goods vehicles will be at the maximum permissible axle loading and traveling at a speed such that the MBEJ is excited partially or notionally in-phase. Fatigue analysis should therefore be based upon not exceeding the stress level at the constant amplitude fatigue limit (CAFL) for the relevant steel S-N curve and the DAF produced by this 1 in 10,000 vehicle. Alternatively, where national bridge design codes use the fatigue cut-off limit at 10^8 cycles, the designer should consider using 80% of the peak DAF. The force profile used in this study was scaled in time to match the truck speed to be simulated.

5.2 Dynamic Amplification Factors

Table 6 presents a summary of the maximum total Dynamic Amplification Factors resulting from each model. It is worth noting that Steenbergen [4] found that DAF values higher than 2 occur easily and that these values are much higher than those prescribed in current bridge design codes.

5.3 DAF Sensitivity - Damping

Further Transient Analysis runs were carried out on the '*As Built*' models to assess the sensitivity of the DAF to damping. **Figures 8 & 9** shows the resulting trend for both the Anzac and Taree MBEJ's.

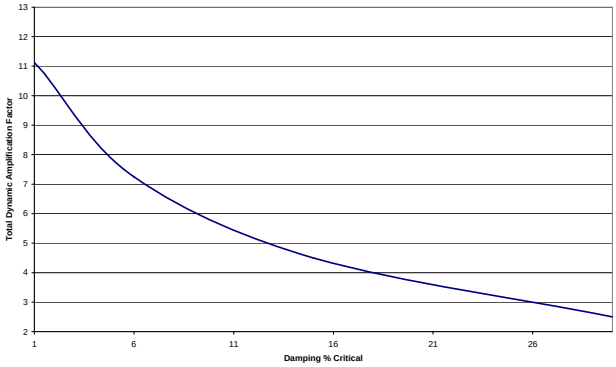

Figure 8 *Dynamic Amplification Factor vs Damping (Anzac)*

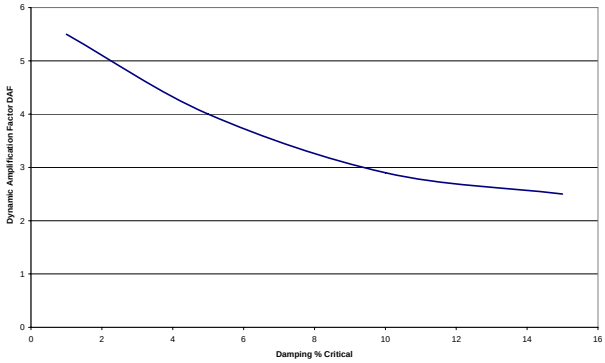

Figure 9 *Dynamic Amplification Factor vs Damping (Taree)*

6. Conclusion

Static and dynamic finite element modelling studies were performed on a hybrid single support bar MBEJ installed in the western abutment of Anzac Bridge and a welded multiple support bar MBEJ installed in one of the Taree Bypass bridges. The studies showed that for these joints:

- There was excellent agreement with experimental modal and strain gauge data.
- A method was developed to apply a virtual truck pass-by based on '*calibration*' of previous quasi-static (slow roll) strain measurements. This '*measured*' force time history was scaled to represent the desired virtual truck pass-by speed. The same force time history was applied to each centre beam with an appropriate time delay to match the virtual truck pass-by speed.
- The DAF was up to 11 for the lightly damped '*as built*' condition of the Anzac MBEJ.
- The DAF was substantially reduced by the modelled installation of modified elastomeric springs and bearings.
- The phenomenon of coupled centre beam resonance was confirmed by FEM as the basis of the dynamic behavior.
- Fatigue analysis should be based upon not exceeding the stress level at the CAFL for the relevant steel S-N curve and the DAF produced by notionally in-phase multiple axle excitation of multiple centre beams. Alternatively, where national bridge design codes use the fatigue cut-off limit at 10^8 cycles, the designer should consider using 80% of the peak DAF.
- All MBEJ designs are probably limited to a minimum DAF around 2.5. This is due to the coupled centre beam resonance phenomenon, in-phase excitation and the practical limitations of providing damping above 15% of critical.

The normal assumption of quasi-static behavior for the single support bar design MBEJ (and variants thereof) and the welded multiple support bar design MBEJ is not sustainable and both bridge designers and modular joint suppliers must think in terms of a fully dynamic system both in the design and in the detailing.

Acknowledgement

All site measurements and data analyses were undertaken by Steve Brown (Heggies Australia Pty Ltd) and his pivotal contribution is gratefully acknowledged.

The author also wishes to thank the Chief Executive of the Roads and Traffic Authority of NSW (RTA) for permission to publish this paper. The opinions and conclusions expressed in this paper do not necessarily reflect the views of the RTA.

References

[1] TSCHEMMERNEGG F., "Messung von Vertikal- und Horizontallasten beim Anfahren, Bremsen und Überrollen von Fahrzeugen auf einem Fahrbahnübergang (Measurement of Vertical and Horizontal Loads due to Accelerating, Braking, and Rolling Vehicles on an Expansion Joint)", *Der Bauingenieur,* 48 (9), Springer-Verlag, 1973, pp. 326-330 (In German).

[2] OSTERMANN M., "Beanspruchung von elastisch gelagerten Fahrbahnübergängen unter Radstoßeinwirkung (Stresses in elastically supported modular expansion joints under wheel load impact)", *Bauingenieur 66*, Springer-Verlag, 1991, pp. 381-389 (In German).

[3] MEDEOT R., "Impact Analysis of Maurer Expansion Joints: DS640 Swivel joist joint and D240 girder grid joint", *Unpublished report prepared on behalf of Maurer Söhne GmbH*, Selvazzano, Italy, 2003, p. 38.

[4] STEENBERGEN M.J.M.M., "Dynamic response of expansion joints to traffic loading", *Engineering Structures,* Vol. 26, No. 12, Elsevier, 2004, pp. 1677-1690.

[5] ROEDER C.W., "Fatigue Cracking in Modular Expansion Joints", *Research Report WA-RD 306.1*, Washington State Transportation Centre, Seattle, WA, U.S.A, 1993, p. 53.

[6] ANCICH E.J., CHIRGWIN G.J., and BROWN S.C., "Dynamic Anomalies in a Modular Bridge Expansion Joint", *ASCE Journal of Bridge Engineering*, Vol. 11, No. 5, 2006, pp. 541-554.

[7] ANCICH E.J., BROWN S.C., and CHIRGWIN G.J., "Modular Deck Joints – Investigations into structural behaviour and some implications for new joints", *Proc. 5th Austroads Bridge Conference* (Hobart, Australia), Austroads, Sydney, NSW, Australia, 2004 (on CD).

Appendix L

Ancich E.J., Chirgwin G.J., Brown S.C. & Madrio H. (2009). Fatigue Sensitive Cope Details in Steel Bridges and Implications from Growth in Heavy Vehicle Loads and Numbers, *Proc. 7th Austroads Bridge Conference*, Auckland, New Zealand.


7th Austroads Bridge Conference
Bridges linking communities
26 - 29 May 2009
Sky City Convention Centre
Auckland, New Zealand
NZ TRANSPORT AGENCY
WAKA KOTAHI
Austroads

Fatigue Sensitive Cope Details in Steel Bridges and Implications from Growth in Heavy Vehicle Loads and Numbers

Eric Ancich[1], Steve Brown[2], Gordon Chirgwin[1] and Huber Madrio[1]

1. *Roads & Traffic Authority of NSW, PO Box 3035, Parramatta NSW 2124*
2. *Heggies Pty Ltd, PO Box 176, Lane Cove NSW 1595*

SYNOPSIS

It is known that 75% of the total Australian road freight task passes through NSW and the Pacific Highway is a major recipient of this freight. There are numerous crossings of major rivers between Newcastle and the Queensland border and until the late 1960's, steel bridges were preferred as lift spans could be easily incorporated in the design.

Over the past 10-15 years, heavy vehicle numbers using the Pacific Highway have increased dramatically, with a stepwise increase in 2001 and exponential growth of about 2% per year otherwise. This growth has been matched by a parallel exponential growth in loads and an even faster growth in axle group repetitions due to the greater utilisation of B-doubles and tri-axle semi-trailers.

Three bridges along the Pacific Highway exhibiting fatigue cracking were investigated using a structural dynamics based approach. The investigations revealed numerous compression/tension stress reversals for each heavy vehicle transit. Whilst the dynamic amplification factor (DAF) for a single controlled heavy vehicle transit was comparable with current Codes, the load effect for fatigue from uncontrolled heavy vehicle traffic significantly exceeds the value that would be predicted using the test vehicle factored for dynamic effects and multiple presence.

A cost effective fatigue life extension modification was proposed and tested on one of the bridges in this study. This "*compliant fastener*" modification in concept reduces the out of plane bending resistance at the stringer-to-cross girder connection, and hence reduces the stress range experienced by the fasteners and cope. In the bridge that was experiencing multiple fatigue and fastener failures every month, no further failures have been recorded in the three years subsequent to installation of the modification.

INTRODUCTION

The Roads and Traffic Authority of NSW (RTA) maintains some 5,000 bridges on the classified road network in New South Wales. Coped stringer to cross girder connections are a common feature of steel truss road bridges in NSW and the RTA has in excess of 60 such bridges. The design is, however, dynamically sub-optimal and a number of bridges along the Pacific Highway are exhibiting fatigue related cracking. The design is further complicated by un-explained variations in implementation. In some bridge designs, an attempt was made to reinstate the coped stringer top flange across the cross girder by bolting or riveting a thick steel plate to each stringer top flange.

Where used, the connection plate has resisted fatigue cracking around the copes but the bridges using the detail only used it for alternate cross girders. Cracking was first observed in the riveted cope connections of Macksville Bridge in 2004. At the time, it was not realised that the cracking was fatigue related. Rather, given the age of the bridge (built 1930's) and changes to the size and volume of heavy vehicles, progressive overloading was considered to be the cause. Subsequently, routine inspections of the 1960's era Kempsey Bridge (See **Figure 1**) identified a number of coped stringer-to-cross girder connections where some of the rivets in the top two rows had been lost. The lost rivets were replaced with high strength bolts and following inspections revealed that the replacement bolts were failing in as little as 6-months. Some failed bolts were recovered and submitted for metallurgical examination. This examination revealed characteristic evidence of fatigue failure (See **Figure 2**).

A literature review indicated that steel bridge designers of this era gave little or no consideration to fatigue. Fatigue design provisions, as we largely know them today, may be traced to AASHTO [1] from 1973. Roeder et al [2] reported similar connection details in US bridges and noted that whilst they were designed as pinned connections they should be regarded as partially restrained connections as they have limited rotational restraint.

Fu *et al* [3] report Australian, Canadian and United States studies of the impact of increased heavy vehicle loading on bridge infrastructure. They concluded that these investigations used largely deterministic approaches and tended to exclude fatigue effects. Imam *et al* [4] undertook a largely theoretical study of riveted rail bridges in the UK. They concluded that fatigue life estimates exhibit the highest sensitivity to detail classification, to S-N predictions in the region of high endurances, and to model uncertainty. This highlighted the importance of field monitoring for old bridges approaching the end of their useful life.

Whilst it was known that 75% of the total Australian road freight task passed through NSW [5, 6] and the Pacific Highway was a major recipient of this freight, little was known about actual heavy vehicle loading on the Pacific Highway. Analysis of weigh-in-motion (WIM) data from Pacific Highway sites indicated that over the past 10-15 years, heavy vehicle numbers using the Pacific Highway have increased dramatically, with a stepwise increase in 2001 and exponential growth of about 2% per year otherwise. This growth has been matched by a parallel exponential growth in loads and an even faster growth in axle group repetitions due to the greater utilisation of B-doubles and tri-axle semi-trailers. A detailed consideration of this traffic data indicates that fatigue has only become important since 1990, but that in the period 1990 to 2004 some 90% of the fatigue life of the deck stringer connection may have been used.

The present study reports extensive dynamic measurements and FE modelling of Kempsey Bridge. The FE model was calibrated [7] using dynamic measurements and then used for a series of "*what if*" studies. Whilst the optimum solution was shown to be the connection plate over the cross girder, there were major difficulties with implementation as the bridge could not be taken out of service. An alternative solution was devised that involved removing the top two rows of rivets in the stringer/cross girder connection and replacing the removed rivets with "*compliant*" fasteners.

Post replacement measurements have validated the FEM predictions and confirmed that, under current traffic volumes and loadings, the fatigue life of Kempsey Bridge has been extended by a further 40 years. In the three years subsequent to installation of the modification no further fatigue failures have been recorded.

Figure 1 Kempsey Bridge

Two other bridges along the Pacific Highway were also investigated using the same structural dynamics based approach. The investigations revealed numerous compression/tension stress reversals for each heavy vehicle transit. Whilst the dynamic amplification factor (DAF) for a single controlled heavy vehicle transit was comparable with current Codes, the load effect for fatigue from uncontrolled heavy vehicle traffic significantly exceeds the value that would be predicted using the test vehicle factored for dynamic effects and multiple presence.

Figure 2 Fatigue affected bolt

PRELIMINARY FINITE ELEMENT MODEL

A preliminary global finite element model was used to identify likely hot spots or weaknesses in the structure. The finite element model was built using MSC.FEA software. The FE model was initially developed as a global modal of the entire truss span 6, which consisted predominately of shell elements and a few beam elements. The geometry was manually entered from work-as-executed drawings of the bridge. Suitable spring elements were used to represent the bridge bearings and piers. **Figure 3** shows a perspective view of the base model.

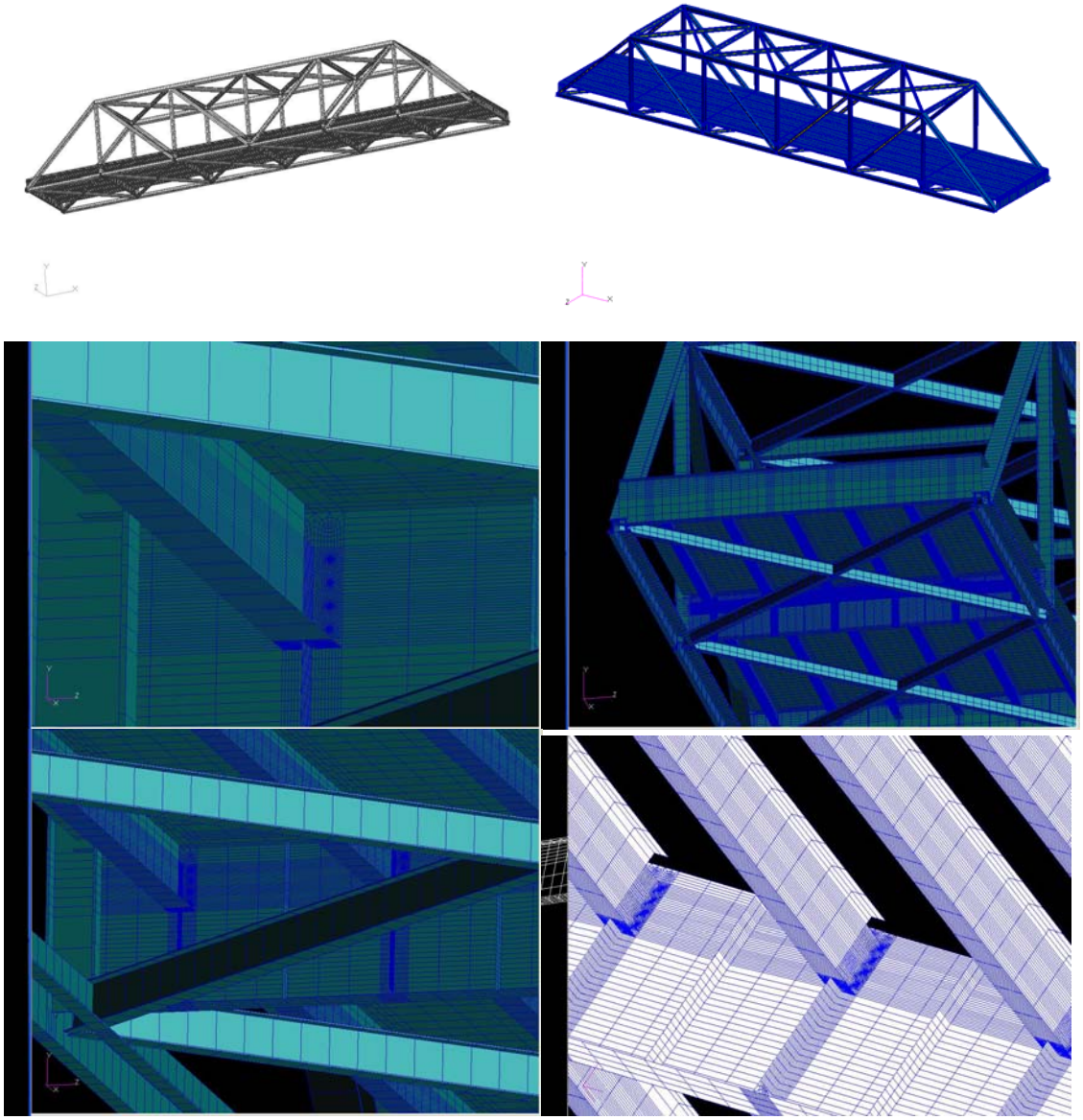

Figure 3 Views of base model for Kempsey Bridge

NORMAL MODE ANALYSIS

Table 1 shows a summary of the resulting natural modal frequencies with a description of the associated mode shapes.

Table 1 Summary of the Resulting Natural Modal Frequencies

Mode No	Mode Shape Description	Natural Frequency from FEM (Hz)	Natural Frequency from EMA (Hz)
1	First vertical bending	3.8	3.6
2	Second vertical bending	7.0	6.5
3	Third vertical bending	9.0	8.7
4	Fourth vertical bending	10.1	10.1
5	Transverse/vertical bending	12.1	11.8
6	Fifth vertical bending	13.3	13.7

Figures 4 - **9** show mode shapes from modes 1 to 6 respectively.

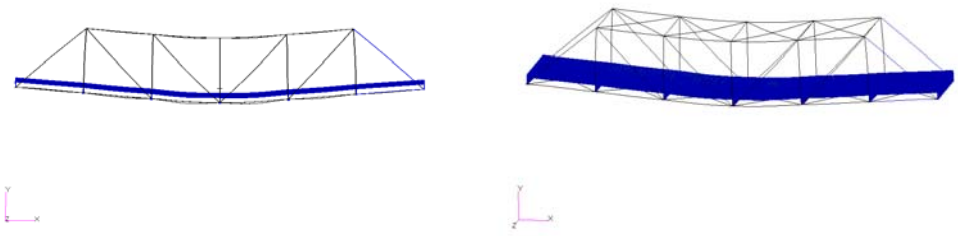

Figure 4 Mode 1 at 3.8 Hz

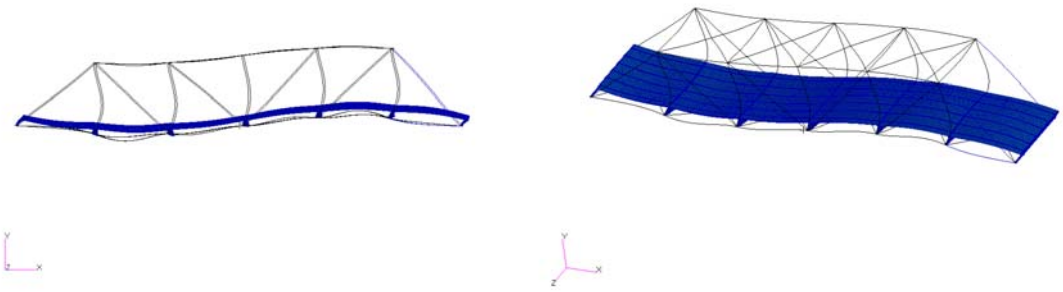

Figure 5 Mode 2 at 7 Hz

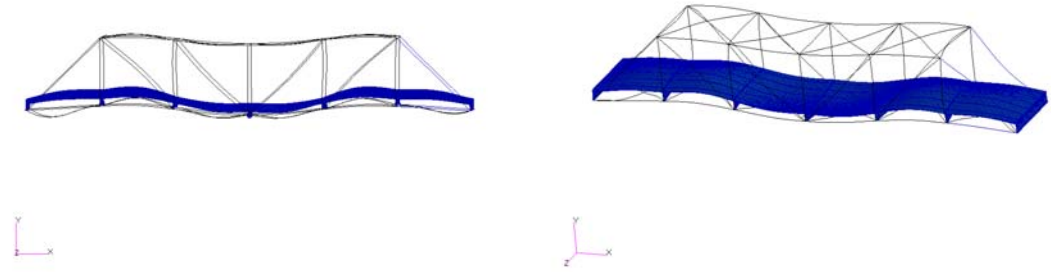

Figure 6 Mode 3 at 9 Hz

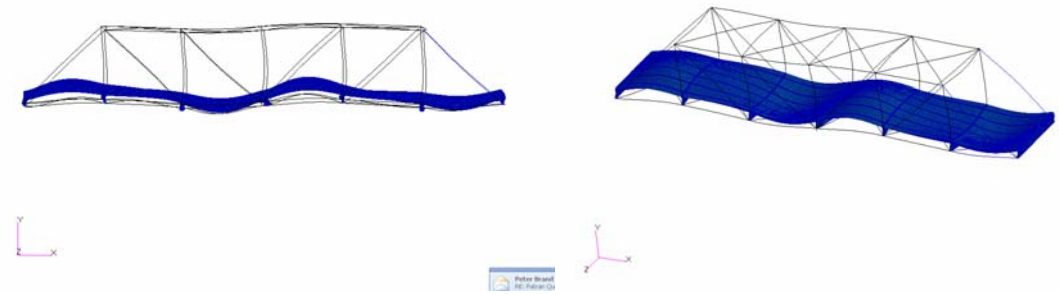

Figure 7 Mode 4 at 10.1 Hz

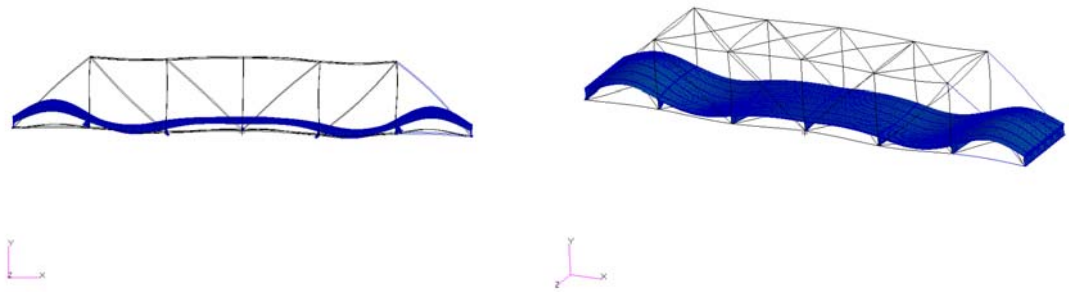

Figure 8 Mode 5 at 12.1 Hz

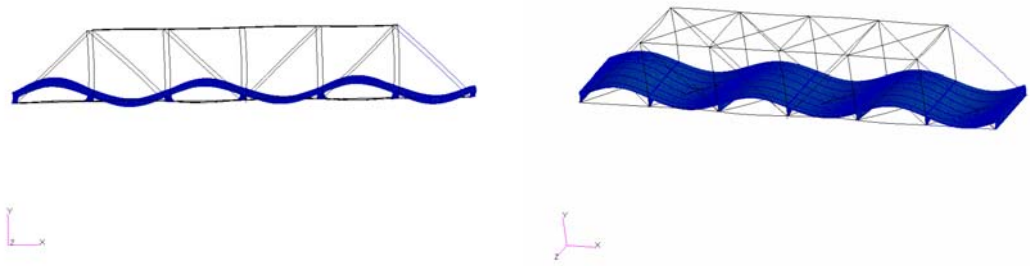

Figure 9 Mode 6 at 13.3 Hz

MODAL ANALYSIS TEST PROCEDURES

Test Description

The measurement and definition of the natural frequencies and mode shapes of a structure is referred to as modal analysis.

Experimental identification of structural dynamic models is usually based on the modal analysis approach. In the classical modal parameter estimation method, frequency response functions are measured under controlled conditions. For many large structures it is not practical, or prohibitively expensive to apply a controlled input force and hence the need arises to identify modes under operating conditions, or from environmental excitation

In this type of analysis, only response data are measurable while the actual loading conditions (input forces) are unknown.

The test procedure and methodology for experimental modal analysis is comprehensively covered by Ewins [8].

For the three bridges studied, the measurement of Frequency Response Functions (FRF's) involved the simultaneous measurement of a reference vibration response and "roving" vibration responses at a large number of locations over the bridge structure.

In these tests the frequency range of interest was a nominal 0 Hz to 25 Hz. The vibration responses were measured at selected locations using an accelerometer attached to the structure with a magnetic base. **Figure 10** shows the typical transducer set-up.

Figure 10 Typical Instrument Setup

The reference response and roving vibration responses were recorded on the eight-channel DAT recorder. Data integrity was checked in real time using the two-channel FFT analyser. **Figure 11** shows the general test setup.

Figure 11 General Test Setup

Subsequently, each frequency response function (FRF) was simultaneously measured using the four-channel FFT analyser and recorded data. Frequency Response Functions (FRF's) were stored on the hard disk drive of a laptop computer.

The type of modal test undertaken is sometimes referred to as an Operational Modal Analysis as the force input is supplied by the operating conditions and response (only) measured.

Figure 12 shows a line drawing of the undeformed structure as produced in the modal software. All reference points were in the vertical direction.

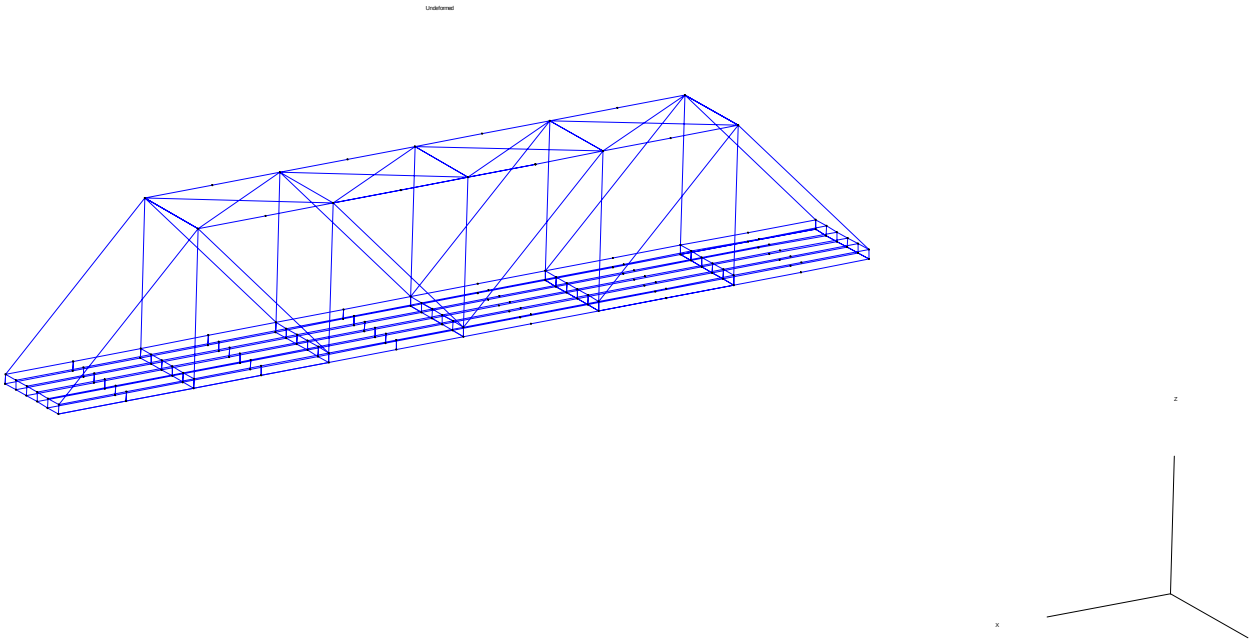

Figure 12 Line Drawing of the Undeformed Structure Showing Measurement Locations

Modal analysis results

Modal Testing

Table 1 shows the resulting frequency tables for the first 6 experimental modes identified compared with similar modes from FEM. It should be noted that the mode shapes presented represent the dominant modes of response of the bridge structure during the one day test period during which time traffic and wind were the major source of excitation.

The measured natural modes of vibration for Kempsey Bridge are shown below.

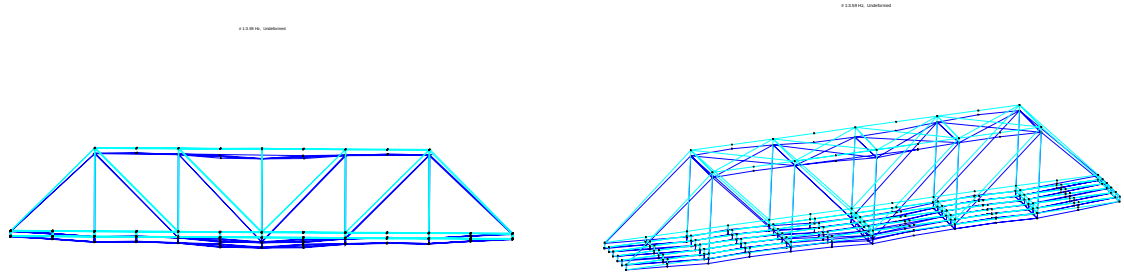

Figure 13 Mode 1 at 2.6 Hz Fundamental Vertical Bending Mode - Vertical movement of the Bays 1 to Bay 6 all in phase, nodes at piers.

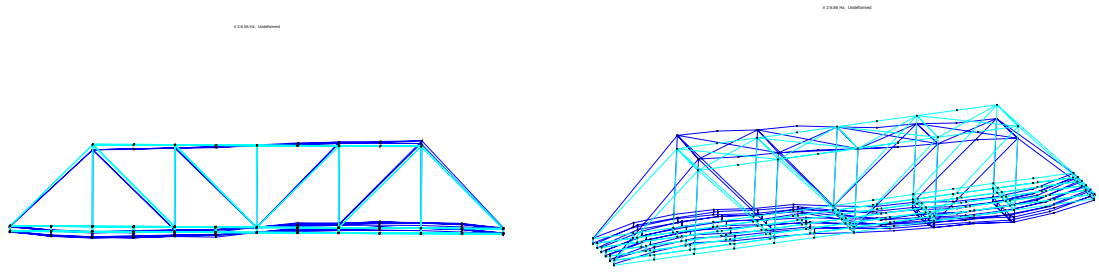

Figure 14 Mode 2 at 6.5 Hz Second Vertical Bending, Bays 1, 2, 3 out of phase with bays 4, 5, 6, nodes at piers and 1 node mid span, i.e. 3 nodes

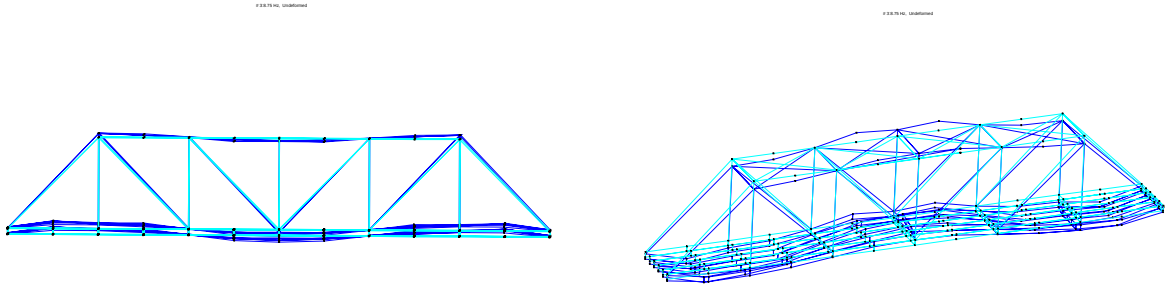

Figure 15 Mode 3 at 8.75 Hz Third Vertical Bending, Bays 1,2, and bays 5,6 out of phase with bays 3,4, (4 nodes)

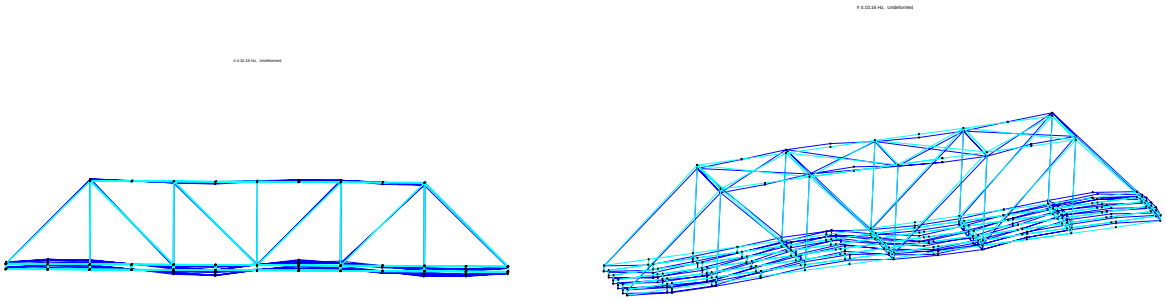

Figure 16 Mode 4 at 10.16 Hz Fourth Vertical Bending, (5 nodes)

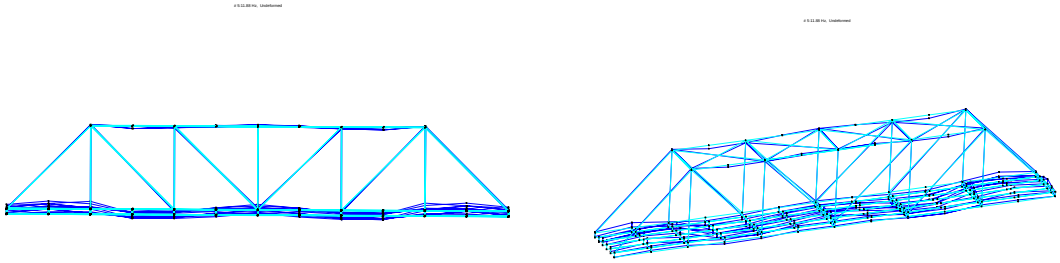

Figure 17 Mode 5 at 11.8 Hz Transverse/ vertical bending Mode – (6 nodes)

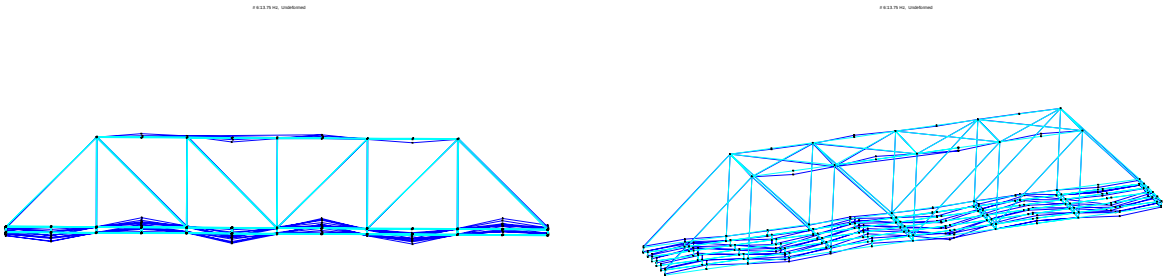

Figure 18 Mode 6 at 13.75 Hz Fifth Vertical Bending, alternate bays out of phase, (7nodes)

STRAIN MEASUREMENTS

Strain gauge measurements were undertaken at sixteen locations. The strain gauge locations were selected based on the resulting “hot spots” from the FEA as well as mode shape results from the EMA. **Figure 19** presents a plan view diagram of the north bound kerb side lane of the Kempsey Bridge and shows the sixteen strain gauge locations (SG1 to SG16). All gauges were of a linear, gel encapsulated type and orientated in the anticipated principal stress direction (i.e. parallel to the long axis of the respective structural members).

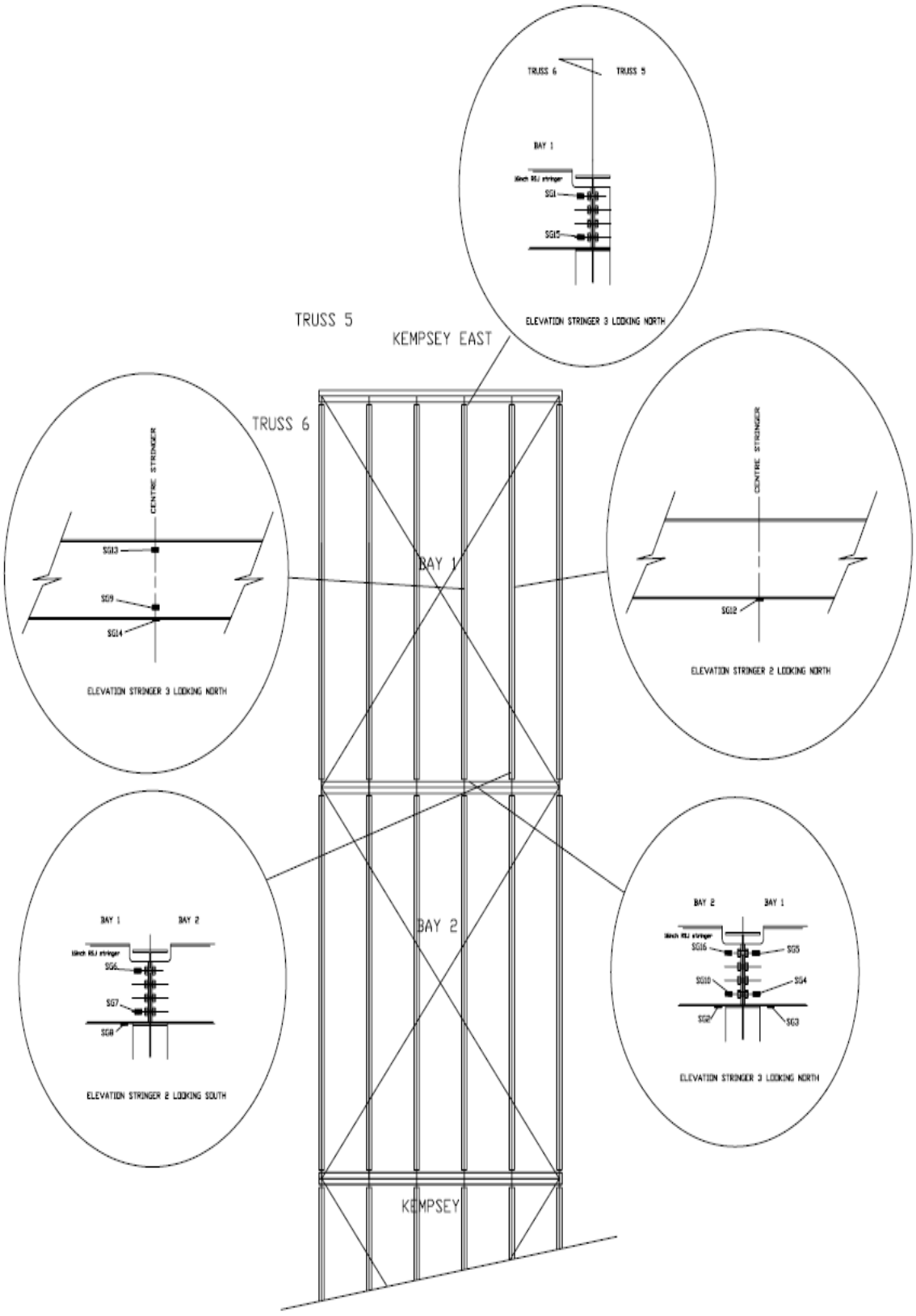

Figure 19 Plan View North Bound kerbside Lane - Sixteen Strain Gauge Locations (SG1 to SG16)

Test Vehicle Loading

Bridge Evaluation & Assessment - Test Truck loading

Axle loads from loading arrangements

Dimensions of Volvo Prime Mover F75155 and Brentwood Low Loader F02726
Test Load Vehicle A

Truck description

Steer axle (tare)	4.26 t	Steer to tandem	3.58 m	Block mass	0.99 t
Tandem (tare)	4.64 t	Spacing of tandem	1.37 m	Space for crane	3.44 m
Trailer (tare at king-pin)	4.28 t	Tandem to tridem	6.70 m	Max reach required	5.99 m
Trailer tridem (tare)	8.66 t	Spacing of tridem	1.27 m	(assumes crane in centre of trailer)	
King pin offset from centre of tandem	0.20 m	Spacing of tridem	1.27 m	Distribution to prime mover	
King-pin to front of trailer	0.63 m	King-pin to centre of tridem	8.85 m	King-pin to steer	5%
Length of tray	11.84 m	Centre of rear axle to end	1.09 m	King-pin to tandem	95%
No of blocks at goose-neck	4	Front of trailer to centre of block	3.60 m		

Block loading

Modular Expansion Joint Testing - ANZAC BRIDGE, WESTERN ABUTMENT

Block Position	Block position 1	2	3	4	5	6	7		Group loads (t) Steer	Tandem	Tridem	Total
								Tare	4.46	8.72	8.66	21.84
Loading level	No of blocks per position							Tare+bl	4.58	11.23	9.99	25.80
1	1	1	0	1	2	2	2	Load 1	4.66	12.83	17.22	34.71
2	2	2	2	2	2	4	2	Load 2	4.82	16.05	20.76	41.64

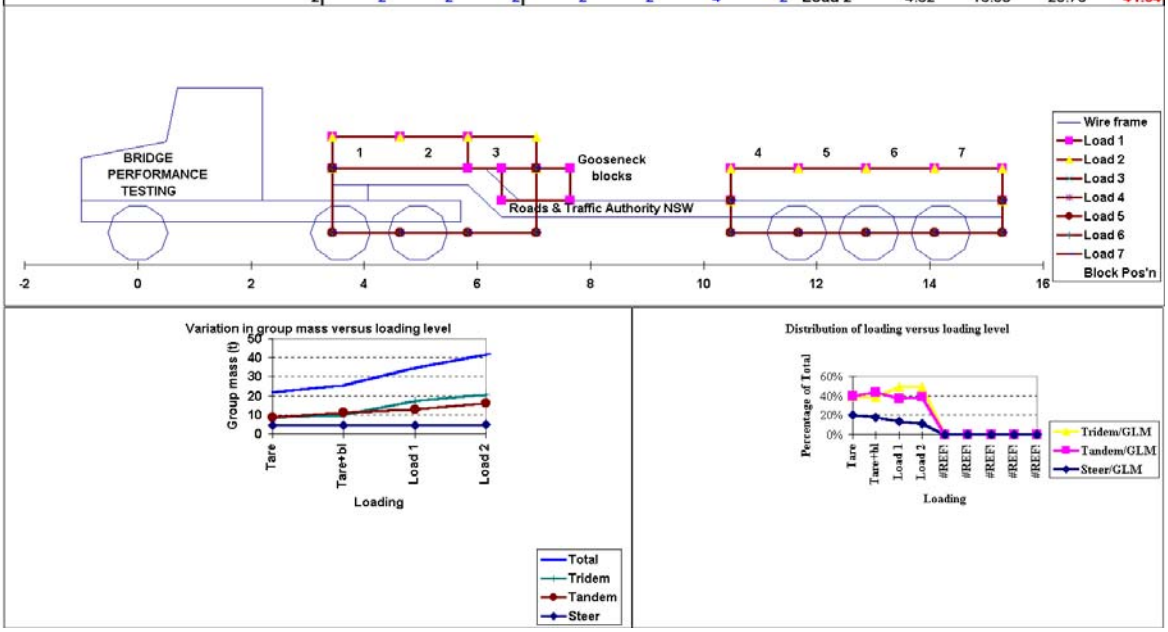

Figure 20 Test Vehicle Loading Arrangement

Figure 21 is a photograph of the test truck used for the controlled tests at all three bridges.

Figure 21 Bridge Load Test Truck

Figure 22 presents a schematic elevation of the bridge deck and kerb in relation to the nominal kerbside lane position and nominal test truck wheel positions.

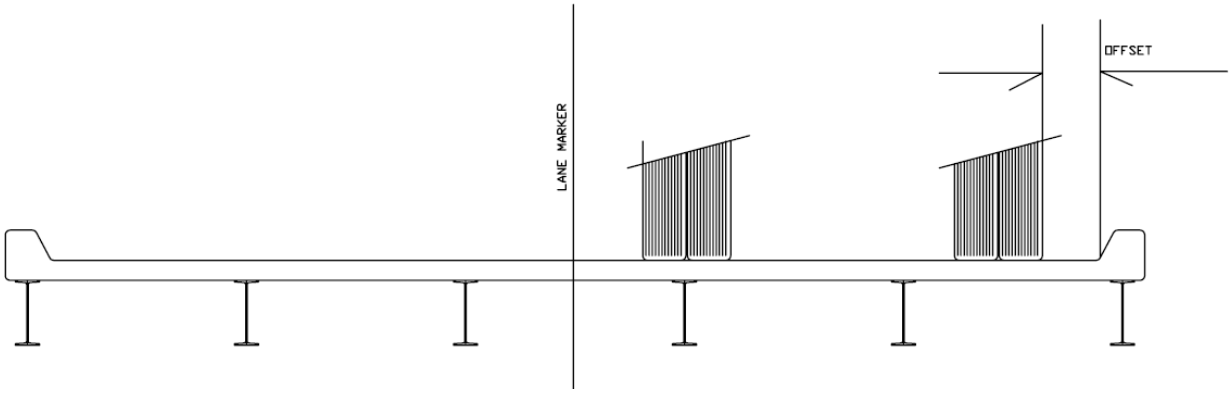

Figure 22 Sectional Elevation of Bridge Deck Showing Nominal Test Truck Position

MEASUREMENT PROCEDURE

Truck Slow Roll

In order to approximate true static strains and displacements, the truck was traversed over the joint at less than 10 km/hr producing negligible dynamic response of the truck or structure. All static and dynamic strains were recorded during this test. The lateral position of the truck was measured after each run by physical measurement of the wheel impression left on a bead of dental paste placed in a transverse direction on the road surface.

Truck Pass-bys

Following as closely as possible to the same line as the slow roll test, the truck was traversed at several speeds in the target speed range of 17 km/hr to 70 km/hr. The actual truck speed for each run was measured using a laser speed gun.

Table 2 presents the target pass-by speeds as well as the measured (actual) pass-by speeds, lateral tracking position, and time of test.

Table 2 Target Speed and Actual Pass-by Speeds

Run No.	Target Speed (Km/hr)	Actual Speed	Offset distance mm
1	18	18	535
2	18	17	570
3	25	27	570
4	25	24	490
5	30	30	560
6	30	31	570
7	36	36	615
8	36	37	580
9	41	41	620
10	46	49	750
11	46	46	685
12	51	51	470
13	54	54	600
14	54	54	410
15	60	59	610
16	60	59	660
17	65	66	655
18	Slow	north	450
19	Slow	reverse	
20	Slow	north	650
21	Slow	reverse	
22	Slow	north	800
23	Slow	reverse	
24	Stopping	north	430

STRAIN MEASUREMENT RESULTS

Strain signals were sampled at a rate of 1 kHz and allowed to run for the entire test sequence. The calibrated strain data was stored directly to disk on a Laptop via an Ethernet connection. The data was subsequently analysed to produce strain versus time plots.

Further analysis included the extraction of the maximum and minimum strain resulting from the passage of the six individual test truck axles. These data were used to calculate dynamic range factors for each strain signal, the calculations were performed for each strain gauge location for each individual axle as well as for all axles.

The positive dynamic amplification factor was calculated as follows:

$$\textbf{Dynamic Amplification Factor (Positive)} = \frac{\text{Maximum Dynamic Strain (same sense as static)}}{\text{Maximum Static Strain}}$$

The negative dynamic range factor was calculated as follows:

$$\textbf{Dynamic Amplification Factor (Negative)} = \frac{\text{Maximum Dynamic Strain (opposite sense as static)}}{\text{Maximum Static Strain}}$$

The total dynamic range factor was calculated as follows:

$$\textbf{Dynamic Amplification Factor} = \frac{\text{Maximum Dynamic Strain - Minimum Dynamic Strain}}{\text{Maximum Static Strain}}$$

Note: The Maximum Static Strain used in the denominator of the above equations was the maximum of the two closest slow roll lateral position results which straddled the lateral position for the run in question. This procedure was used to reduce the possibility of DAF over estimation.

RESULTS AND DISCUSSIONS

Slow Roll Results

Table 3 presents a summary of the resulting maximum strains and stresses from slow roll tests.

Table 3 Summary of Resulting Strains and Stresses From Slow Roll Pass-bys

	Maximum Strain (με)	Minimum Strain (με)	Maximum Strain Range (με)	Maximum Stress (MPa)	Minimum Stress (MPa)	Peak-Peak Stress Range (MPa)
sg1	57	-30	78	11	-6	16
sg15	25	-10	35	5	-2	7
sg13	1	-62	64	0	-12	13
sg9	134	-17	151	27	-3	30
sg14	163	-19	182	33	-4	36
sg12	174	-21	190	35	-4	38
sg5	350	0	348	70	0	70
sg4	55	0	56	11	0	11
sg3	0	-124	122	0	-25	24
sg16	170	-37	204	34	-7	41
sg10	29	-5	33	6	-1	7
sg2	0	-162	156	0	-32	31
sg6	95	-22	117	19	-4	23
sg7	77	-12	88	15	-2	18
sg8	0	-203	194	0	-41	39

Figure 23 shows sample strain time histories for a slow roll strain measurement for all gauges, during this slow roll the truck was briefly stopped at the mid span positions indicated by the diagram of the truck. The flat spots in the traces are at times when the truck was stationary.

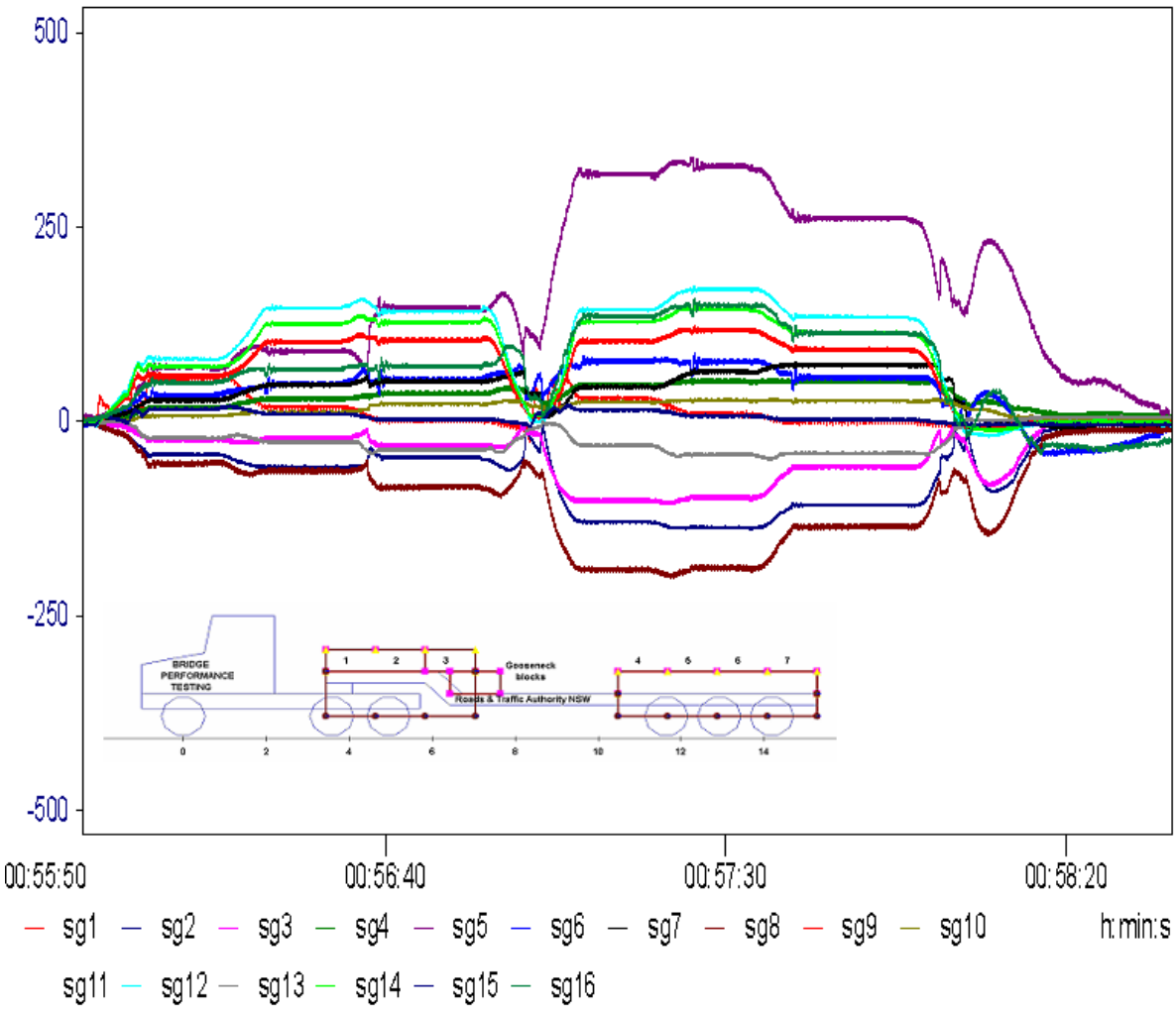

Figure 23 Sample Strain Time history all gauges

NEUTRAL AXIS OF STRINGERS AND COMPOSITE BEAM EFFECTS

The slow roll results were used to plot the position of the neutral axis of the stringers. **Figure 24** below shows the resulting normal stress diagram and apparent position of the neutral axis of the beam for a mid span location as well as for the cope connection.

It is clear that at the mid span stringer location the neutral axis is quite close to the geometric centre of the beam, which is an indication that the concrete deck is providing little composite effect, i.e. the concrete deck and stringer act almost as independent beams.

At the cope connection, the neutral axis is remarkably almost at the bottom flange of the stringer indicating, (not good for a moment connection), indicating a complete lack of composite effect as well as a severely limited moment carrying ability. These measurements appear to confirm theoretical results reported by Roeder *et al* [9].

Calculation of the moment of inertia for the complete stringer and reduced stringer at the cross girder connection predicted a ratio of approximately 3.6. The calculated increase in stress to support the same moment is approximately 4, (from y/I ratio).

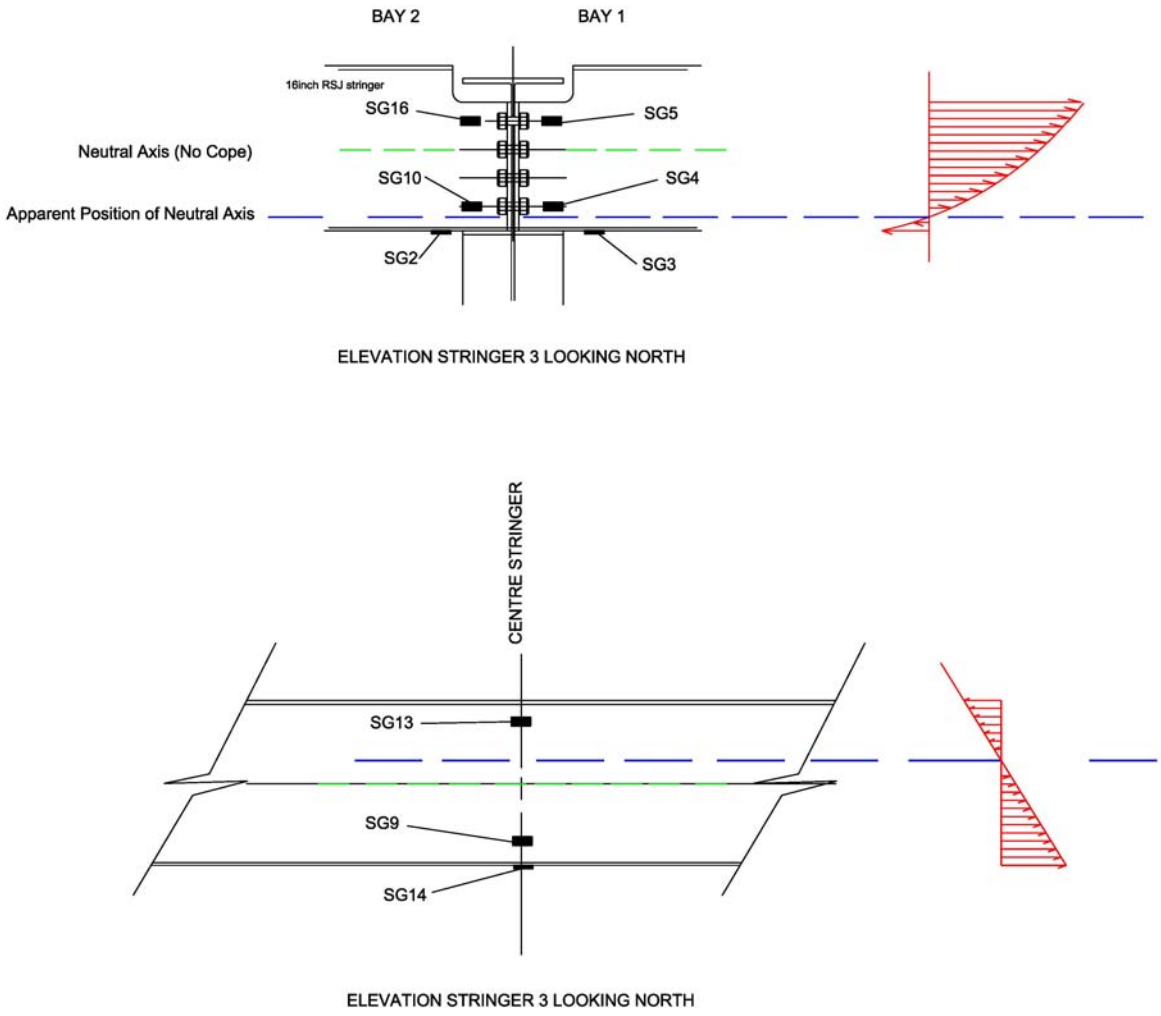

Figure 24 Stringer Diagrams Showing Measured Position of Neutral Axis

MAXIMUM STRAINS AND HYSTERESIS DURING PASS-BYS

Figures 26 to 31 below show sample slow roll results for all gauges. The figures include a diagram of the test truck scaled and positioned with respect to each group of gauges, i.e. at any instant in time, x axis, the truck position with respect to the gauge, can be found by projecting a vertical line at the point in strain and time in question. It is easy to pick this out from SG1, in Figure 21, as each strain event correlates with each axle passing above the gauge.

Figure 24 demonstrates that for the stringer mid span (bottom trace) there are two main peak strain events for the truck passby,), i.e. prime-mover tandem (tractor) axles mid span and trailer tridem mid span.

Figure 25 shows that there are three main peaks in strain the additional peak occurring when the tridem is mid span of bay 2, the extreme maxima occurs when axle 5 is mid span bay 1 and the prime-mover (tractor) is approx mid span bay2, i.e. the stringer connection receives an additive tensile strain from the load in the adjacent bay.

The maximum strain at SD5, top cope connection, occurs when the prime-mover (tractor) and trailer have straddled the cross girder.

It is also apparent that for most if not all strain gauges a hysteresis effect occurs, this is most apparent on **Figure 25, Figure 26** and **Figure 27**, marked as an offset. Such an effect is most likely due to a stick slip mechanism which probably occurs at the stringer/deck interface, this is again evidence of no composite beam effect, i.e. no effective shear connection between stringers and deck, once the load has passed the strain does not return to the same state as before the load is applied.

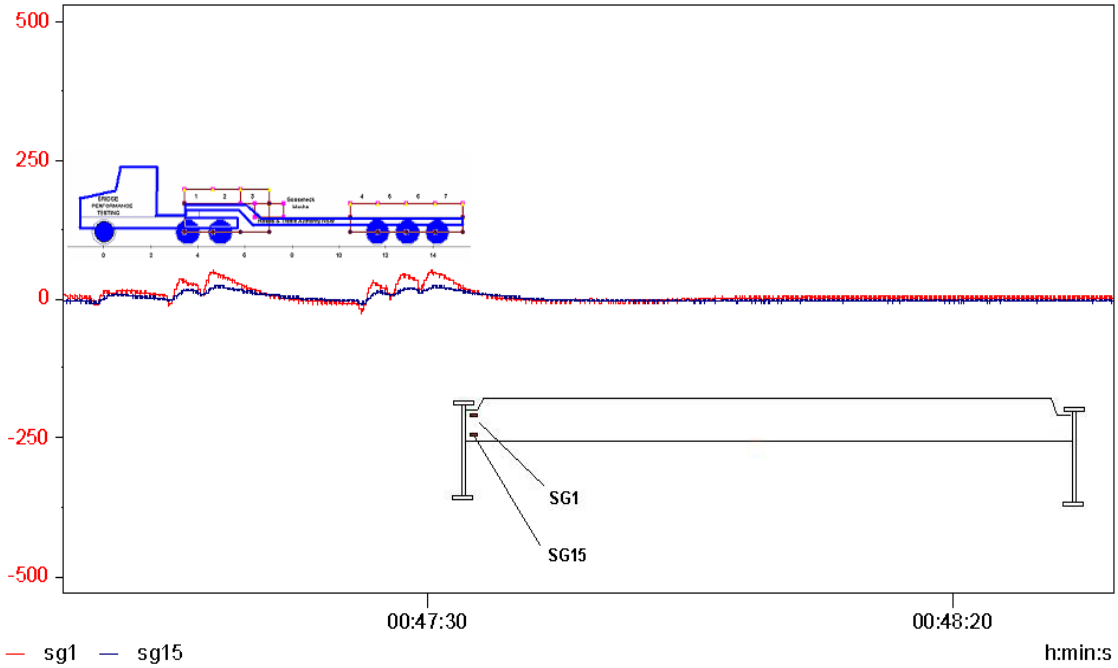

Figure 25 Slow Roll Strain time Histories For Group 1 Gauges, (stringer line 3, see also Figure 19 for locations)

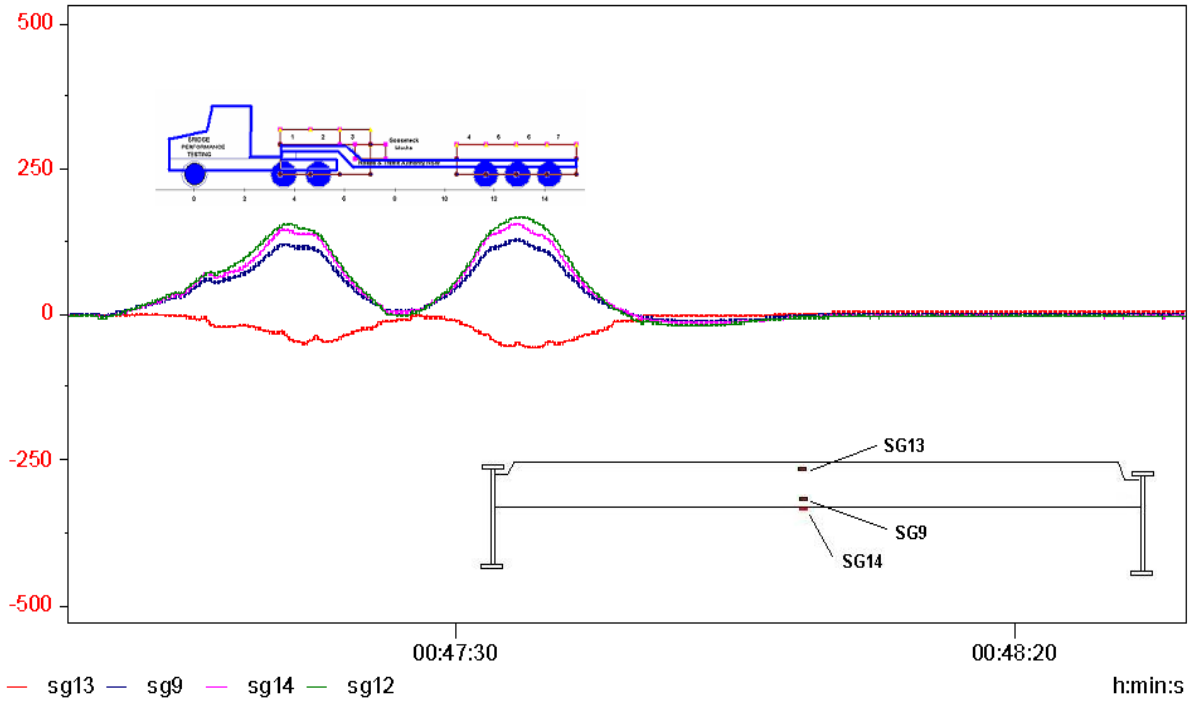

Figure 26 Slow Roll Strain time Histories For Group 2 Gauges, (SG9, SG13 and SG14 on stringer line 3, SG12 as SG14 but on stringer line 2, see also Figure 19 for locations)

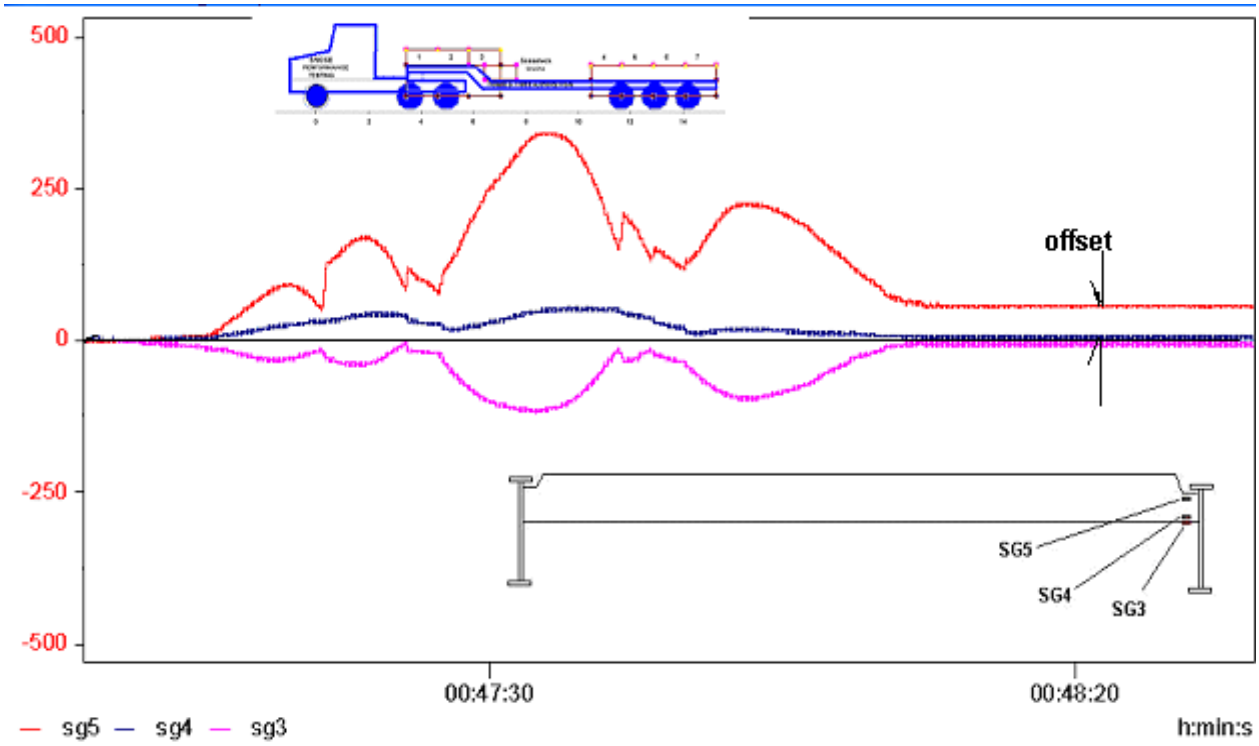

Figure 27 Slow Roll Strain time Histories For Group 3 Gauges, (stringer line 3, see also Figure 19 for locations)

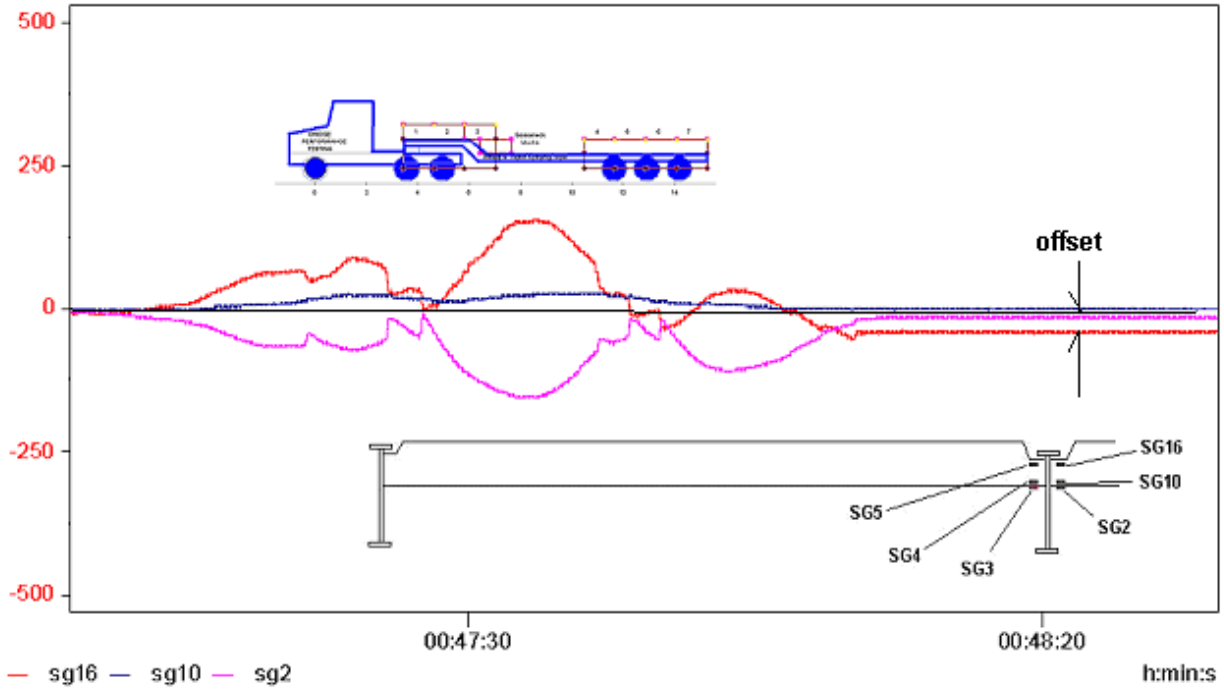

Figure 28 Slow Roll Strain time Histories For Group 4 Gauges, (stringer line 3, see also Figure 19 for locations)

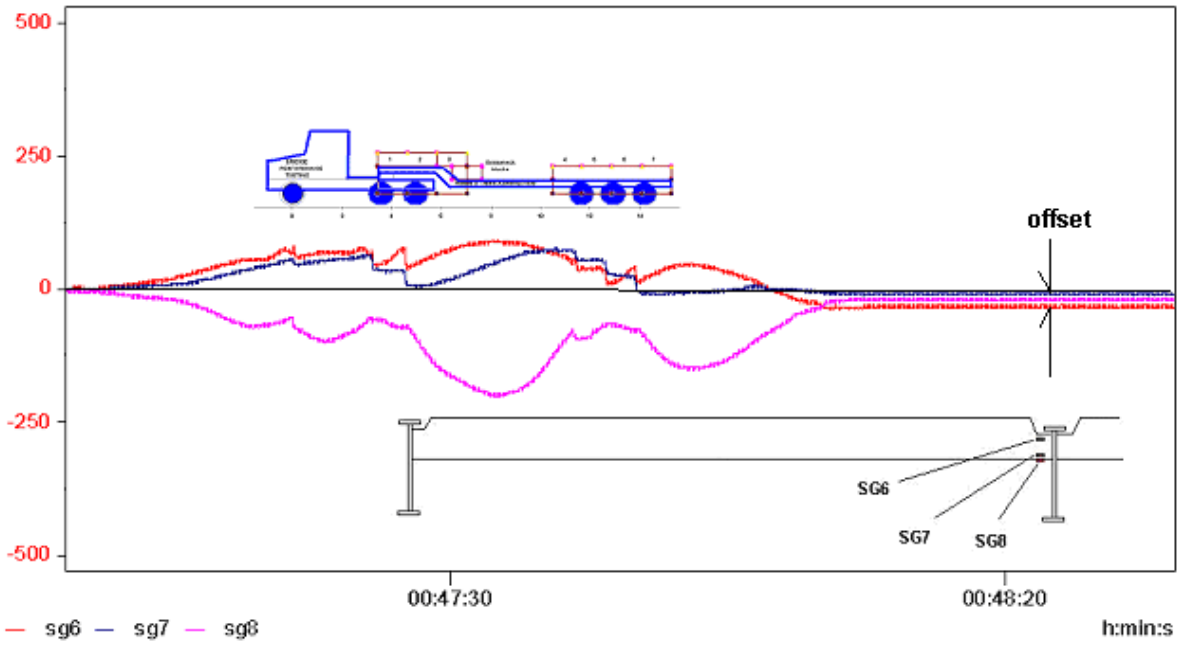

Figure 29 Slow Roll Strain time Histories for Group 5 Gauges, (stringer line 2, see also Figure 19 for locations)

DYNAMIC STRAIN RESULTS

Table 4 presents a summary of the resulting maximum strains, stresses and dynamic amplification factors from all controlled tests at Kempsey Bridge.

Table 4 Summary of Resulting Strains, Stresses and Dynamic Amplification Factors

Location	Strain (με)			Stress (MPa)			DAF's		
	Max.	Min.	Range	Max.	Min.	Range	+ve	-ve	Range
sg1	57	-45	87	11	-9	17	1.1	-0.9	1.1
sg15	29	-20	39	6	-4	8	1.1	-0.8	1.1
sg13	9	-78	76	2	-16	15	1.3	-0.2	1.3
sg9	148	-36	176	30	-7	35	1.1	-0.3	1.2
sg14	181	-34	211	36	-7	42	1.1	-0.2	1.2
sg12	178	-37	212	36	-7	42	1.0	-0.2	1.1
sg5	372	-119	472	74	-24	94	1.1	-0.3	1.4
sg4	66	-19	76	13	-4	15	1.2	-0.3	1.4
sg3	18	-138	140	4	-28	28	1.2	-0.2	1.2
sg16	170	-121	252	34	-24	50	1.0	-0.8	1.3
sg10	31	-20	41	6	-4	8	1.1	-0.7	1.2
sg2	12	-185	184	2	-37	37	1.2	-0.1	1.2
sg6	106	-64	163	21	-13	33	1.2	-0.7	1.6
sg7	77	-34	98	15	-7	20	1.0	-0.4	1.1
sg8	1	-231	222	0	-46	44	1.1	0.0	1.2

Figure 30 shows sample strain time history for group 3 gauges i.e. SG5 SG4 and SG3, at slow roll and a typical 59kph pass-by. These plots demonstrate that the dynamic response, is a combination of localised stress effects as well as global stresses i.e. the dynamic strain time histories from gauges at the cope show similar general shape to the slow roll strain time histories but at an amplified level. In addition, a more global dynamic effect can be seen on the lower plot, which is the dynamic build up in strain prior to the arrival of the truck on the span instrumented with strain gauges, due predominately in this case to excitation of the fundamental vertical bending mode of the truss span.

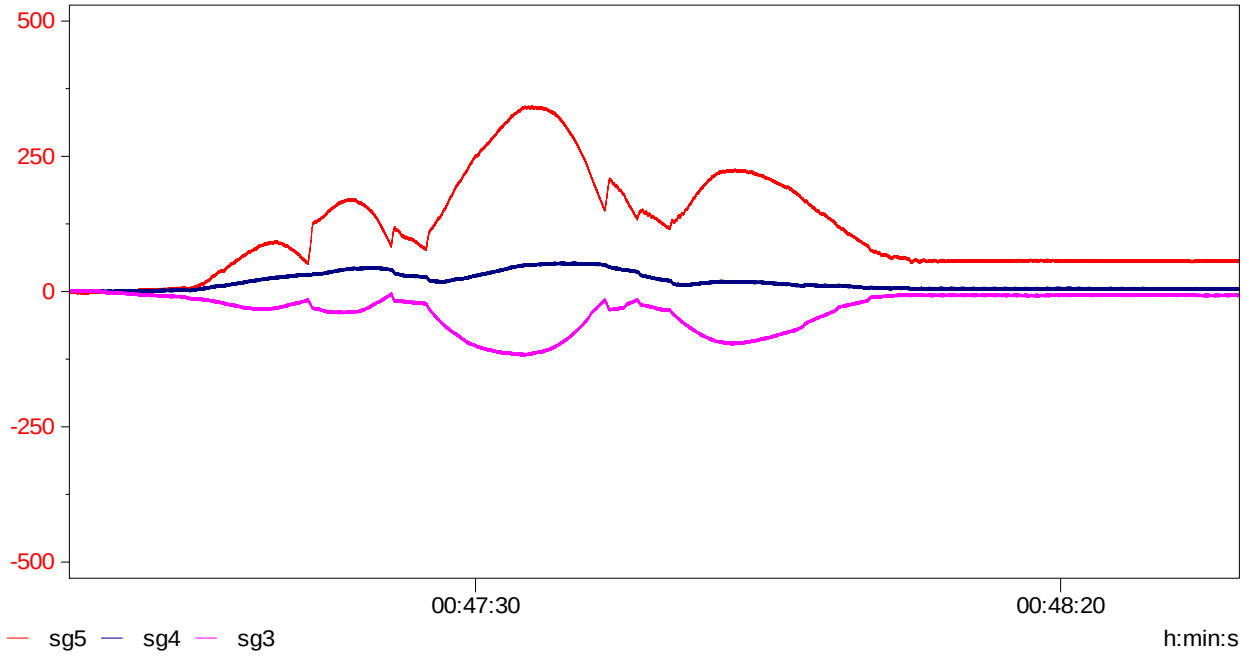

Figure 30(a) Sample Strain Time History Module 5 Gauges, slow roll

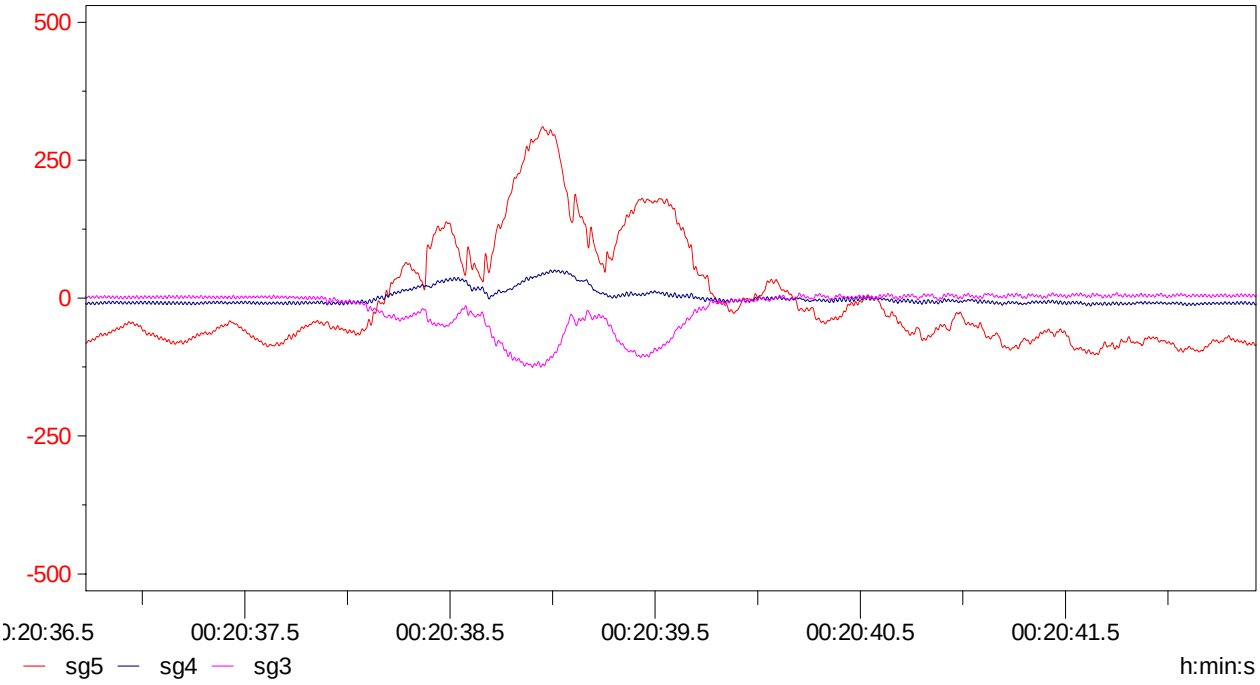

Figure 30(b) Sample Strain Time History Module 5 Gauges, 59km/hr

LONG TERM STRAIN MEASUREMENTS AND RAIN FLOW CYCLE COUNTING

Table 5 below shows an abridged summary of the maximum strain range recorded for each gauge from the controlled (legal axle load and legal speed) pass-bys and from the uncontrolled 7 days of traffic for all three tested bridges. It is apparent from these results that analysis or fatigue design based on legal load limits alone would very much under estimate the actual dynamic service loads.

Table 5 Summary of Maximum Recorded Stress Ranges (All Bridges)

Bridge Location	Strain Gauge Location No.	Component Description	Stress Range From Controlled Tests (MPa)	Stress Range Recorded under Traffic (MPa)	Apparent Maximum Amplification from Traffic (note 1)
Dennis	Sg4	Top Web	75	84	1.1
	Sg6	Bottom Web	15	34	2.3
Hexham	Sg14	Top Web	19	56	3.0
	Sg15	Bottom Web	20	48	2.4
	Sg21	Top Web	16	48	3.0
	Sg22	Bottom Web	9	32	3.6
Kempsey	sg5	Top Web	94	128	1.4
	sg4	Bottom Web	15	24	1.6
	sg3	Bottom Flange	28	48	1.7
	sg10	Bottom Web	8	16	1.9
	sg2	Bottom Flange	37	56	1.5
	sg6	Top Web	33	56	1.7
	sg7	Bottom Web	20	32	1.6
	sg8	Bottom Flange	44	56	1.3

Note: Numbers include effects from multiple presence

FINITE ELEMENT MODELLING – FINE MESH RESULTS

A fine mesh model was refined to assess the potential effects of concept fatigue life extension options. Concept options proposed can be placed in two main categories, 1) **Stringer stiffening** and 2) **Compliant stringer cross girder connections**.

As-Built Connection Detail

The as-built condition was first modelled and a static analysis carried out for the live load as per controlled strain measurements. **Figure 31** presents modelling results for the as-built condition.

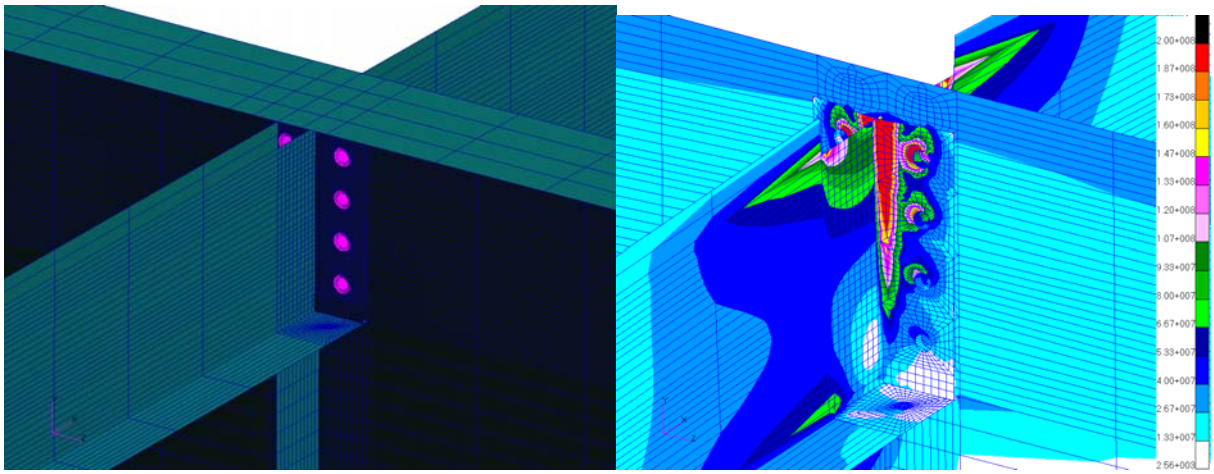

Figure 31 Fine Mesh Model For As Built Connection Detail, base model left, Stress contour results right.

STRINGER STIFFENING OPTIONS

Stringer Top Flange Replacement- This option involved plating over the stringer top flanges at the cross girders to effectively replace the top flange cut away to clear the cross girder top flange. **Figure 32** shows a sample stress contour output for this concept.

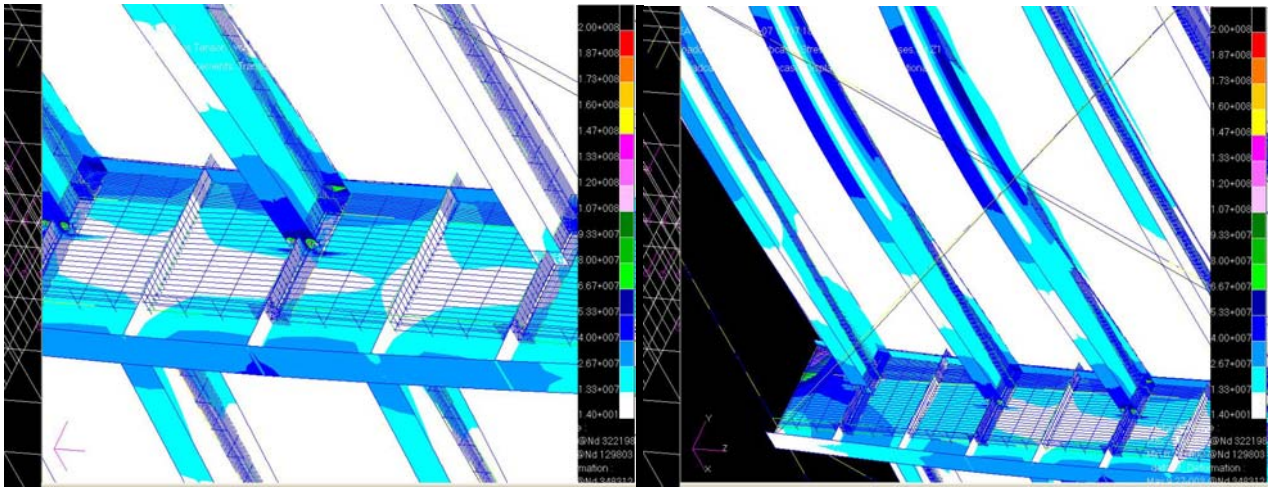

Figure 32 Sample Stress Contour Plots For Stringer top Plate replacement Option

COMPLIANT CONNECTION OPTIONS

Flexible Bolted Connections/Bearings- These options require the replacement of the top two, three or four rows of connection fasteners with a flexible assembly. Ideally these assemblies would allow some axial movement of the stringer flange whilst maintaining lateral restraint. The concept compliant connection options were modelled with an axial stiffness of 100KN/mm. **Figure 33** shows a sample stress contour plot.

The compliant connection may be seen as a variation of the rivet removal damage limitation method investigated by Roeder *et al* [10]. The principal difference appears to be in the plane of removal. Roeder removed rivets from the connection through the web of the stringer and the present study replaced rivets (with compliant fasteners) through the web of the cross girder.

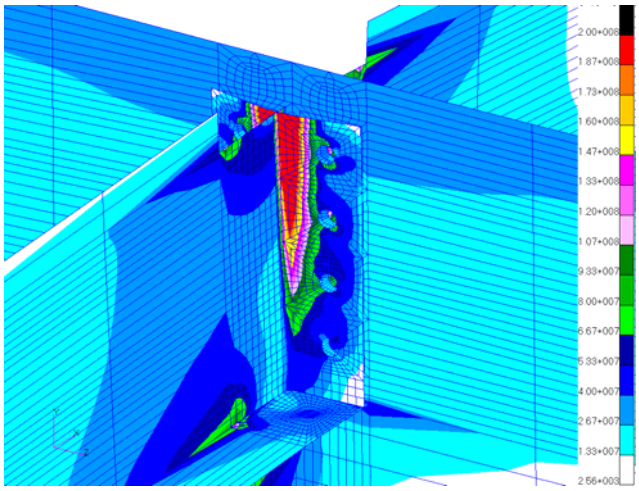

Figure 33 Sample Stress Contour Plot, Compliant Connection Option

Bolt Removal - Removal of the top 2 and 4 rows of bolts/rivets has also been modelled. **Figure 34** shows stress contour plots for these conditions.

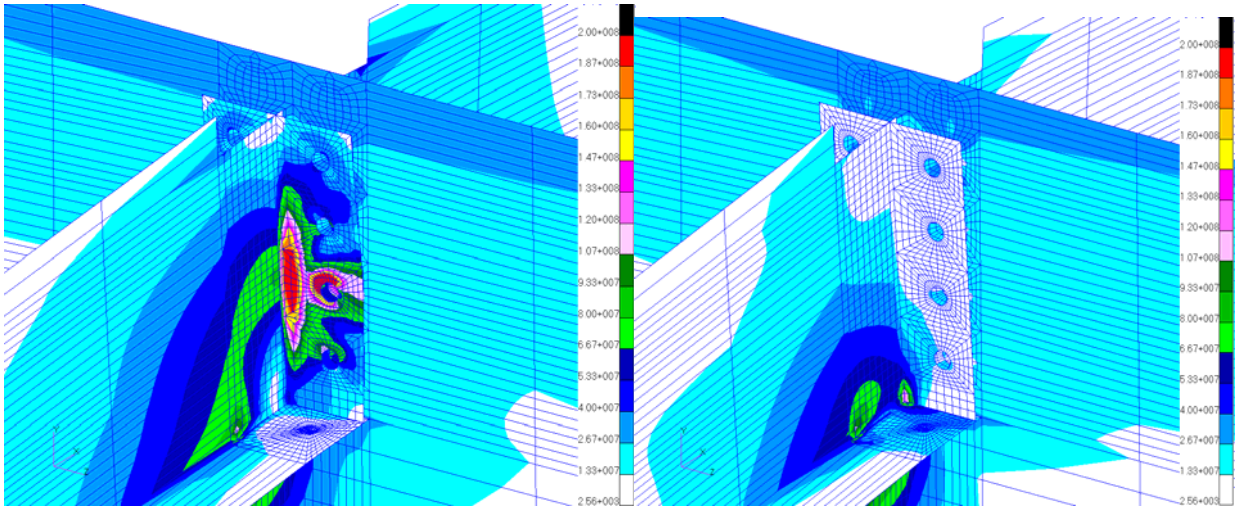

Figure 34 Sample Stress Contour Plots: 2 rows bolts removed left: 4 rows bolts removed right

POST MODIFICATION MEASUREMENTS

Whilst the stringer top flange stiffening option offered the optimum solution, there were operational constraints that operated against its implementation. The compliant fastener option was initially trialled in one span. Strain measurements were recorded under traffic for each connection arrangement tested.

The following connection arrangements were tested

TEST A no bolts in top 2 rows ie 4 bolts out

TEST B 2 hard bolts RHS flange (cracked flange)

TEST C 4 hard bolts top two rows ie fully bolted as per pre modification

TEST D compliant bolts, (zero pre tension)

TEST E compliant bolts in top two rows (half turn pre tension). Recordings were subsequently analysed to produce time histories for a sample number of heavy vehicle pass-bys, the ratio of mid span stringer strain to the maximum strain at each gauge was calculated for each pass by.

Stress concentration Factors

Table 6 presents a summary of the resulting maximum stress concentration factors from the above test series.

Table 6 Summary of Resulting Stress Concentration Factors From Test Series

Test	Description of Test	Maximum Stress Concentration Factor	Position of Maximum Stress	Reduction in Stress due to Modification (%)	Predicted increase in Fatigue Life (x)
A	no bolts in top 2 rows ie 4 bolts out	1.3	SG5	45	6.1
B	2 hard bolts RHS flange (cracked flange)	1.2	SG5	50	8.1
C	4 hard bolts top two rows ie fully bolted as per pre modification	2.4	SG3	0	1.0
D	compliant bolts, zero pre tension	1.4	SG3	41	5.1
E	compliant bolts in top two rows, half turn pre stress	1.6	SG3	33	3.3

Figure 35 shows a sample strain time history for the as built connection, ie hard bolted with all fasteners in place. **Figure 36** shows a sample strain time history for the modified connection as proposed, i.e. top four bolts with compliant washers, pre tension one half turn. The figures clearly demonstrate the significant stress reduction associated with the modification.

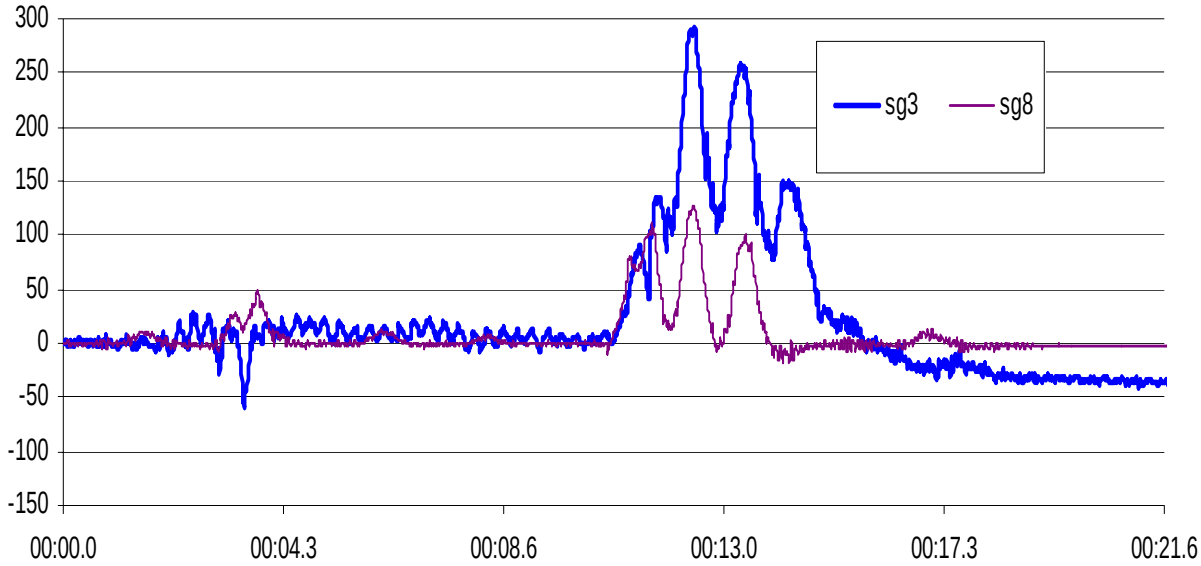

Figure 35 Sample Strain Time History – As Built (Test C)

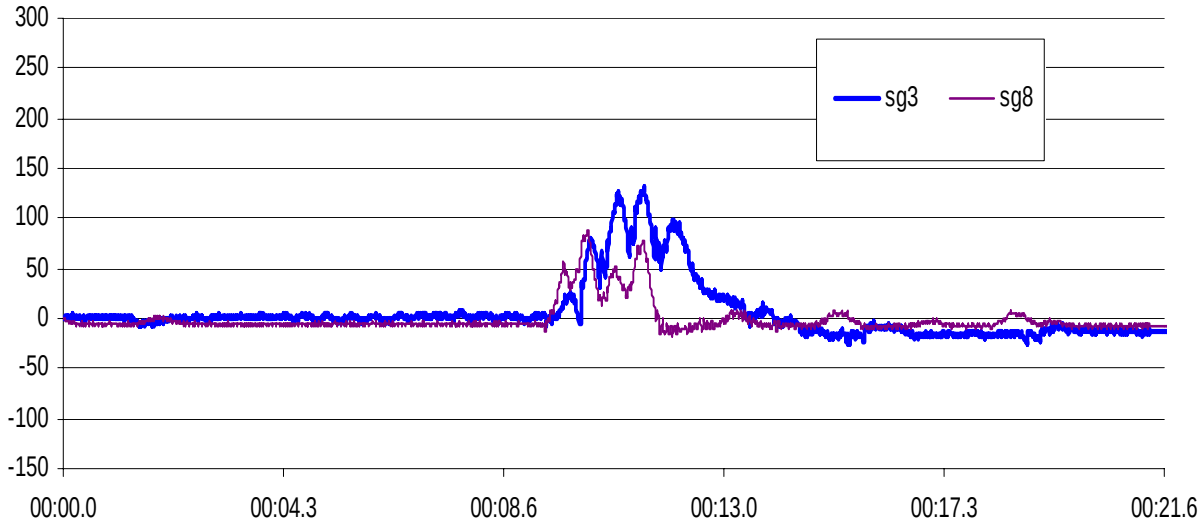

Figure 36 Sample Strain Time History – Installed Modification (Test E)

TRAFFIC DATA ANALYSIS

Analysis of Weigh-In-Motion (WIM) Data

The load spectrum data for each WIM station were converted to the ADESA applicable to relevant bridges using the minus rule. The resulting Average Daily Equivalent Standard Axle (ADESA) load spectra were then plotted to structure the initial data groups. The data groups listing were individually tested using F-test and Student T-test, and statistically analysed for homogeneity using ANOVA. The data groups were subjected to a follow-up test using Tukey's Test. Final grouping of data was done after a series of follow-up tests. An attempt was also made to transform the weighted percentages of the resulting ADESA load spectra into arcsin values for each WIM station. All samples of the arcsin transformed ADESA percentages were then analysed using ANOVA. The results showed that the data were homogeneous.

Calculation of ESA from WIM Data

The ESA applicable to bridges based on WIM data for the first half of 2006 was calculated using the minus rule formula, derived as follows:

$$f_f^3 = \frac{f_m^3 \times 2 \times 10^6}{n_{sc}}$$

$$n_{sc} = \frac{f_m^3}{f_f^3} \times 2 \times 10^6$$

$$N_{sc} = \sum_i n_{sci}$$

$$N_{sc} = \sum_i \frac{f_{mi}^3}{f_f^3} \times 2 \times 10^6$$

Proportional Correlation

$$f_{mi} \propto L_i$$

$$f_f \propto L_f$$

$$N_f = \sum_i \left(\frac{L_i}{L_f} \right)^3 n_i$$

$$\frac{N_f}{N_V}$$

$$\frac{N_f}{N_G}$$

$$\frac{N_f}{N_A}$$

Where:

N_f = Equivalent standard axle (ESA) for the period

L_i = Mass of Axles x Number in group

L_f = Standard Load (160 kN, assumed)

n_i = Count for the period

N_V = Total number of Vehicles

N_G = Total Groups

N_A = Total Axles

Cumulative ESA data for the period 1980-2006 are shown graphically as Figure 37. These data confirm the exponential growth in loads and an even faster growth in axle group repetitions due to the greater utilisation of B-doubles and tri-axle semi-trailers. The ESA approach differs from the truck weight histogram (TWH) and wheel weight histogram (WWH) method suggested by Fu *et al* [6]. However, the methodology is considered to be broadly similar.

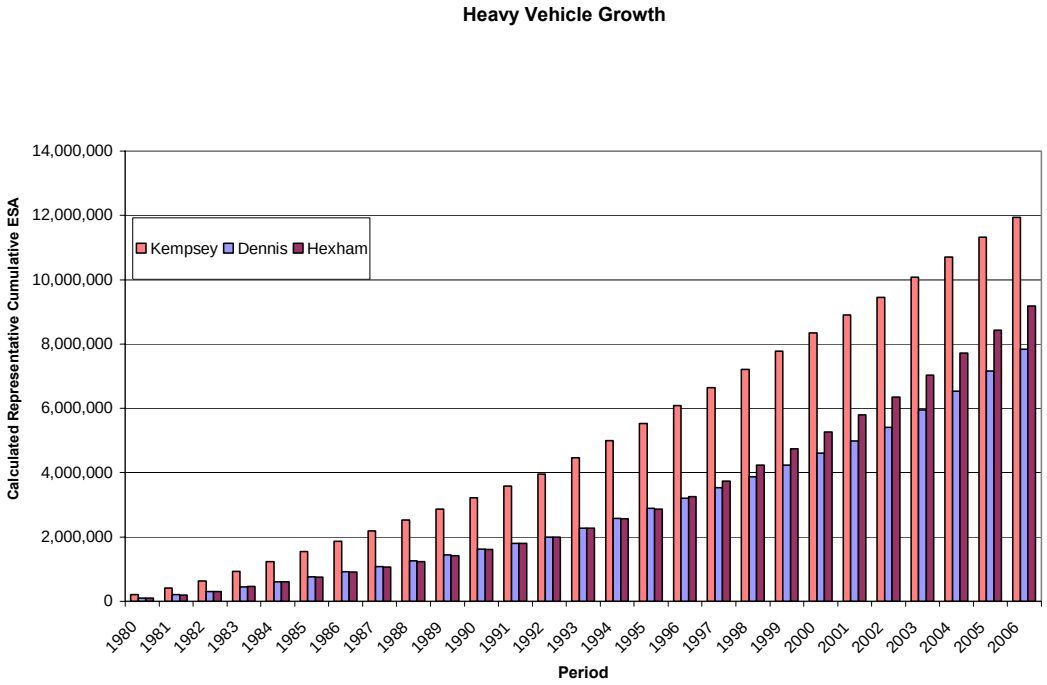

Figure 37 Representative Cumulative ESA

CONCLUSION

The basic failure mechanism at the stringer/cross girder connection involves the inability of the stringer to transmit and/or react live and dead load induced bending moments. From this study, it is clear that the neutral axis of the stringer (at the cross girder) is almost at the bottom flange, (at mid span the neutral axis is approx 2/3 up the web, so a small composite beam effect only exists between the stringers and the concrete deck).

Due to the vast reduction in moment of inertia of the stringer at the cross girder, (i.e. a factor of 3.6), the bending stiffness is greatly reduced and the stringer probably behaves (and deflects) more like a simply supported beam attempting to rotate the stringer flange out of plane. It is also apparent that the “fixed end” and/or “continuous” nature of the stringer does little to assist the stringer to carry load, some indirect evidence of this can be seen in **Figure 24** (note the very small compression that occurs mid span of the stringer when the tridem has passed to bay 2, SG14, this is really the third peak in the strain which is much greater and in the opposite sense for SG5 and would be greater for SG14 if the stringer was truly continuous). Analysis of the speed runs demonstrate that these conclusions are similar but with generally higher strains due to dynamic amplification.

In summary the as-built stringer connection detail is **poor** from both a **static and dynamic** perspective. The detail is **not stiff** or **strong enough** to act as a **fixed end** or form a **continuous** beam, neither is it **flexible enough** to **allow out of plane rotation**, (without high stress) and allow the stringer behave as a simply supported beam.

Possible solutions for this problem that have been identified thus far are placed in two main categories

Stiffening, which would include the top flange replacement concepts as well as the stringer truss type stiffening, such concepts would take bending stresses away from the stringer/cross girder connections and/or reduce mid span stringer deflections as well as out of plane rotation, bolts/rivets would probably remain as is.

Compliant Fastening, i.e. concepts which allow the out of plane rotation at the stringer support points and allow the stringer to act more as a simply supported beam, have a clear advantage of much lower cost than the stiffening options, and were achieved with access from under the bridge, i.e. no lane closures.

Analysis of weigh-in-motion (WIM) data confirm that bridge loadings are increasing due to exponential growth in loads and an even faster growth in axle group repetitions due to the greater utilisation of B-doubles and tri-axle semi-trailers. These data and the apparent load effect for fatigue from uncontrolled heavy vehicle traffic significantly exceeds the value that would be predicted using the test vehicle factored for dynamic effects and multiple presence.

ACKNOWLEDGEMENT

The authors wish to thank the Chief Executive of the Roads and Traffic Authority NSW for permission to publish this paper. The opinions and conclusions expressed in this paper do not necessarily reflect the views of the RTA.

REFERENCES

1. AASHTO, “Standard Specification for Highway Bridges”, American Association of State Highway and Transportation Officials, 15th Edition, Washington, DC, USA, 1973.
2. ROEDER C.W., MACRAE G.A., ARIMA K., CROCKER P.N. & WONG S.D., “Fatigue Cracking of Riveted Steel Tied Arch and Truss Bridges”, *Research Report WA-RD 447.1,* Washington State Transportation Center, Seattle, USA, 1998.
3. Roads & Traffic Authority of NSW. “Blueprint - RTA Corporate Plan 2008 to 2012”, *RTA Publication 07.329*, Sydney, Australia, 2008.
4. IMAM, B.M., RIGHINIOTIS T.D. & CHRYSSANTHOPOULOS M.K., “Probabilistic Fatigue Evaluation of Riveted Railway Bridges”, *J. Bridge Engineering,* ASCE, 13(3), 237-244, 2008.
5. GARGETT D., HOSSAIN A. & COSGROVE D., “Interstate Freight on States’ Roads”, *Proc. 29th Australasian Transport Research Forum*, Surfers Paradise, Australia, 2006.
6. FU G., FENG J., DEKELBAB W., MOSES F., COHEN H. & MERTZ D., “Impact of Commercial Vehicle Weight Change on Highway Bridge Infrastructure”, *J. Bridge Engineering,* ASCE, 13(6), 556-564, 2008.

7. MORASSI A. & TONON S., “Dynamic Testing for Structural Identification of a Bridge”, *J. Bridge Engineering,* ASCE, 13(6), 573-585, 2008.

8. EWINS D.J. “Modal Testing: Theory, Practice & Application (2nd Edition)”, *Research Studies Press*, Hertfordshire, UK, 163-276, 1999.

9. ROEDER C.W., MACRAE G.A., KALOGIROS A.Y. & LELAND A., “Fatigue Cracking of Riveted, Coped, Stringer-to-Floorbeam Connections”, *Research Report WA-RD 494.1,* Washington State Transportation Center, Seattle, USA, 2001.

10. ROEDER C.W., MACRAE G.A., LELAND A. & ROSPO A., “Extending the Fatigue Life of Riveted Coped Stringer Connections”, *J. Bridge Engineering,* ASCE, 10(1), 69-76, 2005.

Appendix M

Ancich E.J. and Brown S.C. (2009). Premature Fatigue Failure in a Horizontally Curved Steel Trough Girder Bridge, *Proc. International Association for Bridge & Structural Engineering (IABSE) Symposium,* Bangkok, Thailand.

IABSE
International Association for Bridge & Structural Engineering

SUSTAINABLE INFRASTRUCTURE
Environment Friendly, Safe and Resource Efficient

33rd IABSE Symposium

Bangkok, Thailand
September 9-11, 2009

Sponsored by:

Ministry of Transport, MOT

PTT Public Company Limited

The Siam Cement Group

Organized by:

Chulalongkorn University, CU

IABSE Thai Group
The Thai Group of IABSE

Asian Institute of Technology, AIT

Premature Fatigue Failure in a Horizontally Curved Steel Trough Girder Bridge

Eric ANCICH
Senior Project Engineer,
Bridge Engineering
Roads & Traffic Authority
Parramatta, Australia
Eric_Ancich@rta.nsw.gov.au

Eric Ancich has over 25 years experience in structural dynamics and manages the delivery of engineering consultant services for bridge rehabilitation and technically unique bridge projects.

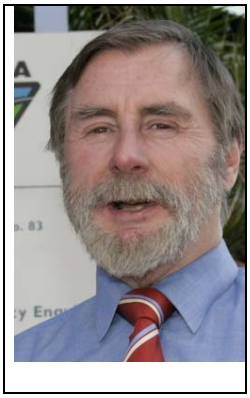

Steve BROWN
Associate
Heggies Pty Ltd
Lane Cove, Australia
Steve.Brown@heggies.com

Steve Brown graduated from the University of Technology, Sydney in 1980 with an honours degree in mechanical engineering. He specialises in the areas of structural dynamics and analytical modelling.

Summary

Fatigue cracking was observed in a three cell, three span, continuously curved steel trough girder bridge in far western NSW. The bridge over the Darling River at Wilcannia had been in service for about 11 years and the fatigue cracks were all associated with asymmetric internal stiffeners.

The bridge was investigated using a structural dynamics based approach and the results showed that the premature fatigue failure was due to the design of the asymmetric internal stiffeners that were not continuous over the full perimeter. As the stiffeners form a partial height U-frame, this allowed the webs, above the stiffeners, and the deck to rack under load. A calibrated FEA model of the bridge was used to investigate a range of solution options including continuing the stiffeners over the full perimeter and the complete removal of the stiffeners. As the confined space inside the box girders was not conducive to welding or cutting, a very unusual and innovative solution using external rib stiffeners was devised, modelled and adopted.

Keywords: High cycle fatigue; Composite box girder bridge; Damping; Finite element method; Modal analysis; Strain measurement.

1 INTRODUCTION

The bridge was designed in 1988 to NAASRA [1]. It generally complies with Section 3 and Clause 7.7.3 provisions of the Code for composite box girder bridges. The origin of the design criteria is the AASHO Standard Specification for Highway Bridges (AASHTO [2]). The design criteria stem from a research and prototype testing of straight bridges of similar construction. Whilst this bridge is described as a trough girder bridge, it is identical to the North American description of a multiple spine composite concrete-steel box girder bridge (Sennah & Kennedy [3]). Figure 1 shows a general view of Wilcannia Bridge with the original 19th Century lift span bridge visible in the background. The bearings for the bridge are pot-type bearings, with two fixed bearings at each pier and one sliding guided bearing and two free sliding bearings at each abutment.

The NAASRA 1976 code provided that "transverse bending stresses resulting from distortion of the girder cross section and from vibration of the bottom flange plate need not be considered" and that " internal diaphragms are not required at points intermediate between support diaphragms".

Concern was raised in early 2002 at the appearance of a number of cracks in the webs of the steel box girders, which had manifested after the relatively short period of approximately eleven years of service.
The cracking appeared to be fatigue related and was restricted to areas immediately adjacent to asymmetric internal stiffeners (See Figure 3). Figure 2 also shows a temporary cross brace that was removed after construction.

Vibration measurements and modal response shape measurements were conducted during September 2002. In addition to the above vibration tests, strain measurements were undertaken at six selected locations which were selected following preliminary analysis of the modal tests. The main aims of the strain measurements were:

- Quantify quasi static and dynamic strain levels due to traffic.
- Determine dynamic amplification factors.
- Determine dominant frequencies of dynamic strains.

Figure 1 presents a photograph of the Wilcannia Bridge

Figure 1 *View of Wilcannia Bridge*

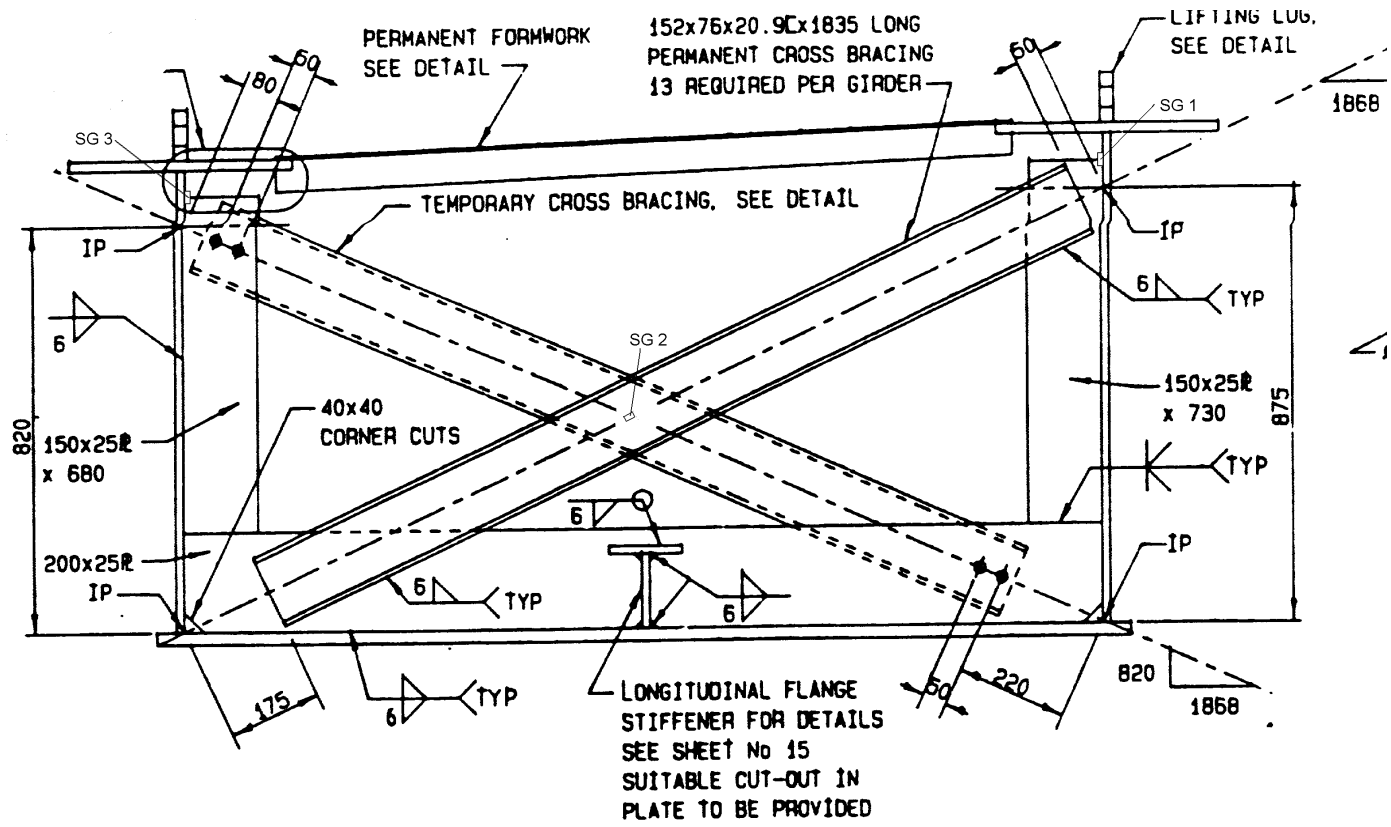

Figure 2 *Asymmetric Internal Stiffeners*

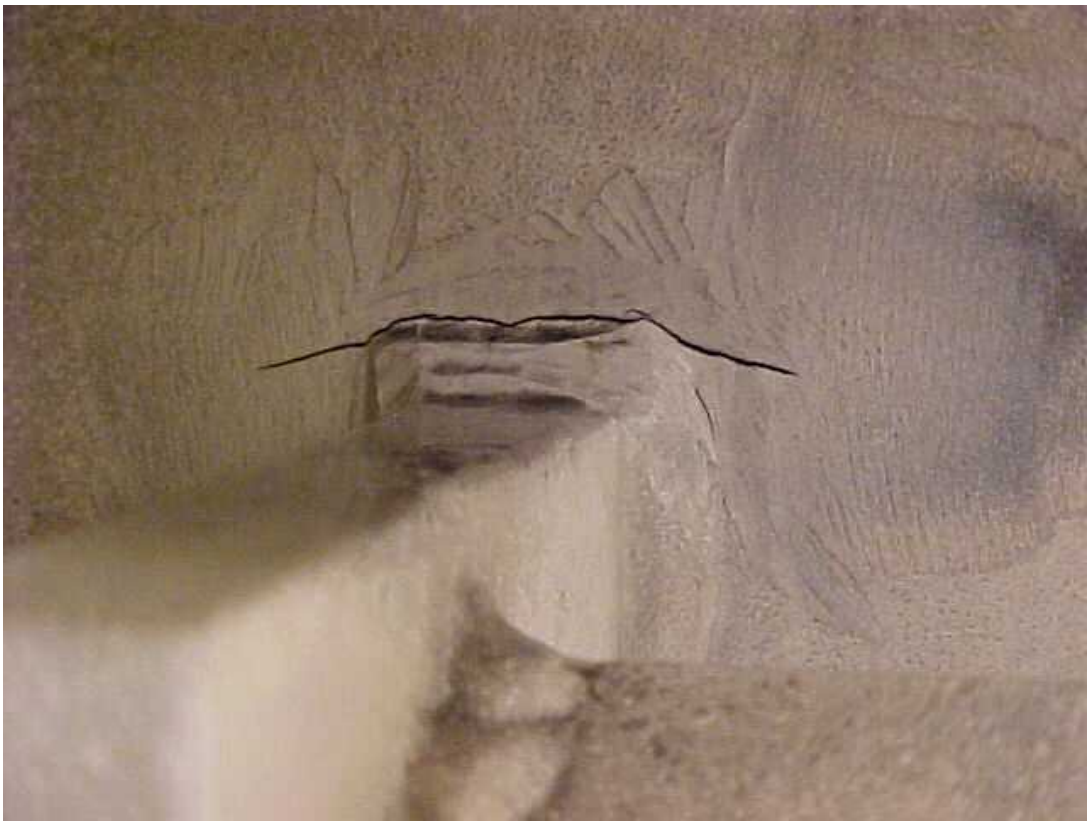

Figure 3 *Typical Cracking above Asymmetric Internal Stiffener*

2 MODAL ANALYSIS TEST PROCEDURES

2.1 Test Description

The measurement and definition of the natural frequencies and mode shapes of a structure is referred to as modal analysis. Experimental identification of structural dynamic models is usually based on the modal analysis approach. In the classical modal parameter estimation method, frequency response functions are measured under controlled conditions. For many large structures it is not practical, or prohibitively expensive to apply a controlled input force and hence the need arises to identify modes under operating conditions, or from environmental excitation. In this type of analysis, only response data are measurable while the actual loading conditions (input forces) are unknown. In the last decade, the problem of output-only modal analysis has typically been approached by applying a peak-picking technique to the auto- and cross- powers of the measured responses, resulting in operational deflection shapes and approximate estimates for the resonance frequencies. A further enhancement of this method was conceived and trialled at Wilcannia which involved the use of an artificially introduced bump. An RTA test truck (GMV approximately 10 tonnes) was traversed across a length of 100mm by 50mm thick hardwood bonded temporarily to the bridge deck for the duration of the modal tests. **Figure 4** shows a photograph of this arrangement. The RTA test truck was driven at approximately 5 km/hr with the rear axle only made to traverse the bump. The bump was located approximately 6m west of mid span (adjacent to measurement location 113).

The test procedure and methodology for experimental modal analysis is comprehensively covered by Ewins [4].

Figure 4 *View of Test Truck and Artificial Bump*

For the bridge studied, the measurement of Frequency Response Functions (FRF's) involved the simultaneous measurement of a reference vibration response and "roving" vibration responses at a large number of locations over the bridge structure. For these tests, the frequency range of interest was nominally 0 Hz to 25 Hz. The vibration responses were measured at selected locations using an accelerometer attached to the structure with a magnetic base. **Figure 5** shows the typical instrumentation set-up.

Figure 5 ***Typical Instrument Set-up***

The reference response and roving vibration responses were recorded on the eight-channel DAT recorder. Data integrity was checked in real time using the two-channel FFT analyser. **Figure 6** shows the general test set-up.

Figure 6 ***General Test Set-up***

The type of modal test undertaken is sometimes referred to as an Operational Modal Analysis as the force input is supplied by the operating conditions and response (only) measured. **Figure 7** shows a line drawing of the undeformed structure as produced in the modal software. All reference points were in the vertical direction.

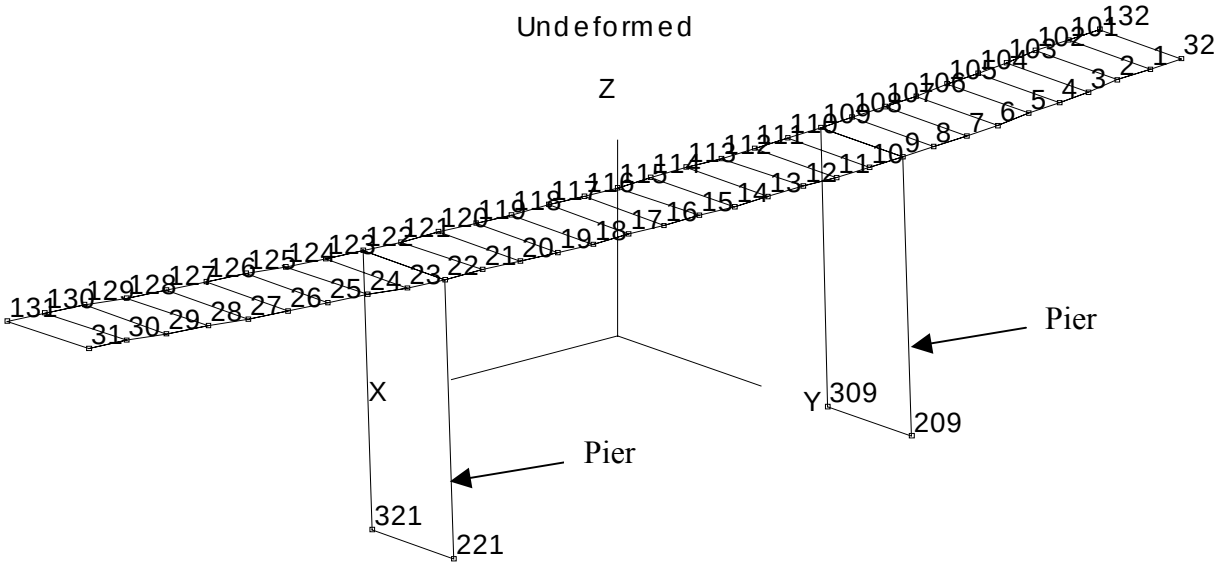

Figure 7 ***Line Drawing of the Undeformed Structure showing Measurement Locations***

2.2 Modal Analysis Results

Table 1 shows the resulting frequency tables for the first 6 experimental modes identified. It should be noted that the mode shapes presented represent the dominant modes of response of the bridge structure during the test period during which time traffic was the major source of excitation.

Table 1 ***Frequency and Damping Table***

Mode No	Centre Frequency (Hz)	Damping (% critical)	Description
1	2.9	0.8	Fundamental vertical bending
2	3.3	0.9	Vertical bending/ Torsional
3	4.7		First torsional
4	5.4		Second Vertical Bending/Torsional
5	6.3		Second Torsional
6	1.34		Horizontal Bending

The natural modes of vibration for the bridge structure are described below.

Mode 1 2.9 Hz Fundamental Vertical Bending Mode - Vertical movement of the Span 1 and Span 3 with out of phase with Span 2. Four nodes and three anti-nodes.

Mode 2 3.3 Hz Vertical Bending/Torsional Mode - Vertical movement of Span 1 and Span 3 with out of phase vertical and torsional motion of Span 2. Four nodes and three anti-nodes.

Mode 3 4.7 Hz First Torsional Bending Mode - Vertical out of phase movement of Span 1 and Span 3 with pure torsion of Span 2

Mode 4 5.4 Hz Second Vertical Bending/Torsional Mode - Vertical movement of the Span 1 and Span 3 in phase with Span 2. Four nodes and three anti-nodes.

Mode 5 6.3 Hz Second Torsional Mode - In phase torsional movement of Span 1, Span 2 and Span 3.

Mode 6 1.34 Hz Horizontal Bending Mode - Likely Horizontal bending of Span 1, Span 2 and Span 3, shape not defined.

2.3 Vibration Spectra

Figure 8 shows a typical narrow band vibration spectrum for the reference measurement location (6Z).

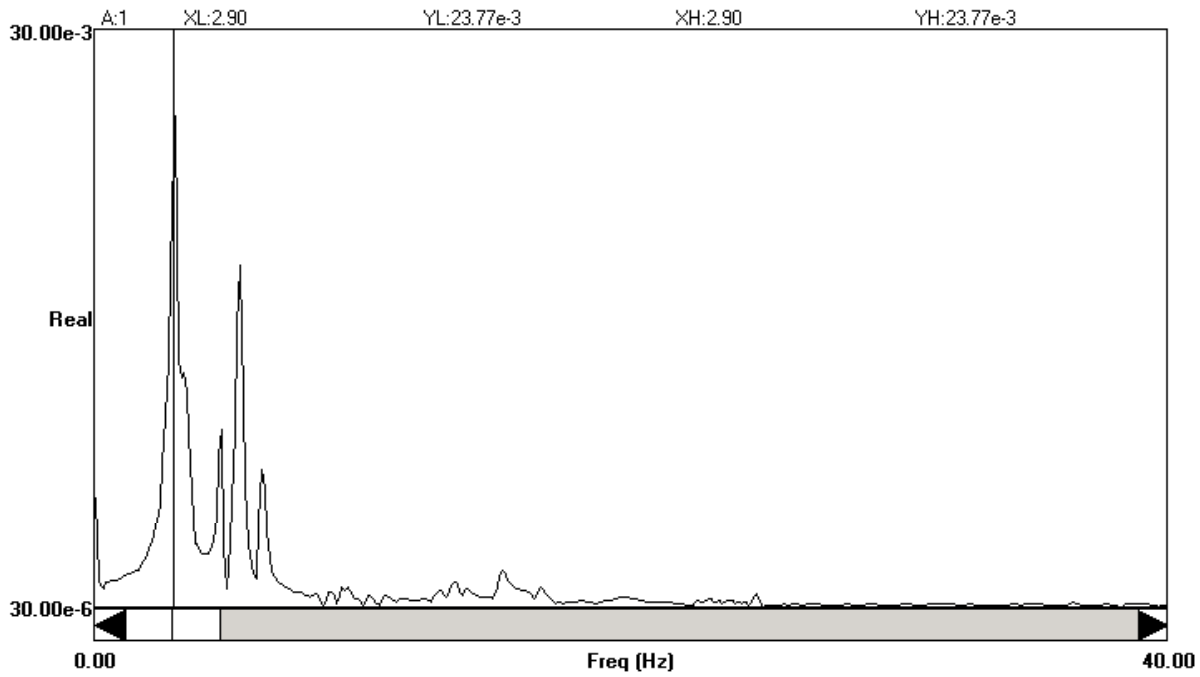

Figure 8 *Typical Narrow Band Vibration Spectrum (Cursor at 2.9 Hz)*

Response shape analysis of the Wilcannia Bridge structure successfully defined several dominant natural modal frequencies and mode shapes of the bridge structure. Mode 2 at 3.3 Hz and mode 3 at 4.7 Hz were identified as having significant potential to induce transverse racking of the box girders due to the significant torsional response of the bridge deck at these frequencies. Modes 1 and 2 were assessed as being very lightly damped exhibiting less than 1% of critical damping. Huang [5] reported that frequencies increase with radius. These data for a bridge with a centreline radius of curvature of 800 metres are very similar to Huang's data for a 244 metre radius and the measured mode shapes are dominated by torsional modes. Okeil & El-Tawil [6] investigated a number of Florida bridges with different length/radius (L/R) ratios. They concluded that for open cross sections, an L/R = 0.087 could be treated as straight. Above this value, they added that the effect of horizontal curvature and the resulting torsional demands could be significant and should be taken into consideration. As the subject bridge has an L/R = 0.11, the present study supports that conclusion.

3 STRAIN GAUGE MEASUREMENTS

3.1 Strain Gauge Locations

Figure 2 is an elevation of the Wilcannia Bridge centre box girder and shows three strain gauge locations (SG1 to SG3), located on or adjacent to asymmetric internal brace No.7. Strain gauges SG 4 to SG 6 were located in a similar plane, 3 meters west of the internal brace No. 7, in virgin metal.

All gauges were of a linear type and orientated in the anticipated principal stress direction (ie perpendicular to the direction of crack propagation).

Figures 9 to **15** are photographs of the strain gauge measurement locations.

Figure 9 ***Strain Gauge Locations Overview***

Figure 10 ***Strain Gauge Location SG1***

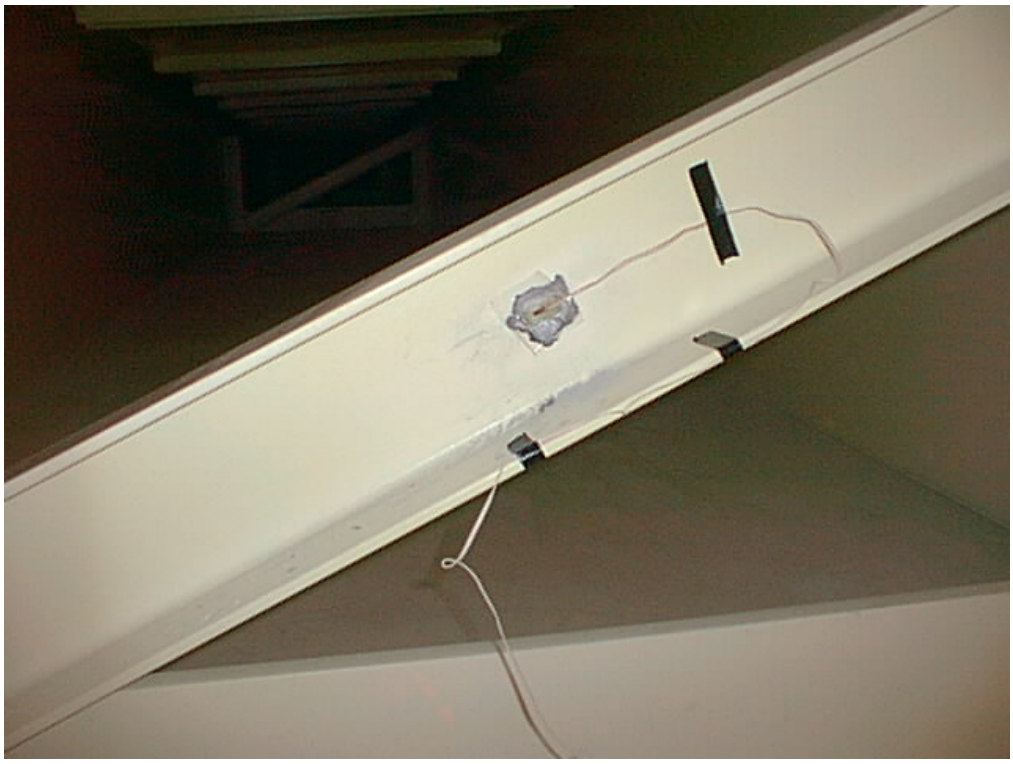

Figure 11 ***Strain Gauge Location SG2***

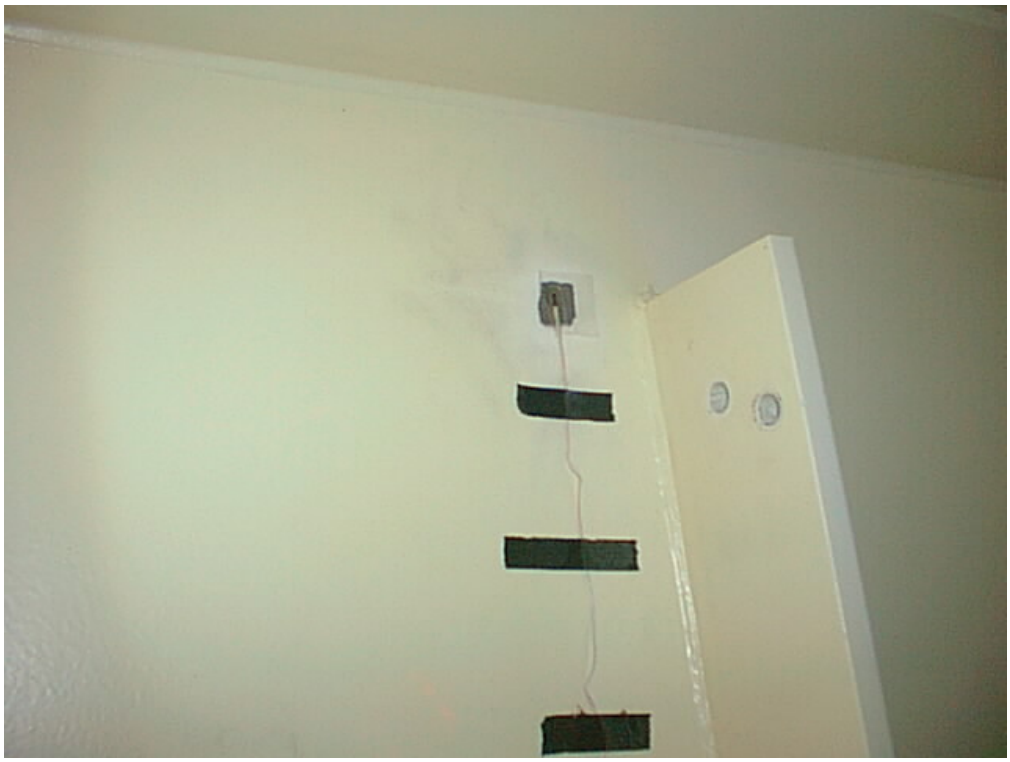

Figure 12 ***Strain Gauge Location SG3***

Figure 13 ***Strain Gauge Location SG4***

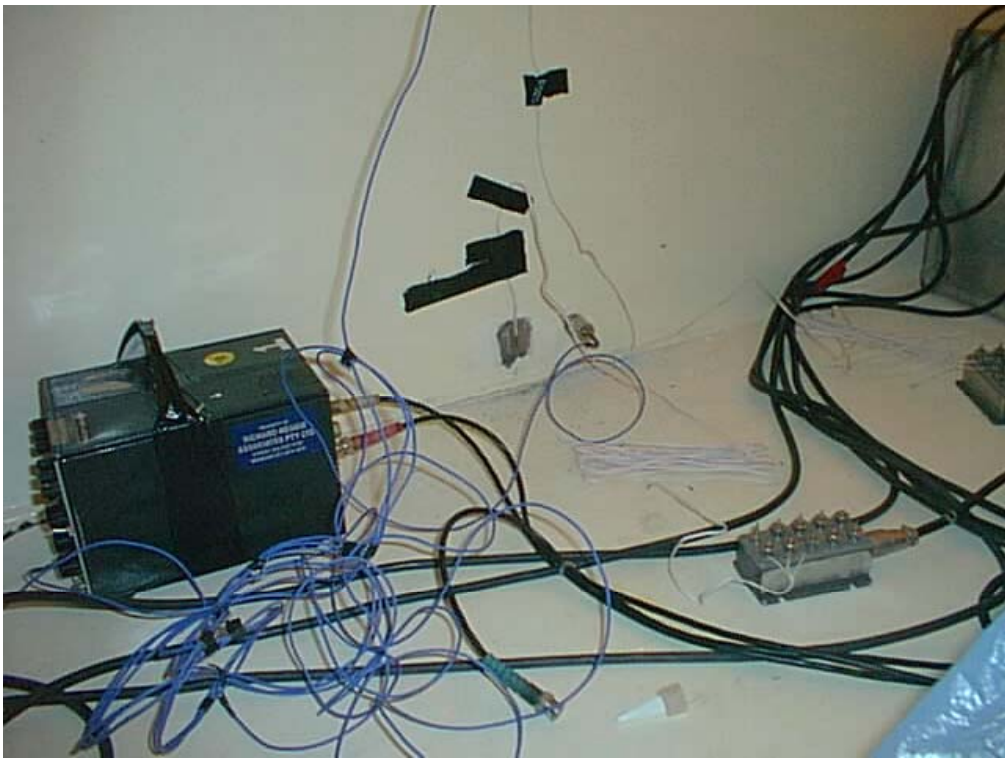

Figure 14 ***Strain Gauge Location SG5***

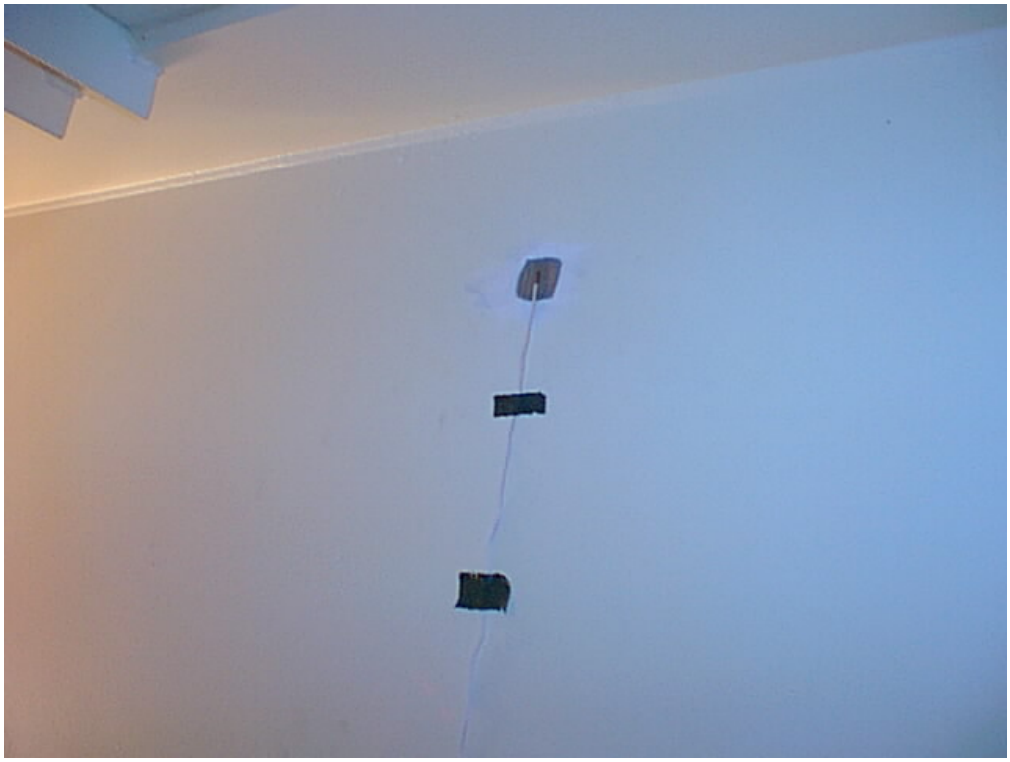

Figure 15 ***Strain Gauge Location SG6***

3.2 Test Vehicle Loading

Figure 16 presents a photograph of the Wilcannia Bridge during strain testing, the west bound lane was closed for the duration of the tests to provide access to the centre box girder, with the east bound lane cleared for the test truck to traverse at selected speeds.

Figure 16 *View of Wilcannia Bridge Access For Strain Tests*

4 MEASUREMENT PROCEDURE

4.1 Truck Slow Roll

In order to approximate true static strains and displacements, the truck was traversed over the joint at less than 1 km/hr producing negligible dynamic response of the truck or structure. All static and dynamic strains and displacements were recorded during this test. At this time the test truck was also slowly traversed over the artificial bump which was placed in front of the rear wheels.

4.2 Truck Pass-bys

The test truck was traversed at several speeds in the target speed range of 10 km/hr to 60 km/hr. The lateral position of the test truck was not recorded during the test runs and Whitton [7] reported some sensitivity in 2D modelling to the lateral position of the test truck on the bridge deck but this sensitivity was not reported by French [8] and Heywood *et al* [9].

Table 2 presents the target pass by speeds.

Table 2 ***Target Test Truck Passby Speeds***

Run Number	Target Speed
1	10 kph
2	15 kph
3	20 kph
4	25 kph
5	30kph
6	35 kph
7	40 kph
8	45 kph
9	50 kph
10	55 kph
11	60kph
12	Slow roll

4.3 Strain and Vibration Measurements

Strain and vibration signals were recorded on the 8-channel DAT-corder which was allowed to run for the entire test sequence. The recorded data was subsequently analysed to produce strain versus time and vibration acceleration versus time plots.

Further analysis included the extraction of the maximum and minimum strain resulting from each test. This data was used to calculate dynamic amplification factors for each strain and displacement signal.

The positive dynamic amplification factor was calculated as follows:

$$\text{Dynamic Amplification Factor (Positive)} = \frac{\text{Maximum Dynamic Strain (same sense as static)}}{\text{Maximum Static Strain}}$$

The negative dynamic amplification factor was calculated as follows:

$$\text{Dynamic Amplification Factor (Negative)} = \frac{\text{Maximum Dynamic Strain (opposite sense as static)}}{\text{Maximum Static Strain}}$$

The total dynamic amplification factor was calculated as follows:

$$\text{Dynamic Amplification Factor (Total)} = \frac{\text{Maximum Dynamic Strain - Minimum Dynamic Strain}}{\text{Maximum Static Strain}}$$

5 RESULTS AND DISCUSSIONS

Table 3 presents a summary of the resulting maximum strains, stresses and dynamic amplification factors for each test. It should be noted that dynamic amplification factor (DAF) is the same as the impact factor plus 100%. Huang [10] undertook static and dynamic strain gauge testing using a calibrated (known axle weight) truck but his results do not identify whether the dynamic strains are associated with any particular modes. **Figure 17** shows that most strain is associated with mode 2 that has a significant torsional component.

Table 3 ***Summary of Resulting Strains, Stresses and Dynamic Amplification Factors***

Test Truck Passby Speed	Transducer Location	Strain and Stress								
		Strain (με)			Stress (MPa)			Dynamic Amplification Factors		
		Max Tensile	Max Compressive	Peak to Peak	Max Tensile	Max Compressive	Peak to Peak	Max Tensile	Max Compressive	Peak to Peak
Slow Roll	SG 1	100	0	100	20	0	20			
	SG 3	0	-40	40	0	-8	8			
10 km/hr	SG 1	129	0	129	26	0	26	1.3	0.0	1.3
	SG 3	0	-44	44	0	-9	9	1.1	0.0	1.1
15 km/hr	SG 1	214	-6	220	43	-1	44	2.1	-0.1	2.2
	SG 3	3	-54	57	1	-11	11	1.4	-0.1	1.4
20 km/hr	SG 1	110	-10	120	22	-2	24	1.1	-0.1	1.2
	SG 3	5	-40	45	1	-8	9	1.0	-0.1	1.1
25 km/hr	SG 1	150	-15	165	30	-3	33	1.5	-0.2	1.7
	SG 3	8	-50	58	2	-10	12	1.3	-0.2	1.5
30 km/hr	SG 1	124	-5	129	25	-1	26	1.2	-0.1	1.3
	SG 3	6	-45	51	1	-9	10	1.1	-0.2	1.3
35 km/hr	SG 1	145	-6	151	29	-1	30	1.5	-0.1	1.5
	SG 3	5	-49	54	1	-10	11	1.2	-0.1	1.4
40 km/hr	SG 1	134	-5	139	27	-1	28	1.3	-0.1	1.4
	SG 3	2	-44	46	0	-9	9	1.1	-0.1	1.2
45 km/hr	SG 1	156	-4	160	31	-1	32	1.6	0.0	1.6
	SG 3	4	-51	55	1	-10	11	1.3	-0.1	1.4
50 km/hr	SG 1	141	-3	144	28	-1	29	1.4	0.0	1.4
	SG 3	5	-51	56	1	-10	11	1.3	-0.1	1.4
55 km/hr	SG 1	140	-4	144	28	-1	29	1.4	0.0	1.4
	SG 3	3	-50	53	1	-10	11	1.3	-0.1	1.3
60 km/hr	SG 1	116	-6	122	23	-1	24	1.2	-0.1	1.2
	SG 3	5	-43	48	1	-9	10	1.1	-0.1	1.2
Impacts	SG 1	100	30	70	20	6	14	1.0	0.3	0.7
	SG 3	-15	-34	19	-3	-7	4	0.9	0.4	0.5
Maximum	All	214	-54	220	35	-11	36	2.2	-0.2	2.2

Note: DAF equals Impact Factor plus 100%

Figure 17 presents a typical strain frequency spectrum. It is also important to note that the relative phase of all strain gauges support a racking (distorsional) response of the box girder due to the quasi-static strain as well as the dominant dynamic strain at approximately 3.4 Hz.

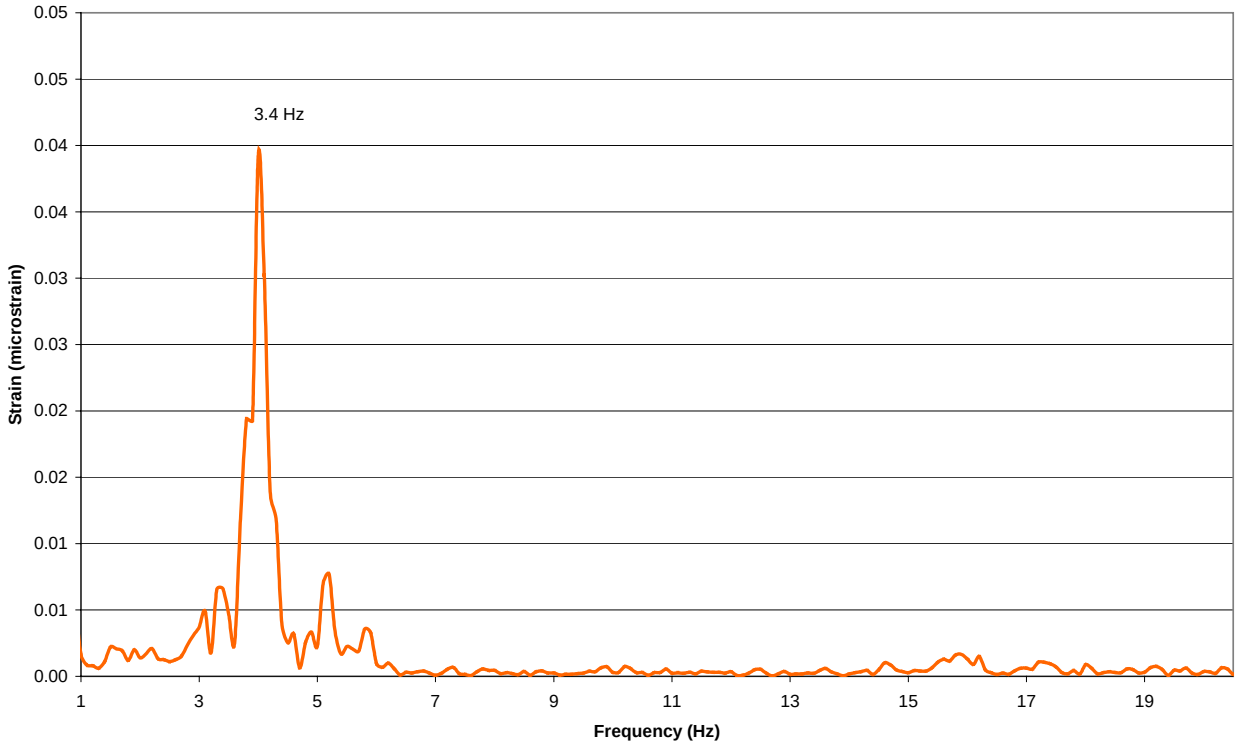

Figure 17 *Typical Strain Spectrum; SG 1; 15 km/hr*

6 TEST TRUCK SUSPENSION VIBRATION

Following the completion of the strain testing, addition vibration tests were undertaken with the main aim to determine fundamental test truck suspension modes. A vibration transducer was positioned on the test truck chassis adjacent to the rear axle in the vertical direction. The test truck was driven at a range of speeds, as well as over bumps, while the chassis vibration was recorded with the 8 channel DAT. These recordings were later analysed to produce vibration spectra for each test condition. **Figure 18** shows a sample vibration spectra from the bump test which clearly shows the presence of fundamental vertical suspension modes centred about 3.3 Hz. It is interesting to note that this suspension mode, while evident, was not strongly excited by coincidence with wheel speed. The strongest vibration response of the test truck vertical suspension mode was due apparently to road deformations rather than wheel speed. Huang [5] assumed that the road profile was the realisation of a random process that could be described by a power spectral density function. These data indicate the presence, in this bridge deck, of a longitudinal profile with periodic corrugations of approximately 1.2 metres in length. Such an observation may partially explain the above strain results in which the 15 km/hr pass-by produced the maximum dynamic strains. It therefore appears that periodic corrugations of the road surface profile over the Wilcannia Bridge excites the truck suspension modes, and consequently the dominant bridge modes, at approximately 3.3 Hz.

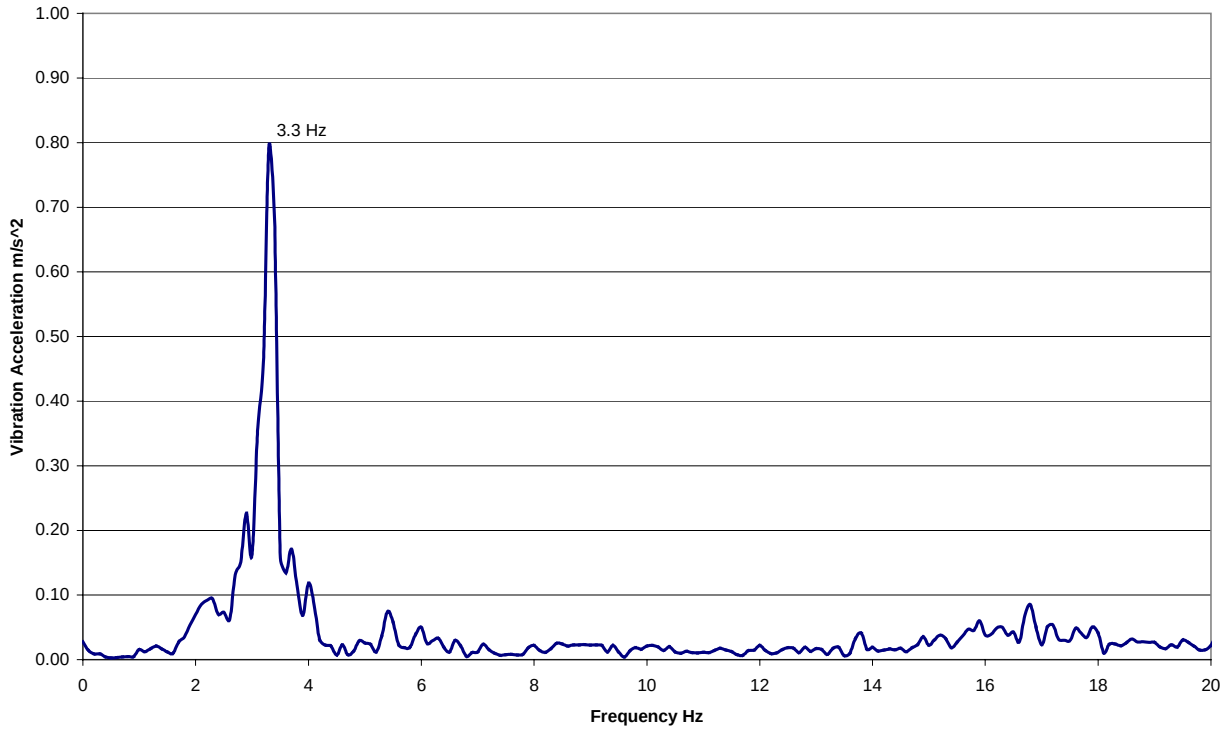

Figure 18 ***Test Truck Vertical Chassis Vibration Spectrum (Bump Test)***

7 FINITE ELEMENT BASE MODEL

The finite element model was built using MSC.FEA NASTRAN PATRAN software. The FE model was initially developed as a global modal of the entire bridge structure, which consisted predominately of shell elements. The geometry was manually entered from the as-built engineering drawings of the bridge. Suitable spring elements were used to represent the bridge bearings and piers. The FE model was calibrated [10] using dynamic measurements and used for a series of "*what if*" studies.

7.1 Normal Mode Analysis

Table 1 shows a summary of the resulting natural modal frequencies with a description of the associated mode shapes. These results are subsequent to FE model optimization and updating.

Table 1 ***Summary of the Resulting Natural Modal Frequencies from FEA and EMA***

Mode No	**Mode Shape Description**	**Natural Frequency From FEM**	**Natural Frequency Of Mode From Experimental Modal Analysis**
1	Fundamental vertical bending	2.9	**2.9**
2	First Torsional	4.8	4.7
3	Second Vertical Bending	5.2	5.4
4	Second Torsional	6.7	6.3

Figures 19 – 22 show mode shapes from mode 1 to mode 4 respectively.

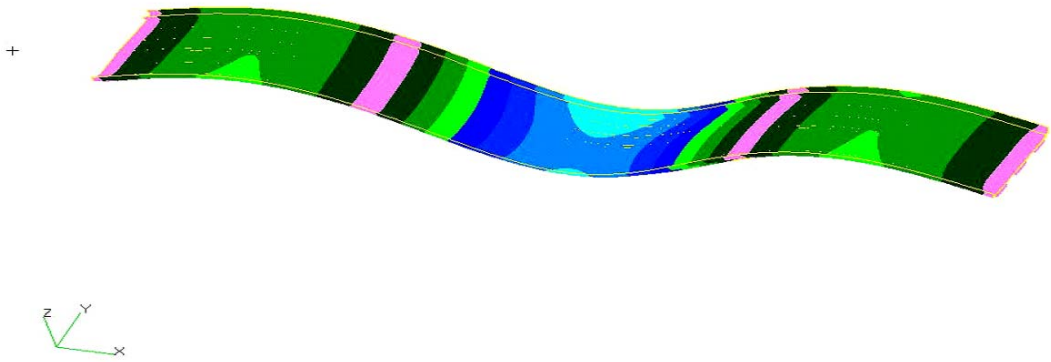

Figure 19 *Mode 1 at 2.9Hz*

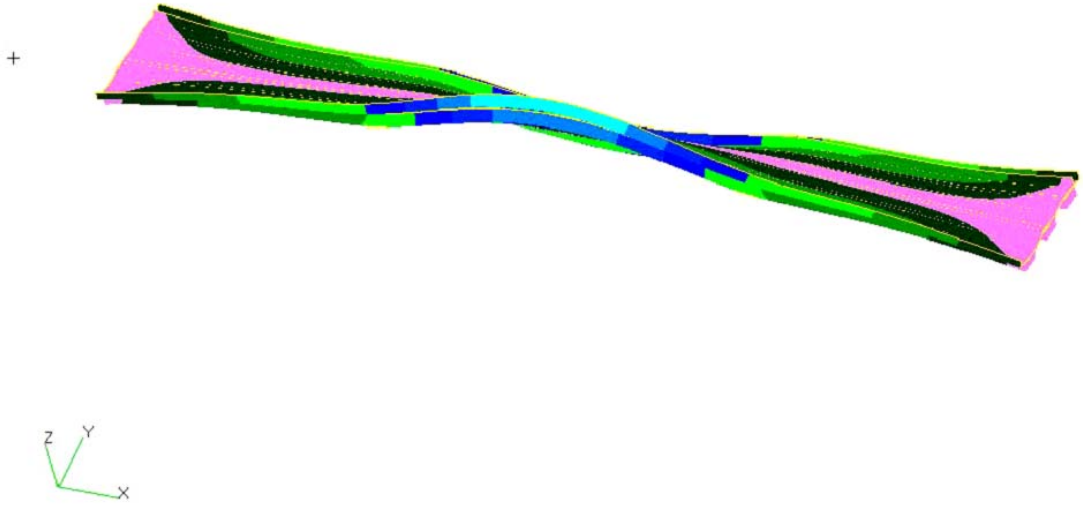

Figure 20 *Mode 2 at 4.8 Hz*

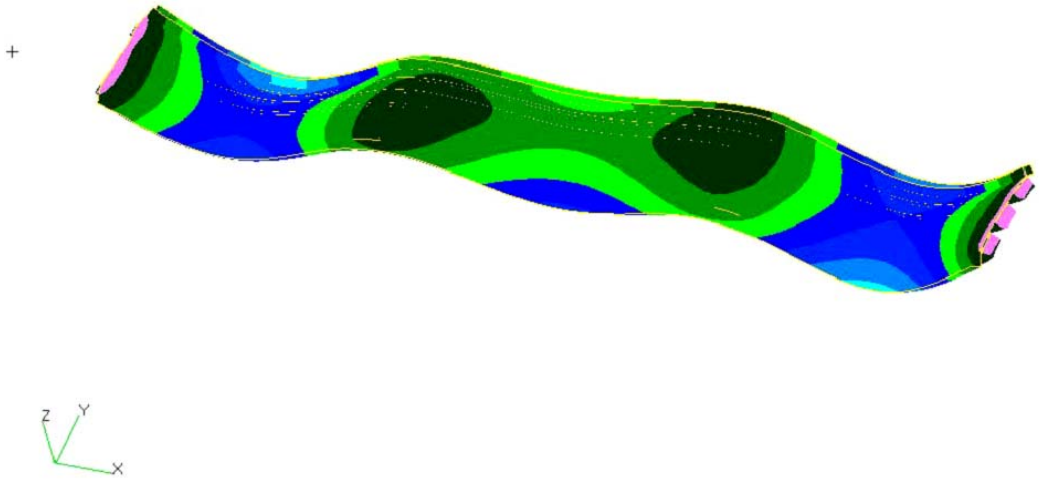

Figure 21 *Mode 3 at 5.2 Hz*

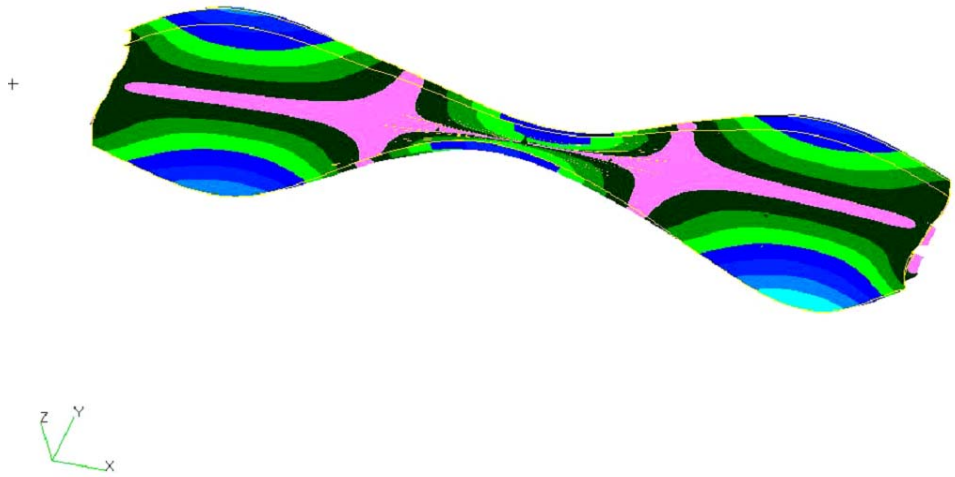

Figure 22 *Mode 4 at 6.7 Hz*

7.2 Static Load Case Analysis

Several static load cases were applied to the model representing a range of possible axle and wheel load arrangements, as well as the test truck configuration used in the trials. Good correlation was found to exist between global stresses in the box girder and relevant strain gauge locations. The FE model over predicted the stress at the crack site strain gauge, however the effects of the existing crack were not modelled. The FE results clearly demonstrated that the global stresses in the bridge were low, ie less than 30MPa. The FE model also demonstrated that the areas of fatigue cracking were the result of a severe stress concentration effect due to the offset connection of the box girder diagonal brace to the side wall of the box girder. **Figure 23** shows a sample stress contour plot for the test truck mid span load case.

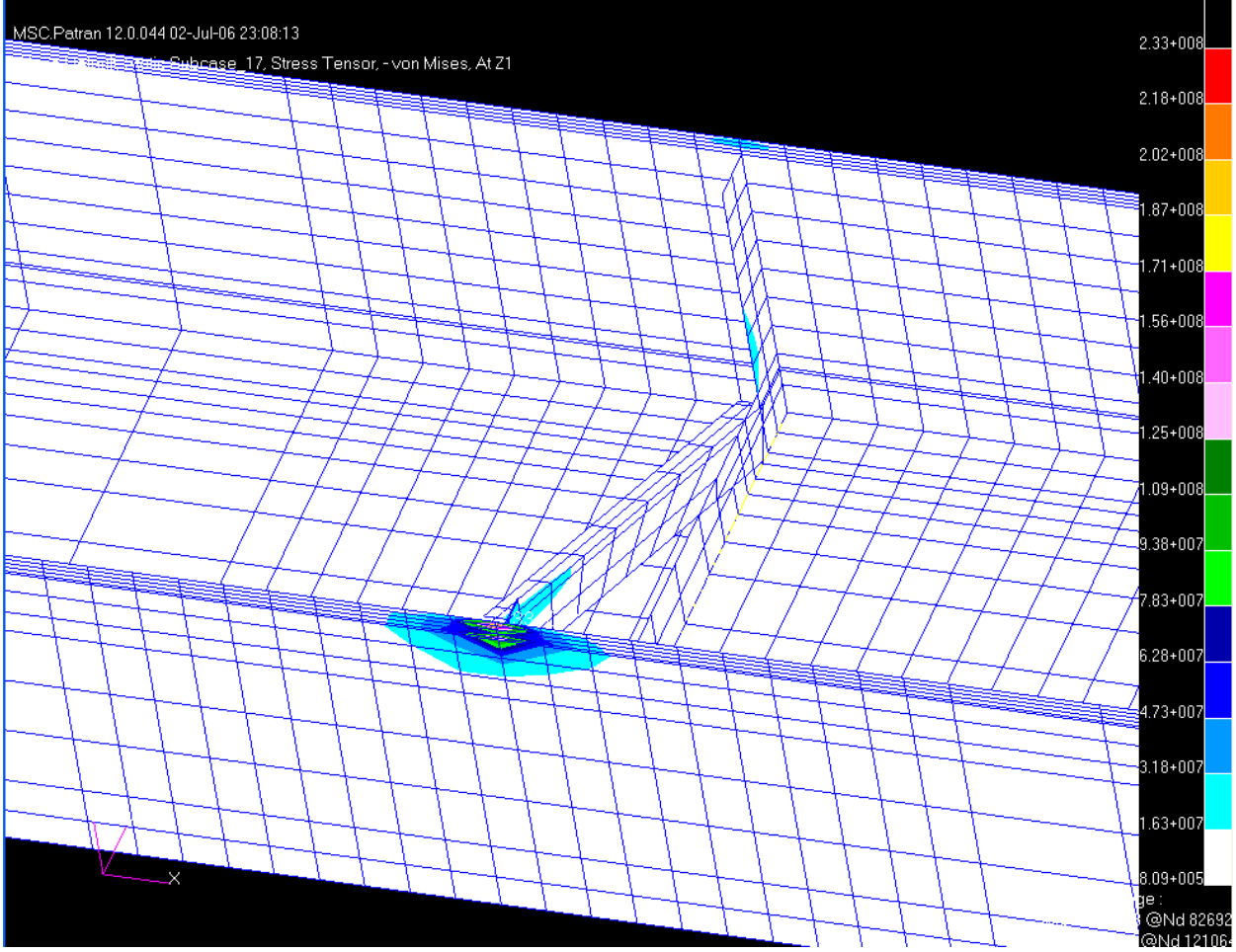

Figure 23 ***Sample Stress Contour Plot Of Box Girder, As Built Condition***

7.3 Modification Options

Several modification options were assessed including bolt on and welded on stiffening ribs. A sample stress contour plot for the bolted stiffener is shown in **Figure 24** and the single external welded stiffening rib in **Figure 25**. It was decided to implement the single external stiffening rib option and this is also shown in **Figure 26**.

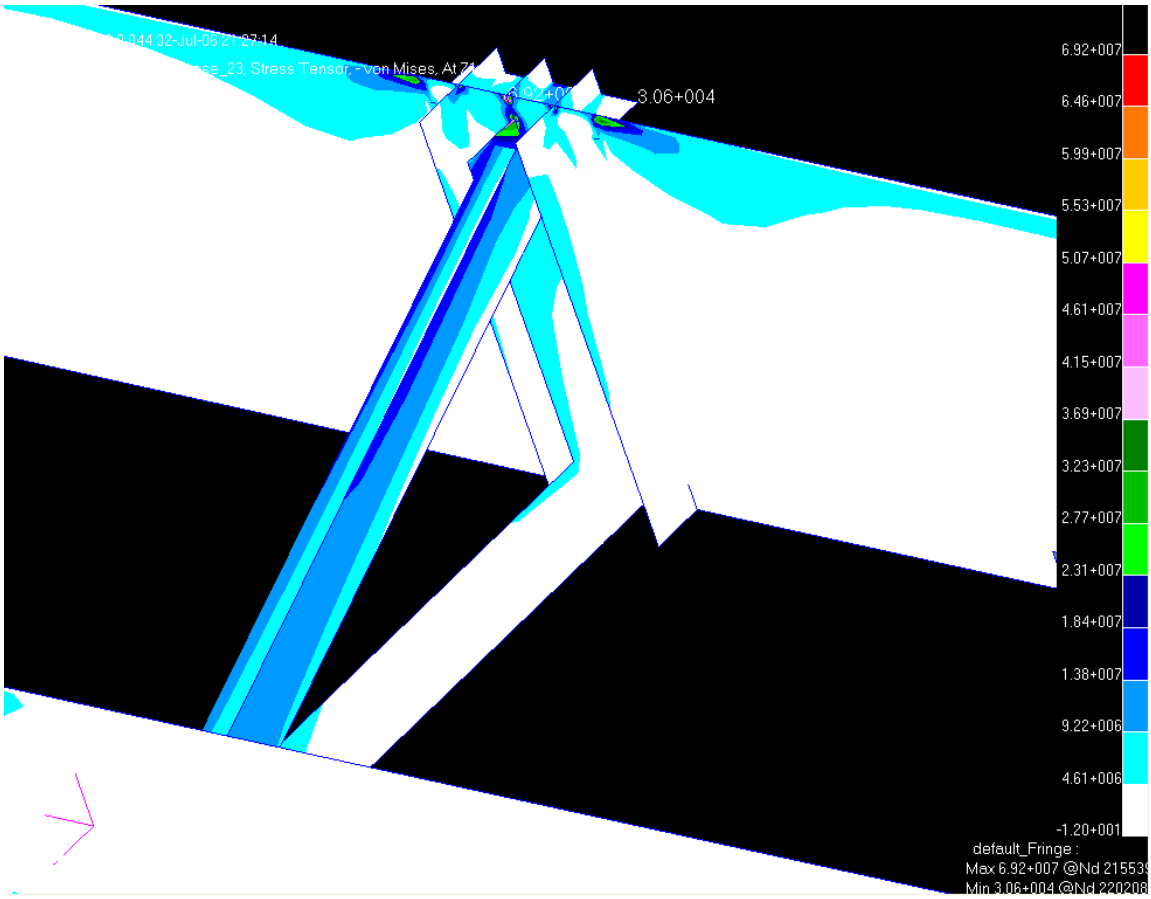

Figure 24 *Sample Stress contour Plot, Three Rib Bolted Stiffener*

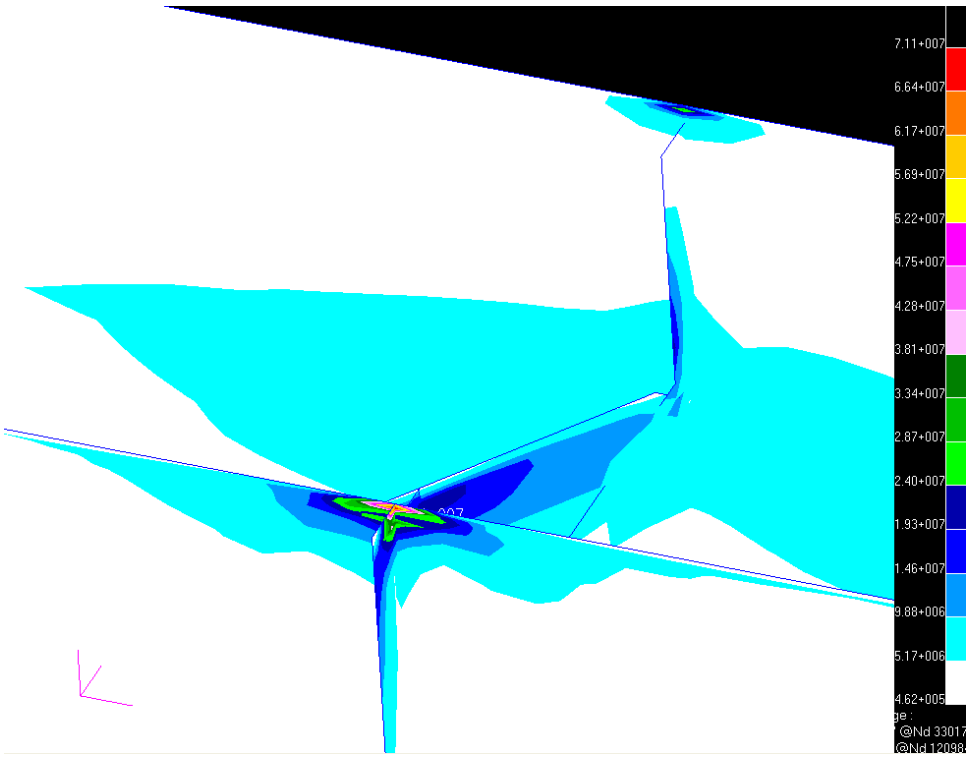

Figure 25 *Sample Stress Contour Plot, Single Rib Welded Stiffener*

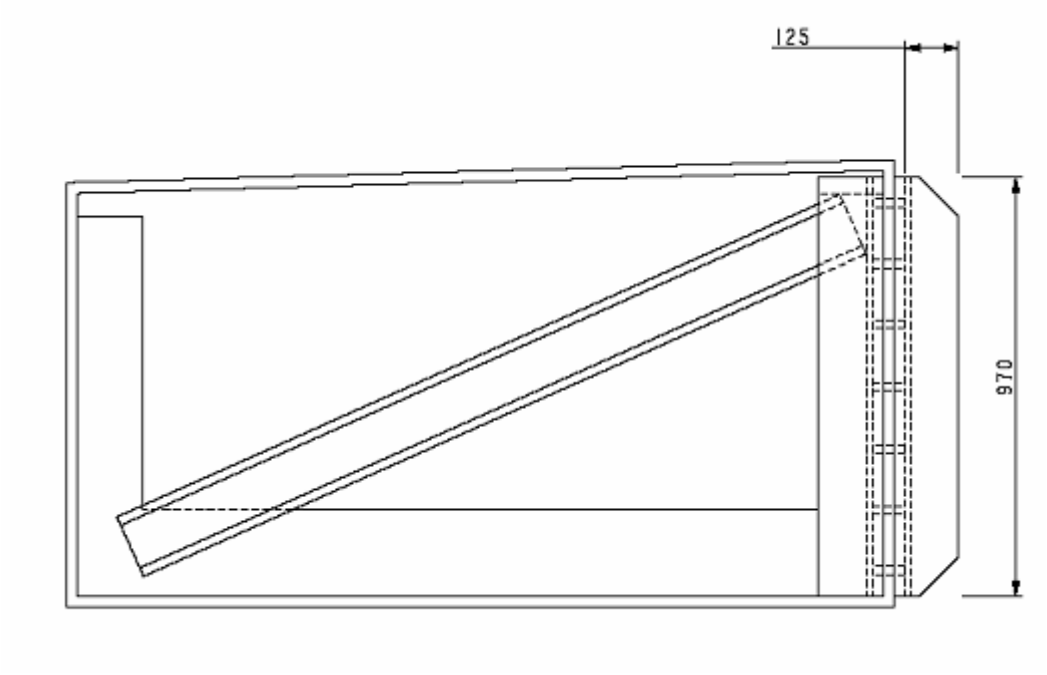

Figure 26 ***Drawing of Single Rib Welded Stiffener***

8. FATIGUE LIFE EXTENSION

The fatigue life extension for the above modification was calculated based on extrapolation of the measured existing life of a nominal 20 years and the cubic stress ratio relationship from appropriate S_N curves. (In this case there is no need to select a detail category as the fatigue life of the "*as is*" detail is known). This technique is simple but conservative as it uses the steepest part of the S-N curve to estimate fatigue life. The predicted additional fatigue life was in excess of 100 years.

9. CONCLUSION

A structural dynamics study of Wilcannia Bridge has experimentally identified the first five vertical bending and/or torsional modes. Static and dynamic strain gauge measurements showed that a peak-to-peak strain of 220 με occurred at heavy vehicle speeds around 15 km/hr. A peak-to-peak DAF of 2.2 was also associated with this speed. It is also important to note that the relative phase of all strain gauges supported a racking (distorsional) response of the box girder due to the quasi-static strain as well as the dominant dynamic strain at approximately 3.4 Hz. This frequency is also associated with periodic corrugations of the road surface profile over the Wilcannia Bridge that excited the truck suspension modes, and consequently the dominant bridge modes, at approximately 3.3 Hz. Whilst this vehicle speed may seem relatively low, the bridge is in a 50 km/hr speed zone and a 15km/hr differential between heavy vehicles passing on the bridge could produce the same dynamic response due to beating. A global FE model of the bridge was developed and calibrated using the empirical data. The calibrated model was then used to investigate a range of modifications to reduce or eliminate fatigue cracking. A single external fin welded to the web at each asymmetric internal stiffeners. The FE modelling indicated that the post-modification fatigue life was in excess of 100 years.

ACKNOWLEDGEMENT

The author wishes to thank the Chief Executive of the Roads and Traffic Authority of NSW (RTA) for permission to publish this paper. The opinions and conclusions expressed in this paper do not necessarily reflect the views of the RTA.

REFERENCES

[1] NAASRA, "National Association of Australian State Road Authorities 1976 Bridge Design Specification", National Association of Australian State Road Authorities, Sydney, NSW Australia, 1976

[2] AASHTO, "Standard Specification for Highway Bridges", American Association of State Highway and Transportation Officials, 14th Edition, Washington, DC, USA, 1969.

[3] SENNAH K.M. & KENNEDY J.B., "State-of-the-Art in Design of Curved Box-Girder Bridges", *J. Bridge Engineering,* ASCE, 6(3), 159-167, 2001.

[4] EWINS D.J. "Modal Testing: Theory, Practice & Application (2nd Edition)", *Research Studies Press*, Hertfordshire, UK, 163-276, 1999.

[5] HUANG D., "Dynamic Analysis of Steel Curved Box Girder Bridges", *J. Bridge Engineering,* ASCE, 6(6), 506-513, 2001.

[6] OKEIL A.M. & EL-TAWIL S., "Warping Stresses in Curved Box Girder Bridges: Case Study", *J. Bridge Engineering,* ASCE, 9(5), 487-496, 2004

[7] WHITTON R. J., "Strengthening Options/Load Capacity – Bridge Over the Darling River at Wilcannia", *RTA Technical Services Report*, Roads & Traffic Authority, Sydney, NSW, Australia, (2003), 23 pp.

[8] FRENCH S., "Review of Cracking Remediation Reports and Recommended Remediation Scope", *Report 024-P1164-009-01*, Unpublished Report by Burns & Roe Worley Pty Ltd submitted to Roads & Traffic Authority of NSW, Sydney, Australia, 2005, 10 pp.

[9] HEYWOOD R., BRANDIS A. & LAND K., "Bridge over Darling River at Wilcannia: Design Review of Steel Trough Girder Web Crack Repairs" *Report 14024*, Unpublished Report by Texcel Pty Ltd submitted to Roads & Traffic Authority of NSW, Brisbane, Australia, 2004, 40 pp.

[10] HUANG D., "Full-Scale Test and Analysis of a Curved Steel-Box Girder Bridges", *J. Bridge Engineering,* ASCE, 13(5), 492-500, 2008

[11] MORASSI A. & TONON S., "Dynamic Testing for Structural Identification of a Bridge", *J. Bridge Engineering,* ASCE, 13(6), 573-585, 2008.

Appendix N

Ancich E.J., Chirgwin G.J., Brown S.C. & Madrio H. (2009). Fatigue Implications of Growth in Heavy Vehicle Loads and Numbers on Steel Bridges, *Proc. International Association for Bridge & Structural Engineering (IABSE) Symposium*, Bangkok, Thailand.

IABSE
International Association for Bridge & Structural Engineering

SUSTAINABLE INFRASTRUCTURE

Environment Friendly, Safe and Resource Efficient

33rd IABSE Symposium

Bangkok, Thailand
September 9-11, 2009

Sponsored by:

Ministry of Transport, MOT

PTT Public Company Limited

The Siam Cement Group

Organized by:

Chulalongkorn University, CU

IABSE Thai Group
The Thai Group of IABSE

Asian Institute of Technology, AIT

Fatigue Implications of Growth in Heavy Vehicle Loads and Numbers on Steel Bridges

Eric ANCICH
Senior Project Engineer
Roads & Traffic Authority
Parramatta, NSW, Australia
Eric_Ancich@rta.nsw.gov.au

Steve BROWN
Associate
Heggies Pty Ltd
Lane Cove, NSW, Australia
Steve.brown@heggies.com

Gordon CHIRGWIN
Supervising Bridge Engineer
(Durability & Materials)
Roads & Traffic Authority
Parramatta, NSW, Australia
Gordon_Chirgwin@rta.nsw.gov.au

Huber MADRIO
Project Engineer
Roads & Traffic Authority
Parramatta, NSW, Australia
Huber_Madrio@rta.nsw.gov.au

SUMMARY

It is known that 75% of the total Australian road freight task passes through NSW and the Pacific Highway is a major recipient of this freight. There are numerous crossings of major rivers between Newcastle and the Queensland border and until the late 1960's, steel bridges were preferred as lift spans could be easily incorporated in the design.

Over the past 10-15 years, heavy vehicle numbers using the Pacific Highway have increased dramatically, with a stepwise increase in 2001 and exponential growth of about 2% per year otherwise. This growth has been matched by a parallel exponential growth in loads and an even faster growth in axle group repetitions due to the greater utilisation of B-doubles and tri-axle semi-trailers.

Three bridges along the Pacific Highway were investigated using a structural dynamics based approach. The investigation revealed numerous compression/tension stress reversals for each heavy vehicle transit. Whilst the dynamic amplification factor (DAF) for a single controlled heavy vehicle transit was comparable with current Codes, the load effect for fatigue from uncontrolled heavy vehicle traffic significantly exceeds the value which would be predicted using the test vehicle factored for dynamic effects and multiple presence.

Keywords: Steel Truss Bridge; High cycle fatigue; Damping; Finite element method; Modal analysis; Strain measurement.

1. INTRODUCTION

The Roads and Traffic Authority of NSW (RTA) maintains some 5,000 bridges on the classified road network in New South Wales. Coped stringer to cross girder connections are a common feature of steel truss road bridges in NSW and the RTA has in excess of 60 such bridges. The design is, however, dynamically sub-optimal and a number of bridges along the Pacific Highway are exhibiting fatigue related cracking. The design is further complicated by un-explained variations in implementation. In some bridge designs, an attempt was made to reinstate the coped stringer top flange across the cross girder by bolting or riveting a thick steel plate to each stringer top flange.

Where used, the connection plate has resisted fatigue cracking around the copes but the bridges using the detail only used it for alternate cross girders. Cracking was first observed in the riveted cope connections of Macksville Bridge in 2004. At the time, it was not realised that the cracking was fatigue related. Rather, given the age of the bridge (built 1930's) and changes to the size and volume of heavy vehicles, progressive overloading was considered to be the cause. Subsequently, routine inspections of the 1960's era Kempsey Bridge (See **Figure 1**) identified a number of coped stringer-to-cross girder connections where some of the rivets in the top two rows had been lost. The lost rivets were replaced with high strength bolts and following inspections revealed that the replacement bolts were failing in as little as 6-months. Some failed bolts were recovered and submitted for metallurgical examination. This examination revealed characteristic evidence of fatigue failure (See **Figure 2**).

A literature review indicated that steel bridge designers of this era gave little or no consideration to fatigue. Fatigue design provisions, as we largely know them today, may be traced to AASHTO [1] from 1973. Roeder et al [2] reported similar connection details in US bridges and noted that whilst they were designed as pinned connections they should be regarded as partially restrained connections as they have limited rotational restraint.

Fu *et al* [3] report Australian, Canadian and United States studies of the impact of increased heavy vehicle loading on bridge infrastructure. They concluded that these investigations used largely deterministic approaches and tended to exclude fatigue effects. Imam *et al* [4] undertook a largely theoretical study of riveted rail bridges in the UK. They concluded that fatigue life estimates exhibit the highest sensitivity to detail classification, to S-N predictions in the region of high endurances, and to model uncertainty. This highlighted the importance of field monitoring for old bridges approaching the end of their useful life.

Whilst it was known that 75% of the total Australian road freight task passed through NSW [5, 6] and the Pacific Highway was a major recipient of this freight, little was known about actual heavy vehicle loading on the Pacific Highway. In addition, until the late twentieth century, the main freight route from Sydney and Newcastle to Brisbane was via the inland New England Highway route. Analysis of weigh-in-motion (WIM) data from Pacific Highway sites indicated that over the past 10-15 years, heavy vehicle numbers using the Pacific Highway have increased dramatically, with a stepwise increase in 2001 and exponential growth of about 2% per year otherwise. This growth has been matched by a parallel exponential growth in loads and an even faster growth in axle group repetitions due to the greater utilisation of B-doubles and tri-axle semi-trailers. A detailed consideration of this traffic data indicates that fatigue has only become important since 1990, but that in the period 1990 to 2004 some 90% of the theoretical fatigue life of the deck stringer connection had been used.

The present study reports extensive dynamic measurements and FE modelling of Kempsey Bridge. The FE model was calibrated [7] using dynamic measurements and then used for a series of "*what if*" studies. Whilst the optimum solution was shown to be the connection plate over the cross girder, there were major difficulties with implementation as the bridge could not be taken out of service. An alternative solution was devised that involved removing the top two rows of rivets in the stringer/cross girder connection and replacing the removed rivets with "*compliant*" fasteners.

Post replacement measurements have validated the FEM predictions and confirmed that, under current traffic volumes and loadings, the fatigue life of Kempsey Bridge has been extended by a further 40 years. In the three years subsequent to installation of the modification no further fatigue failures have been recorded.

Figure 1 ***Kempsey Bridge***

Two other bridges along the Pacific Highway were also investigated using the same structural dynamics based approach. The investigations revealed numerous compression/tension stress reversals for each heavy vehicle transit. Whilst the dynamic amplification factor (DAF) for a single controlled heavy vehicle transit was comparable with current Codes, the load effect for fatigue from uncontrolled heavy vehicle traffic significantly exceeds the value that would be predicted using the test vehicle factored for dynamic effects and multiple presence.

Figure 2 ***Fatigue affected bolt***

2. PRELIMINARY FINITE ELEMENT MODEL

A preliminary global finite element model was used to identify likely hot spots or weaknesses in the structure. The finite element model was built using MSC.FEA software. The FE model was initially developed as a global modal of the entire truss span 6, which consisted predominately of shell elements and a few beam elements. The geometry was manually entered from work-as-executed drawings of the bridge. Suitable spring elements were used to represent the bridge bearings and piers. **Figure 3** shows a perspective view of the base model.

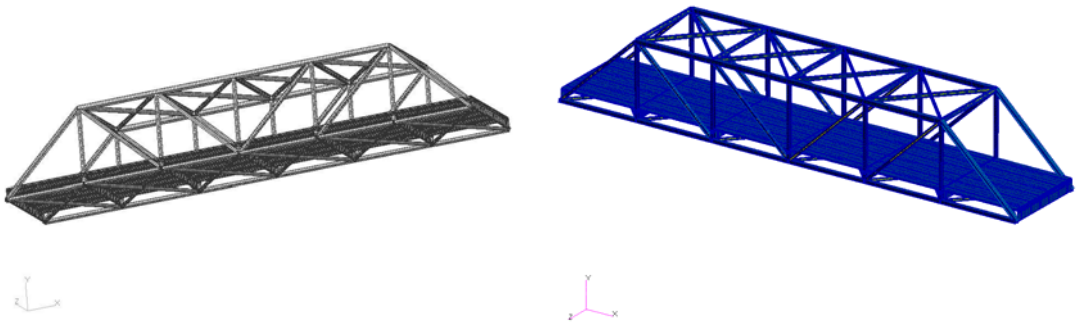

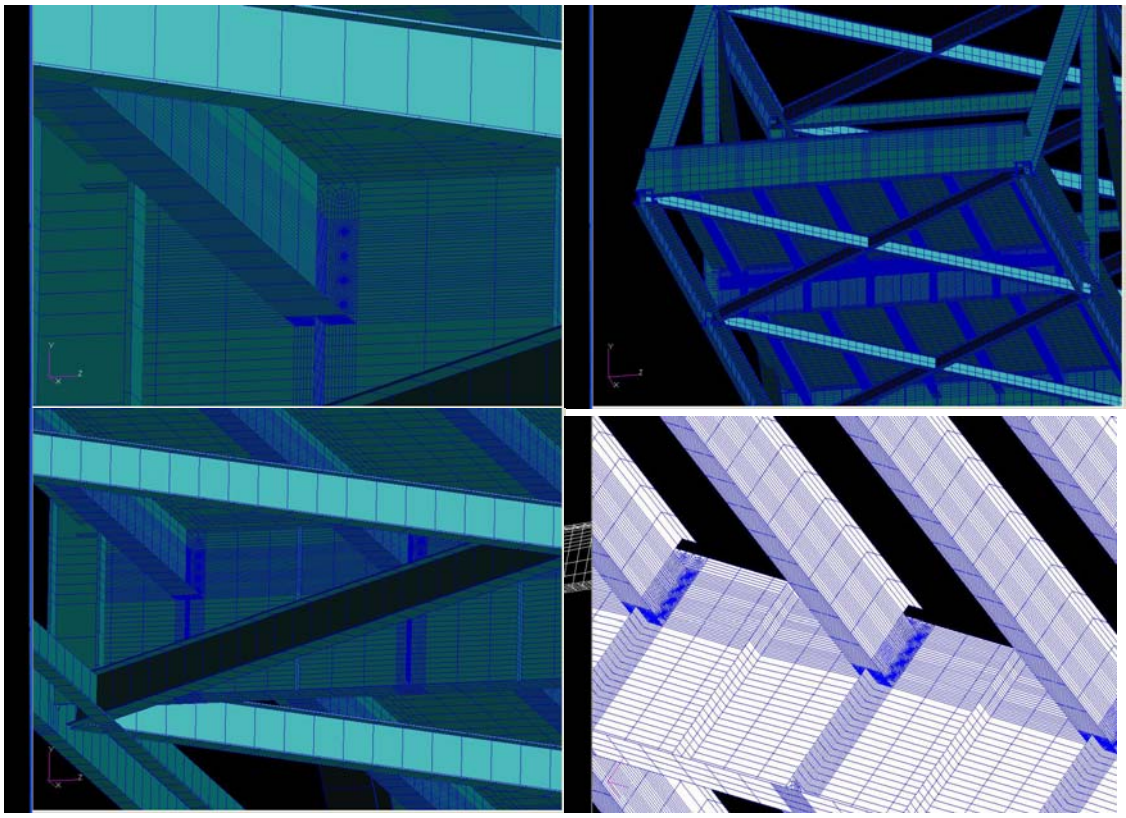

Figure 3 *Views of base model for Kempsey Bridge*

3. NORMAL MODE ANALYSIS

Table 1 shows a summary of the resulting natural modal frequencies with a description of the associated mode shapes.

Table 1 ***Summary of the Resulting Natural Modal Frequencies***

Mode No	Mode Shape Description	Natural Frequency from FEM (Hz)	Natural Frequency from EMA (Hz)
1	First vertical bending	3.8	3.6
2	Second vertical bending	7.0	6.5
3	Third vertical bending	9.0	8.7
4	Fourth vertical bending	10.1	10.1
5	Transverse/vertical bending	12.1	11.8
6	Fifth vertical bending	13.3	13.7

Figures 4 - 9 show mode shapes from modes 1 to 6 respectively.

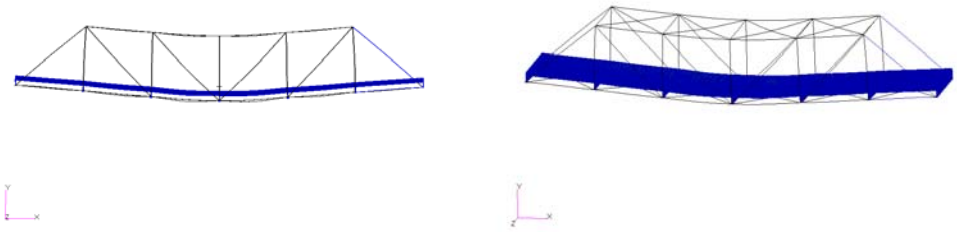

Figure 4 ***Mode 1 at 3.8 Hz***

Figure 5 ***Mode 2 at 7 Hz***

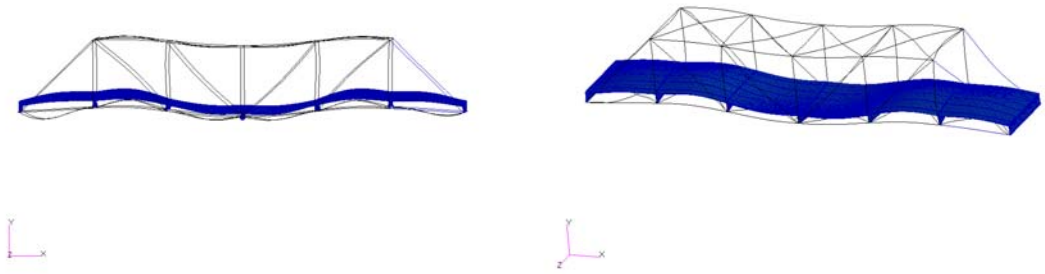

Figure 6 *Mode 3 at 9 Hz*

Figure 7 *Mode 4 at 10.1 Hz*

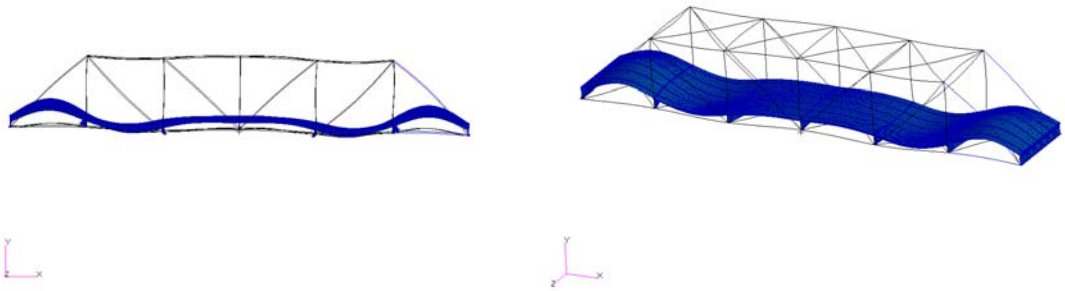

Figure 8 *Mode 5 at 12.1 Hz*

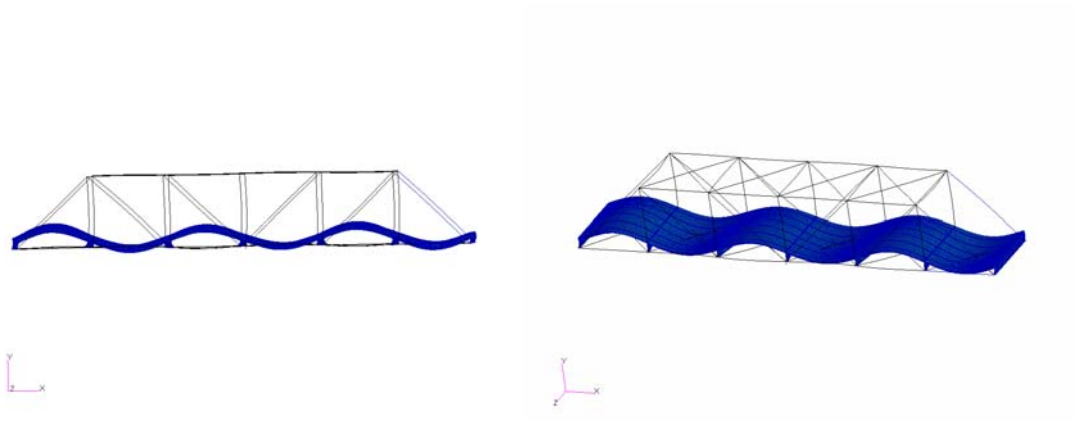

Figure 9 *Mode 6 at 13.3 Hz*

4. MODAL ANALYSIS TEST PROCEDURES

4.1 Test Description

The measurement and definition of the natural frequencies and mode shapes of a structure is referred to as modal analysis. Experimental identification of structural dynamic models is usually based on the modal analysis approach. In the classical modal parameter estimation method, frequency response functions are measured under controlled conditions. For many large structures it is not practical, or prohibitively expensive to apply a controlled input force and hence the need arises to identify modes under operating conditions, or from environmental excitation. In this type of analysis, only response data are measurable while the actual loading conditions (input forces) are unknown. The test procedure and methodology for experimental modal analysis is comprehensively covered by Ewins [8]. For the three bridges studied, the measurement of Frequency Response Functions (FRF's) involved the simultaneous measurement of a reference vibration response and "roving" vibration responses at a large number of locations over the bridge structure. In these tests the frequency range of interest was a nominal 0 Hz to 25 Hz. The vibration responses were measured at selected locations using an accelerometer attached to the structure with a magnetic base. **Figure 10** shows the typical transducer set-up.

Figure 10 *Typical Instrument Setup*

The reference response and roving vibration responses were recorded on the eight-channel DAT recorder. Data integrity was checked in real time using the two-channel FFT analyser. **Figure 11** shows the general test set-up.

Figure 11 *General Test Set-up*

Subsequently, each frequency response function (FRF) was simultaneously measured using the four-channel FFT analyser and recorded data. Frequency Response Functions (FRF's) were stored on the hard disk drive of a laptop computer. The type of modal test undertaken is sometimes referred to as an Operational Modal Analysis as the force input is supplied by the operating conditions and response (only) measured. **Figure 12** shows a line drawing of the undeformed structure as produced in the modal software. All reference points were in the vertical direction.

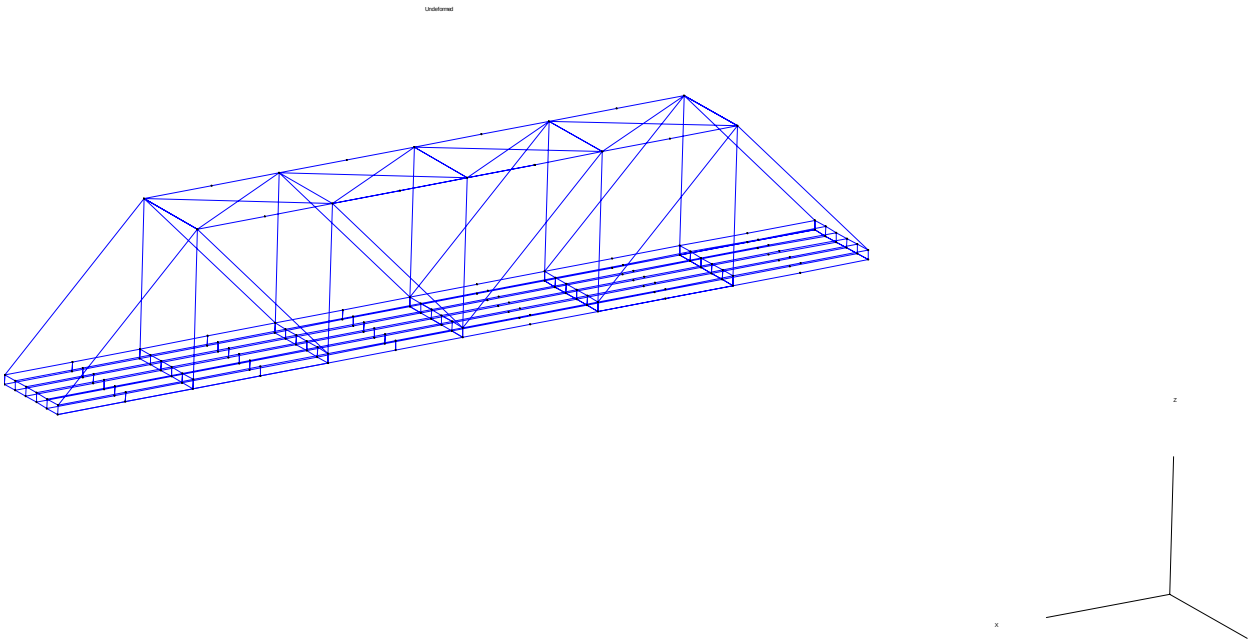

Figure 12 *Line Drawing of the Undeformed Structure Showing Measurement Locations*

4.2 Modal analysis results

4.2.1 Modal Testing

Table 1 shows the resulting frequency tables for the first 6 experimental modes identified compared with similar modes from FEM. It should be noted that the mode shapes presented represent the dominant modes of response of the bridge structure during the test period during which time traffic and wind were the major source of excitation.

The measured natural modes of vibration for Kempsey Bridge are shown below.

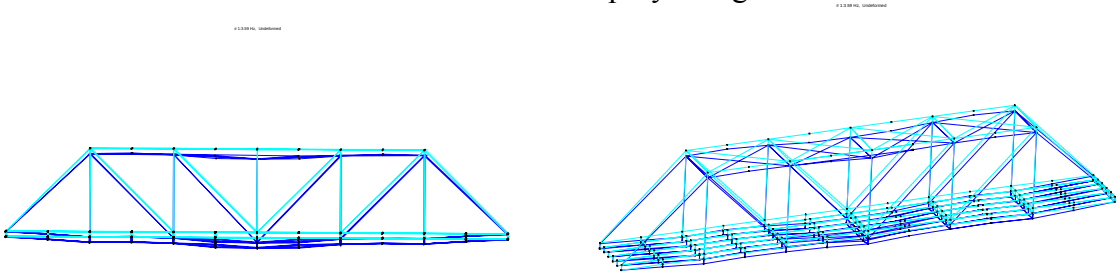

Figure 13 *Mode 1 at 2.6 Hz Fundamental Vertical Bending Mode - Vertical movement of the Bays 1 to Bay 6 all in phase, nodes at piers*

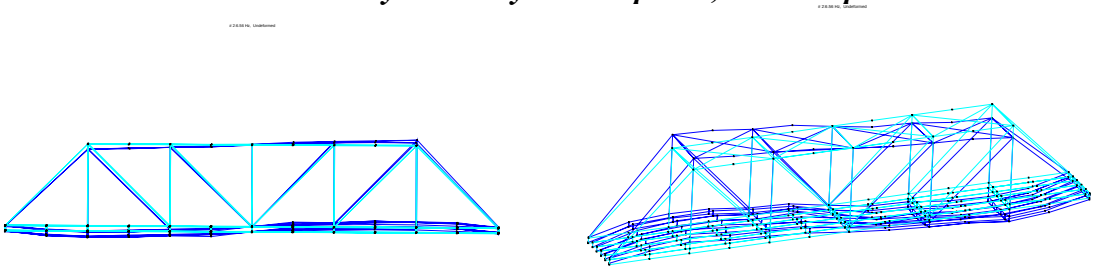

Figure 14 *Mode 2 at 6.5 Hz Second Vertical Bending, Bays 1, 2, 3 out of phase with bays 4, 5, 6, nodes at piers and 1 node mid span, i.e. 3 nodes*

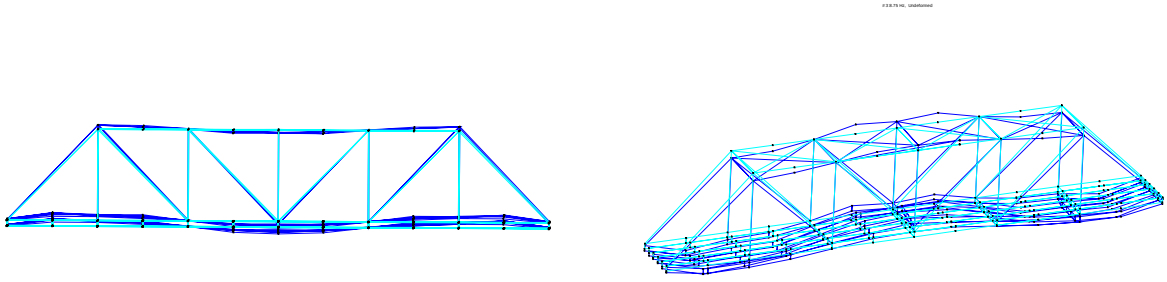

Figure 15 *Mode 3 at 8.75 Hz Third Vertical Bending, Bays 1,2, and bays 5,6 out of phase with bays 3,4, (4 nodes)*

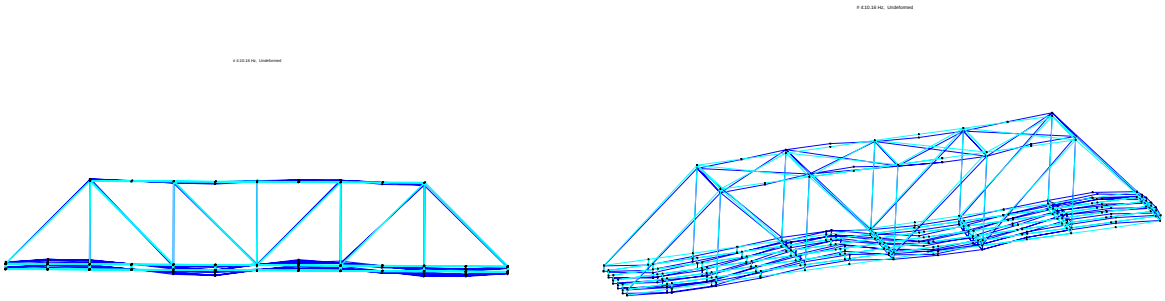

Figure 16 *Mode 4 at 10.16 Hz Fourth Vertical Bending, (5 nodes)*

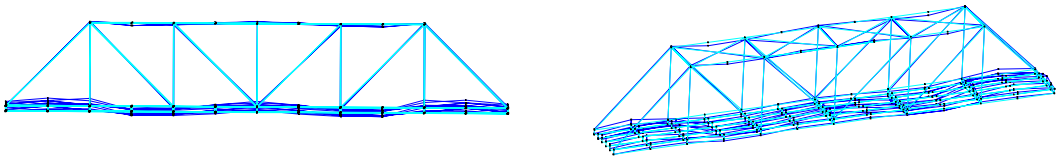

Figure 17 *Mode 5 at 11.8 Hz Transverse/ vertical bending Mode – (6 nodes)*

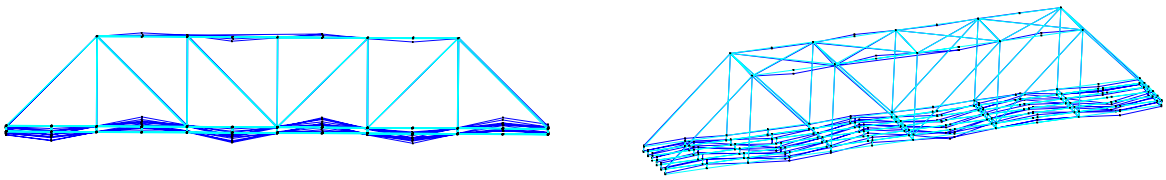

Figure 18 *Mode 6 at 13.75 Hz Fifth Vertical Bending, alternate bays out of phase, (7nodes)*

5. STRAIN MEASUREMENTS

Strain gauge measurements were undertaken at sixteen locations. The strain gauge locations were selected based on the resulting "*hot spots*" from the FEA as well as mode shape results from the EMA. **Figure 19** presents a plan view diagram of the northbound kerb side lane of the Kempsey Bridge and shows the sixteen strain gauge locations (SG1 to SG16). All gauges were of a linear, gel encapsulated type and orientated in the anticipated principal stress direction (i.e. parallel to the long axis of the respective structural members).

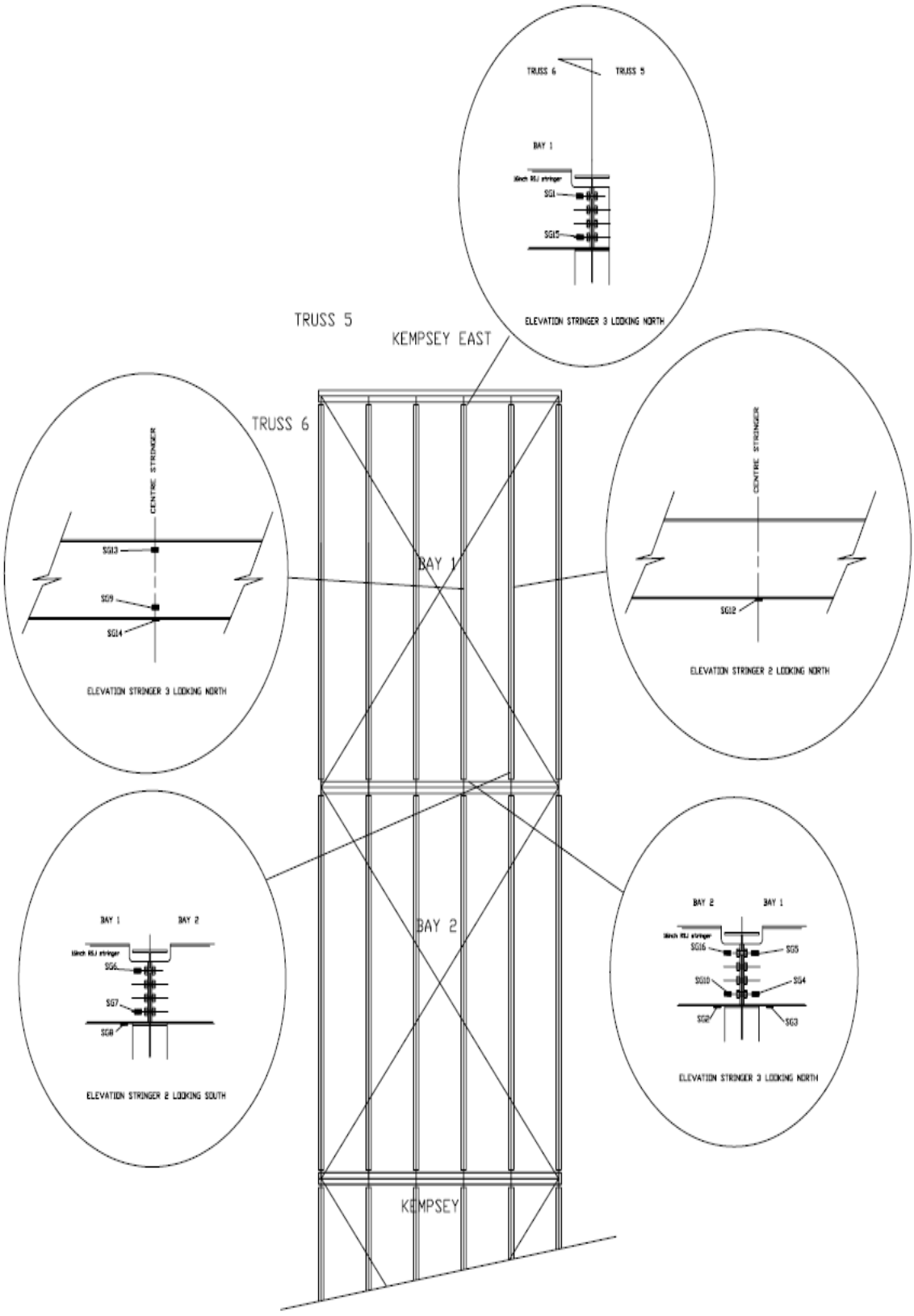

Figure 19 ***Plan View North Bound kerbside Lane - Sixteen Strain Gauge Locations (SG1 to SG16)***

5.1 Test Vehicle Loading

Bridge Evaluation & Assessment - Test Truck loading

Axle loads from loading arrangements

Dimensions of Volvo Prime Mover F75155 and Brentwood Low Loader F02726
Test Load Vehicle A

Truck description

Steer axle (tare)	4.26 t	Steer to tandem	3.58 m	Block mass	0.99 t
Tandem (tare)	4.64 t	Spacing of tandem	1.37 m	Space for crane	3.44 m
Trailer (tare at king-pin)	4.28 t	Tandem to tridem	6.70 m	Max reach required	5.99 m
Trailer tridem (tare)	8.66 t	Spacing of tridem	1.27 m	(assumes crane in centre of trailer)	
King pin offset from centre of tandem	0.20 m	Spacing of tridem	1.27 m	Distribution to prime mover	
King-pin to front of trailer	0.63 m	King-pin to centre of tridem	8.85 m	King-pin to steer	5%
Length of tray	11.84 m	Centre of rear axle to end	1.09 m	King-pin to tandem	95%
No of blocks at goose-neck	4	Front of trailer to centre of block	3.60 m		

Block loading

Modular Expansion Joint Testing - ANZAC BRIDGE, WESTERN ABUTMENT

Block Position	Block position 1	2	3	4	5	6	7		Group loads (t) Steer	Tandem	Tridem	Total
								Tare	4.46	8.72	8.66	21.84
Loading level	No of blocks per position							Tare+bl	4.58	11.23	9.99	25.80
1	1	1	0	1	2	2	2	Load 1	4.66	12.83	17.22	34.71
2	2	2	2	2	2	4	2	Load 2	4.82	16.05	20.76	41.64

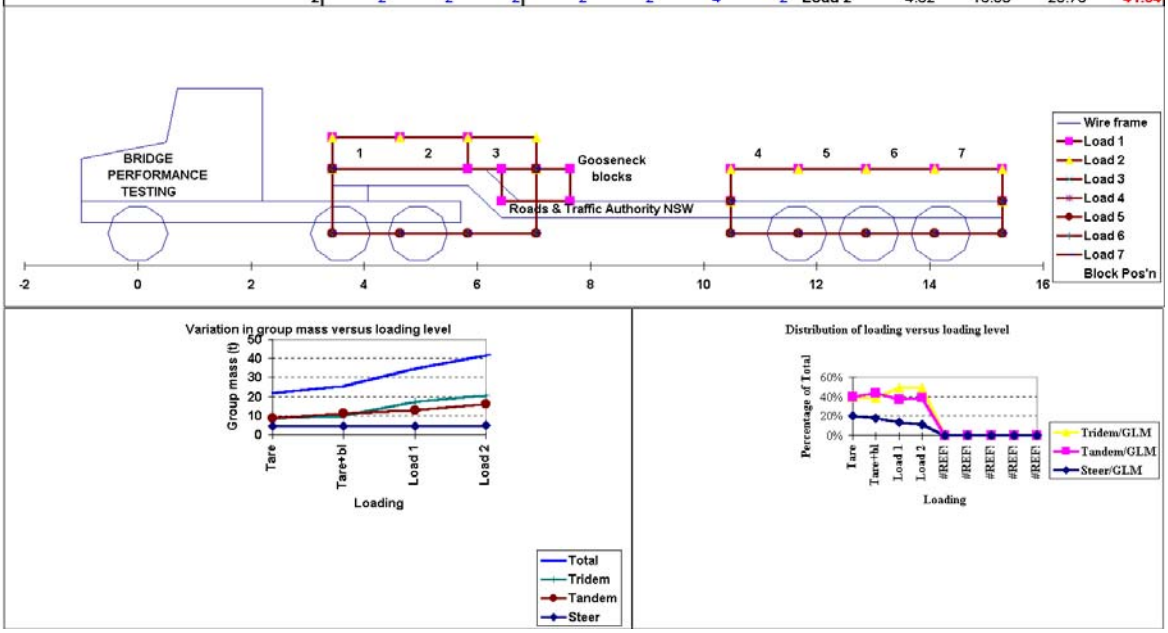

Figure 20 *Test Vehicle Loading Arrangement*

Figure 21 is a photograph of the test truck used for the controlled tests at all three bridges.

Figure 21 ***Bridge Load Test Truck***

Figure 22 presents a schematic elevation of the bridge deck and kerb in relation to the nominal kerbside lane position and nominal test truck wheel positions.

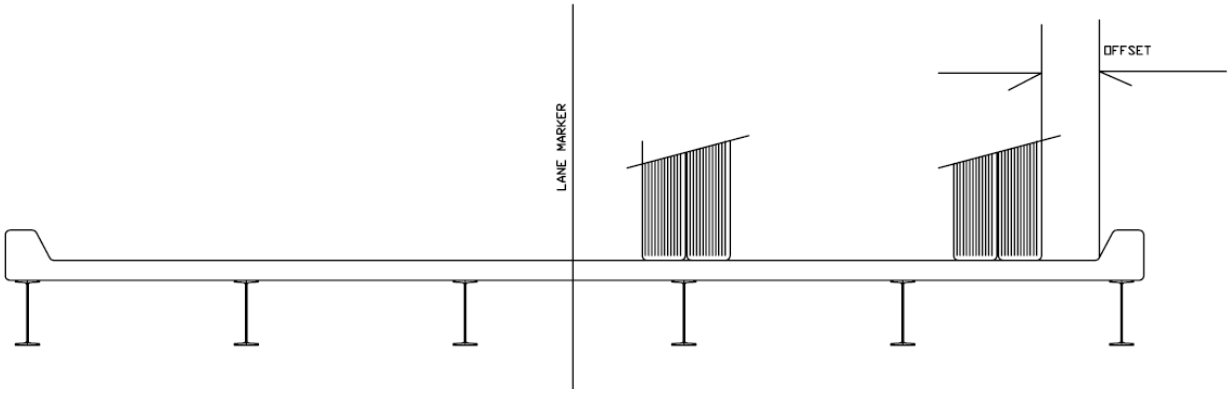

Figure 22 ***Sectional Elevation of Bridge Deck Showing Nominal Test Truck Position***

5.3 Measurement Procedure

Truck Slow Roll

In order to approximate true static strains and displacements, the truck was traversed over the joint at less than 10 km/hr producing negligible dynamic response of the truck or structure. All static and dynamic strains were recorded during this test. The lateral position of the truck was measured after each run by physical measurement of the wheel impression left on a bead of dental paste placed in a transverse direction on the road surface.

Truck Pass-bys

Following as closely as possible to the same line as the slow roll test, the truck was traversed at several speeds in the target speed range of 17 km/hr to 70 km/hr. The actual truck speed for each run was measured using a laser speed gun.
Table 2 presents the target pass-by speeds as well as the measured (actual) pass-by speeds, lateral tracking position, and time of test.

Table 2 ***Target Speed and Actual Pass-by Speeds***

Run No.	Target Speed (Km/hr)	Actual Speed	Offset distance mm
1	18	18	535
2	18	17	570
3	25	27	570
4	25	24	490
5	30	30	560
6	30	31	570
7	36	36	615
8	36	37	580
9	41	41	620
10	46	49	750
11	46	46	685
12	51	51	470
13	54	54	600
14	54	54	410
15	60	59	610
16	60	59	660
17	65	66	655
18	Slow	north	450
19	Slow	reverse	
20	Slow	north	650
21	Slow	reverse	
22	Slow	north	800
23	Slow	reverse	
24	Stopping	north	430

6. STRAIN MEASUREMENT RESULTS

Strain signals were sampled at a rate of 1 kHz and allowed to run for the entire test sequence. The calibrated strain data was stored directly to disk on a Laptop via an Ethernet connection. The data was subsequently analysed to produce strain versus time plots. Further analysis included the extraction of the maximum and minimum strain resulting from the passage of the six individual test truck axles. These data were used to calculate dynamic range factors for each strain signal and the calculations were performed for each strain gauge location for each individual axle as well as for all axles. The positive dynamic amplification factor was calculated as follows:

$$\textbf{Dynamic Amplification Factor (Positive)} = \frac{\text{Maximum Dynamic Strain (same sense as static)}}{\text{Maximum Static Strain}}$$

The negative dynamic range factor was calculated as follows:

$$\textbf{Dynamic Amplification Factor (Negative)} = \frac{\text{Maximum Dynamic Strain (opposite sense as static)}}{\text{Maximum Static Strain}}$$

The total dynamic range factor was calculated as follows:

$$\textbf{Dynamic Amplification Factor} = \frac{\text{Maximum Dynamic Strain - Minimum Dynamic Strain}}{\text{Maximum Static Strain}}$$

Note: The Maximum static strain used in the denominator of the above equations was the maximum of the two closest slow-roll lateral position results that straddled the lateral position for the run in question. This procedure was used to reduce the possibility of DAF over estimation.

7. RESULTS AND DISCUSSIONS

Slow Roll Results

Table 3 presents a summary of the resulting maximum strains and stresses from slow roll tests.

Table 3 ***Summary of Resulting Strains and Stresses From Slow Roll Pass-bys***

	Maximum Strain (με)	**Minimum Strain (με)**	**Maximum Strain Range (με)**	**Maximum Stress (MPa)**	**Minimum Stress (MPa)**	**Peak-Peak Stress Range (MPa)**
sg1	57	-30	78	11	-6	16
sg15	25	-10	35	5	-2	7
sg13	1	-62	64	0	-12	13
sg9	134	-17	151	27	-3	30
sg14	163	-19	182	33	-4	36
sg12	174	-21	190	35	-4	38
sg5	350	0	348	70	0	70
sg4	55	0	56	11	0	11
sg3	0	-124	122	0	-25	24
sg16	170	-37	204	34	-7	41
sg10	29	-5	33	6	-1	7
sg2	0	-162	156	0	-32	31
sg6	95	-22	117	19	-4	23
sg7	77	-12	88	15	-2	18
sg8	0	-203	194	0	-41	39

Figure 23 shows sample strain time histories for a slow roll strain measurement for all gauges, during this slow roll the truck was briefly stopped at the mid span positions indicated by the diagram of the truck. The flat spots in the traces are at times when the truck was stationary.

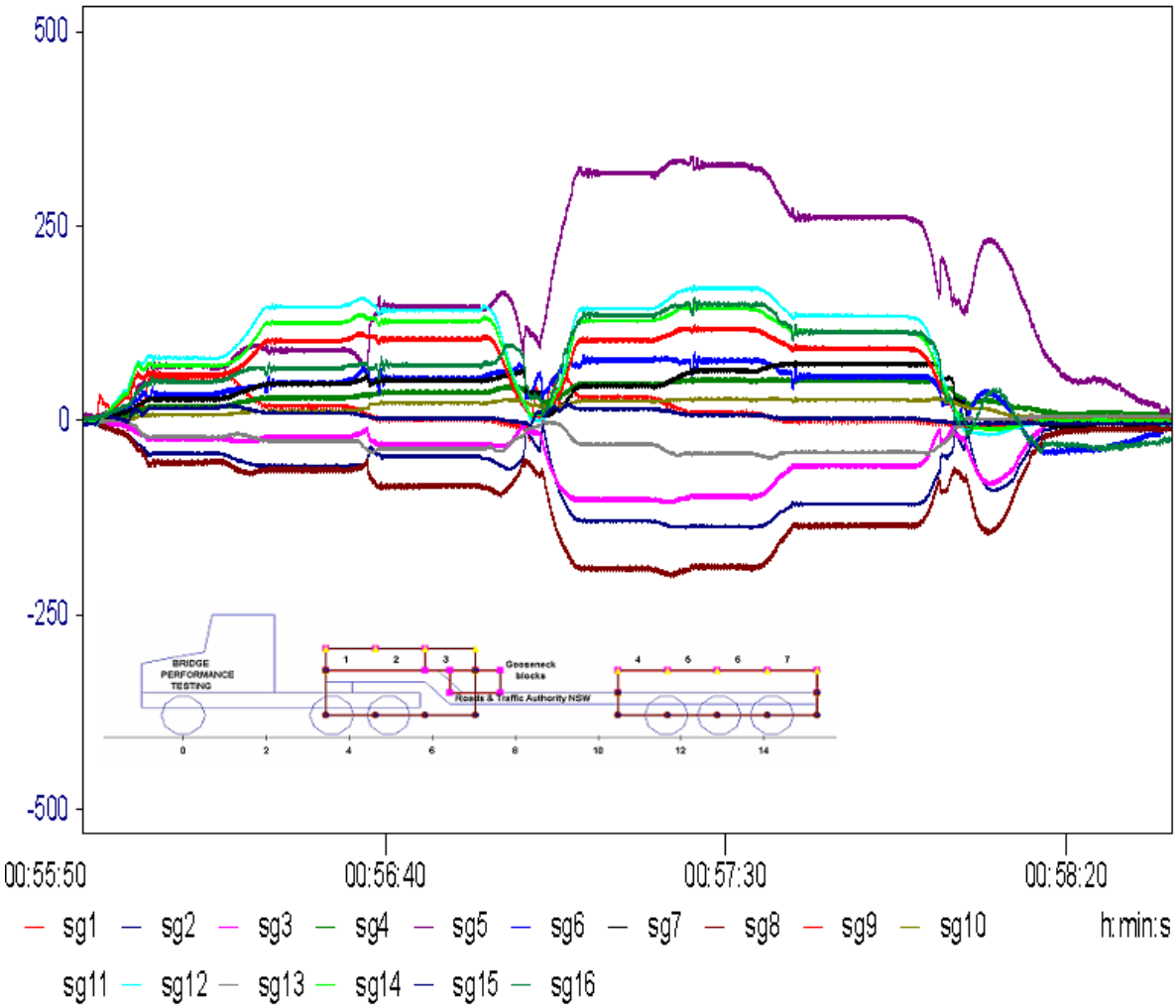

Figure 23 *Sample Strain Time history all gauges*

8. NEUTRAL AXIS OF STRINGERS AND COMPOSITE BEAM EFFECTS

The slow roll results were used to plot the position of the neutral axis of the stringers. **Figure 24** below shows the resulting normal stress diagram and apparent position of the neutral axis of the beam for a mid span location as well as for the cope connection. It is clear that at the mid span stringer location the neutral axis is quite close to the geometric centre of the beam, which is an indication that the concrete deck is providing little composite effect, i.e. the concrete deck and stringer act almost as independent beams. At the cope connection, the neutral axis is remarkably almost at the bottom flange of the stringer indicating, (not good for a moment connection), indicating a complete lack of composite effect as well as a severely limited moment carrying ability. These measurements appear to confirm theoretical results reported by Roeder *et al* [9]. Calculation of the moment of inertia for the complete stringer and reduced stringer at the cross girder connection predicted a ratio of approximately 3.6. The calculated increase in stress to support the same moment is approximately 4, (from y/I ratio).

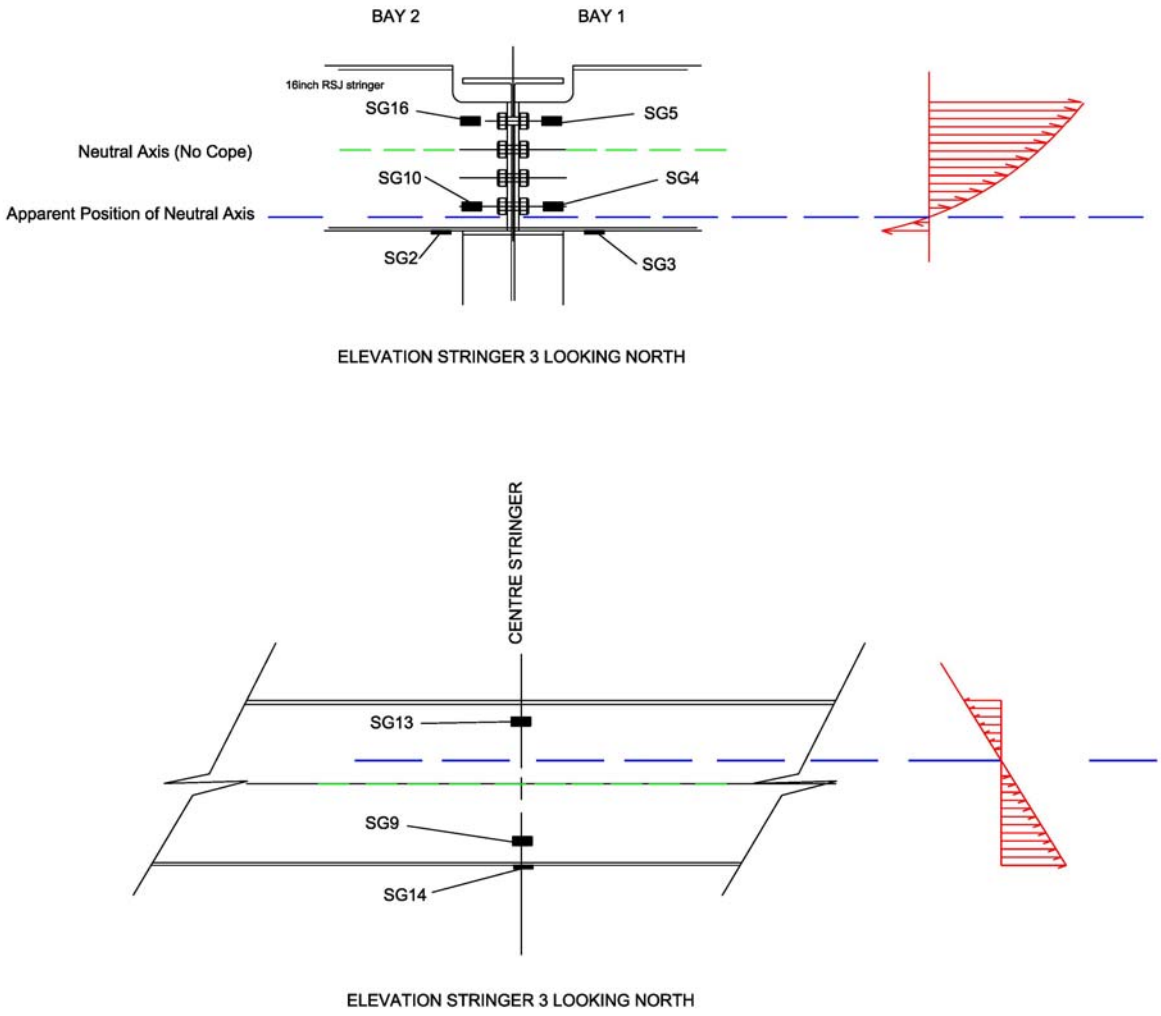

Figure 24 ***Stringer Diagrams Showing Measured Position of Neutral Axis***

9. MAXIMUM STRAINS AND HYSTERESIS DURING PASS-BYS

Figures 26 to 31 below show sample slow roll results for all gauges. The figures include a diagram of the test truck scaled and positioned with respect to each group of gauges, i.e. at any instant in time, x axis, the truck position with respect to the gauge, can be found by projecting a vertical line at the point in strain and time in question. It is easy to pick this out from SG1, in Figure 21, as each strain event correlates with each axle passing above the gauge. **Figure 24** demonstrates that for the stringer mid span (bottom trace) there are two main peak strain events for the truck passby,), i.e. prime-mover (tractor) tandem axles mid span and trailer tridem mid span. **Figure 25** shows that there are three main peaks in strain the additional peak occurring when the tridem is mid span of bay 2, the extreme maxima occurs when axle 5 is mid span bay 1 and the prime-mover (tractor) is approx mid span bay2, i.e. the stringer connection receives an additive tensile strain from the load in the adjacent bay. The maximum strain at SD5, top cope connection, occurs when the prime-mover (tractor) and trailer have straddled the cross girder. It is also apparent that for most if not all strain gauges a hysteresis effect occurs, this is most apparent on **Figure 25, Figure 26** and **Figure 27**, marked as an offset. Such an effect is most likely due to a stick slip mechanism which probably occurs at the stringer/deck interface, this is again evidence of no composite beam effect, i.e. no effective shear connection between stringers and deck, once the load has passed the strain does not return to the same state as before the load is applied.

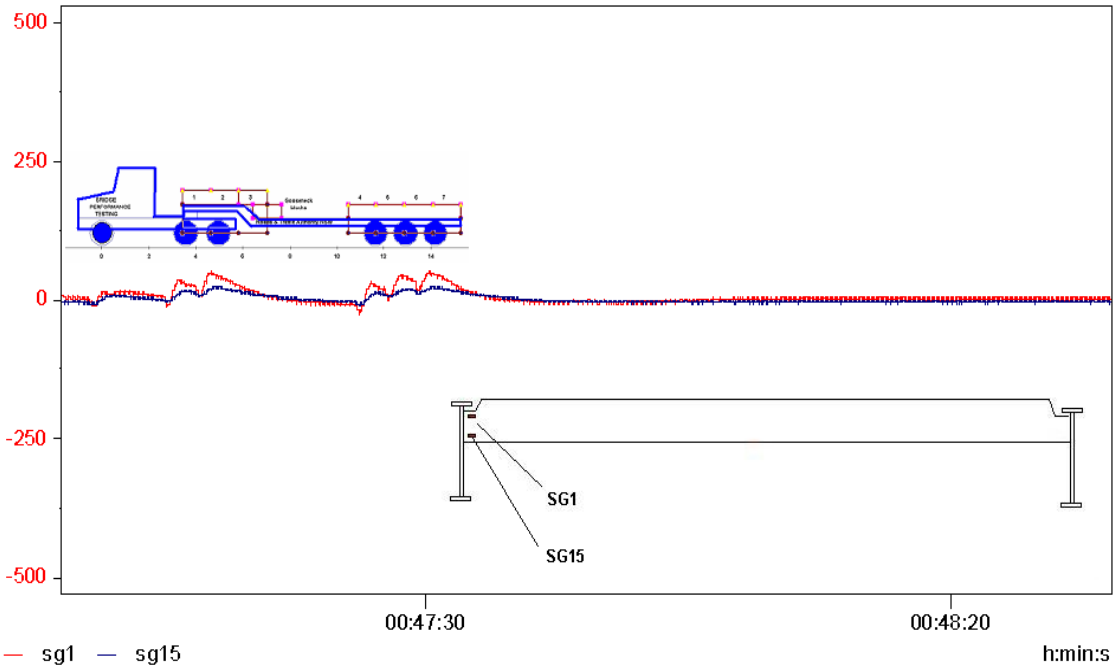

Figure 25 *Slow Roll Strain time Histories For Group 1 Gauges, (stringer line 3, see also Figure 19 for locations)*

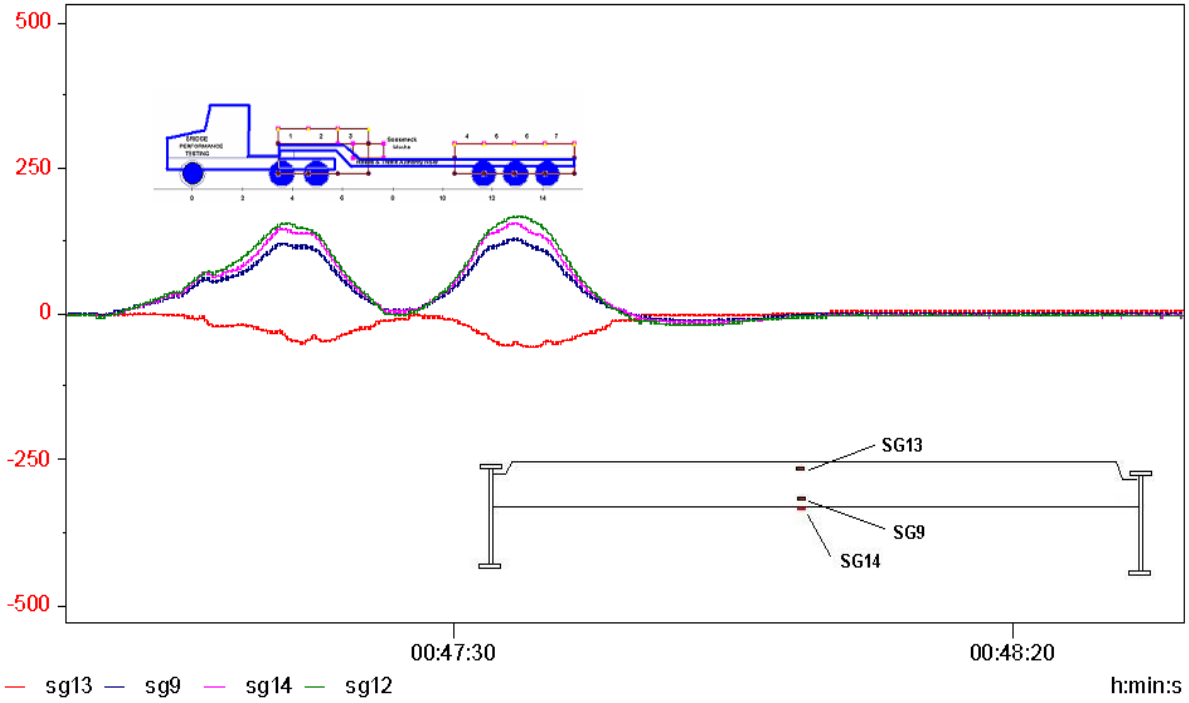

Figure 26 *Slow Roll Strain time Histories For Group 2 Gauges, (SG9, SG13 and SG14 on stringer line 3, SG12 as SG14 but on stringer line 2)*

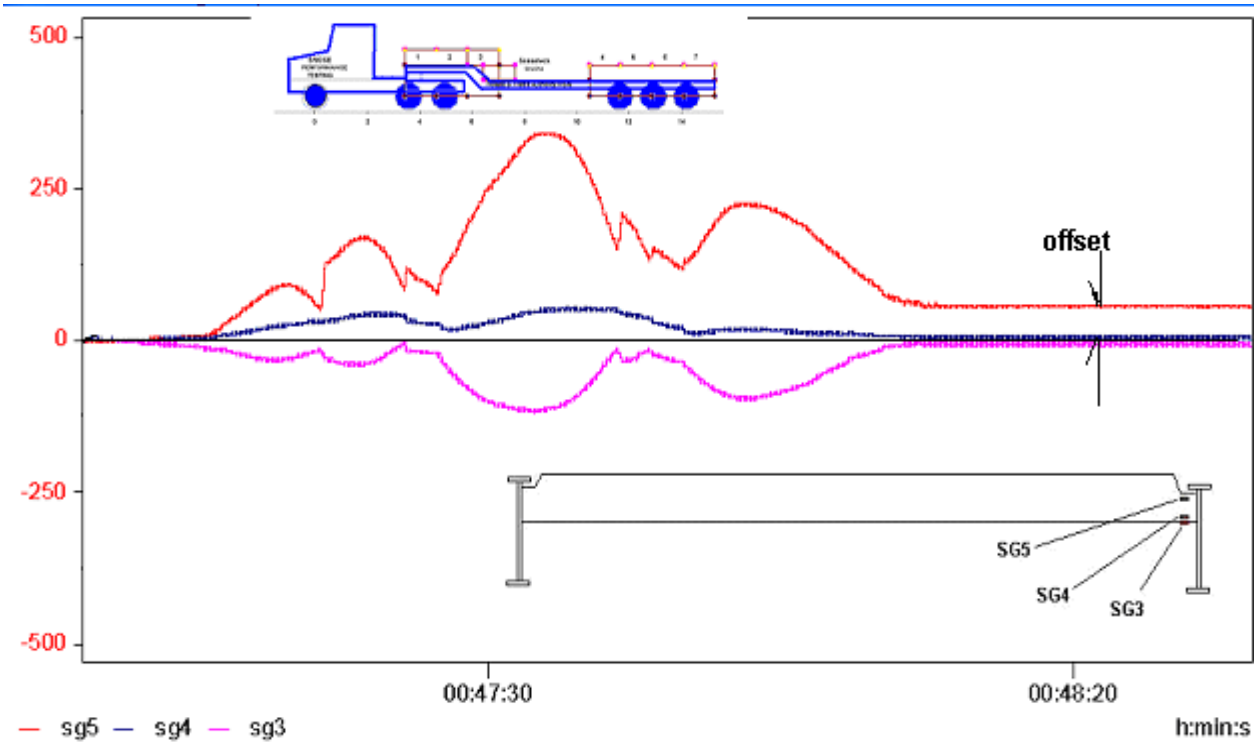

Figure 27 *Slow Roll Strain time Histories For Group 3 Gauges, (stringer line 3)*

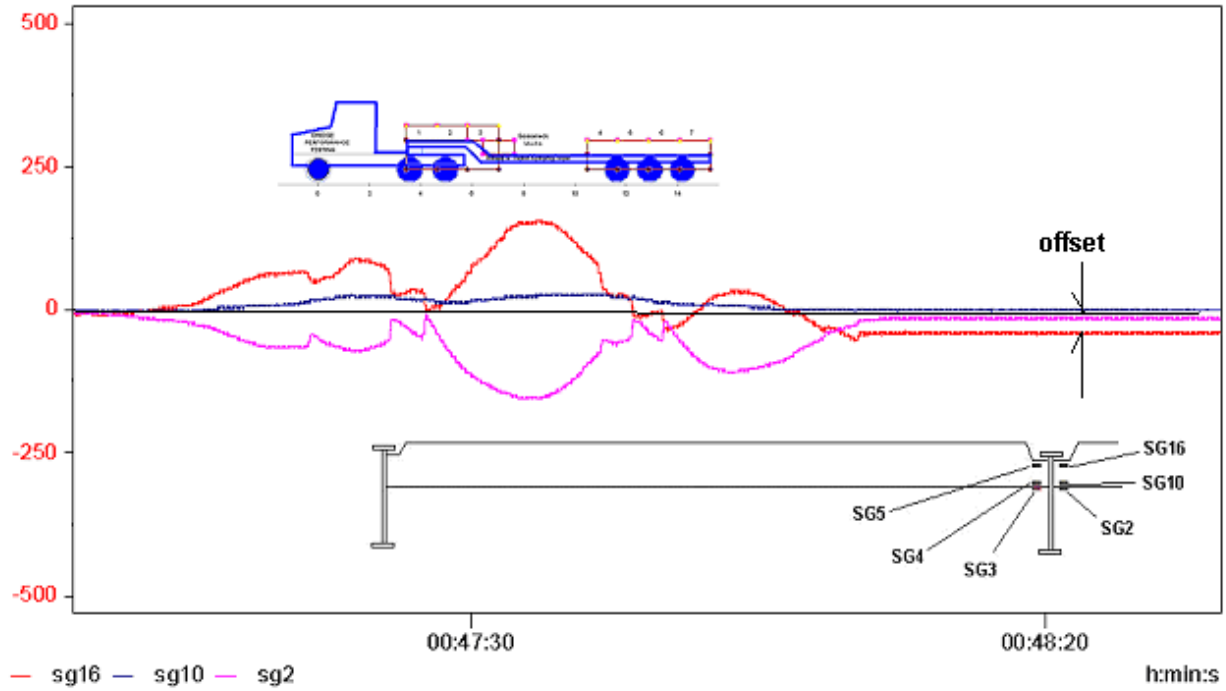

Figure 28 *Slow Roll Strain time Histories For Group 4 Gauges, (stringer line 3)*

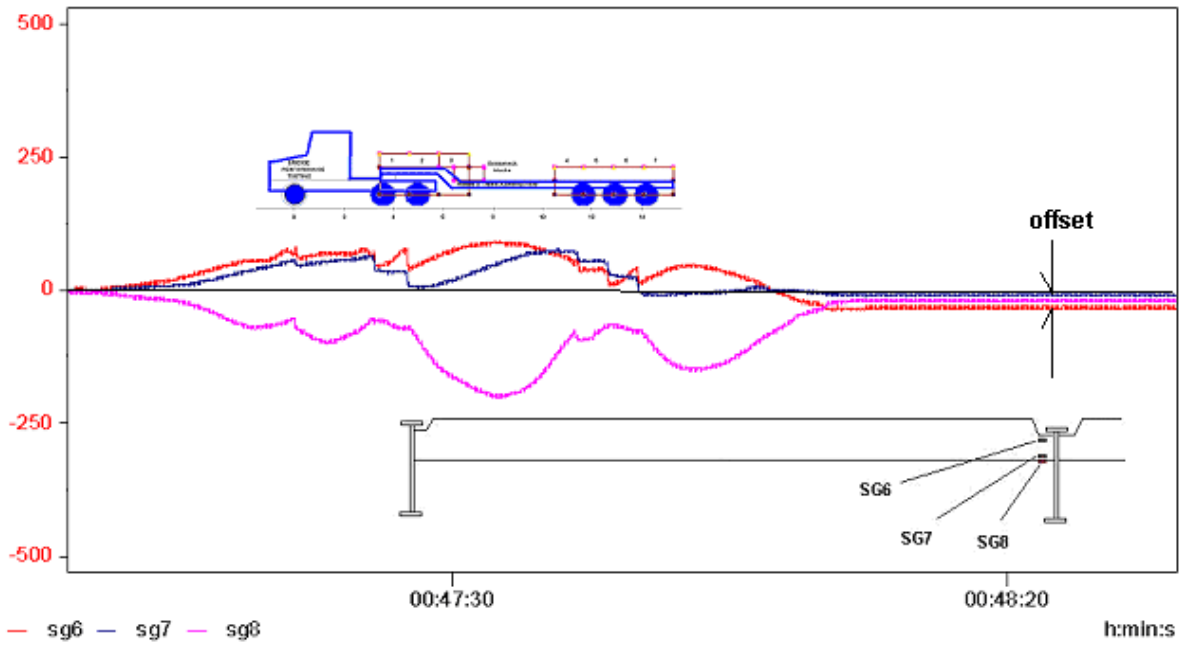

Figure 29 *Slow Roll Strain time Histories for Group 5 Gauges, (stringer line 2)*

10. DYNAMIC STRAIN RESULTS

Table 4 presents a summary of the resulting maximum strains, stresses and dynamic amplification factors from all controlled tests at Kempsey Bridge. It should be noted that DAF is identical to the impact factor plus 100%.

Table 4 *Summary of Resulting Strains, Stresses and Dynamic Amplification Factors*

Location	Strain (με)			Stress (MPa)			DAF's		
	Max.	Min.	Range	Max.	Min.	Range	+ve	-ve	Range
sg1	57	-45	87	11	-9	17	1.1	-0.9	1.1
sg15	29	-20	39	6	-4	8	1.1	-0.8	1.1
sg13	9	-78	76	2	-16	15	1.3	-0.2	1.3
sg9	148	-36	176	30	-7	35	1.1	-0.3	1.2
sg14	181	-34	211	36	-7	42	1.1	-0.2	1.2
sg12	178	-37	212	36	-7	42	1.0	-0.2	1.1
sg5	372	-119	472	74	-24	94	1.1	-0.3	1.4
sg4	66	-19	76	13	-4	15	1.2	-0.3	1.4
sg3	18	-138	140	4	-28	28	1.2	-0.2	1.2
sg16	170	-121	252	34	-24	50	1.0	-0.8	1.3
sg10	31	-20	41	6	-4	8	1.1	-0.7	1.2
sg2	12	-185	184	2	-37	37	1.2	-0.1	1.2
sg6	106	-64	163	21	-13	33	1.2	-0.7	1.6
sg7	77	-34	98	15	-7	20	1.0	-0.4	1.1
sg8	1	-231	222	0	-46	44	1.1	0.0	1.2

Figure 30 shows sample strain time history for group 3 gauges i.e. SG5 SG4 and SG3, at slow roll and a typical 59kph pass-by. These plots demonstrate that the dynamic response, is a combination of localised stress effects as well as global stresses i.e. the dynamic strain time histories from gauges at the cope show similar general shape to the slow roll strain time histories but at an amplified level. In addition, a more global dynamic effect can be seen on the lower plot, which is the dynamic build up in strain prior to the arrival of the truck on the span instrumented with strain gauges, due predominately in this case to excitation of the fundamental vertical bending mode of the truss span.

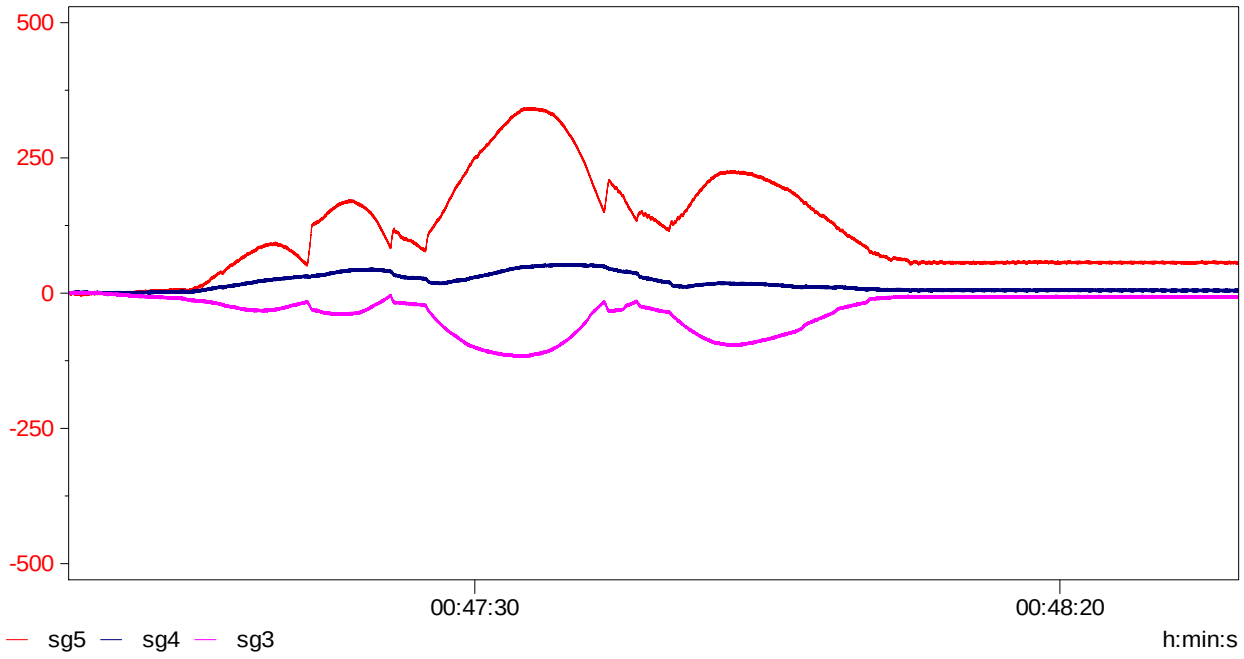

Figure 30(a) ***Sample Strain Time History Module 5 Gauges, slow roll***

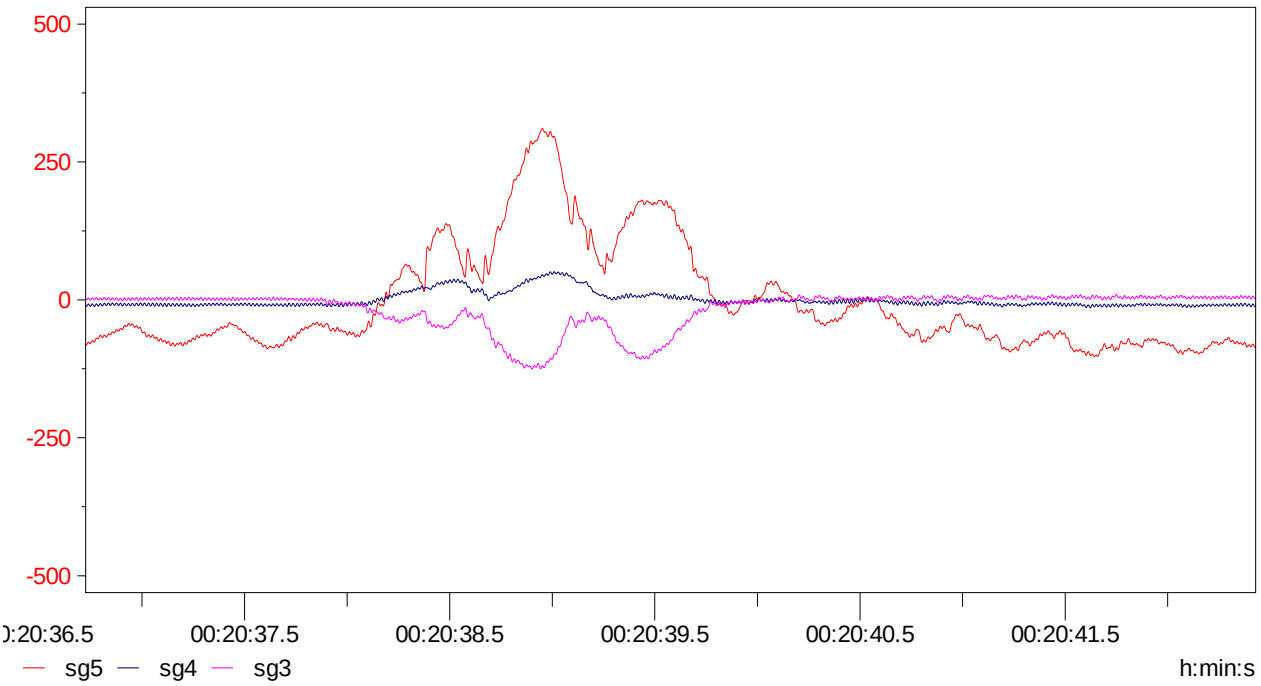

Figure 30(b) ***Sample Strain Time History Module 5 Gauges, 59km/hr***

11. LONG TERM STRAIN MEASUREMENTS AND RAIN FLOW CYCLE COUNTING

Table 5 below shows an abridged summary of the maximum strain range recorded for each gauge from the controlled (legal axle load and legal speed) pass-bys and from the uncontrolled 7 days of traffic for all three tested bridges. It is apparent from these results that analysis or fatigue design based on legal load limits alone would very much under estimate the actual dynamic service loads.

Table 5 *Summary of Maximum Recorded Stress Ranges (All Bridges)*

Bridge Location	Strain Gauge Location No.	Component Description	Stress Range From Controlled Tests (MPa)	Stress Range Recorded under Traffic (MPa)	Apparent Maximum Amplification from Traffic (note 1)
Dennis	Sg4	Top Web	75	84	1.1
	Sg6	Bottom Web	15	34	2.3
Hexham	Sg14	Top Web	19	56	3.0
	Sg15	Bottom Web	20	48	2.4
	Sg21	Top Web	16	48	3.0
	Sg22	Bottom Web	9	32	3.6
Kempsey	sg5	Top Web	94	128	1.4
	sg4	Bottom Web	15	24	1.6
	sg3	Bottom Flange	28	48	1.7
	sg10	Bottom Web	8	16	1.9
	sg2	Bottom Flange	37	56	1.5
	sg6	Top Web	33	56	1.7
	sg7	Bottom Web	20	32	1.6
	sg8	Bottom Flange	44	56	1.3

Note: Numbers include effects from multiple presence

12. FINITE ELEMENT MODELLING – FINE MESH RESULTS

A fine mesh model was refined to assess the potential effects of concept fatigue life extension options. Concept options proposed can be placed in two main categories, 1) **Stringer stiffening** and 2) **Compliant stringer cross girder connections**.

As-Built Connection Detail

The as-built condition was first modelled and a static analysis carried out for the live load as per controlled strain measurements. **Figure 31** presents modelling results for the as-built condition.

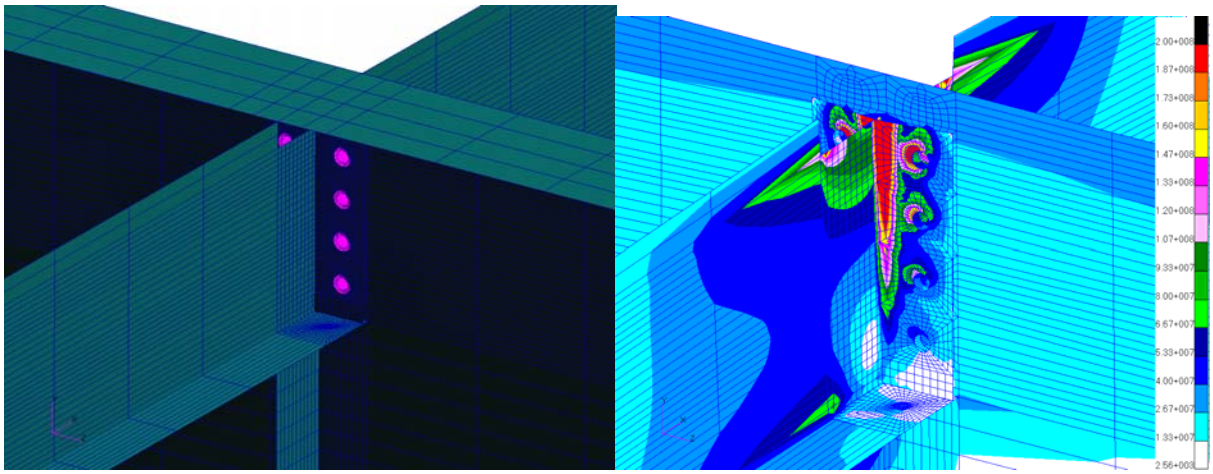

Figure 31 *Fine Mesh Model For As Built Connection Detail, base model left, Stress contour results right*

13. STRINGER STIFFENING OPTIONS

Stringer Top Flange Replacement- This option involved plating over the stringer top flanges at the cross girders to effectively replace the top flange cut away to clear the cross girder top flange. **Figure 32** shows a sample stress contour output for this concept.

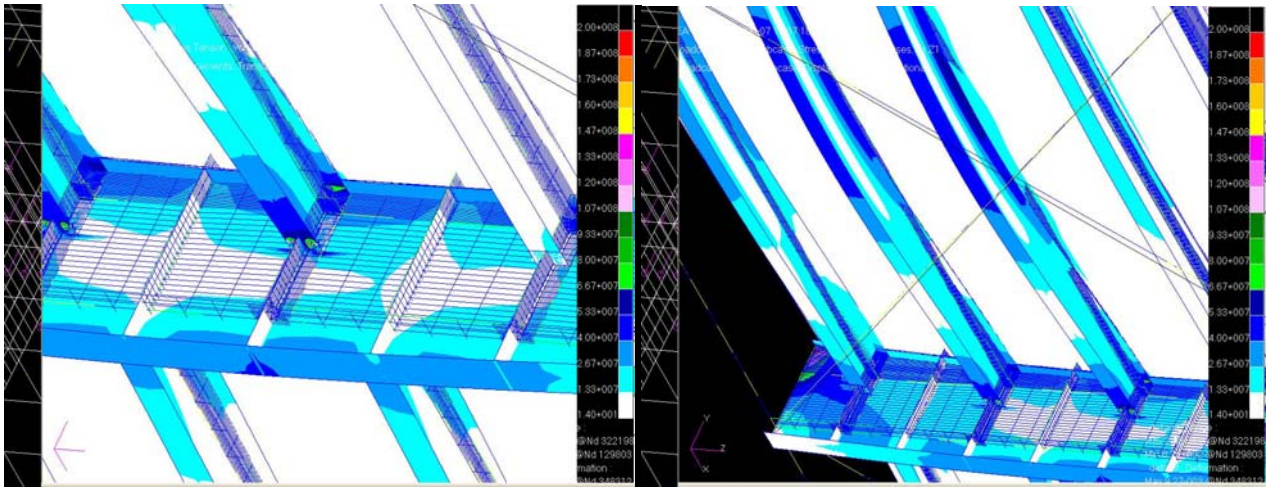

Figure 32 *Sample Stress Contour Plots For Stringer top Plate replacement Option*

14. COMPLIANT CONNECTION OPTIONS

Flexible Bolted Connections/Bearings- These options require the replacement of the top two, three or four rows of connection fasteners with a flexible assembly. Ideally these assemblies would allow some axial movement of the stringer flange whilst maintaining lateral restraint. The concept compliant connection options were modelled with an axial stiffness of 100KN/mm. **Figure 33** shows a sample stress contour plot. The compliant connection may be seen as a variation of the rivet removal damage limitation method investigated by Roeder *et al* [10]. The principal difference appears to be in the plane of removal. Roeder removed rivets from the connection through the web of the stringer and the present study replaced rivets (with compliant fasteners) through the web of the cross girder.

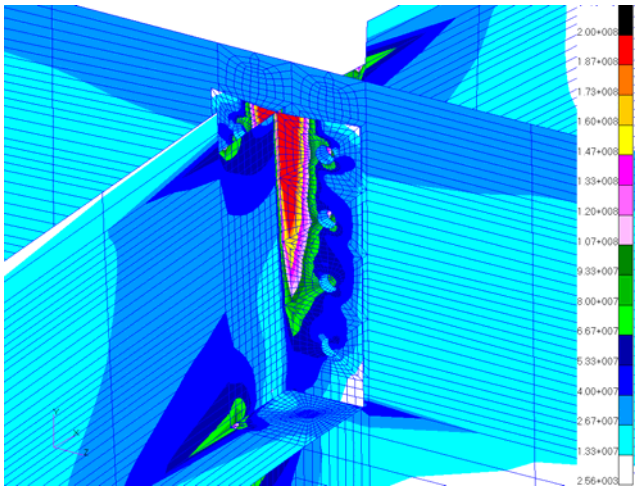

Figure 33 ***Sample Stress Contour Plot, Compliant Connection Option***

Bolt Removal - Removal of the top 2 and 4 rows of bolts/rivets has also been modelled. **Figure 34** shows stress contour plots for these conditions.

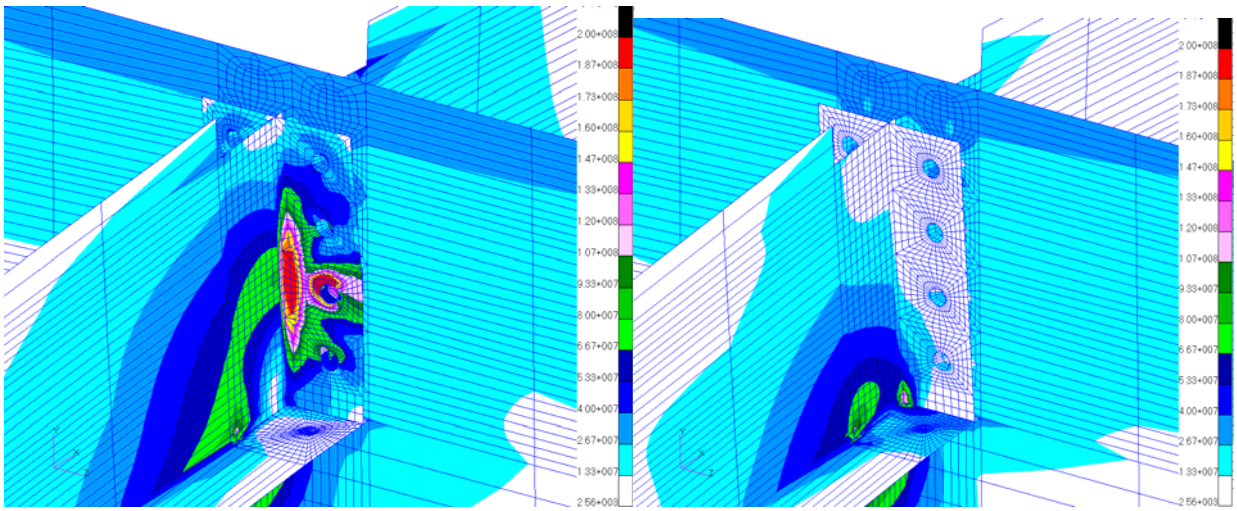

Figure 34 ***Sample Stress Contour Plots: 2 rows bolts removed left: 4 rows bolts removed right***

15. POST MODIFICATION MEASUREMENTS (DENNIS)

Figure 35 shows typical strain histories due to ambient traffic prior to modification and **Figure 36** shows typical strain histories due to ambient traffic after modification. Inspection of the data for SG2 reveals that a strain range of around 250 με (150 to -100) has been changed to around 227 με (45 to -182) but the strain is now mostly compressive.

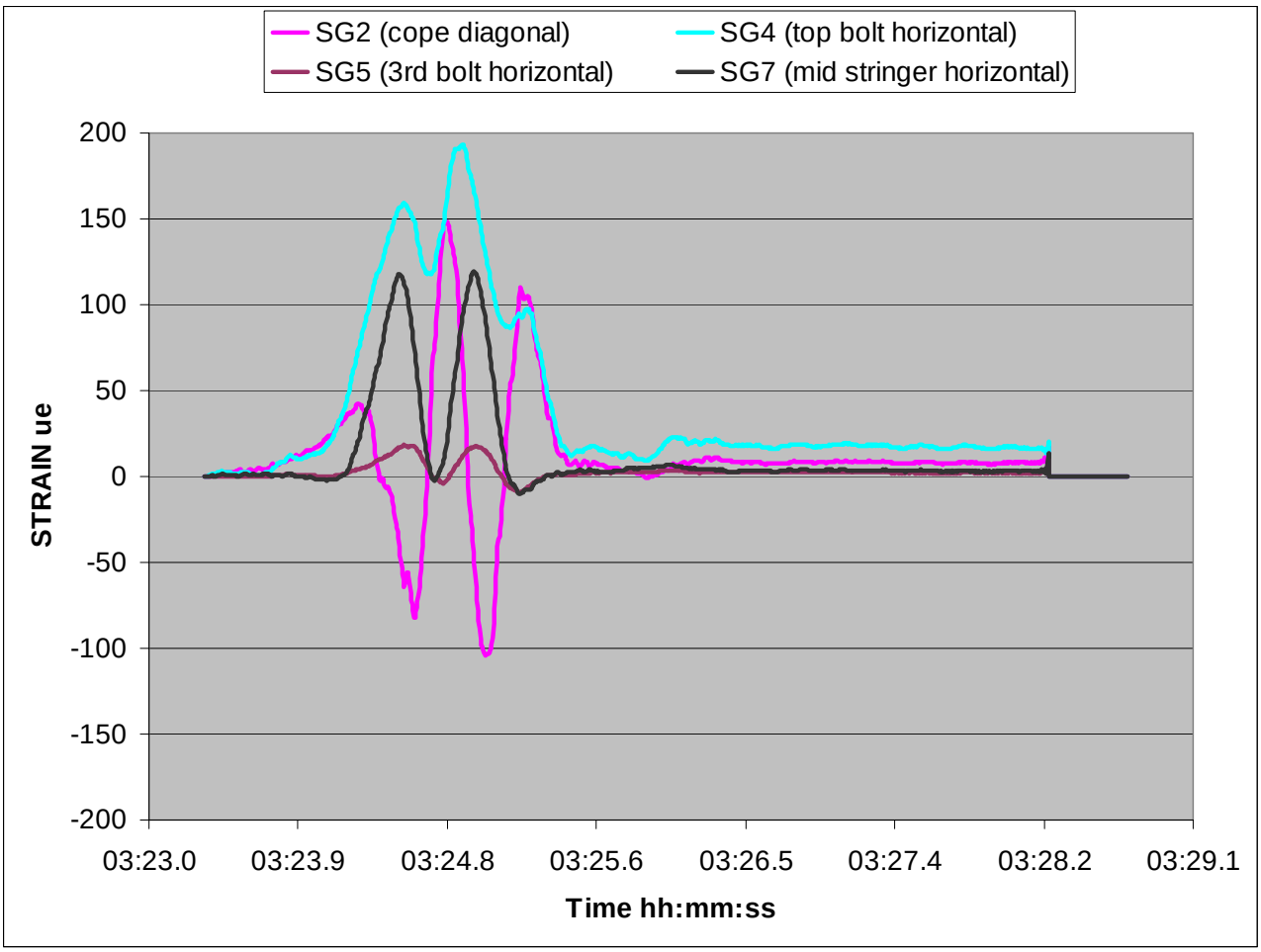

Figure 35 *Typical Strain Time Histories – Pre Modification (Ambient Traffic)*

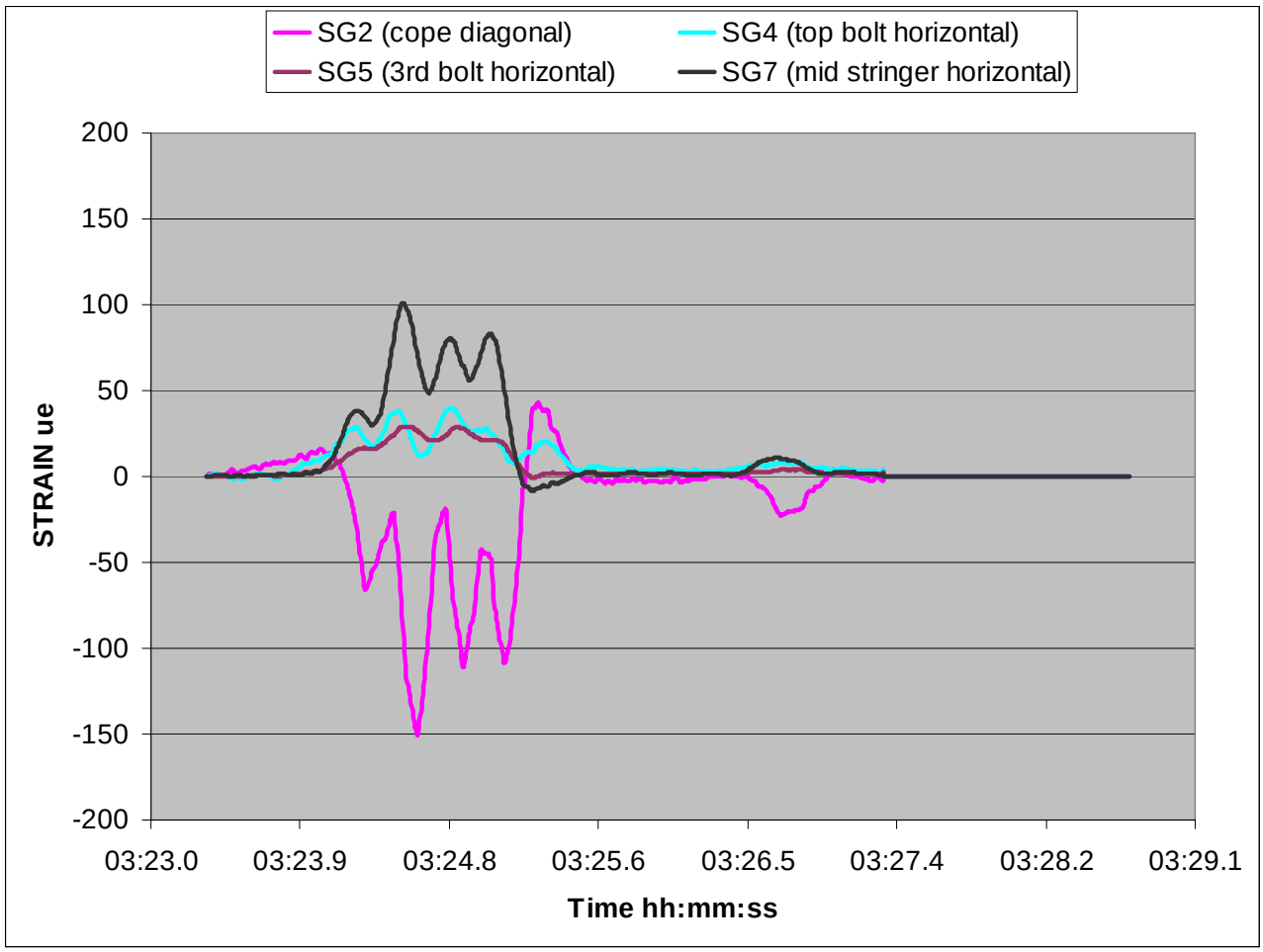

Figure 36 *Typical Strain Time Histories – Post Modification (Ambient Traffic)*

Figure 37 shows the percentage reduction in stress range for both the compliant bolt option and the removal of the top two rows of bolts. For this figure, stress reduction was calculated as the maximum strain range at each gauge divided by the maximum strain range at gauge SG7 (stringer mid-span). **Figure 38** shows the percentage reduction in tensile stress for both the compliant bolt option and the removal of the top two rows of bolts. For this figure, stress reduction was calculated as the maximum tensile strain at each gauge divided by the maximum strain range at gauge SG7 (stringer mid-span). These data show a clear benefit for the compliant bolt modification. At the stringer flange and bolted connection both the strange range and tensile stress cycles are significantly reduced. For welded connections the reduction in strain range is used to assess the fatigue life benefit. At the cope while the strain range is reduced by approximately 20% the tensile strain cycles are reduced by approximately 70%. For non welded details (ie the cut out at the cope) it is likely that the fatigue life is more sensitive to reduction in tensile load cycles rather than simply the stress range.

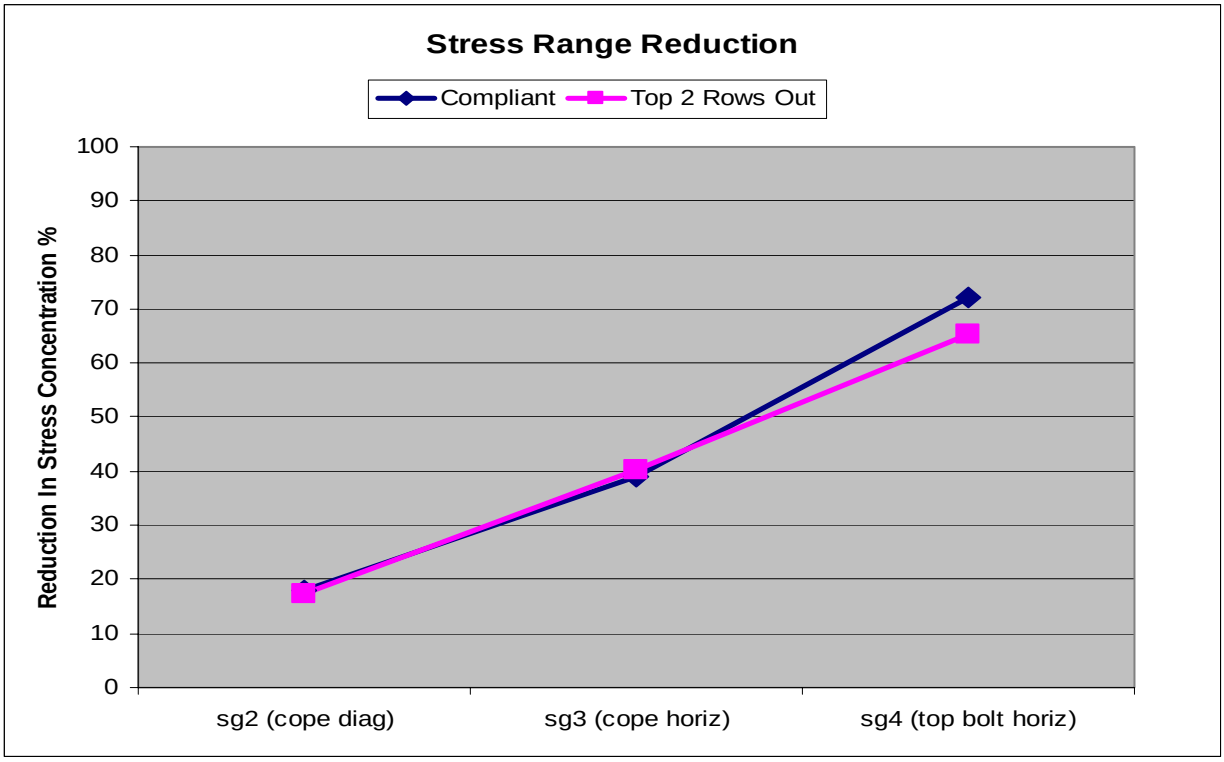

Figure 37 *Typical Stress Range Reduction*

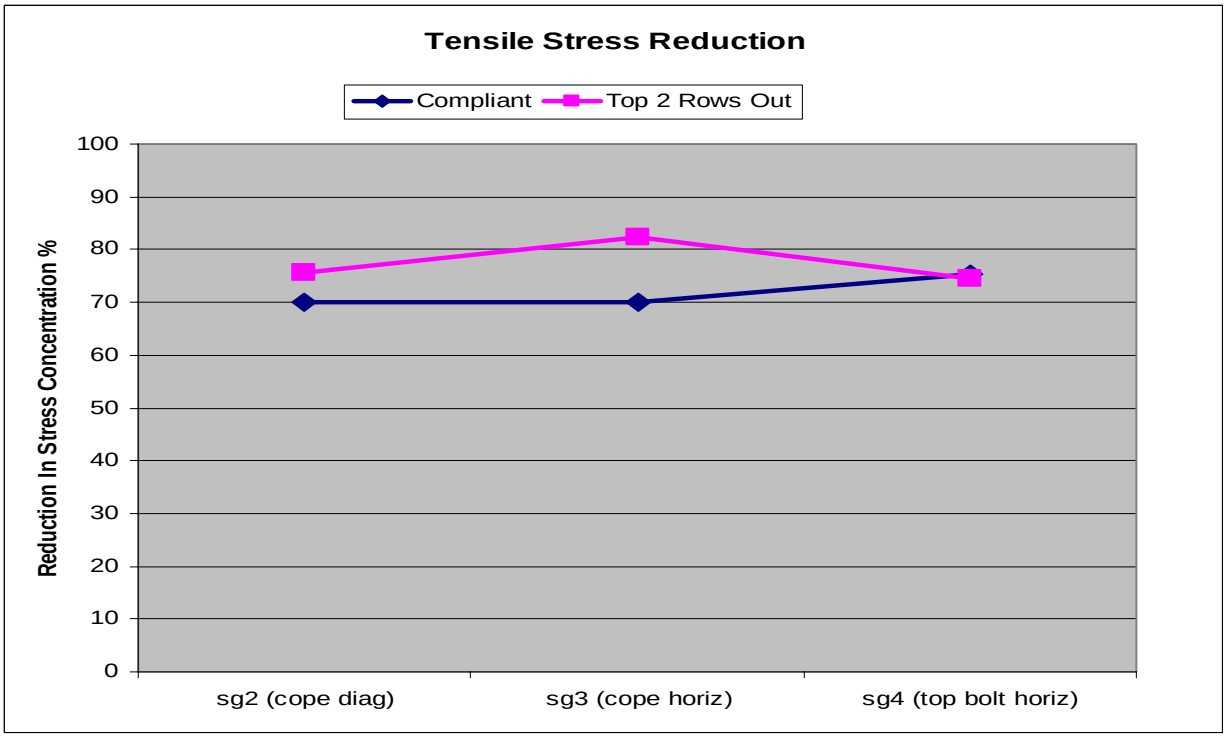

Figure 38 *Typical Tensile Stress Reduction*

16. POST MODIFICATION MEASUREMENTS (KEMPSEY)

Whilst the stringer top flange stiffening option offered the optimum solution, there were operational constraints that operated against its implementation. The compliant fastener option was initially trialled in one span. Strain measurements were recorded under traffic for each connection arrangement tested. The following connection arrangements were tested:

TEST A no bolts in top 2 rows ie 4 bolts out
TEST B2 hard bolts RHS flange (cracked flange)
TEST C4 hard bolts top two rows ie fully bolted as per pre modification
TEST D compliant bolts, (zero pre tension)
TEST E compliant bolts in top two rows (half turn pre tension). Recordings were subsequently analysed to produce time histories for a sample number of heavy vehicle pass-bys, the ratio of mid span stringer strain to the maximum strain at each gauge was calculated for each pass by.

Stress concentration Factors

Table 6 presents a summary of the resulting maximum stress concentration factors from the above test series.

Table 6 ***Summary of Resulting Stress Concentration Factors From Test Series***

Test	Description of Test	Maximum Stress Concentration Factor	Position of Maximum Stress	Reduction in Stress due to Modification (%)	Predicted increase in Fatigue Life (x)
A	no bolts in top 2 rows ie 4 bolts out	1.3	SG5	45	6.1
B	2 hard bolts RHS flange (cracked flange)	1.2	SG5	50	8.1
C	4 hard bolts top two rows ie fully bolted as per pre modification	2.4	SG3	0	1.0
D	compliant bolts, zero pre tension	1.4	SG3	41	5.1
E	compliant bolts in top two rows, half turn pre stress	1.6	SG3	33	3.3

Figure 35 shows a sample strain time history for the as built connection, ie hard bolted with all fasteners in place. **Figure** shows a sample strain time history for the modified connection as proposed, i.e. top four bolts with compliant washers, pre tension one half turn. The figures clearly demonstrate the significant stress reduction associated with the modification.

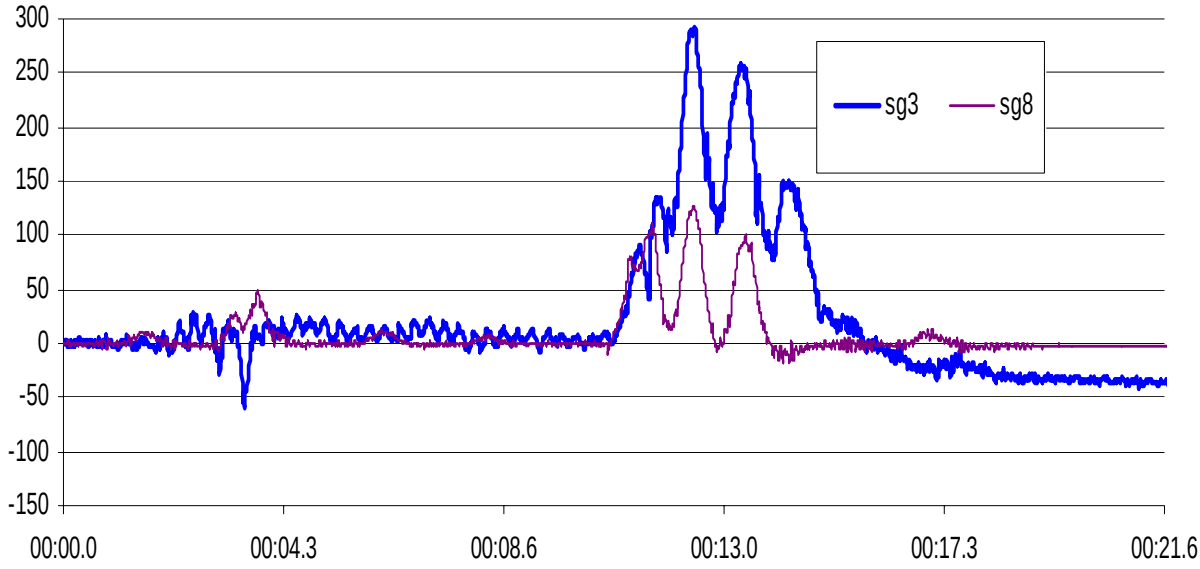

Figure 35 ***Sample Strain Time History – As Built (Test C)***

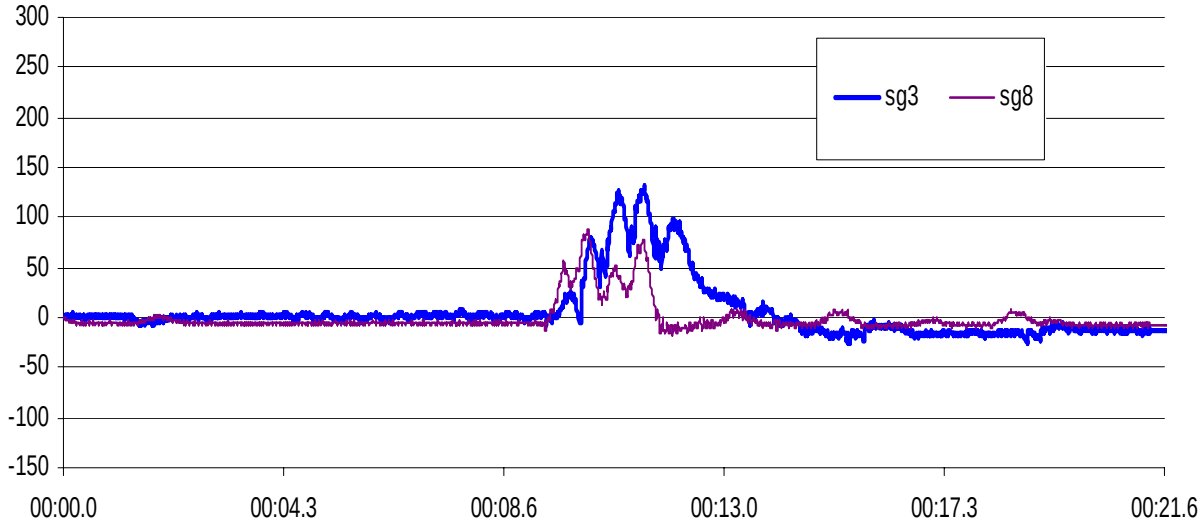

Figure 39 ***Sample Strain Time History – Installed Modification (Test E)***

17. TRAFFIC DATA ANALYSIS

Analysis of Weigh-In-Motion (WIM) Data

The load spectrum data for each WIM station were converted to the ADESA applicable to relevant bridges using the minus rule. The resulting Average Daily Equivalent Standard Axle (ADESA) load spectra were then plotted to structure the initial data groups. The data groups listing were individually tested using F-test and Student T-test, and statistically analysed for homogeneity using ANOVA. The data groups were subjected to a follow-up test using Tukey's Test. Final grouping of data was done after a series of follow-up tests. An attempt was also made to transform the weighted percentages of the resulting ADESA load spectra into arcsin values for each WIM station. All samples of the arcsin transformed ADESA percentages were then analysed using ANOVA. The results showed that the data were homogeneous.

Calculation of ESA from WIM Data

The ESA applicable to bridges based on WIM data for the first half of 2006 was calculated using the minus rule formula, derived as follows:

$$f_f^3 = \frac{f_m^3 \times 2 \times 10^6}{n_{sc}}$$

$$n_{sc} = \frac{f_m^3}{f_f^3} \times 2 \times 10^6$$

$$N_{sc} = \sum_i n_{sci}$$

$$N_{sc} = \sum_i \frac{f_{mi}^3}{f_f^3} \times 2 \times 10^6$$

Proportional Correlation

$$f_{mi} \propto L_i$$

$$f_f \propto L_f$$

$$N_f = \sum_i \left(\frac{L_i}{L_f} \right)^3 n_i$$

Where:

N_f = Equivalent standard axle (ESA) for the period

L_i = Mass of Axles x Number in group

L_f = Standard Load (160 kN, assumed)

n_i = Count for the period

$\frac{N_f}{N_V}$

N_V = Total number of Vehicles

$\frac{N_f}{N_G}$

N_G = Total Groups

$\frac{N_f}{N_A}$

N_A = Total Axles

Cumulative ESA data for the period 1980-2006 are shown graphically as Figure 37. These data confirm the exponential growth in loads and an even faster growth in axle group repetitions due to the greater utilisation of B-doubles and tri-axle semi-trailers. The ESA approach differs from the truck weight histogram (TWH) and wheel weight histogram (WWH) method suggested by Fu *et al* [6]. However, the methodology is considered to be broadly similar.

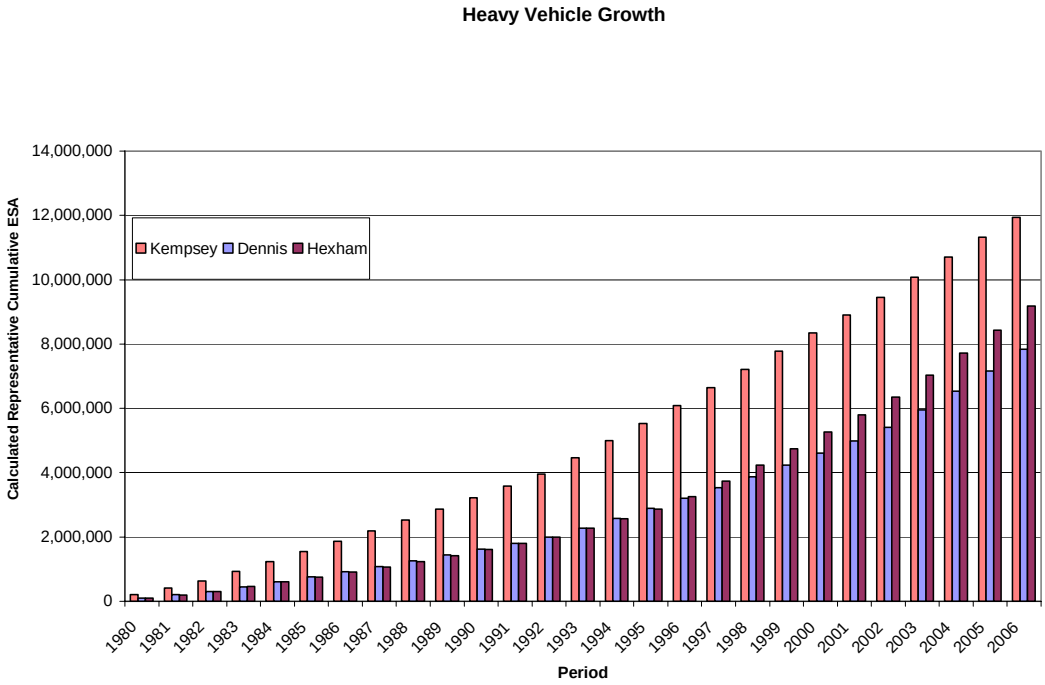

Figure 40 ***Representative Cumulative ESA***

18. CONCLUSION

The basic failure mechanism at the stringer/cross girder connection involves the inability of the stringer to transmit and/or react live and dead load induced bending moments. From this study, it is clear that the neutral axis of the stringer (at the cross girder) is almost at the bottom flange, (at mid span the neutral axis is approx 2/3 up the web, so a small composite beam effect only exists between the stringers and the concrete deck). Due to the vast reduction in moment of inertia of the stringer at the cross girder, (i.e. a factor of 3.6), the bending stiffness is greatly reduced and the stringer probably behaves (and deflects) more like a simply supported beam attempting to rotate the stringer flange out of plane. It is also apparent that the "fixed end" and/or "continuous" nature of the stringer does little to assist the stringer to carry load, some indirect evidence of this can be seen in **Figure 24** (note the very small compression that occurs mid span of the stringer when the tridem has passed to bay 2, SG14, this is really the third peak in the strain which is much greater and in the opposite sense for SG5 and would be greater for SG14 if the stringer was truly continuous). Analysis of the speed runs demonstrates that these conclusions are similar but with generally higher strains due to dynamic amplification.

In summary, the as-built stringer connection detail is poor from both a static and dynamic perspective. The detail is not stiff or strong enough to act as a fixed end or form a continuous beam, neither is it flexible enough to allow out of plane rotation, (without high stress) and allow the stringer behave as a simply supported beam. Possible solutions for this problem that have been identified thus far are placed in two main categories. Stiffening, which would include the top flange replacement concepts as well as the stringer truss type stiffening, such concepts would take bending stresses away from the stringer/cross girder connections and/or reduce mid span stringer deflections as well as out of plane rotation, bolts/rivets would probably remain as is.

Compliant Fastening, i.e. concepts which allow the out of plane rotation at the stringer support points and allow the stringer to act more as a simply supported beam, have a clear advantage of much lower cost than the stiffening options, and were achieved with access from under the bridge, i.e. no lane closures. Analysis of weigh-in-motion (WIM) data confirm that bridge loadings are increasing due to exponential growth in loads and an even faster growth in axle group repetitions due to the greater utilisation of B-doubles and tri-axle semi-trailers. These data and the apparent load effect for fatigue from uncontrolled heavy vehicle traffic significantly exceed the value that would be predicted using the test vehicle factored for dynamic effects and multiple presence.

ACKNOWLEDGEMENT

The authors wish to thank the Chief Executive of the Roads and Traffic Authority NSW for permission to publish this paper. The opinions and conclusions expressed in this paper do not necessarily reflect the views of the RTA.

REFERENCES

1. AASHTO, "Standard Specification for Highway Bridges", American Association of State Highway and Transportation Officials, 15th Edition, Washington, DC, USA, 1973.
2. ROEDER C.W., MACRAE G.A., ARIMA K., CROCKER P.N. & WONG S.D., "Fatigue Cracking of Riveted Steel Tied Arch and Truss Bridges", *Research Report WA-RD 447.1,* Washington State Transportation Center, Seattle, USA, 1998.
3. Roads & Traffic Authority of NSW. "Blueprint - RTA Corporate Plan 2008 to 2012", *RTA Publication 07.329*, Sydney, Australia, 2008.
4. IMAM, B.M., RIGHINIOTIS T.D. & CHRYSSANTHOPOULOS M.K., "Probabilistic Fatigue Evaluation of Riveted Railway Bridges", *J. Bridge Engineering,* ASCE, 13(3), 237-244, 2008.
5. GARGETT D., HOSSAIN A. & COSGROVE D., "Interstate Freight on States' Roads", *Proc. 29th Australasian Transport Research Forum*, Surfers Paradise, Australia, 2006.
6. FU G., FENG J., DEKELBAB W., MOSES F., COHEN H. & MERTZ D., "Impact of Commercial Vehicle Weight Change on Highway Bridge Infrastructure", *J. Bridge Engineering,* ASCE, 13(6), 556-564, 2008.
7. MORASSI A. & TONON S., "Dynamic Testing for Structural Identification of a Bridge", *J. Bridge Engineering,* ASCE, 13(6), 573-585, 2008.
8. EWINS D.J. "Modal Testing: Theory, Practice & Application (2nd Edition)", *Research Studies Press*, Hertfordshire, UK, 163-276, 1999.
9. ROEDER C.W., MACRAE G.A., KALOGIROS A.Y. & LELAND A., "Fatigue Cracking of Riveted, Coped, Stringer-to-Floorbeam Connections", *Research Report WA-RD 494.1,* Washington State Transportation Center, Seattle, USA, 2001.
10. ROEDER C.W., MACRAE G.A., LELAND A. & ROSPO A., "Extending the Fatigue Life of Riveted Coped Stringer Connections", *J. Bridge Engineering,* ASCE, 10(1), 69-76, 2005.